29 November 2013 | $10

# Science

AAAS

## EDITORIAL



## NEWS OF THE WEEK



## NEWS & ANALYSIS



## NEWS FOCUS



## LETTERS



## BOOKS *ET AL.*



## POLICY FORUM



## PERSPECTIVES



## *SCIENCE* PRIZE ESSAY



CONTENTS continued >>

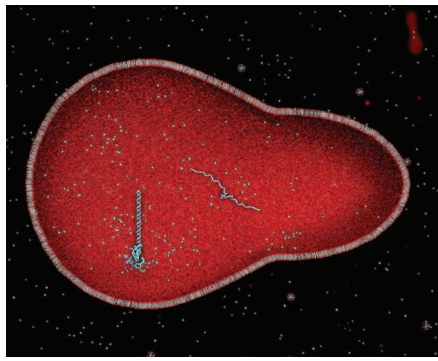

pages 1032 & 1098

page 1043

## ON THE WEB THIS WEEK

**>> *Science* Podcast**
Listen to stories on the top children's books of 2013, what newlyweds know about their prospects for happiness, authorship for sale in China, and more.

**>> Find More Online**
Check out *Science* Express, our podcast, videos, daily news, our research journals, and *Science* Careers at **www.sciencemag.org**.

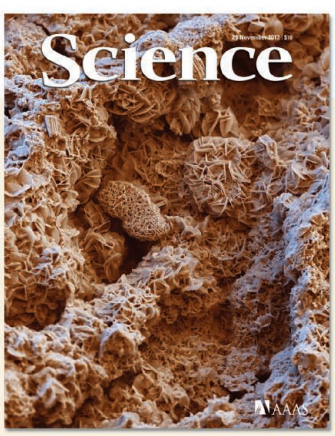


## COVER

Color-enhanced scanning electron micrograph of rust (iron oxide) on painted sheet metal (width of image field: 41.3 micrometers). When activated by a thin carbon layer doped with nitrogen atoms, iron oxide proves to be an efficient catalyst for selective hydrogenation of nitroarenes to anilines, a process that previously required noble metals. See pages 1054 and 1073.

***Image: Eye of Science/Science Source***

## DEPARTMENTS

## RESEARCH ARTICLES



## REPORTS



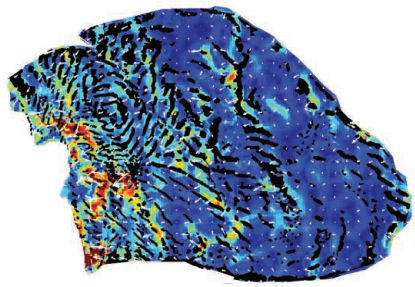

page 1086

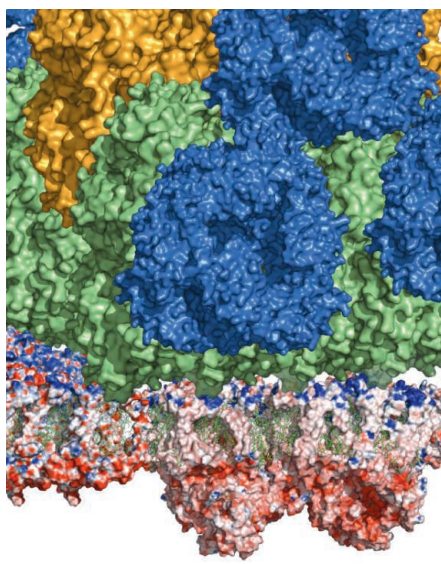

page 1104

CREDIT: (BOTTOM) COURTESY OF HAIJUN LIU

**SCIENCE (ISSN 0036-8075) is published weekly on Friday, except the last week in December, by the American Association for the Advancement of Science, 1200 New York Avenue, NW, Washington, DC 20005.** Periodicals Mail postage (publication No. 484460) paid at Washington, DC, and additional mailing offices.  Domestic individual membership and subscription (51 issues): $149 ($74 allocated to subscription). Domestic institutional subscription (51 issues): $990; Foreign postage extra: Mexico, Caribbean (surface mail) $55; other countries (air assist delivery) $85. First class, airmail, student, and emeritus rates on request. Canadian rates with GST available upon request, GST #1254 88122. Publications Mail Agreement Number 1069624. **Printed in the U.S.A.**

**Change of address:** Allow 4 weeks, giving old and new addresses and 8-digit account number. **Postmaster:** Send change of address to AAAS, P.O. Box 96178, Washington, DC 20090–6178. **Single-copy sales:** $10.00 current issue, $15.00 back issue prepaid includes surface postage; bulk rates on request. **Authorization to photocopy** material for internal or personal use under circumstances not falling within the fair use provisions of the Copyright Act is granted by AAAS to libraries and other users registered with the Copyright Clearance Center (CCC) Transactional Reporting Service, provided that $30.00 per article is paid directly to CCC, 222 Rosewood Drive, Danvers, MA 01923. The identification code for *Science* is 0036-8075. *Science* is indexed in the *Reader's Guide to Periodical Literature* and in several specialized indexes.

EDITED BY STELLA HURTLEY

## Deep Impact?

On 15 February 2013, the Russian district of Chelyabinsk, with a population of more than 1 million, suffered the impact and atmospheric explosion of a 20-meter-wide asteroid—the largest impact on Earth by an asteroid since 1908. **Popova *et al.*** (p. 1069, published online 7 November; see the Perspective by **Chapman**) provide a comprehensive description of this event and of the body that caused it, including detailed information on the asteroid orbit and atmospheric trajectory, damage assessment, and meteorite recovery and characterization.

## Lighter Hydrogenation Catalysts

Enzymes have evolved to use abundant metals such as iron, cobalt, and nickel for redox catalysis. However, synthetic catalysis has generally relied on the rarer, heavier relatives of these elements: ruthenium, rhodium, iridium, palladium, and platinum (see the Perspective by **Bullock**). **Friedfeld *et al.*** (p. 1076) used high-throughput screening to show that the right cobalt precursor can be activated for asymmetric hydrogenation catalysis by using the traditional ligands developed for the precious metals. **Zuo *et al.*** (p. 1080) focused on iron, demonstrating a highly effective asymmetric transfer hydrogenation catalyst that uses a ligand rationally designed after careful mechanistic study. **Jagadeesh *et al.*** (p. 1073) prepared supported iron catalysts that selectively reduce nitro substituents on aromatic rings to amines, thereby facilitating the preparation of a wide range of aniline derivatives.

## Remembrance of Places Past

The hippocampus has two major roles in cognition. Place-responsive neurons form a context-sensitive cognitive map, firing more strongly when an animal traverses specific regions of its environment. Both humans and animals thus need the hippocampus to learn their way around novel environments. Similarly, the hippocampus is critical for our ability to remember a specific event in space and time. It has thus been suggested that the spatial and memory functions of the hippocampus reflect a common architecture. Recording from neurosurgical patients playing a virtual reality memory game, **Miller *et al.*** (p. 1111) found that the recall of events was indeed associated with reinstatement of the place-firing of neurons activated as the subjects navigated through the environment.

## Foil-Forged Images

X-ray diffraction is widely used to determine molecular geometries and can often distinguish mirror image isomers (enantiomers), which generally requires well-ordered crystals. **Herwig *et al.*** (p. 1084) report an imaging technique to characterize enantiomers in the gas phase. A succession of ionization events were induced by passage through a carbon foil that culminated in a Coulomb explosion of mutually repelling nuclei. The trajectories of these nuclei precisely reflected the original molecular structure.

## Cholesterol and Cancer

Obesity and high cholesterol levels are associated with an increased risk of breast cancer in postmenopausal women. **Nelson *et al.*** (p. 1094) found that a specific metabolite of cholesterol, 27-hydroxycholesterol (27HC), promoted tumor growth and metastasis in mouse models of mammary cancer by serving as a partial agonist for the estrogen receptor and the liver X receptor. The most aggressive human breast cancers were found to express the highest level of the enzyme that converts cholesterol to 27HC, suggesting that 27HC produced within tumors (in addition to circulating 27HC) may contribute to tumorigenesis.

## Banding Together

It is important to understand how and where the Antarctic Ice Sheet and underlying ground are coupled, if we want to predict the glacial contribution to sea level rise. **Sergienko and Hindmarsh** (p. 1086, published online 7 November) used observations of ice surface velocities, ice surface elevations, and bed elevations to perform inverse calculations of basal shear stress. Areas of high basal stress were distributed in riblike patterns embedded in much larger areas of no basal shear stress, which may affect the rates at which ice is discharged into the ocean.

## Deciphering Hepatitis C

Hepatitis C virus is a major cause of liver disease and cancer. Two envelope glycoproteins, E1 and E2, form a heterodimer that facilitates infection. The envelope proteins have been difficult to crystallize, hindering vaccine development. **Kong *et al.*** (p. 1090) designed an E2 core glycoprotein construct and solved the crystal structure of the glycosylated protein in complex with a broadly neutralizing antibody. The host cell receptor binding site was identified by electron microscopy and mutagenesis. The findings should help in future drug and vaccine design.

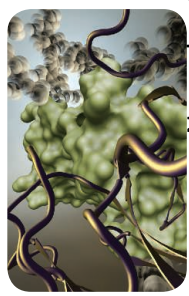

## Don't Ape Protein Variation

Changes in DNA and messenger RNA (mRNA) expression levels have been used to estimate evolutionary changes between species. However protein expression levels may better reflect selection on divergent and constrained phenotypes. **Khan *et al.*** (p. 1100, published online 17 October; see the Perspective by **Vogel**) measured the differences among and within species between mRNA expression and protein levels in humans, chimpanzees, and rhesus macaques, identifying protein transcripts that seem to be under lineage-specific constraint between humans and chimpanzees.

## Newlywed Game?

The extent to which our "gut" feelings influence our social interactions has been a matter of debate. Social psychologists have sometimes been criticized for their reliance on short-term analyses of undergraduates as test subjects. **McNulty *et al.*** (p. 1119) measured explicit and implicit attitudes of newlywed couples toward one another twice a year for 4 years. Over time, the implicit or unaware evaluations of the relationship predicted changes of marital satisfaction, whereas the explicit or conscious evaluations did not.

CREDITS (TOP TO BOTTOM): EDUARD KALININ; CHRISTINA CORBACI/THE SCRIPPS RESEARCH INSTITUTE





Published by AAAS

*Additional summaries*

## Keeping Quiet

Many bacteria overcome antibiotic treatment by expressing proteins that confer antibiotic resistance, for instance, efflux pumps. But when a strain that expresses these antibiotic resistance proteins encounters an environment containing the corresponding drug, the resistance against the drug may paradoxically become silenced in many cells. In this case, a fraction of a population of genetically identical cells will grow in the presence of antibiotics while other subpopulations fail to grow at all. **Deris *et al.*** (p. 1068) show that this bistable response arises from a built-in global feedback originating in antibiotic-mediated inhibition of growth, which reduces the expression of proteins that protect against growth inhibition. The resulting populations of dormant cells can exceed 50%, among otherwise identical resistance-expressing cells. This is important for antimicrobial treatment strategies because many bacterial cells may remain vulnerable to an antibiotic even when they apparently display strong resistance to it.

## Protecting Self-Replicating RNA?

The potential for self-replication makes RNA an attractive candidate as a primordial catalysis in the origin of life. Catalysis may have occurred in some kind of compartment, possibly a fatty acid vesicle. However, RNA catalysis generally requires high levels of magnesium, which are incompatible with fatty acid vesicle integrity. **Adamala and Szostak** (p. 1098) screened magnesium chelators and found that several—including citrate, isocitrate, and oxalate—could maintain the membrane stability of fatty acid vesicles in the presence of $Mg^{2+}$. Citrate also allowed $Mg^{2+}$-dependent RNA synthesis within protocell-like vesicles, while at the same time protecting RNA from $Mg^{2+}$-catalyzed degradation.

## Neuronal Activity and Dendrite Development

How does the developing brain establish the correct connections? **Matsui *et al.*** (p. 1114, published online 31 October) discovered an activity-dependent transcription mechanism during mouse and ferret visual cortex development that controls the direction of dendrite orientation, allowing dendrites to steer toward active axons and away from inactive axons. This mechanism enables the construction of polarized neuronal shapes for integration into neural circuits with the required fine-scale architecture to process subtle activity patterns, a property underlying complex behavior.

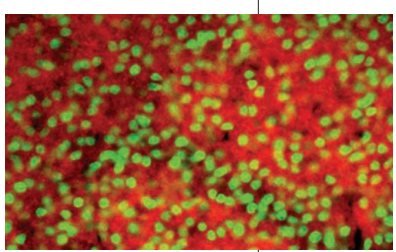

## Complexing Photosynthesis

Photosynthesis operates through a series of protein complexes that harvest sunlight and turn it into chemical energy. The separate complexes—including photosystems I and II, phycobilisome antennae, and reaction centers—are understood for a number of photosynthetic organisms; however, the large-scale organization and interactions between them are less clear. Using protein cross-linking, **Liu *et al.*** (p. 1104) demonstrate how the individual components are organized when present as a megacomplex in the cyanobacterium *Synechocystis* PCC 6803. Time-resolved fluorescence spectroscopy indicated that the phycobilisomes transfer energy to both photosystems, which is consistent with their molecular arrangement.

## It Takes a Few

Persistent maintenance of long-term potentiation (LTP) of glutamatergic synapses and long-term memory requires neuronal nuclear signaling that leads to gene transcription. It is unclear whether signaling produced at a single dendritic spine can be transmitted into the nucleus to regulate gene transcription. Using two-photon glutamate uncaging in combination with two-photon fluorescence lifetime imaging, **Zhai *et al.*** (p. 1107) show that induction of LTP in only three to seven dendritic spines in a hippocampal pyramidal neuron can trigger activation of nuclear extracellular signal–regulated kinase and downstream transcription factors cyclic adenosine monophosphate response element–binding protein and E26-like transcription factor-1. Thus, signaling initiated in each dendritic spine can be transmitted into the nucleus to regulate gene transcription. Furthermore, biochemical signaling in multiple dendritic branches was integrated to activate the nuclear signaling.

CREDIT: MASAHARU OGAWA

Wei Yang is president of the National Natural Science Foundation of China and a professor in the Institute of Applied Mechanics at Zhejiang University, Hangzhou, China. E-mail: yangwei@nsfc.gov.cn.

# Research Integrity in China

CHINA'S RESEARCH CAPACITY HAS GROWN DRAMATICALLY IN THE PAST DECADE, AN EXPANSION THAT is reshaping the landscape of global scientific investigation. This rapid growth has not necessarily been accompanied by an equally measured promotion of the cultural norms of the scientific enterprise. Most troubling is a lack of research integrity, which may hinder China's growth in original science, damage the reputation of Chinese academics, and dampen the impact of science developed in China.

An unhealthy research environment in China is being driven by several factors. In many research-intensive universities and institutions, competitive research grants constitute oversized fractions of their budgets, providing an economic incentive for ethical violations. Misconduct is also inadvertently encouraged by the use of quantitative rather than qualitative measures of merit, which can lure young scientists to climb the academic ladder by stepping outside ethical boundaries. Performance-based subsidiary income is a policy that can entice scientists to act unethically. And there is a talent hierarchy in academia that encourages scientists to overblow their findings.

The good news is that several pivotal events over the past decade mark the long march toward research integrity in China. The first event at the beginning of the 21st century was to ban multiple submissions of a paper to journals, after clarifying a delicate issue of the translation rights for bilingual submissions. The copyright law was also revised to allow a longer embargo period to accommodate the review time required for technical papers. The allegations of whistleblowers, mostly anonymous, have led to a majority of crackdowns, as evidenced by my own handling of more than 80% of research misconduct cases at Zhejiang University. In addition, action by the media to expose research misconduct, ranging from plagiarism and retractions in the He Haibo event, to the fraudulent "Hanxin" computer chips, has stoked a hostile public intolerance for misconduct, prompting politicians to acknowledge that a serious problem exists.

There is now a massive education effort by the China Association for Science and Technology (CAST) and Ministry of Education (MoE) to train graduate students, postdoctoral fellows, and young faculty in research ethics. There is a new emphasis on a code of ethics, put forth by the Chinese Academy of Sciences (CAS), CAST, and the National Natural Science Foundation of China (NSFC), to guide researchers in the life sciences. Major universities as well as CAS have revised the criteria for promotion to emphasize the quality of research contributions rather than the number of publications by a researcher. And since 1998, there has been active censoring by the NSFC of scientists who submit plagiarized grant applications. This campaign has resulted in a decline of 70% in the fraction of alleged application misconduct over the past 14 years. At a press conference in August 2013, the NSFC revealed six cases of misconduct discovered by comparing submitted and funded proposals, including a "proposal for sale," similar to manuscripts for sale described in the News story on p. 1035. Moreover, in 2012, the Chinese government began other surveillance and inspections of submitted research proposals to complement the efforts of research funding agencies in safeguarding the ethical use of research dollars.

Help from the global science community has been an important factor in promoting integrity in China. For example, a dialogue between the American Association for the Advancement of Science and CAST has focused on drafting guidelines and casebooks to prevent misconduct. The movement of cultivating standards for scientific integrity by the Global Research Council is also gaining momentum in China and other nations.

Many challenges lie ahead in achieving zero tolerance for unethical behavior. China is still grappling with the incorporation of panel reviewers, promotion committees, and prize nominators in the systems that award grants and titles. The development of good science in China should accomplish three goals: to produce original breakthroughs, to advance understanding from discoveries made elsewhere, and to gain global influence. None of this can happen until the scientific enterprise is healthy and credible.

**— Wei Yang**

10.1126/science.1247700





*Published by AAAS*

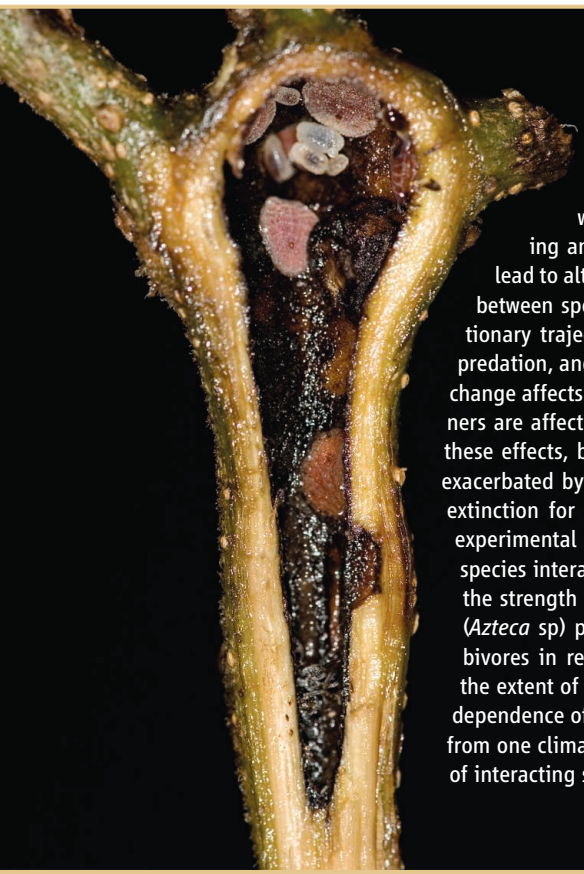

ECOLOGY

## Relationship Trajectories

Changing climates cause shifts in the geographical distributions of species and in their abundance, as well as in their biological features, such as the timing and duration of reproductive seasons. These shifts can lead to alterations in the strength and effects of the interactions between species in ecological communities, and hence to evolutionary trajectories. Northfield and Ives model how competition, predation, and mutualism are affected by coevolution when climate change affects interacting partners in different ways. When the partners are affected in conflicting ways, coevolution tends to mitigate these effects, but where the effects are nonconflicting, they can be exacerbated by coevolution and can even increase the likelihood of extinction for one or both partners. Their models suggest various experimental scenarios for investigating how coevolution drives species interactions under climate change. Pringle *et al.* show how the strength of a mutualistic interaction, in which the tropical ant (*Azteca* sp) protects a plant (*Cordia alliodora*) against insect herbivores in return for receiving sugar from the plant, varies with the extent of water stress. When less water is available, the mutual dependence of the two partners is increased, illustrating how a shift from one climatic regime to another might alter the future relations of interacting species. — AMS

*PlOS Biol.* **11**, e1001685; e1001705 (2013).

NEUROSCIENCE

## Too Soon

Familial dysautonomia arises from the inappropriate splicing of an mRNA that encodes a kinase inhibitor; this affects sensory and autonomic functions of the peripheral nervous system, and those affected die young. George *et al.* have looked at the function of the inhibitor in the neural crest lineage, which is the source of much of the peripheral nervous system. In mice without the inhibitor, there were fewer than normal neurons in the superior cervical ganglia and dorsal root ganglia (DRG). Particularly depleted were neurons expressing the neurotrophin receptor TrkA. Their analysis of embryonic mouse development showed that the inhibitor was present in progenitor cells and in postmitotic neurons representing the second wave of neurogenesis in the DRG, the wave that produces TrkA-positive nociceptors and thermoreceptors. Without the inhibitor, this subgroup of progenitors differentiates too early, resulting in a precocious excess of these sensory neurons but depleting progenitors, so that the numbers of neurons fail to keep pace with subsequent development. — PJH

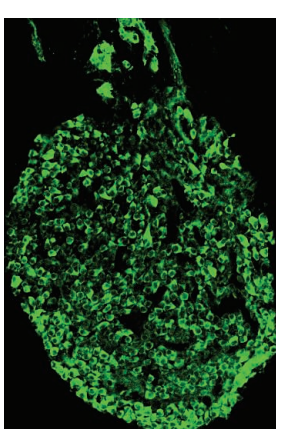

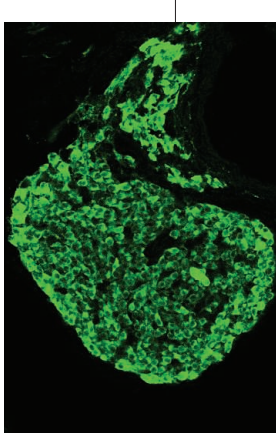

*Proc. Natl. Acad. Sci. U.S.A.* **110**, 10.1073/pnas.1308596110 (2013).

PLANETARY SCIENCE

## Teasing Out the Plume

On 9 October 2009, the second stage of the rocket that launched the Lunar Reconnaissance Orbiter plunged into the Cabeus crater on the south pole of the Moon, lifting a plume of debris, dust, and vapor that contained water. The plume and its contents were detected by the Lunar Crater Observation and Sensing Satellite Shepherding Spacecraft that followed the impacting rocket stage into the crater (see Research Articles, 22 October 2010, p. 463). Apart from a sodium enhancement in the exosphere of the Moon, no Earth-based detections were reported, even though observations were attempted. Strycker *et al.* used a principal-components analysis to tease out the impact plume from visible images obtained on 9 October 2009 with the Agile camera on the Astrophysical Research Consortium 3.5-m telescope at the Apache Point Observatory in New Mexico, USA. Their analysis reveals that the plume had separate low- and high-angle components, as suggested by previous results from laboratory work but not verified by the observations made by the Shepherding Spacecraft. The study also confirms that the concentration of water ice in the regolith at the impact site is about 6% by mass. — MJC

*Nat. Commun.* **4**, 2620 (2013).

BIOPHYSICS

## Pattern Sensing

More than 60 years ago, Alan Turing described how self-regulated biological patterns could arise in his reaction-diffusion model: An activator and a repressor interact and diffuse at different rates. Payne *et al.* developed a synthetic system to implement this model by engineering two circuits into bacteria: (i) a mutant T7 RNA polymerase that activates its own promoter plus cyan fluorescent protein (CFP), and (ii) an inhibitory circuit containing the gene for lysozyme, which inhibits T7 RNA polymerase and was linked to the fluorescent mCherry protein. The T7 RNA polymerase induced expression of LuxI, which is involved in the synthesis of acyl-homoserine lactone (AHL). High concentrations of AHL induced LuxR expression, which in turn induced the expression of T7 lysozyme, resulting in the inhibition of the T7 RNA promoter. Microcolonies, launched from individual cells, displayed a CFP core and an mCherry ring. Modeling studies incorporating the metabolic burdens imposed by the circuits suggested that cell growth and gene expression were linked so that the activation signal acted as a timing

CREDITS (TOP TO BOTTOM): JEFFREY C. MILLER; L. GEORGE *ET AL.*, *PROCEEDINGS OF THE NATIONAL ACADEMY OF SCIENCES* **110**, 46 (30 OCTOBER 2013)

mechanism that enabled the colony to sense its environment. The larger the environment, the longer it took for the activating signal to reach a critical concentration that triggered pattern formation and the larger the ring. — BJ

*Mol. Syst. Biol.* **9**, 697 (2013).

CELL BIOLOGY

## Muscle Mitophagy

Mitochondrial injury triggers an adaptive compensatory response: Signals emanating from damaged mitochondria activate cytoprotective cascades that restore cellular homeostasis. Identifying cytoprotective factors has been difficult, in part because of the heterogeneity of tissue culture models of mitochondrial distress. Owusu-Ansah *et al.* have established a *Drosophila* model in which modest muscle mitochondrial perturbation was associated with the induction of genes required for cytoprotection and cell maintenance. A synthetic lethal screen for increased life span and preserved muscle function uncovered components of the mitochondrial unfolded protein response ($UPR^{mt}$) and a homolog of insulin-like growth factor–binding protein 7, which indirectly facilitates mitophagy—the removal of damaged mitochondria. Overexpression of $UPR^{mt}$ genes in fly muscles preserved mitochondrial function and delayed age-related locomotory impairment. — SMH

*Cell* **155,** 699 (2013).

EDUCATION

## Evaluating Computer Scoring

The preferred way to evaluate science students' argumentation and communication skills is through written essays and oral interviews. Because these assessment methods are time-consuming for teachers, automated grading machines are being developed. Beggrow *et al.* tested the knowledge of 104 undergraduate students exposed to varying amounts of biological evolution content by using three types of assessment: an oral interview with two researchers; a written, open-response assessment scored by both a human and a computer; and a multiple-choice test scored by a computer. Regression and correlation analysis of the data, showed that the multiple-choice test results were most weakly correlated with interview results, whereas the computer-graded written test had the strongest correlation with oral interview results. This suggests that multiple-choice tests are not the best way to evaluate students' debate and communication skills and should be replaced with computer-graded short-answers essays. — FB

*J. Sci. Educ. Technol.* 10.1007/s10956-013-9461-9 (2013).

PHYSICS

## Interface Pseudogap

The superconductivity of copper oxide compounds, which in some cases can persist to temperatures above 100 K, is inextricably connected to the pseudogap phase, a range of energies that has very few electronic states associated with it. This phase appears well above the superconducting critical temperature $T_c$, and its origin is still under debate. It could be a consequence of a competing order or simply a precursor to superconductivity. Richter *et al.* studied the behavior of the electronic density of states (DOS) of a different superconducting

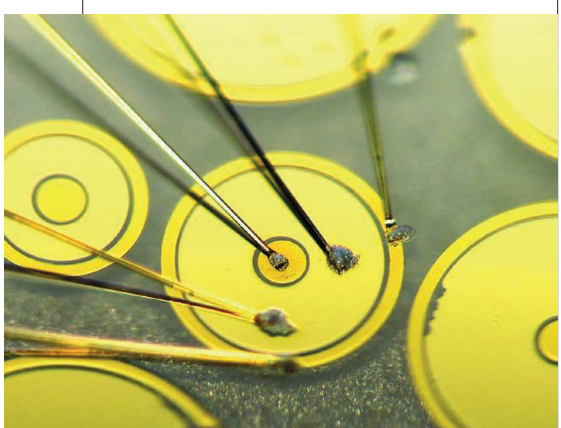

system: the two-dimensional gas that appears at the interface between the insulators $SrTiO_3$ and $LaAlO_3$. Tunneling into the layer while modulating its carrier density by applying a gate voltage, the authors observed an energy gap in the DOS that behaved in a similar manner to the pseudogap in high-$T_c$ copper oxide superconductors. Like the pseudogap, a gap in the DOS grows monotonically with carrier depletion and persists to temperatures far above the $T_c$. This similarity is surprising given the differences between the electronic structures of the two systems. What they do have in common, however, is dimensionality. Although copper oxides are three-dimensional compounds, they are layered, and most of the action happens in the two-dimensional planes. The authors thus suggest that the copper oxides' characteristic phase diagram might be related to the nature of two-dimensional superconductivity. — JS

*Nature* **502**, 528 (2013).

CREDIT: C. RICHTER *ET AL.*, *NATURE* **502**, 7472 (24 OCTOBER 2013) © NATURE PUBLISHING GROUP



Published by AAAS

## AROUND THE WORLD

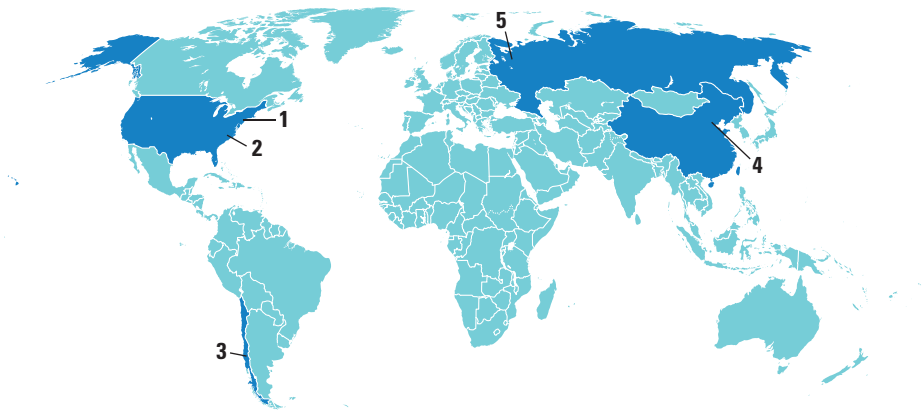


New York City **1**

### 'Dueling Dinos' Fail to Sell

The New York auction house Bonhams pulled a controversial fossil from the auction block last week when the final offer fell short of the seller's minimum price. The specimen includes two dinosaurs, from the families Ceratopsidae and Tyrannosauridae, discovered in 2006 in Montana by commercial fossil hunter Clayton Phipps. The two were found touching, with missing teeth and shattered chest bones suggestive to some of mortal combat, so Phipps dubbed them "The Dueling Dinosaurs."

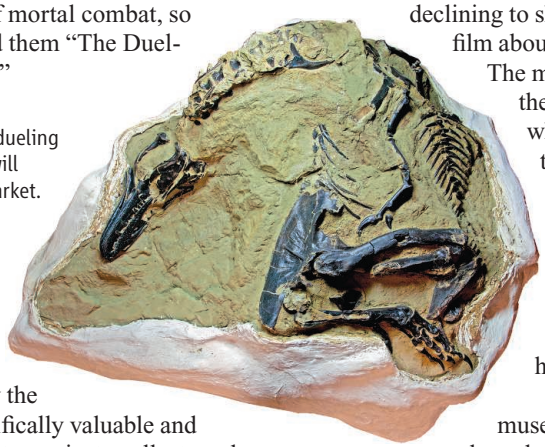

**No takers.** The "dueling dinosaur" fossil will remain on the market.

Phipps is legally entitled to sell his discovery, but some paleontologists say the fossil is scientifically valuable and fear it will fall to a private collector who won't allow detailed study. If that happens, "then someone might as well walk up to it with a sledgehammer and turn it to dust," says paleontologist Thomas Carr of Carthage College in Kenosha, Wisconsin.

The final offer of $5.5 million didn't meet Phipps's asking price (somewhere between $5.5 million and $7 million), but Bonhams representatives are confident the fossil will eventually sell and say that several public institutions are interested. **http://scim.ag/_dino**

**Science LIVE**

Join us on Thursday, 5 December, at 3 p.m. EST for a live chat with experts on **whether animals should have legal rights**. **http://scim.ag/science-live**

Raleigh **2**

### Science Museum in Tiff Over Climate Change Film

The North Carolina Museum of Natural Sciences has sparked controversy by declining to show an hourlong film about rising sea levels. The museum is run by the state government, which has been hostile to action on climate change, but Director Emlyn Koster denies avoiding the topic. "I have a track record of dealing with these issues head on," he says.

Last month, the museum was asked to show the film *Shored Up* as part of its weekly Science Café. Director Ben Kalina says he hoped the screening would spark dialogue, because the museum is across the street from the state Capitol.

On 13 November, Koster declined, saying the film was not suitable by itself for the complex and controversial topic. "I take him at his word when he says they have a robust way of treating these issues," says social scientist Michael Orbach of Duke University's Marine Lab in Beaufort, North Carolina, of Koster's decision, but he wonders how and when the museum will tackle the subject. **http://scim.ag/_NCfilm**

Santiago **3**

### Guanacos Enlisted for Restoration

Centuries after being hunted to extinction in central Chile, the guanaco will return next month as part of the country's first rewilding project. Scientists hope the llamalike animal, still roaming wild in the north and south, will help restore the espinal, a semiarid ecosystem used to raise livestock and viewed by many Chileans as hopelessly degraded.

**Homecoming.** Guanacos in a Chilean breeding facility will soon be released to restore the espinal.

Ecologist Meredith Root-Bernstein of the University of Oxford in the United Kingdom and her colleagues recently discovered that the espino, a spiny tree that dominates the landscape, grew back more robustly after a good pruning, a likely adaptation to munching guanacos—the espinal's only native large herbivores. Reintroduced guanacos could return withered espinos to health, making the espinal shadier and more hospitable to both wild animals and economically important livestock. "Instead of putting a domestic animal in a wild landscape, we're putting a wild animal in a domestic landscape," Root-Bernstein explains.

The team will move six guanacos into a fenced region of the espinal and monitor the ecosystem to determine if more should be added elsewhere.

### THEY SAID IT

**"For America, this is our last chance to be first, and even the very movement of planets seems to be saying 'Go.'"**

—Report from billionaire Dennis Tito's Inspiration Mars Foundation on a manned flyby mission proposed for the 2017 alignment of Mars and Earth.

CREDITS (TOP TO BOTTOM): MEREDITH ROOT-BERNSTEIN; CK PREPARATIONS



Published by AAAS

## Random Sample

### A Message in the Sand

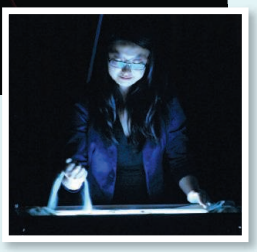

Usually, lengthy newspaper or magazine stories win the Communications Award of the American Society of Tropical Medicine and Hygiene (ASTMH). But this year's winner was a surprise: A story told using sand and light by Shelly Xie, a student at the University of Texas Southwestern Medical Center in Dallas.

As a biology undergrad at Stanford University, Xie studied schistosomiasis, a little-known parasitic disease that kills an estimated 300,000 annually. She decided to use her time at The Senior Reflection, a Stanford program that lets life science students explore the arts, to raise awareness. Xie's medium is sand animation, in which artists use their hands to draw images in a thin layer of sand atop a lightbox. Her striking 10-minute performance, which includes music and narration (http://bit.ly/1eiFmSd), tells the story of a young Ghanaian mother suffering from schistosomiasis. Xie performed it at a TEDx event in Livermore, California, in June.

"People are very surprised how much they can learn about science through this art form," says Xie, who—besides a trophy and $2000—won a trip to the ASTMH annual meeting in Washington, D.C., where she performed a new piece on hookworm disease.

Beijing **4**

## Chinese Leaders Call For Academic Reform

Scientists in China have found something to cheer about within a lengthy 15 November document from Communist Party leaders: a long hoped-for reform of the country's academy membership system. Beyond the expected plans for economic and legal overhaul, the document called for changes to the election, management, and retirement policies for Chinese Academy of Sciences (CAS) members, known as *yuanshi*. With the prestige of being a *yuanshi* come special privileges, such as a lifetime appointment. The system has come under criticism amid scandals, including attempted bribery for membership.

Some doubt that the move will fix fundamental problems in Chinese academia. "Top-down interference will only produce the opposite results," says Cao Cong, a sociologist at the University of Nottingham in the United Kingdom, who specializes in China's scientific community.

What the reform will entail is not yet clear. An adviser to CAS who asked to remain anonymous says he suspects the academy was caught off-guard by such a high-level show of disapproval, but will likely present a timeline for reform measures at a meeting next June.

**http://scim.ag/_CAS**

Arkhangelsk Oblast, Russia **5**

## ESA Targets Magnetic Mysteries

A constellation of three satellites launched by the European Space Agency on 22 November will map Earth's magnetic field in unprecedented detail. The mission, called Swarm, will probe the sources of the field, why it changes, and how it protects Earth from the solar wind.

The ever-shifting magnetic field comes mostly from molten iron churning in Earth's outer core, but also from rocks in the crust, ocean currents, and particle flows in the atmosphere. Understanding this field is essential for satellite navigation and mineral prospecting as well as predicting space weather—the field acts as a protective bubble, deflecting the charged particles that stream past Earth in the solar wind.

The car-sized satellites, launched together from the Plesetsk spaceport in Russia, carry magnetic and electric field sensors to tease out magnetic field sources around the globe.

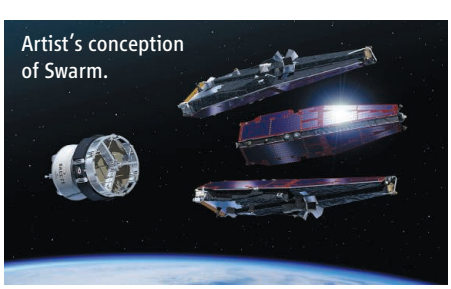

Artist's conception of Swarm.

## BY THE NUMBERS

**72%** Portion of scientists who feel it is "very important" that scientific papers be freely accessible to the public, according to 254 respondents to an online survey conducted by *Science*. **http://scim.ag/survOA**

**29, 32** Successive records set last week for number of satellites deployed in a single launch, aboard NASA's Minotaur 1 and Russia's Dnepr rocket, respectively.

## NEWSMAKERS

### Sequencing Pioneer Dies at 95

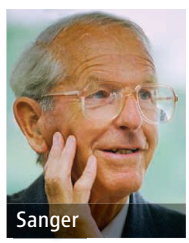

Sanger

Double Nobel Prize–winning British biochemist **Frederick Sanger** died on 19 November at the age of 95. The ever self-effacing scientist, who turned down the offer of knighthood, spent his whole career at the University of Cambridge in the United Kingdom and the Laboratory of Molecular Biology, also in Cambridge.

When he began studying the protein insulin in the mid-1940s, biochemists thought that proteins were amorphous. Through meticulous amino acid mapping, Sanger showed that insulin, and presumably other proteins, had a precise structure—a conclusion that won him the 1958 Nobel Prize in chemistry.

He went on to develop methods for sequencing RNA and DNA: His 1977 "dideoxy" chain-termination method dramatically speeded sequencing and won him a share of the 1980 Nobel chemistry prize. The technique was later used to sequence the human genome. Sanger is one of only four people to win two Nobel Prizes and the only person to win two chemistry prizes. In 1992, the United Kingdom's new sequencing laboratory near Cambridge was named the Sanger Centre in his honor.

"Fred was an inspiration to many, for his brilliant work, for his quiet determination and for his modesty. He was an outstanding investigator, with a dogged determination to solve questions that have led to transformations in how we perceive our world," said Mike Stratton, director of what is now the Wellcome Trust Sanger Institute, in a statement.

SPACE SCIENCE

# Chinese Mission Ushers in New Era of Lunar Exploration

**BEIJING**—Shortly after the sun rises next month over the Bay of Rainbows, a lava plain on the moon's near side, a Chinese spacecraft will seek out a safe landing spot, cut its engines 3 meters above the surface, and settle onto a carpet of 3-billion-year-old dust. If all goes well, Chang'e-3 will be the first spacecraft to make a soft landing on the moon since the Soviet Union's Luna-24 in 1976.

Chang'e-3 is "an important milestone" on China's quest to send a crewed mission to the moon by 2030, says David Kring, a geologist at the Lunar and Planetary Institute in Houston, Texas. A robotic rover, the first of its ilk in 40 years, is the mission's showiest technology. But Chang'e-3 has a "robust" science mission as well, Kring says. Managed by the National Space Science Center of the Chinese Academy of Sciences (CAS) in Beijing, the science payload will study the lunar crust underfoot and the Earth and stars overhead. Center Director General Wu Ji was at the Xichang Satellite Launch Center in Sichuan province last week, overseeing final tests of the instruments. "They all work very well," he says.

The lander's premier instrument is a wide-angle extreme ultraviolet camera that will continuously observe Earth's plasmasphere—its halo of ionized gases—and the tail of comet ISON as it swings by next month. Because the sun is in an active phase, regularly unleashing flares and coronal mass ejections, "we may have good chance to see a dynamic plasmasphere," Wu says. The lander also has a near-ultraviolet telescope, expected to make the first detailed observations of stars and galaxies from the moon's surface.

China has not announced the launch date, but analysts say liftoff is likely on 2 December, which would set up the most favorable approach to the Bay of Rainbows, also known as Sinus Iridum. After the lander sets down around 16 December, the rover will detach from its side and roll down a metal gangway. During a lunar day, which lasts about two Earth weeks, the solar-powered, 140-kilogram rover (*Yutu*, or jade hare, is leading in a public naming contest) will perambulate up to 200 meters an hour on its six wheels, snapping photos and probing surface geochemistry with a particle excitation x-ray spectrometer and an infrared spectrometer attached to a robotic arm.

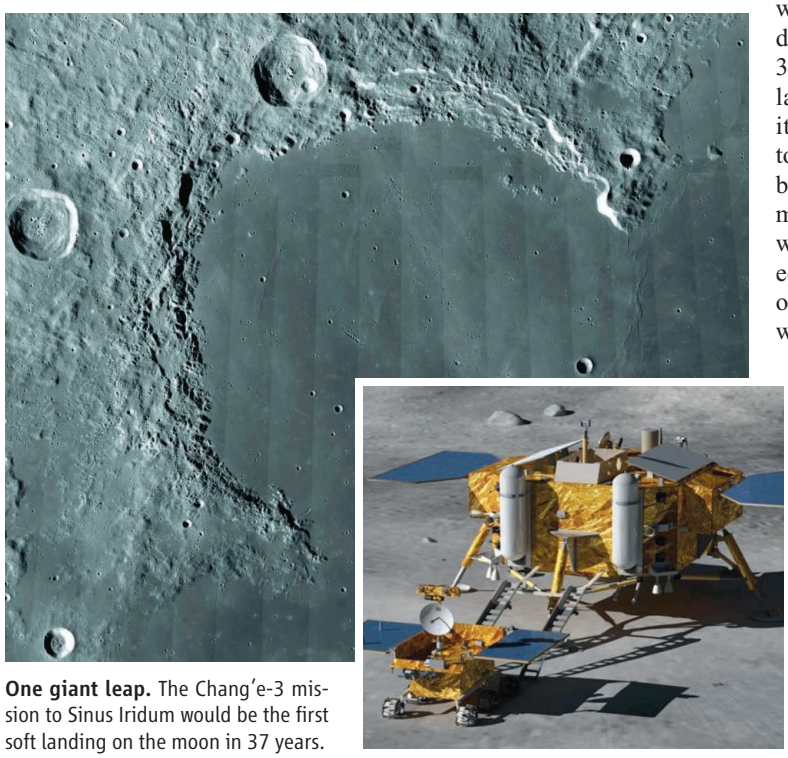

**One giant leap.** The Chang'e-3 mission to Sinus Iridum would be the first soft landing on the moon in 37 years.

Mounted on its undercarriage is a ground-penetrating radar—another lunar first—that will record echoes in the very high frequency and ultrahigh frequency bands from as much as 100 meters deep, Wu says. This imaging could help shed light on Sinus Iridum's complex history, says Xiao Long, a lunar geologist at the China University of Geosciences in Wuhan. Forged from ancient impacts and lava flows, the 235-kilometer-wide basin may include rock blasted from the mantle, he says. Chang'e-3, Xiao says, should "get a glimpse of the moon's past and deep structure."

For a mission with a bevy of firsts, "the challenges are immense," says Ouyang Ziyuan, senior adviser to China's lunar exploration program. One is surviving the long lunar night, when temperatures plummet as low as –180°C. The rover will "go to sleep," using the radioactive warmth of a plutonium-238 generator to keep vital circuits from freezing, says Jia Yang, the spacecraft's deputy chief engineer at the Beijing Institute of Spacecraft System Engineering. The rover "is like a child to me," says Jia, who has been working on the project since its conception a decade ago. "Now it has grown up and is going to make its mark on the world."

Jia and others hope the lander and rover will survive beyond their design lives of 6 months and 3 months, respectively. If the lander makes it to August, its cameras could image a total eclipse, as Earth passes between our sun and the moon. Only the outer corona will be visible during the eclipse, providing "a superb opportunity to study solar winds," says Ping Jinsong, an astronomer here at CAS's National Astronomical Observatories.

Chang'e-3 may also spark a bit of unorthodox Chinese–U.S. cooperation. The two nations don't have any formal joint space projects. But as the landing and the rover kick up clouds of dust, NASA's Lunar Atmosphere and Dust Environment Explorer, or LADEE, now in orbit, should get a bird's eye view—and some insights into the moon's mantle of dust.

If Chang'e-3 goes well, Ouyang says, China will "speed up the next phase of lunar exploration." Chang'e-4 will reprise the current mission possibly in 2016. The next major event would be Chang'e-5, which aims to return dust and rock samples to Earth as early as 2018, he says. Meanwhile, U.S. lunar scientists admit to feeling envious. "China," Kring says, "will gain a capability the United States no longer has."

**–JANE QIU AND RICHARD STONE**

Jane Qiu is a writer in Beijing.

CREDITS (TOP TO BOTTOM): NASA/GSFC/ARIZONA STATE UNIVERSITY; CHINA ACADEMY OF SPACE TECHNOLOGY



Published by AAAS

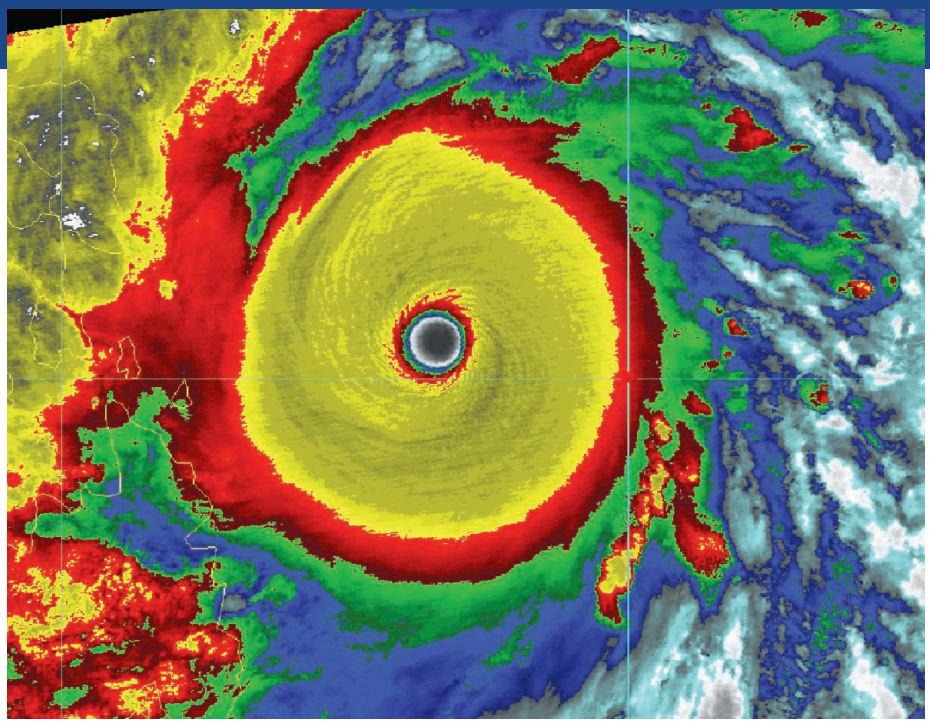

**Feeding the monster.** Unusually warm Pacific waters supercharged Haiyan.

CLIMATOLOGY

# Clues to Supertyphoon's Ferocity Found in the Western Pacific

Tropical storm watchers agree that Haiyan was probably the strongest typhoon to make landfall when it slammed into the Philippines on 8 November, packing winds of up to 314 kilometers per hour. What gave Haiyan, which killed thousands and displaced millions, its deadly wallop?

Researchers think they have at least a partial answer to that question: unusually warm subsurface Pacific waters east of the Philippines. A related phenomenon—rising sea levels in the western Pacific—likely abetted Haiyan's devastating storm surge, which caused more deaths than the winds themselves.

Typhoons draw heat from the ocean for the energy that generates their winds. Typically, as a storm's winds increase, they stir up deeper, cooler ocean waters that temper its strength. This cooling effect "is nature's brake to stop typhoons from intensifying," says I-I Lin, a specialist in typhoon-ocean interactions at National Taiwan University in Taipei.

Drawing on data from satellite observations and Argo floats—thousands of instrumented, subsurface probes that measure ocean temperature, salinity, and current speeds—Lin and others have documented a steady 2-decade rise in subsurface temperatures in the western North Pacific and a bulging warm water layer. The warmer and thicker that subsurface layer, the more heat is available to feed a storm. Oceanographers use a measure called the Tropical Cyclone Heat Potential (TCHP) to quantify the heat reservoir. Lin and colleague Iam-Fei Pun reported online on 3 September in *Geophysical Research Letters* that the TCHP where most cyclones develop in the western North Pacific has increased 10% since the early 1990s (see graph). While surface waters along Haiyan's path were only slightly warmer than normal, waters down to 100 meters were 3° warmer than the historical average. So as Haiyan churned up western Pacific waters, it drew more wind-intensifying heat, Lin says.

Other factors contributed to Haiyan's intensity. "The genesis location was very important," says Il-Ju Moon, a marine meteorologist at Jeju National University in South Korea who studies how ocean heat influences typhoons. Haiyan originated around 5° latitude north of the equator and was at about 10° when it hit land. "The ocean heat content is very high in that region," Moon says. And starting more than 3000 kilometers east of the Philippines gave Haiyan plenty of open water over which to strengthen.

Haiyan was a speed demon as well. "It was flying over the water" at 32 kilometers per hour, Lin says, nearly twice as fast as most typhoons travel. "Why it moved so fast is unknown," she adds. Researchers speculate that a fast-moving storm passes by before its churn pulls energy-sapping deeper, cooler water to the surface. In any case, "the warmer the subsurface layer, the faster the moving speed, the smaller the cooling effect," Lin says. "It's like a car without a brake, only an accelerator."

The warm bulge in the western North Pacific is the result of stronger easterly trade winds. This phenomenon also aggravated Haiyan's storm surge. In addition to blowing heat westward, the winds are literally piling up water in the western Pacific, where the cumulative sea-level rise over the past 20 years exceeds 20 centimeters, says Bo Qiu, an oceanographer at the University of Hawaii, Manoa. "It is likely that the elevated sea level contributed to the flood and inundation problems" in the Philippines, he says.

While many observers blame Haiyan's destructive power on climate change, tropical storm experts say there is little hard evidence of a link. "It is possibly natural variability," Lin says. Nor is it certain that the western Pacific has become a supertyphoon breeding ground. Although warmer subsurface waters might raise the risk, Lin says, atmospheric conditions may not always cooperate.

**–DENNIS NORMILE**

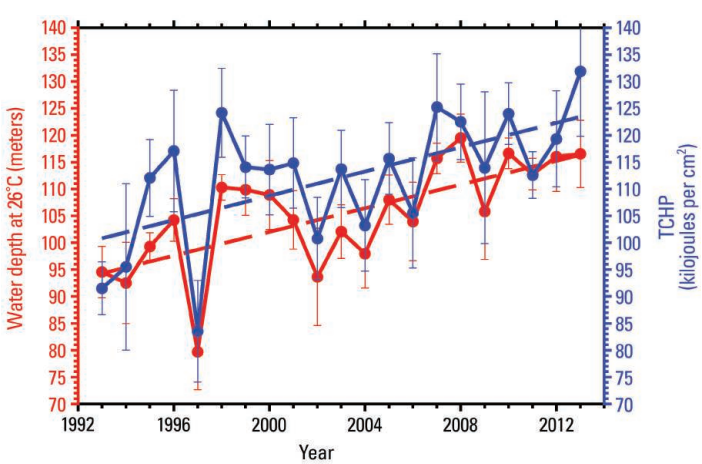


**Heated situation.** Over 2 decades, a thickening layer of warm water (red) increased the storm-driving heat potential (blue) at the latitudes Haiyan traversed.

CREDITS (TOP TO BOTTOM): JOHN KNAFF, NOAA/NESDIS/RAMMB, CSU/CIRA; I-I LIN





Published by AAAS

CANCER

# Cholesterol Forges Link Between Obesity and Breast Cancer

Cholesterol, the fat molecule that builds up in our arteries and contributes to heart attacks and strokes, has another nasty trick up its sleeve. When metabolized by the body, it turns into a potent estrogenlike molecule that spurs the growth of breast cancer in mice, and perhaps in people. That's the conclusion of a pair of surprising studies that shed new light on the link between obesity and cancer. "No one had thought of it before. It raises a new potential strategy" for treating breast cancer and perhaps other cancers, too, says breast cancer researcher Myles Brown of the Dana-Farber Cancer Institute in Boston, who was not involved with the research.

Obesity is as powerful a factor as smoking in raising the risk of some cancers. Researchers suspect several mechanisms: For example, fat tissue pumps out tumor-nurturing molecules such as estrogen, which drives the growth of the most common type of breast cancer. Many obese people have diabetes, and insulin and a related hormone may spur cancer cell growth as well.

Elevated cholesterol in the blood, common in obese people, has also been linked to breast and other cancers. The risk is particularly high for women past menopause, who otherwise should be partially protected against breast cancer because their bodies have stopped making much estrogen. One clue to cholesterol's role in cancer emerged a few years ago from collaborating researchers at the University of Texas (UT) Southwestern Medical Center in Dallas and Duke University School of Medicine in Durham, North Carolina. They discovered that a cholesterol metabolite called 27-hydroxycholesterol (27HC) mimics estrogen in certain tissues. This inspired team members Philip Shaul at UT Southwestern and molecular pharmacologist Donald McDonnell at Duke, working independently, to explore whether 27HC spurs breast cancer growth.

Their hunch paid off: In papers published by McDonnell's group this week in *Science* on page 1094 and by Shaul's team in *Cell Reports* on 7 November, the teams report that in a petri dish, human breast cancer cells grew faster when dosed with 27HC. The compound also spurred tumors to grow faster and larger in mice that had been implanted with human cancer cells or engineered to spontaneously develop breast tumors. Most intriguingly, McDonnell says, his team showed that 27HC also appears to dramatically hasten the spread, or metastasis, of breast tumors to other organs.

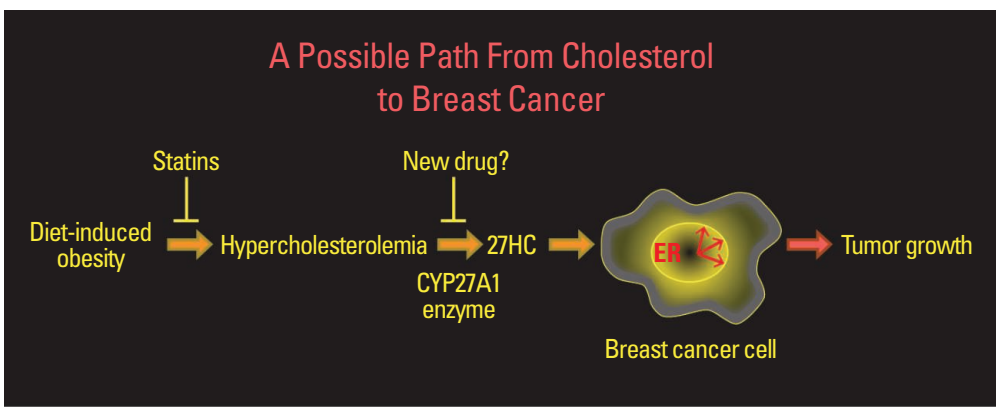


**Fat-cancer link.** In obese women, cholesterol turns into a metabolite, 27HC, that may act on the estrogen receptor (ER) to spur the growth of breast cancer. Statins or a new drug could disrupt this process at two different points.

When McDonnell's group turned to human breast tissue samples, they found that more aggressive tumors had higher levels of an enzyme called CYP27A1, which converts cholesterol into 27HC. Tumors appear to get the chemical both from the blood and from the conversion of cholesterol in tumor cells and tumor-infiltrating immune cells.

> *"It's a link and it's pretty much unanticipated."*
>
> —DONALD MCDONNELL, DUKE UNIVERSITY

Data from 66 women with estrogen-positive breast cancer supported a 27HC link as well, Shaul reports: Women with cancer had significantly more 27HC in their normal breast tissue than controls and even more in their tumors. Both groups also found that breast cancer patients with low tumor levels of CYP7B1, an enzyme that breaks down 27HC, did not live as long as women with the highest levels. The bottom line, McDonnell says, is that some estrogen-driven breast tumors may rely on 27HC to grow when estrogen isn't available.

To explore how all this might relate to dietary cholesterol, McDonnell's group implanted breast cancer cells in mice engineered to develop high cholesterol blood levels when they eat a lot of fat. Those on a high-fat diet had more 27HC in their blood and had tumors that were 30% larger after 15 days than mice on a control diet. This effect could be blocked by giving the animals statins, which lower blood cholesterol levels, or an experimental compound that inhibits CYP27A1, the enzyme that converts cholesterol into 27HC (see diagram).

The findings have several possible implications for patients, McDonnell says. First, lowering cholesterol with dietary changes or statins could reduce a women's breast cancer risk or slow tumor growth. (Indeed, some studies have found that women who are taking statins when they develop breast cancer live longer than those who aren't on statins.) Second, a drug that blocks CYP27A1 might help prevent or treat breast cancer. Shaul adds that 27HC could also help explain why aromatase inhibitors, which decrease estrogen production, don't work for some breast cancer patients.

The work helps solve a puzzle, says molecular biologist Peter Tontonoz of the University of California, Los Angeles. "They're among just a few papers offering specific insights into the mechanism linking lipid levels to tumor growth," he says. Brown adds, however, that the relative importance of 27HC compared to other obesity-related drivers of cancer isn't yet clear. McDonnell agrees: "I bet they're all contributing," he says. "But it's a link and it's pretty much unanticipated." His and Shaul's groups are now looking at 27HC's role in other hormone-driven cancers—in particular, endometrial cancer. Shaul's group has already found that this cancer, too, grows faster in a petri dish if supplied with 27HC, suggesting another cancer-cholesterol connection.

–JOCELYN KAISER

CREDIT: D. MCDONNELL/DUKE UNIVERSITY





Published by AAAS

CREDIT: DARPA

**Restorer.** After guiding a DARPA effort to create a brain-controlled prosthetic arm, Geoffrey Ling wants to enlist scientists to fix injured brains.

NEWSMAKER INTERVIEW: GEOFFREY LING

# DARPA Aims to Rebuild Brains

On 11 November, a momentary slip set the rumor mill spinning at the Society for Neuroscience meeting in San Diego, California. At a press conference for the Brain Research through Advancing Innovative Neurotechnologies (BRAIN) Initiative, a National Institutes of Health (NIH) official suggested that the Defense Advanced Research Projects Agency (DARPA) planned to develop technology that transfers memory from one brain to another.

Geoffrey Ling, deputy director of the Defense Sciences Office and program manager for one of DARPA's new BRAIN projects, was horrified: "I said, 'What!? No, we're restoring memory, and she says, 'Oh yeah, that's what I meant to say.' " But the genie was out of the bottle—by the end of the day even Tom Insel, director of the National Institute of Mental Health, was spreading the word about Vulcan mind meld–esque memory transfer. "It's wild," he told *Science*.

The confusion was understandable: In contrast to NIH, which held a series of open meetings over the summer to discuss its BRAIN research goals, DARPA has until recently kept plans for its $70 million portion of the project under wraps. And although brain-to-brain memory transfer isn't on the agency's to-do list, its actual goals are still wildly ambitious. So far, DARPA has released two calls for grant applications, with at least one more likely: The first, called SUBNETS (Systems-Based Neurotechnology for Emerging Therapies), asks researchers to develop novel, wireless devices, such as deep brain stimulators, that can cure neurological disorders such as posttraumatic stress (PTS), major depression, and chronic pain. The second, RAM (Restoring Active Memory), calls for a separate wireless device that repairs brain damage and restores memory loss.

In San Diego, *Science* sat down with Ling, a neurologist and former Army colonel who specialized in traumatic brain injuries while in the military, to talk about the projects. The following has been edited for brevity and clarity; an extended version is online at http://scim.ag/DARPAbrains.

–EMILY UNDERWOOD

**Q: Why did DARPA get involved in the BRAIN project?**

**G.L.:** It's really focused on our injured warfighters, but it has a use for civilians who have stress disorders and civilians who also have memory disorders from dementia and the like. But at the end of the day, it is still meeting [President Barack Obama's] directive. Of all the things he could have chosen—global warming, alternative fuels—he chose this, so in my mind the neuroscience community should be as excited as all get-up.

**Q: Why does SUBNETS focus on deep brain stimulation (DBS)?**

**G.L.:** We've opened the possibility of using DBS but we haven't exclusively said that. We're challenging people to go after neuropsychiatric disorders like PTS [and] depression. We're challenging the community to come up with something in 5 years that's clinically feasible. DBS is an area that has really been traditionally underfunded, so we thought what the heck, let's give it a go—in this new BRAIN Initiative the whole idea is to go after the things that there aren't 400 R01 grants for—and let's be bold, and boy, if it works, fabulous.

**Q: For RAM, why did DARPA choose to focus on memory, and what kinds of memory do you hope to restore?**

**G.L.:** All these [injured] guys and gals want to go back into the service. A lot of them can go back because we've got good prosthetic legs, and now we've got the prosthetic arm that's really close to being FDA [Food and Drug Administration] approved. But the thing with brain-injured guys—the thing that really keeps them out—is they can't remember how to do certain motor tasks like drive a car or operate machinery. Now I don't know if we are at that point, but if we can fix hearts, and we can fix badly broken bones, why can't we fix part of the brain? If you had to pick an area of the brain that you can fix, the memory area is the most obvious because motor-task memory is really pretty well-worked out in preclinical models. Declarative memory is very different than associative memory and emotional memory—that stuff, nobody even knows



Published by AAAS

anything about it—but when you look at the work in rodents with memory motor tasks, you say ok, it's still a big step but it's rational.

**Q: Does collaboration with the National Science Foundation (NSF) and NIH mean overlapping funding priorities?**

**G.L.:** No, but we like to think they're synergistic and complementary. There are scientists—you and I know them—who think big. They think, "I can do this if I only have the means to do it. Where am I going to get the means? Do I go to NIH, do I go to NSF? No." DARPA is saying, "You want $20–30 million? We'll give you $20–30 million." What I'm hoping is that we'll get two or three teams of really bold leaders who are doing this thing with different approaches. When you do that, you get a real big leader who now, instead of giving me 20% of time on a grant, is going to give 50% time, or 60% time because this is what they've lived their career for. You want these guys full of tension because if this is going to cure people, I'd be working on it night and day—I wouldn't take a damn vacation, would you? What DARPA is saying is here's your chance. Here's the golden ring—who's brave enough to step up and actually grab it?

SCIENCE EDUCATION

# New Head of Advocacy Group Plans to 'Fight the Good Fight'

Ann Reid has reconstructed a notorious flu virus in the lab and shaped science policy in the United States and in Europe. In January, she will put on a new hat—as first responder to attacks on high-quality science education.

Last week, Reid was named executive director of the National Center for Science Education (NCSE). She will succeed Eugenie Scott, who is retiring after spending 26 years building the small, Oakland, California–based organization into a feisty and powerful defender of the teaching of evolution and climate change in U.S. public schools.

"Our role is to fight the good fight," Reid says about the center's mission. "I don't think there's anything more important than having every child receive a good science education." The center's 15-person staff, she says, serves as "the fire department or FEMA [Federal Emergency Management Agency]" in helping local scientists, educators, and parents combat efforts to undermine science-based instruction. "As Genie likes to say, 'We don't put out the fire. But we pass out the fire extinguishers.' "

Reid would like to expand the 4000-member organization by appealing to any academic and industry scientist "who understands how important it is for children to have great science teachers." She also hopes to attract support from private foundations and government agencies with interests that dovetail with the center's mission.

"I think [the center is] the most effective group working at the grassroots level," says Jay Labov, senior adviser for education and communications at the National Academies' National Research Council (NRC) in Washington, D.C. "The work they did in the Dover case was just spectacular; I'm not sure the ruling would have been the same without their help," Labov says, referring to a federal judge's 2005 decision to reject a Pennsylvania school district's attempt to force teachers to present intelligent design as a viable alternative to evolution in science courses (*Science*, 6 January 2006, p. 34).

**Firefighter.** Ann Reid is the new director of the National Center for Science Education.

Reid, 54, took a circuitous path to her new job. A college graduate at 19, Reid earned a master's degree in international studies from Johns Hopkins University in Baltimore, Maryland, before working in Paris for the Organisation for Economic Co-operation and Development. "I was 21 and I wanted to change the world—today!" she says.

But the realm of international diplomacy turned out to be less exciting—and less satisfying—than she had imagined. "I found the policy work to be very frustrating," she says. "It simply wasn't evidence-based. Decisions were being made based on political rhetoric."

Returning to the United States, Reid accepted an entry-level lab technician position at the Walter Reed Army Medical Center in Silver Spring, Maryland. The job led to a 20-year research career, including her leading role in sequencing the virus that caused the 1918 flu pandemic. The work, by a team at the Armed Forces Institute of Pathology, helped scientists recreate the virus. "We finished sequencing the virus in 2004, after 7 years of work," she notes. "Now you could do it on your lunch hour."

She eventually left bench science and returned to the policy arena, first as a program manager at the National Academies and most recently as director of the American Academy of Microbiology (AAM) within the American Society for Microbiology. An NRC report on metagenomics also led to her first formal foray into science education, as co-author with Labov on a 2007 paper titled "A Call for Bringing a New Science into the Classroom (While It's Still New)."

"Ann is an expert at navigating the science-policy-society interface," says microbiologist Bonnie Bassler of Princeton University, who chairs AAM's board of governors. "Plus, she has a knack for making complicated subjects understandable to broad audiences. She will bring rigor and a passion for science to her new role."

**–JEFFREY MERVIS**

CREDIT: CHRIS CONDAYAN/AMERICAN SOCIETY FOR MICROBIOLOGY



Published by AAAS

CREDIT: INHUA PHOTO/LI GA/SIPA USA

**Bird in hand?** If quail harbor H7N9, it might be possible to eradicate the deadly virus.

PUBLIC HEALTH

# Tense Vigil in China as Nasty Flu Virus Stirs Back to Life

**BEIJING**—As flu season bears down, the world is warily eyeing China. A novel H7N9 avian flu strain emerged here in March, infecting at least 135 people and killing 45 before petering out in the summer. Now it is back, with four human cases in southern China in the past month. More cases are a certainty, and researchers, public health experts, and vaccinemakers are preparing for the remote but real possibility that H7N9 will explode into a pandemic.

For now, the signs are reassuring. Sustained human-to-human transmission would be needed for H7N9 to cause widespread illness. But so far, there have been only a handful of possible instances of people infecting each other. In 70% of cases, victims are believed to have picked up the virus directly from live poultry, says Masato Tashiro, head of a World Health Organization (WHO) flu collaborating center in Tokyo. H7N9 is "still looking for ways to adapt well to humans," says George Gao, deputy director-general of the Chinese Center for Disease Control and Prevention (China CDC).

Disturbingly, however, the signatures of the H7N9 strains isolated from the four new cases show that the virus is evolving rapidly. Les Sims, an animal disease consultant in Palm Grove, Australia, says that H7N9 appears to be swapping genes with other avian flu strains in poultry, adding additional genetic variation to the naturally high mutation rate of any flu virus.

For researchers watching the virus's genetic moves, Tashiro says, "the most important question" is which mutations would enable the virus to spread in people's coughs and sneezes, like seasonal flu. Virologist Ron Fouchier at Erasmus MC in Rotterdam, the Netherlands, and others authored a letter that appeared online in *Science* on 7 August advocating a way to find out: gain-of-function studies that would give H7N9 the genetic wherewithal to spread through the air, in a secure facility. Many scientists oppose creation of such a strain, which might set off a pandemic if it were released. Fouchier says he has not embarked on an H7N9 gain-of-function study.

In the meantime, China is girding for an eventful winter. China CDC researchers have given staff members at nearly 1000 hospitals and labs a crash course in how to detect the virus in patients. Respiratory samples are collected daily from hospitals and tested for H7N9, says Shu Yuelong, director of the Chinese National Influenza Center here.

A far tougher task is tracing H7N9's movements in the environment. "What has been lacking is an understanding of exactly where this virus is in the poultry sector," says Malik Peiris, a virologist at the University of Hong Kong's School of Public Health. The virus causes no discernible symptoms in poultry, making infections difficult to spot. Another puzzle is why so few birds test positive for the virus. China's National Avian Influenza Reference Laboratory in Harbin had only a handful of positive hits in some 84,000 poultry samples it collected this spring (*Science*, 26 April, p. 414). "Biologically, that's really difficult to explain," Peiris says.

Scientists are divided on whether China should permanently shutter its live poultry markets. Doing so is clearly effective: In four cities that temporarily closed markets in spring—Shanghai, Hangzhou, Huzhou, and Nanjing—human H7N9 cases were effectively snuffed out, according to a report last month in *The Lancet*. But Chinese consumers generally shun packaged meat. In the absence of a pandemic, they would never accept permanent closure, Gao says: "You cannot change culture." He favors closing markets a day or two a week for disinfection.

One intriguing possibility may not require China to kick its live poultry habit. H7N9 may be hiding out in a particular species kept in smaller numbers in the markets, such as quail. Six of H7N9's eight gene segments—what Peiris calls its "genetic engine"—are derived from another family of bird flu viruses, H9N2. Some H9N2 strains that bind well to human receptors have been detected in quail, Fouchier says. He notes that so far, few quail from China's poultry markets have been tested for H7N9. If H7N9 turns out to be a quail virus, it could be spreading from a small number of poultry holdings or a small area of China, offering hope that "the virus can still be eradicated at the original source," Fouchier says.

If eradication fails and H7N9 does mutate into a pandemic strain, health officials hope a vaccine will be ready to ward off disaster. Labs in the WHO network now have six H7N9 seed stocks—a version of the virus that can be grown in large quantities as the basis for a vaccine. Chinese labs are awaiting approval for clinical trials; meanwhile, some Japanese drug manufacturers have begun clinical trials.

European and U.S. researchers are further along. Novartis, based in Switzerland, has announced that 85% of 400 adults enrolled in a clinical trial of an H7N9 vaccine candidate showed some protective immune response. In September, the U.S. National Institutes of Health launched clinical trials of another vaccine candidate. And earlier this month, Novavax, a Maryland-based company, published encouraging results from an H7N9 vaccine clinical trial online in *The New England Journal of Medicine*. "We don't know if a vaccine will be necessary," Tashiro says. Everyone would prefer that it isn't.

**–CHRISTINA LARSON**



Published by AAAS

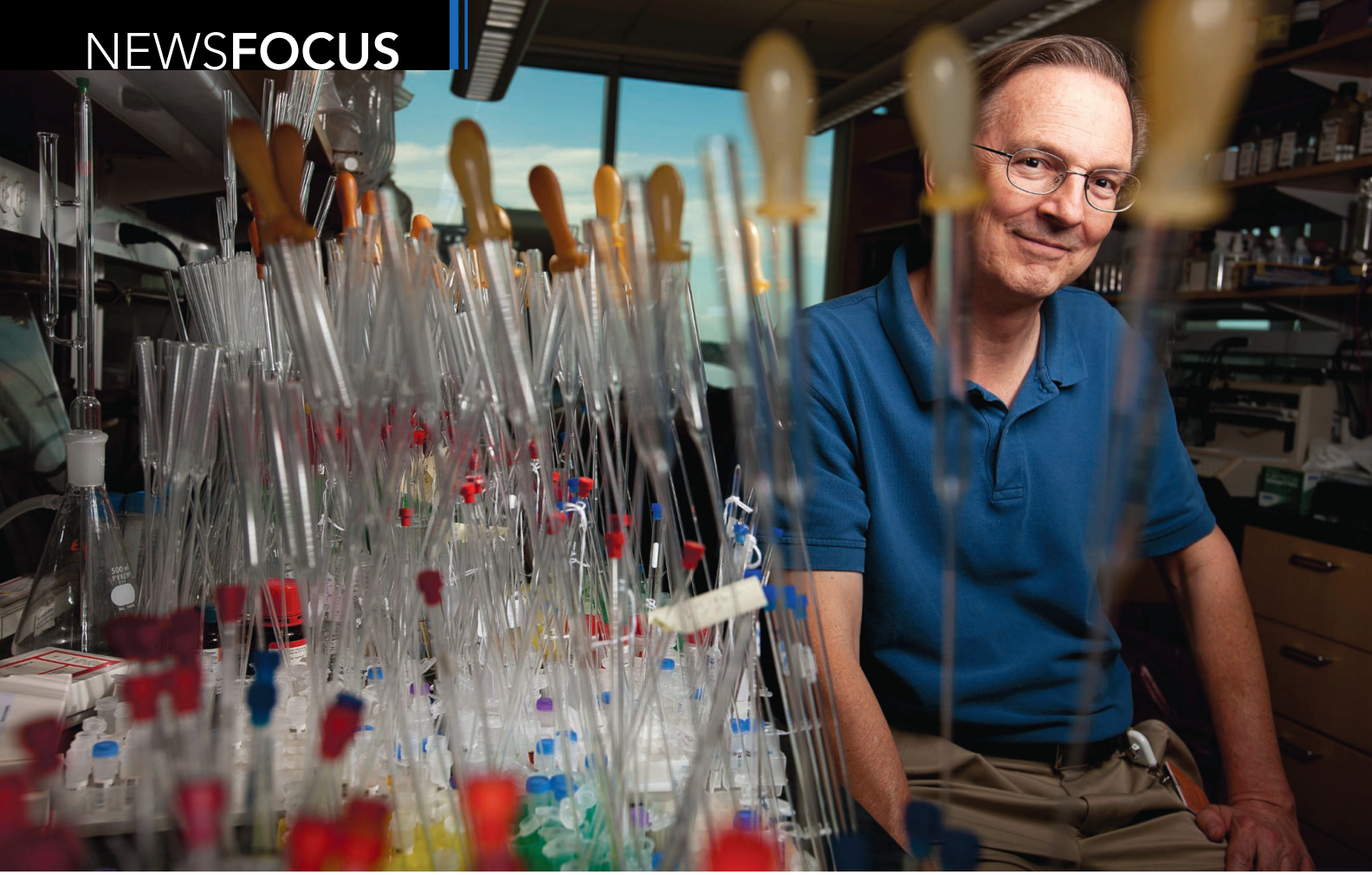

# The Life Force

**Step by grueling step, Jack Szostak is pushing through the barriers that keep him from his goal: making living cells from scratch in the lab**

Jack Szostak knows he'll never realize his ultimate scientific dream. But if he pulls off number two on his list, "it will go down in history as the greatest experimental achievement ever," says John Sutherland, an organic chemist at the Medical Research Council's Laboratory of Molecular Biology in Cambridge, U.K. Not bad for a backup.

Szostak, a molecular biologist at Harvard University and Massachusetts General Hospital in Boston, has already accomplished some spectacular science. He shared the 2009 Nobel Prize in physiology or medicine for helping to reveal the role of telomeres, the end bits of chromosomes that help protect genetic instructions during cell division. But more than a decade ago, Szostak shifted his lab's focus to exploring how life on Earth may have gotten its start. He would dearly love to know the recipe for the primordial soup in which it all began some 4 billion years ago. That recipe is almost assuredly lost to history. "We don't have a time machine," Szostak says. "We can't go back."

So he hopes to do the next best thing: fiddle around with a few ingredients of his own and watch as they spontaneously assemble themselves into genes inside simplified cells that copy themselves and demonstrate the first emergent signs of Darwinian evolution. The origin of life. Again. Only this time in a lab.

A lab demonstration wouldn't prove that life emerged the same way, Szostak says, but it would begin to tell a plausible story about how chemistry made the transition to biology. "If we can do that, to me it would give us a pretty good understanding of how life got started."

It's a big if. But on page 1098, Szostak and Katarzyna Adamala, his former graduate student and now a postdoctoral associate at the Massachusetts Institute of Technology in Cambridge, report taking a major step in that direction. For the first time, they found a recipe that promotes RNA copying inside primitive "protocells." It's not life in the lab—not yet—but other origin-of-life researchers are watching closely, says Gerald Joyce, a chemist and origin-of-life researcher at the Scripps Research Institute in San Diego, California. "You never want to bet against Jack," Joyce says. "He has a really good nose for where to go."

For an RNA-containing protocell to display Darwinian evolution, Szostak says eight large problems must be surmounted (see table, p. 1034). His lab has already solved three, and he says it is closing in on another three. That leaves two to go. "It's tantalizing," Szostak says. "We're close." And he's not the only one who thinks so. "I'd be hugely surprised if we don't get to that [during my career]," says Matthew Powner, a former postdoctoral assistant of Szostak's who now runs his own lab at University College London. "There is tangible excitement that this can be solved and this will mean something big."

## In the beginning

In tackling the origin of life, Szostak is taking on one of the biggest questions humanity has ever asked—second only to the origin of the universe itself. For millennia, it lay in the realm of philosophy, theology, and alchemy. Science got in on the act in a systematic way in the mid-20th century, after researchers discovered the structures of DNA and RNA and

CREDIT: BRYCE VICKMARK/*THE NEW YORK TIMES*/REDUX



Published by AAAS

**Creation scientist.** Jack Szostak is working to recreate a recipe that transformed chemistry into biology.

their central role in coding for proteins, the chemical workhorses of the cell. In a host of now-classic experiments, scientists probed how potential building blocks of life such as amino acids and nucleic acids could be synthesized from simple compounds under conditions thought to have prevailed on early Earth. Progress was rapid and spirits high. "Laboratories will be creating a living cell within ten years," Colin Pittendrigh, an American biologist, predicted in 1967.

Then things got complicated. Researchers realized that creating the raw ingredients of life wasn't enough: They also needed to explain how those compounds assembled themselves and evolved into the sophisticated living cells on Earth today. Life required not just the right ingredients, but also the right molecular tools. In the late 1960s, a trio of biologists—Francis Crick, Carl Woese, and Leslie Orgel—independently proposed that RNA could serve two roles. What came to be known as the "RNA World" hypothesis holds that RNA existed long before DNA, catalyzed its own reproduction, and helped give life its start. Others believed RNA wasn't up to the task and proposed alternatives for the earliest biochemistry, developing the "peptide world," "lipid world," and "metabolism first" scenarios for life's origin. Conferences on the subject became shouting matches. "They all fought each other tooth and nail," Sutherland says. "People wondered, 'How on Earth do you solve this problem?' "

Throughout most of history, the answer had been simple: divine intervention. Szostak, though, takes pleasure in pushing back the borders of the supernatural. "To me it's very satisfying to find natural explanations for problems that were so complex that people had to resort to magic," he says. But he insists that he is not a philosopher; he simply likes to solve problems at the lab bench.

Szostak has had a practical bent for most of his life. The eldest child of an aeronautical engineer father and a mother who held down various jobs, he grew up in Ottawa and Montreal. As a child, his parents took him to church and Sunday school but weren't particularly devout themselves. "When I was 12, I said I'm not going to do that anymore," Szostak says; his parents seemed more relieved than anything else.

In his teens, Szostak became absorbed in chemistry. His mother was working as a librarian for a chemical company and used to bring home ingredients for his basement lab. His early experiments left "a few little scars," Szostak says. But he chuckles, "I still have all my fingers."

After earning an undergraduate degree at McGill University in Montreal in 1972, Szostak moved to Cornell University to work with biologist Ray Wu. Wu's lab was racing to synthesize DNA fragments that could detect messenger RNA—the form of RNA that carries copies of genes to ribosomes, which translate their code into proteins. Wu's lab lost out by a few months to British biologist Michael Smith. Szostak didn't come in second often after that.

> **"The big picture is it's not an RNA world, a peptide world, a lipid world. It only works if everything is connected."**
>
> —JOHN SUTHERLAND, MRC LABORATORY OF MOLECULAR BIOLOGY

After setting up his own lab, Szostak plunged into the burgeoning field of genetics. He helped develop the yeast artificial chromosome, a technique that was widely used to identify, clone, and manipulate genes. He identified the specialized sequences of telomeres and helped show how they aid in cell division and how telomeres contribute to cell aging, hereditary diseases, and cancer.

Szostak's success brought other researchers flocking to work with telomeres. "The field was getting crowded," Szostak says. "I thought maybe it was time to do something different." He drew inspiration from experiments by Thomas Cech of the University of Colorado, Boulder, and Sidney Altman of Yale University, for which they won their own Nobel in 1989. In the early 1980s, Cech and Altman found that RNA not only serves as a genetic mail carrier but can also catalyze chemical reactions. Because that role was previously thought to be the sole domain of proteins, the finding bolstered the RNA World hypothesis.

In the early 1990s, Szostak switched his lab's focus to RNA catalysts, known as ribozymes. He and his colleagues invented a scheme for evolving new ribozymes in the lab, in a process known as in vitro selection. (Joyce's group at Scripps carried out similar work.) In 1995, Szostak and former students Eric Ekland and David Bartel used the technique to produce the first RNA catalyst capable of welding two other pieces of RNA together. A year later, Ekland and Bartel announced that they had found an RNA catalyst capable of serving as an RNA polymerase, the enzyme that living cells use to produce new copies of an RNA strand.

RNA was proving increasingly versatile, with multiple roles previously reserved for DNA and proteins. In 2000, researchers at Yale discovered that even the catalytic heart of the ribosome is an RNA-based ribozyme. Here was a possible relic of the RNA World, strongly supporting the idea that early life ran on RNA and only later evolved the ability to build chemically superior proteins.

Szostak found himself thinking more and more about the RNA World. The hypothesis had its problems, he realized. "RNA brings with it a lot of baggage," Szostak says. It is a fragile molecule, so researchers would need to explain how it could have survived conditions on early Earth. They would also need to explain how long RNA chains formed, were copied, split apart, and sent to daughter cells—the cycle of replication that is basic to life.

CREDIT: JANET IWASA/UNIVERSITY OF UTAH

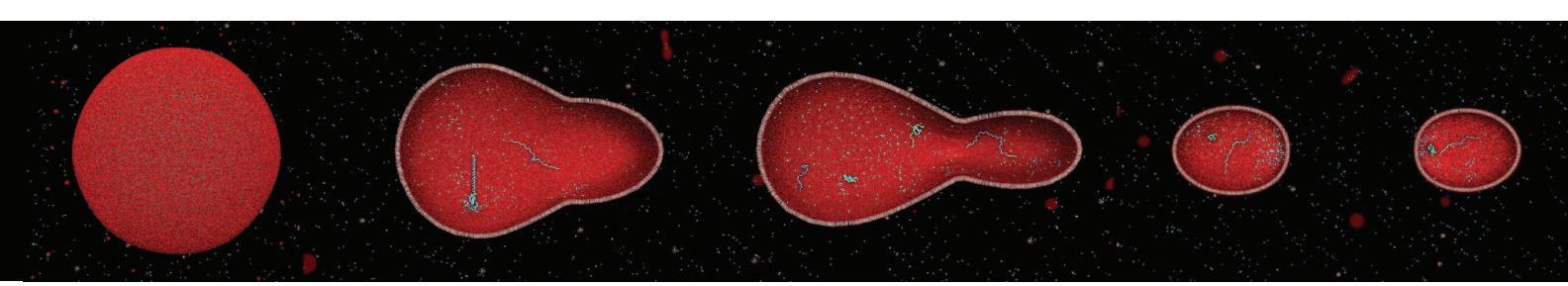

**Divide and conquer.** Protocells that assemble themselves and split might undergo Darwinian evolution.



Published by AAAS

Most fundamentally, it wasn't at all clear how an RNA fragment drifting around in a warm pond or stuck on a fleck of mineral could have spawned variants that would have reproduced more or less rapidly, allowing "fitter" variants to outcompete others. What allowed primordial RNA to *evolve*?

**All of the above**

After numerous conversations with other origin-of-life researchers, Szostak became convinced that RNA couldn't have done it alone. The molecules needed to be isolated and confined. Some sort of cell membrane probably was needed, both to concentrate the ingredients of life and to promote a Darwinian process. "If [chemistry] is compartmentalized, you keep molecules related by descent together," Szostak explains. If an RNA-containing protocell arises and can grow and divide better than its neighbors can, it can pass its advantages to its progeny. The protocells would allow fitter molecules to flourish, in true Darwinian fashion.

"I thought, 'Well, I've never worked on membranes before,' " Szostak says. " 'Maybe it's time to do so.' " Protocell membranes, he knew, must have been very different from those of modern cells. Current cell membranes are made from fats called phospholipids and are all but impenetrable to key ingredients of life such as amino acids and nucleic acids. Without the modern biochemical apparatus of protein-based pores and pumps, nutrients cannot get in and waste products can't get out.

Szostak and his students found an alternative. They discovered that far simpler fatty acid molecules could form leaky cell-like spheres that allowed ions, amino acids, and nucleic acids to diffuse in. In 2008, Szostak's team reported that RNA nucleotides, or building blocks, could enter these cells and then form growing RNA chains that were too big to diffuse back out. A year later, Szostak and his graduate student Ting Zhu found that adding extra fatty acid molecules to the mix caused existing protocells to grow. Then, modest shear forces—such as those that protocells might experience when flowing through a column of warm water near a volcanic vent—would stress the large spheres until they divided, and any RNA inside them would be partitioned among the daughter cells. Yet another paper showed that RNA or peptide catalysts would speed the incorporation of additional fatty acid molecules into protocells, promoting their growth. Crude as they were, fatty acid vesicles appeared to be up to the job.

What about the other key component, RNA? Advances both in Szostak's lab and elsewhere showed that, with the right mix of ingredients, individual RNA nucleotides would bind to a sister "template" strand in a copying process without the enzymes required inside modern cells. That was good news—but researchers couldn't make it happen inside a protocell.

The biggest problem was that one of the most important ingredients for copying an RNA template without added enzymes is charged magnesium ions ($Mg^{2+}$). Take away $Mg^{2+}$ and the reaction proceeds so slowly, it's hard to imagine how it could have been relevant to early life. But $Mg^{2+}$ has downsides. The ions rip apart fatty acid protocells and shred growing RNA chains as fast as they build them up.

Adamala says she tried adding hundreds of different compounds and short peptides to the mix. "Nothing worked," she says. "It was very frustrating." But then she turned to metal-binding compounds called chelators, and one gave her the result she was looking for. In their current paper, Adamala and Szostak report that when they added a bit of a simple citric acid derivative called citrate to the mix, they got a perfect Goldilocks result. The citrate bound the $Mg^{2+}$ ions tightly enough to keep the ions from tearing apart either the RNA or the fatty acid membranes, but loosely enough to give the $Mg^{2+}$ ions leeway to copy a template RNA strand.

"It's a beautiful paper," Sutherland says. Citrate itself is a tantalizing solution, he says. It also plays a key metabolic role in modern cells, which suggests that it, too, could be a molecular fossil left over from early evolution.

Equally important, Sutherland says, is that for the first time, all the various pieces of the protolife puzzle seem to be coming together. "The big picture is it's not an RNA world, a peptide world, a lipid world. It only works if everything is connected," Sutherland says. George Cody, an organic geochemist at the Carnegie Institution for Science in Washington, D.C., agrees. "In the beginning, all these had to be in play," he says.

Next, Szostak says, his team must overcome two large hurdles: The researchers must show how individual RNA bases could have become chemically "activated" so they would readily bind to growing RNA strands. Then they must demonstrate how RNA strands can duplicate without a starter template strand to help the nucleotides come together to form the complementary strand. Sutherland thinks these are solvable problems. "There's no reason it shouldn't be possible to recreate [a replicating cell]," he says.

Even if Szostak's experiment works, there will still be plenty of unanswered questions. Among them: What prebiotic processes would have produced the RNA nucleotides and other mix of ingredients that would have gone into an early protocell? It's also not clear that an evolving protocell made in the lab would have any broader significance, says Ramanarayanan Krishnamurthy, an organic chemist at Scripps. "Pushing its relevance to what happened 4 billion years ago is a risky thing."

But Szostak argues that such dismissals are too facile. Such a "cell" would help define the chemistry that must have been involved at some level to get a self-replicating system going. Sutherland likens it to a crossword puzzle. As you begin to fill in words in some of the open squares, the options narrow for the words that intersect each known word. The puzzle shrinks, making subsequent answers easier. For someone aiming to show that the puzzle of life's origin didn't solve itself by magic, that would be a satisfying result indeed.

**–ROBERT F. SERVICE**

## Steps Toward an Evolving RNA Protocell

| Challenge | Status |
|---|---|
| 1. Enable RNA template copying to proceed despite strands with random backbone linkages | ✓ |
| 2. Enable paired RNA strands to separate without high temperatures | ✓ |
| 3. Keep metal ions (needed to copy RNA) from destroying protocells and RNA strands | ✓ |
| 4. Improve accuracy of copying RNA without enzymes | Recent progress |
| 5. Speed up rate of copying RNA without enzymes | Recent progress |
| 6. Keep RNA strands from quickly reforming duplexes after they separate | Recent progress |
| 7. Chemically "activate" RNA nucleotides to bond to a growing strand | Not demonstrated |
| 8. Enable RNA to form in protocells without primer template strands | Not demonstrated |

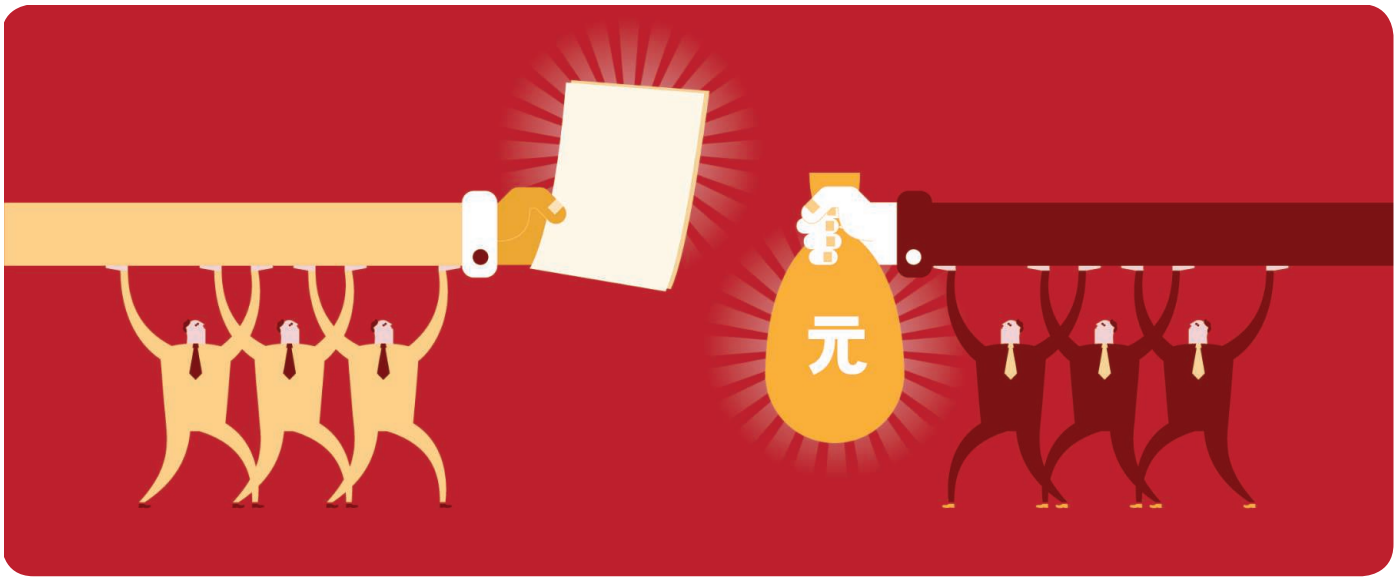


# China's Publication Bazaar

A *Science* investigation has uncovered a smorgasbord of questionable practices including paying for author's slots on papers written by other scientists and buying papers from online brokers

**SHANGHAI, CHINA—**The e-mail arrived around noon from the mysterious sender "Publish SCI Paper," with the subject line "Transfer co-first author and co-corresponding author." A message body uncluttered with pleasantries contained a scientific abstract with all the usual ingredients, bar one: author names. The message said that the paper, describing a potential strategy for curbing drug resistance in cancer cells, had been accepted by Elsevier's *International Journal of Biochemistry & Cell Biology*. Now its authorship was for sale.

"There are some authors who don't have much use for their papers after they're published, and they can be transferred to you," a sales agent for a company called Wanfang Huizhi told a *Science* reporter posing as a scientist. Wanfang Huizhi, the agent explained, acts as an intermediary between researchers with forthcoming papers in good journals and scientists needing to snag publications. The company would sell the title of co–first author on the cancer paper for 90,000 yuan ($14,800). Adding two names—co–first author and co–corresponding author—would run $26,300, with a deposit due upon acceptance and the rest on publication. A purported sales document from Wanfang Huizhi obtained by *Science* touts the convenience of this kind of arrangement: "You only need to pay attention to your academic research. The heavy labor can be left to us. Our service can help you make progress in your academic path!"

Online
**sciencemag.org**
Podcast interview with author Mara Hvistendahl (http://scim.ag/pod_6162).

On 6 July, a few weeks after our conversation with the sales agent took place, the paper appeared online in the *International Journal of Biochemistry & Cell Biology*. The print version followed in September, roughly when the agent said it would. The title and abstract had undergone minor revisions from the e-mail solicitation.

But the list of authors was transformed. On the published paper, two first authors share the honor. (Our reporter did not pay for authorship.) Interviews with authors and with the journal's editors confirmed that a first author was added on 11 June, approximately a week after our reporter received the abstract; all deny knowledge of anyone having paid for authorship. Following an inquiry from *Science*, an investigation by the *International Journal of Biochemistry & Cell Biology* found that a total of four authors had been added, and two dropped. (The exuberant agent had erred on one detail during our June conversation with her: By then, the paper had undergone one round of review, but had not yet been accepted. The resubmitted version with a different author lineup was accepted soon after.)

Earlier this month, *Science* told Wanfang Huizhi about our undercover operation. In an e-mailed response, Huang Wei, who identified himself as Wanfang Huizhi's manager, denied that his firm sells authorship. The sales document that *Science* had obtained was not authentic, he said, because it did not bear his company's official seal. Wanfang Huizhi helps authors with "language polishing, editing, and submission of manuscripts," he wrote, so it is "very probable" that the cancer paper's authors had sought editing help from the firm. Our reporter may have encountered a rogue employee or former employee who had "gone through irregular channels" to hawk authorship on the side, Huang wrote. He stated that Wanfang Huizhi would investigate the matter.

The sales agent's offer is far from an anomaly in China's publishing scene. A 5-month investigation by *Science* has uncovered a flourishing academic black market involving shady agencies, corrupt scientists, and compromised editors—many of them operating in plain view. The commodity: papers in journals indexed by Thomson Reuters' Science Citation Index (SCI), Thomson Reuters' Social Sciences Citation Index, and Elsevier's Engineering Index. *Science* has documented authorship fees ranging from $1600 to $26,300. At the high end, fees exceed the annual salary of some Chinese assistant professors. But SCI papers—particularly those published in journals with a high impact factor—are so critical to getting promotions that researchers shell out. As Fan Dongsheng,

a neurologist and former vice president of Peking University Third Hospital, puts it: "People are sparing no expense in order to get published in international journals."

The options include not just paying for an author's slot on a paper written by other scientists but also self-plagiarizing by translating a paper already published in Chinese and resubmitting it in English; hiring a ghostwriter to compose a paper from faked or independently gathered data; or simply buying a paper from an online catalog of manuscripts—often with a guarantee of publication.

Offering these services are brokers who hawk titles and SCI paper abstracts from their perches in China; individuals such as a Chinese graduate student who keeps a blog listing unpublished papers for sale; fly-by-night operations that advertise online; and established companies like Wanfang Huizhi that also offer an array of above-board services, such as arranging conferences and producing tailor-made coins and commemorative stamps. Agencies boast at conferences that they can write papers for scientists who lack data. They cold-call journal editors. They troll for customers in chat programs. "SCI papers transfer: papers about cervical cancer; head and neck cancer; kidney cancer; stomach cancer; nano-materials," reads a chat message to one editor. They set up toll-free hotlines.

Some of the journals in which brokered papers appear belong to Chinese publishers, whereas others are located overseas and owned by publishing giants. Although the agencies market themselves to researchers in fields like medical research, in which time constraints make satisfying promotion requirements especially difficult, scientists in a range of disciplines—even those who publish on academic honesty and publishing ethics—say they have been approached. Nearly all the editors and researchers in China whom *Science* contacted about SCI paper-selling agencies were aware of their existence.

*Science* looked into 27 agencies that trade in SCI papers. Our targets included agencies identified by scientists we interviewed and others we found using Baidu, a popular Chinese Web search engine. Inputting "publish SCI paper" in Baidu pulls up dozens of agencies with websites brazenly touting the sale of papers for publication in SCI-ranked journals. "Ghostwrite and ghost-publish papers…SCI paper publishing," reads one typical description. We targeted the top search results. We also looked into agencies that had purchased ads on Baidu and posted in online publishing forums, focusing on those that seemed most established. Scientists and journal editors in China, many of them speaking under condition of anonymity, helped round out our portrait of the business.

Posing as graduate students and scientists, *Science* reporters contacted the selected agencies by phone or via the Chinese messaging service QQ, inquiring about buying authorship on a paper or paying the company to write a paper. A mere five of the 27 companies we contacted refused to write papers or broker authorship. We also tracked individual papers. Some were advertised for sale ahead of publication and have not yet appeared. Others appeared in reputable journals several months after they were proffered.

Academic honesty has been a hot-button issue in China for years, and officials hoping to project a more international image have repeatedly vowed to address it. Since coming to power in March, President Xi Jinping has spearheaded a broad attack on corruption, with the government taking aim at a spectrum of misbehavior that ranges from bribing officials to pharmaceutical company payoffs (*Science*, 2 August, p. 445). The campaign has spilled over into scientific publishing: In September, police disguised as gas company employees busted seven people who, operating out of a Beijing apartment, offered space in fake journals and collected publication fees from scientists. Their victims blew up to $650 in fees for papers that never saw the light of day.

But most of the corrupt publishing practices that *Science* investigated have no clear victims; scientists, brokers, and some journal editors all benefit. What is at risk, say prominent researchers in China, is China's wider achievement in science. The country has become a powerhouse in scientific publishing: The number of SCI Expanded papers originating in China skyrocketed from 41,417 in 2002 to 193,733 in 2012, ranking it second in the world, after the United States. Corrupt publication practices taint that achievement. "[Some scientists] are publishing better and better papers and getting into top-notch journals, but in the end they don't even know what their papers say," says Cao Zexian, a physicist at the Chinese Academy of Sciences' Institute of Physics in Beijing. "They spend a lot of money hiring researchers to write them."

> "People are **sparing no expense** in order to get published in international journals."
>
> —Fan Dongsheng, Peking University Third Hospital

## Skewed incentives

Chinese-language journals are a prime outlet for the paper-sellers. "The number of articles appearing in Chinese-language journals that has been sold is very high," says one journal editor in Beijing. Many companies investigated by *Science* offer to sell papers in Chinese-language journals. The purported Wanfang Huizhi sales document delineates the cost of buying articles in "core journals"—a select group of Chinese-language journals ranked by either Peking University, Nanjing University, or the Institute of Scientific and Technical Information of China.

For most Chinese scientists, however, the gold standard is English-language journals, especially the 3746 ranked by SCI, a database of citations introduced in 1963 by the Institute for Scientific Information. Thomson Reuters, which now owns the institute, uses the index to compute each journal's "impact factor," a tally of how many times the average article in a journal is cited in a given year. Thomson Reuters bills impact factors as a way to compare journals within fields. Evaluating individual researchers by the impact factor of the journals they publish in is "not something that we advocate," says Nicholas Stipp, business development director with Thomson Reuters in Beijing.

But in China, "SCI papers have become the yardstick to promote scientists," says Cong Cao, an expert on Chinese science policy at the University of Nottingham in the United Kingdom. The number of papers a researcher has published in SCI-ranked journals over a 5-year period is often the deciding factor in promotions—and typically only papers on which the candidate is a first author or corresponding author count.


Published by AAAS

## An Aura of Legitimacy

China's SCI paper-selling agencies mimic legitimate services that help scientists struggling with English. In the 1990s, as science took off in Japan, editing outfits emerged to help polish English writing. Today, scientific language editing is a profitable sector, with established companies like American Journal Experts, Edanz, Editage, and Enago serving the global market. Besides editing, such companies offer additional services at various stages of the publication process, from suggesting appropriate journals to helping craft a cover letter. Some also edit for content and provide translation services.

For the most part, journals recognize that they benefit by receiving more polished manuscripts. Some publishers now recommend specific editing companies, and the companies offer a discount to those journals' contributors in return.

The paper-selling agencies flourish in the aura of these reputable businesses. A Baidu search for "SCI paper editing" brings up Editage and Enago—beneath a banner ad for MicroSCI, a company that goes a step further by gathering data and writing papers for scientists, according to a representative. For some scientists, it may be difficult to tell the difference. Many paper-selling agencies contacted by *Science* appear professional and well-staffed. Several have registered with China's Industrial and Commercial Bureau. To assure clients that all of their information will be kept confidential, the agencies prepare contracts emblazoned with government-issued seals.

But any similarities to mainstream editing companies end there. MicroSCI sells its services on Taobao.com, the Chinese answer to eBay, and it is one of several agencies that guarantee a client's paper will be published, according to a sales agent. Guaranteeing publication is an alarm bell, says Benjamin Shaw, chief operating officer for Edanz in Beijing: "It makes me uncomfortable that some companies offer this. We always take care to educate authors that we can only guarantee language quality and that journal editors make the final publication decision." (MicroSCI did not respond to repeated interview requests.) The fees charged by SCI paper-selling companies raise eyebrows as well. Edanz charges $325 on average for language editing. Compare that with the $26,200 an agent with the outfit Ketong Editing and Translation says it charges for authorship on a paper targeted at a high-impact Western journal.

**–M. H.**

(Publications in Chinese core journals can be credited toward promotions as well, but a researcher usually must amass many more of them during a short period to meet requirements.) Some universities require Ph.D. students to publish one or more SCI papers to graduate. Incentive schemes have yielded an environment in which scientists "focus on quantity, not quality," wrote Lin Songqing, an editor with the Chinese Academy of Sciences in Wuhan, in a paper in *Learned Publishing* in January. (A running joke in China now is that SCI stands for Stupid Chinese Idea.)

Pressure to publish is especially acute for medical researchers. Even for doctors, of whom the vast majority in China work in government hospitals or clinics, securing a promotion can hinge on writing SCI papers—regardless of how many patients they see.

With the stakes so high, ways of gaming the system have cropped up. Researchers who are "eager for quick success or maybe have a low academic level" turn to SCI paper brokerages, says Zhang Yuehong, editor of the *Journal of Zhejiang University-SCIENCE* in Hangzhou and an advocate for improving journal oversight in China. (The journal is not indexed in SCI.) By passing off bought papers as legitimate research, she says, "they replace pearls with fish eyes."

Because many promotion schemes in China simply tally up a researcher's total SCI publications without regard to impact factor, some paper-selling agencies target journals with negligible impact factors; a spot in SCI is enough. But Chinese institutions dole out lavish rewards ranging into the tens of thousands of dollars for publishing in highly rated journals—meaning that researchers who pay agencies for papers may get a return on their investment.

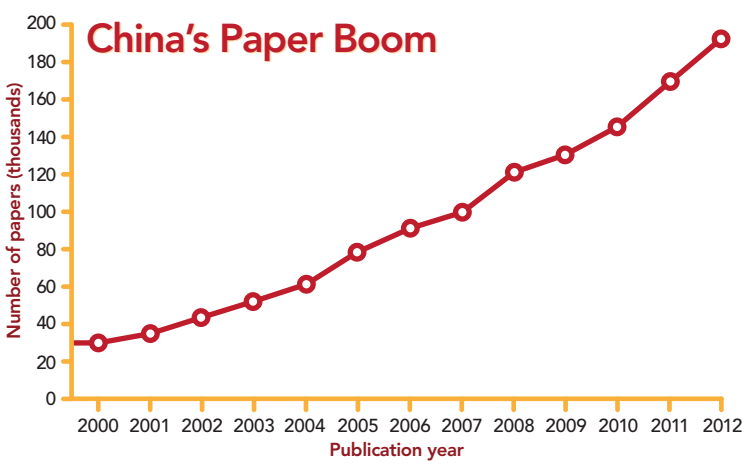


**Speaking volumes.** Since 2000, Chinese papers have increased sixfold in Thomson Reuters' SCI Expanded, a database of more than 8500 journals.

CREDIT: THOMSON REUTERS

### The paper-pushers

At one end of the spectrum of services offered by China's SCI-paper cottage industry, companies will translate into English a paper published in a Chinese journal. (The purported Wanfang Huizhi document specifies that researchers should avoid submitting Chinese-language papers whose abstracts can be found in PubMed.) In another arrangement called *daixie,* or "ghostwriting," a scientist will hire an agency to write a paper—a task sometimes farmed out to graduate students—and ensure its publication in a specified journal. Too busy to format papers, prepare citations and graphs according to a journal's specifications, analyze statistics, submit your paper, and answer queries from editors when a paper is in proofs? SCI Science Paper Service Center can handle all of the above, brags its website.

Several agencies claim they collaborate with specific journals indexed in SCI to guarantee publication. A representative for one company, Haixin, was blunt about the collaborations: "We rely on our *guanxi*"—a Chinese concept evoking relationships often deepened by exchanging gifts. "To put it simply, we give them money." At least three companies offer to assist scientists who have written a paper and want to ensure its publication. Other firms claim to purchase a set number of pages in journals. Several agencies specified both the journal and issue in which a paper would appear—even though the paper had yet to be written.

An editor at one SCI journal in China says the journal regularly receives multiple submissions from a single e-mail address. It rejects them under the assumption that the papers are ghostwritten. Other agencies may seek out journal editors willing to enter an arrangement. One editor, who worked for 6 years at a Chinese journal listed in


Published by AAAS

Elsevier's Engineering Index, says that in that time he was approached by scientists in need of papers about 10 times. "They asked me to add their names to the papers of another author," hinting that he would be compensated for the favor. Later, as his own 5-year review approached as a professor, an editor at an SCI Expanded journal offered him an author's slot on a paper in exchange for ghostwriting another paper.

Other editors say they have never heard of counterparts collaborating on paper-selling deals, and that for an editor at an internationally ranked journal the risks of being on the take are too high. "Many editors are trying hard to improve the quality of their journals, and they hate this kind of fraud," says the former Engineering Index journal editor. "Maybe a small group is engaged in this kind of activity." But, he continues, "It completely destroys the academic environment."

One seeming conduit for paid publication is the *Chinese Medical Journal*, an open-access journal published by the Chinese Medical Association. Agents at eight of the companies we contacted claim they can arrange publication in the journal, for fees ranging from $1600 to $4600. Until *Science* reached the journal's managing director, Wang Mouyue, by phone in late October, the "links" section on the journal's homepage featured the logo of Sciedit, a Guangzhou-based agency whose representative sent a *Science* reporter an abstract of a paper that was purportedly for sale. But Wang told *Science* it is "impossible" that *Chinese Medical Journal* editors take payments for ensuring a paper's publication. "China's paper-selling market is very large, and there's every sort of agency imaginable out there. But our journal hasn't cooperated with any agency in order to sell articles." The Sciedit logo was later removed from the journal's website. A man who identified himself only as Mr. Wang and claimed to be Sciedit's owner declined to answer questions about collaboration with the *Chinese Medical Journal*.

## Full service

Some agencies claim they not only prepare and submit papers for a client: They furnish the data as well. "IT'S UNBELIEVABLE: YOU CAN PUBLISH SCI PAPERS WITHOUT DOING EXPERIMENTS," boasts a flashing banner on Sciedit's website.

One timesaver: a ready stock of abstracts at hand for clients who need to get published fast. Jiecheng Editing and Translation entices clients on its website with titles of papers that only lack authors. An agency representative told an undercover *Science* reporter that the company buys data from a national laboratory in Hunan province.

For scientists who have qualms about attaching their names to data of questionable provenance, many agencies offer to write meta-analyses or review papers, based on already-published data. The fact that review articles can be written without gathering original data has made them wildly popular in China, says Deborah Yang, marketing and sales director for China for Editage, a reputable international editing company, in Shanghai. From 2003 to 2011, the number of meta-analyses from China listed in PubMed increased more than 16 times faster than did meta-analyses from the United States, far outstripping the overall rise in papers from China. Sciedit's Mr. Wang says the reference on his agency's website to publishing without doing experiments refers to meta-analyses. "We don't write [papers], we just help with revisions and language polishing," he wrote in an e-mail to *Science*.

A customer service representative with H&G IES told an undercover *Science* reporter that the agency could write a paper and guarantee publication in an international journal. Reached by phone, Kevin Chang, chief editor at H&G IES, elaborated: "If a person doesn't have any data or an article, what we can do at the most is to write a review paper. … We don't make up data." Chang was more cautious in a later e-mail, stating that H&G IES provides only "editing and consulting services, not writing." The customer service representative, he explained, was "under-trained."

There may be less to many of these agencies than meets the eye. H&G IES's website advertises its "US Root, Global Reach" and, until *Science* reached Chang, claimed to have representatives serving France, Germany, Japan, Korea, Spain, and Vietnam. But its website includes content only in English and Chinese, and the lone telephone number listed until recently was a Google Voice number. Chang did not respond to questions about the company's size.

The Chinese paper-selling agencies also inhabit a murky legal space, as several agency representatives acknowledged in chats with an undercover *Science* reporter. But, at least in some cases, they seem to deliver on their promises. On 21 August 2012, Core Editing advertised authorship for sale on 12 papers listed on its blog. Eight were meta-analyses; the other four were original research. Of the dozen, at least two have since been published by Chinese authors in SCI journals.

Corresponding authors of the two papers—one published in *OncoTargets and Therapy* and the other in the *Canadian Journal of Neurological Sciences*—did not respond to repeated interview requests. An e-mail to the address connected to the QQ messaging service number on Core Editing's blog elicited this reply: "I apologize if the blog's content inadvertently violated certain writers' rights…. If the famous Science Magazine goes so far as to be interested in a personal blog, isn't it making a big fuss over a small issue?" The page advertising papers for sale has since been deleted.

In those two cases, the brokered papers had not yet been submitted, raising the possibility that any original authors may have transferred

CREDIT: ADAPTED FROM AKINDO/ISTOCKPHOTO.COM



Published by AAAS

the authorship to Core Editing's clients. In an e-mail to *Science*, Hans-Joachim Schmoll, editor-in-chief of *OncoTargets and Therapy*, wrote that his journal is investigating the paper and will consider retracting it if the investigation shows its authorship to be suspect. Robert Chen, editor of the *Canadian Journal of Neurological Sciences,* told *Science* that his journal will pursue a similar course of action.

Another common brokerage method is bringing on authors after a paper has gone through peer review. Such an approach takes advantage of journal policies allowing authors to be added at late stages—a change sometimes legitimately necessary because of issues raised by reviewers. Such practices have contributed to a boom in co–first authors and co–corresponding authors in China, says Cao Zexian—so common, he jokes, that they're "a Chinese invention."

At the *International Journal of Biochemistry & Cell Biology*, the overhaul of the author list in the paper purportedly brokered by Wanfang Huizhi went unnoticed. Typically, if new authors are brought on, the corresponding author is expected to explain the change to the editor handling the paper. That didn't happen with the cancer paper, Joanna Kargul, the journal's managing editor, wrote in an e-mail to *Science*: "The authorship change slipped the radar of the reviewers and the handling editor."

Outside China, ignorance of the methods used by agencies may prevent editors from spotting brokered papers. Schmoll notes that many editors struggle to evaluate the flood of papers from China: "We don't know the universities, we don't know the clinics, we don't know the research institutions." He adds: We have to either reject everything or evaluate [papers] as normal."

"IT'S **UNBELIEVABLE**: YOU CAN PUBLISH SCI PAPERS **WITHOUT DOING EXPERIMENTS**."

—Banner on Sciedit's website

## Winds of change?

At a publishing conference sponsored by the China Association for Science and Technology in Hangzhou last September and attended by editors from across China, Thomson Reuters' Stipp was the star of the show. As he clicked through PowerPoint slides explaining how journals are selected for the Web of Science, the broad citation database that encompasses SCI, audience members crowded the screen, snapping photos. A slide showing a huge leap in the number of Chinese journals listed brought hearty applause.

Globally, the past few years have seen a growing shift away from science's overreliance on impact factors. In May, 155 scientists from 78 scientific organizations signed the San Francisco Declaration on Research Assessment, a document drafted at the December 2012 meeting of the American Society for Cell Biology (*Science*, 17 May, p. 787). The declaration advocates abandoning the use of journal impact factors to assess individual researchers. Chinese science leaders are steering in that direction (see Editorial, p. 1019). Thomson Reuters is working with the National Natural Science Foundation of China, the science ministry's Institute of Scientific and Technical Information of China, and the Ministry of Education to introduce other evaluation measures for authors, such as total paper citations and number of patents awarded.

One way to more explicitly combat paper-selling is to beef up authorship requirements. Following recurring revelations of pharmaceutical company ghostwriting at international medical journals over the past decade, several leading journals adopted more stringent standards, requiring that each author detail his or her involvement in the research upon submission. Some journals ask for one of the authors to serve as a "guarantor" of a paper's integrity and authorship from inception to publication. And editors say an increasing number of journals based in China warn authors that they are not affiliated with any paper-selling companies.

Basing academic evaluation on peer review rather than on impact factors would also curtail fraud, argues Jianwu Tang, an ecologist at the Marine Biological Laboratory in Woods Hole, Massachusetts, who conducts research part of the year in China. "In a specific field, our colleagues know pretty much what we are doing," he notes. Others say that scientists caught in publication scams should face stricter punishments. For now, agencies and their clients are operating with impunity. Under China's current setup, says one editor, "what you gain [by buying papers] is more than you lose if you are found to commit academic fraud."

As for the paper whose abstract the Wanfang Huizhi agent sent our reporter, the authors offered a range of explanations for the late changes in the author list. Asked about the decision to add a second first author, corresponding author Wang Xuedong of the Fifth People's Hospital of Wuxi and the Affiliated Hospital of Nanjing Medical University in Wuxi responded in an e-mail: "The entire submission was prepared by the first author, so I'm not very clear about the situation you mentioned." He explained that the first author had suggested adding as a co–first author a former classmate who had helped with the work. As to how the Wanfang Huizhi agent could have described authorship on the paper as for sale, he wrote: "We do not know through what channels the agency obtained the abstract to our paper."

The original first author, Wang Qingping of Shaoxing Hospital of China Medical University in Shaoxing, denied that the authorship change had been his idea. Reached by telephone, he said, "The co–first author's name was added after discussion among the other authors. It was not my decision alone." In response to an e-mailed copy of the abstract obtained from Wanfang Huizhi, he wrote that he was shocked at the suggestion that 90,000 yuan ($14,800) had changed hands: "You don't mean [Japanese] yen?"

Wang Yu, the new first author whose name appears in the slot that the agent claimed was for sale, remains a mystery. The Southwest Hospital of the Third Military Medical University in Chongqing, listed on the paper as her affiliation, did not provide her telephone number. There's no trace of her online, apart from a few doctor review sites. The paper in the *International Journal of Biochemistry & Cell Biology* appears to be Wang Yu's first publication in an SCI journal. An unintended consequence was her debut in *Science* as well.

**–MARA HVISTENDAHL**

With reporting by Li Jiao and Ma Qionghui.



Published by AAAS





# LETTERS

*edited by Jennifer Sills*

## The More Parasites, the Better?

S. ALTIZER *ET AL.*'S REVIEW "CLIMATE CHANGE AND INFECTIOUS DISeases: From evidence to a predictive framework" (2 August, p. 514) suggests that increased temperatures will favor several attributes of virulent pathogens that will adversely affect host health. Altizer *et al.* predict a decline in parasite biodiversity but overlook an important problem: This loss could have dire consequences to ecosystems.

Parasite diversity benefits ecosystems by regulating host population dynamics, increasing connectivity and stability in food webs (*1*) and decreasing community-level disease risk. For example, increased parasite richness reduced transmission of the virulent trematode *Ribeiroia* to amphibian hosts by more than 50% (*2*). This decrease in disease risk may be due to either increased parasite competition within intermediate hosts (*2*) or antiparasite immune responses increasing immune genetic diversity in hosts (*3*). Pathogens can also have a mediating effect on interspecific competition between shared hosts, as in the case of *Anolis gingivinus* lizards in the Caribbean, which exclude sister species *A. wattsi* except when their competitive ability is diminished by the presence of *Plasmodium azurophilum* (*4*). Parasites likely mediate such interactions largely through immune costs, with hosts trading off resource use between immune responses and reproduction and growth (*5*). Thus, although some virulent parasite populations may increase with climate change, we anticipate that the loss of parasite biodiversity will result in more widespread and unpredictable threats to ecosystem health. We therefore call for further research into parasite ecology and host-parasite coextinctions as tools for quantifying ecosystem vulnerability to climate change.

**Frog with parasite-induced (*Ribeiroia ondatrae*) limb malformation.** Increased parasite diversity reduced the transmission of *Ribeiroia* to amphibian hosts.

**COLIN J. CARLSON,[1] CARRIE A. CIZAUSKAS,[2] KEVIN R. BURGIO,[3] CHRISTOPHER F. CLEMENTS,[4] NYEEMA C. HARRIS[1]***

[1]Environmental Science, Policy and Management, University of California, Berkeley, Berkeley, CA 94704, USA. [2]Department of Ecology and Evolutionary Biology, Princeton University, Princeton, NJ 08544, USA. [3]Department of Ecology and Evolutionary Biology, University of Connecticut, Storrs, CT 06269, USA. [4]Department of Animal and Plant Sciences, University of Sheffield, Sheffield, S10 2TN, UK.

*Corresponding author. E-mail: nyeema@berkeley.edu

**References**

1. K. D. Lafferty, A. P. Dobson, A. M. Kuris, *Proc. Natl. Acad. Sci. U.S.A.* **103**, 11211 (2006).
2. P. T. J. Johnson, D. L. Preston, J. T. Hoverman, B. E. Lafonte, *Proc. Natl. Acad. Sci. U.S.A.* **110**, 16916 (2013).
3. G. Froeschke, S. Sommer, *PLOS ONE* **7**, 2 (2012).
4. J. J. Schall, *Oecologia* **92**, 1 (1992).
5. I. Colditz, *Parasite Immunol.* **30**, 2 (2008).

## Open Data: Crediting a Culture of Cooperation

ALTHOUGH THE QUESTION OF WHO PAYS FOR open data is important ("Who will pay for public access to research data?", F. Berman and V. Cerf, Policy Forum, 9 August, p. 616), a greater challenge lies in implementing the institutional and cultural changes required before data from government-sponsored research can be openly shared.

The Office of Science and Technology Policy (OSTP) has ordered U.S. federal agencies to formulate plans to share federally funded science data (*1*). This reflects a fundamental shift in the social contract between scientists and society. While seeking to strengthen science, the order also seeks better use of data to promote economic innovation, improve cross-disciplinary efforts, and address "grand challenge" societal problems such as global climate change and urban violence.

The OSTP memo correctly notes that public availability of atmospheric data enabled commercial weather services and severe weather prediction. Yet many data, tools, and models in the geosciences are held by a mix of individual investigators, national data centers, university-based initiatives, and commercial labs, embedded in institutional arrangements that actively reward holding onto data and maximizing individual outcomes in a competitive environment. NSF's EarthCube project, a long-term strategic initiative to build the cyber infrastructure for integrating data, tools, and models in the geosciences, illustrates the challenges and benefits of community engagement and institutional alignment (*2*).

The push for open data goes beyond the question of who pays. It challenges science to create a more cooperative culture that aligns credit and rewards with sharing data, tools, and models.

CREDIT: BRETT A. GOODMAN, PIETER T. J. JOHNSON/WIKIMEDIA COMMONS

**BURCU BOLUKBASI,[1*] NICHOLAS BERENTE,[2*] JOEL CUTCHER-GERSHENFELD,[1,3*] LESLIE DECHURCH,[4*] COURTNEY FLINT,[5*] MICHAEL HABERMAN,[6*] JOHN LESLIE KING,[7*†] ERIC KNIGHT,[8*] BARBARA LAWRENCE,[9*] ETHAN MASELLA,[10*] CHARLES MCELROY,[11*] BARBARA MITTLEMAN,[12*] MARK NOLAN,[13*] MELANIE RADIK,[10*] NAMCHUL SHIN,[14*] CHERYL A. THOMPSON,[13*] SUSAN WINTER,[15*] ILYA ZASLAVSKY,[16*] M. LEE ALLISON,[17‡] DAVID ARCTUR,[18‡] JENNIFER ARRIGO,[19‡] ANTHONY K. AUFDENKAMPE,[20‡] JAY BASS,[21‡] JIM CROWELL,[22‡] MIKE DANIELS,[23‡] STEPHEN DIGGS,[24‡] CHRISTOPHER DUFFY,[25‡] YOLANDA GIL,[26‡] BASIL GOMEZ,[27‡] SARA GRAVES,[28‡] ROBERT HAZEN,[29‡] LESLIE HSU,[30‡] DANIE KINKADE,[31‡] KERSTIN LEHNERT,[30‡] CHRIS MARONE,[32‡] DON MIDDLETON,[23‡] ANDERS NOREN,[33‡] GENEVIEVE PEARTHREE,[17‡] MOHAN RAMAMURTHY,[34‡] ERIN ROBINSON,[35‡] GEORGE PERCIVALL,[36‡] STEPHEN RICHARD,[17‡] CELINA SUAREZ,[37‡] DOUG WALKER[38‡]**

[1]School of Labor and Employment Relations, University of Illinois at Urbana-Champaign, Champaign, IL 61820, USA. [2]Terry College of Business, University of Georgia, Athens, GA 30602, USA. [3]National Center for Supercomputing Applications, University of Illinois at Urbana-Champaign, Urbana, IL 61801, USA. [4]Industrial/Organizational Psychology, School of Psychology, Georgia Institute of Technology, Atlanta, GA 30332, USA. [5]Department of Sociology, Social Work and Anthropology, Utah State University, Logan, UT 84322, USA. [6]Illinois Informatics Institute, University of Illinois at Urbana-Champaign, IL 61820, USA. [7]School of Information, University of Michigan, Ann Arbor, MI 48109, USA. [8]Discipline of Work and Organisational Studies, University of Sydney Business School, 2006, Australia. [9]Management and Organization, Anderson School of Management, University of California at Los Angeles, Los Angeles, CA 90095, USA. [10]Library and Technology Services, Brandeis University, Waltham, MA 02453, USA. [11]Design and Innovation, Weatherhead School of Management, Case Western Reserve University, Cleveland, OH 44103, USA. [12]Nodality, Inc., South San Francisco, CA 94080, USA. [13]Graduate School of Library and Information Sciences, University of Illinois at Urbana-Champaign, Champaign, IL 61820, USA. [14]Seidenberg School of Computer Science and Information Systems, Pace University, New York, NY 10038, USA. [15]College of Information Studies, University of Maryland, College Park, MD 20742 USA. [16]San Diego Super Computing Center, University of California at San Diego, La Jolla, CA 92093, USA. [17]Arizona Geological Survey, Tucson, AZ 85701, USA. [18]Jackson School of Geosciences, University of Texas at Austin, Austin, TX 78712, USA. [19]Consortium of Universities for the Advancement of Hydrologic Science, Inc., Medford, MA 02155, USA. [20]Stroud Water Research Center, Avondale, PA 19311, USA. [21]COMPRES and University of Illinois at Urbana-Champaign, Champaign, IL 61820, USA. [22]School of Earth and Space Exploration, Arizona State University, Phoenix, AZ 85004, USA. [23]Computing, Data and Software Facility, Earth Observing Laboratory, National Center for Atmospheric Research, Boulder, CO 80301, USA. [24]Scripps Institution of Oceanography, La Jolla, CA 92037, USA. [25]Department of Civil and Environmental Engineering, Penn State University, University Park, PA 16802, USA. [26]Information Sciences Institute, University of Southern California, Marina del Rey, CA 90292, USA. [27]Department of Geography, University of Hawaii at Manoa, Honolulu, HI 96822, USA. [28]Computer Science Department, The University of Alabama in Huntsville, Huntsville, AL 35899, USA. [29]Deep Carbon Observatory, Carnegie Institution for Science, Washington, DC 20015, USA. [30]Lamont-Doherty Earth Observatory, Columbia University, Palisades, NY 10964, USA. [31]Woods Hole Oceanographic Institution, Woods Hole, MA 02543, USA. [32]Department of Geosciences, The Pennsylvania State University, University Park, PA 16802, USA. [33]Department of Earth Sciences, University of Minnesota, Minneapolis, MN 55455, USA. [34]Unidata, University Corporation for Atmospheric Research, Boulder, CO 80301, USA. [35]Foundation for Earth Science, Raleigh, NC 27612, USA. [36]The Open Geospatial Consortium, Wayland, MA 01778, USA. [37]Department of Geosciences, University of Arkansas, Fayetteville, AR 72701, USA. [38]Department of Geology, University of Kansas, Lawrence, KS 66045, USA.

*Members of Project on Stakeholder Alignment in Complex Systems (NSF SciSPR-STS-OCI-GEO-INSPIRE 1249607, "Enabling Transformation in the Social Sciences, Geosciences, and Cyberinfrastructure")

†Corresponding author. E-mail: jlking@umich.edu

‡Principal Investigators for NSF EarthCube End-User PI Workshops (NSF EAR-124039).

**References**

1. OSTP, Expanding Public Access to the Results of Federally Funded Research (www.whitehouse.gov/blog/2013/02/22/expanding-public-access-results-federally-funded-research).
2. EarthCube (www.earthcube.org).

## Open Data: A Sustainable Model

IN THEIR POLICY FORUM "WHO WILL PAY FOR public access to research data?" (9 August, p. 616), F. Berman and V. Cerf describe some ways to increase public access to research data within the existing budget. Their call for action for joint effort among the private, public, and academic sectors is entirely appropriate and timely. However, thus far, this kind of collaboration remains very limited.

Research data must be hosted somewhere, new biological information must be curated, and services must be managed. All these incur substantial costs. Yet, the research community conventionally expects that access to data should be free. I agree that cultural change is needed. Berman and Cerf, assuming a small data-access fee on par with buying music on the Internet, proposed a broader adoption of the payment model. However, some databases of high community value that have lost their public funding support have had to resort to a subscription model. For example, Human Gene Mutation Database (www.hgmd.cf.ac.uk) and Kyoto Encyclopedia of Genes and Genomes (www.genome.jp/kegg) are now charging about US$3000 to $5000 annually for each academic research group. These prices are substantially more than the cost of subscribing to digital versions of a newspaper or paying for music on iTunes. Precedents such as these suggest that the cost would be unaffordable for some research groups.

How can a mature database remain both financially sustainable and accessible to a broad community of users? Every day, scientists use these databases as starting points for in-depth analysis, learning about the data and deriving incremental findings. Perhaps it is time for the subscription-based databases to adopt a curator reward system in which access fees are reduced in exchange for a certain amount of quality curation. If this model were successful, scientists who were unable to pay could help improve the databases in exchange for continuous access. This could be a win-win economic model for both scientists and database managers.

**JING-WOEI LI**

School of Life Sciences, The Chinese University of Hong Kong, Hong Kong SAR. E-mail: marcoli@cuhk.edu.hk

## Ethics Tests for Trials

IN HIS NEWS & ANALYSIS STORY "CLINICAL trials paused as India adopts new rules" (26 July, p. 327), Y. Bhattacharjee discusses the new regulations put in place to protect clinical trial participants. Ethics committees responsible for approving clinical trial protocols play a key role in participant safety. It should be deemed unethical to enroll patients in a clinical trial that has a low probability of generating meaningful information, no matter how promising a new investigational therapy. Thus, the ethics committee should always critically evaluate clinical trial protocols for their probability of success.

To make sure these evaluations occur, ethics committees should include or consult qualified statisticians. Ethics committees should ensure that clinical study protocols are adequately powered to succeed and that the underlying assumptions used in power calculations are reasonable. Only then should clinical trials be allowed to proceed in India, or the rest of the world.

**DEEPAK B. KHATRY**

Arlington, VA 22205, USA. E-mail: khatryd7@gmail.com

FOR YOUNGER READERS

# Some Suggestions from 2013—The SB&F Prizes Finalists

If you wish to spark an interest in science among younger readers, the finalists for the 2014 *Science Books and Films* Prizes for Excellence in Science Books may provide some tinder. The prizes, sponsored by AAAS and Subaru, honor books that promote an understanding and appreciation of science in children and young adults. The 125 books considered for the 2014 prizes were published between September 2012 and August 2013. The judges will pick a hands-on science book and a title from each of three age-based categories: for readers in grades K–4, for those in grades 5–8, and for high school students. Once again, the four titles shortlisted for the young adult award were written for the general public.

Short descriptions of the 13 finalists chosen by panels of librarians, scientists, and science literacy experts follow. Longer reviews have appeared or been scheduled in *Science Books and Films*. The winners will be announced in February at the AAAS Annual Meeting in Chicago.

The finalists are expected to clearly and accurately present scientific concepts. We hope that they will also entice children and young adults.

## Children's Science Picture Book

**It's Our Garden: From Seeds to Harvest in a School Garden.** George Ancona. Candlewick, Somerville, MA, 2013. 48 pp. $16.99, C$20, £10.49. ISBN 9780763653927.

You might think gardens are for growing vegetables, but they can be so much more. Inspired by a third-grade teacher, a New Mexico elementary school turned its garden into a year-round interdisciplinary project, which prompts as many smiles as its playground. In the best of scientific traditions, students plan, do, observe, and record. In their arid location, rainfall capture and solar-generated power deliver water when needed. Water also serves as a heat reservoir to keep sensitive tomato plants warm through chilly desert nights. School and community bond over sustenance enriched by lemon cucumbers, walking onions, and the traditional Indian "three sisters" (corn, pinto beans, and squash). Ancona's photoessay is graced with the students' drawings of the plants, the insects that keep the garden thriving, and the wildlife that finds it home. Good for elementary-school readers, the book may also inspire adults to help organize gardens for their children's schools. **– Pamela J. Hines**

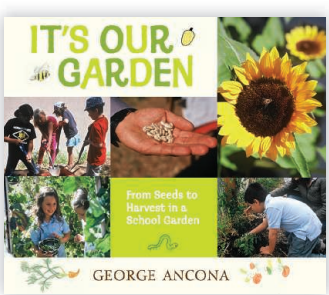


**Things That Float and Things That Don't.** David A. Adler, illustrated by Anna Raff. Holiday House, New York, 2013. 32 pp. $16.99, £10.59. ISBN 9780823428625.

Lift two different objects, and it should be pretty easy to tell which is heavier. Look at two objects that differ in size; it will be easy to know which is larger. But when it comes to the ratio of mass to volume, the density, it can be harder to judge which object might float and which one won't. Raff's illustrated characters test pennies, ice cubes, aluminum foil, soap, and apples as well as clay in a lump and after being shaped into a boat. The use of only imperial measurements may limit the book's geographic audience. A bigger problem is that although kids may relate to an object that weighs 62 pounds, they are less likely to have a sense of how much space a cubic foot of water occupies, and one wishes he had used a smaller base volume. Adler's narrative challenges readers to become junior experimenters as they first guess and then test whether various objects will float in water. For example, a loose ball of aluminum will float. But by crushing it to reduce its volume without changing its weight, you can make it sink; this shows how experiments should be done. I just wish that, when encouraging children to test objects in the sink, Adler had cautioned against letting small things go down the drain. **– Marc Lavine**

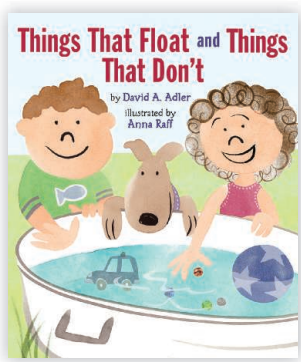


**Too Hot? Too Cold?: Keeping Body Temperature Just Right.** Caroline Arnold, illustrated by Annie Patterson. Charlesbridge, Watertown, MA, 2013. 32 pp. $17.95. ISBN 9781580892766. Paper, $7.95, £6.99. ISBN 9781580892773.

Set a thermostat just a few degrees too cold or hot, and there will be no shortage of complaints. But put the same people on a sun-soaked beach or fresh-packed ski slope, and they'll enjoy the temperate extremes. "Warm-

CREDIT: PETER AND MARIA HOEY/WWW.PETERHOEY.COM



Published by AAAS

blooded" (endothermic) animals, including mammals and birds, can regulate their temperatures in response to their surroundings, whereas "cold-blooded" (ectothermic) ones cannot and must exploit their environment. The contrast between these responses forms the thread Arnold uses to tie together and explain how humans and other animals keep their temperature just right. The large ears on the fennec fox, the panting of a dog, and the sweating of exercising humans are all examples of mammals' cooling tricks; they may generate heat by shivering or the conversion of brown fat to energy. In contrast, cold-blooded animals may expose more surface area to heat or cool up, by, respectively, capturing more sunlight or letting the heat escape. The author also discusses body shape, coverings such as hair and fur, burrowing into the ground, hibernating, and the need to migrate. The presentation of content in bite-sized chunks with many helpful illustrations makes the book appropriate for a wide range of ages. It can be described as a hot success or a cool read—either way, it gets its audience's temperature just right. **– Marc Lavine**

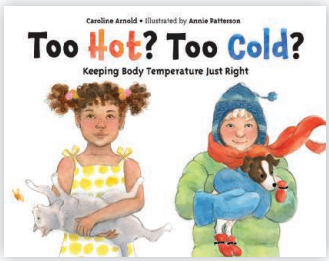


## Middle Grades Science Book

**Eruption! Volcanoes and the Science of Saving Lives.** Elizabeth Rusch, photographs by Tom Uhlman. Houghton Mifflin Harcourt, Boston, 2013. 80 pp. $18.99, £11.72. ISBN 9780547503509.

Erupting volcanoes, some of the most visually captivating subjects on Earth, provide an ideal subject with which to first engage students in Earth science. Yet middle school curricula too often focus on simple definitions of rock and mineral types. Grasping the science behind understanding eruptions and the social consequences is not as well appreciated or easily discussed in the classroom. Writer Rusch and photographer Uhlman tackle this problem head on by weaving sophisticated scientific topics such as satellite imaging, seismology, and early warning systems together with dramatic stories and photographs of narrow escapes, pyroclastic flows, and beautiful scenery. Furthermore, they do not shy away from less photogenic yet critically important topics such as uncertainty, risk assessment, and even science diplomacy. The narrative focuses on a team from the U.S. Volcano Disaster Assistance Program working with scientists in the Philippines and Indonesia on Mount Pinatubo and Mount Merapi, respectively, expertly portraying the research behind volcano monitoring efforts that eventually saved tens of thousands of lives. The book will reward not just aspiring volcanologists but also any young readers interested in the benefits of science to society. **– Nicholas S. Wigginton**

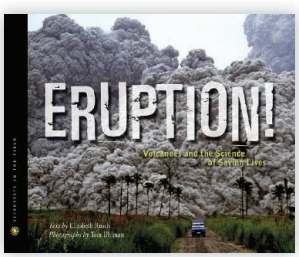


**The Skull in the Rock: How a Scientist, a Boy, and Google Earth Opened a New Window on Human Origins.** Lee R. Berger and Marc Aronson. National Geographic, Washington, DC, 2012. 64 pp. $18.95, C$21.50, £12.99. ISBN 9781426310102.

In this slim volume, the authors merge the hunt for human ancestry with the excavation of paleoanthropologist Berger's past. Their account serves as both an autobiography of an adventurer and a basic introduction to working out the puzzle of the origins of humans in Africa. It begins in the hills near Johannesburg, South Africa, with Berger's son spotting the first fragment of what turned out to be a nearly complete fossil skeleton of a previously unknown species, *Australopithecus sediba* (a major find in the hominid tree). It then takes us back to the roots of the father and son's searching nature by revisiting Berger's past as a young boy growing up in Georgia. The story traces his family's tendency to restless and imaginative pursuits, starting with his wildcatting grandfather. In addition, the authors offer step-by-step explanations of paleontological techniques using photographs from the field and laboratory. Many other pictures and reconstructions depict the fossil bones, past and present environments of the Cradle of Humankind World Heritage Site, and our ancient relatives themselves. **– Sarah Crespi**

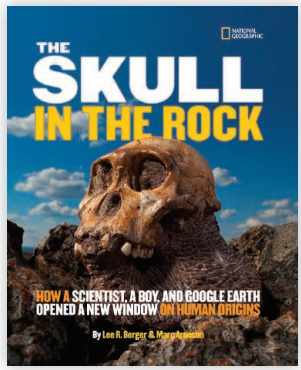


**Wild Horse Scientists.** Kay Frydenborg. Houghton Mifflin Harcourt, Boston, 2012. 80 pp. $18.99, £11.72. ISBN 9780547518312. Scientists in the Field.

Several hundred sturdy wild horses thrive on the dune grasses among the shifting sands of the barrier islands of the mid-Atlantic states. Paradoxically, protecting the herds and giving the horses a natural habitat depended on discovering how to control their fertility. Population management strategies developed for the wild mustangs of Wyoming have been applied to the horses of Assateague Island (Maryland and Virginia). The key lay in proteins coating pig eggs, used to generate a vaccine called PZP (porcine zona pellucida) that stimulates the mare's immune system to make antibodies against her own eggs and thus prevent fertilization (and thus birth). Jay Kirkpatrick, the reproductive physiologist who helped pioneer the approach, is nervous when he pulls the trigger to fire the painless dart used to deliver the vaccine. He has spent time learning how to tell the feelings of horses by their actions; discovering that fecal samples are easier to collect than urine samples; and tracking the horses' births, relationships, and deaths (including that of a favorite named Voodoo). Taking a long view of population genetics allows the scientists and managers to maintain the herds' genetic diversity even while reducing fertility. The book is full of interesting facts and details, which Frydenborg supplements with helpful maps and textboxes that explain the evolution, migration, and domestication of horses. The many color photographs bring to life the researchers and the horses they care for.

**– Pamela J. Hines and Alexander Lerner Hines**

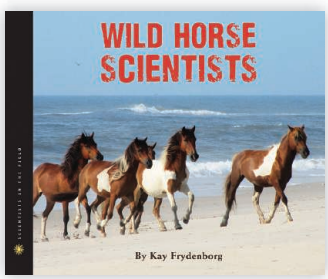


## Hands-On Science Book

**Beyond the Solar System: Exploring Galaxies, Black Holes, Alien Planets, and More.** Mary Kay Carson. Chicago Review Press, Chicago, 2013. 135 pp. Paper, $18.95, £15.99. ISBN 9781613745441.

Targeting readers 9 years old and up, Carson provides (in the words of a cover tagline) "a history with 21 activities." Proceeding from early stargazers to recent discoveries of alien planets and dark energy, her narrative emphasizes researchers who made the discoveries. For some, it offers insights into the social and political forces that affected their lives and their work. Historical portraits and photographs accompany these minibiographies, and color images (many from the Hubble Space Telescope and the Chandra X-ray Observatory) depict distant galaxies and nebulae. For kids (or their parents)

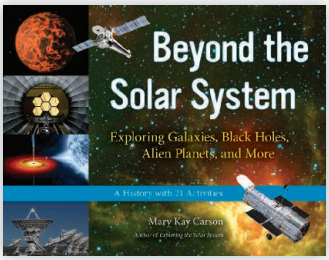


desiring more details, the author supplies a timeline, a glossary, a list of websites, and suggestions for additional reading. But the book stands out from other introductions to the field because of the activities, all of which use simple and easy-to-find materials. These hands-on projects illuminate some challenging concepts, such as how astronomers search for exoplanets and Einstein's theory of space-time. **– Barbara R. Jasny**

**Look Up!: Bird-Watching in Your Own Backyard.** Annette LeBlanc Cate. Candlewick, Somerville, MA, 2013. 64 pp. $15.99, C$18, £9.87. ISBN 9780763645618.

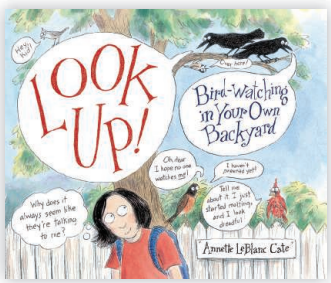


One of the easiest ways to get children to appreciate the world in which we live is to help them understand their local ecosystem. Cate embraces the philosophy that you do not have to be an expert naturalist to appreciate nature in your neighborhood. Pointing out that unless we know what is usually around us we will fail to notice when something is different, she doesn't simply discuss looking at birds but also offers an introduction to how to observe your environment. Told primarily through amusing, information-rich cartoon drawings interspersed amid longer sections of text, the book clearly guides children through the basics of bird-watching. Besides learning how to start in their own yard, they will find some enticing homages to the diversity and behavior of our feathered friends. **– Laura M. Zahn and Elliot S. Richter**

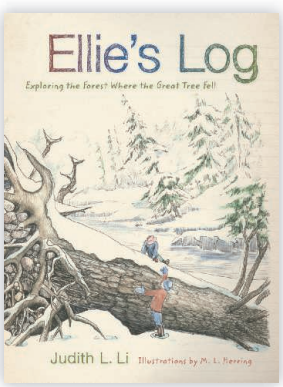


**Ellie's Log: Exploring the Forest Where the Great Tree Fell.** Judith L. Li, illustrations by M. L. Herring. Oregon State University Press, Corvallis, 2013. 112 pp. Paper, $16.95, £10.59. ISBN 9780870716966.

A winter storm fells a huge Douglas fir near Ellie's home in the Oregon Cascades. She and a friend repeatedly return to the site over the following months, and Ellie records their discoveries about the local biota and ecology in a field notebook. Li's (fictional) story is enlivened by Herring's colored pen-and-ink renderings of the area's plants, mammals, insects, and birds along with pages from the notebook. Rather than specifying a series of activities for its intended readers (ages 8 to 12 years), the book appeals to their curiosity. It should inspire them to look closely at nature wherever they are—and to keep logs of their own observations. **– Sherman J. Suter**

## Young Adult Science Book

**Frankenstein's Cat: Cuddling Up to Biotech's Brave New Beasts.** Emily Anthes. Scientific American/Farrar Straus Giroux, New York, 2013. 253 pp. $26, C$30. ISBN 9780374158590. Oneworld, London, Paper, £8.99. ISBN 9781851689682.

What child doesn't grow up loving or longing for a pet? Don't we all want our animal companions to be unique and healthy? Anthes uses this fact to hook readers into considering why humans are compelled to alter animal physiology. Through selective breeding, medicine, and habitat destruction, for many centuries people have intentionally (and often unintentionally) shaped animals and their behaviors. Advances in biomedical science and engineering have enabled us to do so faster than ever. Anthes weaves a timely and up-to-date discussion of scientific, legal, economic, and ethical issues of altering animals and their environment. Her account traverses a range of examples, including genetically engineered glowing fish, cloning of farm animals and pets, custom prosthetics for dolphins and dogs, wildlife tracking, antibiotics produced in goat milk, and cyborg spies fashioned from insects. She encourages readers to examine their own feelings about conflicting attitudes toward animal welfare and self-preservation, explaining that everyone is willing to accept some degree of exploitation of animals (whether that is by using them as a source of food, clothing, drug testing, companionship, or entertainment). Ultimately, she reasons that society is on an inescapable course and that we should embrace advances in biotechnology as a means of improving animal lives along with our own. Through her approachable and informative style, Anthes provides a rich look into our interactions with our furry friends—and our slimy ones too. **– Jason Berndt**

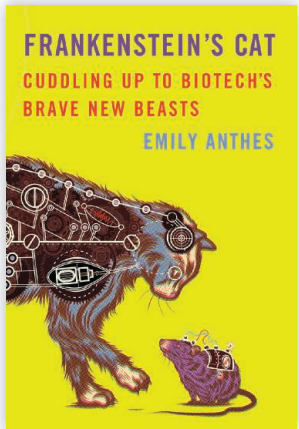


**Gulp: Adventures on the Alimentary Canal.** Mary Roach. Norton, New York, 2013. 348 pp. $26.95, C$28.50. ISBN 9780393081572. Oneworld, London. Paper, £11.99. ISBN 9781851689934.

It has been said—at times by the author herself—that Roach is a 12-year-old boy trapped in a grown woman's body. Her latest book follows the mastication and digestion of that 12-year-old, with delightfully diverting sidetracks along the way. She leads readers on a logical yet unpredictable path through our bodies and their relations with food, beginning with smell and going all the way to the inevitable conclusion. This is perhaps the quintessential bathroom book, with easily digestible chunks of content, which some may consider to be in poor taste. As she notes, "Humans, even physiologists, don't like to think about food once they've begun to process it. The same chanterelle and Gorgonzola galette that had the guests swooning is, after two seconds in the mouth, an object of universal revulsion." But Roach is a master of tackling taboo subjects head-on, with such bluntness, humor, variety,* and depth of research that one can't help but be drawn in. People seem either to love or hate Roach's writing. This book will not disappoint those in the former camp. **– Yael Fitzpatrick**

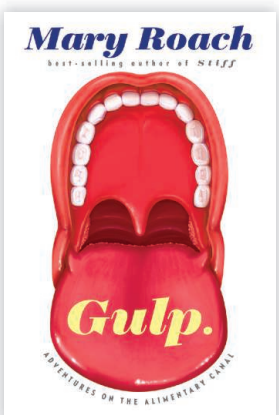


*And it wouldn't be a Mary Roach book without a plethora of idiosyncratic footnotes. One of the 125 I counted may have permanently ruined a particular Beatles' song for me.

**Mirror Earth: The Search for Our Planet's Twin.** Michael D. Lemonick. Walker, New York, 2012. 303 pp. $26, £19.99. ISBN 9780802779007.

Lemonick's absorbing book chronicles the quest for a planet like our own. The search started in earnest in the mid-1990s, after two Swiss astronomers announced the first discovery of a planet orbiting a Sun-like star. Before that, it was thought that detecting planets around other stars would be too difficult,

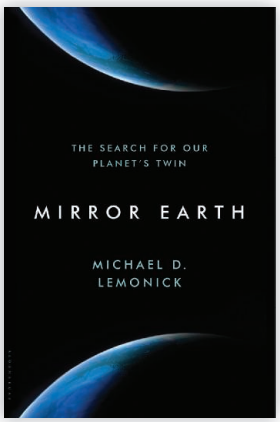


if not impossible, and thus very few astronomers were engaged in the activity. Indeed, the Swiss pair who announced that first discovery were not trying to find planets; they just chanced upon one. However, their find set off a frantic race. Its principal goal is the detection of a planet with the same size and same mass as Earth, orbiting at a distance from its star such that the temperature at its surface allows for liquid water and perhaps even for the existence of life. The author talked to and spent time with several of the key players in this still-unfolding race, including the early pioneers. Their stories—their dreams and hopes, their successes and failures, as well as their rivalries and friendships—take center stage alongside the science, enlivening the narrative and bringing out the human aspects of scientific enquiry. **– Maria Cruz**

**Letters to a Young Scientist.** Edward O. Wilson. Liveright, New York, 2013. 245 pp. $21.95, C$23, £14.99. ISBN 9780871403773.

Since Wilson retired from teaching at Harvard in 1996, he has published a new book nearly every year. This year brought a slim volume (divided into

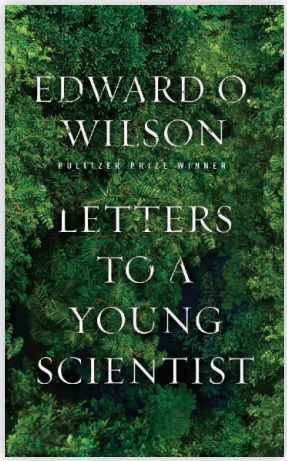


a prologue and 20 chapters) crafted as 21 letters addressed to readers who are considering degrees in science—and, he assumes, a research career. Of course, the author encourages anyone interested in becoming a scientist to pursue the necessary education and training, stating, "The world needs you—badly." The title and dust-jacket text suggest that he discusses all areas of science, but the book, unsurprisingly, reflects Wilson's focus on and interest in biodiversity. As with Wilson's other books, readers will learn a lot about ants. Along with advice, they will find numerous autobiographical anecdotes about the successes and occasional disappointments of his own career. The first of Wilson's five principles for choosing the right field of study is to "put passion ahead of training." He believes that passion will help overcome setbacks, although he never mentions what those hurdles may be or offers advice on how to overcome them. The book is not a storehouse of practical information for aspiring researchers, but it does convey Wilson's positive outlook and hopes for the future. **– Trista Wagoner**

10.1126/science.1247708

FOR YOUNGER READERS

# From the UK—Finalists for the Royal Society's Young People's Book Prize

The Royal Society's Young People's Book Prize draws attention to books that effectively communicate science to readers up to age 14. Publishers were invited to submit for consideration titles that first appeared in English in 2012 and whose content, narrative, or theme incorporates substantial science.

A jury of adults—chemist John Goodby (University of York), neuroscientist Jenny Read (Newcastle University), science blogger Grrlscientist, science teacher Schazia Lydon (Challney High School for Boys, Luton), and science communicator Simon Watt (BBC Channel 4)—trimmed the list of nominations down to six finalists. Although these differ in terms of the topics covered and the age group targeted, each succeeds at combining text and design to effectively present science.

The shortlisted titles were distributed to nearly 90 judging panels in schools and youth groups from around the United Kingdom. On the basis of the combined decisions of these panels of young readers, the £10,000 prize was awarded 11 November to Rob Lloyd Jones's *Look Inside Space*. (Each of the other finalists received £1000.) Although your own young readers may have a different preference, all six books should aid the Royal Society's goal of promoting interest "in the joy, wonder and excitement of scientific discovery."

**Buzzing.** Anneliese Emmans Dean. Brambleby, Luton, Bedfordshire, UK, 2012. 160 pp. £14.99, $16.99. ISBN 9781908241078.

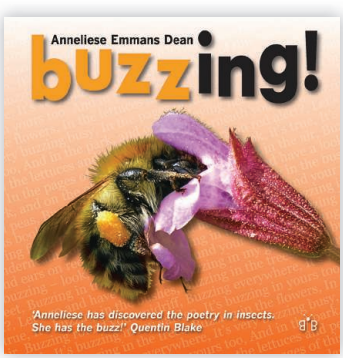


This is a book for British schoolchildren wanting to identify any monstrous minibeast French invaders that proclaim "I am 'ere in your jardin." It will arm students with plenty of doggerel for terrifying foreign invertebrates as well as numerous native ones. For each, Dean offers a few facts, including the animals' names—both formal and less so, such as Charlie the earthworm, Errol the earwig, and Ariadne the garden spider—together with brief (but too often unsatisfying) comments on their biology. The real stars of the book are its rhymes. The author has inherited the mantle of established zoological versifiers Walter Garstang (*Larval Forms and Other Zoological Verses*) and Dick King-Smith (*Alphabeasts*)—both very funny as well—and added to the canon of "the Ballad of the Veliger" and the "clippety cloppety wappity" with the claims of Kiera the flesh-fly, for whom "Only the best corpse/Will do for my brood." Dean ranges across an eclectic mix of species, in no particular order. Her enthusiasm for the minibeasts of Britain's gardens cannot be denied, saving caveats for the invaders: "Harlequin, Harlequin/You are not welcome in/Blighty, your fightin'/Has us in a spin." **– Caroline Ash**

**The Elements.** Dan Green. Scholastic, New York, 2012. 112 pp. $15.99. ISBN 9780545330190. £10.99, ISBN 9781407131559. Discover More.

Packed full of spectacular images, from crystal caves and the explosion of




Published by AAAS

the Hindenburg airship to a periodic table featuring photos of elements in their pure form, Green's visual feast provides a snapshot of chemical elements and their roles and impacts in the world around us. Chemistry emerges not as the dry subject it is often perceived to be but rather as integral to our lives and universe. The book encourages browsing rather than linear reading: One finds some full-spread photos accompanied by only a small caption, allowing the visual message to be absorbed, whereas other pages are chock-full of images and snippets of text. These cover, for example, the composition of Earth's interior, the role of calcium in building materials and in biominerals such as bone, and the properties and uses of gold. At times, the layout makes the main message hard to extract. Purchasers receive a unique code that allows them to download a companion interactive digital book, which provides further information on the various groups of elements in the periodic table and encourages readers to collect objects (or photos of objects) containing different elements. The strong focus on technology on the cover and through the early pages seems likely to narrow the book's appeal. That is unfortunate, because the scope of the author's survey is actually much broader.


**– Julia Fahrenkamp-Uppenbrink**

**Don't Flush: Lifting the Lid on the Science of Poo and Wee/ The Scoop on Poop: Lifting the Lid on the Science of Poo and Pee.** Mary Platt and Richard Platt, illustrated by John Kelly. Kingfisher, London, 2012. 48 pp. £10.99. ISBN 9780753433997. Paper, $7.99. ISBN 9780753469231.

Adults have a strong aversion to human waste, known as the "yuck factor," that makes it difficult to talk about. Yet parents know that many children often are fascinated by, or at least curious about, what they flush down the toilet. Because excrement is a valuable tool for scientists—from studying public health through fecal microbiology to using fossil feces to discover the behavior of extinct species—a children's science book on the subject is full of learning possibilities. The book offers a fun and informative romp, led by the Poo Crew, through the science of all things "poo and wee."* Kelly's humorous illustrations and the Platts' witty text leave little to the imagination—in a good way—yet are filled with interesting and accurate facts. Lacking a through-going narrative, the book can easily be read in short parts and on occasion, as opposed to in one sitting. Surprisingly, even though the book spans 48 pages, it suffers a bit from packing too much in too tightly. The authors note several historical instances of people making use of human and animal waste; this information is timely given a recent renewed interest by scientists and engineers in using wastewater as a resource. Moreover, these many facts and details (including a glossary of "Dirty Words") might just help parents address their own yuck factor and embrace discussing all of the fascinating things about poo and wee—but still not at the dinner table.

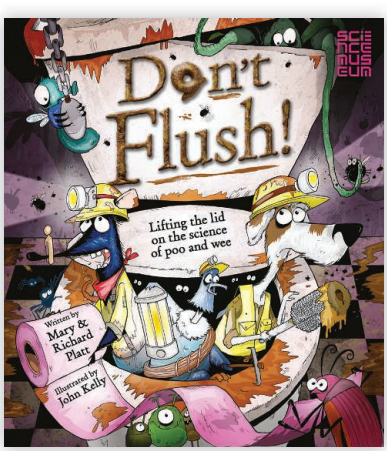


**– Krista R. Wigginton and Nicholas S. Wigginton**

*Note: Or, in the U.S. edition, "poo and pee."

**Build the Human Body.** Richard Walker, illustrated by Mark Ruffle and Galia Bernstein. Templar, Dorking, Surrey, UK, 2012. 28 pp. £14.99. ISBN 9781848777507. Silver Dolphin, Charlotte, NC, 2012. $19.95. ISBN 9781607104131.

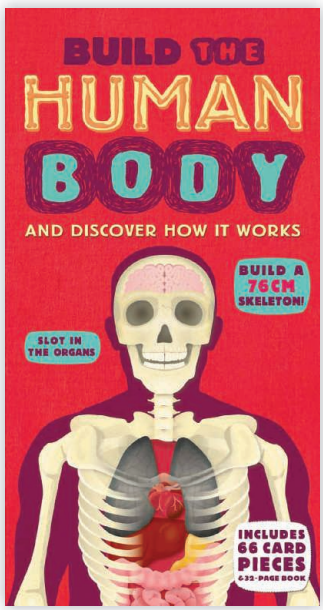


Human anatomy is complex. Molecules, cells, tissues, bones, and organs all must come together in just the right way. Walker offers an ideal method for getting budding scientists to appreciate all these intricate connections: constructing their own model body. Between the book's covers, one finds a hands-on, 66-piece, three-dimensional puzzle of a human skeleton, which entices readers to actively engage with our physiological systems. The paginated section serves primarily as a guide to the puzzle building, although you wouldn't necessarily realize that supporting role if you looked at it alone. Full of beautiful illustrations and plenty of trivia, this manual takes readers through each of the human body's major systems, introducing major concepts and themes, while still keeping the tone light and appealing. Although the collection could not be further from a standard schoolbook on anatomy, anyone who works through both the puzzle and text will gain a firm grasp on the subject.

**– Melissa McCartney**

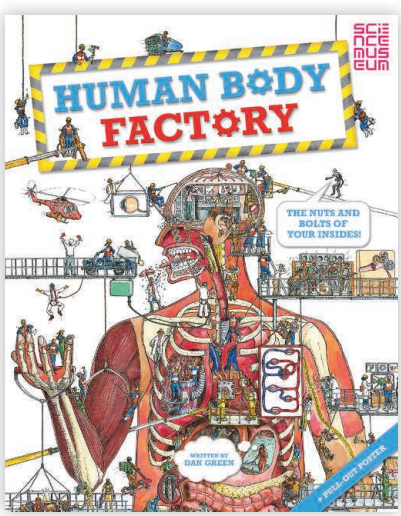


**Human Body Factory.** Dan Green, illustrated by Edmund Davis. Kingfisher, London, 2012. 48 pp. £9.99. ISBN 9780753431672. $16.99. ISBN 9780753468081.

In this cartoon exploration of the human body, skin, endocrine system, circulation, and so on are presented in big, colorful illustrations that span—and often completely fill—each two-page spread. Hordes of technicians (ear-canal cleaners, bile chefs, ninja killer T cells, and even sperm swim coaches) and a plethora of machines (e.g., fork lifts, conveyor belts, minisubmarines, and helicopters) are depicted running the brain, immune system, liver, and other systems as a series of interconnected (and visually hyperkinetic) factories. Green explains the workings of the body simply and clearly (at a level suitable for adolescents) through the speech and thought bubbles of the microsized workers along with a healthy scattering of humorous asides, aided by tons of visual jokes and puns in Davis's pictures. Great fun to browse, the book is a rich mine of


Published by AAAS

information about physiology. Regrettably, many of the finely detailed drawings are simply too small—and too busy—to let one easily appreciate the artist's clever visual ideas. And the speech and thought bubbles too often obstruct the graphics, criminally forcing the drawings into the background.

**– Guy Riddihough**

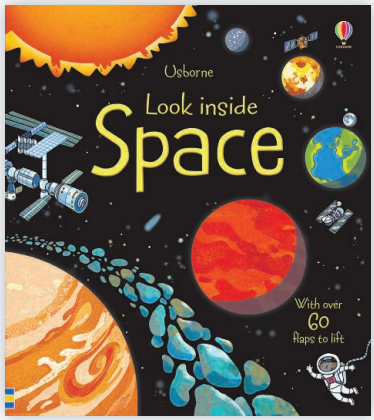


**Look Inside Space.** Rob Lloyd Jones. Usborne, London, 2012. 14 pp. £9.99, $14.99, C$18.95. ISBN 9781409523383.

Young readers intrigued by space will be captivated by this engaging tour of the universe. Brightly colored illustrations and concise captions explain the surface of the Moon, life on the International Space Station, how stars and planets are created, and the composition of the Milky Way. A solar system centerfold provides factoids about each planet, asteroids, and comets. Another spread samples the history of stargazing and space exploration. The board-book's more than 80 flaps open to display answers to questions (the Moon orbits Earth because "gravity pulls small objects to big ones"), additional tidbits ("About a million Earths could fit inside the Sun"), and occasional enthusiastic remarks (under a space station porthole: "Amazing view!"). Lifting some flaps reveals another underneath them. Such nested flaps are best used in describing the Moon's phases and conveying a feeling of discovery that seems appropriate to space missions such as Galileo and Voyager 1. Most important, the book unflinchingly reveals the unknown: "No one knows just how big space is, not even the very best scientists." With so much still to discover, readers may find themselves eager to lift the flap with the book's final question: "How can I become an astronaut?"

**– Jennifer Sills**

10.1126/science.1247709

## BROWSINGS

**Rosie Revere, Engineer.** Andrea Beaty, illustrated by David Roberts. Abrams, New York, 2013. 32 pp. $16.95, C$18.95, £10.99. ISBN 9781419708459.

Rosie dreams of becoming an engineer. Then her favorite uncle laughs at her snake-repelling cheese hat. And after the cheese-copter she builds so that her great-great-aunt (who'd helped assemble airplanes during World War II) can fly crashes to the ground, she vows, "Never! Not ever again will I try to build something." But her aunt proclaims that flop a "perfect first try"—because, as engineers well know, the road to success is paved with failures. Told through Beaty's rhymes and Roberts's playful art, this tale of creativity and persistence will delight readers five and (way) up.

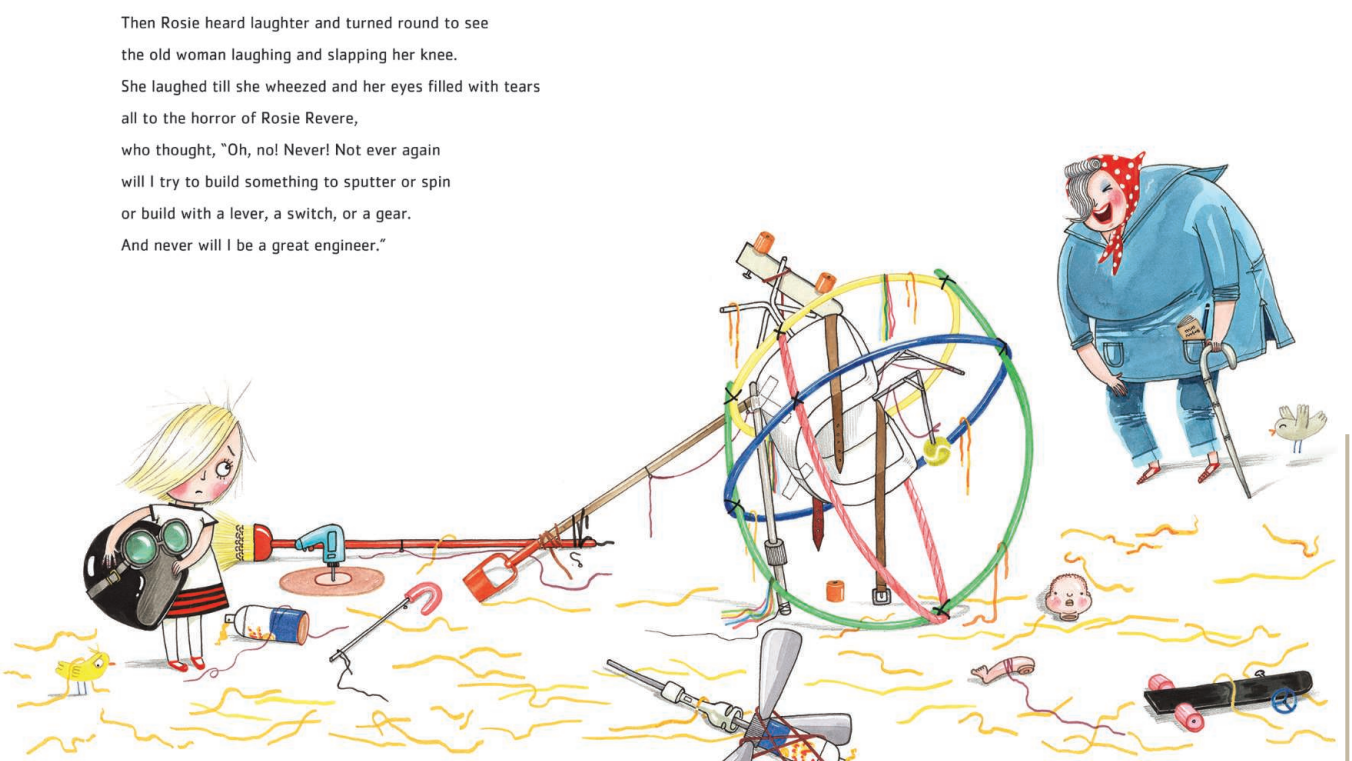


CREDIT: COURTESY ABRAMS BOOKS FOR YOUNG READERS

SPACE LAW

# International Cooperation on Human Lunar Heritage

Protecting Apollo sites is laudable. Making them U.S. National Parks is not.

**Henry R. Hertzfeld* and Scott N. Pace**

The U.S. Apollo Space Program was a premier technological accomplishment of the 20th century. Preserving the six historic landing sites of the manned Apollo missions, as well as the mementos and equipment still on the Moon from those and other U.S. (e.g., Ranger and Surveyor) and Soviet Union (e.g., Luna) missions is important. Some of the instruments on the lunar surface are still active, monitored, and provide valuable scientific information. But recent government and private-sector plans to explore and potentially use lunar resources for commercial activity raise questions about the use of the Moon and potential accidental or purposeful threats to the historic sites and scientific equipment there. Although some steps to protect these sites have been proposed, we suggest a better way, drawing on international, not U.S. unilateral, recognition for the sites.

Less than 2 years before the first footsteps on the lunar surface on 20 July 1969 (see the image), the United Nations Outer Space Treaty (OST) was drafted, ratified, and came into force (*1*). Article II of the OST [ck] the international standard that outer space, the Moon, and other celestial bodies would not be subject to claims of sovereignty from any nation by any means, including appropriation. The OST prohibits ownership of territory or its appropriation by any state party to the treaty, which includes the United States, Russia, and 126 other nations. It does not prohibit the use of the Moon and its resources. In fact, the treaty emphasizes the importance of freedom of access to space for any nation and the importance of international cooperation in space exploration. These principles of the space treaties have enabled gains in science and technology and have contributed to international stability in space.

New attention is being focused on the lunar surface. China has an active Moon exploration program and is considering sending astronauts (taikonauts) to the Moon. Private firms are contemplating robotic missions that could land in the vicinity of the historical sites of Apollo and other missions. Although we might assume the best of intentions for such missions, they could irreparably disturb the traces of the first human visits to another world.

**Neil Armstrong stepping on the lunar surface** during the Apollo 11 mission in 1969. [Image has been digitally processed from scans made by Roger Ressmeyer from the original flight film.]

NASA has taken steps to protect the lunar landing sites and equipment and to initiate a process to create recognized norms of behavior. In July 2011, guidelines were issued for private companies competing in the Google Lunar X Prize that established detailed requirements for avoiding damage to U.S. government property on the Moon (*2*).

H.R. 2617, The Apollo Lunar Landing Legacy Act, was introduced into the U.S. Congress on 8 July 2013 (*3*). In essence, it proposes to designate the Apollo landing sites and U.S. equipment on the Moon as a U.S. National Park with jurisdiction under the auspices of the U.S. Department of the Interior.

Although the bill acknowledges treaty obligations of the United States, it would create, in effect, a unilateral U.S. action to control parts of the Moon. This would create a direct conflict with international law and could be viewed as a violation of U.S. commitments under the OST. It would be an ineffective way of protecting historical U.S. sites, and it fails to address interests of other states that have visited and will likely visit the Moon. It is legally flawed, unenforceable, and contradictory to our national space policy and our international relations in space (*4*).

There is a better way for the United States to protect its historic artifacts and equipment on the Moon. The first step is to clearly distinguish between U.S. artifacts left on the Moon, such as flags and scientific equipment, and the territory they occupy. The second is to gain international, not unilateral, recognition for the sites upon which they rest.

Aside from debris from crash landings (by Japan, India, China, and the European Space Agency), there are only two nations with "soft-landed" equipment on the lunar surface: the United States and Russia. China has plans to soft-land Chang'e 3 on the Moon in December 2013. All three nations (and any others wishing to participate) have much to gain and little or nothing to lose from a multinational agreement based on mutual respect and mutual protection of each other's historical sites and equipment.

## Legal Issues

Although ownership of planets, the Moon, and celestial bodies is prohibited, ownership of equipment launched into space remains with the nation or entity that launched the equipment, wherever that equipment is in the solar system. Under the OST, that nation is both responsible and liable for any harmful acts that equipment may create in space. There are no prescribed limits on time or the amount of damage a nation may have to pay.

The U.S. government therefore still owns equipment it placed on the Moon. Ownership has the associated right of protecting the equipment, subject to using necessary and proportional means for protection. But, because no nation can claim ownership of the territory on which equipment rests, there is an open issue of how to control the spots on the Moon underneath that equipment, because the site is integral to the historical significance. In H.R. 2617, establishment of Apollo sites as a unit of the U.S. National Park System could be interpreted as a declaration of territorial sovereignty on the Moon, even

Space Policy Institute, Elliott School of International Affairs, The George Washington University, Washington, DC 20052, USA.

*Corresponding author: hrh@gwu.edu

CREDIT: NASA–APOLLO/DIGITAL VERSION BY SCIENCE FACTION





Published by AAAS

though ensuing paragraphs specify the Park's components as the "artifacts on the surface of the Moon" at those sites. This problem needs international legal clarification, achievable via a formal agreement among those nations that have the technological ability to directly access the Moon (*5*).

Section 6(a) raises another legal issue. The bill proposes that the Secretary of the Interior shall administer the park in accordance with laws generally applicable to U.S. National Parks. It also requires the Secretary to act in accordance with applicable international law and treaties. The U.S. National Park System Act states that the Parks are "managed for the benefit and inspiration of all the people of the United States" (*6*). The OST clearly emphasizes that the exploration and use of space by nations is to benefit all peoples. The laws and space policies of the United States have always emphasized peaceful uses of space and the benefits of space for humankind. It may not be possible to implement and execute provisions of this Bill without raising important and fundamental questions about these contradictions between the language of the treaty and the mandates of our National Park Service.

A third legal issue is raised in section (6)(c)(2) that allows private donations and cooperative agreements to "provide visitors centers and administrative facilities within reasonable proximity to the Historical Park." This implies future private use of the Moon under rights granted by the U.S. government. Unilateral granting of lunar territorial rights to private individuals and implicit sovereign protection of that territory violates the OST.

Finally, section 8 of the bill requires the Secretary of the Interior to submit the Apollo 11 lunar landing site to the United Nations Educational, Scientific, and Cultural Organization (UNESCO) for designation as a World Heritage Site. This violates Article II of the OST. All current World Heritage Sites are located on sovereign territory of nations. The only exception is a separate treaty that allows UNESCO to designate underwater sites (such as sunken ships) as protected cultural sites (*7*). These designations are very limited, and although the convention has been ratified by 43 nations, the United States, Russia, and China are not among them. Thus, any new treaty of this type specifically for outer space would have little chance of being ratified by the major space-faring nations.

### A Proposal to Protect Lunar Sites

Although a new U.N. treaty for space artifacts of significant cultural and historic importance may be reasonable someday, this would start a very long process with unknown outcomes. Such a treaty could be delayed to a point beyond the time when nations and/or companies may be active on the Moon (*8*).

Our suggested alternative is to create a bilateral agreement between the United States and Russia, offered as a multilateral agreement to other nations with artifacts on the Moon. This would be more legally expedient, politically sustainable, and would more likely meet and exceed the stated goals of the bill. It would also emphasize the important role of national laws to implement and enforce these international space agreements.

Any nation with assets on the lunar surface will endeavor to protect those assets. This creates a situation where those nations have a timely, current, and common interest incorporating important implications for peaceful uses of outer space; scientific research and the advancement of knowledge; and cultural and heritage value, either presently or in the foreseeable future.

The United States, Russia, and China all engage in multilateral cooperative space programs. They share many economic and trade dependencies adding to the international importance of promoting cooperation in space and commerce. In spite of today's charged political environment, an agreement of the type we propose may still be possible to negotiate because it focuses on the culture of space, the use of space to benefit humankind, and the archaeological record of our civilization. It specifically would not touch sensitive issues of real property rights, export controls, human rights, or the weaponization of outer space.

Cooperation on recognizing and protecting each other's interests in historical sites and on equipment and artifacts also has no significant security, prestige, or technological impediments. It reinforces the basic principles of the existing space treaties, avoids declarations of sovereignty on the Moon, and encourages multilateral cooperation resulting in a more stable and predictable environment for private activities on the Moon.

The best mechanism for implementing a new agreement would be direct negotiations at highest levels of government in the United States, Russia, and China, with priority to include Russian sites in a proposal that protects U.S. sites. It could be included in meetings of heads of state of those nations, either jointly or sequentially among the three nations. Such an agreement could be executed in a relatively short period of time, setting precedents for peaceful and coordinated research, exploration, and exploitation of the Moon (*9*).

An international agreement on lunar artifacts among the United States, Russia, and China would be a far superior and long-lasting solution than the unilateral U.S. proclamation in H.R. 2617. Enforcement of the agreement would be through each nation's national laws, applying to those entities subject to the jurisdiction or control of the agreement members. Each nation's property would be protected and preserved. Other nations should be free to join the agreement, and particularly encouraged to do so if they have the ability to access the Moon. An important result would be to develop a new level of trust among nations that could then lead to more comprehensive future cooperative agreements on space, science, exploration, commerce, and the use of the Moon and other celestial bodies.

### References and Notes


1. The Treaty on Principles Governing the Activities of States in the Exploration and Use of Outer Space, including the Moon and Other Celestial Bodies [General Assembly resolution 2222 (XXI), annex]—adopted on 19 December 1966, opened for signature on 27 January 1967, entered into force on 10 October 1967.
2. NASA's Recommendations to Space-Faring Entities: How to Protect and Preserve the Historic and Scientific Value of U.S. Government Lunar Artifacts, 20 July 2011. In mid-2012, the X Prize Foundation incorporated NASA's recommendations into its master agreement with the teams, and four contractors were awarded a NASA subcontract to develop a Planetary Protection Plan. In this way, a U.S. government agency's internal regulations are brought into an international context because there are non-U.S. entities competing for that prize.
3. House of Representatives, U.S. Congress, H.R. 2617, Apollo Lunar Landing Legacy Act, 8 July 2013.
4. Executive Office of the President, U.S. National Space Policy of the United States (Executive Office, Washington, DC, 2010).
5. Other solutions to protecting facilities in areas where there is no sovereignty include geosynchronous orbit slots administered by the U.N. International Telecommunications Union, and the Antarctica System of Treaties allowing national research facilities to be placed and maintained there.
6. 16 U.S. Code 1a-1, 39 Stat 535, 25 August 1916, as amended.
7. The UNESCO Convention on the Protection of the Underwater Cultural Heritage was adopted on 2 November 2001 by the plenary session of the 31st General Conference (Doc. 31C/24) with 88 votes in favor, 4 against, and 15 abstentions.
8. The United Nations Committee on Peaceful Uses of Outer Space (UNCOPUOS) is the international body that has drafted the space treaties. The 1979 Agreement Governing the Activities of States on the Moon and Other Celestial Bodies, "Moon Treaty," has to date only been ratified or signed by 19 nations. The United States, Russia, and China are not parties to it.
9. The term "exploitation" is found in the Moon Treaty and specifically suggests possible commercial use of the Moon. Because the Moon Treaty has not been ratified by most major space-faring nations, allowing for commercial activities in this proposed agreement could be an important incentive.


10.1126/science.1243607

ASTRONOMY

# Calibrating Asteroid Impact

The airburst over the Russian city of Chelyabinsk earlier this year provides a calibration point to assess the possible damage due to asteroid strikes.

**Clark R. Chapman**

An asteroid impact on Earth about 65 million years ago caused a mass extinction, opening an opportunity for mammals and, eventually, human beings to evolve. We could suffer the dinosaurs' fate this century, but chances are extremely tiny. More realistic, though less catastrophic, threats come from much more numerous but much smaller near-Earth asteroids (NEAs). NEA impacts with the potential to kill millions of people, like the very largest floods, earthquakes, and hurricanes, occur far less than 1% as often as such natural terrestrial calamities. Indeed, truly dangerous NEA impacts, discounting mere meteorites that puncture roofs, occur so rarely that none have been reliably observed until this year. On page 1069, Popova *et al*. (*1*) describe the impact and atmospheric explosion of a 20-m-wide NEA over the Russian city of Chelyabinsk (population 1.2 million) on 15 February 2013, the first NEA impact disaster in modern history.

An order of magnitude more energetic airburst in 1908 over the remote Tunguska region of Siberia was witnessed by few people, but two decades elapsed before the first scientific expedition reached the site. Chelyabinsk, with an explosive energy of half-a-megaton of TNT, is the largest known impact since Tunguska (although one or two larger remote impacts might have been missed or marginally detected many decades ago).

Despite scientific studies of the impact hazard (*2*), the impact frequencies of small NEAs (1 to 100 m in diameter) remain poorly known, and the potential lethality and damage to infrastructure and the environment remain speculative, relying on theory based on only partially relevant data from 1960s nuclear tests and the 1994 impacts of fragments of Comet Shoemaker-Levy 9 into Jupiter. Thus, Chelyabinsk presents the first opportunity to calibrate the impact hazard by direct observations of the consequences. Instead of waiting two decades to get to the site, researchers (including many among the 59 in Popova *et al*.'s "Chelyabinsk Airburst Consortium") arrived within hours or days, and returned during subsequent weeks and months, to collect data while meteorites were still in the snow and eyewitness memories were still sharp.

CREDIT: KYODO VIA AP IMAGES

**Making an impact.** A photo of the point of impact in the frozen lake from which a half-ton fragment of the meteorite that exploded in the skies of Chelyabinsk was later recovered.

Chelyabinsk alone cannot greatly improve our knowledge of impact frequencies, but it does augment suspicions that Earth is being struck more frequently than we thought. After all, Tunguska, estimated to be a once-in-1000-year event, occurred just over a century ago and now a 20-m NEA just struck, thought to be a once-in-100-year event. There are other indications of higher impact frequencies, but they are counterbalanced by extrapolations from the recent Near-Earth Object Wide-Field Infrared Survey Explorer (NEOWISE) survey of NEAs (*3*) suggesting fewer small NEAs.

The prime contribution of Popova *et al*.'s study of the Chelyabinsk airburst is direct observation of the damage. A NASA study (*4*) had concluded that airbursts by NEAs up to 10 times more massive than Chelyabinsk would be essentially harmless. It was argued (*5*) that those predictions, based on stationary nuclear tests, ignored the downward momentum of an impacting NEA, which causes its airburst to descend dangerously toward the ground. Actually, Chelyabinsk struck at an unusually shallow angle, just 18°, so the airburst at ~30 km altitude had little downward momentum and damage was widely distributed along and to the sides of a path roughly 100 km long. Impact at a more typical, higher angle, would have concentrated more serious damage near ground zero. Therefore, emergency management officials should note that any predicted impacts by NEAs even several times less massive than Chelyabinsk should be taken very seriously, perhaps meriting evacuation.

Although Chelyabinsk-sized impacts now happen without warning (only 0.01% of such small NEAs have been discovered), at least one soon-to-be-operational search program, Asteroid Terrestrial-Impact Last Alert System (ATLAS) (*6*), can potentially discover up to half of small NEAs as they approach Earth, providing perhaps days to weeks of advance warning.

The Chelyabinsk airburst killed nobody, despite occurring over an unusually densely populated region. Nevertheless, over 1600 people requested medical assistance at hospitals (~0.1% of the population). Several times as many suffered less serious injuries (sunburn

Department of Space Studies, Southwest Research Institute, 1050 Walnut Street, Suite 300, Boulder, CO 80302, USA. E-mail: cchapman@boulder.swri.edu



Published by AAAS

and temporary blindness or deafness), according to in-person interviews in ~50 towns and Internet-questionnaire surveys (1754 respondents, mostly from the city). The worst injuries were cuts and bruises from flying glass. Some people noticed the brilliant flash (many times brighter than the Sun), rushed to windows, perhaps remaining to gaze at the contrail, and were unprepared for the shock wave that arrived a couple of minutes later. Over 7300 buildings were damaged, mainly with broken windows. Popova *et al*. collected abundant, valuable reports of observations (sounds and smells) and damage for social scientists, engineers, and emergency managers to study.

The Chelyabinsk event was surely a disaster, comparable in casualties and damage to some events that in the United States are presidentially declared disasters. However, it was modest in scale compared with other headline-grabbing disasters like the November 2013 typhoon in the Philippines. Small NEA impacts remain a tiny natural hazard. However, because time and location of a future impact may be predicted with great accuracy, the local emergency manager can now know from Chelyabinsk the potential dangers and can take prudent measures.

Popova *et al*. also describe the physical and compositional characteristics of the recovered meteorites. Mineralogical, compositional, and isotopic analyses demonstrate that Chelyabinsk is an unusually strongly shocked LL chondrite. Although just 8% of ordinary chondrites (the most common meteorite in museums) are of the LL (iron-poor) type, they are abundant among NEAs [e.g., Itokawa, from which dust samples were returned (*7*)] and in the inner asteroid belt. Popova *et al*. determine a trajectory for the Chelyabinsk asteroid consistent with its being derived from the large Flora family of asteroids in the inner belt. They suggest that Chelyabinsk may have been unusually weak and more heterogeneous than most meteorites, but all research groups must compare notes and converge on a definitive description of this meteorite.

The largest fragment proceeded westward toward a lake where a 7-m-wide hole appeared in the ice (see the figure). Popova *et al*. show a video record of it striking the lake's surface. On 16 October 2013, the half-ton fragment was removed from a depth of 20 m. Although just a tiny fraction of the asteroid's estimated original mass of 13,000 metric tons has been recovered, much will be gleaned from this best-ever observed meteorite fall, thanks to security and dashboard cameras. Meanwhile, efforts proceed to find other dangerous NEAs before they find us. The privately funded Sentinel mission (*8*) may launch in 2018 to provide a census of 90% of NEAs larger than 140 m (and many smaller ones), and the ATLAS project may soon provide advance warning of future Chelyabinsk-like impacts, which may be more dangerous, and perhaps more probable, than had previously been estimated.

**References**


1. O. P. Popova *et al*., *Science* **342**, 1069 (2013); 10.1126/science.1242642.
2. National Research Council, *Defending Planet Earth: Near-Earth-Object Surveys and Hazard Mitigation Strategies* (National Academies Press, Washington, DC, 2010).
3. A. Mainzer *et al*., *Astrophys. J.* **743**, 156 (2011).
4. Near-Earth Object Science Definition Team, *Study to Determine the Feasibility of Extending the Search for Near-Earth Objects to Smaller Limiting Diameters* (NASA, Washington, DC, 2003).
5. M. Boslough, D. Crawford, *Int. J. Impact Eng.* **35**, 1441 (2008).
6. J. L. Tonry, *Publ. Astron. Soc. Pac.* **123**, 58 (2011).
7. T. Nakamura *et al*., *Science* **333**, 1113 (2011).
8. B612 Sentinel Mission; b612foundation.org/sentinel-mission


10.1126/science.1246250

EVOLUTION

# Protein Expression Under Pressure

Cellular protein concentrations are generally under stronger evolutionary pressure than mRNA concentrations.

**Christine Vogel**

Which is more conserved across species—the concentrations of proteins or the concentrations of the messenger RNAs (mRNAs) that encode them? When examining orthologous genes, it's protein concentrations that are more similar to each other. This observation was first made in worm and fly (*1*), and later for eight organisms ranging from bacteria to yeast, plant, and human (*2*). However, because the measurement platforms, data sets, and cell samples were heterogeneous in these studies, it has been difficult to separate possible biological trends from technical artifacts. On page 1100 of this issue, Khan *et al*. (*3*) show that the biological trend is very real. The authors show that protein concentrations from identical cell types across three primate species are under stronger evolutionary constraints than the respective mRNA expression levels.

New York University, Center for Genomics and Systems Biology, New York, NY 10003, USA. E-mail: cvogel@nyu.edu

Khan *et al*. subjected lymphoblastoid cell lines from humans, chimpanzees, and rhesus macaques (five of each) to RNA sequencing and mass spectrometry–based proteomics experiments. Protein and mRNA concentrations were quantified for ~3400 proteins across at least three individuals from each species, controlling strictly for variation across replicates, ambiguous quantification, and artifacts introduced by extremely high- or low-abundance genes. The authors found that the expression is more tightly controlled for orthologous proteins compared to corresponding mRNAs (see the figure).

Evolutionarily, this observation seems obvious: Proteins are the cell's workhorses, and for proper cellular function, one would expect their concentrations to be firmly set at desired levels. Khan *et al*. demonstrate that protein concentrations diverge at a slower rate than mRNA concentrations, suggesting higher evolutionary constraints. These constraints may be larger for some protein functions than for others. Due to mass spectrometry's bias toward high-abundance proteins, it remains to be seen how the observation holds true for less-abundant proteins, such as transcription factors.

One hypothesis to explain the conservation of protein concentrations is inspired by work on the chaperone heat shock protein 90 (HSP90), which supports proper folding of protein substrates. HSP90 can act as an evolutionary capacitor and enable the accumulation of mutant proteins across a cell population to provide a repository of functional variants when needed (*4*). This explanation can now be extended to possible capacitor roles in gene expression regulation. On the basis of Khan *et al*.'s observation, protein concentrations may be assumed to vary less across a population of cells than the respective mRNA concentrations—i.e., protein concentrations are buffered—and the regulation of transcription and therefore mRNA abundances are allowed to evolve more freely. Indeed, this is what Khan *et al*. conclude from their data, and it is consistent with the previously

observed rapid divergence of transcription regulation (*5*). Similar to sequence variants accumulating under HSP90 function, variants of mRNA expression levels may provide a repository for regulatory adaptation if the cell population is under selection pressure. Single-cell studies that resolve the variation of mRNA and protein concentrations across individual cells will be needed to show if this interpretation holds true.

But how is the conservation of protein concentrations achieved? Several observations point to possible explanations, and the answer may lie in a combination of these. For example, mRNA concentrations appear to be often regulated in a switchlike manner, turning transcription on or off, without much attention to exact concentrations (*6*). Translation, in turn, may be much more finely regulated: MicroRNAs (miRNAs), for example, have very small individual effects on protein abundances (*7*, *8*). Similarly, other translation regulators, such as RNA-binding proteins, have also small effects on protein concentrations, as with the RNA-binding protein human antigen R (*9*). These data point to a highly combinatorial mode of action for these translation regulators that may counterbalance large variations in transcript concentrations (*10*).

Furthermore, buffering of expression divergence at the mRNA level will likely require extensive feedback between the different steps of protein synthesis. Such coupling has been observed in several circumstances (*11*). To regulate protein concentrations and counteract variations introduced at the mRNA level, the cell would have to sense the levels of transcription (how much mRNA is present), and adjust translation and protein degradation accordingly. Conversely, once desired protein concentrations are achieved, the cell may reduce translation (and transcription) or increase protein degradation to maintain proteostasis. The existence of such feedback mechanisms could also explain the large number of possible translation regulators that have now been found: The human genome encodes at least 800 miRNA genes (*12*), and possibly ~1000 RNA-binding proteins (*13*). However, in most cases, the mechanisms of regulatory feedback between the different processes of protein synthesis are unknown, and we do not yet understand the extent to which coupling is positive or negative—i.e., whether processes are working in the same or opposite directions.

Part of the observation by Khan *et al*. can be explained by simple mathematics. In their data (but also in general), mRNA concentrations vary by three to four orders of magnitude. In comparison, protein concentrations cover four to six orders of magnitude, suggesting an amplification step at the level of translation: A single mRNA may be translated ten, hundreds, or thousands of times before being degraded. Because the resulting protein and mRNA concentrations are compared at a logarithmic scale, the amplification step alone can partly explain the observation, even when acting randomly. Indeed, there may be a very large variation in mammalian translation and degradation rates (*14*). While explaining some of the observed trends, this logic produces another intriguing question: How would the cell decide which rate to use for a particular mRNA species? Innovative techniques for measuring translation and protein degradation rates will have to provide answers (*14*, *15*).

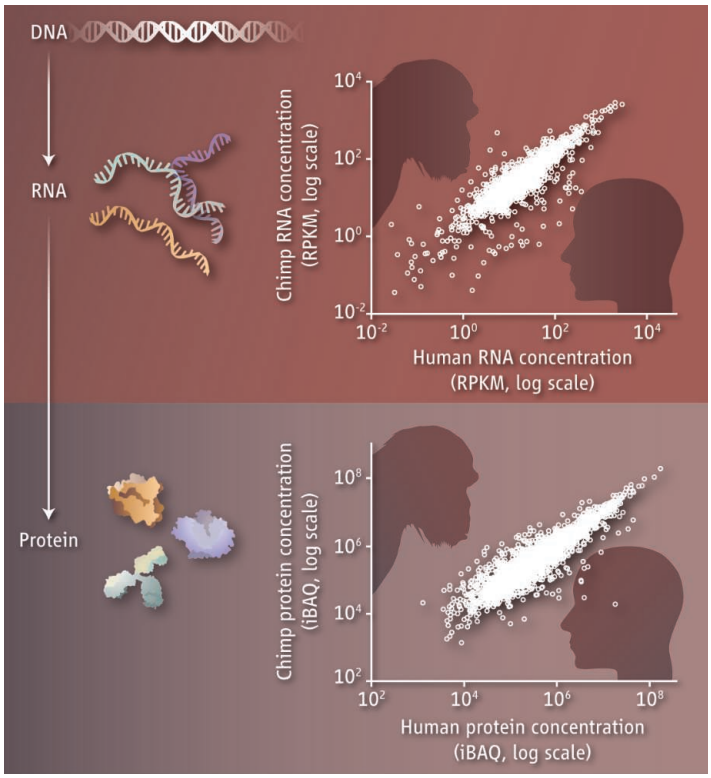


**Protein versus mRNA expression.** Absolute concentrations of mRNA are more divergent between chimpanzee and human than absolute protein concentrations, suggesting tighter evolutionary constraints on protein abundances. Graphs are generated from table S8 in (*3*). Protein concentrations were determined by intensity-based absolute quantification (iBAQ) of mass spectrometry data; mRNA concentrations were measured by reads per kilobase of transcript per million mapped reads (RPKM) from RNA-sequencing data, as described in (*3*).

Khan *et al*.'s observation points to several future analyses. We still lack a basic understanding of the fundamental principles of gene expression regulation, starting from simple descriptions of the absolute concentrations of mRNA and proteins in different cells, across tissues, and conditions—it is unclear how mRNA expression and protein abundance are coordinated in dynamic systems responding to a stimulus. In addition, these concentration measurements should now be extended to estimates of underlying rates of synthesis and degradation of mRNA and proteins. Despite the availability of large-scale methods for determining these rates (*14*, *15*), such experiments are still rare. One next step would involve measurements of translation in parallel to protein and mRNA concentrations. The regulation of protein synthesis is a complex process involving at least two levels (transcription and translation, plus the respective degradation), and deconvoluting these processes from observed protein and mRNA concentration measurements is all but trivial, requiring new models, molecular tools, and computational approaches—many of which are under way.

CREDIT: H. MCDONALD/*SCIENCE*

### References and Notes

1. S. P. Schrimpf *et al*., *PLOS Biol.* **7**, e48 (2009).
2. J. M. Laurent *et al*., *Proteomics* **10**, 4209 (2010).
3. Z. Khan *et al*., *Science* **342**, 1100 (2013); 10.1126/science.1242379.
4. C. Queitsch, T. A. Sangster, S. Lindquist, *Nature* **417**, 618 (2002).
5. P. Khaitovich *et al*., *Science* **309**, 1850 (2005).
6. A. Raj, C. S. Peskin, D. Tranchina, D. Y. Vargas, S. Tyagi, *PLOS Biol.* **4**, e309 (2006).
7. D. Baek *et al*., *Nature* **455**, 64 (2008).
8. M. Selbach *et al*., *Nature* **455**, 58 (2008).
9. S. Lebedeva *et al*., *Mol. Cell* **43**, 340 (2011).
10. C. Vogel, E. M. Marcotte, *Nat. Rev. Genet.* **13**, 227 (2012).
11. O. Dahan, H. Gingold, Y. Pilpel, *Trends Genet.* **27**, 316 (2011).
12. I. Bentwich *et al*., *Nat. Genet.* **37**, 766 (2005).
13. A. Castello *et al*., *Cell* **149**, 1393 (2012).
14. B. Schwanhäusser *et al*., *Nature* **473**, 337 (2011).
15. A. J. Howden *et al*., *Nat. Methods* **10**, 343 (2013).

**Acknowledgments:** C.V. acknowledges funding by the New York University (NYU) Whitehead Fellowship and the NYU University Research Challenge Grant.

10.1126/science.1247833

CHEMISTRY

# Abundant Metals Give Precious Hydrogenation Performance

Iron- or cobalt-based catalysts have outperformed traditional precious metal catalysts in several hydrogenation reactions.

**R. Morris Bullock**

Homogeneous catalysts based on precious metals have enabled highly selective synthesis of organic compounds. Precious metal catalysts including ruthenium (Ru), rhodium (Rh), and platinum (Pt) have been superstars of both homogeneous and heterogeneous catalysis. In recent years, increasing efforts have been devoted to the design and discovery of homogeneous catalysts that incorporate base metals, such as iron (Fe) and cobalt (Co) (*1*–*3*) (see the figure). Catalytic hydrogenations are one of the extraordinary success stories of homogeneous catalysis, and three reports in this issue describe remarkable progress in the use of Earth-abundant metals as catalysts for hydrogenations. Hydrogenations are conceptually simple—$H_2$ is added across a C=C or C=O double bond—but mechanistic studies have revealed considerable complexity with respect to how the metal catalyzes hydrogenations (*4*). On page 1080, Zuo *et al*. (*5*) report iron catalysts for asymmetric hydrogenation of C=O bonds. On page 1076, cobalt catalysts for asymmetric hydrogenation of C=C bonds are described by Friedfeld *et al*. (*6*). On page 1073, Jagadeesh *et al*. (*7*) report on nanoscale iron catalysts for synthesis of functionalized anilines through hydrogenation of nitroarenes.

Given that precious metal catalysts work so well for hydrogenations, why replace them? First, precious metals are expensive, largely because of their low abundance. The price of Pt is typically >$40 per gram, whereas the price of Fe is often quoted by the kilogram or ton. The price comparison becomes even more favorable for Fe when considering the much higher atomic weight of Pt relative to Fe, so comparison of cost per mole is more appropriate. Second, precious metals such as Pt and Rh are more toxic than Fe by two or more orders of magnitude. Finally, although the catalysts described in this issue are of particular interest for synthesis of high-value chemicals, the broad concept is equally applicable to catalysis that might be implemented on a much larger scale. In the context of energy science (*8*), the impetus for developing catalysts based on Earth-abundant metals reflects the need for usage on a global scale. If we eventually want to replace all automobiles that use gasoline (and produce carbon dioxide emissions) with cars powered by hydrogen fuel cells that require Pt catalysts, there is not enough Pt on the planet to accomplish that goal, whereas it could be achieved with the development of efficient fuel cells that use Fe catalysts (*9*).

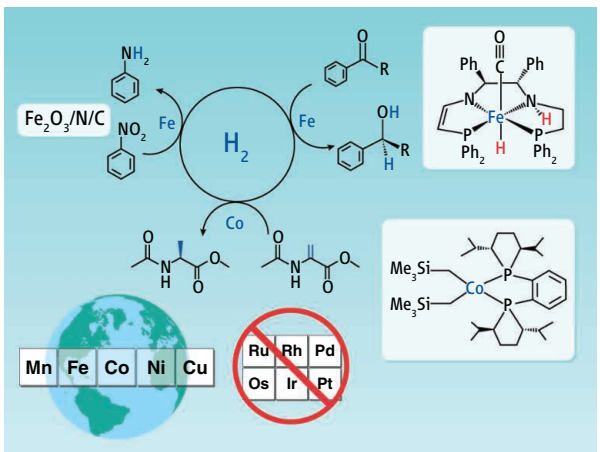


**Elevating base metals for catalysis.** Catalytic hydrogenations typically use precious metals that are usually not abundant on Earth, such as ruthenium (Ru), rhodium (Rh), palladium (Pd), osmium (Os), iridium (Ir), and platinum (Pt). Three studies report on practical catalytic hydrogenations based on iron (Fe) and cobalt (Co) complexes and compounds, which, like other base metals such as manganese (Mn), nickel (Ni), and copper (Cu), are abundant. Clockwise from the bottom, the catalysts developed by Friedfeld *et al*., Jagadeesh *et al*., and Zuo *et al*. are illustrated; the atoms in blue are directly part of the reaction (in the Zuo *et al*. catalyst, hydrogen is derived from an alcohol). Abbreviations: Me, methyl; Ph, phenyl; R, alkyl.

The Fe catalyst reported by Zuo *et al*. is the culmination of detailed studies of kinetics and mechanisms of Fe catalysts over several years. The previous efforts of Morris and co-workers on Fe complexes with tetradentate ligands led to an understanding of how to achieve high reactivity and high enantioselectivity for asymmetric transfer hydrogenations of ketones (*10*). Zuo *et al*. report turnover frequencies (completed catalytic cycles per unit time) as high as 200 $s^{-1}$ (at 28°C) at 50% conversion; those remarkably high rates exceed those reported for Ru catalysts (*11*). Enantiomeric excesses (ee values) of the chiral alcohol obtained from these Fe catalysts are >99% for some substrates. These Fe complexes do not use $H_2$ gas directly but transfer $H_2$ from isopropyl alcohol. The mechanism for these catalytic reactions involves delivery of a proton from an N-H bond and a hydride from an Fe-H bond. Noyori *et al*. developed many hydrogenation catalysts using Ru and termed this type of ionic hydrogenation mechanism "metal-ligand bifunctional catalysis" (*12*).

Asymmetric hydrogenation of C=C bonds is widely used in the pharmaceutical and agrochemical industries, but such reactions typically rely on precious metal catalysts, with Rh (*4*) and iridium (Ir) (*13*, *14*) being the prominent examples. Friedfeld *et al*. report Co complexes with chiral diphosphine ligands that are fast, efficient catalysts for production of single enantiomers. Reactions at 23°C under $H_2$ pressure led to hydrogenated products, with several examples providing >90% ee. Many potential catalysts were tested by high-throughput screening of 10 cobalt precursors and 192 phosphines. Chiral diphosphines were added to Co(II) complexes such as $(pyridine)_2Co(CH_2SiMe_3)_2$, giving $(diphosphine)Co(CH_2SiMe_3)_2$ (Me = methyl). The active catalyst presumably has Co-H bonds that are generated after cleavage of the Co-C bonds of $(diphosphine)Co(CH_2SiMe_3)_2$. In addition to the obvious difference of using Co rather than Rh, it is notable that the catalyst precursor is a paramagnetic Co(II) complex, whereas the metal complexes commonly encountered with precious metals are typically diamagnetic.

Jagadeesh *et al*. synthesized heterogeneous Fe catalysts that obviate the need for precious metals for the hydrogenation of nitroarenes, providing a route to substituted aniline derivatives that are important inter-

Center for Molecular Electrocatalysis, Pacific Northwest National Laboratory, P.O. Box 999, K2-57, Richland, WA 99352, USA. E-mail: morris.bullock@pnnl.gov

CREDIT: C. SMITH



Published by AAAS

mediates for many industrial reactions. They explored several nitrogen-containing ligands, a variety of pyrolysis temperatures, and different supports. Their best catalyst was prepared by pyrolysis of iron(II) acetate and phenanthroline at 800°C on carbon supports. A remarkable feature is that the nitro group is selectively hydrogenated in the presence of aldehydes, ketones, and C=C bonds. Although the mechanism of their catalyst is not known, it must involve several steps, as two N-O bonds must be cleaved in addition to the formation of the N-H bonds of the product. Characterization of the catalyst particles revealed $Fe_2O_3$ nanoparticles, which suggests that some form of "nano-rust" is the catalyst, but the nitrogen-doped layers around the particles of $Fe_2O_3$ indicate that nitrogen arising from the phenanthroline is incorporated into the support.

These three papers do not merely report proof-of-principle results; they describe catalysts based on inexpensive metals that exhibit impressive activities and selectivities that are comparable to, or even exceed, those of well-established catalysts based on precious metals. None of the new catalysts were designed by keeping the ligands and oxidation states the same as those on a precious metal catalyst while simply changing the metal; rather, their design relies on understanding and exploiting their characteristic reactivity. The striking diversity of approaches, all ultimately fruitful, illustrates that there is no exclusive single "recipe" for success in developing catalysts based on cheap metals—an observation that is encouraging to chemists seeking to design and develop catalysts based on abundant, inexpensive metals.

### References and Notes


1. R. M. Bullock, Ed., *Catalysis Without Precious Metals* (Wiley-VCH, Weinheim, Germany, 2010).
2. C. Bolm, *Nat. Chem.* **1**, 420 (2009).
3. S. Enthaler, K. Junge, M. Beller, *Angew. Chem. Int. Ed.* **47**, 3317 (2008).
4. C. R. Landis, J. Halpern, *J. Am. Chem. Soc.* **109**, 1746 (1987).
5. W. Zuo, A. J. Lough, Y. F. Li, R. H. Morris, *Science* **342**, 1080 (2013).
6. M. R. Friedfeld *et al., Science* **342**, 1076 (2013).
7. R. V. Jagadeesh *et al., Science* **342**, 1073 (2013).
8. N. S. Lewis, D. G. Nocera, *Proc. Natl. Acad. Sci. U.S.A.* **103**, 15729 (2006).
9. T. R. Simmons, V. Artero, *Angew. Chem. Int. Ed.* **52**, 6143 (2013).
10. A. A. Mikhailine, M. I. Maishan, A. J. Lough, R. H. Morris, *J. Am. Chem. Soc.* **134**, 12266 (2012).
11. R. Noyori, *Angew. Chem. Int. Ed.* **41**, 2008 (2002).
12. R. Noyori, M. Yamakawa, S. Hashiguchi, *J. Org. Chem.* **66**, 7931 (2001).
13. S. Bell *et al.*, *Science* **311**, 642 (2006).
14. M. C. Perry *et al.*, *J. Am. Chem. Soc.* **125**, 113 (2003).


**Acknowledgments:** The author's work in this area is supported as part of the Center for Molecular Electrocatalysis, an Energy Frontier Research Center funded by the U.S. Department of Energy, Office of Science, Basic Energy Sciences. Pacific Northwest National Laboratory is operated by Battelle for the U.S. Department of Energy.

10.1126/science.1247240

ENGINEERING

# Devices for Low-Resource Health Care

Devices designed for low-resource settings can improve access to life-saving health care around the world.

**Rebecca Richards-Kortum and Maria Oden**

Most of the world receives health care in low-resource settings (see the figure), yet medical technologies are designed to be used mainly in high-resource settings, where designers take for granted basic infrastructure that supports their safe use and effective distribution. The corridors of many hospitals in low-resource settings are lined with donated medical equipment, but up to three-quarters of these devices do not work, often due to lack of spare parts or consumables (*1*). As a result, most of the world's population lacks access to life-saving technologies developed decades ago, including infant incubators, oxygen concentrators, and simple laboratory diagnostics. In this Perspective, we review the challenges of developing and translating medical technologies and highlight promising new technologies to improve health in low-resource settings.

Low-resource settings present challenging design constraints, including inadequate electricity and clean water, limited funding, weak supply chains, lack of trained users, and lack of technology management policies (*1*, *2*). Alarms and fail-safe features that make devices safe in high-resource settings can be damaged in harsh environmental conditions, causing devices to fail or be unsafe in low-resource settings. Efforts to design new technologies for low-resource settings have generally been more successful than attempts to adapt existing technologies by removing costly or complex features (*1*, *3*). Designs that eliminate or minimize cost of consumables may be most sustainable. Because consumables are often reused in low-resource settings, designers should ensure that they can be cleaned safely.

Evaluating technology performance presents further challenges in low-resource clinics. It is difficult to design ethical trials of potentially life-saving appropriate technologies when the benefits of counterpart technologies in high-resource settings are well documented. Moreover, collecting accurate data in understaffed clinics is challenging.

Successful product design requires multidisciplinary partnerships. There are many benefits to engaging local innovators, yet opportunities for quality engineering education in low-resource settings are limited, especially in Africa (*4*). Many efforts have identified unmet clinical needs in low-resource settings, but it can be difficult to identify early-stage industrial partners to develop a parallel business case. Engaging partners working to strengthen regional health systems can assist in wider-scale implementation.

A growing number of academic programs, nongovernmental organizations, and companies are addressing these challenges (*2*). Here, we highlight successful efforts and remaining barriers for several technologies.

Birth asphyxia contributes to more than a quarter of neonatal deaths in low-resource settings (*5*). To address this problem, Laerdal, a medical company that specializes in life-saving equipment, developed affordable, reusable neonatal resuscitation tools, including an easily cleanable bulb suction device to clear the infant's airway and a manual resuscitator with a self-inflating bag. To train providers to recognize and treat birth asphyxia, Laerdal developed NeoNatalie, an electricity-free, low-cost neonatal simulator that mimics chest rise with mechanical ventilation (*6*).

Bioengineering Department, Rice University, 6100 Main Street, Houston, TX 77005, USA. E-mail: rkortum@rice.edu


**Challenging health care settings.** Photos of a neonatal unit at an Ethiopian district hospital (**A**) and in a laboratory at a health center in the Democratic Republic of the Congo (**B**) illustrate the difficult conditions often found in low-resource settings. To be successful, new device designs must address the challenges of limited physical infrastructure, low economic resources, lack of consumables, and lack of tools and maintenance personnel. The early phases of technology development should emphasize clinical, scientific, and private-sector partnerships to enable sustainable implementation.

With global input, the American Academy of Pediatrics developed a training curriculum for these technologies called Helping Babies Breathe (HBB) (*6*). Implementation of HBB in Tanzania reduced early neonatal mortality by 47% (*5*).

HBB is being implemented in more than 50 countries and is a part of the World Health Organization (WHO) Essential Newborn Care Course (*6*). Studies of HBB show that even with a simple technology, there is a need for ongoing training and mentoring to change clinical management and patient outcomes (*5*, *6*). HBB's success illustrates the importance of partnerships that couple design, education, and efforts to improve health systems; early engagement of partners ensures that design constraints are set to facilitate future integration of a technology into the health system.

Premature birth is the leading cause of newborn death. Over half of premature babies struggle to breathe; in the developed world, this is easily treated using continuous positive airway pressure, in which pressurized air and oxygen are gently delivered through nasal prongs. At $6000, continuous positive airway pressure machines designed for high-resource settings are too costly for most developing-world hospitals. Recently, we reported a $400 continuous positive airway pressure system that delivers the same therapeutic flow and pressure as systems used in high-resource settings (*7*). The device was designed with analog electronics to ensure that it would be robust. In 1 year of clinical evaluation of five devices at a central hospital in Malawi, no device failed, whereas 40% of study oxygen concentrators regularly used in the ward failed when circuit boards were damaged by line voltage spikes (*8*). Often, technologies such as the oxygen concentrators designed for high-resource settings fail when used in low-resource settings because of the large mismatch between the context for design and that for actual use (*1*).

Global efforts to expand access to HIV care have led to a need for improved laboratory diagnostics for HIV-infected patients. In particular, protocols to initiate and monitor therapy with antiretroviral drugs require $CD4^+$ T cell counts. The gold standard for CD4 testing is flow cytometry, but these devices are expensive and complex (*3*). Developers first attempted to meet this need by modifying existing flow cytometers to reduce cost. For example, the BD FACSCount is a low-cost flow cytometer, but it requires skilled operators and frequent calibration (*3*). Alternative technologies have been designed explicitly to meet the needs of low-resource settings. For example, the Alere PIMA device uses a fixed-volume, static cytometer and can run on battery or solar power (*3*, *9*). It cannot be maintained or repaired on site, but the company maintains local inventory stocks to swap out nonfunctional devices (*3*). Despite the limitations of both approaches, introduction of point-of-care CD4 testing with these devices has improved patient care in low-resource settings, increasing the proportion of patients who initiate the necessary treatment and decreasing time to receive necessary therapy (*10*).

In 2012, a WHO expert panel proposed that point-of-care CD4 technologies should be affordable (<$5), sensitive (99%), specific (98%), user-friendly (requiring minimal operator training), rapid and robust (<1 hour, no special temperature requirements for shipping or storage, no operator calibration, minimal routine maintenance), equipment-free (battery operated and no moving parts), and deliverable (commercially available and approved) (*3*). No CD4 devices yet meet these criteria (*3*, *9*, *11*), and some devices fail frequently in the field (*11*). CD4 devices explicitly designed for low-resource settings more closely approach the target specifications for use at the point of care than simplified versions of designs originally developed for high-resource settings (*3*).

Efforts to improve laboratory diagnostics for *Mycobacterium tuberculosis* (MTB) led to the recent introduction of GeneXpert. Designed to provide sample-to-answer nucleic acid testing for MTB and drug resistance using polymerase chain reaction amplification, the assay has shown improved sensitivity compared to microscopy (*12*). However, laboratory temperatures exceeded the operational range for GeneXpert more than 10% of the time in four of six sites in one multicountry study (*12*). Moreover, the subsidized price for each Xpert test cartridge in low-resource settings ranges from $10 to $17, much higher than the $3 South African National Health Laboratory Service charge for standard fluorescence microscopy, which includes overhead, supplies, and personnel costs (*13*). While the Xpert test offers important benefits, the hardware and consumables are expensive; it is often more challenging for health systems to sustain the cost of consumables than to purchase one-time hardware costs.

Approaches that minimize the cost of consumables may be the most sustainable; as an alternative to reduce the cost of consumables for laboratory tests, diagnostic tests made of paper show considerable promise. Clinical evaluation of a paper-based device to measure liver function demonstrated accurate results with an estimated per-test cost of $0.10, well below the $4 per-test cost of existing commercial assays (*14*). Whole blood is applied to the device, and plasma

CREDIT: NEONATAL WARD, REBECCA RICHARDS-KORTUM; LABORATORY, CARL BOSE/UNIVERSITY OF NORTH CAROLINA


Published by AAAS

passes through a filter that retains red and white blood cells to layers of paper containing colorimetric reagents. Fluid flow within the paper is directed by patterned hydrophobic barriers that are easily created using a wax-based printer and heat source. Results can be documented, analyzed, and transmitted with a cell phone camera, and devices can be safely disposed of by incineration. Paper-based tests to amplify and detect nucleic acids have been reported recently (*15*).

Health care innovation should be available to all the world's citizens, but technical and economic barriers remain. Low-resource settings present challenging constraints that require design for context, safety, reusability, and reparability. The current landscape of appropriate technologies reflects a reaction to economic incentives, largely shaped by philanthropic efforts rather than market forces. Often these funding mechanisms favor technical innovation over simplicity, and resulting technologies are too costly and difficult to maintain at scale. Alternative approaches that explicitly design technologies to function in settings that lack resources for consumables, effective distribution systems, supply chains, and technology management programs and that incorporate early private sector partnerships are needed. In parallel, efforts to develop and support innovators in low-resource settings must be strengthened. Partnerships that focus on developing and disseminating integrated packages of technologies that address focused areas (such as technologies for the neonatal unit) can navigate technical and implementation barriers more efficiently than single technologies.

**References and Notes**


1. World Health Organization, Medical Devices: Managing the Mismatch. An Outcome of the Priority Medical Devices Project (World Health Organization, Geneva, 2010); http://whqlibdoc.who.int/publications/2010/9789241564045_eng.pdf.
2. S. R. Sinha, M. Barry, *N. Engl. J. Med.* **365**, 779 (2011).
3. M. T. Glynn, D. J. Kinahan, J. Ducrée, *Lab Chip* **13**, 2731 (2013).
4. P. Matthews, L. Ryan-Collins, J. Wells, H. Sillem, H. Wright, Africa-UK Engineering for Development Partnership, A Summary Report: Engineers for Africa: Identifying Engineering Capacity Needs in Sub-Saharan Africa (Royal Academy of Engineering, London, 2012); www.raeng.org.uk/news/publications/list/reports/RAEng_Africa_Summary_Report.pdf.
5. G. Msemo *et al.*, *Pediatrics* **131**, e353 (2013).
6. H. L. Ersdal, N. Singhal, *Semin. Fetal Neonatal Med.* 10.1016/j.siny.2013.07.001 (2013).
7. J. Brown *et al.*, *PLOS ONE* **8**, e53622 (2013).
8. J. Brown *et al.*, *Low-Cost, Highly Effective Respiratory Support: Reducing Neonatal Death in Rural Malawi*, Saving Lives at Birth Development Exchange, Washington, DC, 19 to 21 July 2013.
9. M. Mwau *et al.*, *PLOS ONE* **8**, e67612 (2013).
10. I. V. Jani *et al.*, *Lancet* **378**, 1572 (2011).
11. M. Bergeron *et al.*, *PLOS ONE* **7**, e41166 (2012).
12. C. C. Boehme *et al.*, *Lancet* **377**, 1495 (2011).
13. G. Meyer-Rath *et al.*, *PLOS ONE* **7**, e36966 (2012).
14. N. R. Pollock *et al., Sci. Transl. Med.* **4**, 152ra129 (2012).
15. B. A. Rohrman, R. R. Richards-Kortum, *Lab Chip* **12**, 3082 (2012).


**Acknowledgments:** We apologize to those authors whose works we could not cover owing to space limitations. R.R.-K. is supported by the NIH (U54A1057156-10, R03EB013973-03, R21CA156704-02), and the Bill and Melinda Gates Foundation; R.R.-K and M.O. are supported by the U.S. Agency for International Development (AID-OAA-A-13-00014). The device reported in (*7*) is the subject of U.S. Provisional Patent Application 61/730,353 (Bubble Continuous Positive Airway Pressure), filed on 27 November 2012.

10.1126/science.1243473

MICROBIOLOGY

# Genomes from Metagenomics

Metagenomic approaches are rapidly expanding our knowledge of microbial metabolic potential.

**Itai Sharon and Jillian F. Banfield**

Evaluation of the functional capacities of microorganisms long relied on laboratory cultivation of individual species. About a decade ago, recovery of draft genomes for a few uncultivated bacteria and archaea from natural communities opened the way for physiological prediction of their environmental roles. Further development of the metagenomics methods used in those early studies now allows the rapid delivery of accurately reconstructed microbial genomes from diverse environmental samples. The resulting knowledge has the potential to revolutionize our understanding of the topology of the tree of life and the metabolic capacities distributed across it. Advances in bioinformatics promise a new era in which comprehensive genetic characterization is sufficiently rapid to find application in diagnostics for medicine, agriculture, forensic science, and biotechnology.

Metagenomics is a cultivation-independent method for studying microbes sampled directly from the natural environment. DNA is extracted and sequenced from one or a series of samples, and the resulting data is analyzed using computational tools. The approach addresses two important needs: It enables analysis of the 99% of microbes in nature that have not yet been cultivated, and it facilitates the study of organisms in the context of their community.

Because the DNA originates from multiple populations, the recovery of genomes from metagenomic data is a complex task. Until recently, genomes were reconstructed only from relatively simple environments with a few abundant genotypes (*1*). The advent of high-throughput DNA sequencing has enabled genomic sampling of much less abundant organisms and characterization of communities with relatively even species abundance levels, but the complexity of data analysis has increased greatly. Newly developed computational tools allow data assembly (*2*) and accurate assignment of genome fragments to specific organisms (*3*, *4*), a process termed binning.

In 2012, Wrighton *et al*. reconstructed 49 genomes with varying completeness levels for bacteria from at least five phyla for which there was almost no prior genomic information (*5*). The authors used a binning method that combines time-series abundance information with sequence compositional characteristics. More recently, Albertsen *et al*. (*6*) used information from multiple samples—an approach similar to that used for analysis of human infant gut microbial consortia (*4*)—to reconstruct 31 genomes with an average estimated genome completeness of 80% from DNA sequence information for an activated sludge bioreactor community. They were able to assemble the complete genome of an organism from the TM7 candidate bacterial phylum (lacking cultivated representatives) into a single contiguous sequence. Complete genomes for organisms that constitute ~1% of the community have also been reconstructed from environments such as the ocean (*3*) and, very recently, from adult human gut (*7*) and sediment (*8*, *9*). These examples demonstrate that metagenome-based genome recovery can now be applied to very complex systems.

Uncertainty about accuracy currently limits wide acceptance of metagenomics-derived

Department of Earth and Planetary Science, University of California, Berkeley, CA 94720, USA. E-mail: jbanfield@berkeley.edu

genomes. Of most concern are the possibilities of incorrect assembly of regions from different genomes into a single sequence and false assignment of assembled fragments to genomes during the binning process. Assembly errors can be addressed using automatic and manual procedures for error correction. Ultimately, the same criterion traditionally used to validate genomes from clonal cultures should be applied: consistent, unambiguous mapping of paired reads across the final sequence. In some cases, the credibility of the derived genomes also can be evaluated by comparison to published genomes for closely related organisms (*4*) or by additional sequencing using long, high-quality DNA sequences (*10*). Binning is an error-prone process that requires special care. Use of information from multiple sources, particularly unique patterns of organism abundance across samples, can reduce error levels substantially (*4*, *5*).

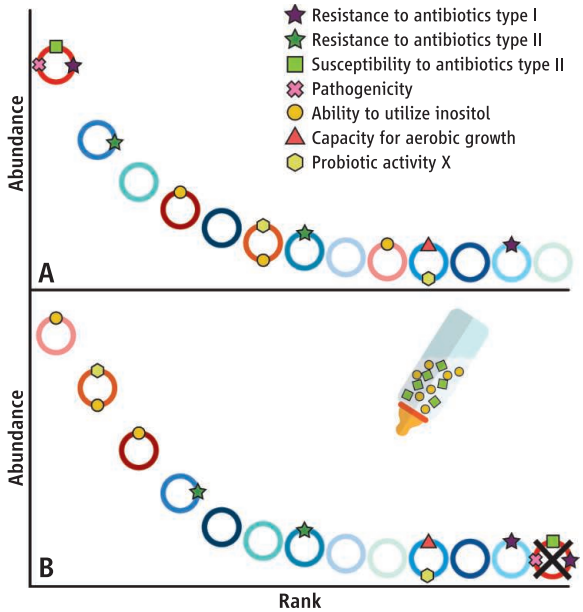


**Treatment by genome-informed microbial selection.** Medical treatments could benefit from knowledge of how microbial capacities are combined in individual organisms. In this hypothetical example, organisms are ranked in order of decreasing abundance. Circles represent genomes. Symbols on the circles indicate traits such as antibiotic resistance or substrate metabolic capacities. Prior to treatment (**A**), organisms with probiotic activity are low in abundance; the most abundant organism is pathogenic. Genome-informed choice of an infant formula containing appropriate antibiotics favors organisms with probiotic activity and eliminates the pathogenic organism (crossed out genome) (**B**).

An alternative to metagenomic approaches is single-cell genomics, in which single cells or cell concentrates are obtained directly from the environment, without cultivation, and sequenced. Recently, Rinke *et al*. (*11*) separated single cells from a variety of natural samples, amplified and sequenced the DNA, and recovered 201 partial genomes, with an estimated average genome completeness of 40%. To our knowledge, no complete genome has yet been achieved for a single cell alone (or by aggregating results from multiple single cells). Genomes generated by single-cell methods are typically very fragmented. In the study of Rinke *et al*., the best-assembled genome, estimated to be 100% complete, remained in 10 pieces; another genome, estimated to be 99% complete, remained in 137 pieces.

For the many genomes from metagenomic data that are initially incomplete (typically because of undersampling), completeness can be improved by additional sequencing. For single-cell genomes, additional sequencing is unlikely to improve the assembly. Metagenomics also does not entail the time-consuming cell manipulation or sorting required in single-cell genomics studies. However, the methods provide subtly different information. A genome derived from metagenomic data represents a population. Currently used assembly algorithms are essentially strain-specific, but there will likely be some nucleotides for which polymorphic variants are detected. Furthermore, a subset of individual sequencing reads will only partially match the consensus sequence if the sampled cell has an inserted or deleted gene. This is advantageous if the researcher is interested in overall population metabolic potential, population structure, diversity, or evolutionary dynamics. On the other hand, single-cell genomics can provide gene variant linkage information that is lost in metagenomic analyses.

As both single-cell genomics and metagenomics gain widespread acceptance, we advocate the use of clearly defined terms to describe genome completeness so as to accurately communicate the success or limitations of the analysis (*12*). A genome should be described as complete or finished only if it is assembled into a single contiguous sequence with no ambiguities or gaps, after careful checking for errors. Genomes assembled into multiple pieces where the fragment order cannot be resolved because of repeated sequences may be termed essentially complete. Following Chain *et al*. (*13*), genomes assembled into multiple pieces without all scaffold connections resolved should be defined as standard draft genomes. In such cases, completeness is typically calculated according to inventories of single-copy genes (*6*, *10*, *11*, *14*). Single-copy genes generally constitute less than 10% of the genes and are unevenly distributed across the genome, thus providing only a rough estimation of completeness.

More robust methods for assessing the completeness of draft genomes are needed. One improvement may involve the use of marker genes that do not tend to cluster together on the genome. Better sampling of microbial genomes from uncultivated organisms will enable refinement of the set of genes considered to be universal. These new genomes will also improve identification of single-copy genes that diverge from known sequences.

Given the important developments in sequencing speed, accuracy, and informatics, high-throughput metagenomic approaches have the potential to revolutionize fields where rapid, accurate, and strain-specific diagnostics are essential. One can imagine, for example, an age of personal microbiomics in which antibiotics are prescribed on the basis of accurate and fast screening of the resistance gene repertoire of the pathogen population (see the figure). Metagenomic insight could enable selective stimulation of desirable microbial populations so as to address medical conditions such as chronic diarrhea or obesity (*15*). More broadly, our understanding of life and its evolutionary history will be dramatically advanced by access to genomes from the numerous, previously unstudied parts of the tree.

**References**

1. G. W. Tyson *et al*., *Nature* **428**, 37 (2004).
2. Y. Peng, H. C. Leung, S. M. Yiu, F. Y. Chin, *Bioinformatics* **28**, 1420 (2012).
3. V. Iverson *et al*., *Science* **335**, 587 (2012).
4. I. Sharon *et al*., *Genome Res.* **23**, 111 (2013).
5. K. C. Wrighton *et al*., *Science* **337**, 1661 (2012).
6. M. Albertsen *et al*., *Nat. Biotechnol.* **31**, 533 (2013).
7. S. C. Di Rienzi *et al*., *eLife* **2**, e01102 (2013).
8. C. J. Castelle *et al*., *Nat. Commun.* **4**, 2120 (2013).
9. R. S. Kantor *et al*., *mBio* **4**, 5 (2013).
10. A. Voskoboynik *et al*., *eLife* **2**, e00569 (2013).
11. C. Rinke *et al*., *Nature* **499**, 431 (2013).
12. E. Mardis *et al*., *Genome Res.* **12**, 669 (2002).
13. P. S. Chain *et al*., *Science* **326**, 236 (2009).
14. B. K. Swan *et al*., *Proc. Natl. Acad. Sci. U.S.A.* **110**, 11463 (2013).
15. V. K. Ridaura *et al*., *Science* **341**, 1241214 (2013).

10.1126/science.1247023

RETROSPECTIVE

# Fred Sherman (1932–2013)

A geneticist championed baker's yeast as a model system and inspired and trained many scientists in the field.

**Susan W. Liebman[1,2] and James E. Haber[3]**

Fred Sherman, a brilliant geneticist who popularized the use of baker's yeast, *Saccharomyces cerevisiae*, as a genetic model system of eukaryotic cells, died on 16 September at the age of 81. Budding yeast are now used at virtually all research centers worldwide, largely due to Fred's efforts and mentoring of many of the leaders in the field. Indeed, Randy Schekman, who shared this year's Nobel Prize in Physiology or Medicine, was introduced to yeast in the Cold Spring Harbor course that Fred taught for 17 summers with his friend and colleague Gerald Fink. Many students and postdoctoral fellows who were trained in Fred's own laboratory also helped shape the field of yeast genetics. Fred taught by example how to think about science, how to do it, and how to enjoy it. He lived life fully, with joy, humor, and dance (ballet), and without ever really separating life from science.

Fred was born in 1932 in Minneapolis, Minnesota, to Jewish Ukrainian immigrant parents. The family lived in a few rooms behind his father's grocery store. "Freddie" (the name on his birth certificate) grew up thinking he was one of richest kids in the world because, unlike his friends, he always had enough to eat. Fred graduated magna cum laude with a B.A. in chemistry from the University of Minnesota in 1953. He obtained his Ph.D. with Robert Mortimer at the University of California, Berkeley in 1958, where he was introduced to yeast and then studied with two other founding yeast geneticists, Herschel Roman at the University of Washington in Seattle, and Boris Ephrussi at the Lab Genetique, Gif-sur-Yvette, France. In 1961, Fred took a faculty position at the University of Rochester in the Department of Radiation Biology and Biophysics, where he remained for his entire career and served as chair of the Department of Biochemistry for 15 years. He often said of this job, "I can't believe they are paying me to do this!"

A long time before DNA could be sequenced, Fred devised a method to deduce

CREDIT: COURTESY OF UNIVERSITY OF ROCHESTER MEDICAL CENTER

the DNA sequence of the first 15 amino acids of the yeast gene *CYC1*, which encodes iso-1-cytochrome c. He did this by isolating and fine-structure mapping many *CYC1* mutations and reverting nonfunctional mutations back to functional, pseudo–wild-type proteins. Changes in these revertants could be identified by sequencing the amino terminus of these proteins, using the laborious chemical process of Edman degradation, carried out with the help of his long-time collaborator, John Stewart. The pattern of amino acid changes from single mutants allowed Fred to establish that the genetic code used in eukaryotes was the same in all key respects with the code that had been deciphered primarily in genetic and biochemical studies with the bacterium *Escherichia coli* and its bacteriophages. He established that AUG was the only start codon in eukaryotic protein translation and that UAA, UAG, and UGA were chain-terminating "nonsense" mutations. He also identified transfer RNA genes by isolating extragenic suppressors of the nonsense mutations and determining the amino acid inserted at the nonsense codon. His work deciphered the rules for transcriptional starts and termination. His deduction of the *CYC1* DNA sequence led to the synthesis of a synthetic oligodeoxyribonucleotide that could for the first time identify the messenger RNA of a specific yeast protein gene. Studying gene structure and function by genetic approaches inevitably led Fred to investigate gene conversion and to make important contributions to understanding mechanisms of recombination.

The importance of Fred's work was recognized by his election to the U.S. National Academy of Sciences in 1985, his receipt of an honorary doctorate from the University of Minnesota in 2002, and his election as a fellow of the American Association for the Advancement of Science in 2006. In 2006, he also was awarded the George W. Beadle Award from the Genetics Society of America in honor of his outstanding contributions to the community of genetics researchers.

Fred's impact on the scientific community extends far beyond his individual scientific achievements and organized service on editorial and society boards and scientific review panels. Unlike many leading scientists, Fred answered his own telephone, where he spent hours each week helping colleagues with all sorts of scientific problems. In these and other conversations, he might ask seemingly naïve questions and then come up with stunningly profound suggestions. Fred promoted a culture of sharing ideas, reagents, and strains that is still prevalent in the yeast community. He loved to travel and shared his ideas all over the world at conferences and at universities where he visited colleagues and gave many seminars. He welcomed many of the students he met abroad into his laboratory for a year or two of critical training before they returned to their home country for successful careers.

No reflection of Fred Sherman would be complete without mention of his inclusiveness. He ate lunch with his students and postdocs most days. Fred used his famous wit and humor to make people feel included and comfortable. For example, he would break the ice with a lonely graduate student at a meeting by asking "How are you doing?" The surprised student would often respond "I'm fine, how are you?" to which Fred would say "Well, I think I'm fantastic. … But not everyone agrees with me."

Fred Sherman was an exemplary scientist. His memory is a blessing for us all.

[1]University of Illinois at Chicago, Chicago, IL, USA. [2]Department of Biochemistry and Molecular Biology, University of Nevada, Reno, NV, USA. [3]Department of Biology and Rosenstiel Basic Medical Sciences Research Center, Brandeis University, Waltham, MA, USA. E-mail: sliebman@unr.edu; haber@brandeis.edu

10.1126/science.1248055

IBI* SERIES WINNER

# Exploring the Evolution of Human Mate Preference

The Evolution of Human Mate Preference, an IBI prize–winning module, uses inquiry to elucidate strategies used by males and females to maximize reproductive fitness.

**Valerie Foster**†

A colleague once told me that, during lectures, 60% of the time college students are thinking about sex. Although attempts to find the source of this statistic resulted in its description as "apocryphal" (*1*), most educators will agree that maintaining student interest during lecture is challenging, and dedicated readers of this series are well aware of the benefits of replacing lecture with inquiry-based instruction (*2*). Asking college students to design experiments to investigate human mate preference engages them in the process of science by appealing to their natural interest in the subject. The Evolution of Human Mate Preference module has been used in a lower-division majors' biology course at a community college. This multiday module gives students experience with researching the primary literature, formulating a testable hypothesis, conducting an experiment, analyzing data, and communicating ideas in a scientific paper or poster. Although some may argue that the development of these skills should begin at the upper division or graduate levels, lower-division students, when given frequent formative assessment and appropriate scaffolding (*2*), are quite successful with this module.

The evolution of human mate preference is an inherently ill-structured problem and, as such, is well suited for a problem-based learning approach (*3*). Mate preference in humans varies substantially with respect to type of trait preferred (e.g., visual, auditory, olfactory, or personality), the interaction between traits, age, time in ovulation cycle, and gender. Furthermore, it is complicated by our advanced cognitive abilities and cultural influences. Students have no difficulty finding a hypothesis of interest see the photos.

This module is taught after students have been introduced to natural selection and other types of microevolutionary mechanisms. Additional interest in the topic is generated by showing videos that contrast intersexual and intrasexual selection and conducting a discussion about the different strategies that male and female animals use to maximize their lifetime reproductive fitness (*4*). Together, we have an uncensored brainstorming session on the differences in mate preferences between men and women.

After reading about sexual selection in their textbook and taking a basic knowledge quiz, students are assigned a primary research article on human mate preference to read. Although any paper of interest will work, Wedekind *et al*. (*5*) is often used because the paper is short and demonstrates an evolutionary benefit of olfactory preference. Because students will be designing their own experiment and writing a paper for the summative assessment, I ask them questions about the scientific process used by the authors and the general format of a primary research article. Students answer these questions as they read the article and we discuss them together.

During class, students conduct their own search of the primary literature to develop a hypothesis of interest and to design an experiment to test it. Although students work in groups of three to four for this module, they must turn in individual proposals

**Pasadena City College students investigate a hypothesis.** Biology majors use creative methods to evaluate the premise that male vocal pitch affects visual preferences of females (pictured clockwise from left: Catherine Velasco, Ashly Ho, Anthony Chen, and Brady Hu).

**Fellow students serve as test subjects.** James Trinh and his group (not pictured) are interested in determining if females place more value on visual or personality traits (pictured clockwise from left: Isis Janilkarn-Urena, Amanda Lopez, Sharon Gautama, and James Trinh).

CREDITS: VALERIE FOSTER

†Natural Sciences Division, Pasadena City College, 1570 East Colorado Boulevard, Pasadena, CA 91106, USA. E-mail: vsfoster@pasadena.edu

*IBI, *Science* Prize for Inquiry-Based Instruction; www.sciencemag.org/site/feature/data/prizes/inquiry/.



Published by AAAS

(see supplementary materials). It has been my experience that the quality of the proposals predicts how students will progress through the rest of the module, which will be important for anticipating issues of classroom management. For example, students who choose an interesting hypothesis and follow the directions on the proposal form usually need minimal assistance during later stages. If students with similar needs are grouped together, class time can be used more efficiently because groups that are farther behind in their inquiry will usually need consultation after more independent groups have had their consultations with the instructor.

Student groups must agree on a hypothesis and experimental design (most use surveys, although any method that can be done in a safe and timely manner is acceptable); they can decide to use one person's idea, combine ideas, or take a completely new direction. A few examples of hypotheses students have chosen include males prefer demure over assertive females, female preference for visual traits in males is augmented by low vocal pitch, and females prefer males whose occupations involve risky, but altruistic, behavior. Pilot studies are conducted with a small sample size (usually $n = 30$) so that students can evaluate the efficacy of their design and make adjustments before launching into the final experiment ($n = 100$). At this step of the module, many students cannot agree on methodology or identify flaws in their design. During the pilot, they may decide to compare two experimental approaches in order to decide which is best to use for the final experiment. Instructors should emphasize that trial and error are natural components of the scientific process.

Before students begin to analyze their data, an Excel workshop is given to illustrate the basic use of a spreadsheet, graphs, and descriptive statistics so that students are able to make sense of a large data set and to communicate their results in a clear manner. Most of the groups understand how they will use the data to evaluate their hypotheses, but some will need help with unexpected results. Instructors need to reassure students that it is acceptable if results do not support the hypothesis, but stress that they should not make excuses in the discussion section of the paper. Rather, they need to explore alternative explanations. Although students are encouraged to collaborate during all steps, including data analysis, writing the paper should be an individual effort.

Frequent formative assessment allows for appropriate scaffolding throughout any problem-based learning activity and is imperative to its success. It is easy for students to feel lost and veer in the wrong direction. Regular communication from the instructor minimizes frustration with the open-ended nature of the problem-based learning process and allows for student-specific guidance in a timely manner (*6*). In this module, formative assessment happens mostly through instructor consultation during the individual literature research and proposal phase, the development of the small group pilot study, evaluation of the pilot results, and final data analysis. Most students will have specific questions and feel comfortable engaging with the instructor, but instructors should make a point to approach students who tend to be shy or may have difficulty grasping new concepts and to ask them questions about their process. Peer critiques can be incorporated when students share their pilot ideas or after writing a first draft of the paper. Metacognitive questions are useful at any stage during or after the module (see supplementary materials). If many students are having issues understanding the same aspect of the project, a mini-lecture or discussion may be appropriate.

Learning challenges can crop up at each stage of this module. Regarding literature searches, students vary in their ability to use effective keywords and may need guidance to choose those that lead to manageable results. In addition, students may need assistance with the jargon used in the sexual selection literature. It is difficult for students to develop a novel hypothesis (see supplementary materials for suggestions). Encouraging them to be creative and prohibiting the replication of published methodology develops their critical thinking skills. Students also need assistance on how to use the literature to support their ideas. I often ask students to think of their hypothesis as a position and the literature as support. Additionally, the experimental design proposed by students might not test their hypothesis adequately. In this case it is advisable to ask students leading questions so that they can identify and solve their own issues.

This module can be modified for adoption in courses such as nonmajors' biology, upper-division evolution, or anthropology. A nonmajors' course usually requires a more guided process with less emphasis on being able to communicate scientifically. Testing a single hypothesis as a class and analyzing the results together actively engages students in the topic of evolution and teaches them critical thinking skills. For an upper-division course, a statistical analysis may be required, and in an anthropology course, a debate may be conducted about the impact of evolutionary versus cultural influences on human mate preference. Application of this module to large lecture sections will be challenging for a single instructor. To provide adequate consultation, the class may have to be split into smaller sections of 30 students. Online interactions could be used if limited class time precludes quality consultation. Finally, the summative assessment can be a group scientific poster instead of an individual paper.

## About the author

**Valerie Foster** is an associate professor at Pasadena City College where she primarily teaches majors' biology. She earned her Ph.D. at the University of California, Irvine, studying the evolution of parental care and sexual selection in zebra finches. Her interest in problem-based learning began as a teaching assistant in graduate school and developed over the years with the support of her colleagues and dean at Pasadena City College.

### References and Notes

1. R. T. Brown, *Studying Psychology: A Manual for Success* (Prentice-Hall College Division, Upper Saddle River, NJ, 1990).
2. C. E. Hmelo-Silver, R. G. Duncan, C. A. Chinn, *Educ. Psychol.* **42**, 99 (2007).
3. C. E. Hmelo-Silver, *Educ. Psychol. Rev.* **16**, 235 (2004).
4. G. F. Miller, in *A Handbook of Evolutionary Psychology Ideas, Issues, and Applications*, C. Crawford and D. Krebs, Eds. (Lawrence Erlbaum Associates, Hillsdale, NJ, 1998).
5. C. Wedekind, T. Seebeck, F. Bettens, A. J. Paepke, *Proc. Biol. Sci.* **260**, 245 (1995).
6. C. Boston, *Pract. Assess., Res. Eval.* **8**, http://PAREonline.net/getvn.asp?v=8&n=9 (2002).

**Acknowledgments:** I thank my Dean, D. Douglass, for his moral and financial support; R. DiFiori for many creative discussions; and several other Pasadena City College faculty for giving me new perspectives during collaborative teaching moments. I also appreciate the early pedagogical opportunities that D. Gallow and R. Berkelhamer provided me at University of California at Irvine.

### Supplementary Materials

www.sciencemag.org/content/342/6162/1060/suppl/DC1

10.1126/science.1230005

**A mixed picture.** Rising natural gas production may have economic benefits for countries like the United States, but will it help or harm efforts to protect the environment?

CREDIT: CORBIS/PAUL SOUDERS

ENERGY & NATURAL RESOURCES

# U.S. Natural Gas Boom Impacting Local Towns and Distant Nations

Thanks to new extraction methods such as hydraulic fracturing, or "fracking," the United States is newly flush with natural gas. After decades of importing a large amount of the nation's gas supply, the country is poised to become a net exporter of this fuel—although the benefits of doing so have been hotly debated.

The U.S. Department of Energy in September approved the development of a new liquid natural gas (LNG) export facility, which would be the fourth of its kind and the third to be approved in the last year. Nineteen other facilities have been proposed, although it's unlikely that they will all be built, due to intensifying global competition, according to Charles Ebinger, senior fellow and director of the energy security initiative at the Brookings Institution.

"There is no question that the scale of the gas revolution is unprecedented," Ebinger said. He and other experts considered the natural gas boom in two recent events at AAAS, where it became clear that the implications of this revolution—both positive and negative—are reaching from small American towns to nations on the other side of the globe. The first discussion, on 16 October, was an annual forum sponsored by Hitachi, Ltd., and co-organized by AAAS and the Brookings Institution.

For now, U.S. natural gas resources are largely staying on the North American continent, which has helped to keep energy prices relatively low in the United States. But countries such as Japan, which imports all of its gas and oil, are eager to take advantage of U.S. exports. Meanwhile, shale gas is set to take off in other regions of the world, such as Australia, the Middle East, and potentially Russia, according to Ebinger.

Greater energy independence for the United States could have implications around the world, said Nobuo Tanaka, global associate for energy security and sustainability at the Institute of Energy Economics, Japan, especially if the U.S. government decides to abandon its traditional role in keeping open oil and gas trade routes such as the Strait of Hormuz, leading out of the Persian Gulf. It is unknown at this point who might take over that role, Tanaka said.

Domestically, shale gas has been a windfall in some regions. In Ohio's 63rd district, an area just north of Youngstown, BP has spent $330 million on lease rights alone, according to state representative Sean J. O'Brien. The region has now become one of the fastest growing areas of the country, as the gas revolution has also brought a return of many manufacturing jobs.

The picture hasn't been completely rosy, however. Locally, O'Brien noted, people have been dealing with secondary effects of fracking, which involves injecting fluid into shale beds at high pressure. More trucks are on the roads, for example, and the burning off of methane produced in the extraction of natural gas can emit chemicals that exacerbate respiratory issues such as asthma.

Ohio is just one of the many locations for which fossil fuel extraction is a new issue, and many of these places are far more populous than previous hot spots for oil and gas, noted Gretchen Goldman, an analyst for the Center for Science and Democracy at the Union of Concerned Scientists.

The federal government has largely stayed out of regulating these new developments in shale gas, leaving the industry with a patchwork of regulations that vary from state to state and sometimes, as in Pennsylvania, town to town. The hands-off approach may work well for states such as Texas, where the regulation of fossil fuel exploration has a long history, Goldman said, but other states without this history may benefit from more federal guidance on managing the risks associated with oil and gas development.

In addition, the implications for the climate are often ignored in discussions of the natural gas rise, in part because this can be such a significant economic opportunity, noted Jonathan Fink, vice president for research and strategic partnerships at Portland State University in Oregon. "The short-term economic positives are drowning out the long-term climate negatives," he said. "How do we better integrate those two perspectives?"

A similar question emerged in another panel discussion at AAAS, on the global energy outlook between now and 2040. The 21 October forum was sponsored by Georgetown University's Program on Science in the Public Interest, AAAS, and the American Chemical Society.

Globally, natural gas consumption is expected to nearly double between 2010 and 2040, according to projections presented by Howard Gruenspecht, Deputy Administrator of the U.S. Energy Information Administration (EIA). Most of that increase will take place outside today's high-income countries—for example, in China and India, where economic growth is projected to drive a surge in energy use, and in the Middle East and Africa, where both economic and population growth are key drivers.

The World Bank sees access to energy services as "a huge global equity issue," said Vivien Foster, sector manager in the Sustainable Energy Department at the World Bank, whose president has joined the U.N. secretary-general as co-chairs of an initiative to achieve universal energy access by 2030.

But will it be possible to "make energy available for all without cooking the planet?" asked moderator Richard Harris of National Public Radio. Natural gas could serve as a bridge away from coal and petroleum-based fuels, because burning it produces less carbon and other pollutants. It is still a fossil fuel, however, and despite its cost advantage relative to alternatives such as nuclear and renewable power, its carbon emissions are higher than those options.

While the use of renewable energy sources is also expected to increase by 2040, particularly in the developed world, wind and solar likely will account for about 10% of the global electricity supply, compared to hydropower at about 15%, according to projections by ExxonMobil. Across all demand sectors, most of the world's use of renewable energy will come from biomass, said Rob Gardner, manager of the Economics and Energy Division of ExxonMobil's Corporate Strategic Planning Department. Likewise, the EIA estimates that without major changes in policy, the portion of the global energy mix coming from fossil fuels will decrease only modestly, from about 85% today to about 75% in 2040.

"It's still pretty much a fossil fuel world unless the world makes [very different] policy decisions," said Gruenspecht.

*–Sarah Zielinski and Kathy Wren*

## AAAS Kavli Science Journalism Award Winners Named

Stories about efforts to prevent the Asian carp from invading the Great Lakes, about evolutionary stress on endangered pupfish in the Mojave Desert, and about the use of "crowdsourcing" to solve tough biological problems are among the winners of the 2013 AAAS Kavli Science Journalism Awards.

**Large Newspaper—(Circulation of 100,000 or more):** Dan Egan, the Milwaukee *Journal Sentinel,* for "Deep Trouble," 19 August, 22 August, and 26 August 2012. The series examined why a seemingly radical solution, damming and reversing the flow of the Chicago River, may be necessary to protect the Great Lakes from the invasive Asian carp.

**Small Newspaper—(Circulation less than 100,000):** Azeen Ghorayshi, *East Bay Express,* for "Warning: Quake in 60 Seconds," 1 May 2013. Ghorayshi reported on the work of a group at the University of California, Berkeley, that has been developing an earthquake warning system, and she pointed out the wide gap between the United States and Japan in deployment of such systems.

**Magazine:** Hillary Rosner, *Wired,* for "Attack of the Mutant Pupfish," December 2012. Rosner described what happened when a few pupfish from a different species managed to infiltrate a refuge designed to preserve the endangered Devil's Hole pupfish in the Mojave Desert.

**Television—(Spot News/Feature Reporting, 20 minutes or less):** Joshua Seftel, NOVA scienceNOW, for "Adrien Treuille Profile," 14 November 2012. Seftel explained how a Carnegie Mellon University computer scientist harnessed the brainpower of thousands of people who play computer games as a way to help solve difficult biological problems such as protein folding.

**Television—(In-Depth Reporting, more than 20 minutes):** Dennis Wells, Linda Goldman, David Royle, Smithsonian Channel, for "Killer in the Caves," 13 March 2013. The winning program followed a bat expert and a wildlife manager in their fight against white-nose syndrome, a disease that is driving little brown bats, one of the most common bat species in the northeastern United States, toward extinction.

**Radio:** Howard Berkes, Andrea de Leon, Sandra Bartlett, NPR, and Chris Hamby, The Center for Public Integrity, for "As Mine Protections Fail, Black Lung Cases Surge" and "Black-Lung Rule Loopholes Leave Miners Vulnerable," 9 July and 10 July 2012. The segments described the resurgence of a disease once thought solved and weaknesses in regulatory science meant to protect coal miners.

**Radio: Certificate of Merit:** Ashley Ahearn, KUOW Public Radio, Seattle, for a three-part series on the potential health and environmental impacts of coal in the Pacific Northwest (11 March and 12 March 2013 and 18 June 2013).

**Online:** Phil McKenna, MATTER, for "Uprising: Can a self-trained scientist solve one of the biggest problems in energy policy?", 21 February 2013. McKenna, writing for an online site dedicated to long-form science journalism, described one man's hunt for natural gas leaks from urban distribution systems and their potential contribution to climate change.

**Children's Science News:** Barbara Lich, *GEOlino* magazine (Germany), for "Kaltwasserkorallen: Ein Paradies am Meeresgrund" ("Cold Water Corals: Paradise on the Seabed"), October 2012. Lich told her young readers about lesser-known cold water corals living hundreds of meters below the surface, a realm only reachable by a crewed submersible. The children's science news award, established in 2005, is the only AAAS Kavli award open to journalists from abroad, as well as the United States.

---

The awards, administered by AAAS since their inception in 1945, go to professional journalists for distinguished reporting for a general audience. The Kavli Foundation provided a generous endowment in 2009 that ensures the future of the awards program.

Independent panels of science journalists pick the winners, who will receive $3000 and a plaque at the 2014 AAAS Annual Meeting in Chicago in February. Learn more about the winning entries at www.aaas.org/sja2013.

*–Earl Lane*

ASSOCIATION AFFAIRS

# AAAS Members Elected as Fellows

In October 2013, the AAAS Council elected 388 members as Fellows of AAAS. These individuals will be recognized for their contributions to science and technology at the Fellows Forum to be held on 15 February 2014 during the AAAS Annual Meeting in Chicago, Illinois. The new Fellows will receive a certificate and a blue and gold rosette as a symbol of their distinguished accomplishments. Presented by section affiliation, they are:

### Section on Agriculture, Food, and Renewable Resources

Patrick F. Byrne, Colorado State Univ.
James J. Giovannoni, USDA-ARS/Boyce Thompson Institute at Cornell
Stewart M. Gray, USDA-ARS/Cornell Univ.
Rodney Allan Hill, Univ. of Idaho
Jonathan D. G. Jones, Univ. of East Anglia/The Sainsbury Laboratory (UK)
James E. Kinder, The Ohio State Univ.
Nora L.V. Lapitan, Colorado State Univ.
Tung-Ching Lee, Rutgers Univ.
John F. Leslie, Kansas State Univ.
Yiqi Luo, Univ. of Oklahoma
Bruce A. McDonald, ETH Zürich (Swiss Federal Institute of Technology)
Debra Mohnen, Univ. of Georgia
John C. Reese, Kansas State Univ.
James N. Seiber, Univ. of California, Davis
M. (Kay) Walker Simmons, USDA-ARS
Jean L. Steiner, USDA-ARS

### Section on Anthropology

Zeresenay Alemseged, California Academy of Sciences
W. Penn Handwerker, Univ. of Connecticut
Hidemi Ishida, Univ. of Shiga Prefecture (Japan)
Lisa Sattenspiel, Univ. of Missouri–Columbia
J. Josh Snodgrass, Univ. of Oregon
Matthew W. Tocheri, Smithsonian Institution National Museum of Natural History

### Section on Astronomy

Donald N. B. Hall, Univ. of Hawaii
Felix J. (Jay) Lockman, National Radio Astronomy Observatory
Nancy D. Morrison, Univ. of Toledo (retired)
Stephen S. Murray, Johns Hopkins Univ./Harvard-Smithsonian Astrophysical Observatory
William H. Press, The Univ. of Texas at Austin

### Section on Atmospheric and Hydrospheric Sciences

Lance F. Bosart, Univ. at Albany, SUNY
William Henry Brune III, Pennsylvania State Univ.
Arnold L. Gordon, Columbia Univ.
Jack A. Kaye, NASA
Ross J. Salawitch, Univ. of Maryland, College Park
Mark H. Thiemens, Univ. of California, San Diego

### Section on Biological Sciences

Alejandro Aballay, Duke Univ. Medical Center
Christopher Aiken, Vanderbilt Univ. School of Medicine
Geneviève Almouzni, Institut Curie (France)
L. Mario Amzel, Johns Hopkins Univ. School of Medicine
Allan Balmain, Univ. of California, San Francisco
Vann Bennett, Duke Univ. Medical Center
Ottar Nordal Bjørnstad, Pennsylvania State Univ.
Paul E. Bock, Vanderbilt Univ. School of Medicine
Alan Richard Brash, Vanderbilt Univ.
James R. Broach, Pennsylvania State Univ. College of Medicine
Jeffrey L. Brodsky, Univ. of Pittsburgh
Barry D. Bruce, Univ. of Tennessee, Knoxville
Linda Marie Brzustowicz, Rutgers Univ.
Ronald S. Burton, Univ. of California, San Diego
Frederic D. Bushman, Univ. of Pennsylvania Perelman School of Medicine
Bradley J. Cardinale, Univ. of Michigan
Dana Carroll, Univ. of Utah School of Medicine
Peter T. Cherbas, Indiana Univ.
Alan Douglas Cherrington, Vanderbilt Univ. School of Medicine
Richard Michael Clark, Univ. of Utah
Garry Thomas Cole, The Univ. of Texas at San Antonio
Philip Arthur Cole, Johns Hopkins Univ. School of Medicine
Keith A. Crandall, The George Washington Univ.
Craig Martin Crews, Yale Univ.
Andrew Dancis, Univ. of Pennsylvania Perelman School of Medicine
Katayoon (Katie) Dehesh, Univ. of California, Davis
Job Dekker, Univ. of Massachusetts Boston Medical School
Concetta Christine DiRusso, Univ. of Nebraska–Lincoln
Walter K. Dodds, Kansas State Univ.
Anne M. Dranginis, St. John's Univ.
Caroline Alice Enns, Oregon Health & Science Univ.
John W. Fleeger, Louisiana State Univ.
J. Kevin Foskett, Univ. of Pennsylvania
Gordon A. Fox, Univ. of South Florida
John V. Freudenstein, The Ohio State Univ.
Robert L. Geahlen, Purdue Univ.
Anne E. Giblin, Marine Biological Laboratory
David Benjamin Goldstein, Duke Univ.
Barry M. Gumbiner, Univ. of Virginia School of Medicine
Steven James Hallam, Univ. of British Columbia (Canada)
Oliver Hankinson, Univ. of California, Los Angeles
Mark Edward Hay, Georgia Institute of Technology
Terry Clyde Hazen, Univ. of Tennessee, Knoxville
John D. Helmann, Cornell Univ.
Wim G. J. Hol, Univ. of Washington
Helen Frances James, Smithsonian Institution National Museum of Natural History
John Gene Jelesko, Virginia Tech
Stefan Peter Jentsch, Max Planck Institute for Biochemistry (Germany)
Norman F. Johnson, The Ohio State Univ.
Patricia A. Johnson, Cornell Univ.
Alan C. Kamil, Univ. of Nebraska–Lincoln
Sophien Kamoun, The Sainsbury Laboratory (UK)
Matthew David Kane, National Science Foundation
William H. Karasov, Univ. of Wisconsin–Madison
Donald W. Kaufman, Kansas State Univ.
John Klironomos, Univ. of British Columbia (Canada)
George M. Langford, Syracuse Univ.
Fred David Ledley, Bentley Univ.
Daniel V. Lim, Univ. of South Florida
Kenneth J. Lohmann, Univ. of North Carolina at Chapel Hill
Jeffrey R. Lucas, Purdue Univ.
Julin N. Maloof, Univ. of California, Davis
Peter Philip Marra, Smithsonian Conservation Biology Institute
Robert E. Maxson Jr., Keck School of Medicine of the Univ. of Southern California
John H. McCusker, Duke Univ. Medical Center
David W. Meinke, Oklahoma State Univ.
David Milton Miller III, Vanderbilt Univ.
Kevin A. Morano, The Univ. of Texas Medical School at Houston
William W. Murdoch, Univ. of California, Santa Barbara
Kenneth H. Nealson, Univ. of Southern California
Carole Ober, The Univ. of Chicago
John J. Obrycki, Univ. of Kentucky
Richard Simon Ostfeld, Cary Institute of Ecosystem Studies
Richard A. Padgett, Cleveland Clinic
Dianna K. Padilla, Stony Brook Univ., SUNY
Tej Krishan Pandita, The Univ. of Texas Southwestern Medical Center
Rohit V. Pappu, Washington Univ. in St. Louis
James Gerard Patton, Vanderbilt Univ.
Daniel Pauly, Univ. of British Columbia (Canada)
David H. Price, Univ. of Iowa
Elizabeth C. Raff, Indiana Univ.
Philip A. Rea, Univ. of Pennsylvania
Matthew R. Redinbo, Univ. of North Carolina at Chapel Hill
Bing Ren, Ludwig Institute for Cancer Research/Univ. of California, San Diego School of Medicine
Michael A. Rex, Univ. of Massachusetts, Boston
David F. Ritchie, North Carolina State Univ.
Marsha Rich Rosner, Univ. of Chicago
Matthew S. Sachs, Texas A&M Univ.
Ranjan Sen, NIH/National Institute on Aging
Tom H. Stevens, Univ. of Oregon
Zucai Suo, The Ohio State Univ.
John J. G. Tesmer, Univ. of Michigan
George F. Vande Woude, Van Andel Institute
Gregory L. Verdine, Harvard Univ.


Published by AAAS

Veronica J. Vieland, Nationwide Children's Hospital
Karen Heather Vousden, Cancer Research UK Beatson Institute
Peter Anthony Weil, Vanderbilt Univ. School of Medicine
Diana E. Wheeler, Univ. of Arizona
Malcolm E. Winkler, Indiana Univ.
Alan E. Winter, Genome British Columbia (Canada)
Sandra L. Wolin, Yale Univ. School of Medicine
Charles Wood, Univ. of Nebraska–Lincoln
Richard D. Wood, The Univ. of Texas MD Anderson Cancer Center
Yuan Zhuang, Duke Univ. Medical Center

### Section on Chemistry

Perla Beatriz Balbuena, Texas A&M Univ.
Kevin D. Belfield, Univ. of Central Florida
Squire J. Booker, Pennsylvania State Univ.
Robert H. Byrne, Univ. of South Florida
Gary S. Calabrese, Corning Incorporated
Seth M. Cohen, Univ. of California, San Diego
Steven D. Conradson, Los Alamos National Laboratory
Katharine Covert, National Science Foundation
Stephen Lawrence Craig, Duke Univ.
Stephen P. Cramer, Univ. of California, Davis/Lawrence Berkeley National Laboratory
Debbie C. Crans, Colorado State Univ.
Norman Marvin Edelstein, Lawrence Berkeley National Laboratory
Ron Elber, The Univ. of Texas at Austin
M. Samy El-Shall, Virginia Commonwealth Univ.
David S. Ginley, National Renewable Energy Laboratory
Yvan Guindon, Institut de recherches cliniques de Montréal (Canada)
Sharon Hammes-Schiffer, Univ. of Illinois at Urbana-Champaign
Bryan F. Henson, Los Alamos National Laboratory
Lyle D. Isaacs, Univ. of Maryland, College Park
Samuel P. Kounaves, Tufts Univ.
Donald M. Kurtz Jr., The Univ. of Texas at San Antonio
Patrick Alan Limbach, Univ. of Cincinnati
Katrina Marie Miranda, Univ. of Arizona
Kenton J. Moody, Lawrence Livermore National Laboratory
Nicos A. Petasis, Univ. of Southern California
Blake Robert Peterson, Univ. of Kansas
Tijana Rajh, Argonne National Laboratory
Charles G. Riordan, Univ. of Delaware
Oliver Sacks, New York Univ. School of Medicine
Peter G. Schultz, Scripps Research Institute
Robert A. Scott, Univ. of Georgia
Lynda Soderholm, Argonne National Laboratory
Nicola A. Spaldin, ETH Zürich (Swiss Federal Institute of Technology)
Kosta Steliou, Boston Univ. School of Medicine
Albert E. Stiegman, Florida State Univ.
Jay A. Switzer, Missouri Univ. of Science and Technology
Bradley M. Tebo, Oregon Health & Science Univ.
Joseph L. Templeton, Univ. of North Carolina at Chapel Hill
Tehshik P. Yoon, Univ. of Wisconsin–Madison
Junfeng (Jim) Zhang, Duke Univ.

### Section on Dentistry and Oral Health Sciences

Troy Edward Daniels, Univ. of California, San Francisco
Matthew Philip Hoffman, NIH/National Institute of Dental and Craniofacial Research
Peter X. Ma, Univ. of Michigan School of Dentistry & College of Engineering
Cindy L. Munro, Univ. of South Florida
John Timothy Wright, Univ. of North Carolina at Chapel Hill

### Section on Education

Joan S. Bissell, California State Univ.
Judy Diamond, Univ. of Nebraska–Lincoln
D. Ellen M. Granger, Florida State Univ.
Catherine E. Milne, New York Univ.
Muriel E. Poston, Pitzer College
C. Gary Reiness, Lewis & Clark College
Patricia E. Simmons, North Carolina State Univ.
Harold B. White III, Univ. of Delaware
Adele Judith Wolfson, Wellesley College

### Section on Engineering

François Baneyx, Univ. of Washington
Mark A. Barteau, Univ. of Michigan
Stephen A. Boppart, Univ. of Illinois at Urbana–Champaign
James J. Collins, Boston Univ.
Harold G. Craighead, Cornell Univ.
Horacio Dante Espinosa, Northwestern Univ.
Glenn H. Fredrickson, Univ. of California, Santa Barbara
Sharon C. Glotzer, Univ. of Michigan
Kenneth E. Goodson, Stanford Univ.
Kevin Edward Healy, Univ. of California, Berkeley
Kanti Jain, Univ. of Illinois at Urbana–Champaign
Ali Khademhosseini, Brigham and Women's Hospital/Harvard Medical School
William P. King, Univ. of Illinois at Urbana–Champaign
Klaus S. Lackner, Columbia Univ.
Robert Samuel Langer, Massachusetts Institute of Technology
Cato Thomas Laurencin, Univ. of Connecticut Health Center
Frances S. Ligler, North Carolina State Univ./Univ. of North Carolina at Chapel Hill
Bruce Ernest Logan, Pennsylvania State Univ.
Hang Lu, Georgia Institute of Technology
Glenn E. Lucas, Univ. of California, Santa Barbara
Mia K. Markey, The Univ. of Texas at Austin
Suresh Menon, Georgia Institute of Technology
Adrienne R. Minerick, Michigan Technology Univ.
Brij M. Moudgil, Univ. of Florida
Carlo Uberto Segre, Illinois Institute of Technology
David N. Seidman, Northwestern Univ.
Shankar Subramaniam, Univ. of California, San Diego
Grétar Tryggvason, Univ. of Notre Dame
Bruce C. Wheeler, Univ. of Florida
Xi-Cheng Zhang, Univ. of Rochester/Huazhong Univ. of Science and Technology (China)

### Section on General Interest in Science and Engineering

Dominique Brossard, Univ. of Wisconsin–Madison
Susan Gaidos, Freelance Science Journalist
Francesca T. Grifo, Union of Concerned Scientists
Julia A. Moore, The Pew Charitable Trusts
Ginger Pinholster, American Association for the Advancement of Science
David F. Salisbury, Vanderbilt Univ.

### Section on Geology and Geography

John A. Agnew, Univ. of California, Los Angeles
Sherilyn Claire Fritz, Univ. of Nebraska–Lincoln
Kevin P. Furlong, Pennsylvania State Univ.
Thomas A. Herring, Massachusetts Institute of Technology
Malcolm Hughes, Univ. of Arizona
Thomas C. Johnson, Univ. of Minnesota Duluth
Alan M. MacEachren, Pennsylvania State Univ.
David Lachlan Meyer, Univ. of Cincinnati
Arnold I. Miller, Univ. of Cincinnati
Jean-Bernard Minster, Scripps Institution of Oceanography, Univ. of California San Diego
Walter Clarkson Pitman III, Lamont-Doherty Geological Observatory
James E. Quick, Southern Methodist Univ.
Henry P. Schwarcz, McMaster Univ. (Canada)

### Section on History and Philosophy of Science

James Bogen, Univ. of Pittsburgh
Jonathan C. Coopersmith, Texas A&M Univ.
Karen A. Rader, Virginia Commonwealth Univ.
Rose-Mary Sargent, Merrimack College

### Section on Industrial Science and Technology

Sudarsanam Suresh Babu, Univ. of Tennessee, Knoxville/Oak Ridge National Laboratory
Martin Keller, Oak Ridge National Laboratory
Proctor Page Reid, National Academy of Engineering
James M. Utterback, Massachusetts Institute of Technology

### Section on Information, Computing, and Communication

Nancy M. Amato, Texas A&M Univ.
Duncan A. Buell, Univ. of South Carolina
Henrik Iskov Christensen, Georgia Institute of Technology
Jeffrey Dean, Google, Inc.
Carla P. Gomes, Cornell Univ.
Ananth Grama, Purdue Univ.
Robert L. Grossman, Univ. of Chicago
Thomas A. Henzinger, Institute of Science and Technology Austria
Charles E. Leiserson, Massachusetts Institute of Technology
Deborah L. McGuinness, Rensselaer Polytechnic Univ.
Sudeep Sarkar, Univ. of South Florida
Alvy Ray Smith, Ars Longa
Mark A. Stalzer, California Institute of Technology

### Section on Linguistics and Language Sciences

Joseph Aoun, Northeastern Univ.
Ian Maddieson, Univ. of New Mexico
Wayne O'Neil, Massachusetts Institute of Technology
Douglas H. Whalen, City Univ. of New York/Haskins Laboratories


Published by AAAS

### Section on Mathematics

Steven F. Ashby, Pacific Northwest National Laboratory
Christian Borgs, Microsoft Research
Robert P. Lipton, Louisiana State Univ.
David C. Manderscheid, The Ohio State Univ.
Qing Nie, Univ. of California, Irvine
Philip Protter, Columbia Univ.
Shmuel Weinberger, Univ. of Chicago

### Section on Medical Sciences

Michael Andreeff, The Univ. of Texas MD Anderson Cancer Center
Carlos L. Arteaga, Vanderbilt Univ. School of Medicine
Robert Daniel Beauchamp, Vanderbilt Univ. School of Medicine
Donald M. Bers, Univ. of California, Davis
James B. Bliska, Stony Brook Univ., SUNY
Marc G. Caron, Duke Univ. Medical Center
John M. Coffin, Tufts Univ. School of Medicine
Timothy L. Cover, Vanderbilt Univ. School of Medicine
Robin L. Davisson, Cornell Univ. College of Veterinary Medicine/Weill Cornell Medical College
George S. Deepe Jr., Univ. of Cincinnati College of Medicine
Ethan Dmitrovsky, The Univ. of Texas MD Anderson Cancer Center
Robert W. Doms, Univ. of Pennsylvania Perelman School of Medicine
Ferric C. Fang, Univ. of Washington School of Medicine
Toren Finkel, NIH/National Heart, Lung and Blood Institute
Walter R. Frontera Roura, Vanderbilt Univ. School of Medicine
Frank Davis Gilliland, Keck School of Medicine of the Univ. of Southern California
James Richard Goldenring, Vanderbilt Univ. School of Medicine/Nashville VA Medical Center
Sandra Lee Hofmann, The Univ. of Texas Southwestern Medical Center
Michael J. Holtzman, Washington Univ. School of Medicine in St. Louis
Michael B. Kastan, Duke Univ.
Karl D. Kieburtz, Univ. of Rochester School of Medicine & Dentistry
Robert J. Lefkowitz, Duke Univ. Medical Center
MacRae Fort Linton, Vanderbilt Univ. School of Medicine
Fu-Tong Liu, Academia Sinica (Taiwan)/Univ. of California, Davis
Kevin C. Kent Lloyd, Univ. of California, Davis School of Medicine
Mark Alan Magnuson, Vanderbilt Univ. School of Medicine
Rob McConnell, Keck School of Medicine of the Univ. of Southern California
Paul B. McCray Jr., Univ. of Iowa Carver College of Medicine
Frederick J. Meyers, Univ. of California, Davis School of Medicine
Charles Emerson Murry, Univ. of Washington
M. Bishr Omary, Univ. of Michigan Medical School
Heloise Anne Pereira, Univ. of Oklahoma Health Sciences Center
Edward F. Plow, Cleveland Clinic
David Robertson, Vanderbilt Univ. School of Medicine
Diane M. Robins, Univ. of Michigan Medical School
Marc Elliot Rothenberg, Univ. of Cincinnati College of Medicine/Cincinnati Children's Hospital
Samuel A. Santoro, Vanderbilt Univ. School of Medicine
Timothy Alan Springer, Boston Children's Hospital/Harvard Medical School
John L. Sullivan, Univ. of Massachusetts Medical School
Luke I. Szweda, Oklahoma Medical Research Foundation
Joel E. Tepper, Univ. of North Carolina at Chapel Hill
David M. Virshup, Duke-NUS Graduate Medical School (Singapore)

### Section on Neuroscience

Scott Thomas Brady, Univ. of Illinois at Chicago
Steven J. Burden, New York Univ. Langone Medical Center
Valina Lynn Dawson, Johns Hopkins Univ. School of Medicine
Bart De Strooper, Katholieke Universiteit Leuven (Belgium)
Gordon L. Fain, Univ. of California, Los Angeles
Herbert M. Geller, NIH/National Heart, Lung and Blood Institute
Bernardino Ghetti, Indiana Univ. School of Medicine
Scott T. Grafton, Univ. of California, Santa Barbara
Nobutaka Hirokawa, Univ. of Tokyo Graduate School of Medicine (Japan)
Ole Isacson, McLean Hospital/Harvard Medical School
Brian K. Kaspar, Nationwide Children's Hospital
Eric Klann, New York Univ.
Theresa M. Lee, Univ. of Tennessee, Knoxville
John E. Lisman, Brandeis Univ.
Joan F. Lorden, Univ. of North Carolina at Charlotte
James O'Connell McNamara, Duke Univ. Medical Center
Lin Mei, Georgia Regents Univ. Medical College of Georgia
Craig Montell, Univ. of California, Santa Barbara
Wolf Singer, Max Planck Institute for Brain Research/ Ernst Strüngmann Institute for Neuroscience (Germany)
Olaf Sporns, Indiana Univ.
Leslie Michels Thompson, Univ. of California, Irvine
Flora M. Vaccarino, Yale Univ. School of Medicine
Berislav V. Zlokovic, Keck School of Medicine of the Univ. of Southern California

### Section on Pharmaceutical Sciences

Joseph Thomas DiPiro, Medical Univ. of South Carolina/Univ. of South Carolina
Richard A. Houghten, Torrey Pines Institute for Molecular Studies
Paul A. Newhouse, Vanderbilt Univ. School of Medicine
Peter Charles Preusch, NIH/National Institute of General Medical Sciences
John A. Secrist III, Southern Research Institute
Miguel Angel Villalona-Calero, The Ohio State Univ.

### Section on Physics

Daniela Bortoletto, Univ. of Oxford (UK)
Édouard Brézin, École Normale Supérieure (France)
Jean-Christophe Charlier, Université catholique de Louvain (Belgium)
Giulia Galli, Univ. of Chicago
Ronald Gilman, Rutgers Univ.
Thomas Glasmacher, Michigan State Univ.
Donald L. Hartill, Cornell Univ.
Beverly Karplus Hartline, Montana Tech
David A. Huse, Princeton Univ.
Andreas S. Kronfeld, Fermi National Accelerator Laboratory
Glen Lambertson, Lawrence Berkeley National Laboratory
M. Cristina Marchetti, Syracuse Univ.
Charles M. Marcus, Univ. of Copenhagen (Denmark)
Laszlo Mihaly, Stony Brook Univ., SUNY
Andrew J. Millis, Columbia Univ.
David Julian Sellmyer, Univ. of Nebraska–Lincoln
Didier Sornette, ETH Zürich (Swiss Federal Institute of Technology)
C. Megan Urry, Yale Univ.
Nikos Varelas, Univ. of Illinois at Chicago

### Section on Psychology

Toni Claudette Antonucci, Univ. of Michigan
Eugene Borgida, Univ. of Minnesota Twin Cities
John P. Capitanio, Univ. of California, Davis/California National Primate Research Center
Leonard H. Epstein, Univ. at Buffalo School of Medicine & Biomedical Sciences, SUNY
Mark Stuart Goldman, Univ. of South Florida
Eileen Kowler, Rutgers Univ.
Helen S. Mayberg, Emory Univ. School of Medicine

### Section on Social, Economic, and Political Sciences

Ann Bostrom, Univ. of Washington
Paul D. Cleary, Yale Univ.
Peter Lange, Duke Univ.
Alberto Palloni, Univ. of Wisconsin–Madison

### Section on Societal Impacts of Science and Engineering

Jay Apt, Carnegie Mellon Univ.
Steven C. Currall, Univ. of California, Davis
Michele S. Garfinkel, European Molecular Biology Organization (Germany)
Joseph R. Herkert, Arizona State Univ.
Anne-Marie Carroll Mazza, National Academy of Sciences

### Section on Statistics

Raymond J. Carroll, Texas A&M Univ.
Keith N. Crank, Retired
Barry R. Davis, The Univ. of Texas School of Public Health
Kim-Anh Do, The Univ. of Texas MD Anderson Cancer Center
Mark Scott Kamlet, Carnegie Mellon Univ.
Bani K. Mallick, Texas A&M Univ.
H. Joseph Newton, Texas A&M Univ.
Stephen W. Pierson, American Statistical Association
Robert T. Smythe, Oregon State Univ.
Michael Stein, Univ. of Chicago


Published by AAAS

# The Innate Growth Bistability and Fitness Landscapes of Antibiotic-Resistant Bacteria

J. Barrett Deris, Minsu Kim, Zhongge Zhang, Hiroyuki Okano, Rutger Hermsen, Alexander Groisman, Terence Hwa*

READ THE FULL ARTICLE ONLINE
http://dx.doi.org/10.1126/science.1237435

Cite this article as J. B. Deris *et al.*, *Science* **342**, 1237435 (2013).
DOI: 10.1126/science.1237435

**Introduction:** Understanding how bacteria harboring antibiotic resistance grow in the presence of antibiotics is critical for predicting the spread and evolution of drug resistance. Because drugs inhibit cell growth and a cell's growth state globally influences its gene expression, the expression of drug resistance is subject to an innate, growth-mediated feedback, leading to complex behaviors that affect both the characterization and the prevention of antibiotic resistance. We characterized the consequences of this feedback for the growth of antibiotic-resistant bacteria.

**Methods:** We studied the growth of *Escherichia coli* strains expressing resistance to translation-inhibiting antibiotics, by using both bulk and single-cell techniques. The growth of each strain was quantified in a broad range of drug concentrations by using time-lapse microscopy (to track the responses of individual cells to antibiotics inside a microfluidic chemostat) and by the enrichment of batch cultures for nongrowing cells. We formulated a quantitative phenomenological model to predict the growth rates of drug-resistant strains in the presence of drugs, based on the well-characterized biochemistry of drug and drug-resistance interactions and on bacterial growth laws that dictate relations between cell growth and gene expression. We tested the model predictions for various drugs and resistance mechanisms by constructing strains that constitutively express varying degrees of drug resistance.

**Results:** In strains expressing a moderate degree of drug resistance, growth rates dropped abruptly above a critical drug concentration, the minimum inhibitory concentration (MIC), whose value increased linearly with the basal level of resistance expression (see figure below, panel A). Cells exhibited growth bistability over a broad range of drug concentrations below the MIC: Isogenic cells expressing drug resistance coexisted in growing and nongrowing states in a homogeneous environment (panel B). Our model accurately predicted the range of drug concentrations in which growth bistability occurred, as well as the growth rates of the growing subpopulation, without any ad hoc fitting parameters. These findings reveal a plateau-like fitness landscape (panel A), which can be used to study the evolution of drug resistance in environments with varying drug concentrations.

**Discussion:** The broad occurrence of growth bistability in drug-resistant bacteria challenges the common notions and measures of drug efficacy and resistance. And because growth bistability can arise without complex regulation when gene expression is coupled to the state of cell growth, similar physiological links may underlie the growth bistability implicated in causing bacterial persistence. The availability of quantitative, predictive models will facilitate the formulation of strategies to limit the efficacy and evolvability of drug resistance.

## FIGURES IN THE FULL ARTICLE



## SUPPLEMENTARY MATERIALS



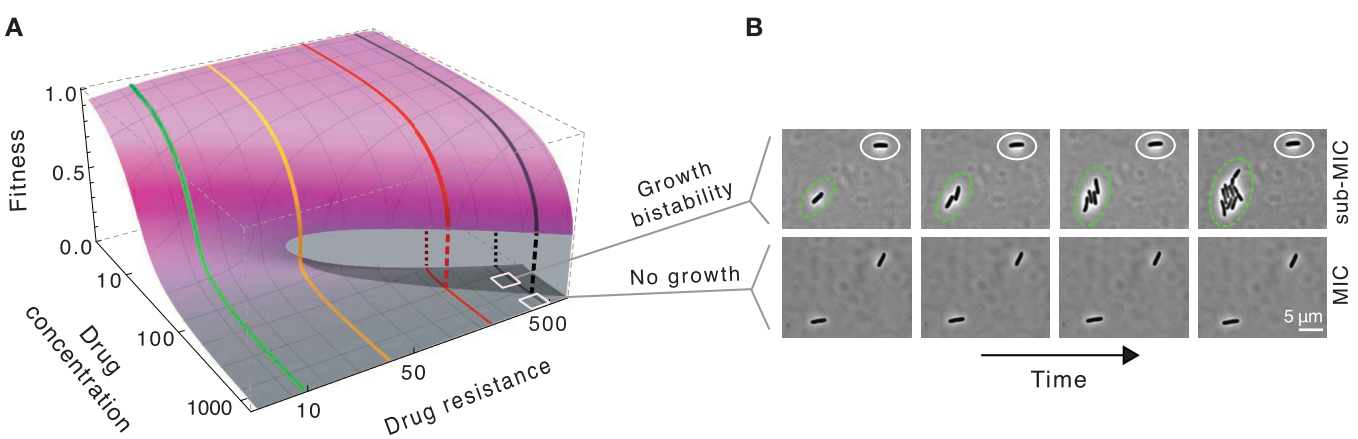


**Fitness landscape and growth bistability.** (**A**) This fitness landscape describes the fitness, or growth rates, of bacterial strains exposed to antibiotics (colored lines indicate the fitness of four example strains). Fitness drops abruptly at high drug concentrations. The shaded area shows a broad region of growth bistability, throughout which we observe that genetically identical cells possessing drug resistance are split into subpopulations of growing and nongrowing cells in response to antibiotics (**B**, top).

The list of author affiliations is available in the full article online.
*Corresponding author. E-mail: hwa@ucsd.edu

# The Innate Growth Bistability and Fitness Landscapes of Antibiotic-Resistant Bacteria

J. Barrett Deris,[1,2]* Minsu Kim,[1]*† Zhongge Zhang,[3] Hiroyuki Okano,[1] Rutger Hermsen,[1,2]‡ Alexander Groisman,[1] Terence Hwa[1,2,3]§

To predict the emergence of antibiotic resistance, quantitative relations must be established between the fitness of drug-resistant organisms and the molecular mechanisms conferring resistance. These relations are often unknown and may depend on the state of bacterial growth. To bridge this gap, we have investigated *Escherichia coli* strains expressing resistance to translation-inhibiting antibiotics. We show that resistance expression and drug inhibition are linked in a positive feedback loop arising from an innate, global effect of drug-inhibited growth on gene expression. A quantitative model of bacterial growth based on this innate feedback accurately predicts the rich phenomena observed: a plateau-shaped fitness landscape, with an abrupt drop in the growth rates of cultures at a threshold drug concentration, and the coexistence of growing and nongrowing populations, that is, growth bistability, below the threshold.

The appearance of bacterial strains with broad antibiotic resistance is becoming an alarming global health concern. The rapidity with which drug resistance has emerged over the past 30 years, for both natural and synthetic antibiotics, exposes a glaring lack of understanding of drug-bacteria interaction and its evolution (*1*, *2*). Although thousands of genetic adaptations that enable drug resistance have been identified, this knowledge has not yet revealed how and when these adaptations will arise, that is, the underlying principles that determine the evolutionary pathways to drug resistance (*3*–*5*).

Although the success of a particular drug-resistant strain might depend on many factors, one of the most basic factors to consider is the nature of bacterial growth during antibiotic treatment. This is especially critical for resistance mechanisms evolved de novo, during early stages of evolution when drug resistance emerges in incremental steps (*3*, *6*, *7*). It is desirable to characterize the interaction between drug and drug resistance in exponentially growing cells because, during an infection, the number of bacteria can increase exponentially for many days (*8*, *9*); indeed, even as the host's immune response reduces the overall number of bacteria, individual bacteria that have yet to be killed are still estimated to grow at typical in vitro rates, doubling up to once or twice per hour for some pathogens (*10*, *11*). However, elucidating this interaction in growing cells is challenging because the expression of drug resistance genes, like the expression of any other gene, is often intimately coupled to the growth status of the bacteria (*12*–*18*).

In particular, translation-inhibiting antibiotics have been shown to reduce the expression of both regulated and constitutively expressed genes because of growth-mediated global effects (*16*, *17*). If one of these gene products provides some degree of antibiotic resistance, then growth inhibition can reduce expression of resistance; the diminished resistance can in turn allow the drug to further inhibit growth in a positive feedback loop (fig. S1), driving the cell into a stable nongrowing state after a transient slowdown in cell growth. Frequently, gene regulatory systems with positive feedback exhibit a switchlike behavior when, for example, intrinsic fluctuations in gene expression exceed some threshold (*19*, *20*). This is often accompanied by bifurcation of a genetically homogeneous culture into two subpopulations with distinct phenotypes, which is called bistability (*19*, *20*). In the context of antibiotic resistance, this would be manifested as a "growth bistability," that is, growing and nongrowing cells coexisting in a homogeneous environment.

[1]Department of Physics, University of California at San Diego, La Jolla, CA 92093–0374, USA. [2]Center for Theoretical Biological Physics, University of California at San Diego, La Jolla, CA 92093–0374, USA. [3]Section of Molecular Biology, Division of Biological Sciences, University of California at San Diego, La Jolla, CA 92093, USA.

*These authors contributed equally to this work.
†Present address: Department of Physics, Emory University, Atlanta, GA 30322, USA.
‡Present address: Theoretical Biology and Bioinformatics Group, Department of Biology, Faculty of Science, Utrecht University, Padualaan 8, 3584 CH Utrecht, Netherlands.
§Corresponding author. E-mail: hwa@ucsd.edu

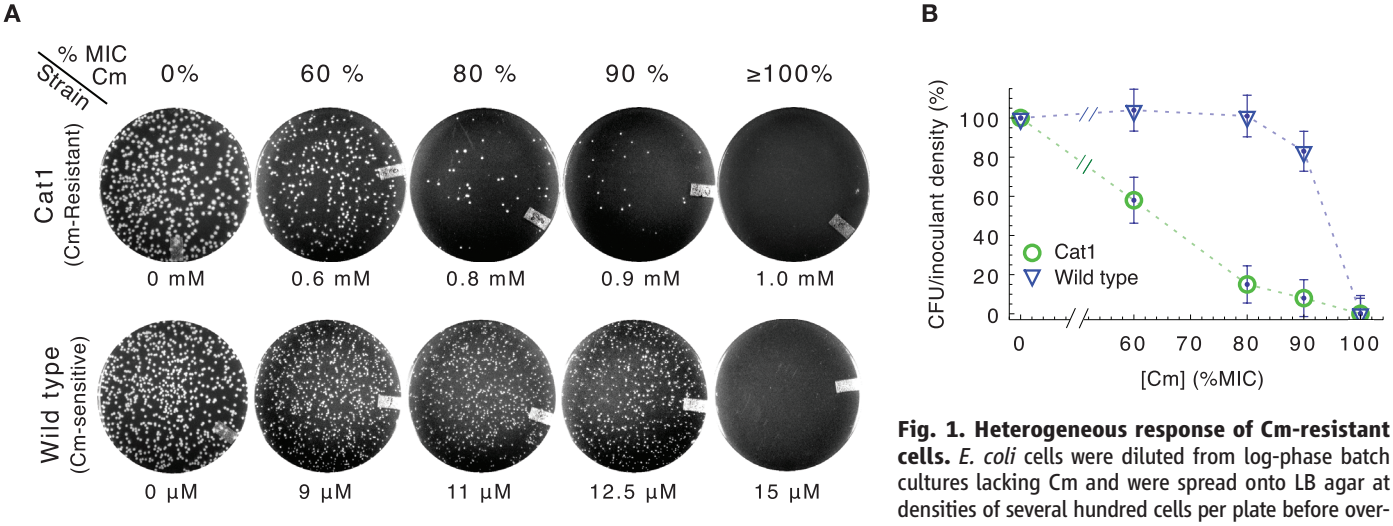


**Fig. 1. Heterogeneous response of Cm-resistant cells.** *E. coli* cells were diluted from log-phase batch cultures lacking Cm and were spread onto LB agar at densities of several hundred cells per plate before overnight incubation at 37°C. (**A**) Typical plate images of Cm-resistant Cat1 (top row) and Cm-sensitive wild-type (bottom row) cells, with Cm concentration indicated below each plate and also given above as approximate fraction of the empirically determined $MIC_{plate}$ for each strain (figs. S2A and S3A). (**B**) Percentage of viable cells grown on Cm-LB plates, CAT-expressing cells (Cat1, green), and wild-type cells (EQ4, blue). Error bars estimate SD of CFU, assuming Poisson-distributed colony appearance.

To characterize the nature of drug–drug resistance interactions and the possible occurrence of growth bistability, we studied the growth of various *Escherichia coli* strains constitutively expressing varying degrees of resistance to translation-inhibiting antibiotics. Our observations at both population and single-cell levels show that drug-resistant strains exhibit many signatures of growth bistability in response to antibiotics, contradicting the naïve expectation that constitutive expression of drug resistance in a population of cells will provide uniform protection against the drug. As will be shown, a heterogeneous effect of antibiotics on genetically identical cells challenges common notions and measures of drug efficacy and resistance and exposes both limitations and opportunities for treatment strategies.

We proceed to develop a simple mathematical model that effectively captures the origins of the observed behaviors and accurately predicts the growth rates of antibiotic-resistant cells in the presence of drugs without invoking any ad hoc fitting parameters. These results reveal a plateau-like fitness landscape that describes an abrupt transition between growth and growth inhibition for strains expressing a broad range of drug resistance subjected to a broad range of drug concentrations. Quantitative knowledge of the fitness landscape is vital for understanding and predicting the evolvability of drug resistance, for example, the acquisition of antibiotic resistance in a stepwise manner.

## Results

### Heterogeneous Responses to Antibiotics

Antibiotic susceptibility is typically assayed by counting the colonies formed after bacteria are spread onto agar plates containing various concentrations of antibiotics (*21*). If these cells exhibit growth bistability, then only the growing fraction of the inoculant cells will form colonies. To test for this heterogeneous response, we characterized the fraction of colonies formed by various strains of *E. coli* growing on agar in the presence of chloramphenicol (Cm), one of the oldest and most-studied translation-inhibiting antibiotics (*22*). We studied strains that express the Cm-resistance enzyme chloramphenicol acetyltransferase (CAT), which modifies and deactivates Cm according to well-characterized biochemistry (*23*). CAT enzymes are expressed constitutively in our strains, just as they (and many other drug-resistance enzymes and pumps) are often found in the wild (*24*–*27*).

Overnight incubation of CAT-expressing strains on Cm agar plates revealed signs of population-level heterogeneity. For one such strain, Cat1 (table S1), the number of colony-forming units (CFU) decreased gradually on plates with increasing Cm concentrations [Fig. 1A (top) and fig. S2B]. Thus, only a fraction of the plated cells formed visible colonies (Fig. 1B, circles), even at concentrations well below the empirical minimal inhibitory concentration at which colony formation is completely inhibited ($MIC_{plate}$, fig. S2A). It is unlikely that heterogeneity arose from spontaneous mutation because repeating the experiment using a single colony isolated at 90% $MIC_{plate}$ produced qualitatively similar results (with CFU decreasing at intermediate drug levels, fig. S2, C and D). In contrast, the CFU count of CAT-less wild-type cells (strain EQ4) remained high until complete inhibition at $MIC_{plate}$ [Fig. 1A (bottom) and fig. S3], indicating that the vast majority of plated cells grew up to the MIC (Fig. 1B, triangles).

### Direct Observation of Growth Bistability by Microscopy

To verify the coexistence of growing and nongrowing cells directly, we used a microfluidic device in which the growth of individual (immotile) cells could be tracked with time-lapse microscopy for extended periods (*28*) as they grew in the presence of Cm. The device provides a steady supply of fresh medium to many growth chambers, whose heights are adjusted to be slightly larger than the width of a single bacterium (~1 μm), allowing cells to grow for up to about nine generations into monolayer colonies in each chamber (fig. S4). Immotile CAT-expressing cells (Cat1m) growing exponentially in Cm-free batch culture were transferred to the microfluidic device and were allowed to continue growing exponentially for several generations before switching to growth medium with Cm (see Materials and Methods). With 0.9 mM Cm (90% of $MIC_{plate}$) in the medium, 70% of the cells stopped growing; nongrowing and growing cells were often observed side by side in the same chamber (Fig. 2A and movie S1). Eventually, it became impossible to track these nongrowing cells that were adjacent to growing populations because of overcrowding. By tracking some nongrowing cells that were far away from growing populations, we observed that this growth bimodality persisted for the duration of observation (up to 24 hours) because cells rarely switched between the growing and nongrowing states at 0.9 mM Cm (less than 1%).

One possible explanation for the sustained presence of nongrowing cells is that these cells did not have the *cat* gene at the beginning of the experiment. To see whether the heterogeneous response observed was due to (unintended) heterogeneity in genotype (for example, contamination), we reduced Cm concentration in the chambers from 0.9 to 0.1 mM, a concentration well above the MIC of Cm-sensitive cells (fig. S3). Many nongrowing cells began growing again, sometimes within ~5 hours of the Cm downshift (Fig. 2B and movie S2), indicating that previously nongrowing cells carried the *cat* gene and were viable [although Cm can be bactericidal at high concentrations (*29*)]. Thus, the population of cells in the nongrowing state was stable at 0.9 mM Cm (at least over the 24-hour period tested) but unstable at 0.1 mM Cm, suggesting that growth bistability might only occur at higher Cm concentrations.

Repeating this characterization for Cat1m cells at different Cm concentrations revealed that the fraction of cells that continued to grow decreased gradually with increasing concentration of the Cm added (Fig. 2C, height of colored bars), qualitatively consistent with the Cm-plating results for Cat1 cells (Fig. 1B). At concentrations up to 0.9 mM Cm, the growing populations grew exponentially, with their growth rate decreasing only moderately (by up to ~50%) with increasing Cm concentrations [Fig. 2, C (hue) and D (green symbols)]. Growing populations disappeared completely for [Cm] ≥ 1.0 mM, marking an abrupt drop in growth between 0.9 and 1.0 mM Cm (green and black symbols in Fig. 2D). This behavior contrasts with that observed for the Cm-sensitive wild type, in which nearly all cells continued growing over the entire range of subinhibitory Cm concentrations tested in the microfluidic device (Fig. 2E). This result is consistent with the response of wild-type cells to Cm on agar plates (Fig. 1), indicating that growth in subinhibitory concentrations of Cm per se does not necessarily generate growth bistability.

### The Abrupt Onset of Growth Bistability

Infrequently, we also observed nongrowing wild-type cells in microfluidic experiments, although their occurrence was not correlated with Cm concentration ($r_s$ ~0.1). This is not surprising because exponentially growing populations of wild-type cells are known to maintain a small fraction of nongrowing cells in the phenomenon called "persistence" (*30*). In the natural course of exponential growth, wild-type cells have been shown to enter into a dormant persister state stochastically at a low rate, resulting in the appearance of one dormant cell in every ~$10^3$ to $10^4$ growing cells (*31*–*33*). It is possible that the growth bistability observed for the CAT-expressing cells in low Cm concentrations is due to such naturally occurring persistence (referred to below as "natural persistence"). This question cannot be resolved by our current microfluidic experiments, which, at a throughput of ~$10^3$ cells, can barely detect natural persistence. We therefore sought a more sensitive method to quantify the conditions that produce growth bistability.

To enhance the sensitivity for detecting nongrowing cells and to probe the population-level behavior of Cat1 cells in batch cultures, we adapted an ampicillin (Amp)–based enrichment assay (*34*) that isolated nongrowing cells from Cm-containing cultures. This enrichment assay (fig. S5) took advantage of the fact that Amp only kills growing cells (*35*), thereby enriching cultures for potentially dormant cells to later be revived in the absence of antibiotics. With the microfluidic device, we verified visually that the cells that stopped growing because of Cm-induced growth bistability could survive Amp treatment, and were viable when antibiotics were removed (fig. S6).

In batch culture enrichment, Cat1 cells that failed to grow in the presence of Cm later appeared as colonies on antibiotic-free agar plates (fig. S7A). Consistent with the results in the microfluidic chamber (Fig. 2C), the fraction of

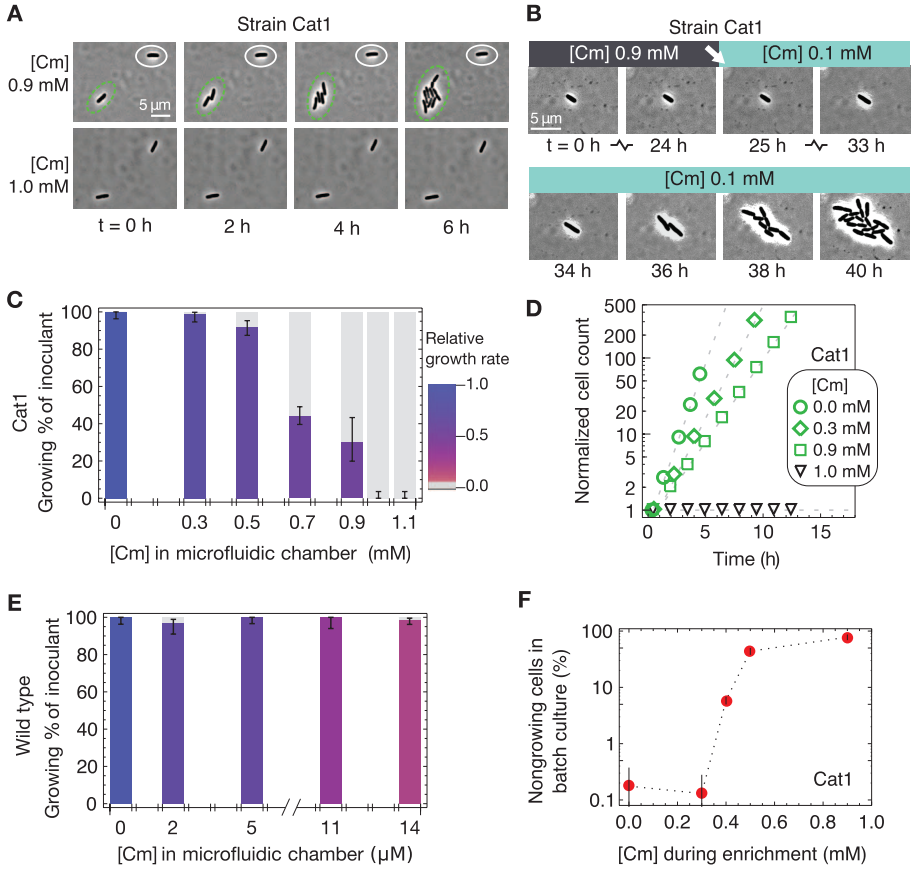


**Fig. 2. Drug-induced growth bistability.** (**A**) Upon increasing Cm concentration from 0 to 0.9 mM in microfluidic chambers (fig. S4), genetically identical Cat1m cells growing exponentially in glucose minimal medium either continued growing (circled in green) or were growth-arrested (circled in white); see movie S1. None of the Cat1m cells grew after adding Cm to 1.0 mM. (**B**) A typical example of the cells that remained dormant throughout the 24 hours during which microfluidic chambers contained 0.9 mM Cm; growth resumed ~8 hours after Cm was reduced to 0.1 mM, which is still well above the MIC of wild-type cells (see movie S2). (**C**) Height of colored bars gives the percentage of Cat1m cells to continue exponential growth in microfluidic chambers upon adding the indicated concentration of Cm; error bars give 95% confidence interval, assuming a binomial distribution. Bar color indicates growth rates of growing cells, with the relative growth rate given by the scale bar on the right. (**D**) Growth curves at different Cm concentrations, given by the size of growing colonies (*y* axis) in the microfluidic device. The deduced growth rates dropped abruptly from 0.35 hour$^{-1}$ (green squares) at 0.9 mM Cm to zero at 1.0 mM Cm (black triangles). (**E**) As in (C), but for immotile wild-type cells (EQ4m) that showed no significant correlation between growth rate and fraction of growing cells ($r_s$ ~0.1). (**F**) Fraction of Cat1 cells remaining after the batch culture Amp-Cm enrichment assay (fig. S5). The results (fig. S7) reveal significant fractions of nongrowing cells well above the basal level of natural persisters (~$10^{-3}$), for [Cm] ≥ 0.4 mM until the MIC of 1.0 mM, above which no cells grew. Error bars estimate SD of CFU, assuming Poisson-distributed colony appearance.

nongrowing cells identified by the enrichment assay at 0.3 mM Cm and below was small (≤$10^{-3}$, Fig. 2F), comparable to the frequencies characterized for natural persistence under similar conditions (*31*, *32*). However, the frequency of cells in the nongrowing state increased substantially at [Cm] ≥ 0.4 mM (Fig. 2F and fig. S7A). We define the minimal coexistence concentration (MCC) as the lowest antibiotic concentration above which coexistence between growing and nongrowing cells appears at frequencies significantly above natural persistence; MCC ≈ 0.35 mM for the strain Cat1. Thus, growth bistability turns large fractions of Cm-resistant cells into Cm-sensitive cells at Cm concentrations between MCC and MIC. In contrast, enriching Cm-sensitive wild-type cells in subinhibitory Cm concentrations reveals that most cells grow; >99% remain sensitive to Amp for all sub-MIC Cm concentrations (fig. S7B), which is consistent with previous findings that cells should only be protected from Amp if Cm completely inhibits growth (*35*–*37*).

### *Growth-Mediated Feedback and Generic Growth Bistability*

If growth bistability exhibited by Cat1 cells was indeed a result of generic growth-mediated feedback, then it should appear generally, not just idiosyncratically for Cm and the specific action of the Cm-modifying enzyme CAT. Toward this end, we tested the growth of a strain (Ta1) constitutively expressing the tetracycline efflux pump TetA (*38*, *39*) in microfluidic chambers with medium containing various concentrations of the drug tetracycline (Tc). As with the growth of strain Cat1 in Cm, Ta1 exhibited coexistence of growing and nongrowing cells for a range of sub-MIC concentrations of Tc and an abrupt drop in its relative growth rate at the MIC (from ~60% of the uninhibited rate to no growth, fig. S8A). In contrast to Tc-resistant cells, none of the wild-type cells stopped growing when exposed to sub-MIC Tc concentrations, even when Tc reduced growth rate by 85% (fig. S8C). These results were similar to those for Cat1 cells in Cm, supporting the hypothesis that growth bistability occurs generically, independent of the mode of drug resistance, as is predicted by growth-mediated feedback (fig. S1).

### *Quantitative Model for Antibiotic-Resistant Growth*

To determine whether growth-mediated feedback could quantitatively account for the occurrence of growth bistability (Figs. 1 and 2), we developed a simple mathematical model to predict the effect of a drug on the growth of cells constitutively expressing drug resistance. We focus here on the Cm-CAT system, whose biochemistry is quantitatively characterized (*23*); (*40*) contains a more general treatment with respect to other antibiotics and resistance mechanisms. The model contains three components, as summarized in Fig. 3A, and can quantitatively predict the dependence of the steady-state growth rate on the Cm concentration of the medium: (i) At steady state, the relation between the internal and external Cm concentration ($[Cm]_{int}$ and $[Cm]_{ext}$, respectively) can be obtained by balancing the rate of Cm influx with the rate of Cm clearance by CAT. (ii) The concentration and, hence, activity of constitutively expressed CAT proteins depends linearly on a cell's growth rate in response to applied Cm as a result of global growth-dependent effects. (iii) The cell's doubling time depends linearly on $[Cm]_{int}$ through the known effect of Cm on translation. Below, we elaborate on each component in some detail.

#### *Balance of Drug Influx and Clearance*

We assume that Cm influx is passive (*41*), as described by Eq. 1 in Fig. 3B, with a permeability κ (table S2). The Cm-CAT interaction is described by Michaelis-Menten kinetics (*23*) parameterized by $K_m$ and $V_{max}$ (Eq. 2 in Fig. 3B). Solving Eqs. 1 and 2 yields an approximate threshold-linear dependence of $[Cm]_{int}$ on $[Cm]_{ext}$ (red line in Fig. 3B). According to this nonlinear relation, $[Cm]_{int}$ is kept relatively low for external concentrations up to ~$V_{max}/\kappa$, the threshold concentration above which Cm influx reaches the maximum capacity of Cm clearance by CAT. Note that this buffering

effect does not require any molecular cooperativity (*40*).

*Growth Rate–Dependent Expression of Constitutive (Unregulated) Genes*

Figure 3C shows that, under translation-limited growth, the expression levels (that is, protein concentrations) of unregulated genes decrease linearly with decreasing growth rate λ (*16*, *42*). This trend contradicts the commonly held expectation that protein concentration should decrease with increasing growth rates, owing to a growth-mediated dilution effect. Instead, the proportionality between expression level and growth rate follows from bacterial growth laws (*16*) and can be understood as a generic consequence of the up-regulation of ribosome synthesis upon translational inhibition, at the expense of the expression of nonribosomal genes (fig. S9). The behavior is shown for translation-inhibited growth in Fig. 3C, with CAT activity ($V_{max}$) of cells constitutively expressing CAT (open green circles) and LacZ activity of cells constitutively expressing LacZ (open black symbols). This result is described by Eq. 3 in Fig. 3C, expressed relative to the CAT activity and growth rate in cells not exposed to drugs (denoted by $V_0$ and $\lambda_0$, respectively). We note that some drug resistance genes are not usually expressed constitutively, but require induction by the target antibiotic (*25*–*27*). However, regulated gene expression is still subject to growth-mediated feedback (*17*, *43*) and may suffer substantial reduction upon increasing the drug concentration. This has been observed for the native Tc-inducible promoter that controls Tc resistance, for growth under sublethal doses of Tc (fig. S10).

*Effect of Translation Inhibition on Cell Growth*

For exponentially growing cells subjected to subinhibitory doses of Cm, the relative doubling time ($\lambda_0/\lambda$) is expected to increase linearly with internal drug concentration $[Cm]_{int}$; see Eq. 4 in Fig. 3D. This relation is a consequence of the characterized effects of Cm on translation (*22*) together with bacterial growth laws, which dictate that the cell's growth rate depends linearly on the translation rate of the ribosomes (fig. S9) (*16*, *44*). Growth data in Fig. 3D verify this quantitatively for wild-type cells. The lone parameter in this relation, the half-inhibition concentration $I_{50}$, is governed by the Cm-ribosome affinity (eq. S6), and its empirical value is well accounted for by the known biochemistry (*22*) (table S2).

### Comparing Model Predictions to Experimental Observations

*The Value of the MIC*

The model based on the above three components contains three parameters: $K_m$, $I_{50}$, and $V_0/\kappa$. The first two are known or measured in this work (table S2), whereas the last one, reflecting the basal CAT activity level ($V_0$), is construct-specific. The model predicts a precipitous drop of growth rate across a threshold Cm concentration, which we identify as the theoretical MIC, whose value depends linearly on $V_0/\kappa$ as given by eq. S28. Empirically, an abrupt drop in growth rate is indeed apparent in the batch culture (fig. S11), yielding an MIC value (0.9 to 1.0 mM) that agrees well with those determined in microfluidics and plate assays. Comparing this empirical MIC value with the predicted dependence of MIC on $V_0/\kappa$ (eq. S28) fixes this lone unknown parameter to a value compatible with an independent estimate, on the basis of the measured CAT activity $V_0$ and indirect estimates of the permeability value κ (table S2).

*Dependence on Drug Concentration*

With $V_0/\kappa$ fixed, the model predicts Cm-dependent growth rates for this strain without any additional parameters (black lines, Fig. 4A). The upper branch of the prediction is in quantitative agreement with the growth rates of Cat1 measured in batch culture [Fig. 4A (solid circles) and fig. S11]. Additionally, when we challenged Tc-resistant strain Ta1 with either Tc or the Tc analog minocycline (Mn) (*39*), the observed growth rates also agreed quantitatively with the upper branch of the respective model predictions (fig. S12). Note also that in the absence of drug resistance or efflux, Eq. 4 predicts a smoothly decreasing growth rate with increasing drug concentration, which we observed for the growth of wild-type cells over a broad range of concentrations (figs. S8C and S12C).

The model also predicts a lower branch with very low growth rates and a range of Cm concentrations below MIC where the upper and lower branches coexist (Fig. 4A, shaded area). We identify the lower edge of this band as the theoretical MCC because a uniformly growing population is predicted for Cm concentrations below this value. Indeed, the occurrence of nongrowing cells for strain Cat1 (Fig. 4A, open diamonds) coincided with the shaded area. Likewise for strain Ta1, respective microfluidic and Amp enrichment experi-

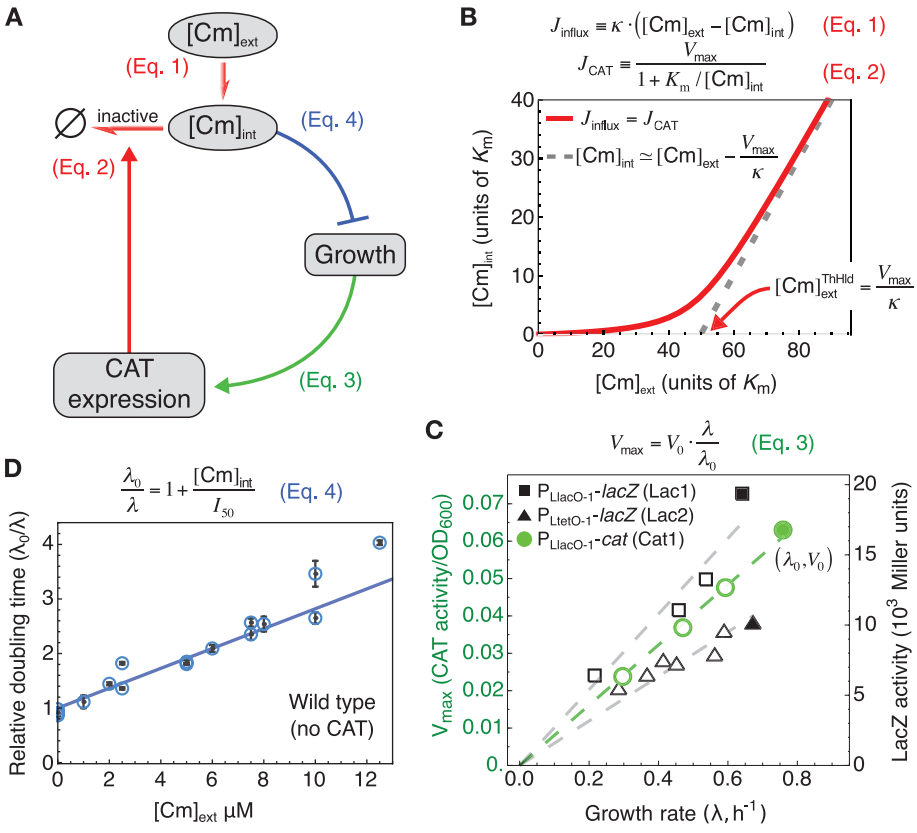


**Fig. 3. Growth-mediated feedback.** (**A**) Components of interactions defining the feedback model. Each link describes a relation substantiated in (B) to (D) (clockwise). (**B**) The relationship between the internal and external Cm concentrations ($[Cm]_{int}$ and $[Cm]_{ext}$, respectively), described by the red line, is obtained by balancing the passive influx of Cm into the cell ($J_{influx}$, Eq. 1) with the rate of Cm modification by CAT ($J_{CAT}$, Eq. 2). This nonlinear relation is characterized by an approximate threshold-linear form, with a "threshold" Cm concentration, $[Cm]_{ext}^{threshold}$ (red arrow), below which $[Cm]_{int}$ is kept low as the capacity for clearance by CAT well exceeds the Cm influx (eq. S12). For $[Cm]_{ext} > [Cm]_{ext}^{threshold}$, CAT is saturated and $J_{influx} \approx V_{max}$ (dashed gray line). (**C**) The expression levels of constitutively expressed CAT (green) and LacZ (black) reporters [reported here in units of activity per OD (*42*)] are proportional to the growth rate with subinhibitory doses of Tc and Cm, respectively. (**D**) The doubling time (blue circles) of wild-type (EQ4) cells grown in minimal medium with various concentrations of Cm increases linearly with [Cm] (Eq. 4). $I_{50}$ (dashed vertical line) gives the Cm concentration at which cell growth is reduced by 50%. Here, $[Cm]_{int} \approx [Cm]_{ext}$ because of the absence of endogenous Cm efflux for wild-type cells in minimal medium (*41*) (see also eq. S9). Each point represents a single experiment; error bars of the doubling times are SEs of inverse slope in linear regression of $\log(OD_{600})$ versus time.

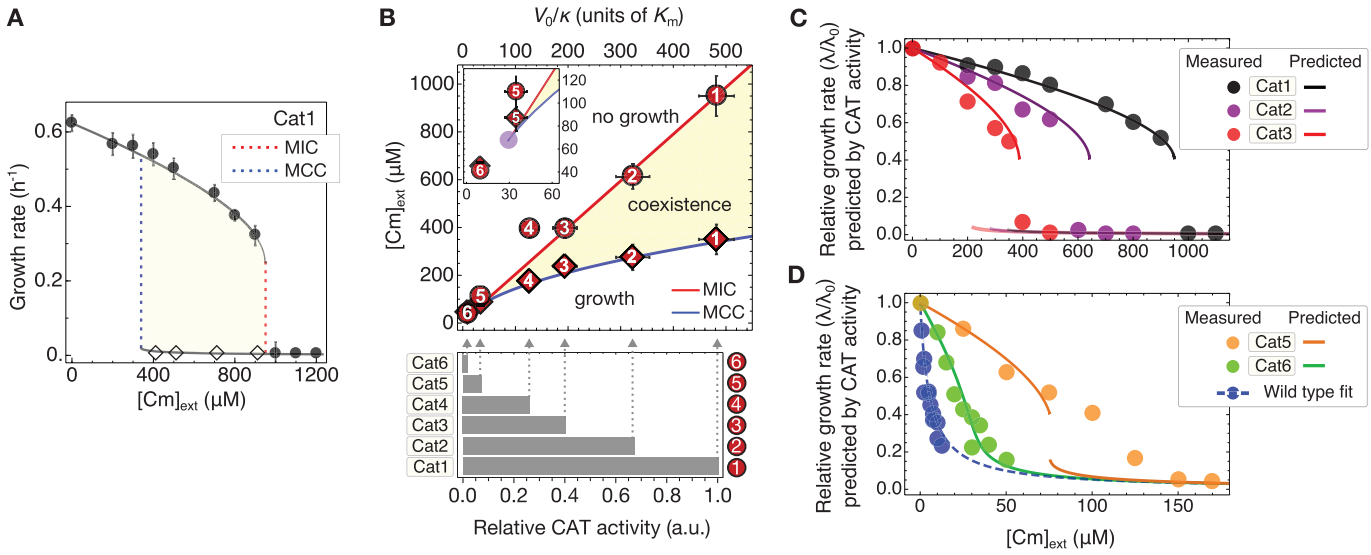


**Fig. 4. Growth rate predictions and phase diagram.** (**A**) The growth rate of Cat1 strain in minimal medium batch culture with varying Cm concentrations (solid circles) agrees quantitatively with the prediction of the growth feedback model (line) on the basis of the measured MIC (dashed red line). Error bars, SD; $n \geq 3$. Dashed blue line is the theoretical MCC. Diamonds indicate drug levels at which enrichment experiments identified significant numbers of nongrowing cells (fig. S7). (**B**) The MCC (blue line) and MIC (red line) predicted by the growth feedback model for strains with different degrees of basal CAT expression ($V_0$) define a phase diagram, with the coexistence of growing and nongrowing populations between the MCC and MIC (beige). MIC (circles, fig. S14) and MCC (diamonds, fig. S15) are measured for strains differing only in their levels of constitutive CAT expression (quantified by the relative CAT activity in the absence of Cm, given by the bar graph below). Error bars, SD; $n \geq 2$. (**C** and **D**) Measured and predicted growth rates (circles and lines of like colors) in minimal medium with varying Cm concentrations for strains of known relative CAT activities; the wild type is shown in blue for reference. Predictions were obtained by solving eq. S28 for $V_0/\kappa$, using the measured MIC for strain Cat1 and the measured relative CAT activity between the different strains [bottom of (B)], without any parameter fitting.

ments with Tc (fig. S8) and Mn (fig. S13) revealed nongrowing cells within the theoretical coexistence region (lower branches in fig. S12).

*Dependence on CAT Expression: Phase Diagram*

The growth-mediated feedback model makes quantitative predictions on how the MIC and MCC depend on the basal CAT expression of the strain ($V_0/\kappa$), as shown in the phase diagram of Fig. 4B. The MIC (red line) is predicted to increase linearly with $V_0/\kappa$, whereas the MCC (blue line) is predicted to increase as $\sqrt{V_0/\kappa}$ (eqs. S28 and S39, respectively). These two lines define a wedge in the parameter space of $[Cm]_{ext}$ and $\sqrt{V_0/\kappa}$, terminating at a bifurcation point (purple point in inset), below which a uniformly growing population is predicted (see eq. S24). We tested these predictions by using five additional strains (Cat2 through Cat6; tables S1 and S3) designed to provide reduced degrees of constitutive CAT expression; see quantitation of $V_0$ for each strain at bottom of Fig. 4B. Assuming that the permeability κ does not differ significantly across these strains, the measured CAT activities give $V_0/\kappa$ for all strains (relative to that of Cat1), as shown by the gray arrows in Fig. 4B. Figure 4B also displays the batch culture MIC (comparable to $MIC_{plate}$ values, fig. S14) and MCC values (fig. S15) obtained for these strains as numbered circles and diamonds, respectively. The model predictions (lines) capture these observations well except close to the bifurcation point (for example, in strain Cat5, inset), without adjusting any parameters. Note that because the feedback model is based on steady-state relations (Eqs. 3 and 4), it is not expected to describe the kinetics of transition into the nongrowing state or its frequency of occurrence, both of which likely depend on complex stochastic processes. However, in all our experiments, we never observed growth bistability at drug concentrations below the predicted MCC.

The CAT activities ($V_0/\kappa$; Fig. 4B, bottom) can also be used to predict growth rate reductions ($\lambda/\lambda_0$) for these strains for concentrations below the MIC. The predictions are plotted together with the data (lines and circles of like colors) in Fig. 4, C and D. The predictive power of the model is rather remarkable because the lines are not fits to the data, but merely solutions to eqs. S15 and S5, using the measured values of $V_0$ as input. Comparable agreements are obtained using the empirical MIC value for each strain (fig. S16). In contrast, an identical model lacking growth-mediated feedback cannot account for the Cm dependence of the growth rates of these strains, particularly the abrupt drop in growth at MIC in strains Cat1 to Cat3 (fig. S17). Even incorporating stochasticity into this deterministic alternative model could not resolve this basic qualitative disagreement with our observations [see (*40*), section 2.5].

### *Fitness Landscapes*

Figure 5A gives the full solution of the model for strains with a range of CAT activity ($V_0/\kappa$) in medium with varying Cm concentrations ($[Cm]_{ext}$). The colored lines reproduce the predicted growth rates of several strains from Fig. 4, C and D, and span a range of behaviors, from subcritical to bistable. Viewing this plot orthogonally, the white line illustrates growth rates in an environment of fixed Cm concentration for strains of different CAT activities. Whereas the CAT activity levels ($V_0$) are determined directly by molecular properties encoded by the genotype, for example, the promoter or ribosomal binding sequences (table S3) and the coding sequence of the *cat* gene, the white line describes a relation between the growth rate and the genotype, and may be regarded as a "fitness landscape." There is such a fitness landscape for each environmental Cm concentration. For $[Cm]_{ext} > [Cm]_{ext}^{crit}$, these fitness landscapes are plateau-shaped, characterized by a threshold level of CAT activity (survival resistance threshold, $V_{SRT}$) across which the growth of the culture changes abruptly (Fig. 5B, diagonal dashed line).

A recent theoretical analysis (*45*) characterizes how bacteria can evolve through plateau-shaped fitness landscapes with drug-dependent survival thresholds and demonstrates how landscape structure can determine the rate at which antibiotic resistance emerges in environments that precipitate rapid adaptation (*45*–*47*); see illustration in Fig. 5B. Specifically, in environments containing a spatial gradient of drug concentrations, the plateau-shaped landscape ensures that a large population of cells is always near an uninhabited niche of higher drug concentration (due to the respectively high and low growth rates on either side of the threshold). Therefore, mutants in this population expand into regions of higher drug

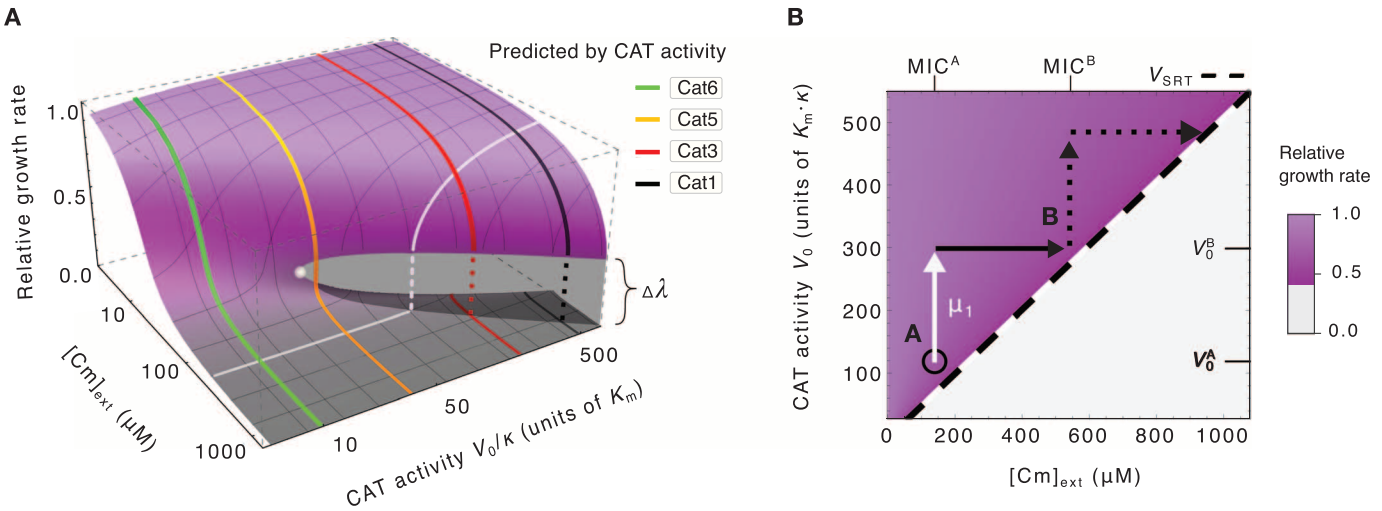


**Fig. 5. Fitness landscapes of drug resistance.** (**A**) Predicted growth rates (height of surface) for arbitrary CAT activity and Cm levels ($V_0$ and $[Cm]_{ext}$, respectively): High (purple surface) and low growth rates (gray surface) overlap in the region of coexistence (growth bistability) that terminates at the bifurcation point (filled white circle). Predictions from Fig. 4, C and D, are reproduced (colored lines). The orthogonal white line illustrates the expected effect of changing CAT activity at a fixed Cm concentration; it can be viewed as a plateau-shaped fitness landscape. (**B**) The survival resistance threshold required for growth, $V_{SRT}$, is predicted to vary linearly with the drug concentration (diagonal black dashed line). For a population initially at point A (black circle) in the phase diagram, that is, with resistance activity $V_0^A$ and surviving in niches with $[Cm]_{ext} < MIC^A$, a mutation ($\mu_1$, white arrow) that increases the resistance activity level to $V_0^B$ can allow the bacteria to "expand its range" (*45*) and proliferate into all niches with $MIC^A \leq [Cm]_{ext} \leq MIC^B$ without competition (solid black arrow). Additional mutations, for example, upstream of the gene at the ribosomal binding sequence (see table S3), or gene amplification events (*69*) provide a simple pathway for sequential expansions into increasingly harsh environments (*45*, *70*).

concentration without competition, and adaptation like this can continue in a ratchetlike fashion to allow the population to survive in increasingly higher concentrations of antibiotics.

## Discussion

The drugs investigated in this study (Cm, Tc, and Mn) are infrequently prescribed today. Because of this, they are among only a handful of antibiotics that remain effective against "pan-resistant" bacteria, that is, those resistant to all other standard drugs and polymyxins, and have been advocated as a last line of defense (*48*, *49*). Therefore, understanding the effect of these drugs on drug resistance expression is critical. More broadly, many other antibiotics also affect gene expression in a variety of bacteria and fungi (*13*, *50*, *51*), raising general questions about the effect of drug–drug resistance interaction on cell growth, the consequences of this interaction on the efficacy of treatment programs, and the long-term evolvability of drug resistance.

We have shown here that for the class of translation-inhibiting antibiotics, the fitness of resistance-expressing bacteria exposed to antibiotics can be quantitatively predicted with a few empirical parameters that are readily determined by the physiological characteristics of the cells. Our minimal model is based on the physiology of drug-cell interactions and the biochemistry of drug resistance. Although it neglects many details, for example, the fitness cost of expressing resistance that may matter when small differences in fitness determine the emergence of resistance (*52*, *53*), this minimal approach already captures the generic existence of a plateau-shaped fitness landscape that can facilitate emerging drug-resistant mutants to invade new territories without competition (*45*). These plateau-shaped fitness landscapes accompany the phenomenon of growth bistability, which arises from positive feedback. As demonstrated here, these positive feedback effects do not require special regulatory mechanisms or any molecular cooperativity and are not limited to a specific enzymatic mechanism of drug resistance. Furthermore, these effects cannot be understood by merely analyzing some local genetic circuits but are instead derived from the global coordination of gene expression during growth inhibition (*16*). Therefore, we expect the growth bistability and the accompanying plateau-shaped fitness landscape to be robust features innate to drug-resistant bacteria.

Growth bistability in drug response has previously been theorized to occur for bacteria lacking drug resistance and for antibiotics with low membrane permeability (*54*). These considerations are not applicable to the systems we study here, because wild-type cells grew homogeneously in the presence of antibiotics tested, and only cells expressing drug resistance exhibited growth bistability when cultured in the presence of antibiotics. The observed growth bistability is also unlikely to arise from a recently described inoculum effect (*55*), in which two separate cultures with identical concentration of certain drugs may exhibit distinct growth rates depending on the culture inoculant density: First, the bacteriostatic drugs investigated here (Cm and Tc) have been shown not to exhibit the inoculum effect (*55*, *56*). Second, the inoculum effect concerns the differences between separate cultures, whereas we observed coexistence of growing and nongrowing subpopulations in a single homogeneous culture.

We also considered the relationship between the drug-induced growth bistability studied here and the phenotypic bistability implicated in natural persistence, identified as the source of many long-term, refractory bacterial infections (*19*, *57*, *58*). These are, first of all, clearly distinct phenomena that nevertheless can be easily be mistaken for one another: The effect we studied is an innate response to drug for cells carrying drug resistance, whereas natural persistence refers to spontaneous entry into the nongrowing state (which can occur in the absence of drugs) for drug-sensitive strains. Also, the frequency of nongrowing cells is typically very low (~0.1%) in natural persistence, but it can be macroscopic (even greater than 80%) for the drug-induced effect. Finally, a cell achieves natural persistence by producing toxin proteins to inhibit its own growth (*33*, *58*), whereas the effect studied here is an obligatory response to applied drugs, rooted deeply in the organization of bacterial growth control (*16*).

However, there also exist important parallels between these two phenomena that cannot be overlooked and may be exploited to understand natural persistence: Researchers have devoted many efforts and resources to understanding the mechanisms underlying bistability in natural persistence, whereas here we show that bistability can arise without complex regulation when gene expression is coupled to the state of cell growth. A similar general strategy may also underlie natural persistence, with cell growth inhibited by a

toxic endogenous gene product whose expression would likely be affected by global growth-dependent effects (*57*–*59*). The precise effects of growth inhibition on gene expression will depend on the specific mode of growth limitations imposed upon cellular metabolism by the various toxin systems (*60*). Characterizing these feedback effects, in the manner we have done here for antibiotic resistance, may yield critical clues needed to formulate a quantitative, physiological understanding of natural persistence.

The fact that drugs can induce growth bistability, that is, antibiotics can have a wildly heterogeneous effect on genetically identical cells in a homogeneous environment, calls into question the current methods of characterizing drug efficacies, which are often performed in bulk growth conditions (*21*). It provides a new perspective on basic notions of drug resistance, including the MIC, which begs for a more careful empirical definition to avoid vast inconsistencies across laboratories (*61*, *62*). Remarkably, large fractions of bacterial cells can remain vulnerable to an antibiotic (that is, stop growing) even though they carry genes providing resistance to it; understanding the mechanisms that force cells into the nongrowing state could enable the development of new treatment strategies against drug-resistant bacteria. On the other hand, heterogeneous effects may require a more careful reexamination of the effectiveness of combinatorial drug treatment (*43*, *63*) because strains resistant to one drug may produce macroscopic fractions of growing and nongrowing cells that respond very differently to a second drug, which may affect the evolution of drug resistance (*63*). The success of the phenomenological model presented here for the class of translation-inhibiting antibiotics gives the hope that predictive models may be similarly developed for other types of drug action, including combinations of drugs, to facilitate the formulation of strategies that limit the efficacy and evolvability of drug resistance.

## Materials and Methods

### Culture and Cell Growth

#### *Media and Chemicals*

Unless noted elsewhere, minimal medium refers to a mixture of 0.4% (w/v) glucose, 20 mM $NH_4Cl$, and "N$^-$C$^-$" buffer (*64*) consisting of 1.0 g of $K_2SO_4$, 17.7 g of $K_2HPO_4$•$3H_2O$, 4.7 g of $KH_2PO_4$, 0.1 g of $MgSO_4$•$7H_2O$, and NaCl (2.0 g/liter), with 6 mM sodium acetate when indicated. Chloramphenicol (Sigma C0378) stock solutions contained Cm at a concentration of either 2 or 25 mg/ml in 70% isopropanol stock solution. Tetracycline hydrochloride (Sigma T4062) stock solutions contained Tc•HCl at a concentration of either 0.1 or 25 mg/ml in deionized $H_2O$; minocycline hydrochloride (Sigma M9511) stock solution contained 10 mM Mn•HCl. These stock solutions were stored at −20°C in the dark and used for preparation of media with various concentrations of antibiotics. Antibiotics were added to the media at the time of experiment as described below, and for Cm, stock concentration was chosen such that the volume added would not exceed 1.5% of total medium volume.

LB agar plates containing Cm were prepared on the day of experiments as follows: After freshly mixed LB agar was autoclaved, 100-ml aliquots were poured into 250-ml Erlenmeyer flasks and cooled to about 50°C. A volume of Cm solution was then pipetted from an appropriate stock into the liquid agar (to achieve the desired concentration), and the mixture was swirled both clockwise and counterclockwise for 10 s. We then poured about 25 ml of medium plus agar into each 100 mm × 15 mm petri dish (Fisherbrand).

#### *Batch Culture Growth*

All batch cultures grew at 37°C in a water bath shaker at 250 rpm (New Brunswick Scientific G76D) with a covered basin to protect photosensitive chemicals (for example, Tc) from degradation and to prevent heat bath from evaporating. Culture growth measurements were performed with unique seed cultures each day. Each 5 ml of seed culture grew to saturation in LB broth from a single colony on an LB plate. Seed cultures were diluted into 5-ml precultures containing minimal media and grown overnight without antibiotic. Except as noted below, experimental cultures were diluted from overnight precultures into 5 ml of minimal medium supplemented with appropriate antibiotics in 20-mm-diameter glass tubes. Experimental cultures were inoculated to an initial optical density ($OD_{600}$) ~0.01, as measured by a Thermo Scientific Genesys 20 spectrophotometer, with a Starna Cells quartz cuvette with a 10-mm light path. At intervals ranging from 40 min to 2 hours, we took 250-µl samples from growing cultures to measure $OD_{600}$. For growth in Tc or Mn, to control for thermolability or photosensitivity (*65*, *66*), we diluted growing cultures 10- to 20-fold into fresh identical media to verify that culture age did not affect growth rate over the course of our experiments.

#### *Growth of Strains Expressing CAT in Cm*

We followed the same procedure as described above, except we began the experiments with ~60-fold lower cell densities in bulk cultures to avoid significant degradation of Cm by CAT during the course of growth. Briefly, experimental cultures were diluted from overnight precultures into a larger volume of 10 ml of minimal medium supplemented with appropriate Cm and acetate in larger 25-mm-diameter glass tubes. From the larger experimental culture volume, we pipetted 1 ml of samples into a Starna Cells quartz cuvette with a 40-mm light path to record OD. Use of the cuvette with longer path length allowed us to observe cultures at fourfold lower densities using the same Genesys spectrophotometer as above. Experimental cultures were inoculated to a maximum initial density of $OD_{600}^{4x}$ ~0.0007 determined by the larger cuvette ($OD_{600}$ ~0.0002). In this manner, we were able to achieve steady exponential growth observable up to at least $OD_{600}^{4x}$ ~0.1 with this cuvette (see green symbols in fig. S11).

### Determination of Growth Rate and MIC

Exponential growth curves for all cultures were fit over about three or more generations of doubling by linear regression of log-OD values; steady state was not assumed until cultures underwent at least two generations of approximately constant exponential growth. When indicated, uncertainty in the calculated growth rate is SE of the resultant slope from the simple linear regression. A growth rate of zero indicates that cultures failed to grow after at least 12 hours or stopped growing within several doublings after addition of antibiotic (for example, see black triangles in fig. S11). If results were ambiguous at a particular Cm concentration, for example, if a culture appeared not to grow for 6 hours and then exhibited fast growth (which occurred rarely), the experiment was repeated in full. For Cm- and Tc-resistant strains, we determined MIC by monitoring the OD of batch cultures as described above (see Fig. 3, B and C, and fig. S11); we determined that cultures contained [Cm] ≥ MIC if cultures failed to grow or if growth rate $\lambda \leq 0.1$ hour$^{-1}$. For strains with high levels of antibiotic resistance (most strains), MIC was unambiguous in that growth was undetectable above some threshold concentration (see, for example, fig. S11). We first determined MICs with antibiotic concentrations set at logarithmic intervals before using finer gradations at linear intervals to achieve a determination within ~10% error. Because our quantitative model is formulated on the basis of growth in batch cultures, we use these MICs determined in batch cultures wherever we provide model predictions or fits. Additionally, the MIC determined on agar plates (called $MIC_{plate}$, see figs. S2 and S13 and methods below) and in the microfluidic device (Fig. 2, C and D) generally agreed with these determinations.

### Growth of Colonies on Agar Plates

#### *Determining CFU on Plates with Cm*

For each strain, cells from log-phase batch cultures grown in minimal medium lacking Cm were diluted with the same medium. We then used sterile glass beads (Kimble, 4 mm) to spread 50 µl of the diluted culture onto an LB-Cm agar plate to achieve a density of several hundred cells per plate (giving rise to several hundred colonies or fewer after incubation, depending on the strain's response to the particular Cm concentration used). Plates were incubated overnight (~18 hours) at 37°C such that colonies formed were easily resolved by the naked eye (see fig. S2, B and C, and Fig. 3B). We used Bio-Rad Gel Doc XR and Quantity One software to photograph plates and count colonies; in many cases, colonies were also counted manually. We calibrated the counting software to agree with manual counts. Plate images were enhanced for brightness and contrast.

*Determination of $MIC_{plate}$*

Similar to above, cells were diluted from log phase in the absence of antibiotics, and 50 µl of diluted culture were spread onto LB-Cm agar plates to achieve a density of about $5\times 10^4$ to $8\times 10^4$ cells per plate before incubation. Plates were incubated overnight (~18 hours) at 37°C to reveal colony formation. $MIC_{plate}$ is taken as the Cm concentration above which colonies appeared at a frequency of less than $\sim 10^{-4}$ per inoculant; the presence or absence of colony growth was readily visually discernable (figs. S2, S3, and S14). We determined $MIC_{plate}$ values for each strain after at least two replicate experiments, and plate images were enhanced for brightness and contrast. These $MIC_{plate}$ values obtained with LB plates for antibiotic-resistant strains were similar to MIC values obtained in batch cultures with minimal media as described above. Coincidence between MIC determined in LB and minimal media has been reported elsewhere (*43*).

### Viability After Amp Enrichment Assays

Cells from overnight batch cultures in drug-free minimal media were diluted into the same fresh media with the indicated concentration of "drug" (Cm or Mn as designated in the text) and incubated for 1 to 2 hours. Cultures were then diluted in identical medium (containing Cm or Mn) with further addition of Amp (100 µg/ml) to an $OD_{600}$ of about $1\times 10^{-3}$ to $2\times 10^{-3}$. At this time, 50-µl aliquots of culture and 100-fold diluted culture were spread onto LB agar plates lacking any antibiotics and incubated overnight, producing plates containing ~500 and $\sim 5\times 10^4$ colonies each. These plates served as a control to monitor CFU at the start of enrichment and allowed us to determine the fraction of cells killed by the enrichment procedure at each drug concentration. After 6 to 7 hours of enrichment in drug and Amp media, 50-µl aliquots of culture and 100-fold diluted culture were again spread onto LB plates without antibiotics for overnight incubation; see fig. S5 for illustration. All plates and batch cultures were incubated at 37°C. Plate images were enhanced for brightness and contrast (figs. S7, S13, and S15).

### Microfluidic Experiments

*Cell Growth in Microfluidic Chambers*

All cultures were grown at 37°C. The growth medium was minimal medium, as described above, and was filtered through 0.45-µm filters before use. The cells were first cultured in LB broth in 20-mm test tubes with shaking (250 rpm) in a water bath (New Brunswick Scientific). After 5 to 6 hours of growth, they were transferred to the growth medium and grew overnight in the same condition (preculture). The preculture was inoculated with fewer than $10^5$ cells/ml so that cells were in an exponential phase at the time of experiment. The next morning, the preculture was diluted in fresh growth medium containing 0.1% BSA (bovine serum albumin; Sigma; BSA prevents cells from binding to surfaces of microfluidic devices) to an $OD_{600}$ of ~0.01 as measured on a Genesys 20 spectrophotometer (Thermo Fisher) with the standard cuvette (16.100-Q-10/Z8.5, Starna Cells Inc.; ~200 µl per measurement). To load cells into the microfluidic device, the diluted preculture was pressurized to 1 to 2 psi at the outlet of the device (fig. S4A). When the channel and growth chambers were completely filled with the preculture, the preculture source was removed, and fresh growth medium was introduced from the inlet of the device.

The microfluidic device was fixed onto a motorized microscope stage equipped with autofocus (ProScan II, Prior) in a fluorescence microscope (Nikon TI-U) that was housed in a microscope incubator (InVivo Scientific). When viewed with a charge-coupled device (CCD) camera (Clara, Andor) with a 60× phase-contrast objective, single cells were dispersed far from each other (more than 100 µm away from each other). Then, −0.5 to −1.5 psi of vacuum were applied from the outlet to bring down the ceiling of the growth chambers and loosely sandwich the cells in place (side view of fig. S4). Because the vacuum induces the fresh medium flow in a channel (flow rate of 50 to 100 µm/s), no additional pressure was applied from the inlet.

After about two generations of unperturbed growth at 37°C in the device, we gently flushed excess cells away to prevent crowding and enable cell tracking, and then introduced growth medium with various concentrations of Cm to the inlet of the device. The 10 to 30 positions that contained a single microcolony in the view (~100 µm × ~100 µm) of the CCD were saved in the motorized stage. Phase-contrast images of the growing cells for each position were recorded two times per doubling. Fluorescence images were taken once per doubling, immediately after the phase-contrast images for each position with a Xenon excitation lamp (Sutter Instrument). The images were analyzed with a custom-built Matlab program. First, the program identified pixel positions occupied by cells with phase-contrast images, obtained the size of a growing colony in time series for each position, and calculated the growth rate of the colony. To quantify fluorescence levels, fluorescence intensities over the cell-occupying area identified by phase-contrast images were averaged.

*Enriching Cm-Resistant Cells with Amp in Microfluidic Chambers*

First, cells that constitutively express green fluorescent protein (GCat1m) were transferred from precultures as described above and grown in medium with 0.7 mM Cm for 8 hours. Initially, 44% of cells grew with a doubling time of 130 min, which is similar to the growth of Cat1m (Fig. 2C). We added Amp (200 µg/ml) to the medium at $t = 9$ hours to kill growing cells (fig. S6). At $t = 24$ hours, all growing cells had stopped growing and lost fluorescence. There were several nongrowing cells that maintained green fluorescence. At $t = 25$ hours, Cm and Amp were removed from the medium. Between $33 \le t \le 37$ hours, the nongrowing cells that maintained their fluorescence throughout the enrichment resumed growth.

### Additional Protocols

Details regarding strain construction, microfluidic device fabrication, CAT, and β-galactosidase assays are described elsewhere (*40*).

#### References and Notes


1. A. J. Alanis, Resistance to antibiotics: Are we in the post-antibiotic era? *Arch. Med. Res.* **36**, 697–705 (2005). doi: 10.1016/j.arcmed.2005.06.009; pmid: 16216651
2. World Health Organization, *The Evolving Threat of Antimicrobial Resistance: Options for Action* (World Health Organization, Geneva, 2012).
3. J. L. Martínez, F. Baquero, D. I. Andersson, Predicting antibiotic resistance. *Nat. Rev. Microbiol.* **5**, 958–965 (2007). doi: 10.1038/nrmicro1796; pmid: 18007678
4. R. C. MacLean, A. R. Hall, G. G. Perron, A. Buckling, The population genetics of antibiotic resistance: Integrating molecular mechanisms and treatment contexts. *Nat. Rev. Genet.* **11**, 405–414 (2010). doi: 10.1038/nrg2778; pmid: 20479772
5. A. G. McArthur *et al.*, The comprehensive antibiotic resistance database. *Antimicrob. Agents Chemother.* **57**, 3348–3357 (2013). doi: 10.1128/AAC.00419-13; pmid: 23650175
6. L. L. Cavalli, G. A. Maccacaro, Chloromycetin resistance in *E. coli*, a case of quantitative inheritance in bacteria. *Nature* **166**, 991–992 (1950). doi: 10.1038/166991a0; pmid: 14796661
7. E. Toprak *et al.*, Evolutionary paths to antibiotic resistance under dynamically sustained drug selection. *Nat. Genet.* **44**, 101–105 (2011). doi: 10.1038/ng.1034; pmid: 22179135
8. D. J. Maskell, C. E. Hormaeche, K. A. Harrington, H. S. Joysey, F. Y. Liew, The initial suppression of bacterial growth in a salmonella infection is mediated by a localized rather than a systemic response. *Microb. Pathog.* **2**, 295–305 (1987). doi: 10.1016/0882-4010(87)90127-6; pmid: 3333801
9. J. C. Batten, R. M. McCune Jr., The influence of corticotrophin and certain corticosteroids on populations of *Mycobacterium tuberculosis* in tissues of mice. *Br. J. Exp. Pathol.* **38**, 413–423 (1957). pmid: 13460186
10. Y. Li, A. Karlin, J. D. Loike, S. C. Silverstein, A critical concentration of neutrophils is required for effective bacterial killing in suspension. *Proc. Natl. Acad. Sci. U.S.A.* **99**, 8289–8294 (2002). doi: 10.1073/pnas.122244799; pmid: 12060772
11. R. Malka, B. Wolach, R. Gavrieli, E. Shochat, V. Rom-Kedar, Evidence for bistable bacteria-neutrophil interaction and its clinical implications. *J. Clin. Invest.* **122**, 3002–3011 (2012). doi: 10.1172/JCI59832; pmid: 22820292
12. J. A. Washington II, The effects and significance of subminimal inhibitory concentrations of antibiotics. *Rev. Infect. Dis.* **1**, 781–786 (1979). doi: 10.1093/clinids/1.5.781; pmid: 396633
13. J. Davies, G. B. Spiegelman, G. Yim, The world of subinhibitory antibiotic concentrations. *Curr. Opin. Microbiol.* **9**, 445–453 (2006). doi: 10.1016/j.mib.2006.08.006; pmid: 16942902
14. C. Tan, P. Marguet, L. You, Emergent bistability by a growth-modulating positive feedback circuit. *Nat. Chem. Biol.* **5**, 842–848 (2009). doi: 10.1038/nchembio.218; pmid: 19801994
15. A. Zaslaver *et al.*, Invariant distribution of promoter activities in *Escherichia coli*. *PLOS Comput. Biol.* **5**, e1000545 (2009). doi: 10.1371/journal.pcbi.1000545; pmid: 19851443
16. M. Scott, C. W. Gunderson, E. M. Mateescu, Z. Zhang, T. Hwa, Interdependence of cell growth and gene expression: Origins and consequences. *Science* **330**, 1099–1102 (2010). doi: 10.1126/science.1192588; pmid: 21097934
17. T. Bollenbach, R. Kishony, Resolution of gene regulatory conflicts caused by combinations of antibiotics. *Mol. Cell* **42**, 413–425 (2011). doi: 10.1016/j.molcel.2011.04.016; pmid: 21596308

18. M. Scott, T. Hwa, Bacterial growth laws and their applications. *Curr. Opin. Biotechnol.* **22**, 559–565 (2011). doi: 10.1016/j.copbio.2011.04.014; pmid: 21592775
19. D. Dubnau, R. Losick, Bistability in bacteria. *Mol. Microbiol.* **61**, 564–572 (2006). doi: 10.1111/j.1365-2958.2006.05249.x; pmid: 16879639
20. W. K. Smits, O. P. Kuipers, J. W. Veening, Phenotypic variation in bacteria: The role of feedback regulation. *Nat. Rev. Microbiol.* **4**, 259–271 (2006). doi: 10.1038/nrmicro1381; pmid: 16541134
21. J. M. Andrews, Determination of minimum inhibitory concentrations. *J. Antimicrob. Chemother.* **48** (suppl. 1), 5–16 (2001). doi: 10.1093/jac/48.suppl_1.5; pmid: 11420333
22. R. J. Harvey, A. L. Koch, How partially inhibitory concentrations of chloramphenicol affect the growth of *Escherichia coli*. *Antimicrob. Agents Chemother.* **18**, 323–337 (1980). doi: 10.1128/AAC.18.2.323; pmid: 6160809
23. J. Ellis, C. R. Bagshaw, W. Shaw, Kinetic mechanism of chloramphenicol acetyltransferase: The role of ternary complex interconversion in rate determination. *Biochemistry* **34**, 16852–16859 (1995). doi: 10.1021/bi00051a036; pmid: 8527461
24. W. V. Shaw, Chloramphenicol acetyltransferase: Enzymology and molecular biology. *CRC Crit. Rev. Biochem.* **14**, 1–46 (1983). doi: 10.3109/10409238309102789; pmid: 6340955
25. H. Harbottle, S. Thakur, S. Zhao, D. G. White, Genetics of antimicrobial resistance. *Anim. Biotechnol.* **17**, 111–124 (2006). doi: 10.1080/10495390600957092; pmid: 17127523
26. T. J. Foster, Plasmid-determined resistance to antimicrobial drugs and toxic metal ions in bacteria. *Microbiol. Rev.* **47**, 361–409 (1983). pmid: 6355806
27. L. J. Piddock, Clinically relevant chromosomally encoded multidrug resistance efflux pumps in bacteria. *Clin. Microbiol. Rev.* **19**, 382–402 (2006). doi: 10.1128/CMR.19.2.382-402.2006; pmid: 16614254
28. A. Groisman *et al.*, A microfluidic chemostat for experiments with bacterial and yeast cells. *Nat. Methods* **2**, 685–689 (2005). doi: 10.1038/nmeth784; pmid: 16118639
29. J. J. Rahal Jr., M. S. Simberkoff, Bactericidal and bacteriostatic action of chloramphenicol against meningeal pathogens. *Antimicrob. Agents Chemother.* **16**, 13–18 (1979). doi: 10.1128/AAC.16.1.13; pmid: 38742
30. J. Bigger, Treatment of staphylococcal infections with penicillin by intermittent sterilisation. *Lancet* **244**, 497–500 (1944). doi: 10.1016/S0140-6736(00)74210-3
31. N. Q. Balaban, J. Merrin, R. Chait, L. Kowalik, S. Leibler, Bacterial persistence as a phenotypic switch. *Science* **305**, 1622–1625 (2004). doi: 10.1126/science.1099390; pmid: 15308767
32. K. Lewis, Persister cells, dormancy and infectious disease. *Nat. Rev. Microbiol.* **5**, 48–56 (2007). doi: 10.1038/nrmicro1557; pmid: 17143318
33. K. Gerdes, E. Maisonneuve, Bacterial persistence and toxin-antitoxin loci. *Annu. Rev. Microbiol.* **66**, 103–123 (2012). doi: 10.1146/annurev-micro-092611-150159; pmid: 22994490
34. H. G. Schlegel, H. W. Jannasch, Enrichment cultures. *Annu. Rev. Microbiol.* **21**, 49–70 (1967). doi: 10.1146/annurev.mi.21.100167.000405; pmid: 4860267
35. R. M. Cozens *et al.*, Evaluation of the bactericidal activity of β-lactam antibiotics on slowly growing bacteria cultured in the chemostat. *Antimicrob. Agents Chemother.* **29**, 797–802 (1986). doi: 10.1128/AAC.29.5.797; pmid: 3089141
36. E. Jawetz, J. B. Gunnison, R. S. Speck, V. R. Coleman, Studies on antibiotic synergism and antagonism: The interference of chloramphenicol with the action of penicillin. *AMA Arch. Intern. Med.* **87**, 349–359 (1951). doi: 10.1001/archinte.1951.03810030022002; pmid: 14810260
37. S. E. Holm, Interaction between β-lactam and other antibiotics. *Rev. Infect. Dis.* **8** (suppl. 3), S305–S314 (1986). doi: 10.1093/clinids/8.Supplement_3.S305; pmid: 3529323
38. D. Schnappinger, W. Hillen, Tetracyclines: Antibiotic action, uptake, and resistance mechanisms. *Arch. Microbiol.* **165**, 359–369 (1996). doi: 10.1007/s002030050339; pmid: 8661929
39. I. Chopra, M. Roberts, Tetracycline antibiotics: Mode of action, applications, molecular biology, and epidemiology of bacterial resistance. *Microbiol. Mol. Biol. Rev.* **65**, 232–260 (2001). doi: 10.1128/MMBR.65.2.232-260.2001; pmid: 11381101
40. See supporting materials and methods in *Science* Online.
41. L. M. McMurry, A. M. George, S. B. Levy, Active efflux of chloramphenicol in susceptible *Escherichia coli* strains and in multiple-antibiotic-resistant (Mar) mutants. *Antimicrob. Agents Chemother.* **38**, 542–546 (1994). doi: 10.1128/AAC.38.3.542; pmid: 8203852
42. Here and elsewhere in the text, "expression level" denotes the intracellular concentration of a protein. This is reported in units of protein activity per OD: Protein activity is proportional to the protein amount. OD units correspond reliably to cell volume (*57*, *67*, *68*).
43. T. Bollenbach, S. Quan, R. Chait, R. Kishony, Nonoptimal microbial response to antibiotics underlies suppressive drug interactions. *Cell* **139**, 707–718 (2009). doi: 10.1016/j.cell.2009.10.025; pmid: 19914165
44. O. Maaløe, in *Biological Regulation and Development*, R. F. Goldberger, Ed. (Plenum Press, New York, 1979), pp. 487–542.
45. R. Hermsen, J. B. Deris, T. Hwa, On the rapidity of antibiotic resistance evolution facilitated by a concentration gradient. *Proc. Natl. Acad. Sci. U.S.A.* **109**, 10775–10780 (2012). doi: 10.1073/pnas.1117716109; pmid: 22711808
46. Q. Zhang *et al.*, Acceleration of emergence of bacterial antibiotic resistance in connected microenvironments. *Science* **333**, 1764–1767 (2011). doi: 10.1126/science.1208747; pmid: 21940899
47. P. Greulich, B. Waclaw, R. J. Allen, Mutational pathway determines whether drug gradients accelerate evolution of drug-resistant cells. *Phys. Rev. Lett.* **109**, 088101 (2012). doi: 10.1103/PhysRevLett.109.088101; pmid: 23002776
48. M. E. Falagas, A. P. Grammatikos, A. Michalopoulos, Potential of old-generation antibiotics to address current need for new antibiotics. *Expert Rev. Anti Infect. Ther.* **6**, 593–600 (2008). doi: 10.1586/14787210.6.5.593; pmid: 18847400
49. Y. Hayashi, D. L. Paterson, The epidemiology of pan/extreme drug resistance, in *Antibiotic Policies*, I. M. Gould, J. W. M. van der Meer, Eds. (Springer, New York, 2011), pp. 27–38.
50. T. Nichterlein *et al.*, Subinhibitory concentrations of β-lactams and other cell-wall antibiotics inhibit listeriolysin production by *Listeria monocytogenes*. *Int. J. Antimicrob. Agents* **7**, 75–81 (1996). doi: 10.1016/0924-8579(96)00014-3; pmid: 18611740
51. M. Niewerth *et al.*, Ciclopirox olamine treatment affects the expression pattern of *Candida albicans* genes encoding virulence factors, iron metabolism proteins, and drug resistance. *Antimicrob. Agents Chemother.* **47**, 1805–1817 (2003). doi: 10.1128/AAC.47.6.1805-1817.2003; pmid: 12760852
52. D. I. Andersson, D. Hughes, Antibiotic resistance and its cost: Is it possible to reverse resistance? *Nat. Rev. Microbiol.* **8**, 260–271 (2010). pmid: 20208551
53. E. Gullberg *et al.*, Selection of resistant bacteria at very low antibiotic concentrations. *PLOS Pathog.* **7**, e1002158 (2011). doi: 10.1371/journal.ppat.1002158; pmid: 21811410
54. J. Elf, K. Nilsson, T. Tenson, M. Ehrenberg, Bistable bacterial growth rate in response to antibiotics with low membrane permeability. *Phys. Rev. Lett.* **97**, 258104 (2006). doi: 10.1103/PhysRevLett.97.258104; pmid: 17280399
55. C. Tan *et al.*, The inoculum effect and band-pass bacterial response to periodic antibiotic treatment. *Mol. Syst. Biol.* **8**, 617 (2012). doi: 10.1038/msb.2012.49; pmid: 23047527
56. M. A. Kohanski, D. J. Dwyer, B. Hayete, C. A. Lawrence, J. J. Collins, A common mechanism of cellular death induced by bactericidal antibiotics. *Cell* **130**, 797–810 (2007). doi: 10.1016/j.cell.2007.06.049; pmid: 17803904
57. S. Klumpp, Z. Zhang, T. Hwa, Growth rate-dependent global effects on gene expression in bacteria. *Cell* **139**, 1366–1375 (2009). doi: 10.1016/j.cell.2009.12.001; pmid: 20064380
58. R. A. Fasani, M. A. Savageau, Molecular mechanisms of multiple toxin–antitoxin systems are coordinated to govern the persister phenotype. *Proc. Natl. Acad. Sci. U.S.A.* **110**, E2528–E2537 (2013). doi: 10.1073/pnas.1301023110; pmid: 23781105
59. C. Lou, Z. Li, Q. Ouyang, A molecular model for persister in *E. coli*. *J. Theor. Biol.* **255**, 205–209 (2008). doi: 10.1016/j.jtbi.2008.07.035; pmid: 18721814
60. C. You *et al.*, Coordination of bacterial proteome with metabolism by cyclic AMP signalling. *Nature* **500**, 301–306 (2013). doi: 10.1038/nature12446; pmid: 23925119
61. J. J. Snell, D. F. Brown, External quality assessment of antimicrobial susceptibility testing in Europe. *J. Antimicrob. Chemother.* **47**, 801–810 (2001). doi: 10.1093/jac/47.6.801; pmid: 11389112
62. P. E. Varaldo, Antimicrobial resistance and susceptibility testing: An evergreen topic. *J. Antimicrob. Chemother.* **50**, 1–4 (2002). doi: 10.1093/jac/dkf093; pmid: 12095999
63. J. B. Michel, P. J. Yeh, R. Chait, R. C. Moellering Jr., R. Kishony, Drug interactions modulate the potential for evolution of resistance. *Proc. Natl. Acad. Sci. U.S.A.* **105**, 14918–14923 (2008). doi: 10.1073/pnas.0800944105; pmid: 18815368
64. L. N. Csonka, T. P. Ikeda, S. A. Fletcher, S. Kustu, The accumulation of glutamate is necessary for optimal growth of *Salmonella typhimurium* in media of high osmolality but not induction of the proU operon. *J. Bacteriol.* **176**, 6324–6333 (1994). pmid: 7929004
65. K. A. Loftin, C. D. Adams, M. T. Meyer, R. Surampalli, Effects of ionic strength, temperature, and pH on degradation of selected antibiotics. *J. Environ. Qual.* **37**, 378–386 (2008). doi: 10.2134/jeq2007.0230; pmid: 18268300
66. T. Stoichev, M. S. Baptista, M. C. P. Basto, V. M. Vasconcelos, M. T. S. D. Vasconcelos, Effects of minocycline and its degradation products on the growth of *Microcystis aeruginosa*. *Ecotoxicol. Environ. Saf.* **74**, 219–224 (2011). doi: 10.1016/j.ecoenv.2010.10.015; pmid: 20965566
67. W. Donachie, A. Robinson, in Escherichia coli and Salmonella typhimurium: *Cellular and Molecular Biology*, F. C. Neidhardt *et al.*, Eds. (American Society for Microbiology, Washington, DC, 1987), pp. 1578–1592.
68. H. E. Kubitschek, W. W. Baldwin, S. J. Schroeter, R. Graetzer, Independence of buoyant cell density and growth rate in *Escherichia coli*. *J. Bacteriol.* **158**, 296–299 (1984). pmid: 6370960
69. L. Sandegren, D. I. Andersson, Bacterial gene amplification: Implications for the evolution of antibiotic resistance. *Nat. Rev. Microbiol.* **7**, 578–588 (2009). doi: 10.1038/nrmicro2174; pmid: 19609259
70. R. Hermsen, T. Hwa, Sources and sinks: A stochastic model of evolution in heterogeneous environments. *Phys. Rev. Lett.* **105**, 248104 (2010). doi: 10.1103/PhysRevLett.105.248104; pmid: 21231560


**Acknowledgments:** We are grateful to R. Austin, L. Chao, M. Ehrenberg, P. Geiduschek, H. Nikaido, S. Klumpp, M. Scott, B. Shaw, Q. Zhang, and members of the Hwa laboratory for comments and suggestions. This work was supported by the NIH through grant R01-GM095903 to T.H., by the NSF, through an NSF Graduate Research Fellowship to J.B.D. and through the Center for Theoretical Biological Physics (PHY0822283), and by the National Cancer Institute via a subcontract of the Physical Science-Oncology program (1 U54 CA143803). R.H. was supported in part by the NWO (Nederlandse Organisatie voor Wetenschappelijk Onderzoek) (VENI 680-47-419). Additional data, including source data for figures, are presented in the supplementary materials. Correspondence and requests for materials should be addressed to T.H. (hwa@ucsd.edu).

## Supplementary Materials

www.sciencemag.org/content/342/6162/1237435/suppl/DC1
Materials and Methods
Figs. S1 to S19
Tables S1 to S5
References (*71*–*121*)
Movies S1 and S2

10.1126/science.1237435

# Chelyabinsk Airburst, Damage Assessment, Meteorite Recovery, and Characterization

Olga P. Popova,[1] Peter Jenniskens,[2,3]* Vacheslav Emel'yanenko,[4] Anna Kartashova,[4] Eugeny Biryukov,[5] Sergey Khaibrakhmanov,[6] Valery Shuvalov,[1] Yurij Rybnov,[1] Alexandr Dudorov,[6] Victor I. Grokhovsky,[7] Dmitry D. Badyukov,[8] Qing-Zhu Yin,[9] Peter S. Gural,[2] Jim Albers,[2] Mikael Granvik,[10] Läslo G. Evers,[11,12] Jacob Kuiper,[11] Vladimir Kharlamov,[1] Andrey Solovyov,[13] Yuri S. Rusakov,[14] Stanislav Korotkiy,[15] Ilya Serdyuk,[16] Alexander V. Korochantsev,[8] Michail Yu. Larionov,[7] Dmitry Glazachev,[1] Alexander E. Mayer,[6] Galen Gisler,[17] Sergei V. Gladkovsky,[18] Josh Wimpenny,[9] Matthew E. Sanborn,[9] Akane Yamakawa,[9] Kenneth L. Verosub,[9] Douglas J. Rowland,[19] Sarah Roeske,[9] Nicholas W. Botto,[9] Jon M. Friedrich,[20,21] Michael E. Zolensky,[22] Loan Le,[23,22] Daniel Ross,[23,22] Karen Ziegler,[24] Tomoki Nakamura,[25] Insu Ahn,[25] Jong Ik Lee,[26] Qin Zhou,[27,28] Xian-Hua Li,[28] Qiu-Li Li,[28] Yu Liu,[28] Guo-Qiang Tang,[28] Takahiro Hiroi,[29] Derek Sears,[3] Ilya A. Weinstein,[7] Alexander S. Vokhmintsev,[7] Alexei V. Ishchenko,[7] Phillipe Schmitt-Kopplin,[30,31] Norbert Hertkorn,[30] Keisuke Nagao,[32] Makiko K. Haba,[32] Mutsumi Komatsu,[33] Takashi Mikouchi,[34] (the Chelyabinsk Airburst Consortium)

The asteroid impact near the Russian city of Chelyabinsk on 15 February 2013 was the largest airburst on Earth since the 1908 Tunguska event, causing a natural disaster in an area with a population exceeding one million. Because it occurred in an era with modern consumer electronics, field sensors, and laboratory techniques, unprecedented measurements were made of the impact event and the meteoroid that caused it. Here, we document the account of what happened, as understood now, using comprehensive data obtained from astronomy, planetary science, geophysics, meteorology, meteoritics, and cosmochemistry and from social science surveys. A good understanding of the Chelyabinsk incident provides an opportunity to calibrate the event, with implications for the study of near-Earth objects and developing hazard mitigation strategies for planetary protection.

Chelyabinsk Oblast experienced an impact that was 100 times more energetic than the recent 4 kT of TNT–equivalent Sutter's Mill meteorite fall (*1*). This was the biggest impact over land since the poorly observed Tunguska impact in 1908, for which kinetic energy estimates range from 3 to 5 (*2*) to 10 to 50 MT (*3*). From the measured period of infrasound waves circum-traveling the globe (*4*), an early estimate of ~470 kT was derived for Chelyabinsk (*5*). Infrasound data from Russia and Kazakhstan provide 570 ± 150 kT; see supplementary materials (SM) section 1.4 (*6*). Spaceborne visible and near-infrared observations (*7*) recorded a total irradiated energy of 90 kT (*5*, *8*), corresponding to a kinetic energy of 590 ± 50 kT using the calibration by Nemtchinov *et al*. (*9*). All values are uncertain by a factor of two because of a lack of calibration data at those high energies and altitudes.

The manner in which this kinetic energy was deposited in the atmosphere determined what shock wave reached the ground. Dash-camera and security camera videos of the fireball (Fig. 1) provide a light curve with peak brightness of –27.3 ± 0.5 magnitude (Fig. 2) (SM section 1.2). The integrated light curve is consistent with other energy estimates if the panchromatic luminous efficiency was 7 ± 3%. Theoretical estimates under these conditions range from 5.6 to 13.2% (*10*).

Calibrated video observations provided a trajectory and pre-atmospheric orbit (Table 1) (SM section 1.1). The fireball was first recorded at 97-km altitude, moving at 19.16 ± 0.15 km/s with entry angle 18.3 ± 0.2° with respect to the horizon, which is slightly faster than reported earlier (*11*). Combined with the best kinetic energy estimate, an entry mass of $1.3 \times 10^7$ kg (with a factor of two uncertainty) and a diameter of 19.8 ± 4.6 m is derived, assuming a spherical shape and the meteorite-derived density of 3.3 g/cm$^3$ based on x-ray computed tomography (SM section 4.2, table S16).

Size and speed suggest that a shock wave first developed at 90 km. Observations show that dust formation and fragmentation started around 83 km and accelerated at 54 km (figs. S16 and S22). Peak radiation occurred at an altitude of 29.7 ± 0.7 km at 03:20:32.2 ± 0.1s UTC (SM section 1.1-2), at which time spaceborne sensors measured a meteoroid speed of 18.6 km/s (*5*). Fragmentation left a thermally emitting debris cloud in this period, the final burst of which occurred at 27.0-km altitude (Fig. 1), with dust and gas settling at 26.2 km and with distinctly higher billowing above that location (fig. S22). The dust cloud split in two due to the buoyancy of the hot gas, leading to two cylindrical vortices (*12*).

Compared with the much larger Tunguska event (*2*, *3*), Chelyabinsk was only on the threshold of forming a common shock wave around the fragments when it broke at peak brightness (SM section 1.2). Fragments were spatially isolated enough to be efficiently decelerated, avoiding the transfer of momentum to lower altitudes and resulting in less damage when the blast wave reached the ground.

### Damage Assessment

In the weeks after the event, 50 villages were visited to verify the extent of glass damage. The resulting map (Fig. 3) demonstrates that the shock wave had a cylindrical component, extending furthest perpendicular to the trajectory. There was little coherence of the shock wave in the forward direction, where the disturbance was of long duration, shaking buildings and making people run outside, but causing no damage.

[1]Institute for Dynamics of Geospheres of the Russian Academy of Sciences, Leninsky Prospect 38, Building 1, Moscow, 119334, Russia. [2]SETI Institute, 189 Bernardo Avenue, Mountain View, CA 94043, USA. [3]NASA Ames Research Center, Moffett Field, Mail Stop 245-1, CA 94035, USA. [4]Institute of Astronomy of the Russian Academy of Sciences, Pyatnitskaya 48, Moscow, 119017, Russia. [5]Department of Theoretical Mechanics, South Ural State University, Lenin Avenue 76, Chelyabinsk, 454080, Russia. [6]Chelyabinsk State University, Bratyev Kashirinyh Street 129, Chelyabinsk, 454001, Russia. [7]Institute of Physics and Technology, Ural Federal University, Mira Street 19, Yekaterinburg, 620002, Russia. [8]Vernadsky Institute of Geochemistry and Analytical Chemistry of the RAS, Kosygina Street 19, Moscow, 119991, Russia. [9]Department of Earth and Planetary Sciences, University of California at Davis, Davis, CA 95616, USA. [10]Department of Physics, University of Helsinki, P.O. Box 64, 00014 Helsinki, Finland. [11]Koninklijk Nederlands Meteorologisch Instituut, P.O. Box 201, 3730 AE De Bilt, Netherlands. [12]Department of Geoscience and Engineering, Faculty of Civil Engineering and Geosciences, Delft University of Technology, P.O. Box 5048, 2600 GA Delft, Netherlands. [13]Tomsk State University, Lenina Prospect 36, Tomsk, 634050, Russia. [14]Research and Production Association "Typhoon," Floor 2, 7 Engels Street, Obninsk, 249032, Russia. [15]Support Foundation for Astronomy "Ka-Dar," P.O. Box 82, Razvilka, 142717, Russia. [16]Science and Technology Center of the Social and Youth Initiatives Organization, 3-12-63 Udal'tsova Street, Moscow, 119415, Russia. [17]University of Oslo, Physics Building, Sem Saelands Vel 24, 0316 Oslo, Norway. [18]Institute of Engineering Sciences Urals Branch of the Russian Academy of Sciences, Komsomolskaya Street 34, Yekaterinburg, 620049, Russia. [19]Center for Molecular and Genomic Imaging, University of California, Davis, Davis, CA 95616, USA. [20]Department of Earth and Planetary Sciences, American Museum of Natural History, New York, NY 10024, USA. [21]Department of Chemistry, Fordham University, Bronx, NY 10458, USA. [22]Astromaterials Research and Exploration Science, NASA Johnson Space Center, Houston, TX 77058, USA. [23]Jacobs Technology, 2224 Bay Area Boulevard, Houston, TX 77058, USA. [24]Institute of Meteoritics, University of New Mexico, Albuquerque, NM 87131–0001, USA. [25]Department of Earth and Planetary Materials Science, Tohoku University, Aramaki, Aoba, Sendai, Miyagi 980-8578, Japan. [26]Division of Polar Earth-System Sciences, Korea Polar Research Institute, 26 Songdomi Rae, Yeonsu-gu, Incheon 406-840, Korea. [27]National Astronomical Observatories, Beijing, Chinese Academy of Sciences, Beijing 100012, China. [28]State Key Laboratory of Lithospheric Evolution, Institute of Geology and Geophysics, Chinese Academy of Sciences, Beijing 100029, China. [29]Department of Geological Sciences, Brown University, Providence, RI 02912, USA. [30]Analytical BioGeoChemistry, Helmoltz Zentrum Muenchen, Ingoldstäter Landstrasse 1, D-85764 Obeschleissheim, Germany. [31]Technical University Muenchen, Analytical Food Chemistry, Alte Akademie 10, D-85354 Freising, Germany. [32]Geochemical Research Center, The University of Tokyo, 7-3-1 Hongo, Bunkyo-ku, Tokyo 113-0033, Japan. [33]Waseda Institute for Advanced Study, Waseda University, 1-6-1 Nishiwaseda, Shinjuku, Tokyo 169-8050, Japan. [34]Department of Earth and Planetary Science, The University of Tokyo, 7-3-1 Hongo, Bunkyo-ku, Tokyo 113-0033, Japan.

*Corresponding author. E-mail: petrus.m.jenniskens@nasa.gov

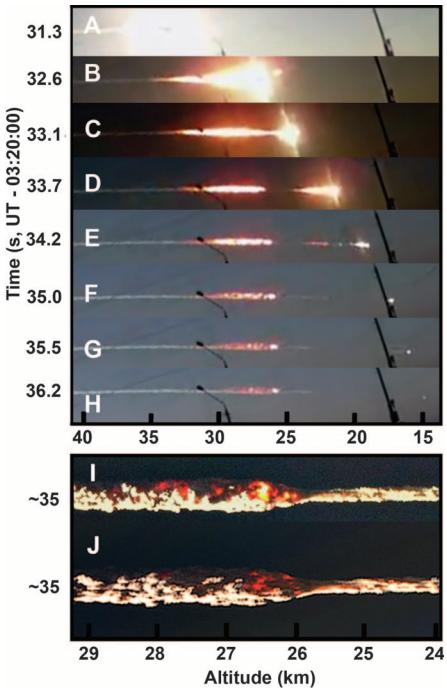


**Fig. 1. Meteoroid fragmentation stages in video taken by A. Ivanov in Kamensk-Uralskiy. (A)** Fireball just before peak brightness, at the moment when camera gain was first adjusted. **(B)** End of main disruption. **(C)** Onset of secondary disruption. **(D)** End of secondary disruption; main debris cloud continues to move down. **(E)** Two main fragments remain. **(F)** Single fragment remains. **(G)** Thermally emitting debris cloud at rest with atmosphere. **(H)** Final fragment continues to penetrate. Meteor moved behind distant lamp posts. **(I** and **J)** Detail of the thermal emission from a photograph by Mr. Dudarev (I) and M. Ahmetvaleev (J), after sky subtraction with high-pass filter and contrast enhancement. Altitude scale is uncertain by ±0.7 km.

**Fig. 2. Fireball visual magnitude irradiance light curve, normalized to 100-km distance.** The bold dashed line shows the model fit to the light curve (SM section 1.2), with thin lines showing total mass of all fragments passing a given altitude (kg) and the altitude-dependent rate of energy deposition as a fraction of the original kinetic energy ($km^{-1}$).

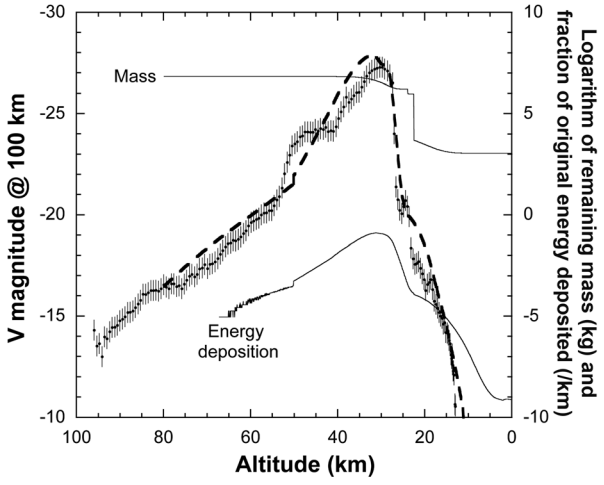


The strength of this shock wave on the ground was modeled (SM section 2.4), assuming that an overpressure of $\Delta p > 500$ Pa was required (*13*). A 520-kT event, with detonations spread over altitudes ranging from 34 to 27 km and 24 to 19 km, would cause damage out to a distance of 120 km with the observed shape (Fig. 3). The fragments that penetrated below 27 km must have contributed to the damage in order to match the shock-wave arrival times (SM section 2.4).

The number of houses damaged per 1000 inhabitants (table S11) (SM section 2.3) falls off with distance from the airburst source ($r$) as $r^{-2.6 \pm 1.2}$, with overpressure calculated to fall off as $r^{-2.4}$ (fig. S39). In Chelyabinsk itself, 3613 apartment buildings (about 44%) had shattered and broken glass, but these were not evenly distributed in the city (fig. S37). Sharp sounds heard after the shock wave also point to the fragmentation's causing a complicated distribution of pressure. Structural damage included the collapse of a zinc factory roof.

Directly below the fireball's path, the shock wave was strong enough to blow people off their feet. In Yemanzhelinsk, window frames facing the trajectory were pushed inwards, and suspended ceilings were sucked down above broken windows (fig. S36G). There was no structural damage to buildings, other than a statue of Pushkin inside the local library, cracked by a blown-out window frame. Cracks in walls were documented in nearby Baturinsky and Kalachevo.

Electrophonic sounds were heard (SM section 1.6), but there was no evidence of an electromagnetic pulse (EMP) under the track in neighboring Emanzhelinka. Due to shock-wave–induced vibrations, electricity and cell phone connectivity was briefly halted in the Kunashaksky district at the far northern end of the damage area. The gas supply was briefly interrupted in some districts because of valves reacting to the vibrations.

People found it painful to look at the bright fireball, but glancing away prevented lasting eye damage. Of 1113 respondents to an Internet survey who were outside at the time, 25 were sunburned (2.2%), 315 felt hot (28%), and 415 (37%) felt warm (SM section 2.2). Mild sunburns were reported throughout the survey area (table S7), reflecting the fact that ultraviolet (UV) flux density falls off as $\sim r^{-2}$. In Korkino, 30 km from the point of peak brightness, one resident reported getting a mild sunburn on the face, followed by peeling of skin. Such effects occur at a minimum erythema dose of ~1000 J/$m^2$ (*14*) of 290- to 320-nm radiation (mostly UV-B). Assuming 6000-K radiation (*9*), the calculated dose would have been ~200 J/$m^2$ at Korkino. Ground reflectance of UV light by snow may have further increased the dose.

Out of the total 1674 collected Internet responses, 374 mention 452 body injuries or inconveniences (SM section 2.2). Of those, 5.3% reported sunburn, 48% eyes hurt, and 2.9% retinal burns. Because of the shock wave, 6.4% reported a concussion or mental confusion, upset, or exhaustion as a result of excessive stress. Flying glass and falling building debris affected a relatively small fraction of respondents: 4.8% reported cuts and 2.9% reported bruises, but no broken bones were reported.

The percentage of people asking for medical assistance (table S10) dropped with distance according to $r^{-3.2 \pm 0.5}$ (SM section 2.1). The majority of injuries (1210) took place in the densely populated Chelyabinsk city, but the highest fraction of people asking for assistance was near the trajectory track in the Korkinsky district (0.16%).

### Meteorite Recovery

Shock radiation contributed to surface heating and ablation but did not completely evaporate all fragments of Chelyabinsk, unlike in the case of Tunguska (*3*). Meteorites of ~0.1 g fell near Aleksandrovka close to the point of peak brightness, masses of ~100 g fell further along the trajectory near Deputatskiy, and at least one of 3.4 kg fell near Timiryazevskiy. One hit the roof of a house in Deputatskiy (fig. S46). Falling-sphere models suggest that they originated at 32- to 26-km altitude (fig. S52), where the meteor model shows rapid fragmentation (fig. S18C). The location of the meteorites is consistent with prevailing northwest winds of 5 to 15 m/s (fig. S24). An estimated 3000 to 5000 kg fell in this area (SM section 3.1).

Two main fragments survived the disruption at 29.7 km. They flared around 24 km, with one falling apart at 18.5 km and the other remaining luminous down to 13.6 km (Fig. 1 and fig. S15). Light-curve modeling (SM section 1.2) suggests that from this material another ~1 ton in larger fragments up to 100 to 400 kg in mass reached the ground. A 7-m-sized hole was discovered in 70-cm-thick ice on Lake Chebarkul (fig. S53A), in line with the trajectory (SM section 1.1). A lakeshore video security camera, pointed to the site, recorded the impact (fig. S53B). Small meteorite fragments were recovered over an area up to 50 m from the impact location (Fig. 4C). Impact models (figs. S18 and S54) suggest a 200- to 1000-kg meteorite would be required to create such a hole. A mass of ≥570 kg was recovered from the lake bed (fig. S53C).

The combined 4 to 6 tons of surviving meteorites is only 0.03 to 0.05% of the initial mass. Seventy-six percent of the meteoroid evaporated, with most of the remaining mass converted into

**Table 1. Atmospheric trajectory and pre-atmospheric orbit for the Chelyabinsk meteoroid, with 2 standard deviation uncertainties.** Angular elements are for equinox J2000.0.

| Atmospheric trajectory | Chelyabinsk | Pre-atmospheric orbit | Chelyabinsk | Itokawa |
|---|---|---|---|---|
| $H_b$ (beginning height, km) | 97.1 ± 1.6 | $T_J$ (Tisserand's parameter) | 3.87 ± 0.24 | 4.90 |
| $H_m$ (peak brightness, km) | 29.7 ± 1.4 | $a$ (semimajor axis, AU) | 1.76 ± 0.16 | 1.324 |
| $H_f$ (disruption, km) | 27.0 ± 1.4 | $e$ (eccentricity) | 0.581 ± 0.018 | 0.280 |
| $H_e$ (end height, km) | 13.6 ± 1.4 | $q$ (perihelion distance, AU) | 0.739 ± 0.020 | 0.953 |
| $V_\infty$ (entry speed, km/s) | 19.16 ± 0.30 | ω (argument of perihelion, °) | 108.3 ± 3.8 | 162.8 |
| $h$ (entry elevation angle, °) | 18.3 ± 0.4 | Ω (longitude of ascending node, °) | 326.4422 ± 0.0028 | 69.1 |
| $a_z$ (entry azimuth angle from south, °) | 283.2 ± 0.4 | $i$ (inclination, °) | 4.93 ± 0.48 | 1.6 |
| $V_g$ (geocentric entry speed, km/s) | 15.3 ± 0.4 | $Q$ (aphelion distance, AU) | 2.78 ± 0.20 | 1.70 |
| $Ra_g$ (geocentric right ascension of radiant, °) | 333.2 ± 1.6 | $T_p$ (perihelion time) | 2012-12-31.9 ± 2.0 | 2013-07-10.8 |
| $Dec_g$ (geocentric declination of radiant, °) | +0.3 ± 1.8 | Epoch (ET) | 2013-02-15.139 | 2013-04-18.0 |

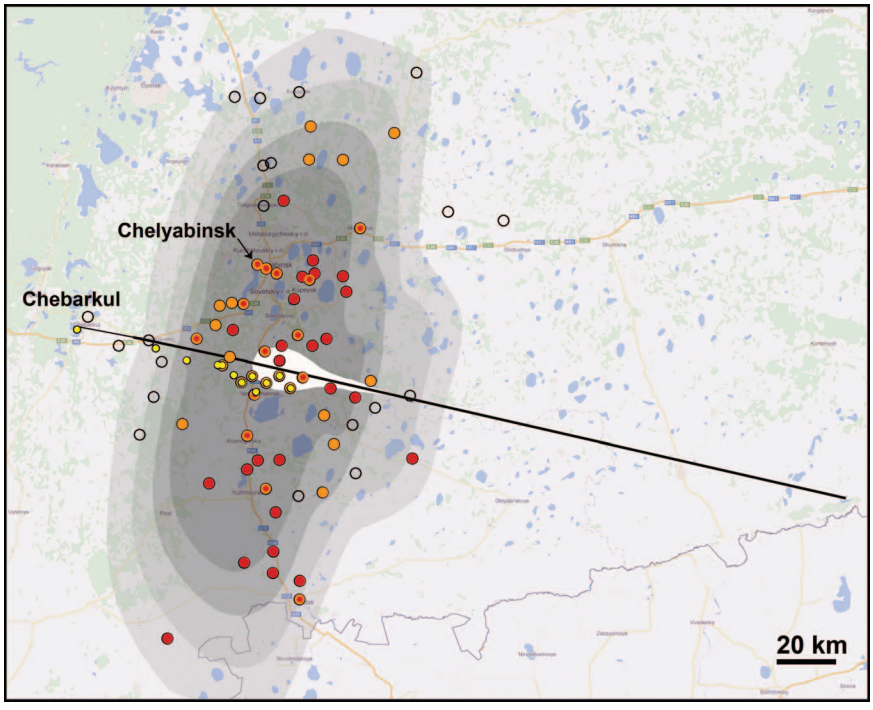


**Fig. 3. Map of glass damage on the ground with models of overpressure.** Field survey data are shown in solid orange circles for reported damage and open black circles for no damage; solid red circles show the most damaged villages in each district, as reported by the government. Each point, irrespective of population density, represents one of many villages or city districts scattered throughout the area. Model contours (with progressive gray scale) represent kinetic energies and overpressures from inside out: 300 kT $\Delta p > 1000$ Pa, 520 kT $\Delta p > 1000$ Pa, 300 kT $\Delta p > 500$ Pa, and 520 kT $\Delta p > 500$ Pa, respectively. Also shown are the locations of meteorite finds (yellow points) and the ground-projected fireball trajectory (black line), moving from 97-km altitude on the right to 14-km altitude on the left. White shows the fireball brightness on a linear scale.

dust (SM section 1.3). Witnesses reported smelling "sulfur" and burning odors over a wide region concentrated near the fireball trajectory, starting about an hour after the fireball and lasting through much of the day (SM section 1.5) (fig. S34).

### Characterization of Recovered Meteorites

The unusually effective fragmentation and small surviving mass may have been caused by structural and material weakness. The asteroid had a lower compressive strength than the ~330 MPa measured for recovered, surviving meteorites (SM section S4.1). The light curve (Fig. 2) is modeled with fragmentation starting at a low 0.2 MPa dynamic pressure but tolerating higher pressure with decreasing fragment size. This is similar to other meteorite falls, where initial weakness was attributed to macroscopic cracks or microscopic porosity (*15*). For Chelyabinsk, however, the physical weakness is not microporosity related. X-ray computed tomography (SM section 4.2) revealed a degree of compaction consistent with the lack of intragranular porosity typical of LL chondrites (*16*).

Some laboratory-broken meteorites fragmented along shock veins (fig. S55), a possible weakness in the material that could have contributed to the abundant dust formation. The meteorite is composed of a breccia (*17*) of mildly shocked lighter clasts and moderately shocked darker clasts with abundant thin to cm-wide shock melt veins (Fig. 4A) (SM section 4.4). A peculiar feature is that some shock veins exhibit a metal layer located ~20 micrometers inside the vein, which follows the outer contours of the vein (Fig. 4B), indicating that metal initially segregated from the most rapidly solidifying rims of the vein. This could contribute to weakness. Metal-rich tendrils also project outward from the vein.

The mineral compositional ranges (SM section 4.4) are slightly larger than those reported before (*18*), but still compatible with a classification as LL5, shock stage S4 (*19*). The classification as LL chondrite is substantiated by oxygen and chromium isotope studies (SM section 4.5 to 4.7), which put the meteorite near the L end of the LL field (*20*, *21*) (Fig. 4D and fig. S68). Iron content and oxidation state also support the LL chondrite classification (Fig. 4E and fig. S58). Rare earth element abundances are more similar to L chondrites (Fig. 4F and table S18), whereas one measuring reflectance spectrum better matches that of H chondrites (fig. S72).

The Chelyabinsk (LL) parent body experienced a substantial thermal and/or collision resetting event 115 ± 21 million years after the formation of the solar system (*25*), not experienced by most other LL chondrites, possibly due to a major impact event near its site of origin on the parent body. The phosphate U-Pb age is 4452 ± 21 million years (SM section 4.8) (fig. S70), much younger than the majority of other ordinary chondrite phosphate ages dated by conventional thermal ionization mass spectrometry methods (*22*, *23*). Perhaps one other piece of evidence for this is the 4.48 ± 0.12 billion years Pb-Pb isochron age of phosphates in a granite-like fragment found in the LL3 to LL6 chondrite regolith breccia Adzhi-Bogdo (*24*), an observed fall in Mongolia in 1949.

Chelyabinsk shows a common orientation of metal grains indicating an impact-related petrofabric (fig. S59), stronger than that seen in any other ordinary chondrite of any shock stage (*26*) (fig. S60). This petrofabric probably reflects the most recent extraterrestrial shock event experienced by the

Chelyabinsk meteoroid. The magnetic susceptibility value is at the upper end of the range for LL type (fig. S61) (*27*), closer to L-type chondrites, suggestive of higher metal content in Chelyabinsk than a typical LL chondrite. However, detailed analysis of the remanent magnetization suggests that a shock event or the conditions of atmospheric entry led to substantial resetting of the remanence (SM section 4.3).

Recent meteoroid heating events are normally recorded by thermoluminescence (TL) (SM section 4.10). In this case, the induced TL level of Chelyabinsk is lower than other petrographic type 5 or 6 chondrites, possibly because shock metamorphism to the level of S4 (30 to 35 GPa) (fig. S79) destroyed feldspar, the mineral phase responsible for the TL signal (*28*). Atmospheric heating did not cause loss of natural TL signal, the steep thermal gradient being consistent with a very thin fusion crust on the measured samples (*29*). The natural TL value is consistent with the meteoroid's having been heated at a perihelion distance of 0.6 to 0.8 astronomical units (AU) (Table 1).

The shock did not remove all organic matter from the meteorite. Methanol-soluble polar organic compounds (SM section 4.11) were detected in impact melt vein and chondrite fractions using electrospray ionization ion cyclotron resonance Fourier-Transform mass spectrometry (*30*). Out of more than 18,000 resolved mass peaks, 2536 could be assigned to compounds containing C, H, N, O, or S. The organic signature is typical of other shocked LL chondrites, showing a higher abundance of oxygen and nitrogen atoms in the impact melt (fig. S83). The presence of oxygenated sulfur is indicated by CHOS compounds containing on average three more oxygen atoms than CHO and CHNO compounds. The high abundance of CHOS compounds in a homologous series across the entire mass range testifies that most of these did not result from terrestrial contamination.

Impact shock–induced fracturing on the Chelyabinsk parent body was followed by melting of metal and sulfides, which are pressure-driven through the cracks. There are cases in which this increased a meteorite's mechanical strength, the residual heat facilitating the process. However, in the case of Chelyabinsk, the production of cracks weakened the meteorite material more than shock melting increased its strength.

### Source and Evolution of the Chelyabinsk Meteoroid

Chelyabinsk adds an LL5 type meteorite to a short list (SM section 1.1) of 18 different types of meteorites with known pre-atmospheric orbits (*1*). Only 8.2% of falls are LL chondrites (*31*). The Chelyabinsk meteorite is of particular interest because it is of the same type as asteroid Itokawa, from which samples were collected by the Hayabusa Mission (*32*). Indeed, both Itokawa and Chelyabinsk have similar low-inclined low-semimajor axis orbits (Table 1), which, according to one model (*33*), imply a 62%, 11%, and 25% probability for Chelyabinsk (and 71%, 0%, and 29% probability for Itokawa) of originating from the secular $\nu_6$ resonance, the 3:1 mean-motion resonance, and the Intermediate Mars Crosser region, respectively. Multiplying these probabilities, assuming all LL chondrites enter the near-Earth object region through the same escape route, there is now an 86% probability that they originated from $\nu_6$. This supports the hypothesis (*34*) that they originated from the inner part of the LL-type (*35*) Flora asteroid family, which straddles the $\nu_6$ resonance in 1.6° to 7.7° inclined orbits (*36*).

As a group, LL chondrites have a cosmic ray exposure age peaking at ~17 million years (*34*). Chelyabinsk, on the other hand, was exposed only since ~1.2 million years ago (SM section 4.12). The responsible breakup that first exposed the Chelyabinsk meteoroid surface to cosmic rays was not likely part of the ongoing collision cascade in the asteroid main belt that followed the formation of the Flora family. Although fast pathways exist that can bring meteoroids from all three resonances into a Chelyabinsk-like orbit in about 0.2 million years, such cases are rare (table S6). More likely, Chelyabinsk was exposed only since being ejected from the resonance, due to breakup from either thermal stresses, rotational spin-up, or tidal forces in terrestrial planet encounters. The required structural weakness may have come from macroscopic cracks or from a weakly consolidated rubble-pile morphology.

If tidal forces disrupted the Chelyabinsk meteoroid (*37*), events were set in motion 1.2 million years ago during what was likely an earlier close encounter with Earth, when a 20-m sized chunk of subsurface Flora-family parent body rubble, rich in shock veins, separated from a larger object. The rest of that rubble could still be part of the near-Earth object population.

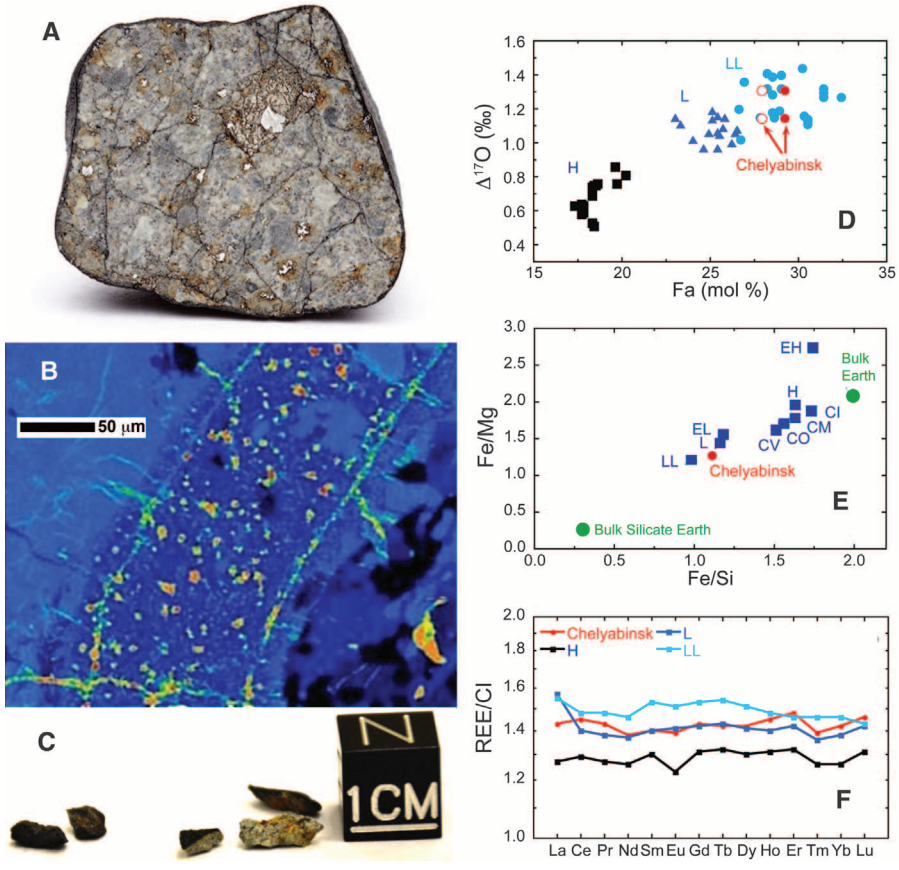


**Fig. 4. Meteorite material properties, chemical and isotopic compositions.** (**A**) Chelyabinsk meteorite (diameter ~4 cm) showing shock veins. (**B**) Fe element map of a shock vein. Note the metal layer (shown in green) located ~20 micrometers inside the vein. (**C**) Meteorite fragments recovered from the ice-covered lake Chebarkul. (**D**) $\Delta^{17}O$ versus Fa molar percent of olivine in Chelyabinsk, compared with other ordinary chondrites of type H, L, and LL (*38*). Fa is defined as molar ratio of Fe/(Fe+Mg) in olivine. Average $\Delta^{17}O$ values from the University of New Mexico (UNM) [1.15 ± 0.06 per mil (‰)] and from the Korea Polar Research Institute (KOPRI) (1.31 ± 0.04‰) for Chelyabinsk likely reflect indigenous heterogeneity in oxygen isotopes. Solid symbols are Fa number measured in this study (SM section S4.3), whereas open symbols are from (*18*). (**E**) Ratio plots of the three major elements (Mg, Si, Fe; together with oxygen >90% of mass) for Chelyabinsk and the main chondrite groups. The bulk Earth and bulk silicate Earth compositions were taken from (*39*), chondrite compositions from (*40*). (**F**) CI chondrite normalized rare earth elemental pattern of Chelyabinsk compared with the average chondrite group compositions of (*38*, *41*).

**References and Notes**

1. P. Jenniskens *et al*., *Science* **338**, 1583–1587 (2012).
2. M. B. E. Boslough, D. A. Crawford, *Ann. N.Y. Acad. Sci.* **822**, 236–282 (1997).
3. V. V. Svetsov, V. V. Shuvalov, in *Catastrophic Events Caused by Cosmic Objects*, V. Adushkin, I. Nemtchinov, Eds. (Springer, Dordrecht, Netherlands, 2008), pp. 227–267.
4. D. R. Christie, P. Campus, in *Infrasound Monitoring for Atmospheric Studies*, A. Le Pichon, E. Blanc, A. Hauchecorne, Eds. (Springer, Dordrecht, Netherlands, 2010), pp. 29–75.
5. D. Yeomans, P. Chodas, Additional Details on the Large Fireball Event over Russia on Feb. 15, 2013. *NASA NEO Program Office Announcement, March 1, 2013* (NASA, Washington, DC, 2013).
6. Materials and methods are available as supporting material on *Science Online*.
7. E. Tagliaferri, R. Spalding, C. Jacobs, S. P. Worden, A. Erlich, in *Hazards Due to Comets and Asteroids, Space Science Series*, T. Gehrels, M. S. Matthews. A. Schumann, Eds., (Univ. of Arizona Press, Tucson, AZ, 1994), pp. 199–220.
8. T. A. Ens, P. G. Brown, W. N. Edwards, E. A. Silber, *J. Atmos. Sol. Terr. Phys.* **80**, 208–229 (2012).
9. I. V. Nemtchinov *et al*., *Icarus* **130**, 259–274 (1997).
10. D. O. Revelle, Z. Ceplecha, *ESA Special Publ.* **495**, 507–512 (2001).
11. J. Borovicka, P. Spurny, L. Shrbeny, Trajectory and orbit of the Chelyabinsk superbolide. CBET 3423, Central Bureau for Astronomical Telegrams, International Astronomical Union (2013); www.icq.eps.harvard.edu/CBET3423.html
12. J. Zinn, J. Drummond, *JGR Space Physics* **110**, A04306 (2005).
13. S. Glasstone, P. J. Dolan, *The Effects of Nuclear Weapons, Third Edition* (U.S. Government Printing Office, Washington, DC, 1977).
14. M.-W. Huang, P.-Y. Lo, K.-S. Cheng, *EURASIP J. Adv. Signal Process.* **2010**, 483562 (2010).
15. O. Popova *et al*., *Meteorit. Planet. Sci.* **46**, 1525–1550 (2011).
16. G. J. Consolmagno, D. T. Britt, R. J. Macke, *Chem. Erde* **68**, 1–29 (2008).
17. A. Bischoff, E. R. D. Scott, K. Metzler, C. A. Goodrich, in *Meteorites and the Early Solar System II*, D. S. Lauretta, H. Y. McSween Jr., Eds. (Univ. of Arizona Press, Tucson, AZ, 2006), pp. 679–712.
18. M. A. Nazarov, D. D. Badyukov, N. N. Kononkova, I. V. Kubrakova, Chelyabinsk Meteoritical Bulletin: Entry for Chelyabinsk; http://www.lpi.usra.edu/meteor/metbull.php?code=57165 (2013).
19. D. Stöffler, K. Keil, E. R. D. Scott, *Geochim. Cosmochim. Acta* **55**, 3845–3867 (1991).
20. R. N. Clayton, T. K. Mayeda, J. N. Goswami, E. J. Olsen, *Geochim. Cosmochim. Acta* **55**, 2317–2337 (1991).
21. A. Trinquier, J.-L. Birck, C. J. Allègre, *Astrophys. J.* **655**, 1179–1185 (2007).
22. C. Göpel, G. Manhès, C. J. Allègre, *Earth Planet. Sci. Lett.* **121**, 153–171 (1994).
23. Y. Amelin, *Science* **310**, 839–841 (2005).
24. K. Terada, A. Bischoff, *Astrophys. J.* **699**, L68–L71 (2009).
25. J. N. Connelly *et al*., *Science* **338**, 651–655 (2012).
26. J. M. Friedrich, J. C. Bridges, M.-S. Wang, M. E. Lipschutz, *Geochim. Cosmochim. Acta* **68**, 2889–2904 (2004).
27. P. Rochette *et al*., *Meteorit. Planet. Sci.* **38**, 251–268 (2003).
28. C. P. Hartmetz, D. W. G. Sears, *Meteoritics* **22**, 400–401 (1988).
29. D. W. Sears, A. A. Mills, *Nat. Phys. Sci (London)* **242**, 25–26 (1973).
30. P. Schmitt-Kopplin *et al*., *Proc. Natl. Acad. Sci. U.S.A.* **107**, 2763–2768 (2010).
31. T. L. Dunn, T. H. Burbine, W. F. Bottke Jr., J. P. Clark, *Icarus* **222**, 273–282 (2013).
32. T. Nakamura *et al*., *Science* **333**, 1113–1116 (2011).
33. W. F. Bottke *et al*., *Icarus* **156**, 339–433 (2000).
34. P. Michel, M. Yoshikawa, *Astron. Astrophys.* **449**, 817–820 (2006).
35. V. Reddy *et al*., *Icarus* **216**, 184–197 (2011).
36. D. Nesvorny, A. Morbidelli, D. Vokrouhlicky, W. F. Bottke, M. Broz, *Icarus* **157**, 155–172 (2002).
37. E. Schunová *et al*., *Icarus* **220**, 1050–1063 (2012).
38. J. Troiano, D. Rumble III, M. L. Rivers, J. M. Friedrich, *Geochim. Cosmochim. Acta* **75**, 6511–6519 (2011).
39. W. F. McDonough, in *The Mantle and Core, Vol. 2, Treatise on Geochemistry*, R. W. Carlson, Ed. (Elsevier-Pergamon, Oxford, 2003), pp. 547–568.
40. J. T. Wasson, G. W. Kallemeyn, *Phil. Trans. R. Soc. London A* **325**, 535–544 (1988).
41. J. M. Friedrich, M.-S. Wang, M. E. Lipschutz, *Geochim. Cosmochim. Acta* **67**, 2467–2479 (2003).



**Acknowledgments:** The Russian Academy of Sciences (RAS) field study of the Chelyabinsk airburst was supported by the Institute for Dynamics of Geospheres and grants of the Federal Targeted Program Scientific and Educational Human Resources of Innovation-Driven Russia and the RAS Presidium Program Fundamental Problems of Investigation and Exploration of the Solar System. The office of Chelyabinsk Oblast Governor Mikhail Yurevich provided assistance. S. Petukhov and I. Talyukin from the Universe History Museum in Dedovsk contributed samples, as did M. Boslough of Sandia National Laboratories. U. Johann (Astrium Satellites GmbH) calculated the Chebarkul hole position from Pléiades 1A satellite observations. D. F. Blake provided use of a petrographic microscope. P.J. acknowledges support from the NASA Near Earth Object Observation Program, Q.Z.Y. and M.E.Z. from the NASA Cosmochemistry Program, and M.G. from the Academy of Finland.


**Supplementary Materials**

www.sciencemag.org/content/342/6162/1069/suppl/DC1
Supplementary Text
Figs. S1 to S87
Tables S1 to S24
References (*42*–*157*)


1 July 2013; accepted 28 October 2013
Published online 7 November 2013;
10.1126/science.1242642




# Nanoscale $Fe_2O_3$-Based Catalysts for Selective Hydrogenation of Nitroarenes to Anilines


**Rajenahally V. Jagadeesh,[1] Annette-Enrica Surkus,[1] Henrik Junge,[1] Marga-Martina Pohl,[1] Jörg Radnik,[1] Jabor Rabeah,[1] Heming Huan,[2] Volker Schünemann,[2] Angelika Brückner,[1] Matthias Beller[1]***



**Production of anilines—key intermediates for the fine chemical, agrochemical, and pharmaceutical industries—relies on precious metal catalysts that selectively hydrogenate aryl nitro groups in the presence of other easily reducible functionalities. Herein, we report convenient and stable iron oxide ($Fe_2O_3$)–based catalysts as a more earth-abundant alternative for this transformation. Pyrolysis of iron-phenanthroline complexes on carbon furnishes a unique structure in which the active $Fe_2O_3$ particles are surrounded by a nitrogen-doped carbon layer. Highly selective hydrogenation of numerous structurally diverse nitroarenes (more than 80 examples) proceeded in good to excellent yield under industrially viable conditions.**


Beginning in the 1950s, the development of organometallic catalysts proceeded to revolutionize organic synthesis at scales ranging from the laboratory bench to the industrial manufacture of fine and bulk chemicals. This success was mainly due to the use of noble metal complexes—for example, palladium, rhodium, ruthenium, and iridium (*1*). However, the high price and limited availability of these precious metals (*2*) have spurred interest in catalysis with more earth-abundant alternatives, especially iron (*3*–*8*). The durability and copious supply of iron salts coupled with their environmentally benign nature and low toxicity make them ideal catalysts. Recently, structurally well-defined molecular iron complexes have been applied successfully in contexts where previously noble metals were required (*9*–*19*). However, most of these homogeneous complexes are rather sensitive and/or incorporate sophisticated (and thus synthetically demanding) ligand systems. In contrast, heterogeneous iron oxides are extremely stable and can be easily recycled. Important applications of heterogeneous iron catalysts include the production of olefins through the Fischer-Tropsch process (*20*, *21*) and the hydrogenation of CO (*22*). Unfortunately, these known catalysts work under drastic conditions (>275°C) and are therefore of limited use for the refinement of more complex substrates. In this context, we report special iron oxide–based catalysts that allow for a general and highly selective hydrogenation of nitroarenes under comparably mild conditions. The resulting anilines constitute key building blocks for the synthesis of fine (agrochemicals, dyes, pigments, and pharmaceuticals) as well as bulk chemicals (polymers) (*23*, *24*). In particular, anilines used in life science applications are often structurally complex molecules decorated with diverse functional groups. Thus, achieving high chemoselectivity is of crucial importance for


[1]Leibniz-Institut für Katalyse e.V. an der Universität Rostock, Albert-Einstein Strasse 29a, D-18059 Rostock, Germany [2]Technische Universität Kaiserslautern, Fachbereich Physik, Erwin-Schrödinger-Strasse 46, D-67663 Kaiserslautern, Germany.

*Corresponding author. E-mail: matthias.beller@catalysis.de

any catalyst development. Among the different known reductions of nitroarenes, catalytic hydrogenation represents the most benign and cost-efficient route (*25*–*31*). Until today, such hydrogenations have been mainly carried out using noble metal catalysts. With respect to chemoselectivity, important advancements have been reported by Corma and co-workers using gold catalysts (*30*) and recently by our group applying $Co_3O_4$-based materials (*31*).

To improve the hydrogenation activity of bulk iron oxides, we explored the synthesis of nanoscale iron oxides supported on nitrogen-doped surfaces. For this purpose, iron nitrogen complexes were prepared by mixing iron(II) acetate in ethanol at room temperature with 1,10-phenanthroline (phen) (for other nitrogen ligands, see the supplementary materials). The resulting metal complex was deposited onto carbon (Vulcan XC72R), titanium dioxide (P25), or aluminum oxide at 60°C followed by pyrolysis at higher temperatures under inert gas atmosphere (for details, see the supplementary materials). Hereafter, the carbon-supported catalysts are labeled as Fe-phen/C-x, where x denotes the pyrolysis temperature.

All the prepared materials were tested for their hydrogenation activity toward the industrially important substrate nitrobenzene in a water-tetrahydrofuran (THF) solvent mixture. Parameters such as pyrolysis temperature, pyrolysis time, type of support, nitrogen ligands, and Fe:ligand molar ratios were systematically investigated (table S1). Neither the homogeneous iron complexes nor supported $Fe(OAc)_2$ without any ligand were active (table S1, entries 1 to 6). Similarly, the material containing supported $Fe(OAc)_2$-phenanthroline without pyrolysis was also not active (table S1, entry 7). However, after pyrolysis the resulting catalysts showed different activity (table S1, entries 8 to 12). On increasing the pyrolysis temperature from 200°C to 800°C, the activity of the resulting catalyst steadily increased. The material pyrolyzed at 800°C (Fe-phen/C-800) showed maximum activity: The benchmark substrate nitrobenzene was hydrogenated to give aniline in excellent yield (98%) (table S1, entry 11). Upon further raising the pyrolysis temperature to 1000°C, the activity of the resulting catalyst decreased (table S1, entry 12). Pyrolysis of the phenanthroline-based iron complexes on $TiO_2$ and $Al_2O_3$ supports also gave active catalyst materials but produced aniline only in lower yields of 49 to 78% (table S1, entries 13 and 14).

To demonstrate the general applicability of the catalyst, we explored the hydrogenation of more than 80 diverse nitroarenes and consistently obtained the corresponding anilines in excellent yields and selectivities (Figs. 1 and 2 and fig. S2). In addition to amino and halogen substituents (the latter present in key agrochemical intermediates), sensitive functional groups such as aldehydes, ketones, nitriles, esters, amides, and olefins were well tolerated without being reduced to any substantial extent. In addition to benchmark substrates, marketed nitro-substituted drugs—for example, Nimodipine, Nilutamide, Nimesulide Flutamide, and Niclosamide—were hydrogenated to the respective amines with high selectivity (Fig. 2). Moreover, amino-benzonitriles, which constitute common building blocks for the chemical industry, could be accessed in up to 88% yield (Fig. 2 and fig. S2).

We then tested a variety of heterocyclic nitro compounds (Fig. 2 and fig. S2). Amino-substituted *N*-heterocycles in particular are important intermediates in the pharmaceutical and agrochemical industries. Again, all the catalytic hydrogenations proceeded smoothly, and we obtained the corresponding heteroaromatic amines in good to excellent yields. To demonstrate the utility of this method, we performed several gram-scale reactions (>20 mmol) for selected substrates (see fig. S4). In all cases, similar yields to the standard 0.5 mmol–scale experiments were obtained.

Next, we investigated the stability and recyclability of the catalyst, which are crucial performance metrics for cost-effective industrial processes. The iron catalyst was recycled and conveniently reused seven times without any reactivation (fig. S3). After the fifth recycling, some gradual decrease in the activity is observed. Nevertheless, full conversion was obtained after prolonged reaction time.

To elucidate reasons for the markedly different catalytic activity of the Fe-phen/C-x catalysts compared with known iron oxides, the effects of pyrolysis temperature and ligand on the structure of the catalysts were investigated in detail by transmission electron microscopy (TEM), x-ray photoelectron spectroscopy (XPS), electron paramagnetic resonance (EPR), and Mössbauer spectroscopy. The TEM image of the inactive Fe-phen/C-400 shows essentially no iron oxide particles; only very small features (<1 nm) of weak contrast within cloudy agglomerates are observed (Fig. 3A). The energy-dispersive x-ray (EDX) analysis (fig. S5C) indicates a rather homogeneous distribution of iron within these agglomerates. However, the active catalyst Fe-phen/C-800 is characterized by $Fe_2O_3$ particles of different size (Fig. 3B and fig. S5D). Their oxidic nature is confirmed by Mössbauer, XPS, and EPR results presented in the supplementary materials. Most of the oxide particles have a size between 20 and 80 nm but occur together with smaller particles of 2- to 5-nm size [Fig. 3B, high-angle annular dark field (HAADF) image].

The iron oxide particles of the active catalyst are surrounded by a shell of 3 to 5 nitrogen-doped graphene layers [marked by arrows in the annular bright field (ABF) image, Fig. 3B]. When the pyrolysis temperature is raised to 1000°C, small particles ($d \leq 5$ nm) collapse into well-faceted larger ones of 50- to 60-nm size, which are shielded by a 10- to 40-nm-thick graphite layer. This is evident from the TEM images of sample Fe-phen/C-1000 in Fig. 3C. Supported iron-nitrogen complexes used in fuel cell applications were reported to have different structures (*32*–*34*).

The growth of particles within the Fe-phen/C series is also supported by EPR and Mössbauer results, which confirm additionally that the Fe particles might have a $\gamma$-$Fe_2O_3$–like structure (see fig. S8). Because no conclusive information on the location of nitrogen in the samples could be obtained by TEM/EDX analysis, due to superposition of C and N signals, XPS studies have been performed (Fig. 4). In nonpyrolyzed Fe-phen/C, two N1s peaks occur at 398.7 eV and 400.1 eV, which are assigned to pyridinic nitrogen and Fe-N centers, respectively (*35*). The former peak might reflect N within the free ligand, whereas the latter

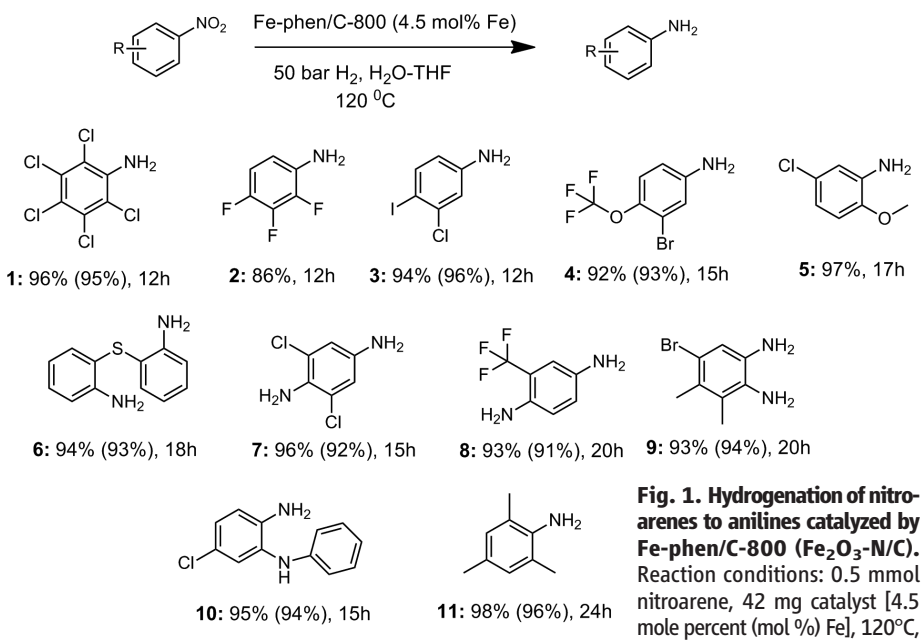


**Fig. 1. Hydrogenation of nitroarenes to anilines catalyzed by Fe-phen/C-800 ($Fe_2O_3$-N/C).** Reaction conditions: 0.5 mmol nitroarene, 42 mg catalyst [4.5 mole percent (mol %) Fe], 120°C, 1:1 water-THF (4 mL), 50 bar $H_2$. Conversion and yields were determined by gas chromatography (GC) using n-hexadecane (100 μL) standard. Yields in parentheses refer to isolated yields. In all cases, complete conversion of nitroarene was observed.

arises from ligand N atoms coordinating to Fe. In Fe-phen/C-400 and, to a more pronounced extent, in the most active catalyst, Fe-phen/C-800, these peaks are shifted to lower binding energies (398.3 eV and 399.3 eV). A similar shift, and even a splitting, of the N1s peak was observed for 2H-tetraphenylporphyrin monolayers in contact with deposited Fe atoms on top. It was assigned to a so-called distorted $FeN_4$ center (*36*), in which the Fe-N distances are slightly different, thus giving rise to the peak splitting. It is probable that similar $FeN_x$ centers are formed with progressing pyrolysis on the surface of the emerging iron oxide particles. The fact that no splitting of the peak at 399.3 eV is observed may be due to a distribution of Fe-N distances that just contributes to the line width. A further N1s peak is observed in sample Fe-phen/C-800 at 401.0 eV, which gains intensity after pyrolysis at 1000°C and which can be assigned to nitrogen in a graphite-like structure (*35*). This suggests that N is incorporated into the support lattice. In the less active catalyst Fe-phen/C-1000, the characteristic peak of $FeN_x$ centers around 399.3 eV disappears, leaving behind only the signals of pyridinic (398.6 eV) and graphite-enclosed nitrogen (401.0 eV). Simultaneously, a loss of nitrogen was observed with rising pyrolysis temperature in both the near-surface region and the bulk, and the surface Fe/N ratio decreased from around 7 in catalysts Fe-phen/C-400 and Fe-phen/C-800 to 3.6 in sample Fe-phen/C-1000 (table S3). These results indicate a decomposition of the $FeN_x$ centers during pyrolysis at 1000°C, accompanied by partial sublimation and incorporation of nitrogen into the support structure.

In contrast to the most active sample, Fe-phen/C-800, the poorly active Fe-bipyridyl/C-800 catalyst shows only one N1s peak typical for pyridinic nitrogen (398.6 eV). No hints for Fe-N centers were found (fig. S9). Moreover, TEM indicates much larger $Fe_2O_3$ particles for this material that consist of several crystallites and that are not surrounded by a graphene layer (fig. S5A). This is also true when the catalyst is prepared in the same way, but without any ligand, in which well-faceted big particles of 100- to 800-nm size are formed [fig. S5B, sample $Fe(OAc)_2$/C-800]. For sample Fe-phen/$Al_2O_3$-800, which is almost as active as sample Fe-phen/C-800 (table S1), XPS points to a very similar nature of the N species, including the presence of $FeN_x$ (fig. S10), whereas TEM/EDX indicates a rather homogeneous distribution of Fe on the support with hardly any pronounced particle formation (fig. S6 B). In contrast, very large needle-like particles are formed in catalyst Fe-phen/$TiO_2$-800, which are covered by a few graphene layers (fig. S6 A) containing $FeN_x$ species as evidenced by XPS (fig. S11).

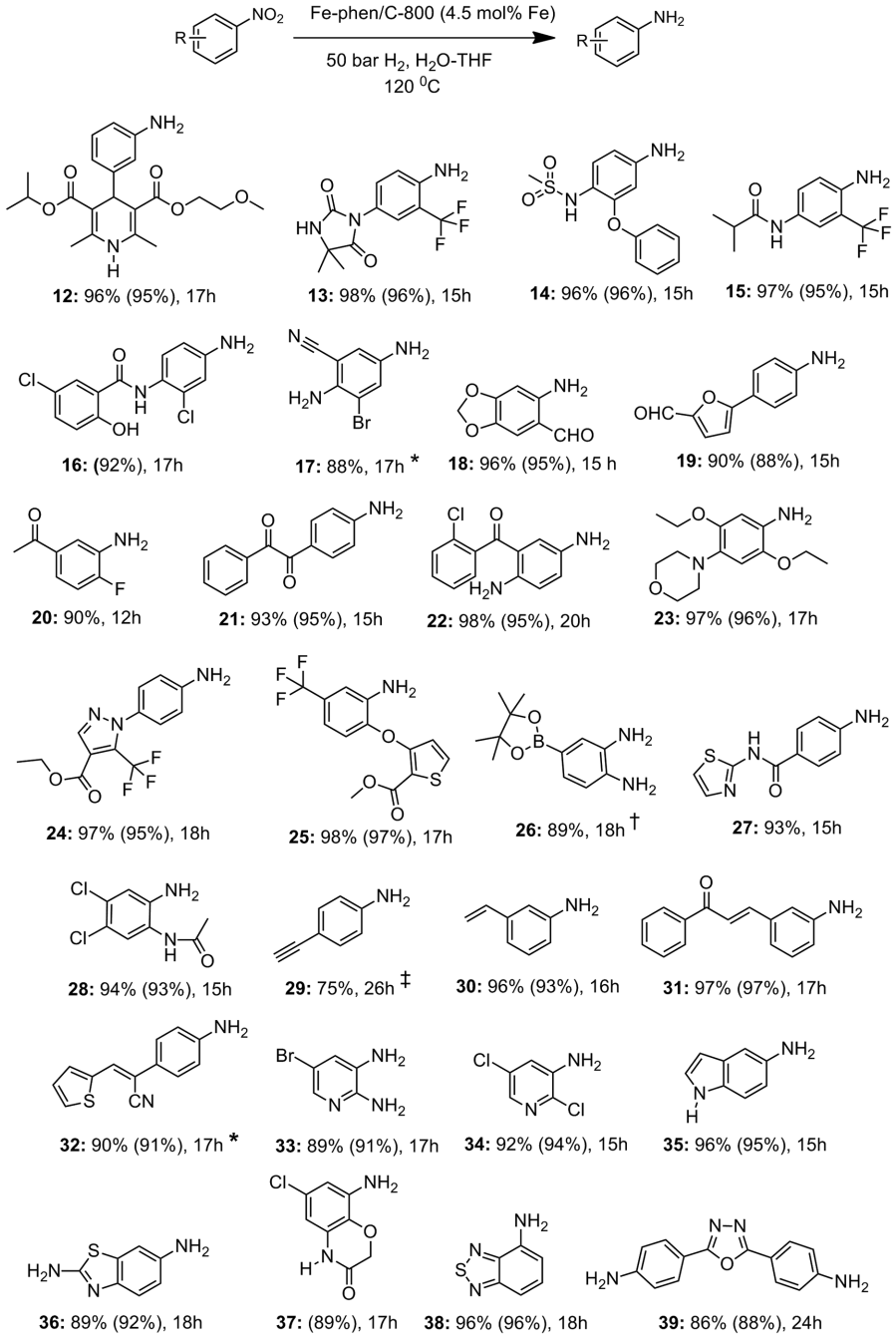


**Fig. 2. Fe-phen/C-800 ($Fe_2O_3$-N/C)–catalyzed hydrogenation of functionalized nitroarenes and nitro-heterocyclic compounds.** Reaction conditions: 0.5 mmol nitroarene, 42 mg catalyst (4.5 mol % Fe), 120°C, 1:1 water-THF (4 mL), 50 bar $H_2$. Conversion and yields were determined by GC using n-hexadecane (100 μL) standard. Yields in parentheses refer to isolated yields. In all cases, complete conversion of nitroarene was observed. *, in 0.5:4 water-THF solvent (4.5 mL). †, in 4 mL *t*-amylalcohol at 130°C. ‡, at 105°C with 60 mg catalyst.

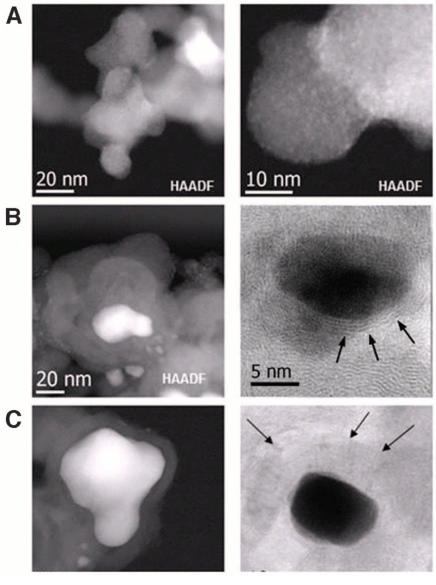


**Fig. 3. HAADF and ABF TEM images of Fe-phen-/C-x catalysts.** (**A**) Fe-phen/C-400. (**B**) Fe-phen/C-800. (**C**) Fe-phen/C-1000.

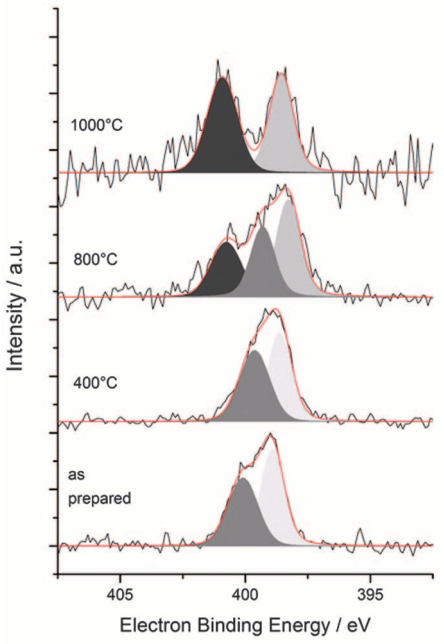


**Fig. 4. XP spectra of the N1s electrons for the Fe-phen/C catalyst as prepared and after different pyrolysis temperatures.**

Comparison of characterization and catalytic results suggests that it is these particular $FeN_x$ centers formed in a narrow range of pyrolysis temperatures around 800°C that govern the unique catalytic activity. The size of the iron oxide particles seems to play a minor role as long as their growth does not reduce the exposed catalytically active surface, as might be the case in catalyst Fe-phen/$TiO_2$-800.

### References and Notes


1. B. Cornils, W. A. Herrmann, *Applied Homogeneous Catalysis with Organometallic Compounds* (Wiley-VCH, ed. 2, Weinheim, Germany, 2002).
2. Johnson Matthey, Platinum Today; www.platinum.matthey.com
3. B. Plietker, *Iron Catalysis in Organic Chemistry* (Wiley-VCH, Weinheim, Germany, 2008).
4. C. Bolm, *Nat. Chem.* **1**, 420 (2009).
5. C. Bolm, J. Legros, J. Le Paih, L. Zani, *Chem. Rev.* **104**, 6217–6254 (2004).
6. S. Enthaler, K. Junge, M. Beller, *Angew. Chem. Int. Ed.* **47**, 3317–3321 (2008).
7. C.-L. Sun, B.-J. Li, Z.-J. Shi, *Chem. Rev.* **111**, 1293–1314 (2011).
8. K. Gopalaiah, *Chem. Rev.* **113**, 3248–3296 (2013).
9. J. L. Fillol *et al.*, *Nat. Chem.* **3**, 807–813 (2011).
10. Y. Hitomi, K. Arakawa, T. Funabiki, M. Kodera, *Angew. Chem. Int. Ed.* **51**, 3448–3452 (2012).
11. A. M. Tondreau *et al.*, *Science* **335**, 567–570 (2012).
12. B. Morandi, E. M. Carreira, *Science* **335**, 1471–1474 (2012).
13. E. T. Hennessy, T. A. Betley, *Science* **340**, 591–595 (2013).
14. A. Boddien *et al.*, *Science* **333**, 1733–1736 (2011).
15. F. Gärtner *et al.*, *Chemistry* **17**, 6425–6436 (2011).
16. K. M. Driller, S. Prateeptongkum, R. Jackstell, M. Beller, *Angew. Chem. Int. Ed.* **50**, 537–541 (2011).
17. C. Ziebart *et al.*, *J. Am. Chem. Soc.* **134**, 20701–20704 (2012).
18. R. V. Jagadeesh *et al.*, *Chem. Commun.* **47**, 10972–10974 (2011).
19. J. R. Cabrero-Antonino, A. Leyva-Pérez, A. Corma, *Chemistry* **19**, 8627–8633 (2013).
20. H. M. T. Galvis *et al.*, *Science* **335**, 835–838 (2012).
21. A. C. J. Koeken, H. M. T. Galvis, T. Davidian, M. Ruitenbeek, K. P. de Jong, *Angew. Chem. Int. Ed.* **51**, 7190–7193 (2012).
22. Z. Yang, S. Guo, X. Pan, X. Jawing, X. Bao, *Environ. Sci.* **4**, 4500–4503 (2011).
23. N. Ono, *The Nitro Group in Organic Synthesis* (Wiley-VCH, New York, 2001).
24. H.-U. Blaser, U. Siegrist, H. Steiner, *Aromatic Nitro Compounds: Fine Chemicals Through Heterogeneous Catalysis* (Wiley-VCH, Weinheim, Germany, 2001).
25. H.-U. Blaser, H. Steiner, M. Studer, *Chem. Cat. Chem.* **1**, 210–221 (2009).
26. J. Li, X.-Y. Shi, Y.-Y. Bi, J.-F. Wei, Z.-G. Chen, *ACS Catal.* **1**, 657–664 (2011).
27. M. Takasaki *et al.*, *Org. Lett.* **10**, 1601–1604 (2008).
28. Y. Motoyama *et al.*, *Chem. Cat. Chem.* **3**, 1578–1581 (2011).
29. V. Pandarus, R. Ciriminna, F. Beland, M. Pagliaro, *Adv. Synth. Catal.* **353**, 1306–1316 (2011).
30. A. Corma, P. Serna, *Science* **313**, 332–334 (2006).
31. F. A. Westerhaus *et al.*, *Nat. Chem.* **5**, 537–543 (2013).
32. E. Proietti *et al.*, *Nat. Commun.* **2**, 416 (2011).
33. W. Li, A. Yu, D. C. Higgins, B. G. Llanos, Z. Chen, *J. Am. Chem. Soc.* **132**, 17056–17058 (2010).
34. M. Lefèvre, E. Proietti, F. Jaouen, J.-P. Dodelet, *Science* **324**, 71–74 (2009).
35. F. Jaouen *et al.*, *ACS Appl. Mater. Interfaces* **1**, 1623–1639 (2009).
36. F. Buchner *et al.*, *J. Phys. Chem. C* **112**, 15458–15465 (2008).


**Acknowledgments:** We gratefully acknowledge the support from the Federal Ministry of Education and Research (BMBF) and the State of Mecklenburg-Vorpommern. We thank the analytical department of the Leibniz-Institute for Catalysis, Rostock for the nuclear magnetic resonance measurements. The Leibniz Institute for Catalysis has filed a patent on the catalysts reported herein. Author contributions: M.B. and R.V.J. planned the project; R.V.J. developed and prepared the catalysts; R.V.J designed and performed all catalytic hydrogenation experiments; R.V.J., M.B., and A.B. wrote the paper; A.-E.S., H.J., and M.B were involved in the development of this class of catalysts; M.-M.P. performed TEM measurements and analysis; J. Radnik did the XPS measurements; J. Rabeah and A.B. conducted EPR measurements; and H.H. and V.S. performed Mössbauer measurements.

### Supplementary Materials

www.sciencemag.org/content/342/6162/1073/suppl/DC1
Materials and Methods
Figs. S1 to S11
Tables S1 to S3
References (*37*–*42*)

17 June 2013; accepted 2 October 2013
10.1126/science.1242005

# Cobalt Precursors for High-Throughput Discovery of Base Metal Asymmetric Alkene Hydrogenation Catalysts

**Max R. Friedfeld,[1] Michael Shevlin,[2] Jordan M. Hoyt,[1] Shane W. Krska,[2] Matthew T. Tudge,[2] Paul J. Chirik[1]**

**Asymmetric hydrogenation of alkenes is one of the most widely used methods for the preparation of single enantiomer compounds, especially in the pharmaceutical and agrochemical industries. For more than four decades, precious metal complexes containing rhodium, iridium, and ruthenium have been predominantly used as catalysts. Here, we report rapid evaluation of libraries of chiral phosphine ligands with a set of simple cobalt precursors. From these studies, base metal precatalysts have been discovered for the hydrogenation of functionalized and unfunctionalized olefins with high enantiomeric excesses, demonstrating the potential utility of more earth-abundant metals in asymmetric hydrogenation.**

Asymmetric hydrogenation of prochiral molecules catalyzed by chiral metal compounds has emerged as one of the most effective and widely used synthetic methods for the preparation of single-enantiomer compounds and has matured into a transformative technology for the pharmaceutical and agrochemical industries (*1*–*3*). This methodology has been applied to the commercial synthesis of the pesticide metolachlor (*4*) as well as routes to the Parkinson's drug L-DOPA (*1*, *5*) and blockbusters, including Pfizer's pregablin (*6*) and Merck's sitagliptin (*7*–*9*). The approval of nonracemic drug candidates by the U.S. Food and Drug Administration (FDA) has increased from 58% in 1992 to 75% in 2006 (*10*) and now constitutes a $15 billion industry (*11*). This history, coupled with ever-shortening periods for market exclusivity for first-in-class drugs (*12*), suggests that asymmetric hydrogenation will continue to be embraced for drug synthesis and manufacture (*9*, *10*, *13*).

Methods for catalyst generation, first reported in 1968 (*14*, *15*), rely on addition of a chiral ligand to a precious metal precursor, which is typically a compound containing rhodium, iridium, or ruthenium. Reliable substitution chemistry coupled with available metal precursors (*16*) has enabled the synthesis of hundreds of precatalysts that can be rationally tuned to overcome challenges encountered with activity and selectivity. Automation of this process has enabled high-throughput experimentation and resulted in the discovery of optimized catalysts and conditions, culminating in the development of asymmetric hydrogenation on an industrial scale (*12*).

Despite these successes, the full potential of asymmetric hydrogenation has yet to be realized.

[1]Department of Chemistry, Princeton University, Princeton, NJ 08540, USA. [2]Department of Process Chemistry, Merck Research Laboratories, Rahway, NJ 07065, USA.

Most precious metal catalysts are effective for only a small class of specifically functionalized olefins that engage in two-point binding to achieve high enantioselectivity, thus limiting the number of substrates that give high enantioselectivity (*17*, *18*). Specialized iridium catalysts have been reported by Pfaltz, and later Andersson and Burgess, that overcome some of these limitations, hydrogenating certain unfunctionalized alkenes with high asymmetric induction (*19*–*21*).

Catalysts that contain earth-abundant elements such as iron and cobalt are attractive because of potential cost and environmental advantages (*22*). The smaller atomic radii of the first-row transition metals and their distinct electronic structures offer opportunities for a new class of catalysts that may expand the utility of asymmetric hydrogenation. Examples of cobalt-catalyzed alkene hydrogenation have been known for some time by using borohydride salts or hydrogen as the terminal reductant, although their substrate scope is limited, and in some cases, the activities and selectivities are not synthetically viable (*23*–*27*). More recently, bis(imino)pyridine–(*28*) and bis(phosphine)amine–ligated (*29*, *30*) cobalt(II) alkyl complexes have been reported that exhibit improved turnover frequencies for the hydrogenation of simple, unactivated terminal and internal alkenes. Our laboratory has reported enantiopure, $C_1$ symmetric variants of the former catalyst class that are effective for the hydrogenation of substituted styrenes with high activity and enantioselectivity (*31*). Modification of the cobalt precatalysts however, requires multistep synthesis and accompanying purification, presenting obstacles for automated high-throughput catalyst evaluation. Discovery of accessible cobalt precursors capable of efficient in situ catalyst formation with common chiral ligands would enable more rapid optimization. Here, we describe the discovery of a variety of cobalt precursors that, in combination with enantiopure bidentate phosphines identified via high-throughput screening, generate base metal precatalysts that are highly active and selective for the asymmetric hydrogenation of both functionalized and unfunctionalized alkenes.

The success of Co(II) complexes in catalytic hydrogenation prompted exploration of precursors with this oxidation state. Budzelaar and coworkers reported the synthesis of $(py)_2Co(CH_2SiMe_3)_2$ (py, pyridine) and displacement of the pyridine ligands by various tridentate N-donor ligands (*32*). These observations inspired examination of the scope of this reaction with chiral phosphines to generate single-enantiomer cobalt precatalysts. Given the commercial availability and success of enantiopure bidentate phosphines in asymmetric catalysis (*2*), 192 commercially available or readily synthesized ligands were assayed for cobalt-catalyzed asymmetric hydrogenation. The hydrogenation of methyl 2-acetamidoacrylate (MAC) was chosen as a representative substrate because of the ubiquity of the unsaturated α-amino acid motif in general, and MAC in particular, in the asymmetric hydrogenation literature (*3*). In a typical experiment, 10 mole percent (mol %) of the phosphine and cobalt precursor were stirred for 20 min followed by removal of the volatiles under vacuum and addition of a 0.041 M tetrahydrofuran (THF) solution of the alkene, followed by pressurization with 500 psi (34 atm) of $H_2$. Relatively high metal-ligand loadings were used in the initial evaluations to maximize the probability for identifying successful combinations. The enantioselectivity of each reaction was assayed by means of chiral supercritical fluid chromatography (SFC) after 20 hours of reaction time. With $(py)_2Co(CH_2SiMe_3)_2$ as the cobalt source, only a few selected phosphines produced reasonable conversion and enantioselectivity. (*R*,*R*)-$^{iPr}$DuPhos and $(py)_2Co(CH_2SiMe_3)_2$ furnished >99% conversion to product in 91.7% enantiomeric excess, with a preference for the (*S*) stereoisomer of the alkane.

To explore the possibility that pyridine might inhibit phosphine coordination and hence catalyst formation, we performed a second high-throughput screen using $CoCl_2$ in combination with two equivalents of $LiCH_2SiMe_3$ and the 192 phosphines evaluated previously. We conducted the asymmetric hydrogenation of MAC using the conditions and analytical techniques described in the preceding paragraph. Selected phosphine-cobalt combinations that produced high conversion and enantioselectivity are highlighted in Fig. 1. A complete listing of the phosphines and their respective yields and enantioselectivities are reported in table S2. Unlike the experiment with $(py)_2Co(CH_2SiMe_3)_2$, this protocol revealed many phosphine-cobalt combinations that furnished both high conversion and enantioselectivity, indicating that pyridine is deleterious for catalyst formation in some cases. Bidentate phosphines with two-carbon atom linkers proved most effective because (*R*,*R*)-QuinoxP*, (*R*,*R*)-$^{Et}$BPE, (*R*,*R*)-$^{iPr}$DuPhos, (*R*,*R*)-BenzP*, and (*S*,*S*′,*R*,*R*′)-TangPhos also yielded the alkane in over 90% conversion and 90% enantioselectivity.

The success of $CoCl_2$ activated with $LiCH_2SiMe_3$ and various chiral bidentate phosphines prompted exploration of other air-stable cobalt(II) precursors. Subsequent experiments were conducted with (*R*, *R*)-$^{iPr}$DuPhos as a representative phosphine because of its commercial availability and widespread use in asymmetric catalysis. Each experiment was conducted with 10 mol % each of the cobalt source and the disphosphine in a 0.041 M THF solution of MAC under 500 psi (34 atm) of $H_2$ at 22°C. A solution of the cobalt precursor and phosphine was mixed in methanol followed by solvent removal in vacuo and reconstitution in THF before addition of 20 mol % of activator. Results with various cobalt sources and activators are highlighted in Fig. 2, and a

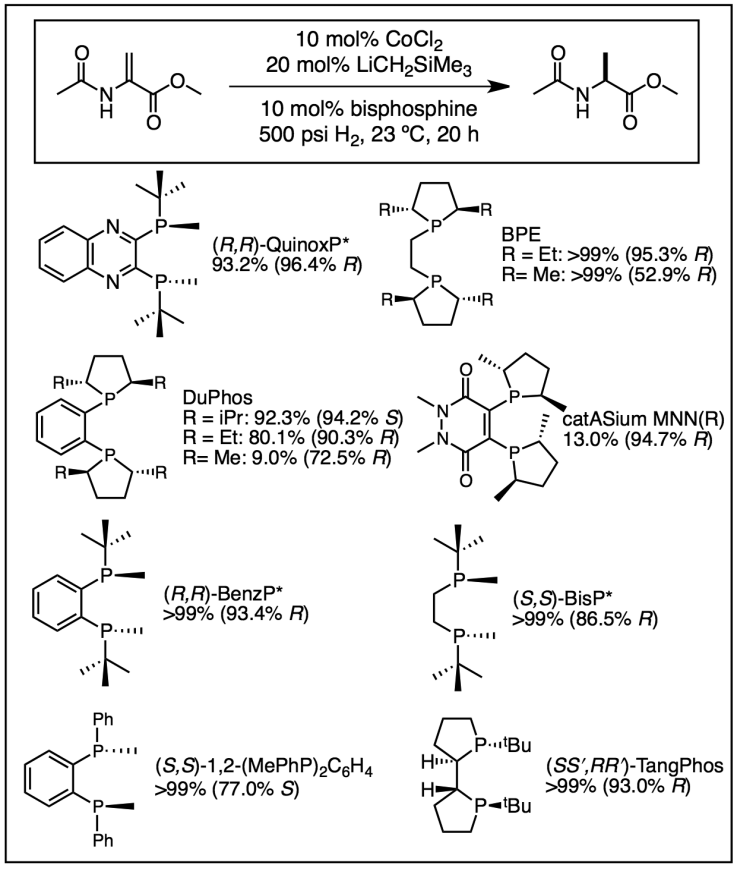


**Fig. 1. Chiral, bidentate phosphines that in combination with $CoCl_2$/2$LiCH_2SiMe_3$ produce high activity and enantioselectivity for the hydrogenation of MAC.** A complete listing of all phosphines evaluated is reported in table S2. Percentages correspond to the conversion to product, whereas those in the parentheses represent the percent enantiomeric excess.

complete listing of results is reported in fig. S23. Various air-stable, commercially available cobalt(II) dihalides and dicarboxylates were examined along with a cobalt(III) precursor, $Co(acac)_3$ (acac, acetylacetonate). A selection of commercially available alkyl and aryl Grigand and zinc reagents were examined as activators. The alkyl lithium reagent $LiCH_2SiMe_3$ was also included for comparison with previous screens.

The data presented in Fig. 2 identified anhydrous cobalt(II) halides and carboxylates as generally effective base metal sources, suggesting favorable phosphine coordination kinetics. Accordingly, (*R*, *R*)-$^{iPr}$DuPhosCoCl$_2$ and (*R*, *R*)-$^{iPr}$DuPhosCo(OBz)$_2$ have been independently prepared and crystallographically characterized (fig. S8). Among the activators examined, $LiCH_2SiMe_3$ and $ClMgCH_2SiMe_3$ were broadly effective, which is likely a result of smooth alkylation chemistry of the in situ–generated phosphine cobalt(II) dihalide or bis(carboxylate) compound. Hydrated cobalt sources were also examined and generated active catalysts, alleviating the requirement for stringently anhydrous reagents. Vacuum was applied after addition of the phosphines and likely removed most if not all of the water liberated from the cobalt source. For both anhydrous and hydrated salts, the chlorides were the most broadly effective, generating highly active and enantioselective catalysts with each activator examined. The results of this evaluation demonstrate that active and often stereoselective base metal catalysts can be generated from a diverse range of air-stable cobalt sources and commercially available activators.

Experiments were also conducted to reduce catalyst loadings. The combination of 1 mol % (*R*,*R*)-$^{iPr}$DuPhos with 1 mol % of $CoCl_2$ activated with two equivalents of $LiCH_2SiMe_3$ was effective for the hydrogenation of MAC, reaching completion in 24 hours with a slightly reduced enantiomeric excess of 91.4%, favoring the (*S*)-enantiomer of the alkane. This configuration of the chiral phosphine ligand also yields the (*S*)-enantiomer of the alkane after hydrogenation of MAC with rhodium catalysts (*33*). Increasing the total concentration of the reaction solution to 0.41 M and performing the hydrogenation with 58.7 psi (4 atm) of $H_2$ produced 98.7% conversion to (*S*)-alkane with 98.6% enantiomeric excess. Similarly, 5 mol % of $Co(OBz)_2$ in combination with 5 mol % of (*R*,*R*)-$^{iPr}$DuPhos and 10 mol % of $LiCH_2SiMe_3$ produced 98.5% conversion and 98.0% enantiomeric excess [(*S*)-alkane] over the course of 6 hours at 22°C with 58.7 psi (4 atm) of $H_2$. Impressive results were also obtained with isolated QuinoxP* cobalt compounds. In the presence of 1 mol % of isolated [(*R*, *R*)-QuinoxP*]Co($CH_2SiMe_3$)$_2$, the hydrogenation of MAC produced >99% conversion (18 hours) to (*R*)-alkane in 99% enantiomeric excess. In a second experiment, two equivalents of pyridine were added relative to the cobalt precursor, and the hydrogenation of MAC under otherwise identical conditions proceeded to 99% conversion with 96.5% enantiomeric excess. Likewise, a similar experiment with isolated [(*R*,*R*)-$^{iPr}$DuPhos]Co($CH_2SiMe_3$)$_2$ and two equivalents of added pyridine (based on Co) also produced 99% conversion and slight reduction of the enantioselectivity to 95.7%. In both cases, these results establish little inhibitory effect of added pyridine on cobalt catalysts for MAC hydrogenation.

In addition to MAC, the combination of (*R*,*R*)-($^{iPr}$DuPhos) with $CoCl_2$ activated with two equivalents of $LiCH_2SiMe_3$ was evaluated for the asymmetric hydrogenation of other functionalized alkenes (Fig. 3). Seeking a base metal–catalyzed route to α-amino acids, the hydrogenation of methyl 2-acetamido-3-phenylacrylate was examined and proceeded to >99% conversion and 92.7% enantiomeric excess in 12 hours at 22°C with 500 psi (34 atm) of $H_2$. Attempts to extend this catalytic protocol to hydrogenation of α-acetamidostyrene again produced excellent activity, reaching >99% conversion to alkane in 15 hours at 22°C. However, a modest enantiomeric excess of 40.8% was obtained, prompting a second iteration of catalyst evaluation. From these experiments, (*S*,*S*)-$^{Et}$DuPhos in combination with $CoCl_2$, activated with two equivalents of $LiCH_2SiMe_3$, was identified as an effective catalyst combination, reaching 99% conversion in 6 hours with 82.0% enantiomeric excess.

The versatility of the high-throughput screening approach and utility of the various cobalt precursors was evaluated in the hydrogenation of *trans*-methylstilbene, an alkene with little coordinating functionality. This class of substrate has proven one of the most challenging in asymmetric hydrogenation, and only a select class of specialized iridium catalysts are capable of achieving both high conversion and enantioselectivity (*34*–*37*). Because of the inhibitory effect of pyridine observed in formation of cobalt catalysts for MAC hydrogenation, $CoCl_2$/2$LiCH_2SiMe_3$ in combination with various chiral phosphines was initially examined. Few acceptable metal-ligand combinations were identified (table S6), and as a consequence, we returned to the initial precursor, (py)$_2$Co($CH_2SiMe_3$)$_2$, which is a more soluble and well-defined compound. A set of experiments was conducted with a library containing 192 chiral bidentate phosphines in combination with 10 mol % (py)$_2$Co($CH_2SiMe_3$)$_2$ with 500 psi (34 atm) of $H_2$ at 22°C. A typical procedure involved premixing the phosphine with (py)$_2$Co($CH_2SiMe_3$)$_2$ followed by removal of all volatile components by evacuation.

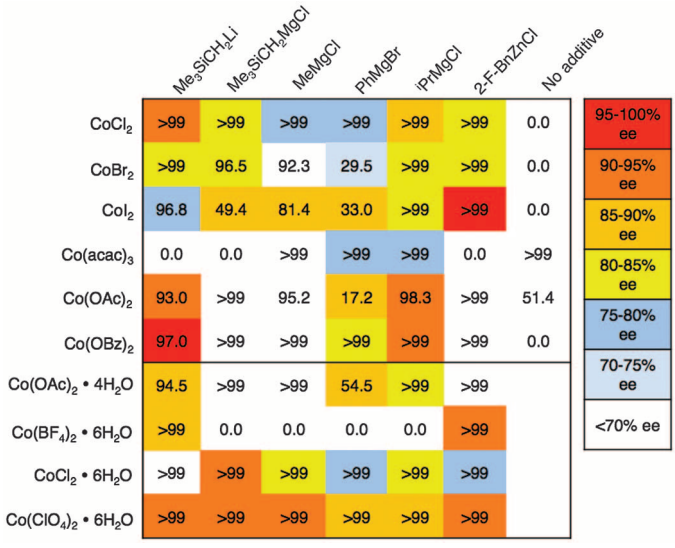


**Fig. 2. Cobalt-catalyzed asymmetric hydrogenation of MAC with air-stable, commercially available precursors with (*R*, *R*)-$^{iPr}$DuPhos.** The numerical values are conversion to alkane, and the color code quantifies the enantioselectivity (ee, enantiomeric excess).

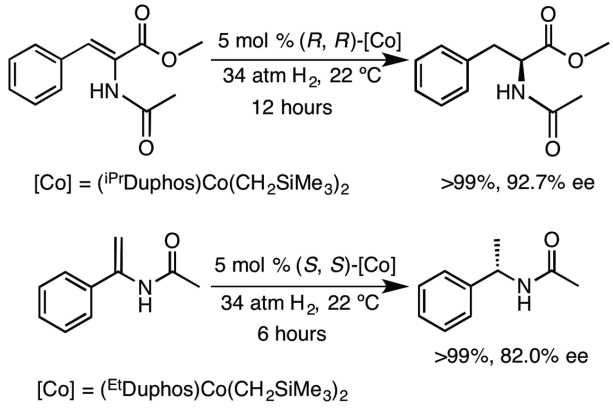


**Fig. 3. Asymmetric hydrogenation of amino acid and enamide derivatives with DuPhos cobalt dialkyl precatalysts.**

Presented in Fig. 4 are examples of phosphine-cobalt combinations that furnished the alkane in highest yields and enantioselectivities, a complete listing of results presented in table S6. Fewer phosphines than the MAC hydrogenations proved effective, highlighting the challenge associated with substrates lacking strongly coordinating functionality. Four-carbon-tethered, principally biaxial type phosphines were most effective, in contrast to MAC hydrogenations, for which two-carbon-linked ligands were preferred. The improved performance observed with the $(py)_2Co(CH_2SiMe_3)_2$ precursor is likely a result of more favorable ligand coordination kinetics with a soluble organometallic compound rather than with an anhydrous salt with an extended structure. Biphep derivative SL-A109-2 (*38*) was identified as an effective ligand for cobalt-catalyzed asymmetric hydrogenation, producing 83.1% conversion and 93.8% enantiomeric excess [(*R*)-alkane] after 20 hours at 22°C (Fig. 4). In a follow-up experiment, a reduced catalyst loading of 5 mol % resulted in an improved conversion and enantiomeric excess of 99 and 89%, respectively. Although higher catalyst loadings were used than for the known iridium catalysts, these results demonstrate that cobalt offers similar substrate versatility when paired with the appropriate phosphine ligand.

Additional studies were conducted to gain insight into the nature of the catalytically active cobalt species for the asymmetric hydrogenation of both MAC and *trans*-methyl stilbene. The success of (*R*,*R*)-$^{iPr}$DuPhos prompted exploration of well-defined cobalt dialkyl complexes with this bis(phosphine). Combination of toluene solutions of $(py)_2Co(CH_2SiMe_3)_2$ and (*R*,*R*)-$^{iPr}$DuPhos followed by filtration and recrystallization from pentane at –35°C furnished orange crystals of (*R*,*R*)-($^{iPr}$DuPhos)$Co(CH_2SiMe_3)_2$ in 95% yield. Likewise, (*R*,*R*)-($^{iPr}$DuPhos)$CoCl_2$ and (*R*,*R*)-($^{iPr}$DuPhos)$Co(OBz)_2$ were isolated as red solids in 97 and 86% yield after addition of the free bis(phosphine) to a THF suspension of $CoCl_2$ or $Co(OBz)_2$, respectively. Magnetic measurements on all three compounds established low-spin Co(II) complexes, with $S = 1/2$ ground states. The solid-state structures were determined by means of x-ray diffraction and confirm the essentially planar geometries about the cobalt atom (fig. S8). The chloride complex is slightly more distorted than the alkyl derivative, with the two halide ligands displaced above and below the idealized cobalt-phosphine plane. The isolated enantiopure cobalt dialkyl complex was evaluated for the asymmetric hydrogenation of MAC and produced quantitative conversion to the alkane with 96.1% enantiomeric excess in 12 hours at 22°C. As with the in situ generated catalysts, the (*S*)-enantiomer of the product was favored.

Experiments were also conducted to explore the coordination chemistry of SL-A109-2 with the cobalt precursors. The solid-state structure of a related cobalt(II) dichloride compound, (SL-A101-1)$CoCl_2$, has been determined (*39*), suggesting a likely 1:1 bis(phosphine):cobalt stoichiometry in the in situ catalytic experiments. To further probe the cobalt-phosphine stoichiometry, the hydrogenation of *trans*-methylstilbene was conducted with 5 mol % of the SL-A109-2/$(py)_2Co(CH_2SiMe_3)_2$ mixture in the presence of an additional equivalent (relative to cobalt) of SL-A109-2. No measureable effect in activity or enantioselectivity was observed in the catalytic hydrogenation. Addition of $(py)_2Co(CH_2SiMe_3)_2$ to a solution containing an equimolar mixture of both enantiomers of SL-A109 generated an active cobalt catalyst that furnished essentially no (<2%) enantioselectivity. In contrast, premixing one enantiomer of the phosphine, SL-A109-2, with $(py)_2Co(CH_2SiMe_3)_2$ followed by an addition of an equimolar quantity of the opposite bis(phosphine) antipode, SL-A109-1, resulted in only a modest erosion of the enantioselectivity to 76%, favoring the expected (*R*)-stereoisomer of the alkane. In a related experiment, performing the catalytic hydrogenation with 5 mol % of cobalt precursor and 10 mol % of SL-A109-2 maintained the enantiomeric excess at 87.6%. These results establish a 1:1 [SL-A109]:[Co] stoichiometry and demonstrate that once the bis(phosphine) is coordinated, it is not sufficiently labile on the time scale of the catalytic hydrogenation to enable exchange with free ligand in solution. Repeating the hydrogenation of *trans*-methylstilbene with 5 mol % of each SL-A109-2 and $(py)_2Co(CH_2SiMe_3)_2$ in the presence of two equivalents of added pyridine lowered the conversion to 17% and the enantioselectivity to 69.8%, demonstrating that unlike in the MAC hydrogenations, pyridine is deleterious for the performance of SL-A109–derived cobalt catalysts used for hydrogenation of largely unfunctionalized olefins (*40*). These observations motivate future studies toward understanding the coordination chemistry of these species so that catalysts with improved performance may be rationally synthesized.

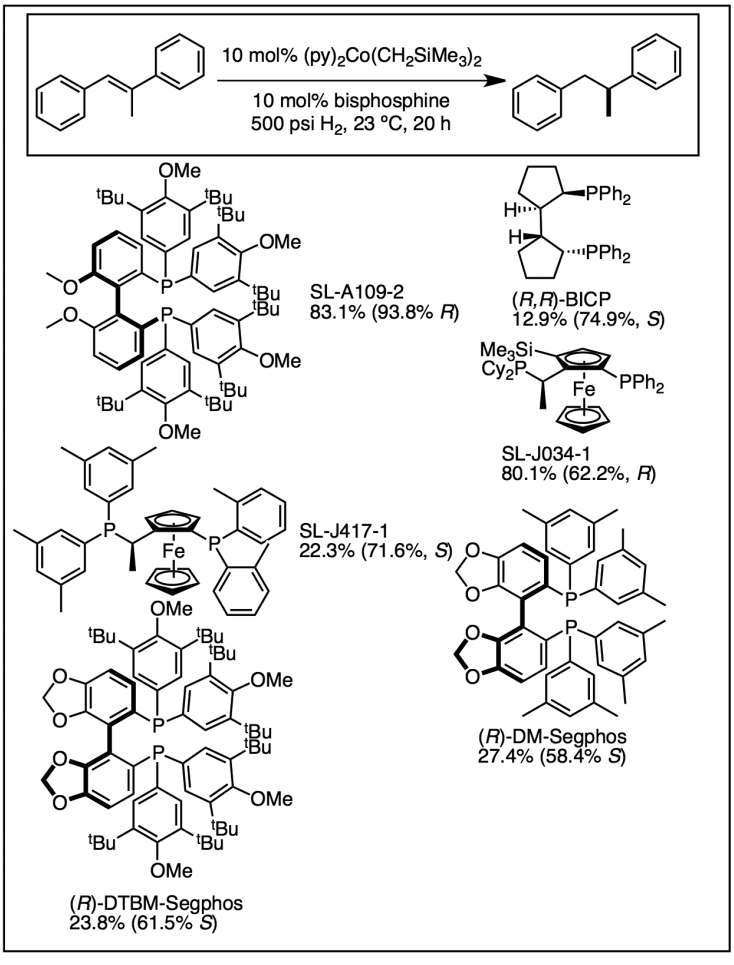


**Fig. 4. Bidentate phosphines that in combination with $(py)_2Co(CH_2SiMe_3)_2$ produce highest activities and selectivities for the asymmetric hydrogenation of *trans*-methylstilbene.** A complete listing of the phosphines evaluated is presented in table S5. Percentages correspond to the conversion to product, whereas those in the parentheses represent the percent enantiomeric excess.

**References and Notes**


1. W. S. Knowles, *Angew. Chem. Int. Ed.* **41**, 1998 (2002).
2. R. Noyori, *Angew. Chem. Int. Ed.* **41**, 2008 (2002).
3. C. A. Busacca, D. R. Fandrick, J. J. Song, C. H. Senanayake, *Adv. Synth. Catal.* **353**, 1825–1864 (2011).
4. H.-U. Blaser, B. Pugin, F. Spindler, M. Thommen, *Acc. Chem. Res.* **40**, 1240–1250 (2007).
5. W. S. Knowles, M. J. Sabacky, B. D. Vineyard, *Chem. Commun.* **1972**, 10 (1972).
6. G. Hoge, *J. Am. Chem. Soc.* **125**, 10219–10227 (2003).
7. Y. Hsiao *et al.*, *J. Am. Chem. Soc.* **126**, 9918–9919 (2004).

8. H. U. Blaser, H.-J. Federsel, Eds., *Asymmetric Catalysis on Industrial Scale: Challenges, Approaches and Solutions* (Wiley-VCH, Weinheim, Germany, ed. 2, 2010).
9. C. S. Shultz, S. W. Krska, *Acc. Chem. Res.* **40**, 1320–1326 (2007).
10. N. B. Johnson, I. C. Lennon, P. H. Moran, J. A. Ramsden, *Acc. Chem. Res.* **40**, 1291–1299 (2007).
11. A. M. Rouhi, *Chem. Eng. News* **82**, 47 (2004).
12. J. A. DiMasi, C. Paquette, *Pharmacoeconomics* **22**, (Suppl 2), 1–14 (2004).
13. A. M. Thayer, *Chem. Eng. News* **85**, 11 (2007).
14. W. S. Knowles, M. J. Sabacky, *J. Chem. Soc. Chem. Commun.* 1445 (1968).
15. L. Horner, H. Siegel, H. Büthe, *Angew. Chem. Int. Ed. Engl.* **7**, 942 (1968).
16. R. R. Schrock, J. A. Osborn, *J. Am. Chem. Soc.* **93**, 2397 (1971).
17. J. Halpern, *Science* **217**, 401–407 (1982).
18. M. T. Ashby, J. Halpern, *J. Am. Chem. Soc.* **113**, 589–594 (1991).
19. S. Bell *et al*., *Science* **311**, 642–644 (2006).
20. J. Mazuela, P. O. Norrby, P. G. Andersson, O. Pàmies, M. Diéguez, *J. Am. Chem. Soc.* **133**, 13634–13645 (2011).
21. M. C. Perry *et al*., *J. Am. Chem. Soc.* **125**, 113–123 (2003).
22. B. Plietker, Ed., *Iron Catalysis in Organic Chemistry: Reactions and Applications* (Wiley-VCH, Weinheim, Germany, 2008).
23. U. Leutenegger, A. Madin, A. Pfaltz, *Angew. Chem. Int. Ed. Engl.* **28**, 60–61 (1989).
24. L. O. Nindakova, F. M. Lebed, Z. Y. Zamazei, B. A. Shainyan, *Russ. J. Org. Chem.* **43**, 1322–1329 (2007).
25. L. O. Nindakova, B. A. Shainyan, *Russ. Chem. Bull. Int. Ed.* **54**, 348–353 (2005).
26. Y. Ogho, S. Takeuchi, Y. Natori, J. Yoshimura, *Bull. Chem. Soc. Jpn.* **54**, 2124 (1981).
27. A. Corma, M. Iglesias, C. del Pino, F. Sánchez, *J. Organomet. Chem.* **431**, 233–246 (1992).
28. Q. Knijnenburg *et al*., *J. Mol. Catal. A.* **232**, 151–159 (2005).
29. G. Zhang, B. L. Scott, S. K. Hanson, *Angew. Chem. Int. Ed.* **51**, 12102–12106 (2012).
30. G. Zhang, K. V. Vasudevan, B. L. Scott, S. K. Hanson, *J. Am. Chem. Soc.* **135**, 8668–8681 (2013).
31. S. Monfette, Z. R. Turner, S. P. Semproni, P. J. Chirik, *J. Am. Chem. Soc.* **134**, 4561–4564 (2012).
32. D. Zhu, F. F. B. J. Janssen, P. H. M. Budzelaar, *Organometallics* **29**, 1897–1908 (2010).
33. M. J. Burk, J. E. Feaster, W. A. Nugent, R. L. Harlow, *J. Am. Chem. Soc.* **115**, 10125–10138 (1993).
34. S. J. Roseblade, A. Pfaltz, *Acc. Chem. Res.* **40**, 1402–1411 (2007).
35. P. G. Cozzi, N. Zimmermann, R. Hilgraf, S. Schaffner, A. Pfaltz, *Adv. Synth. Catal.* **343**, 450–454 (2001).
36. X. Cui, K. Burgess, *Chem. Rev.* **105**, 3272–3296 (2005).
37. T. L. Church, P. G. Andersson, *Coord. Chem. Rev.* **252**, 513–531 (2008).
38. The last number in the name indicates the enantiomer of the ligand. SL-A109-1 corresponds to the (*R*) enantiomer, whereas SL-A109-2 is the (*S*) antipode.
39. S. Gischig, T. M. Schmid, G.Consiglio, http://webcsd.ccdc.cam.ac.uk/display_csd_search_results.php?xml_temp_file=/temp/text_numeric_query_04163190013723027145 1cbad7a67a84.xml&identifier=NALPIA.
40. Similarly, performing the hydrogenation of *trans*-methylstilbene with 5 mol % each of SL-A109-2 and $(py)_2Co(CH_2SiMe_3)_2$ without removal of the volatiles, and hence in the presence of two equivalents of pyridine, lowered the conversion and enantioselectivity to 50 and 51%, respectively, indicating that incomplete removal of the volatile byproducts in catalyst generation could also be deleterious to overall performance.



**Acknowledgments:** We thank the U.S. National Science Foundation for a Grant Opportunities for Academic Liaison with Industry (GOALI) grant (CHE-1265988) between Princeton and Merck. M.R.F. thanks the National Science Foundation for a Graduate Research Fellowship (DGE-1148900). We also thank Z. Turner, S. Semproni, and G. Margulieux (Princeton University) for assistance with x-ray crystallography and B. Chen, J. Cuff, L. Joyce, Z. Pirzada, W. Schafer, and H. Wang (Merck) for assistance with chiral assays. Metrical parameters for the solid-state structures are available free of charge from the Cambridge Crystallographic Data Centre under the reference numbers CCDC 958430, 958431, and 958432. P.J.C., M.R.F., and J.M.H. along with Princeton University have filed a U.S. patent application (13/838,835) for the compounds disclosed in this work.


**Supplementary Materials**

www.sciencemag.org/content/342/6162/1076/suppl/DC1
Materials and Methods
Figs. S1 to S27
Tables S1 to S6
References (*41*–*46*)


22 July 2013; accepted 7 October 2013
10.1126/science.1243550


# Amine(imine)diphosphine Iron Catalysts for Asymmetric Transfer Hydrogenation of Ketones and Imines


**Weiwei Zuo, Alan J. Lough, Young Feng Li, Robert H. Morris***



**A rational approach is needed to design hydrogenation catalysts that make use of Earth-abundant elements to replace the rare elements such as ruthenium, rhodium, and palladium that are traditionally used. Here, we validate a prior mechanistic hypothesis that partially saturated amine(imine)diphosphine ligands (P-NH-N-P) activate iron to catalyze the asymmetric reduction of the polar bonds of ketones and imines to valuable enantiopure alcohols and amines, with isopropanol as the hydrogen donor, at turnover frequencies as high as 200 per second at 28°C. We present a direct synthetic approach to enantiopure ligands of this type that takes advantage of the iron(II) ion as a template. The catalytic mechanism is elucidated by the spectroscopic detection of iron hydride and amide intermediates.**


Metal-based homogeneous catalysts are used in the pharmaceutical, fragrance, flavoring, and fine chemicals industries for the synthesis of enantiomerically pure organic molecules such as alcohols, amines, and amino acids (*1*). Rare and expensive late transition metals such as ruthenium and rhodium have typically been used in this context (*2*–*4*). Iron is an element essential to life and is abundant in mineral ores, in contrast to these precious metals, and thus its use is preferable for economic and health reasons. Recent research has shown that suitably designed ligands can activate iron complexes so that their catalytic turnover frequency rivals or surpasses that of industrial catalysts (*5*–*7*). We describe here an exceptionally efficient class of catalysts for the preparation of enantioenriched alcohols and amines.

Our previous synthetic and mechanistic studies of the iron(II)-based transfer hydrogenation precatalyst (*S*,*S*)-[$Fe(CO)(Br)(PAr_2CH_2CH{=}NCHPhCHPhN{=}CHCH_2PAr_2)$]$BPh_4$ **C** (Fig. 1) suggested that one imine linkage of the bis(imine)diphosphine ligand (P-N-N-P) of **C** was reduced by hydride addition from isopropoxide in a slow activation step (Fig. 1, reaction 3) to produce complexes within the catalytic cycle. These were postulated to be iron amide and iron hydride complexes on the basis of computational chemistry and the trapping of these reactive intermediates by use of hydrogen chloride in ether to give complex **F** (reaction 6). Preliminary results showed that complex **F** with an amine(imine)diphosphine ligand (P-NH-N-P) was a more active catalyst precursor than **C** (*8*, *9*). This system reduced acetophenone at turnover frequencies up to 15 $s^{-1}$ at 30°C; until the present work, this was an unrivaled rate for the transfer hydrogenation of ketones under these conditions (*8*). On this basis, we hypothesized that the direct synthesis of complexes such as **F** containing an unsymmetrical P-NH-N-P ligand would lead to more active catalysts.

A key step toward this goal was the selective synthesis of enantiopure tridentate ligands P-NH-$NH_2$ (**1a** and **1b**) by an iron(II)-assisted method (Fig. 2, reactions 7 and 8). The starting compounds are air- and water-stable dimeric phosphonium salts **A** that are readily prepared with a variety of substituents at phosphorus (in green in Fig. 2); in the present case, these are phenyl and *meta*-xylyl. The latter group is often effective at increasing the selectivity of catalysts (*2*, *9*). These phosphonium dimers release reactive α-phosphinoacetaldehyde species when they are treated with base (NaOMe) and undergo Schiff-base condensation with an enantiopure diamine at iron(II) to form complexes with two tridentate ligands incorporating phosphine, imine, and amine donors (*10*). The optimum reaction conditions include the use of the enantiopure diamine (*S*,*S*)-$NH_2CHPhCHPhNH_2$ [(*S*,*S*)-dpen] and a slight excess of the phosphonium dimer, 0.65 equiv.

These iron complexes are treated with lithium aluminum hydride to reduce the imine linkages and then hydrolyzed to release the enantiopure compounds **1a** and **1b** in high yields. This method is superior to other reductive amination methods that either would require an excess of the expensive diamine or would result in a mixture of amine products. The ligands are produced in ~90% purity and are used directly in the next step.

These ligands enable the direct synthesis (via Fig. 2, reaction 9) of a range of catalyst precursors


Department of Chemistry, University of Toronto, 80 Saint George Street, Toronto, Ontario M5S 3H6, Canada.

*Corresponding author. E-mail: rmorris@chem.utoronto.ca

as exemplified by the three compounds **2a** to **2c**. Reaction 9 is analogous to reaction 2 of Fig. 1 where the iron(II) acts as a template to produce one isomer from the multicomponent reaction. Here, the α-phosphinoacetaldehyde released from compound **A** (with phenyl, *para*-tolyl, or xylyl substituents at phosphorus) condenses with the P-NH-$NH_2$ ligand **1a** or **1b** [rather than the (*S*,*S*)-dpen used previously] at iron(II), thereby leading to an iron complex with the desired partially saturated P-NH-N-P framework. The latter is then treated with 1 atm of carbon monoxide and sodium chloride in acetone to give the new iron complexes **2a** to **2c** in acceptable overall yields (30 to 42%). Remarkably, only one diastereomer is formed, as indicated by the $^{31}P\{^1H\}$ nuclear magnetic resonance (NMR) spectra; for example, complex **2a** when dissolved in $CD_2Cl_2$ produces two doublet resonances at 58.0 and 62.6 ppm with $^2J_{PP}$ = 40 Hz. An x-ray diffraction study of a single crystal of **2b** revealed the expected structure with chloride trans to carbonyl in an octahedral complex of Fe(II). The presence of the amine and imine groups is confirmed by the shorter N-C bond length for the latter group: N(2A)-C(3A) = 1.486 Å, N(1A)-C(5A) = 1.256 Å (these distances have estimated standard deviations of 0.007 Å). The amino proton and the chloro ligand are located on opposite sides of the coordination plane defined by the Fe, N, and P atoms.

When these complexes are treated with at least 2 equiv of potassium tertiary butoxide ($KO^tBu$) base, very reactive, oxygen-sensitive catalysts are released for the hydrogenation of ketones by the transferring of hydrogen from the solvent isopropanol (Fig. 3). Two features distinguish these catalysts from the ones that we have reported earlier (*7*, *9*, *11*, *12*): (i) No induction period is observable, and (ii) the rate of conversion at 28°C is substantially higher. Turnover frequencies (TOF) of >200 $s^{-1}$ (720,000 $hour^{-1}$) at 50% conversion are observed for some substrates (see Table 1), with complete conversion [turnover number (TON) up to 6100] attained in seconds. This exceeds the TOF observed for fast transfer hydrogenation catalysts based on ruthenium and osmium (*R*,*S*)-Josiphos complexes that in basic isopropanol reduce acetophenone to (*R*)-1-phenylethanol in 89 to 92% enantiomeric excess (ee) with TOF up to 89 $s^{-1}$ at 60°C (*13*). The ruthenium complex $RuCl_2$(*R*-tol-binap)[(*R*,*R*)-dpen] [tol-binap is 2,2′-bis(di-4-tolylphosphino)-1,1′-binaphthyl] in basic isopropanol catalyzes the pressure hydrogenation (at 45 atm, 30°C) of acetophenone to (*S*)-1-phenylethanol at 80% ee and at a TOF of 63 $s^{-1}$, whereas a ruthenium(II) complex with a P-NH-NH-P ligands catalyzes the same reaction with a TOF of 92 $s^{-1}$ but at 60°C and with low ee (*14*). The activity of the iron complexes rivals that of enzymes such as liver alcohol dehydrogenase, which transfers a hydride from a zinc ethoxide active site to a pyridinium substrate (*15*), or a synthetic iron-based hydrogenase where dihydrogen is oxidized to protons and electrons (*16*).

A comparison of the utility of the precursors **2a** to **2c** in the hydrogenation of acetophenone (Table 1, top left) under standard conditions (acetophenone:$KO^tBu$:**2** ratio = 6100:8:1) demonstrates that complex **2b** with *para*-tolyl groups provides the highest TOF; complex **2c** with xylyl groups on the phosphorus atoms provides the highest ee values of the (*R*)-1-phenylethanol. The use of **2a** or **2b** results in an erosion of ee over time; **2c** has the advantage of minimal erosion of ee. The racemization of product alcohol by the **2b** system can be minimized by using a less active system containing less base in the ratio of concentrations 6100:2:1 (third entry of Table 1 with a TOF of 12 $s^{-1}$). The reduction of 3,5-bistrifluoromethylacetophenone in 90% ee for **2a** and 98% ee for **2c** is particularly noteworthy, as the (*R*) alcohol product of this reaction serves as an intermediate for the synthesis of an efficient neurokinin 1 ($NK_1$) antagonist for use as an aprepitant to combat nausea associated with cancer chemotherapy (*17*).

Complex **2a** was an effective precatalyst for the efficient reduction of a broad range of aryl ketones (Table 1). It was also active toward alkyl ketones, which are kinetically and thermodynamically less prone to react. Pyridine and furan heterocycles were tolerated, albeit with a drop in enantioselectivity. The reduction of *trans*-4-phenyl-3-buten-2-one initially yields the unsaturated alcohol with relatively low enantioselectivity (40% ee). The reduction of the C=C double bond on the initially formed unsaturated alcohol occurs later, eventually affording the saturated alcohol. The chemoselectivity for the polar C=O versus the nonpolar C=C double bonds is consistent with an outer-sphere proton plus hydride transfer, as shown in Fig. 3. Complex **2a** also catalyzes the transfer hydrogenation of imines activated with the *N*-(diphenylphosphinoyl) group in >99% ee and at rates greater than 100 times those of previously reported iron catalysts (*18*, *19*).

The proposed highly reactive catalysts **3**, **3′**, and **4** (Fig. 3) were characterized by NMR and infrared spectroscopy. The spectra are quite consistent with the structures predicted recently using density functional theory (DFT) calculations where **3** was described as square pyramidal at iron(II) with a carbonyl in the apical position, and the tetradentate ligand unsymmetrical with neutral phosphorus donors, anionic nitrogen donors, and different groups, one saturated $–CH_2CH_2–$ and one unsaturated –CH=CH–, linking the phosphorus with the nitrogen on each side (*20*). Complexes **3** and **3′** were generated as a mixture by reacting complex **2a** with 2 equiv of $KO^tBu$ in

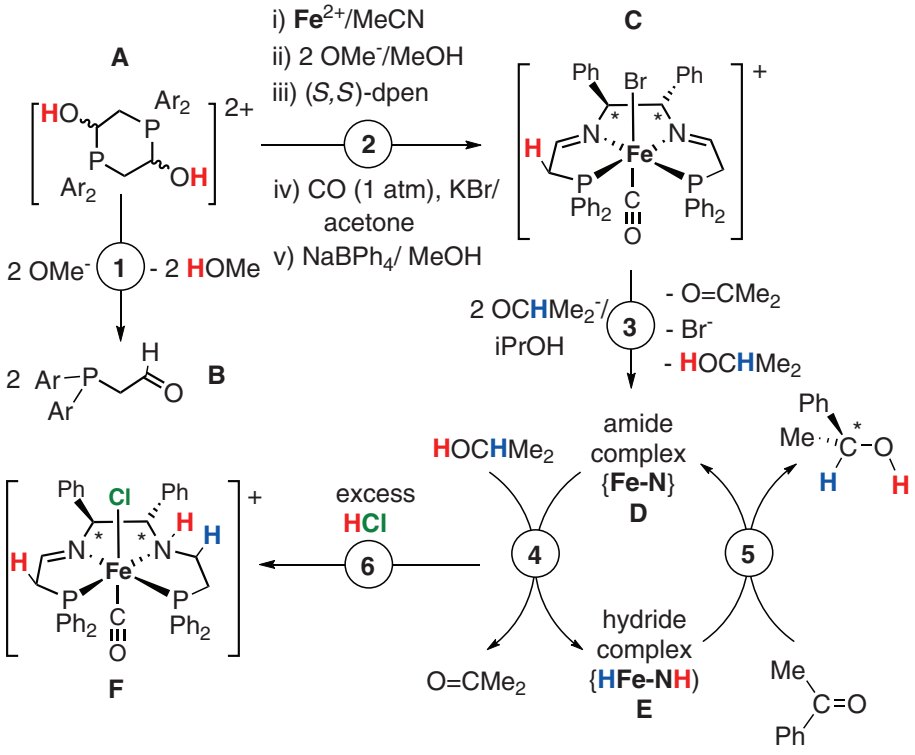


**Fig. 1. Reactions established by previous iron catalyst research.** (**1**) Reaction of the phosphonium salt **A** with base produces α-phosphinoacetaldehyde **B**. (**2**) Reaction of 2 equiv of **B** (Ar = Ph) with 1 equiv of the diamine (*S*,*S*)-$NH_2$CHPhCHPh$NH_2$ [(*S*,*S*)-dpen] at Fe(II) followed by treatment with CO and KBr in acetone and then treatment with $NaBPh_4$ in MeOH precipitates the bis(imine)diphosphine iron(II) complex **C** as the $BPh_4^-$ salt. (**3**) Reaction of isopropoxide with this precatalyst **C** in isopropanol causes its slow activation, a process that is proposed to involve the deprotonation of one side of the ligand and addition of hydride to the imine on the other side, producing an amide species **D**. (**4** and **5**) These reactions constitute the catalytic cycle where the transfer of hydrogen from isopropanol solvent to acetophenone, giving (*R*)-1-phenylethanol is catalyzed by a postulated iron amide **D** and hydride **E**. (**6**) Reaction of the active species **D** and **E** with HCl in ether gives the chloride salt **F** with the amine(imine)diphosphine ligand reduced on the right side as drawn. Here, the active protonic hydrogens are colored red and hydridic hydrogens blue. Ar, aryl; Ph, phenyl; Me, methyl; iPrOH, isopropanol.

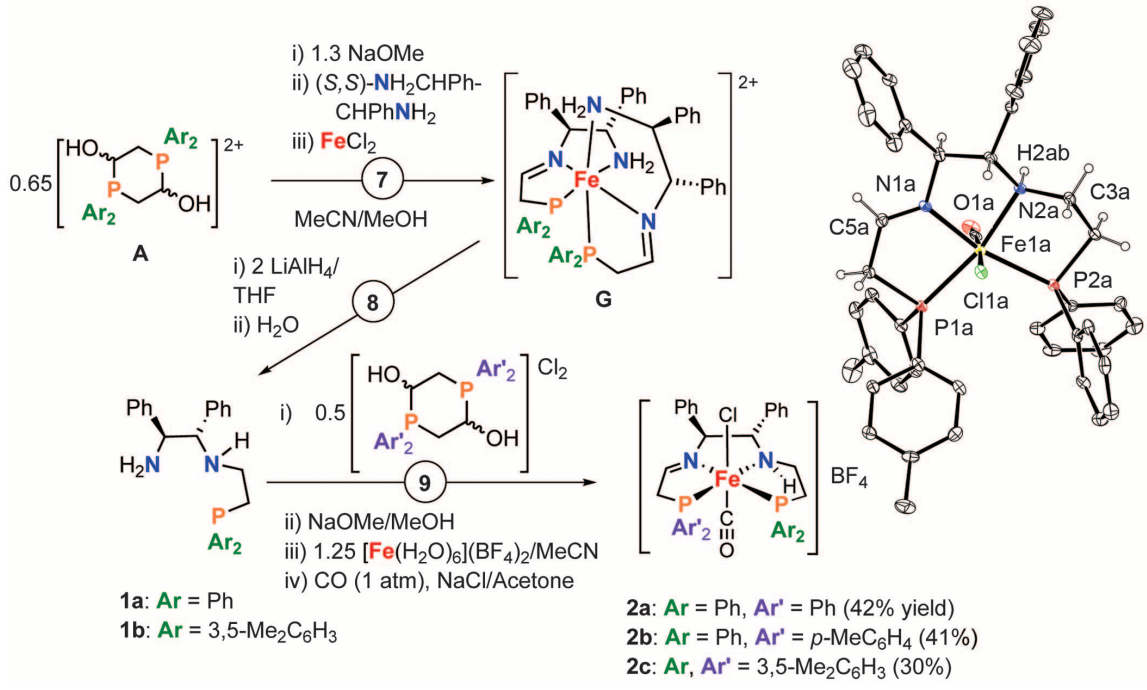


**Fig. 2. Iron(II)-assisted synthesis of enantiopure phosphinediamine ligands 1a and 1b (reactions 7 and 8) and iron (II)-templated synthesis of enantiopure catalyst precursors 2a to 2c (reaction 9).** The molecular structure of the cation of complex **2b** (right) was determined by single-crystal x-ray diffraction. The thermal ellipsoids are plotted at 50% probability; some hydrogens are removed for clarity.

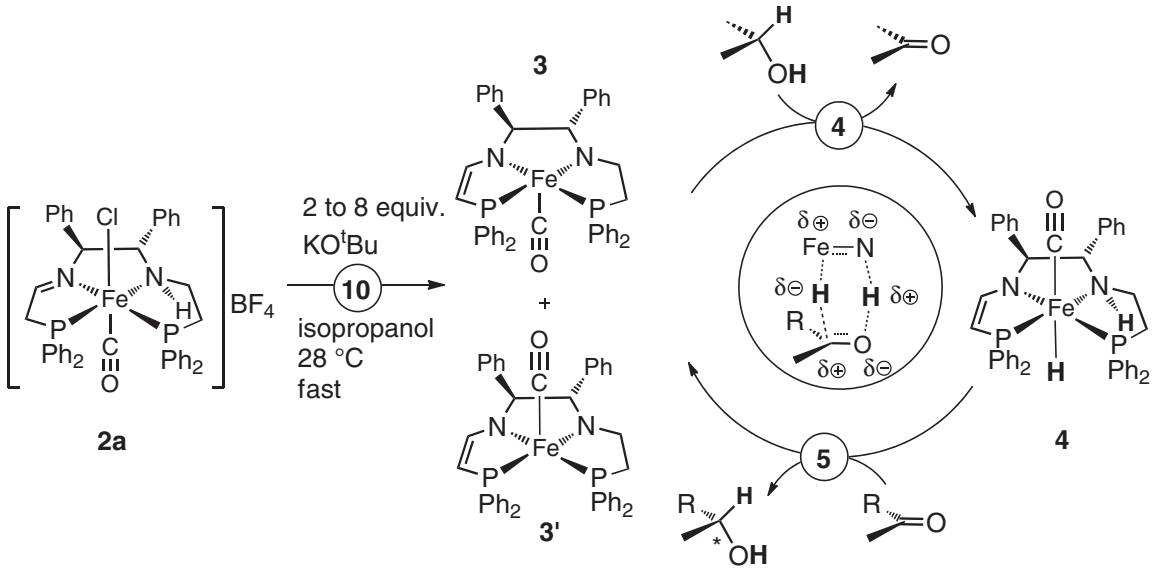


**Fig. 3. Proposed mechanism.** The amido-eneamido complex **3** and its isomer **3′** and the amine-eneamido-hydride complex **4**, corresponding to catalysts **D** and **E** of Fig. 1, are generated when complexes **2a** to **2c** are treated with base in isopropanol solvent. The structures of catalysts **3** and **4** were proposed in a previous theoretical (DFT) study (*20*) and are verified in the current work by NMR.

tetrahydrofuran (THF) at room temperature, evaporating the solvent, and extracting the product with $C_6D_6$ for NMR analysis. The $^{31}P\{^1H\}$ NMR spectrum provides evidence for two diastereomers: (i) a major one displaying two doublets at 75.8 and 85.3 ppm with a $^2J$(P,P) coupling constant of 28 Hz and (ii) a minor one with a similar pattern of doublets at 77.8 and 83.4 ppm with $^2J$(P,P) of 31 Hz. The $^1H$ and $^{13}C$ NMR spectra allowed complete assignment of the hydrogen and carbon nuclei in the major diastereomer, all consistent with either of the structures **3** or **3′** shown in Fig. 3 (see supplementary materials). The other isomer is likely to have the carbonyl on the opposite apex of the square pyramid, as shown.

The mixed isomers of **3** were highly active for the asymmetric transfer hydrogenation of acetophenone to 1-phenylethanol (*R*) in isopropanol without the addition of base. About 60% of the substrate was reduced at room temperature within 10 min with 82% ee. No induction period was observed, and the reaction profile is similar to that obtained when only 2 equiv of base were used with complex **2a**. These observations are consistent with our previous hypothesis that the neutral amido-(ene-amido) complex **3** is the active catalyst for the transfer hydrogenation of ketone substrates using the bis(imine) iron(II) carbonyl complex **C** as the catalyst precursor in basic isopropanol (*8*).

The reaction of a mixture of **3** and **3′** with isopropanol in the absence of substrate led, within 1 min, to a mixture of **3** and the hydride complex **4** (Fig. 3). Complex **4** displayed a characteristic $^1H$ NMR resonance for the FeH at –2.25 ppm (dd, $^2J_{HP}$ = 70.0 and 70.8 Hz). A second hydride grew in more slowly in the absence of substrate with a resonance at –9.23 ppm (dd, $^2J_{HP}$ = 78.6 and 79.8 Hz). The ratio between the two hydride diastereomers is greater than 5:1 with the –2.25 ppm signal predominating. Both of the two hydride species were characterized by NMR spectroscopy, including $^1H$, $^{31}P\{^1H\}$ $^1H$-$^1H$ correlation spectroscopy, heteronuclear single-quantum coherence, and nuclear Overhauser effect spectroscopy, in $C_6D_6$ (see supplementary material). The major isomer has the structure shown in Fig. 3.

The addition of acetophenone to the $C_6D_6$ solution of the hydride mixture immediately led to the disappearance of the hydride signals and the corresponding phosphorus resonances and the generation of free 1-phenylethanol. This is fully consistent

**Table 1. Transfer hydrogenation of ketones and imines catalyzed by complexes 2a to 2c.** General conditions for ketones: [Cat] = $6.73 \times 10^{-5}$ M, [KO$^t$Bu] = $5.45 \times 10^{-4}$ M, [ketone] = 0.412 M, [$^i$PrOH] = 12.4 M, 28°C; for imines: [Cat, **2a**] = $5.89 \times 10^{-4}$ M, [KO$^t$Bu] = $4.71 \times 10^{-3}$ M, [imine] = $5.89 \times 10^{-2}$ M, [$^i$PrOH] = 12.4 M, 28°C. The absolute configurations were obtained by gas chromatography or high-performance liquid chromatography by comparison to known standards.

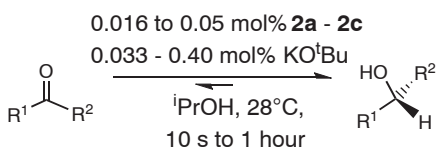


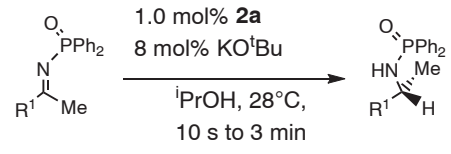


| Comparison of catalysts | 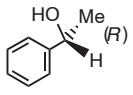 | | | 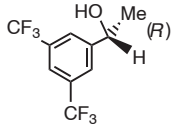 | | Amine products using **2a** | 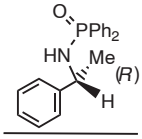 | 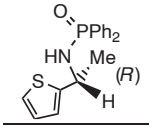 |
|---|---|---|---|---|---|---|---|---|
| | **2a** | **2b** | **2b*** | **2c** | **2a** | **2c**† | **2a** | **2a** |
| Time to equil.: | 180 s | 180 s | 1000 s | 180 s | 180 s | 10 s | 20 s | 180 s |
| Yield: | 82% | 83% | 83% | 82% | 99% | 100% | 100% | 100% |
| TON at equil.: | 5000 | 5100 | 5100 | 5000 | 6060 | 2000 | 100 | 100 |
| TOF at 50% conv.: | 119 $s^{-1}$ | 152 $s^{-1}$ | 12 $s^{-1}$ | 70 $s^{-1}$ | 147 $s^{-1}$ | 200 $s^{-1}$ | 10 $s^{-1}$ | 5 $s^{-1}$ |
| ee at 10 s: | 88% | 86% | 86% | 92% | 91% | 98% | >99% | >99% |
| ee at equil.: | 78% | 70% | 80% | 90% | 90% | 98% | >99% | >99% |

| Alcohol products using **2a** | 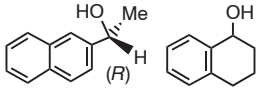 |  | 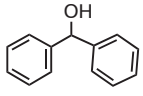 |  | 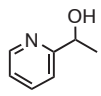 | 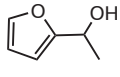 | 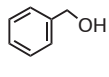 | 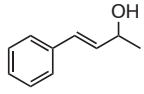 |
|---|---|---|---|---|---|---|---|---|
| Time to equil.: | 180 s | 1 h | 10 min | 1 h | 6 min | 6 min | 25 s | 4 min |
| Yield: | 84% | 73% | 88% | 67% | 98% | 84% | 99% | 55% |
| TON at equil.: | 5140 | 4470 | 5400 | 4100 | 6000 | 5140 | 6060 | 3370 |
| TOF at 50% conv.: | 158 $s^{-1}$ | 4 $s^{-1}$ | 38 $s^{-1}$ | 3 $s^{-1}$ | 100 $s^{-1}$ | 61 $s^{-1}$ | 242 $s^{-1}$ | 14 $s^{-1}$ |
| ee at 10 s: | 92% | 34% | - | 57% | 25% | 51% | - | 40% |
| ee at equil.: | 83% | 33% | - | 54% | 24% | 31% | - | 40% |

*[Cat, **2b**] = $6.73 \times 10^{-5}$ M, [KO$^t$Bu] = $1.35 \times 10^{-4}$ M, [substrate] = 0.412 M, [$^i$PrOH] = 12.4 M, 28°C. †Ketone: Cat ratio = 2000:1 to prevent poisoning by the acidic alcohol product.

with the mechanism shown in Fig. 3. The mixture of **3** and **4** can be generated in isopropanol by reaction of **2a** with base before the addition of substrate, but this mixture must be used for catalysis within 2 min to obtain the same activity and enantioselectivity as the standard method. The stereochemical configuration of the final alcoholic product is predicted and observed to be *R* on the basis of a hydride transfer from **4** to the ketone hydrogen-bonded to the N-H with the larger group of the ketone (e.g., R is aryl or naphthyl in Fig. 3) directed to the less bulky diamine side of the catalyst.

As in Noyori-type catalysts (*21*), the addition of excess base, at least up to 8 equiv relative to the catalyst, causes an increase in turnover frequency, as shown in Table 1 for catalyst **2b** where a TOF of 152 $s^{-1}$ is obtained with 8 equiv of base, versus 12 $s^{-1}$ with 2 equiv. Our group had proposed that this excess of base protects the basic amide and hydride reactants by reducing the hydrogen ion concentration in the alcohol medium (*22*). It might also serve to catalyze the substitution of unreactive octahedral amine complexes (*23*) by amine deprotonation (*24*).

The catalyst systems described here represent versatile, well-understood, extremely active asymmetric reduction catalysts based on a nonprecious metal. The new ligands permit efficient multicomponent synthesis of a very wide range of highly active iron catalysts with varied structural features. In principle, the mirror image catalysts can also be made in the same way using the commercially available diamine (*R*,*R*)-dpen, and these can be used to make the (*S*) forms of the alcohols or amines.

### References and Notes


1. W. S. Knowles, R. Noyori, *Acc. Chem. Res.* **40**, 1238–1239 (2007).
2. R. Noyori, T. Ohkuma, *Angew. Chem. Int. Ed. Engl.* **40**, 40–73 (2001).
3. S. Bell *et al.*, *Science* **311**, 642–644 (2006).
4. W. A. Nugent, T. V. RajanBabu, M. J. Burk, *Science* **259**, 479–483 (1993).
5. A. M. Tondreau *et al.*, *Science* **335**, 567–570 (2012).
6. K. Junge, K. Schröder, M. Beller, *Chem. Commun.* **47**, 4849–4859 (2011).
7. R. H. Morris, *Chem. Soc. Rev.* **38**, 2282–2291 (2009).
8. A. A. Mikhailine, M. I. Maishan, A. J. Lough, R. H. Morris, *J. Am. Chem. Soc.* **134**, 12266–12280 (2012).
9. P. E. Sues, A. J. Lough, R. H. Morris, *Organometallics* **30**, 4418–4431 (2011).
10. A. A. Mikhailine, E. Kim, C. Dingels, A. J. Lough, R. H. Morris, *Inorg. Chem.* **47**, 6587–6589 (2008).
11. A. A. Mikhailine, R. H. Morris, *Inorg. Chem.* **49**, 11039–11044 (2010).
12. P. O. Lagaditis, A. J. Lough, R. H. Morris, *J. Am. Chem. Soc.* **133**, 9662–9665 (2011).
13. W. Baratta *et al.*, *Organometallics* **29**, 3563–3570 (2010).
14. V. Rautenstrauch, X. Hoang-Cong, R. Churlaud, K. Abdur-Rashid, R. H. Morris, *Chem. Eur. J.* **9**, 4954–4967 (2003).
15. A. Kohen, R. Cannio, S. Bartolucci, J. P. Klinman, *Nature* **399**, 496–499 (1999).
16. T. Liu, D. L. Dubois, R. M. Bullock, *Nat. Chem.* **5**, 228–233 (2013).
17. K. M. J. Brands *et al.*, *J. Am. Chem. Soc.* **125**, 2129–2135 (2003).
18. A. A. Mikhailine, M. I. Maishan, R. H. Morris, *Org. Lett.* **14**, 4638–4641 (2012).
19. S. Zhou *et al.*, *Angew. Chem. Int. Ed.* **49**, 8121–8125 (2010).
20. D. E. Prokopchuk, R. H. Morris, *Organometallics* **31**, 7375–7385 (2012).
21. C. A. Sandoval, T. Ohkuma, K. Muñiz, R. Noyori, *J. Am. Chem. Soc.* **125**, 13490–13503 (2003).
22. K. Abdur-Rashid *et al.*, *J. Am. Chem. Soc.* **124**, 15104–15118 (2002).
23. F. Basolo, R. G. Pearson, *Mechanisms of Inorganic Reactions* (Wiley, New York, 1967).
24. J. M. John, S. Takebayashi, N. Dabral, M. Miskolzie, S. H. Bergens, *J. Am. Chem. Soc.* **135**, 8578–8584 (2013).



**Acknowledgments:** Supported by NSERC Discovery and RTI grants (R.H.M.), the University of Toronto, and a proof-of-principle grant from the Green Centre Canada. We thank D. Prokopchuk for DFT calculations, A. Mikhailine for preceding work and for providing a phosphonium dimer compound, and T. Burrow and D. Burns for NMR support. Crystallographic data for **2b** are available free of charge from the Cambridge Crystallographic Data Centre under reference number 954477. R.H.M. is listed as an inventor on a patent filed in relation to the work described herein.


### Supplementary Materials

www.sciencemag.org/content/342/6162/1080/suppl/DC1
Materials and Methods
Figs. S1 to S32
Table S1


9 August 2013; accepted 7 October 2013
10.1126/science.1244466

# Imaging the Absolute Configuration of a Chiral Epoxide in the Gas Phase

Philipp Herwig,[1]* Kerstin Zawatzky,[2]* Manfred Grieser,[1] Oded Heber,[3] Brandon Jordon-Thaden,[1] Claude Krantz,[1] Oldřich Novotný,[1,4] Roland Repnow,[1] Volker Schurig,[5] Dirk Schwalm,[1,3] Zeev Vager,[3] Andreas Wolf,[1] Oliver Trapp,[2]† Holger Kreckel[1]†

In chemistry and biology, chirality, or handedness, refers to molecules that exist in two spatial configurations that are incongruent mirror images of one another. Almost all biologically active molecules are chiral, and the correct determination of their absolute configuration is essential for the understanding and the development of processes involving chiral molecules. Anomalous x-ray diffraction and vibrational optical activity measurements are broadly used to determine absolute configurations of solid or liquid samples. Determining absolute configurations of chiral molecules in the gas phase is still a formidable challenge. Here we demonstrate the determination of the absolute configuration of isotopically labeled (*R*,*R*)-2,3-dideuterooxirane by foil-induced Coulomb explosion imaging of individual molecules. Our technique provides unambiguous and direct access to the absolute configuration of small gas-phase species, including ions and molecular fragments.

In 1847, Louis Pasteur realized that crystals of tartaric acid can come in two different shapes, which are nonsuperimposable mirror images of one another. He was able to sort them and dissolve them separately, and he found that the respective liquids rotate the axis of linearly polarized light in opposite directions. These simple experiments may be considered the birth of modern stereochemistry. A much greater challenge is to relate the sense of rotation of the polarization axis (the optical activity) to the handedness of the underlying microscopic molecular structure, which is referred to as the absolute configuration. Emil Fischer, who postulated the lock-and-key model of enzyme interactions in 1894 (*1*), realized that it was impossible to infer the absolute configuration from macroscopic models, and thus he arbitrarily defined dextrorotatory glucose as having *d*-configuration. It took more than 50 years until his guess was confirmed in 1951 when Bijvoet introduced anomalous single-crystal x-ray diffraction (XRD) to determine the absolute configuration of sodium rubidium tartrate (*2*). To this date, anomalous XRD is still the method of choice for absolute configuration measurements in crystalline samples.

More recently, vibrational circular dichroism (VCD) and vibrational Raman optical activity (ROA) have been used intensely to determine absolute configurations (*3*–*9*). Advances in computational chemistry allow simulating and predicting the spectral difference between the enantiomers by ab initio calculations. Lahav *et al*. introduced stereoselective habit modifications of crystals forming conglomerates to determine absolute configurations by surface interactions (*10*, *11*). Furthermore, microscopic techniques can be used to determine the sense of chirality of surface adsorbed molecules (*12*). All of the above methods have been used for important contributions, and an entire atlas of stereochemical information can be found in the literature (*13*). Nevertheless, difficulties remain for molecules that do not contain heavy atoms, and misassignments still occur, even in state-of-the-art laboratory studies (*14*). Moreover, to this date, the direct visualization of the absolute configuration of selected enantiomers in the gas phase has been elusive.

To address this stereochemical challenge, we developed the idea of using the foil-induced Coulomb explosion imaging (CEI) technique (*15*) to determine the handedness of a sample of individual chiral gas-phase molecules. In CEI experiments, the binding electrons of fast molecular ions are stripped off during passage through an ultrathin diamond-like carbon foil. The remaining positively charged atoms experience strong Coulomb repulsion, which leads to a magnification of the molecular structure that is recorded with modern imaging techniques (Fig. 1).

Very recently, Pitzer *et al*. (*16*) independently reported a similar approach using cold target recoil ion momentum spectroscopy (COLTRIMS) after laser-induced Coulomb explosion. In these studies, an effusive molecular beam is ionized by intense laser light. For this approach, sophisticated laser systems with sufficiently high intensities and repetition rates are necessary, owing to the rather inefficient ionization process. As the Coulomb explosion is triggered by 40-fs-long laser pulses, the time scale for the successive removal of the electrons is slow with respect to the vibrational movements of lighter species, like hydrogen and deuterium, within a given molecule. Therefore, those light nuclei cannot be considered static during the ionization process (*16*), which presently limits the technique to molecules made of heavier atoms. Moreover, large quantities of chiral gases are required, and thus only measurements with racemic mixtures of bromochlorofluoromethane and isotopically chiral bromodichloromethane were reported.

The foil-induced Coulomb explosion method described here, by contrast, requires only small sample amounts of chiral molecules (less than 100 mg was used for the present experiments). Given the well-known electron loss cross sections in fast atomic collisions (*17*), the ionization process due to electron stripping in the foil has a very high efficiency. Moreover, the ionization of all atomic fragments occurs simultaneously upon impact on the foil, within the first femtosecond (*15*). This is considerably faster than molecular vibration and rotation, and the position of all nuclei can be considered frozen during the stripping process. As we demonstrate here, this enables us to perform experiments with fundamental molecular species like epoxides, where the stereochemical information is carried by light atoms exclusively.

The CEI technique relies on time- and position-sensitive detection of all relevant fragments resulting from single-molecule breakup events [details of the experimental setup are given in (*18*, *19*)], and it has been used successfully to infer accurate information on the structure of diatomic molecules and simple polyatomics (*20*–*22*). To extend its range to species complex enough to exhibit chirality, we introduced ultrathin charge conversion

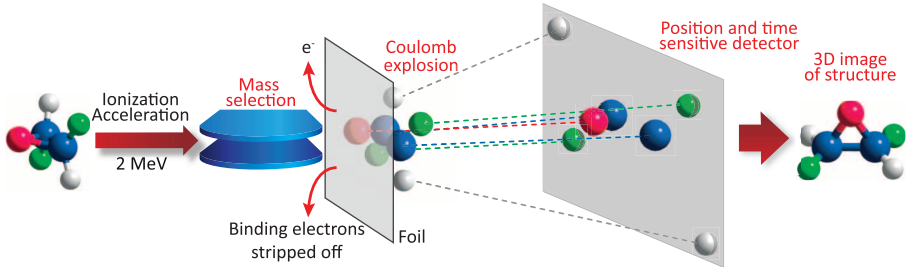


**Fig. 1. Determination of the absolute configuration of chiral molecules by foil-induced Coulomb explosion imaging.** Chiral molecules are ionized and accelerated, followed by mass selection to investigate only selected molecular ions or fragments. The Coulomb explosion is triggered by passing the molecules through an ultrathin stripping foil. The resulting charged atomic ions are recorded by a detector with high spatial and temporal resolution, revealing the molecular structure.

[1]Max-Planck-Institut für Kernphysik, 69117 Heidelberg, Germany. [2]Organisch-Chemisches Institut, Ruprecht-Karls Universität Heidelberg, 69120 Heidelberg, Germany. [3]Department of Particle Physics and Astrophysics, Weizmann Institute, 76100 Rehovot, Israel. [4]Columbia Astrophysics Laboratory, Columbia University, New York, NY 10027, USA. [5]Institut für Organische Chemie, Eberhard Karls Universität Tübingen, 72076 Tübingen, Germany.

*These authors contributed equally to this work.
†Corresponding author. E-mail: holger.kreckel@mpi-hd.mpg.de (H.K.); trapp@oci.uni-heidelberg.de (O.T.)

foils in front of both microchannel plate (MCP) detectors to increase the detection efficiency and developed improved parallel amplifiers to provide cross-talk–free multihit capabilities for each detector.

To meet the particular challenge of determining the absolute configuration of a molecule composed of lighter atoms, we chose *trans*-2,3-dideuterooxirane (compound **1**, Fig. 2A) as our target molecule. For this fundamental epoxide, the chiral character is introduced by two deuterons. The chosen compound **1** is a relatively rigid molecule and shows rotational symmetry ($C_2$), making the two stereogenic centers equivalent. Ionization of **1** by electron impact (fig. S5) does not affect the stereogenic centers, e.g., by bond dissociation. Moreover, unintended inversion of one of the stereogenic centers, e.g., by accidental exchange of the positions of H and D, results in the formation of achiral *cis*-2,3-dideuterooxirane, which would lead to an achiral contribution but not jeopardize the outcome of the experiment. Likewise, statistical double inversion would lead to a racemic sample accompanied by the formation of the achiral *cis*-2,3-dideuterooxirane isomer.

Samples of (*R*,*R*)-2,3-dideuterooxirane (***R*,*R*)-1** were prepared (*23*, *24*) according to an optimized eight-step synthetic protocol (fig. S4). The key step of the synthesis (Fig. 2B) is the enantioselective epoxidation of **2** by a modified semicatalytic Sharpless procedure (*25*) using titanium(IV) tetraisopropoxide, (+)-diisopropyl tartrate, and *tert*-butyl hydroperoxide. The configuration of the epoxide formed by the Sharpless asymmetric epoxidation is predictable, because the conversion is controlled by the configuration of the tartrate in the active complex. Therefore, under the reaction conditions described here, the (*S*,*S*)-configured epoxide **3** is formed with an enantiopurity of 97.5% (enantiomeric ratio). Mild oxidation of the alcohol by a Parikh-Doering reaction (*26*), employing a pyridine sulfur trioxide complex, gives the corresponding aldehyde in excellent yield. This step was followed by decarbonylation of the aldehyde group by stoichiometric reaction with the Wilkinson catalyst (*27*) $RhCl(PPh_3)_3$, under conservation of the stereogenic center at C2 of (***S*,*S*)-4**. Finally, (***R*,*R*)-1** is released as a gas by deprotection of the triphenylsilyl group using tetraethylammonium fluoride.

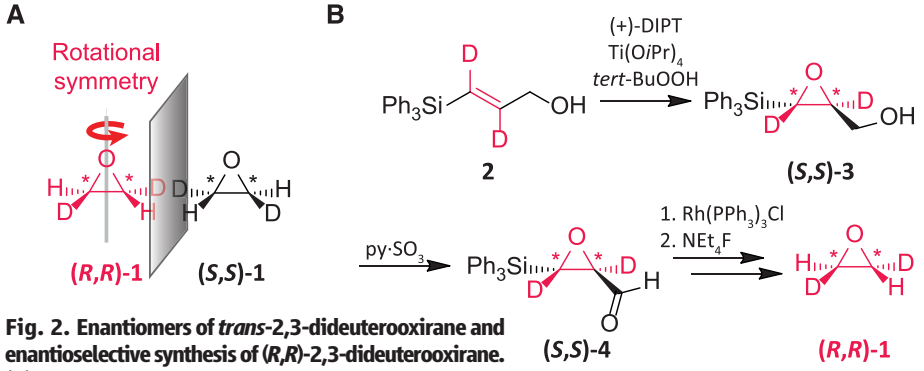


**Fig. 2. Enantiomers of *trans*-2,3-dideuterooxirane and enantioselective synthesis of (*R*,*R*)-2,3-dideuterooxirane.** (**A**) Enantiomers of *trans*-2,3-dideuterooxirane. The rotational symmetry is indicated by the rotation axis. (**B**) Asymmetric synthesis of the target molecule (*R*,*R*)-2,3-dideuterooxirane (***R*,*R*)-1** via a catalytic Sharpless epoxidation of deuterated allyl alcohol **2** as the key step of the synthetic sequence.

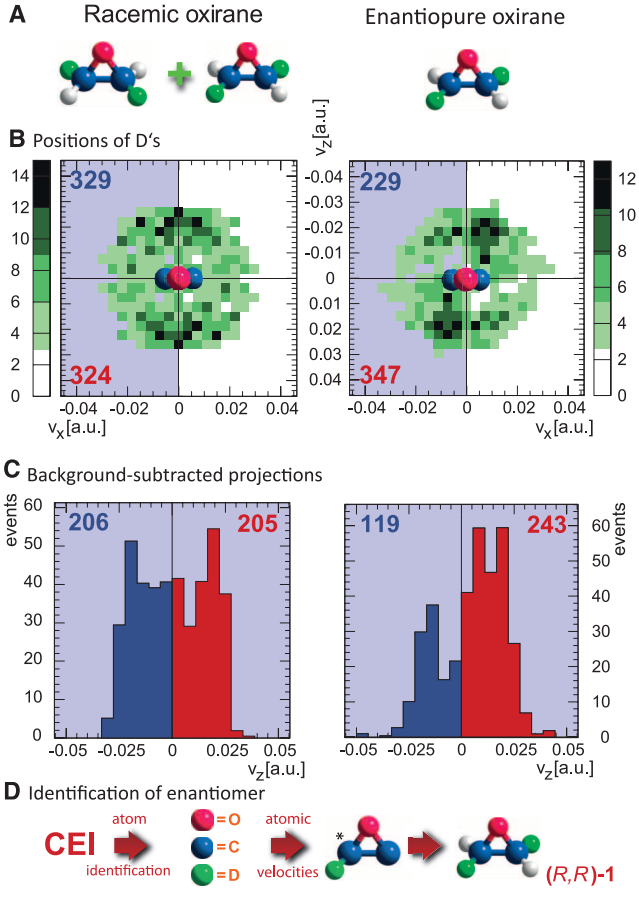


**Fig. 3. Imaging results and absolute configuration of *trans*-2,3-dideuterooxirane 1.** (**A**) CEI measurements were carried out for both enantiopure and racemic **1**. (**B**) Distribution of the D-atom velocities in the $v_x$-$v_z$ plane. This plane contains both C atoms and is oriented perpendicular to the C-O-C plane (the O atom, facing the viewer, is colored red). A distinct difference between racemic and enantiopure **1** is visible in the direction of the D-atom velocities. Accumulated event counts are given for relevant quadrants. (**C**) Projection of the blue areas onto the $v_z$ axis after subtraction of systematic background (see text and supplementary materials for definition). Whereas racemic **1** shows no propensity in the sign of $v_z$, the enantiopure sample reveals a clear precedence toward positive $v_z$ values. (**D**) The imaging results of enantiopure **1** unambiguously identify the configuration as (***R*,*R*)-1**.

The imaging results for both the racemic and the enantiopure oxirane (***R*,*R*)-1** samples are compared in Fig. 3. The coordinate system for each individual event is chosen such that the two C-atom

To obtain direct three-dimensional images of the *trans*-2,3-dideuterooxirane molecules, we ionized samples of racemic and enantiopure **1** in a standard cold cathode ion source. The resulting $C_2H_2D_2O^+$ ions were accelerated to 2.0 MeV, mass-selected, and then magnetically guided onto a thin (~5 nm) carbon foil (Fig. 1). Upon impact on the foil, the binding electrons are stripped off within less than a femtosecond, during which the position of the nuclei can be considered frozen. Behind the foil, the mutual Coulomb potential energy is rapidly converted to kinetic energy. For each individual molecular breakup, a dedicated detector system records the particle distances and impact times, which are proportional to the asymptotic velocities of the Coulomb explosion process. Because the purely repulsive dissociation conserves the handedness, the fragment velocities reflect the chirality of the molecules before fragmentation. As for the heavier atoms various charge states emerge from the foil, we used a magnetic separation field to select and separate the $C^{2+}$ and $O^{2+}$ charge states and to direct them onto a rectangular MCP detector at small deflection angles, whereas the $D^+$ ions were deflected more strongly onto a second, round detector (the $H^+$ ions were diverted outside of the detector region, fig. S1). By reversing the magnetic deflection in the data analysis, we reconstructed the three-membered C-O-C skeleton for events containing all three heavy fragments in the respective $X^{2+}$ charge state. Then the velocity of a single $D^+$ ion of the same event was determined with respect to this skeleton, defining the handedness of the corresponding stereogenic center. To rule out systematic uncertainties and detector effects, we performed control measurements with racemic *trans*-2,3-dideuterooxirane (fig. S3).

velocities lie on the $v_x$ axis, and the velocity of the C-O-C center of mass lies on the positive $v_y$ axis. The breakup velocity of the D atom is projected into the $v_x$-$v_z$ plane. The resulting distributions (Fig. 3B) reveal a clear difference in the absolute configuration of the two samples. Through the rotational symmetry of 2,3-dideuterooxirane (Fig. 2A), each event leads to two entries in the measured distribution, such that each half plane contains all information. To obtain a quantifiable parameter for the certainty with which we can determine the handedness of the enantiopure sample, we projected the blue area ($v_x < 0$) onto the $v_z$ axis (Fig. 3C). In this representation, a negative sign of $v_z$ corresponds to (*S*,*S*) symmetry, whereas a positive sign corresponds to (*R*,*R*) symmetry. Although events with both signs are seen (owing to molecular vibration and racemization induced in the ion source), this plot clearly identifies the enantiopure sample as (*R*,*R*)-2,3-dideuterooxirane (***R*,*R*)-1** with a statistical confidence level of 5σ. A systematic source of background, due to overlapping detector regions for $C^{2+}$ and $O^{2+}$, has been simulated and subtracted for Fig. 3C (see supplementary materials).

Our work uses direct imaging of a small gas-phase chiral compound to assign its sense of chirality. This offers a universal and self-consistent pathway to determine the absolute configuration of chemical species that may not be accessible by other methods. Imaging of chiral ionic species, as demonstrated here, can be combined with mass spectroscopic techniques to preselect molecules of a desired mass/charge ratio. Mass selectivity is an important feature of our approach, as it would enable us to measure gases containing large amounts of impurities, up to samples containing only small traces of chiral molecules. Furthermore, because we mass-select also the atomic fragments after Coulomb explosion and measure them in coincidence, this would permit us to discriminate against unwanted contamination by molecules with the same total mass but different atomic constituents. It would also be possible to store the ions between the initial ionization and the CEI measurement to accumulate and select a desired species or reaction product. Ion storage at cryogenic temperatures could be used to suppress internal excitations and thus provide more rigid molecular structures, which would make quantifiable measurements of the sample purity and the degree of racemization possible. Compared to macroscopic analysis techniques, only small quantities of the chiral species are needed, and neither optical activity nor crystalline samples are required. The foil-induced ionization process is universal and, as it does not rely on laser interactions or high sample densities, potentially can be applied to neutrals, ions, and radicals alike. With these properties, direct imaging of more complex chiral molecules can be envisioned in the future. Chemical compounds could be mass-selected at high resolution before their chiral properties are determined by applying ion-beam imaging. This paves the way for promising concepts of chiral sequencing and for highly efficient analysis of the absolute configuration of molecular fragments and reaction products.

By providing direct snapshots of selected enantiomers, our approach gives access to the absolute configuration of small gas-phase molecules, fully independent of quantum-chemical calculations. In addition, it offers broader intellectual merit in the direct visualization of a property as fundamental as chirality, on a molecular level.

### References and Notes


1. E. Fischer, *Ber. Dtsch. Chem. Ges* **27**, 2985–2993 (1894).
2. J. M. Bijvoet, A. F. Peerdeman, A. J. van Bommel, *Nature* **168**, 271–272 (1951).
3. P. J. Stephens, *J. Phys. Chem.* **89**, 748–752 (1985).
4. T. B. Freedman, X. Cao, R. K. Dukor, L. A. Nafie, *Chirality* **15**, 743–758 (2003).
5. P. J. Stephens, F. J. Devlin, J.-J. Pan, *Chirality* **20**, 643–663 (2008).
6. L. D. Barron, M. P. Bogaard, A. D. Buckingham, *J. Am. Chem. Soc.* **95**, 603–605 (1973).
7. J. Haesler, I. Schindelholz, E. Riguet, C. G. Bochet, W. Hug, *Nature* **446**, 526–529 (2007).
8. L. D. Barron, A. D. Buckingham, *Chem. Phys. Lett.* **492**, 199–213 (2010).
9. Y. He, B. Wang, R. K. Dukor, L. A. Nafie, *Appl. Spectrosc.* **65**, 699–723 (2011).
10. L. Addadi *et al*., *Nature* **296**, 21–26 (1982).
11. Z. Berkovitch-Yellin, L. Addadi, M. Idelson, L. Leiserowitz, M. Lahav, *Nature* **296**, 27–34 (1982).
12. H. Fang, L. C. Giancarlo, G. W. Flynn, *J. Phys. Chem. B* **102**, 7311–7315 (1998).
13. W. Klyne, J. Buckingham, *Atlas of Stereochemistry—Absolute Configurations of Organic Molecules* (Chapman & Hall, London, 1978), vols. 1 and 2.
14. Y. Inokuma *et al*., *Nature* **495**, 461–466 (2013).
15. Z. Vager, R. Naaman, E. P. Kanter, *Science* **244**, 426–431 (1989).
16. M. Pitzer *et al*., *Science* **341**, 1096–1100 (2013).
17. V. S. Nikolaev, *Sov. Phys. Usp.* **8**, 269–294 (1965).
18. R. Wester *et al*., *Nucl. Instrum. Methods Phys. Res. A* **413**, 379–396 (1998).
19. R. Wester *et al*., *J. Chem. Phys.* **116**, 7000 (2002).
20. B. Jordon-Thaden *et al*., *Phys. Rev. Lett.* **107**, 193003 (2011).
21. P. Herwig *et al*., *Phys. Rev. A* **87**, 062513 (2013).
22. L. Lammich *et al*., *Phys. Rev. A* **69**, 062904 (2004).
23. J. M. Schwab, C.-K. Ho, *J. Chem. Soc. Chem. Commun.* (11): 872 (1986).
24. J. M. Schwab, T. Ray, C.-K. Ho, *J. Am. Chem. Soc.* **111**, 1057–1063 (1989).
25. Y. Gao *et al*., *J. Am. Chem. Soc.* **109**, 5765–5780 (1987).
26. J. R. Parikh, W. von E. Doering, *J. Am. Chem. Soc.* **89**, 5505–5507 (1967).
27. D. Evans, J. A. Osborn, F. H. Jardine, G. Wilkinson, *Nature* **208**, 1203–1204 (1965).


**Acknowledgments:** This work was supported by the Max-Planck Society and the Ruprecht-Karls Universität Heidelberg. O.N. was supported, in part, by grants from NASA and the NSF. H.K. and O.T. were supported by the European Research Council under Grant Agreements StG 307163 and StG 258740, respectively. D.S. acknowledges support by the Weizmann Institute through the Joseph Meyerhoff program. We thank B. F. Straub for support in the quantum-chemical calculations and F. Rominger for x-ray structure analysis. We thank G. Helmchen and H. Wadepohl for helpful discussions. We are grateful for the support from the Max-Planck-Institut für Kernphysik accelerator staff, and we thank O. Koschorreck for assistance with the CEI detector electronics. Metrical parameters for the crystal structures of compounds [**triphenylsilyl propargyl alcohol, 2,** (***S*,*S*)-3** and (***S*,*S*)-4**] are available free of charge from the Cambridge Crystallographic Data Centre under reference numbers CCDC 964292, CCDC 964293, CCDC 964294, and CCDC 964295, respectively.

### Supplementary Materials

www.sciencemag.org/content/342/6162/1084/suppl/DC1
Materials and Methods
Figs. S1 to S5
Appendix
References (*28*–*36*)

27 September 2013; accepted 29 October 2013
10.1126/science.1246549

# Regular Patterns in Frictional Resistance of Ice-Stream Beds Seen by Surface Data Inversion

**Olga V. Sergienko[1]* and Richard C. A. Hindmarsh[2]**

**Fast-flowing glaciers and ice streams are pathways for ice discharge from the interior of the Antarctic Ice Sheet to ice shelves, at rates controlled by conditions at the ice-bed interface. Using recently compiled high-resolution data sets and a standard inverse method, we computed basal shear stress distributions beneath Pine Island and Thwaites Glaciers, which are currently losing mass at an accelerating rate. The inversions reveal the presence of riblike patterns of very high basal shear stress embedded within much larger areas with zero basal shear stress. Their colocation with highs in the gradient of hydraulic potential suggests that subglacial water may control the evolution of these high–shear-stress ribs, potentially causing migration of the grounding line by changes in basal resistance in its vicinity.**

Observations from satellite and aircraft-based platforms show that the ice streams in Amundsen Sea Embayment are the greatest contributors to Antarctic ice-sheet mass loss (*1*, *2*), including Pine Island Glacier (PIG) and Thwaites Glacier (Fig. 1). In contrast to PIG, which flows in a trough whose lateral walls provide resistance to ice flow in addition to its bed, Thwaites is unconfined, with most resistance to its gravity-driven flow coming from its bed. The flux of ice through the grounding line, which determines the rate at which glaciers contribute to

[1]Program in Atmospheric and Oceanic Sciences, Princeton University, 201 Forrestal Road. Princeton, NJ 08540, USA. [2]British Antarctic Survey, High Cross, Madingley Road, Cambridge CB3 0ET, UK.

*Corresponding author. E-mail: osergien@princeton.edu

sea level, is controlled by the rate of ice flow (*3*) and strongly depends on basal conditions immediately upstream of the grounding line (*4*). Direct observations of basal conditions by drilling through the ice, which illuminate the processes by which beds provide resistance to flow, have been performed at a very few point locations on Antarctic ice streams (*5*). Repeating such point observations over extensive areas to understand the basal mechanics of ice flow is logistically unfeasible. One resolution of this problem is to perform inversions of glacier surface observations to determine the spatial distributions of basal resistance (*6*–*8*).

The basal resistance of ice streams is highly variable in space (*9*), but the causes of this heterogeneity are not well understood. Mostly, it is attributed to changes in the underlying geology; for example, variations in the sediment thickness or differences in the bed roughness (*10*), but there are also theoretically based suggestions that intrinsic variability of the ice-stream basal hydrological system can play an important role (*11*). The widespread presence of subglacial water under Antarctic ice streams has been observed directly by probing the bed through boreholes (*12*) and indirectly by observing changes in ice surface elevation (*13*). Water drainage is controlled by hydraulic potential gradients that can be estimated on the basis of hydrostatic assumptions. Subglacial sediments may be dilated, and internal deformation of these sediments can contribute substantially to basal ice motion, as can the slip of ice over a sediment bed or a hard rock bed. Models of the subglacial system are constrained by a very few direct observations and inferences from radar and seismic geophysical surveys.

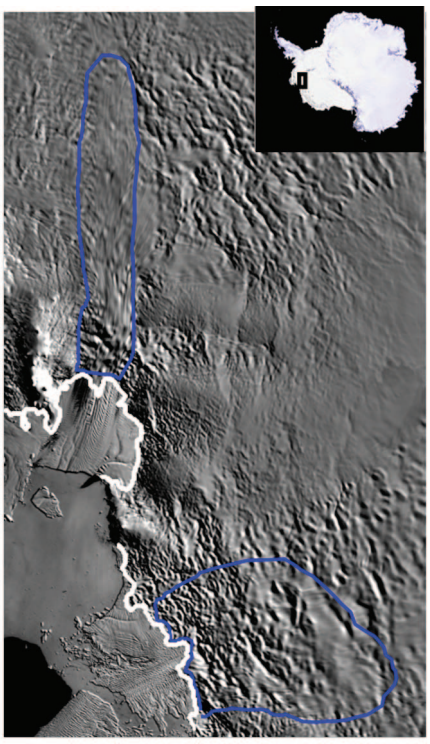

**Fig. 1. Location of the study area.** Blue lines outline the domains of ice streams where inversions were performed. The white line is the location of the grounding line.

Developments in satellite and airborne observing systems have allowed a wealth of measurements over ice sheets to be made in the past few decades. These observations have been compiled, and in some circumstances synthesized with earlier observations, into high-resolution data sets. The recently released very high-resolution data sets of ice surface velocity (900 m resolution) (*14*), ice surface elevations (*15*), and bed elevations (*16*) (both with 1-km gridding) were used by us to infer basal shear stress under PIG and Thwaites by means of a standard inverse technique based on the control method (*6*). To take advantage of such high-resolution data, the forward ice flow model is based on the three-dimensional treatment of the ice momentum balance [all components of the stress tensor are included in the Stokes equations (*17*)], in contrast to a previously used vertically integrated approach that assumes negligible vertical shear stresses (*9*). A description of the inversion procedure is provided in the supplementary materials (SM) section 1.

Inverted basal shear stresses (Figs. 2A, 3A, and 4A) show a much more variable spatial distribution than that previously resolved (*17*). Extensive areas beneath both PIG and Thwaites have basal shear stress very close to zero, apart from confined riblike patterns with very high basal shear stress (~200 to 300 kPa). The number of such traction ribs is significantly larger under Thwaites than under PIG; they also vary substantially in size, from several kilometers to tens of kilometers (the longest being ~50 km). In contrast to PIG, where ribs tend to concentrate in a ~40-km zone near the grounding line, the ribs under Thwaites occupy a much larger area, extending ~100 km from the grounding line. On PIG, the ribs align with ~30° with respect to the direction of ice flow (Figs. 3B and 4B) and on Thwaites ~40° to 60° (Fig. 2B). The inverted spatial patterns (i.e., rib spacing and the difference in basal shear magnitudes over the ribs and between them) are robust features and are insensitive to specifics of the inverse method (SM section 1.2). The distributions of the width, length, and spacing for both glaciers are shown in figs. S1 and S2; the mean width is ~2.2 km (~1.3 ice thicknesses), the mean length is ~6 km (~3.5 ice thicknesses), and the mean distance between the ribs is 6.5 km (~3.6 ice thicknesses) on PIG and ~3 km (~2 ice thicknesses), ~11 km (~7 ice thicknesses) and ~3.7 km (~2.4 ice thicknesses) on Thwaites, respectively. There is a higher concentration of ribs on Thwaites in areas with topographic highs (Fig. 2C), whereas there is no such correspondence between rib locations and topography on PIG (Figs. 3C and 4C).

For the both ice streams, strong correspondence is observed between the locations of the high-basal-traction ribs and locations with large magnitudes of the gradient of hydraulic potential, $\vec{\nabla}\Phi = \vec{\nabla}p_i + \rho_w g\vec{\nabla}B$ (*18*), where $\vec{\nabla}$ is the gradient operator, $p_i$ is ice overburden pressure, $\rho_w$ is the density of subglacial water, $g$ is the acceleration due to gravity, and $B$ is bed elevation. As Figs. 2D, 3D, and 4D show, the majority of the ribs with high basal shear stress are located within areas of high magnitudes of the hydraulic potential gradient. Conversely, areas with low magnitudes of the hydraulic potential gradient have very few ribs. Within the ribs, the correlation coefficients between basal shear stress and the hydraulic potential gradient are 0.68 for PIG and 0.63 for Thwaites. These results suggest that subglacial water may play a role in the rib formation. Because both high driving stress and high hydraulic gradients are determined by high surface slopes, the association of high hydraulic potential gradients with the ribs is not surprising. Basal resistance is expected to be strongly related to effective pressure (the difference between ice overburden and subglacial water pressure), with high effective pressure associated with high basal resistance. Because high effective pressure is probably correlated with lower hydraulic conductivity (*11*), a higher hydraulic potential gradient is to be expected. The low-conductivity ribs dam the water behind them, creating low effective pressure zones. There may be substantial lateral routing of subglacial water, arising from strong hydraulic conductivity variations.

As our results show, there is no strong evidence that basal traction ribs arise from bedrock geological control. We note the possibility that basal shear stress ribs are related to the newly observed geomorphological forms called megaribs (*19*), because the horizontal scale of these geomorphological features is consistent with our inversion results of ice-stream ribbing; however, these features are topographically subtle and may be difficult to detect beneath thick ice. Traction ribs are so far undetected by direct geophysical observations, so that inferences about their dynamics are necessarily rather general. Several studies have suggested that subglacial landforms are created by a pattern-forming instability (*20*, *21*). In particular, a theory exists (*20*, *22*) that quantitatively models the formation of and wavelength of ribbed moraines, which are long ridges a few kilometers broad that lie transverse to ice flow, up to 10 m high, separated from each other by a few hundred meters (*22*). The model describes the coupled flow of ice and till.

The instability mechanism stems from increased effective pressure on the upstream side of till bumps. Although increased effective pressure inhibits till flux, the increased basal shear stress needed to discharge the ice flow overcomes this, and till flux increases in zones of high normal pressure (*21*, *23*). We hypothesize that the basal traction ribs we observe under PIG and Thwaites arise from similar dynamic instabilities at the bed of these glaciers, leading to a pattern-formation process. From this viewpoint, the basal traction ribs arise from the long-term evolution of dynamic

instabilities, manifesting themselves as bed-friction variation arising from variations in the effective pressure in space. They may be instabilities in sediment thickness or water pressure, or coupled instabilities in both.

Ribbed moraines are more closely spaced than the traction ribs we observe, but a closely related model of the physical environment can also predict rib initiation with spacing of around 10 km under suitable parameter combinations (SM section 2). The additional features of the model include an evolving upper surface of the glacier and coupled subglacial water flow with an effective-pressure–dependent conductivity (*11*). Exploratory modeling suggests the formation timescales of 50 to 100 years are feasible (SM section 2). The inclusion of water flow affects the predicted phasing of water pressure and thereby effective pressure, and quantitatively affects the character of the instability. In our model, the timescale for the formation of these features is minimally the

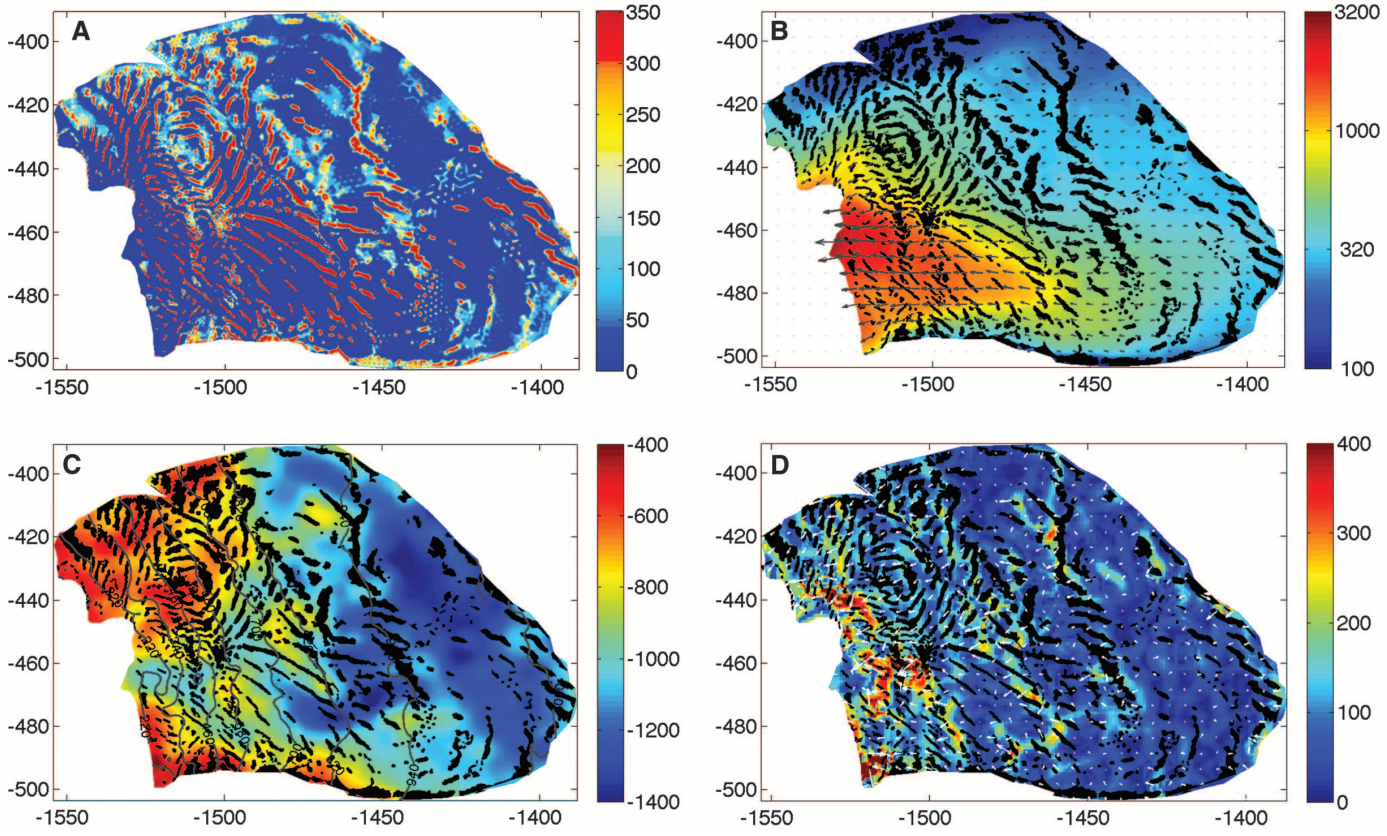


**Fig. 2. Thwaites Glacier.** (**A**) Inverted basal shear stress (in kilopascals). (**B**) Observed ice surface speed (in meters per year); arrows are velocity vectors. (**C**) Ice-stream geometry; colors show bed elevation and contour lines show surface elevation. (**D**) Gradient of the hydraulic potential (in pascals per meter). White arrows show directions of subglacial water flow. Black patches in (B) to (D) are locations with basal shear stress greater than 100 kPa.

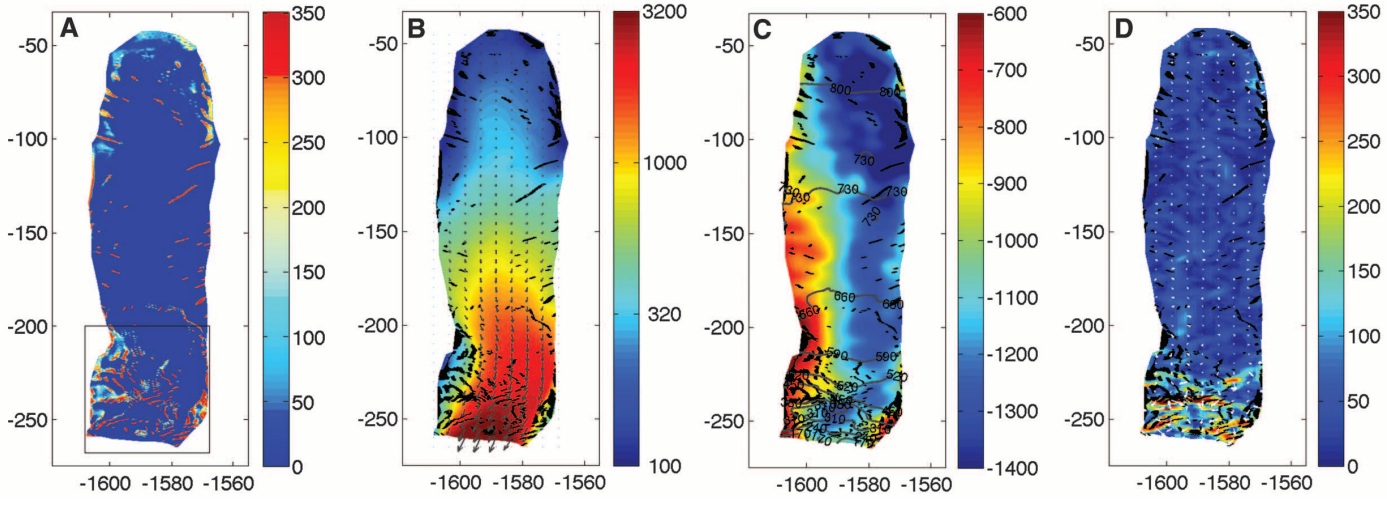


**Fig. 3. PIG.** Panels are the same as in Fig. 2.

time taken for the flowing ice to traverse the features (*21*, *23*), which is on the order of years to decades in PIG or Thwaites.

On the basis of these modeling results, we suggest that the ribs start to form under conditions of low coupling between ice and bed, with relatively low effective pressure. The instability evolves, increasing the contrast in effective pressure, which leads to the formation of the riblike structures we observe in the inversions. This instability is conditional and does not occur if most basal motion is due to sliding over till rather than till deformation, a possible explanation for the absence of ribs as seen in the upper reaches of the PIG main trough. The feasibility of this is supported by modeling of the rib initiation phase (SM section 2). The proposed mechanism is a hypothesis, and there may be other, yet unknown, mechanisms that control the formation of ribs.

The fact that basal shear stress exhibits riblike patterns in the vicinity of the grounding lines of PIG and Thwaites has important consequences for the stability and dynamics of the grounding lines. Both glaciers have inland-sloping over-deepened beds. The grounding lines in such geometric configurations are thought to be inherently unstable (*4*). Although the lateral boundaries of PIG and its floating tongue may stabilize its grounding line by providing resistance to ice flow additional to basal shear stress, Thwaites and its floating tongue lack such lateral boundaries, and resistance to ice flow emanates mostly from basal friction on its grounded part. Regardless of the mechanism responsible for rib formation, there is a possibility of their temporal and spatial variability through, for instance, flooding of some of these ribs and the reduction of their basal shear stress. The present spatial configuration of basal resistance in these ice streams is not immutable and, if our hypothesis is correct, can potentially change over decades to centuries in response to changes in ice-sheet geometry or water input.

Although changes in the individual ribs located far from the grounding line may not substantially affect the large-scale ice flow, changes in basal shear stress distributions in the vicinity of the grounding line inevitably cause variations in ice flow and its flux through the grounding line, triggering its migration, with consequent changes in ice discharge to the ocean. We argue, therefore, that the retreat of the grounding line could potentially be triggered not only by warm ocean waters through increased sub–ice-shelf melting downstream of the grounding lines (*24*), but also by ice and subglacial water dynamics upstream of the grounding lines.

The results presented here shed light on the complex structure of the subglacial environment in the vicinity of the grounding lines and under ice streams in general. Our results suggest that the explanation for the spatial variability of bed resistance may arise from internal variability at the ice-stream bed. The presence of the ribs is inferred in this study from the surface observations by means of inverse methods. Further advances in understanding require direct observations of the subglacial environment through comprehensive geophysical surveys.

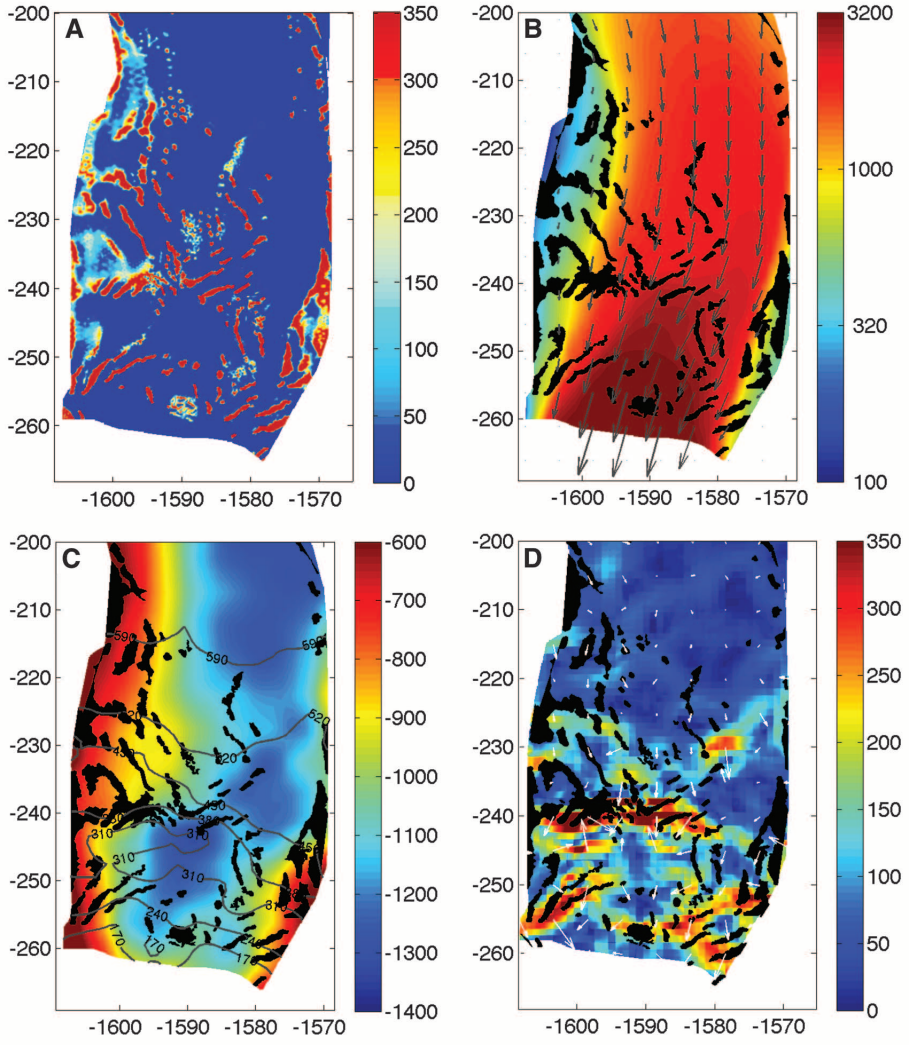


**Fig. 4. Zoom of PIG in the region outlined by the black rectangle in Fig. 3A.** Panels are the same as in Fig. 2.


### References and Notes

1. E. Rignot *et al.*, *Nat. Geosci.* **1**, 106–110 (2009).
2. H. D. Pritchard, R. J. Arthern, D. G. Vaughan, L. A. Edwards, *Nature* **461**, 971–975 (2009).
3. J. Weertman, *J. Glaciol.* **13**, 3 (1974).
4. C. Schoof, *J. Geophys. Res.* **112**, 227 (2007).
5. H. Engelhardt, N. Humphrey, B. Kamb, M. Fahnestock, *Science* **248**, 57–59 (1990).
6. D. R. MacAyeal, *J. Glaciol.* **39**, 91 (1993).
7. I. Joughin, D. MacAyeal, S. Tulaczyk, *J. Geophys. Res.* **109**, B09405 (2004).
8. O. V. Sergienko, R. A. Bindschadler, P. L. Vornberger, D. R. MacAyeal, *J. Geophys. Res.* **113**, F04010 (2008).
9. D. R. MacAyeal, *J. Geophys. Res.* **94**, 4071 (1989).
10. R. G. Bingham, M. J. Siegert, *Geophys. Res. Lett.* **34**, L21504 (2007).
11. R. C. A. Hindmarsh, *J. Glaciol.* **44**, 589 (1998).
12. H. Engelhardt, B. Kamb, *J. Glaciol.* **43**, 207 (1997).
13. L. Gray *et al.*, *Geophys. Res. Lett.* **32**, L03501 (2005).
14. E. Rignot, J. Mouginot, B. Scheuchl, *Science* **333**, 1427–1430 (2011).
15. J. Bamber, J. L. Gomez-Dans, J. Griggs, *Antarctic 1 km Digital Elevation Model (DEM) from Combined ERS-1 Radar and ICESat Laser Satellite Altimetry* (National Snow and Ice Data Center, Boulder CO, USA, 2009)
16. P. Fretwell *et al.*, *Cryosphere* **7**, 375–393 (2013).
17. M. Morlighem *et al.*, *Geophys. Res. Lett.* **37**, 1–6 (2010).
18. R. Shreve, *J. Glaciol.* **11**, 205 (1972).
19. S. L. Greenwood, J. Kleman, *Quat. Sci. Rev.* **29**, 1894–1910 (2010).
20. R. C. A. Hindmarsh, *J. Glaciol.* **44**, 285 (1998).
21. A. C. Fowler, *Proc. R. Soc. London Ser. A* **465**, 681 (2009).
22. P. Dunlop, C. D. Clark, R. C. A. Hindmarsh, *J. Geophys. Res.* **113**, F03005 (2008).
23. C. Schoof, *J. Fluid Mech.* **570**, 227 (2007).
24. A. Shepherd, D. Wingham, E. Rignot, *Geophys. Res. Lett.* **31**, L23402 (2004).


**Acknowledgments:** This research is supported by NSF grant CMG-0934534 and the British Antarctic Survey Polar Science for Planet Earth program. We thank anonymous referees for their valuable comments and suggestions.

### Supplementary Materials

www.sciencemag.org/content/342/6162/1086/suppl/DC1
Methods
Figs. S1 to S5
Table S1
References (*25*–*30*)

29 July 2013; accepted 23 October 2013
Published online 7 November 2013;
10.1126/science.1243903

# Hepatitis C Virus E2 Envelope Glycoprotein Core Structure

Leopold Kong,[1,2,3] Erick Giang,[4] Travis Nieusma,[1] Rameshwar U. Kadam,[1] Kristin E. Cogburn,[1,4] Yuanzi Hua,[1] Xiaoping Dai,[1] Robyn L. Stanfield,[1,2,3] Dennis R. Burton,[2,3,4] Andrew B. Ward,[1,2,3]* Ian A. Wilson,[1,2,3,5]* Mansun Law[4]*

Hepatitis C virus (HCV), a *Hepacivirus*, is a major cause of viral hepatitis, liver cirrhosis, and hepatocellular carcinoma. HCV envelope glycoproteins E1 and E2 mediate fusion and entry into host cells and are the primary targets of the humoral immune response. The crystal structure of the E2 core bound to broadly neutralizing antibody AR3C at 2.65 angstroms reveals a compact architecture composed of a central immunoglobulin-fold β sandwich flanked by two additional protein layers. The CD81 receptor binding site was identified by electron microscopy and site-directed mutagenesis and overlaps with the AR3C epitope. The x-ray and electron microscopy E2 structures differ markedly from predictions of an extended, three-domain, class II fusion protein fold and therefore provide valuable information for HCV drug and vaccine design.

Hepatitis C virus (HCV) was discovered in 1989 as the causative agent of non-A, non-B hepatitis (*1*). It is estimated that 2 to 3% of the world population is infected with HCV (*2*), and, in the United States, it has overtaken human immunodeficiency virus 1 (HIV-1) as a cause of death (*3*). A prophylactic vaccine could help control the HCV pandemic, but its development has been technically challenging because of the viral genome's high sequence variability (*4*) as well as limitations in animal models (*5*, *6*). The envelope glycoprotein E2 is the main target for neutralizing antibody (NAb) responses, but it is also the most variable antigen in HCV (*7*). E2 forms a heterodimer with the other HCV envelope glycoprotein, E1, to mediate cell entry and fusion. Several broadly neutralizing antibodies (bNAbs) have been isolated against E2, raising hopes for the rational design of a broadly effective vaccine (*8*–*10*).

Structural characterization of HCV envelope glycoproteins would inform vaccine and drug design but has been challenging because of the difficulty in obtaining homogenous protein preparations. In HCV envelope glycoproteins, N-linked glycans constitute nearly 50% of the E1 and E2 protein ectodomain molecular weight (11 and 4 N-linked glycosylation sites in E2 and E1, respectively), and a high proportion of the expressed glycoproteins form aberrant disulfide cross-linked aggregates (*11*–*13*). On the basis of computational models, E2 was predicted to be a class II fusion protein characterized by a highly extended conformation (~110 to 130 Å) of three predominantly β-sheet domains (*12*, *14*).

To gain insight into the HCV E2 structure, which corresponds to residues 384 to 746 of the viral polyprotein (E1 is residues 192 to 383), we designed and expressed 41 different soluble E2 constructs and screened 7 of the well-behaved constructs (*15*) with various E2-specific Fabs in crystallization trials. Crystals diffracting to 2.65 Å (table S1 and fig. S2) were grown from an E2 core [(E2c), spanning residues 412 to 645; see supplementary materials (*15*)] in mammalian cells [human embryonic kidney (HEK) 293F] with the HCV prototypic strain H77 sequence in complex with bNAb AR3C Fab (*4*, *8*). The engineered E2c had truncations at the N and C termini, substitution of the potentially flexible variable region 2 (VR2, residues 460 to 485) with a Gly-Ser-Ser-Gly linker, and removal of N448 and N576 (where N is Asn) glycosylation sites of E2 (fig. S3) (*15*). E2c maintains a native E2 fold as verified by binding to a panel of monoclonal antibodies (mAbs) specific to conformational epitopes in E2 and to the CD81 receptor and by functional inhibition of HCV infection, presumably through receptor competition (fig. S1). Two equivalent E2 complexes (A and B) compose the crystal asymmetric unit, making extensive crystal contacts with each other between two sides of E2 and the heavy-chain constant domain of AR3C (fig. S2) (*16*).

Overall, the E2c structure is globular but contains many regions with no regular secondary structure despite the presence of eight disulfide bonds. In fact, nearly 62% of all E2c residues are either in loops or disordered (Fig. 1 and fig. S3). The disordered regions are at the E2c N terminus (residues 412 to 420), a short segment (spanning positions 454 to 491) surrounding the severely truncated E2 VR2, and a loop (586 to 596). Flexibility is also observed for six N-linked glycans in E2c: N417 and N423 are completely disordered; N532, N540, and N623 have only one ordered *N*-acetylglucosamine (GlcNAc); and N556 has two ordered GlcNAcs. Glycan N430 in the crystal interface can be modeled as $Man_6GlcNAc_2$ (where Man is mannose). Despite flexibility in parts of the structure, E2c has an overall well-defined architecture consisting of a central β sandwich flanked by front and back layers consisting of loops, short helices, and β sheets.

The E2 β sandwich (residues 492 to 566) contains four strands designated as the inner sheet (g, f, c, and c′) and two strands exposed to solvent designated as the outer sheet (e and b) (Fig. 1 and fig. S4). The overall strand connectivity places it within the C2 set of immunoglobulin (Ig) folds, which are characterized by the presence of the c′ strand in the inner sheet, as in CD4 domain 2, instead of the d strand in the outer sheet, as in, for example, the C1 set (*17*, *18*) (fig. S4). The loop connecting strands c′ to e contains 17 amino acids and exhibits a bilobed structure that extends from a narrow stalk formed by the N and C termini. The C-terminal lobe contains receptor binding residues ($Tyr^{527}$, $Trp^{529}$, $Gly^{530}$, and $Asp^{535}$) and is adjacent to the front layer that also contains key receptor binding residues (Fig. 1) (*19*) [see (*15*) for a detailed structural description of the front and back layers].

The Ig-fold β sandwich is the only structural element in E2c that is shared with presumed structural homologs that include class II viral fusion proteins, which have a three-domain architecture (domains I to III) (fig. S4). Ig folds are found in domain III of fusion envelope proteins from flaviviruses [e.g., tick-borne encephalitis virus (TBEV) and West Nile virus] (*20*, *21*), domain III of E1 fusion proteins, all domains of E2 proteins from rubivirus (rubella) (*22*) and alphaviruses (e.g., Chikungunya and Sindbis viruses) (*23*, *24*), and E2 domain B from pestivirus (bovine viral diarrhea virus) (*25*, *26*). However, the compact HCV E2c protein, which maximally spans ~50 Å, does not adopt the extended three-domain class II fusion protein fold (Fig. 1C), which measures 100 to 120 Å (*27*).

To confirm that full-length E2 is also compact and to visualize regions that are absent in the E2c crystal structure, we analyzed the complete E2 ectodomain (E2ΔTM, residues 384 to 717) bound to Fab AR3C by negative-stain electron microscopy (EM). Asymmetry of the complex resulting from the protruding Fab allowed for unambiguous fitting of the E2c-Fab AR3C crystal structure into the 16-Å resolution EM three-dimensional (3D) reconstruction, leaving ~30% of the EM volume unassigned (Fig. 1D), which is consistent with the expected 21% difference in mass between fully glycosylated E2c-Fab AR3C and E2ΔTM-Fab AR3C (*28*). The EM reconstruction accounts for most of the E2ΔTM protein and likely some of its N-linked glycans (Fig. 1D). Overall, the EM reconstruction shows that the E2ΔTM construct also displays a compact globular shape, confirming that the complete E2 ectodomain also does not adopt the highly extended, three-domain class II fusion fold (Fig. 1C).

The EM reconstruction enables us to approximately define regions of E2 that are absent in the E2c structure (Fig. 1D). The disordered and trun-

[1]Department of Integrative Structural and Computational Biology, The Scripps Research Institute, La Jolla, CA 92037, USA. [2]International AIDS Vaccine Initiative Neutralizing Antibody Center, The Scripps Research Institute, La Jolla, CA 92037, USA. [3]Scripps Center for HIV/AIDS Vaccine Immunology and Immunogen Discovery, The Scripps Research Institute, La Jolla, CA 92037, USA. [4]Department of Immunology and Microbial Science, The Scripps Research Institute, La Jolla, CA 92037, USA. [5]Skaggs Institute for Chemical Biology, The Scripps Research Institute, La Jolla, CA 92037, USA.

*Corresponding author. E-mail: mlaw@scripps.edu (M.L.); abward@scripps.edu (A.B.W.); wilson@scripps.edu (I.A.W.)

cated N-terminal region (residues 384 to 421), which includes hypervariable region 1 (HVR1), likely fits into a bulb of density next to the β sandwich, consistent with epitope mapping of Fab AR1A (*8*), which identified $Thr^{416}$, as well as $Val^{538}$ and $Asn^{540}$ on the top sheet of the β sandwich, as key interacting residues. The region (residues 454 to 491), which is largely truncated in the E2c construct, contains VR2 (460 to 485) and the N476 glycan and is readily accommodated in the EM density on the opposite face of the β sandwich. The largest portion of EM density not accounted for by the crystal structure is situated behind the back layer and VR3, where extensive crystal contacts are made between two E2 subunits in the asymmetric unit of the crystal structure. The 73-residue C-terminal stalk region that is also absent in the E2c construct would fit at this location, forming a final layer to the overall protein architecture.

In the crystal structure, E2c is bound to antibody AR3C, which belongs to a group of bNAbs that recognize antigenic region 3 (AR3) of E2 and crossneutralizes HCV genotypes by blocking CD81 receptor binding (*8*). The crystal structure defines the common surface that these bNAbs recognize, revealing a prime target for vaccine design. Within the binding interface, Fab AR3C buries 828 $Å^2$ of E2 protein surface and 161 $Å^2$ of E2 glycans (Fig. 2). Overall, residues that are 80 to 100% conserved across HCV genotypes make up 86% of the buried surface area in the AR3C epitope (Fig. 2C), including critical residues previously identified by alanine scanning mutagenesis (*8*). The epitope is relatively flat, encompassing most of the front layer, a serpentine stretch of residues 421 to 446, and a portion of the CD81 receptor binding loop. The protein-protein interface is composed mainly of the heavy-chain variable domain (86%), which corroborates data indicating that AR3C binding activity is not compromised when its light chain is swapped (fig. S1 and Fig. 2). The bNAb interaction is dominated by the CDR H3 loop, which buries a strand of highly conserved residues near the E2 N terminus in the front layer and $Trp^{529}$ in the CD81 receptor binding loop, together accounting for 44% of the total buried surface (Fig. 2). Antibody binding to the N-terminal strand is mediated by main-chain interactions (fig. S5), thus tolerating sequence variation in E2. The CDR H3 loop adopts a β-hairpin fold and is stabilized by a disulfide (*29*), which is encoded in 17% of human Ig heavy chain diversity gene 2 (IGHD2) germline alleles (*30*) (fig. S5), suggesting similar antibodies could be raised by vaccination. The CDR H1 and H2 loops of AR3C are encoded by the germline IGHV1-69 gene, which has been used in bNAbs against several viruses, including influenza (*31*) and HIV-1 (*32*). CDR H2 loops encoded by this heavy-chain variable gene ($V_H$ 1-69) have a hydrophobic tip, which tends to interact with hydrophobic clusters on the antigen and has been proposed as a primordial pattern recognition receptor (*33*). CDR H2 also interacts with hydrophobic residues on the N-terminal side of the front layer and, together with the CDR H1 loop, contacts hydrophobic residues on the α1 C terminus [see (*15*) for discussion of α1 recognition and antibody AR3C germline genes].

CD81 receptor binding residues identified in prior mutagenesis studies (fig. S3) (*19*, *34*) mainly mapped to the AR3C epitope; however, some

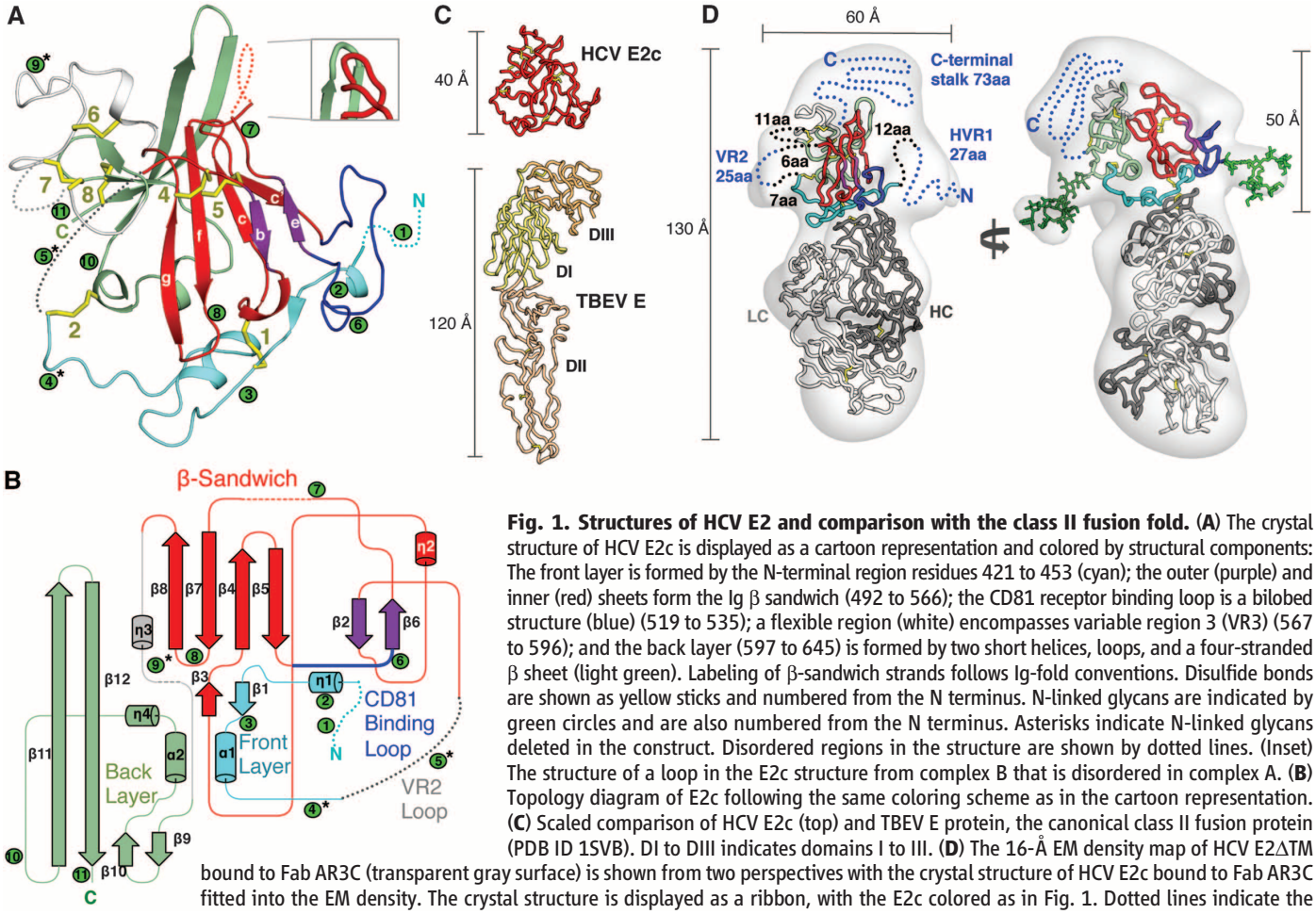


**Fig. 1. Structures of HCV E2 and comparison with the class II fusion fold.** (**A**) The crystal structure of HCV E2c is displayed as a cartoon representation and colored by structural components: The front layer is formed by the N-terminal region residues 421 to 453 (cyan); the outer (purple) and inner (red) sheets form the Ig β sandwich (492 to 566); the CD81 receptor binding loop is a bilobed structure (blue) (519 to 535); a flexible region (white) encompasses variable region 3 (VR3) (567 to 596); and the back layer (597 to 645) is formed by two short helices, loops, and a four-stranded β sheet (light green). Labeling of β-sandwich strands follows Ig-fold conventions. Disulfide bonds are shown as yellow sticks and numbered from the N terminus. N-linked glycans are indicated by green circles and are also numbered from the N terminus. Asterisks indicate N-linked glycans deleted in the construct. Disordered regions in the structure are shown by dotted lines. (Inset) The structure of a loop in the E2c structure from complex B that is disordered in complex A. (**B**) Topology diagram of E2c following the same coloring scheme as in the cartoon representation. (**C**) Scaled comparison of HCV E2c (top) and TBEV E protein, the canonical class II fusion protein (PDB ID 1SVB). DI to DIII indicates domains I to III. (**D**) The 16-Å EM density map of HCV E2ΔTM bound to Fab AR3C (transparent gray surface) is shown from two perspectives with the crystal structure of HCV E2c bound to Fab AR3C fitted into the EM density. The crystal structure is displayed as a ribbon, with the E2c colored as in Fig. 1. Dotted lines indicate the main portions of E2ΔTM that are absent in the E2c crystal structure. The numbers of amino acids (aa) in the missing regions are shown. Blue dotted lines show regions in E2ΔTM that are not in the E2c construct, and black dotted lines indicate regions that are in the E2c construct but are disordered in the crystal structure. Two protrusions in the EM density are in the vicinity of N-linked glycan sites and high-mannose glycans (green ball and sticks) are modeled at those positions. Measurements of dimensions are rounded to the nearest 10. LC, light chain; HC, heavy chain.

were also found in the β sandwich. To determine the location of the binding site, we performed site-directed mutagenesis and negative-stain EM. First, mutagenesis-driven modeling based only on the published putative receptor interacting residues indicated three possible binding sites: one side of the β-sandwich, an isolated portion of the CD81 receptor-binding loop, and the front layer (Fig. 3A and table S2). Thus, mutations were introduced to the full-length E1E2 heterodimer (Fig. 3B). Mutations that totally abrogated CD81 binding were addition of glycosylation sites at position 442 or 428 or a Lys-to-Tyr mutation at position 427 (L427Y) in the front layer. A P525R, but not P525A (P, Pro; R, Arg; A, Ala), mutation in the N-terminal lobe of the CD81 receptor-binding loop greatly reduced binding, suggesting that it may either bind CD81 or be involved in the correct folding of the C-terminal lobe for binding CD81 via $Tyr^{527}$, $Trp^{529}$, $Gly^{530}$, and/or $Asp^{535}$ (*19*). Together with previous mutagenesis data

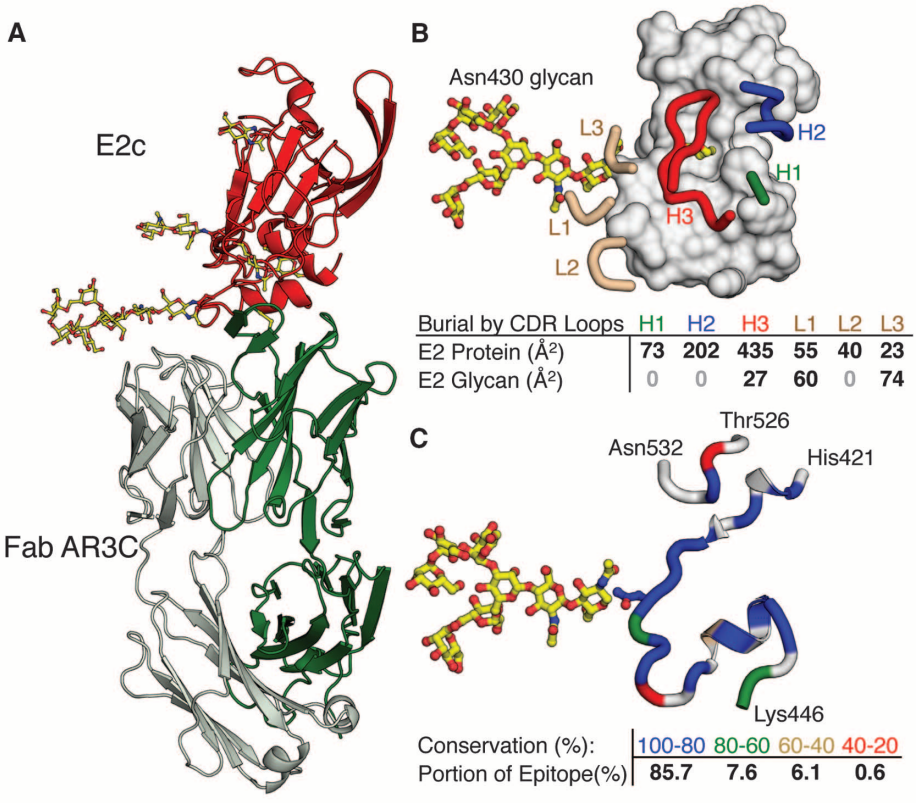


**Fig. 2. HCV E2 interaction with Fab AR3C.** (**A**) Overall structure of E2c (red) bound to Fab AR3C is displayed as a cartoon representation with the heavy and light chains of Fab colored dark and light green, respectively. N-linked glycans are shown in a ball-and-stick representation with carbon, oxygen, and nitrogen atoms colored yellow, red, and blue. (**B**) Interactions between Fab AR3C and E2c. The CDR loops of AR3C are displayed as thick tubes over the gray molecular surface of E2. A relatively unusual disulfide bond in CDR H3 for known human antibody structures is shown in yellow. The N430 glycan that interacts mainly with the light chain of AR3C is shown in yellow and red. Below the diagram is a table listing the surface areas buried on E2 by the different CDR loops. (**C**) The AR3C epitope on E2 is shown as a cartoon representation from the same perspective as in (B) and colored according to sequence conservation. Residues that are not buried by AR3C are colored gray. Below is a table listing the fractions of the surface on the E2 core protein with respect to sequence conservation (binned and color coded) that are buried by AR3C.

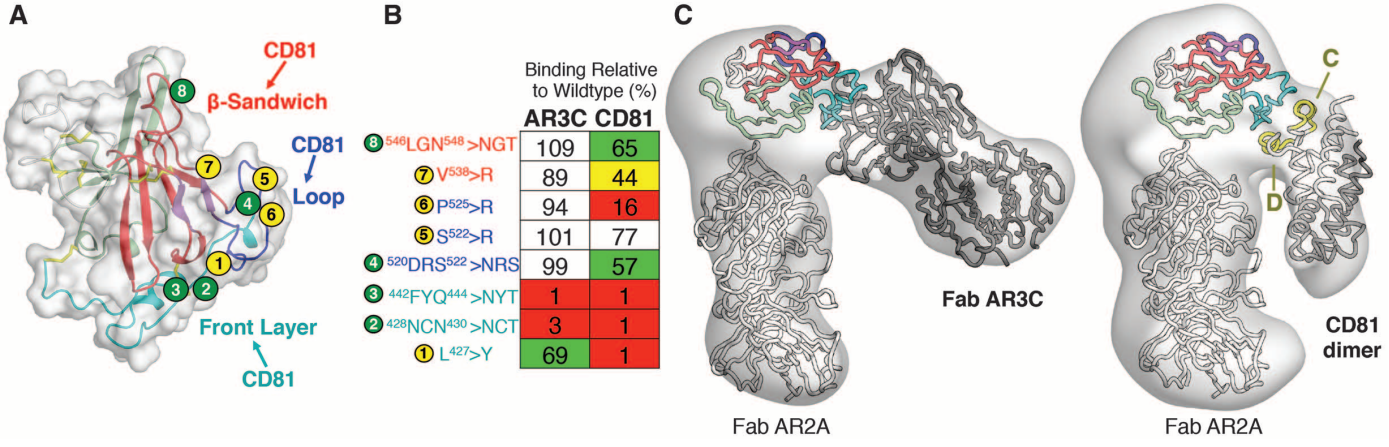


**Fig. 3. CD81 receptor binding site.** (**A**) Three potential CD81 binding sites on E2 were indicated from previously published alanine-scanning results (*19*): a surface on the β sandwich, the top of the CD81 binding loop, and the front layer. E2 mutations used to evaluate the possible binding sites are shown as circles numbered from the N terminus. A yellow circle indicates substitution by a bulky amino acid, and a green circle indicates the introduction of an N-linked glycosylation site. E2 is depicted as a cartoon within its molecular surface and colored as in Fig. 1A. (**B**) The substitutions shown in (A) are described, and their effects on CD81 and Fab AR3C binding are tabulated. Numbers indicate % binding of CD81 or Fab AR3C to variants relative to wild-type E1E2 in an enzyme-linked immunosorbent assay (ELISA). Binding is color coded: 0 to 25%, red; 26 to 50%, yellow; 51 to 75%, green; >75%, white. C, Cys; D, Asp; F, Phe; G, Gly; Q, Gln;S, Ser; T, Thr; and V, Val. (**C**) Negative-stain EM reconstructions of deglycosylated E2ΔTM bound to Fabs AR2A and AR3C (left) or bound to Fab AR2A and CD81 dimer (right). The crystal structure of E2c bound to Fab AR3C and a model of Fab AR2A displayed as ribbons are fitted within the electron density. E2c is colored as in Fig. 1. Helices C and D of CD81 are highlighted in yellow because they contain residues important for binding to E2 (*34*). In the CD81 complex, the density suggests that a CD81 dimer is present as in CD81 crystal structures (*35*, *36*).

(*19*), these results suggest that CD81 interacts with the front layer and the CD81 receptor binding loop (Fig. 3, A and B, and fig. S6).

To further delineate the receptor binding site, we performed negative-stain EM on a ternary complex of deglycosylated E2ΔTM, the large external loop (LEL) of CD81, and Fab AR2A (Fig. 3C and fig. S7). Docking of the E2c crystal structure into the 19-Å resolution EM reconstruction was aided by determination of the Fab AR2A interaction in the 20-Å EM reconstruction of E2ΔTM bound to Fabs AR2A and AR3C (Fig. 3C, left). The EM density for CD81 was too extensive for a monomer but consistent with a CD81 dimer, similar to that in CD81 crystal structures (*35*, *36*). One of the CD81 monomers interacts with the E2c front layer, consistent with the mutagenesis data (Fig. 3C and fig. S8). Only one orientation of the CD81 dimer has a reasonable fit to the EM density (*37*) and results in helices C and D being adjacent to E2 α1 and CD81 receptor binding loop. These helices contain critical E2-interacting residues (*34*). Therefore, CD81 binds to the same surface as AR3C and some other bNAbs (*8*), suggesting that it is a site of vulnerability that could be exploited in immunogen design. This exposed surface is relatively hydrophobic, has relatively low sequence variability, and is free of N-linked glycans (Fig. 4 and fig. S9). This site may also include residues 412 to 420, which are disordered in the crystal structure but are bound by bNAbs HCV1 and AP33 (*38*, *39*). However, similar to HIV-1 envelope glycoprotein 120 and influenza hemagglutinin, HCV E2 contains multiple highly variable regions (HVR1, VR2, and VR3) (*40*) and N-linked glycans to escape from immune recognition (Fig. 4 and fig. S9). For example, an extensive glycan shield masks an exposed face on the E2 surface from NAbs via 7 of the 11 N-linked glycans on E2 (Fig. 4 and fig. S9). Also, on the opposite side of the β sandwich, a relatively hydrophobic surface is likely occluded by the N-terminal HVR1 (fig. S9); deletion of HVR1 is not lethal to the virus and greatly increases the sensitivity of the virus to antibody neutralization (*41*). Lastly, between the glycosylated and HVR1-occluded faces of E2, a separate oblong surface, formed by the outer sheet of the β sandwich and portions of VR3 (Fig. 4 and fig. S9) with relatively high sequence variability, is recognized by several weakly or non-NAbs (*8*). These non-NAbs can bind soluble recombinant E1E2 at high affinity (*8*), suggesting their epitopes must be occluded on the virus.

Until recently, HCV was the sole identified member of the *Hepacivirus* genus in the *Flaviviridae* family. Nonprimate hepaciviruses have now been identified in dogs, horses, and rodents, providing insights into the evolution of this viral genus (*42*). Despite sharing a common Ig fold, the compact globular HCV E2 structure distinguishes HCV from the related virus genera *Pestivirus* and *Flavivirus* that have extended, multidomain envelope-protein structures, undermining the proposals of E2 as a class II fusion protein (*12*, *14*). To determine whether the *Hepacivirus* envelope protein uses a novel fusion mechanism will require structural characterization of E1 and the E1E2 complex in the context of the virus. However, the E2 structure and the characterization of broadly neutralizing epitopes and the CD81 binding site provide new opportunities for HCV vaccine and drug design.

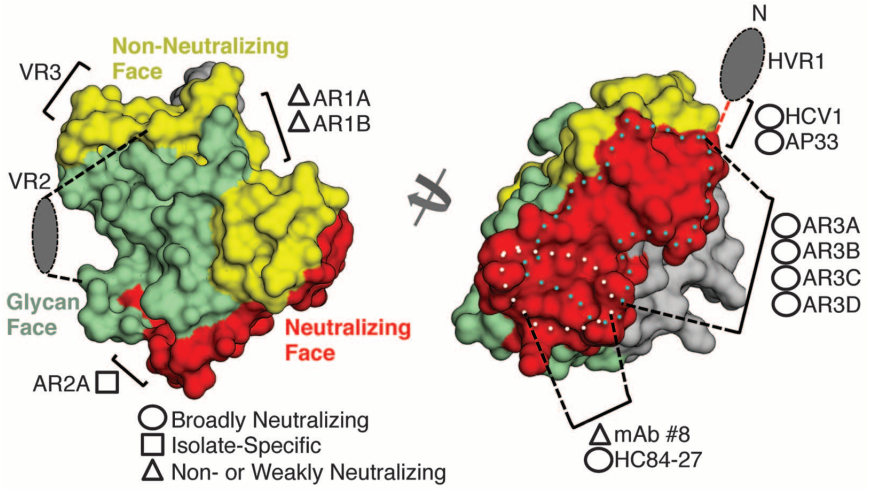


**Fig. 4. HCV E2 antigenic surface.** The E2c structure is displayed as a molecular surface colored according to different antigenic properties described in the text. Missing HVR1 and VR2 regions are represented as colored ovals and labeled. The mAb binding sites mapped from alanine scanning studies or from crystal structures bound to peptides, as described in the main text, are indicated. On the neutralizing face (**right**), three antigenic regions are shown: residues 412 to 423 (red dashed line connecting HVR1 and the rest of E2), the AR3C epitope in the front layer that overlaps with the CD81 binding site (cyan dotted line), and α1 in the front layer (white dotted line). The gray surface is relatively hydrophobic and conserve and may be an occluded zone covered by HVR1 in the full-length E2 protein, as suggested by the EM reconstruction of E2ΔTM (Fig. 1C).

## References and Notes


1. Q. L. Choo *et al.*, *Science* **244**, 359–362 (1989).
2. D. Lavanchy, *Liver Int.* **29** (suppl. 1), 74–81 (2009).
3. K. N. Ly *et al.*, *Ann. Intern. Med.* **156**, 271–278 (2012).
4. C. Kuiken, P. Hraber, J. Thurmond, K. Yusim, *Nucleic Acids Res.* **36**, D512–D516 (2008).
5. M. Houghton, S. Abrignani, *Nature* **436**, 961–966 (2005).
6. E. Billerbeck, Y. de Jong, M. Dorner, C. de la Fuente, A. Ploss, *Curr. Top. Microbiol. Immunol.* **369**, 49–86 (2013).
7. C. Kuiken, P. Simmonds, *Methods Mol. Biol.* **510**, 33–53 (2009).
8. M. Law *et al.*, *Nat. Med.* **14**, 25–27 (2008).
9. T. J. Broering *et al.*, *J. Virol.* **83**, 12473–12482 (2009).
10. Z. Y. Keck *et al.*, *PLOS Pathog.* **8**, e1002653 (2012).
11. J. P. Michalak *et al.*, *J. Gen. Virol.* **78**, 2299–2306 (1997).
12. T. Krey *et al.*, *PLOS Pathog.* **6**, e1000762 (2010).
13. J. Whidby *et al.*, *J. Virol.* **83**, 11078–11089 (2009).
14. A. T. Yagnik *et al.*, *Proteins* **40**, 355–366 (2000).
15. Materials and methods and supplementary text are available as supplementary materials on *Science* Online.
16. Complex A has better defined electron density and lower B values, likely from additional crystal contacts between the tips of glycan N430 and a neighboring symmetry mate (fig. S2); the same glycan in complex B is mostly disordered. The N430 interaction may explain why enzymatic deglycosylation, which typically aids crystallization, does not produce crystals.
17. D. M. Halaby, A. Poupon, J. Mornon, *Protein Eng.* **12**, 563–571 (1999).
18. One difference from the standard C2-set connectivity is the absence of strand a from the outer sheet of the E2 β sandwich, which could be due to disorder or to truncation of E2 VR2 in the construct. A more important difference is the absence of a canonical disulfide connecting outer and inner sheets at strands b and f that is present in most Ig folds, although observed together with C2-set strand connectivity in some bacterial, actinoxanthine-like, and fibronectin III–like domains comprising the C3, C4, and FN3 sets. However, the E2 β sandwich has disulfides linking the loop before strand b with strand g (residues 494 to 564) and strand c with strand f (508 to 552), which are typically observed in the C2 set but not for the C3, C4, or Fn3 sets. This unique disulfide system found in the E2 β sandwich may have constrained the rotational angle between inner and outer sheet strands to be nearly parallel, rather than the –30° offset commonly observed in Ig folds. Together, these features suggest the E2 β sandwich is similar to the C2 set but with differences such as lack of strand a, lack of disulfide connection between strands b and f, and lack of –30° offset between front and back sheets that prevent finding significant matches with equivalent strand connectivity to other structures in the Protein Data Bank (PDB) using structural homology programs DALI and FATCAT (*15*).
19. A. M. Owsianka *et al.*, *J. Virol.* **80**, 8695–8704 (2006).
20. F. A. Rey, F. X. Heinz, C. Mandl, C. Kunz, S. C. Harrison, *Nature* **375**, 291–298 (1995).
21. G. E. Nybakken *et al.*, *Nature* **437**, 764–769 (2005).
22. R. M. DuBois *et al.*, *Nature* **493**, 552–556 (2013).
23. J. E. Voss *et al.*, *Nature* **468**, 709–712 (2010).
24. L. Li, J. Jose, Y. Xiang, R. J. Kuhn, M. G. Rossmann, *Nature* **468**, 705–708 (2010).
25. K. El Omari, O. Iourin, K. Harlos, J. M. Grimes, D. I. Stuart, *Cell Rep.* **3**, 30–35 (2013).
26. Y. Li, J. Wang, R. Kanai, Y. Modis, *Proc. Natl. Acad. Sci. U.S.A.* **110**, 6805–6810 (2013).
27. M. C. Vaney, F. A. Rey, *Cell. Microbiol.* **13**, 1451–1459 (2011).
28. This calculation assumes all N-linked glycans are $Man_9GlcNAc_2$ because of the kifunensine treatment during protein production.
29. J. C. Almagro *et al.*, *J. Mol. Recognit.* **25**, 125–135 (2012).
30. This calculation was made from searching the International Immunogenetics Information System (IMGT) database on 27 March 2013. There were $n = 8832$ IGHD germline genes in the database, of which 1514 contained the disulfide motif.
31. D. C. Ekiert *et al.*, *Science* **324**, 246–251 (2009); 10.1126/science.1171491.
32. T. Zhou *et al.*, *Nature* **445**, 732–737 (2007).
33. D. Lingwood *et al.*, *Nature* **489**, 566–570 (2012).

34. H. E. Drummer, K. A. Wilson, P. Poumbourios, *J. Virol.* **76**, 11143–11147 (2002).
35. K. Kitadokoro *et al.*, *EMBO J.* **20**, 12–18 (2001).
36. K. Kitadokoro *et al.*, *Biol. Chem.* **383**, 1447–1452 (2002).
37. At this resolution, we have approximated the known CD81 dimer structure into the EM reconstruction, but some differences are apparent that will need higher-resolution structure information to discern subtle differences in free and bound conformations of CD81.
38. L. Kong *et al.*, *J. Virol.* **86**, 13085–13088 (2012).
39. L. Kong *et al.*, *Proc. Natl. Acad. Sci. U.S.A.* **109**, 9499–9504 (2012).
40. HVR1 has been defined as the most variable region of the HCV genome. However, relative to the entire genome, VR2 and VR3 are not considered hypervariable. Here, we define these regions as variable with respect to E1 and E2 proteins only and not with respect to the rest of the HCV genome.
41. D. Bankwitz *et al.*, *J. Virol.* **84**, 5751–5763 (2010).
42. A. Kapoor *et al.*, *mBio* **4**, e00216-13 (2013).

**Acknowledgments:** We thank H. Tien, T. Clayton, and M. C. Deller for help in setting up crystallization screens using the CrystalMation and Douglas robots; J. Robbins for help with protein purification; N. Laursen for useful discussions on refinement; L. Jaroszewski for help in analyzing the HCV E2c protein fold; P. Verdino for discussion of Ig folds; and J. P. Verenini for help in manuscript formatting. This work is supported by NIH grants AI079031 and AI080916 (to M.L.), AI071084 (to D.R.B.), and AI084817 and U54 GM094586 (to I.A.W.) and the Skaggs Institute (I.A.W.). L.K. is grateful to the American Foundation for AIDS Research for a Mathilde Krim Fellowship in Basic Biomedical Research, and R.U.K., to the Swiss National Science Foundation for a postdoctoral fellowship. The EM data were collected at the U.S. National Resource for Automated Molecular Microscopy (NRAMM) at the Scripps Research Institute, which is supported by the NIH through the National Center for Research Resources' P41 program (RR017573) at the National Center for Research Resources. X-ray data sets were collected at the Stanford Synchrotron Radiation Lightsource (SSRL) beamline 12-2, a Directorate of the Stanford Linear Accelerator Center National Accelerator Laboratory and an Office of Science User Facility operated for the U.S. Department of Energy (DOE) Office of Science by Stanford University. The SSRL Structural Molecular Biology Program is supported by the DOE Office of Biological and Environmental Research; NIH's National Center for Research Resources, Biomedical Technology Program (P41RR001209); and the National Institute of General Medical Sciences (NIGMS). Coordinates and structure factors for the E2c complex with Fab AR3C have been deposited with the Protein Data Bank under accession code 4MWF. The EM reconstruction densities for the E2ΔTM-Fab AR3C, E2ΔTM-Fab AR3C-Fab AR2A, and E2ΔTM-FabAR2A-CD81 LEL complexes have been deposited with the Electron Microscopy Data Bank under accession codes EMD-5759, EMD-5760, and EMD-5761, respectively. Antibodies and expression vectors used in this work are available from the authors (contact M.L.) under a materials transfer agreement with the Scripps Research Institute. The content is the responsibility of the authors and does not necessarily reflect the official views of the NIGMS, National Cancer Institute, or NIH. This is manuscript 24038 from the Scripps Research Institute. The authors declare no competing financial interests.

**Supplementary Materials**

www.sciencemag.org/content/342/6162/1090/suppl/DC1
Materials and Methods
Supplementary Text
Figs. S1 to S11
Tables S1 and S2
References (*43*–*74*)

29 July 2013; accepted 17 October 2013
10.1126/science.1243876

# 27-Hydroxycholesterol Links Hypercholesterolemia and Breast Cancer Pathophysiology

**Erik R. Nelson,[1] Suzanne E. Wardell,[1] Jeff S. Jasper,[1] Sunghee Park,[1] Sunil Suchindran,[2] Matthew K. Howe,[1] Nicole J. Carver,[1] Ruchita V. Pillai,[1] Patrick M. Sullivan,[3] Varun Sondhi,[4] Michihisa Umetani,[4] Joseph Geradts,[5] Donald P. McDonnell[1]***

Hypercholesterolemia is a risk factor for estrogen receptor (ER)–positive breast cancers and is associated with a decreased response of tumors to endocrine therapies. Here, we show that 27-hydroxycholesterol (27HC), a primary metabolite of cholesterol and an ER and liver X receptor (LXR) ligand, increases ER-dependent growth and LXR-dependent metastasis in mouse models of breast cancer. The effects of cholesterol on tumor pathology required its conversion to 27HC by the cytochrome P450 oxidase CYP27A1 and were attenuated by treatment with CYP27A1 inhibitors. In human breast cancer specimens, CYP27A1 expression levels correlated with tumor grade. In high-grade tumors, both tumor cells and tumor-associated macrophages exhibited high expression levels of the enzyme. Thus, lowering circulating cholesterol levels or interfering with its conversion to 27HC may be a useful strategy to prevent and/or treat breast cancer.

Obesity and the metabolic syndrome are risk factors for estrogen receptor (ER)–positive breast cancer in postmenopausal women (*1*, *2*). This has been attributed to increases in circulating insulin and insulin-like growth factors, local production of estrogens in adipose tissue, and the influence of adipokines and inflammatory cytokines on tumors and their microenvironment (*3*). Recently, hypercholesterolemia, an established comorbidity of obesity, has been identified as an independent risk factor for breast cancer in postmenopausal women (*4*–*6*). Whereas studies of the impact of 3-hydroxy-3-methylglutaryl coenzyme A reductase inhibitors (statins) on breast cancer risk have yielded equivocal results (*7*), there is strong evidence that disease-free survival is improved in breast cancer survivors who are taking statins before diagnosis (*8*, *9*).

It has been proposed that the beneficial effects of statins in breast cancer result from their ability to directly inhibit cell proliferation. This hypothesis is difficult to reconcile with the observation that statin concentrations of 1 to 200 μM are required to inhibit cancer cell proliferation in vitro, whereas the extrahepatic levels of statins do not normally exceed 10 to 200 nM in humans (*10*–*12*). An alternative explanation is that tumor cell growth is negatively affected by reducing the levels of circulating cholesterol. Of importance in this regard are the recent observations that the oxysterol 27-hydroxycholesterol (27HC), an abundant primary metabolite of cholesterol, is a selective estrogen receptor modulator (SERM) and liver X receptor (LXR) agonist that exerts a spectrum of activities in bone and the cardiovascular system in mice (*13*–*16*). Furthermore, we performed a comprehensive analysis of the molecular pharmacology of 27HC in cellular models of breast cancer, revealing that 27HC exhibited significant ER and LXR partial agonist activity at concentrations expected to be found in humans (figs. S1 to S3) (*17*). These findings prompted us to evaluate the extent to which 27HC affects tumor pathophysiology in animal models of breast cancer.

The first objective of our studies was to determine whether or not the estrogenic activity of 27HC was sufficient to promote the growth of MCF7 cell–derived breast xenografts when propagated in ovariectomized mice. The estrogen dependency of this model was demonstrated by showing that 17β-estradiol (E2), but not vehicle treatment, promoted tumor growth (Fig. 1A and fig. S4). 27HC also promoted the growth of these tumors, and this activity was inhibited by cotreatment with the pure antiestrogen ICI 182,780, or upon cessation of 27HC supplementation. Gene expression studies revealed a potential association between 27HC exposure and the development of tamoxifen resistance (fig. S1A), prompting an evaluation of the pharmacology of 27HC in a mouse model of tamoxifen resistance (TamR) (*18*). In this model, as in the tumors of patients with tamoxifen-resistant disease, tamoxifen exhibits robust agonist activity. It was significant, therefore, that 27HC promoted tumor growth as well as, or better than, tamoxifen or E2 in this model (Fig. 1B).

Next, we evaluated the impact of 27HC on tumor pathology in an immune-competent mouse

[1]Department of Pharmacology and Cancer Biology, Duke University School of Medicine, Durham, NC 27710, USA. [2]Duke Institute for Genome Sciences and Policy, Duke University, Durham, NC 27708, USA. [3]Division of Geriatrics, Department of Medicine, Duke University School of Medicine, Durham, NC 27710, USA. [4]Departments of Pediatrics and Pharmacology, University of Texas Southwestern Medical Center, Dallas, TX 75390, USA. [5]Department of Pathology, Duke University School of Medicine, Durham, NC 27710, USA.

*Corresponding author. E-mail: donald.mcdonnell@duke.edu

mammary tumor virus–polyoma middle T-antigen (MMTV-PyMT) model. These mice, which express the MMTV-PyMT transgene, develop spontaneous ERα-positive mammary adenocarcinomas that metastasize to the lung (*19*, *20*). For these studies, the MMTV-PyMT mice were crossed onto a CYP7B1$^{+/+}$ or CYP7B1$^{-/-}$ background. The cytochrome p450 monooxygenase CYP7B1 is responsible for the catabolism of 27HC. In CYP7B1$^{-/-}$/MMTV-PyMT mice, plasma and intratumoral 27HC concentrations were ~three times higher than in CYP7B1$^{+/+}$/MMTV-PyMT control mice. Tumor latency was dramatically reduced in the CYP7B1$^{-/-}$ mice (Fig. 1C). Once palpable tumors formed, they grew at a significantly increased rate in CYP7B1$^{-/-}$ mice compared with CYP7B1$^{+/+}$ mice (Fig. 1D). Treatment of CYP7B1$^{-/-}$ mice with ICI 182,780 resulted in tumor growth rates similar to those in a CYP7B1$^{+/+}$ background, confirming the role of ER in this process. In a separate study, at the time of tumor detection, CYP7B1$^{+/+}$/MMTV-PyMT mice were treated daily with placebo, 27HC, E2, or the synthetic LXR agonist GW3965. As shown in Fig. 1E, treatment with E2 or 27HC significantly increased the growth of tumors compared with vehicle, whereas GW3965 slightly retarded tumor growth when compared to placebo, a result that mirrors the responses observed in vitro (fig. S2, B and C). The tumor-promoting effects of 27HC were also confirmed in a second murine model of ER-positive breast tumors. For this study, E0771 cells, derived from a spontaneous mammary tumor in C57BL/6 mice, were propagated syngenically in ovariectomized mice. In this model, tumor growth was increased by either E2 or 27HC supplementation, and the activity of 27HC could be inhibited by cotreatment with ICI 182,780. The LXR agonist GW3965 decreased tumor growth (Fig. 1F). Assessment of gene expression in the MMTV-PyMT model indicated that markers for proliferation, macrophage infiltration, angiogenesis, and invasion were increased in mice treated with 27HC (fig. S5). Elevated expression of both ER and LXR target genes was also observed. These studies confirm the ER and LXR agonist activity of 27HC and implicate ER as the mediator of the effects of this oxysterol on primary tumor growth.

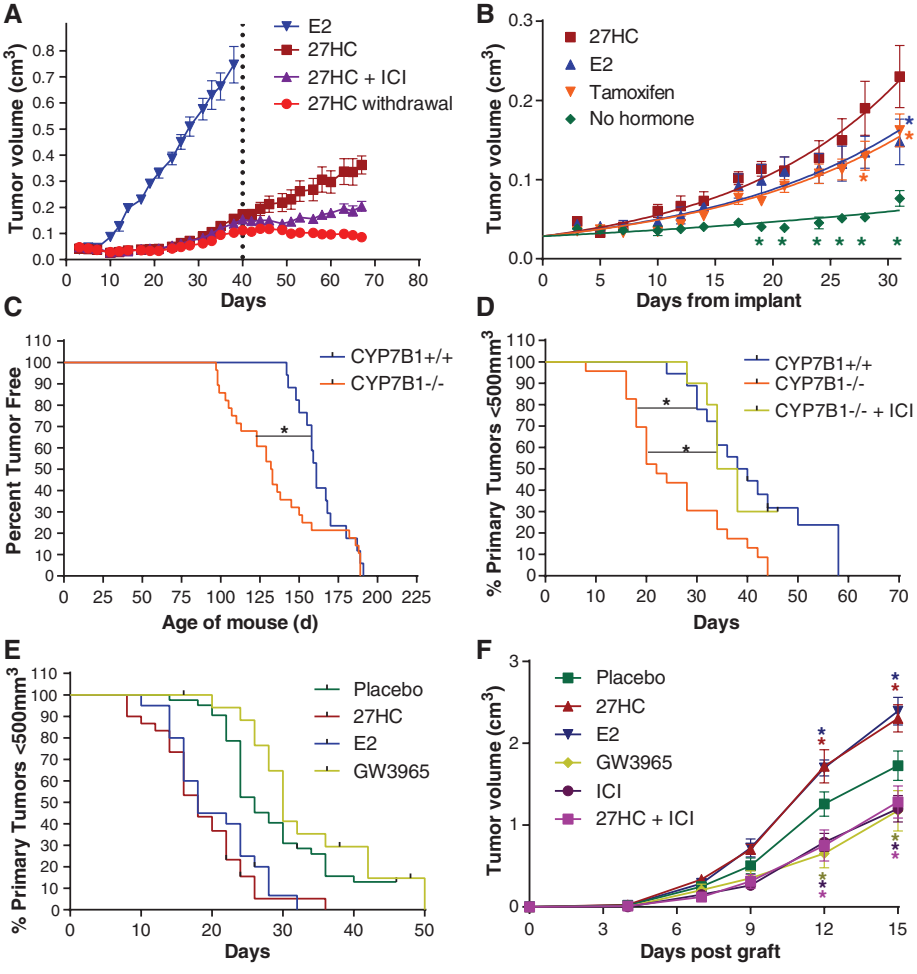


**Fig. 1. The oxysterol 27HC increases tumor growth in several animal models of ER-positive breast cancer.** (**A**) The estrogenic activity of 27HC is sufficient to support the growth of human MCF7 cell xenografts when propagated in ovariectomized mice. MCF7 cells were injected into the axial mammary pad of ovariectomized, immunocompromised mice, and the mice were administered 27HC by daily injection or given an E2 pellet, as indicated. At day 40, the 27HC-treated mice were randomized into three groups: continued 27HC, 27HC + the antiestrogen ICI 182,780 (ICI), or vehicle treatment (27HC withdrawal) [mean ± SEM (error bars), $n$ = 9 to 10 replicates]. (**B**) 27HC supports the growth of tamoxifen-resistant, MCF7 cell–derived breast tumors. Tamoxifen-resistant MCF7 cells (TamR) were injected into ovariectomized, immunocompromised mice. The mice were treated for 30 days with E2 (pellet), tamoxifen (pellet), 27HC (injection), or without supplementation. Colored asterisks indicate significant differences from 27HC-treated tumors (mean ± SEM, $P < 0.05$, $n = 5$ to 9). The latency (**C**) and growth (**D**) of tumors in the MMTV-PyMT mouse model of breast cancer was evaluated in mice in which catabolism of 27HC is attenuated (CYP7B1$^{-/-}$ background). Significance between curves is indicated by a connecting black line and an asterisk ($P < 0.05$, $n = 10$ to 28). d, days. (**E**) Tumor growth in MMTV-PyMT mice is increased by 27HC and attenuated by LXR agonists. MMTV-PyMT mice were injected daily with either 27HC, E2, GW3965, or vehicle as indicated. The growth of tumors in the 27HC- and E2-treated mice were significantly different from those grown in placebo- and GW3965-treated animals ($P < 0.05$, $n = 110$ total). (**F**) The growth of the ER-positive E0771 murine cell-derived xenografts was stimulated by 27HC when grown syngenically. Treatments were by injection as indicated. Colored asterisks indicate significant difference from placebo at the selected time point (mean ± SEM, $P < 0.05$, $n = 7$).

Given the role of CYP7B1 in 27HC catabolism, we considered that differences in its expression might track with outcomes in ER-positive breast cancers. To address this question, we evaluated CYP7B1 mRNA expression in several different human breast cancer data sets and determined that its elevated expression is associated with better survival outcome in luminal A types ($P = 0.0469$) (fig. S6A). This is an important finding as, in general, luminal A breast cancers generally express ER and are most likely to respond to ER antagonists or aromatase inhibitors and would be expected to be influenced by the estrogenic activity of 27HC.

Expression of CYP27A1 (cytochrome p450 oxidase required for the conversion of cholesterol to 27HC) mRNA in breast tumors did not correlate with outcome in this disease, prompting a closer examination of CYP27A1 protein expression in tumors (fig. S6B). Previously, it has been determined that CYP27A1 is highly expressed in macrophages (*21*). Our studies revealed that, regardless of where macrophages reside in human breast tissue (benign versus malignant or intraductal versus stromal), they consistently stain strongly for CYP27A1 protein (fig. S7). The well-established correlation between macrophage infiltration and breast cancer outcome raises the possibility that macrophage-produced 27HC may be able to support the growth of ER-positive breast tumors (*22*). To test this hypothesis, we evaluated whether conditioned media from bone-derived macrophages could support the growth of ER-positive breast cancer cells and whether

media quality was influenced by CYP27A1 activity. We found that (i) macrophage conditioned media stimulated MCF7 cell proliferation and that this activity was inhibited by ICI 182,780, and (ii) the basal effect of conditioned media from CYP27A1$^{-/-}$ macrophages on MCF7 cell proliferation was increased by 27HC supplementation (fig. S8). Importantly, the ability of conditioned media to support the growth of MCF7 cells was compromised when macrophages were treated with two different CYP27A1 inhibitors [GI268267X and GW273297X (*23*)], and the effects of these inhibitors could be reversed by adding 27HC. These data suggest that local production of 27HC by tumor-associated macrophages is likely to have a considerable impact on tumor pathology.

In addition to macrophages, we also found that CYP27A1 protein was expressed, to varying degrees, in cancer cells themselves (fig. S9). More specifically, we determined that increased expression of this enzyme was observed in higher-grade tumors (estimated odds ratio: 6.7, confidence interval: 1.7 to 27, $P = 0.0007$) (Table 1 and fig. S9). Thus, in addition to paracrine production from macrophages, autocrine production of 27HC by cancer cells is likely to influence tumor pathology.

Recently, it was reported that a diet high in both fat and cholesterol decreases latency and increases tumor growth and metastasis in MMTV-PyMT mice (*24*). It has also been shown that tumor xenografts grew faster when propagated in the hyperlipidemic *Apoe*$^{-/-}$ mouse model (*25*). Because a high-fat, high-cholesterol diet was used in both of these studies, the specific contribution of cholesterol (or its metabolites) on tumor biology could not be assessed. To directly address this question, we evaluated tumor pathology in the MMTV-PyMT model as a function of a high-cholesterol diet (HCD). In this study, CYP27A1$^{+/+}$/MMTV-PyMT mice were fed a HCD from weaning and developed palpable tumors earlier than mice on a control diet (Fig. 2A). Furthermore, once tumors were detected, they grew at a faster rate in mice on a HCD compared with mice on a control diet (Fig. 2B). We confirmed that the intratumoral concentrations of 27HC in HCD-fed mice were elevated and reflect the levels observed in human patients without any known genetic predisposition to elevated cholesterol (*15*, *26*) (fig. S10). However, in CYP27A1$^{-/-}$/MMTV-PyMT mice, in which 27HC is undetectable, we observed that tumor latency was increased and tumor growth decreased when mice were fed a control diet, and the effect of HCD on tumor pathology was negated in the CYP27A1 null background (Fig. 2, A and B). Importantly, the impaired growth of mammary tumors in CYP27A1$^{-/-}$ mice could be restored to that observed in CYP27A1 intact mice by daily injection of 27HC from the point of detection of a palpable tumor. These data indicate that 27HC, and not cholesterol per se, is pathologic in breast tumors.

Unlike humans, mice do not normally become hypercholesterolemic when fed a high-fat diet (HFD). Therefore, we made use of an *APOE3* targeted replacement mouse model, in which the mouse *Apoe* gene has been replaced with the human *APOE3* allele (*27*). A HFD significantly increases circulating levels of both total cholesterol and 27HC in these mice. Importantly, the elevated 27HC can be decreased by treatment with a CYP27A1 inhibitor (GW273297X) (fig. S11). Using the ER-positive E0771 model, we demonstrated that tumors grew faster in HFD *APOE3* mice compared with mice on a control diet and that tumor growth was attenuated by treatment with GW273297X administered by daily injection (Fig. 2C). As plasma 27HC concentrations are correlated with circulating cholesterol (*26*), we tested whether inhibition of de novo cholesterol synthesis would affect tumor growth. Indeed, we found that oral administration of the statin atorvastatin reduced the level of circulating cholesterol and attenuated the en-

**Table 1. Overexpression of CYP27A1 increases the likelihood of a higher tumor grade.** Results of immunohistochemical analysis of CYP27A1 expression in human breast cancer tissue microarrays are shown. CYP27A1 expression was determined to be low or high and correlated with tumor grade, estrogen receptor (ER), progesterone receptor (PR), or human epidermal growth factor receptor 2 (HER2) status. A Fisher's exact test was used to determine *P* values for the likelihood of association. Ordinal logistic regression was used to estimate the odds ratio. *N*, sample number; N/A, not applicable (because sample number is too small).

| | | Grade | | | ER | | PR | | HER2 | |
|---|---|---|---|---|---|---|---|---|---|---|
| | *N* | 1 | 2 | 3 | + | − | + | − | + | − |
| CYP27A1 (low) | 48 | 19% | 65% | 17% | 81% | 19% | 73% | 27% | 8% | 92% |
| CYP27A1 (high) | 11 | 0% | 45% | 55% | 71% | 29% | 68% | 32% | 0% | 1% |
| *P* value | | | 0.02 | | 0.02 | | 0.03 | | 0.19 | |
| Odds ratio | | | 6.7 | | 0.19 | | 0.21 | | N/A | |

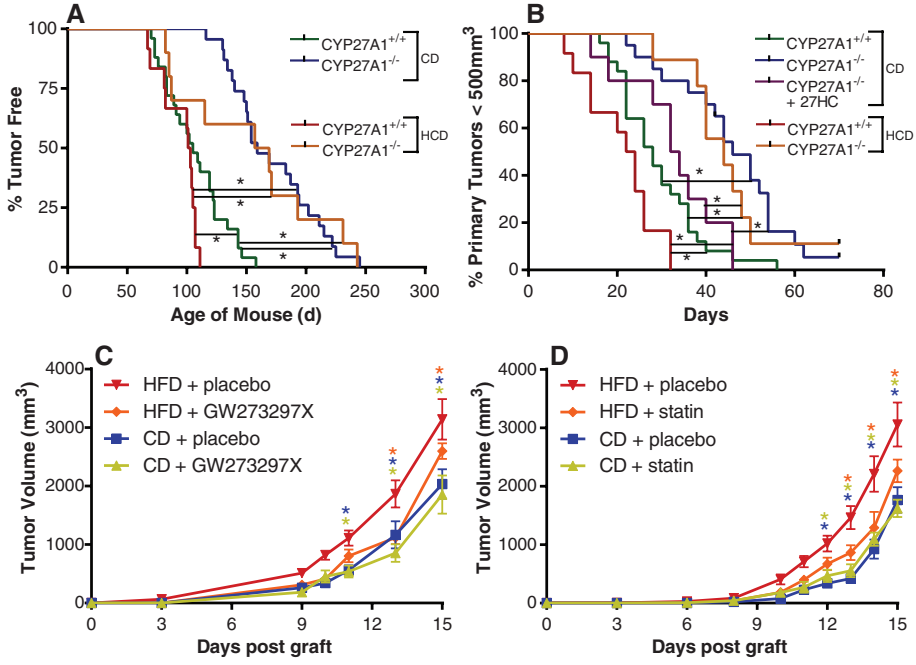


**Fig. 2. Genetic or pharmacological inhibition of 27HC production attenuates hypercholesterolemia-promoted tumor growth in mice.** The latency and growth of tumors in the MMTV-PyMT mouse model of breast cancer were evaluated in mice in which the conversion of cholesterol into 27HC was inhibited by disruption of the *CYP27A1* gene (CYP27A1$^{-/-}$). For this study, MMTV-PyMT mice were bred onto a CYP27A1$^{+/+}$ or a CYP27A1$^{-/-}$ background. (**A**) Tumor latency and (**B**) tumor growth were measured in mice on a control diet (CD) or a high-cholesterol diet (HCD) from weaning. Note that in the tumor growth studies, daily injection of 27HC overcame the inhibitory effect of CYP27A1 deletion. Significance between curves is indicated by a connecting black line and an asterisk ($P < 0.05$, $n = 9$ to 25). Growth of the ER-positive E0771 murine cell–derived grafts was evaluated in syngeneic *APOE3* mice fed a control diet or a HFD after coadministration of (**C**) the CYP27A1 inhibitor GW273297X (or vehicle) or (**D**) the statin atorvastatin (or vehicle), as indicated. Asterisks indicate statistically significant differences with the HFD + placebo group (mean ± SEM, $P < 0.05$, $n = 6$ to 12).

hanced tumor growth associated with a HFD (Fig. 2D and fig. S12). MMTV-PyMT mice on a HFD do not develop hypercholesterolemia, and tumor growth in these animals was indistinguishable from those on a control diet (fig. S13). Thus, in this *APOE3* mouse model, a HFD enhances tumor growth, an effect that can be partially reversed by treatment with agents that inhibit the biosynthesis of cholesterol or 27HC.

We next addressed whether 27HC affected metastasis in the MMTV-PyMT model. As shown in Fig. 3A, a greater number of metastatic foci were observed in lungs from mice treated with daily 27HC injections compared with mice injected with vehicle alone. Metastasis was evaluated when total tumor volume had reached 2 $cm^3$. The effect of 27HC on metastasis in this model was confirmed by measuring lung PyMT mRNA expression. By this measure, decreased metastasis was observed in the CYP27A1$^{-/-}$ mice, with increased metastasis being evident in the CYP7B1$^{-/-}$ mice. A similar relation between elevated 27HC and metastasis (as assessed by PyMT mRNA expression) was observed in mice receiving daily injections of 27HC (Fig. 3B). In contrast to the effects on the growth of primary tumors (above), the actions of 27HC on metastasis do not appear to involve ER, as treatment of animals with E2 was without effect in this model. Conversely, whereas LXR activation attenuates E2-dependent breast cancer cell proliferation in vitro and in the tumor models described above, the LXR agonist GW3965 increased lung metastasis, albeit less efficiently than 27HC. We conclude from these studies that LXR activation by 27HC increases tumor metastasis and that these activities occur independently of ER.

Gene expression analysis revealed that 27HC and LXR agonists induce the expression of several genes involved in epithelial-to-mesenchymal transition (EMT) (fig. S14). In addition, breast cancer cell lines treated in vitro with 27HC or with a synthetic LXR agonist adopt a spindle-like morphology, which mirrors the increased expression of vimentin, Snail1, and FAPα, established markers of EMT (Fig. 3C and fig. S14). To examine the in vivo relevance of these observations, we assessed the impact of 27HC treatment on the metastatic potential of ER-negative, LXR-positive Met1 cells. We determined that when these cells were pretreated in vitro with 27HC and injected intravenously into animals, they readily metastasized to the lung (Fig. 3D). These results are consistent with the hypothesis that 27HC, acting through LXR, increases lung metastasis secondary to effects on EMT.

We have shown the pathologic actions of cholesterol on ER-positive breast cancer require its conversion to 27HC. Further, it was demonstrated that the actions of 27HC on primary tumor growth are dependent on ER, whereas its actions in metastasis require LXR. These results may have implications for both the treatment and prevention of breast cancer. The SERMs tamoxifen and raloxifene were recently approved in the United States as breast cancer chemopreventive agents in postmenopausal women at high risk for the disease. These agents can have adverse side effects and may not be well suited for women at average risk of breast cancer. However, our data suggest that a reduction in breast cancer risk may also be achieved by lowering total cholesterol; further, these data highlight the need for additional studies to evaluate the efficacy of this approach. Studies to evaluate the impact of lowering cholesterol on response to endocrine therapy in breast cancer are also warranted. Finally, the observation that LXR, but not ER, is required for metastasis in mice with elevated 27HC highlights the potential relevance of our findings to other cancers in which LXR expression is apparent.

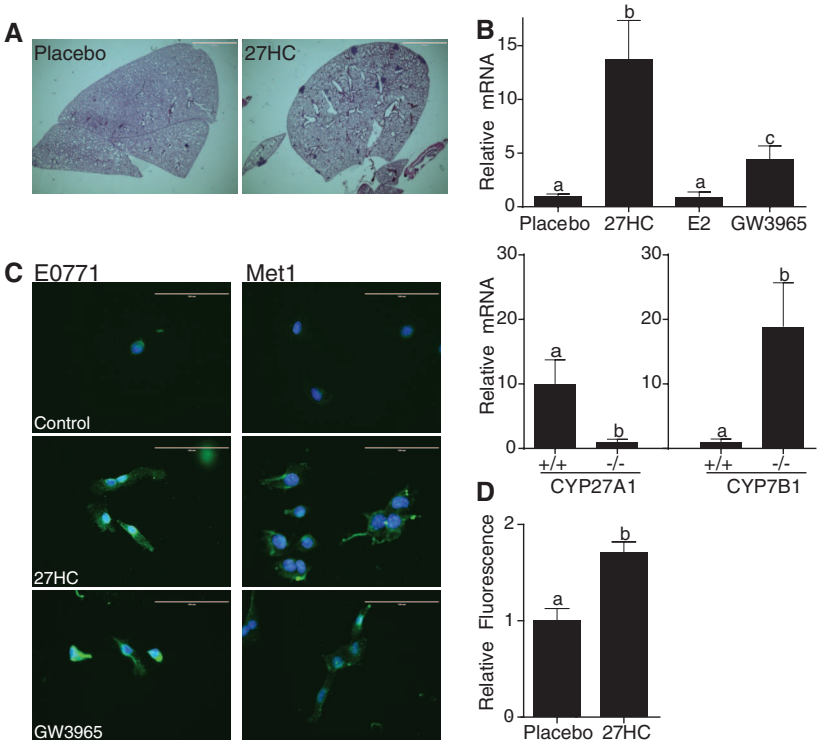


**Fig. 3. Increased metastasis of breast cancer cells to lung is observed in mice in which circulating 27HC is elevated.** (**A**) Representative lung sections from MMTV-PyMT mice reveal an increased number of metastatic lesions after injection of 27HC or placebo. Metastasis was evaluated when the total tumor volume had reached 2 $cm^3$. Scale bars, 2 mm. (**B**) Quantification of PyMT mRNA, a surrogate for mammary tumor cell metastasis, in MMTV-PyMT-mice in which circulating 27HC production is inhibited (CYP27A1$^{-/-}$ background) or increased (CYP7B1$^{-/-}$). Lowercase letters (a to c) denote statistical significance (mean ± SEM, $P < 0.05$, $n = 4$ to 13). (**C**) Both 27HC and the LXR agonist GW3965 induce the expression of vimentin and induce EMT-like morphological changes in E0771 breast cancer cells in vitro. Overlaid images of green (vimentin) and blue (4′,6-diamidino-2-phenylindole nuclear stain). All images were adjusted to 90% brightness and 100% contrast. Scale bars, 100 μm. (**D**) Cell-intrinsic effects of 27HC on the metastatic potential of E0771 breast cancer cells. E0771 cells, tagged by expressing infrared florescence protein, were treated in vitro for 72 hours with 27HC or vehicle and injected into the tail veins of syngeneic mice. Twenty-eight days later, lung colonization was evaluated by assessing fluorescence in harvested lungs (mean ± SEM, $P < 0.05$, $n = 5$).

### References and Notes


1. F. Bianchini, R. Kaaks, H. Vainio, *Lancet Oncol.* **3**, 565–574 (2002).
2. I. Capasso *et al.*, *Cancer Biol. Ther.* **10**, 1240–1243 (2010).
3. A. G. Renehan, D. L. Roberts, C. Dive, *Arch. Physiol. Biochem.* **114**, 71–83 (2008).
4. N. F. Boyd, V. McGuire, *J. Natl. Cancer Inst.* **82**, 460–468 (1990).
5. M. Ferraroni *et al.*, *Int. J. Epidemiol.* **22**, 772–780 (1993).
6. C. M. Kitahara *et al.*, *J. Clin. Oncol.* **29**, 1592–1598 (2011).
7. K. Undela, V. Srikanth, D. Bansal, *Breast Cancer Res. Treat.* **135**, 261–269 (2012).
8. T. P. Ahern *et al.*, *J. Natl. Cancer Inst.* **103**, 1461–1468 (2011).
9. S. F. Nielsen, B. G. Nordestgaard, S. E. Bojesen, *N. Engl. J. Med.* **367**, 1792–1802 (2012).
10. K. K. Chan, A. M. Oza, L. L. Siu, *Clin. Cancer Res.* **9**, 10–19 (2003).
11. J. G. Gerber *et al.*, *J. Acquir. Immune Defic. Syndr.* **39**, 307–312 (2005).
12. W. W. Wong, J. Dimitroulakos, M. D. Minden, L. Z. Penn, *Leukemia* **16**, 508–519 (2002).
13. C. D. DuSell *et al.*, *Endocrinology* **151**, 3675–3685 (2010).
14. C. D. DuSell, M. Umetani, P. W. Shaul, D. J. Mangelsdorf, D. P. McDonnell, *Mol. Endocrinol.* **22**, 65–77 (2008).
15. E. R. Nelson *et al.*, *Endocrinology* **152**, 4691–4705 (2011).

16. M. Umetani *et al.*, *Nat. Med.* **13**, 1185–1192 (2007).
17. Materials and methods are available as supplementary materials on *Science* Online.
18. C. E. Connor *et al.*, *Cancer Res.* **61**, 2917–2922 (2001).
19. C. T. Guy, R. D. Cardiff, W. J. Muller, *Mol. Cell. Biol.* **12**, 954–961 (1992).
20. E. Y. Lin *et al.*, *Am. J. Pathol.* **163**, 2113–2126 (2003).
21. M. Hansson, E. Ellis, M. C. Hunt, G. Schmitz, A. Babiker, *Biochim. Biophys. Acta* **1593**, 283–289 (2003).
22. A. Sica *et al.*, *Semin. Cancer Biol.* **18**, 349–355 (2008).
23. M. A. Lyons, A. J. Brown, *Lipids* **36**, 701–711 (2001).
24. G. Llaverias *et al.*, *Am. J. Pathol.* **178**, 402–412 (2011).
25. N. Alikhani *et al.*, *Oncogene* **32**, 961–967 (2013).
26. R. Karuna *et al.*, *Atherosclerosis* **214**, 448–455 (2011).
27. P. M. Sullivan *et al.*, *J. Biol. Chem.* **272**, 17972–17980 (1997).

**Acknowledgments:** This work was funded by the NIH [grants K99CA172357 (E.R.N.) and R37DK048807 (D.P.M.)] and the U.S. Department of Defense (DOD) [grants BC085585 (E.R.N.) and DOD BC094960 (D.P.M.)]. The content of this paper is solely the responsibility of the authors and does not necessarily represent the official views of the NIH or DOD.

Expression profiling data on 27HC in MCF7 cells were uploaded to Gene Expression Omnibus (GEO) (accession no. GSE46924) and were part of a larger study (GEO accession no. GSE35428).

**Supplementary Materials**

www.sciencemag.org/content/342/6162/1094/suppl/DC1
Materials and Methods
Supplementary Text
Figs. S1 to S14
References (*28*–*33*)

13 June 2013; accepted 25 October 2013
10.1126/science.1241908

# Nonenzymatic Template-Directed RNA Synthesis Inside Model Protocells

**Katarzyna Adamala[1,2] and Jack W. Szostak[1]***

**Efforts to recreate a prebiotically plausible protocell, in which RNA replication occurs within a fatty acid vesicle, have been stalled by the destabilizing effect of $Mg^{2+}$ on fatty acid membranes. Here we report that the presence of citrate protects fatty acid membranes from the disruptive effects of high $Mg^{2+}$ ion concentrations while allowing RNA copying to proceed, while also protecting single-stranded RNA from $Mg^{2+}$-catalyzed degradation. This combination of properties has allowed us to demonstrate the chemical copying of RNA templates inside fatty acid vesicles, which in turn allows for an increase in copying efficiency by bathing the vesicles in a continuously refreshed solution of activated nucleotides.**

The RNA world hypothesis suggests that the primordial catalysts were ribozymes (*1*, *2*), whereas biophysical considerations suggest that the primordial replicating compartments were membranous vesicles composed of fatty acids and related amphiphiles (*3*, *4*). However, the conditions required for RNA replication chemistry and fatty acid vesicle integrity have appeared to be fundamentally incompatible (*5*) (fig. S1). Both ribozyme-catalyzed and nonenzymatic RNA copying reactions require high (50 to 200 mM) concentrations of $Mg^{2+}$ (or other divalent) ions (*6*), but $Mg^{2+}$ at such concentrations destroys vesicles by causing fatty acid precipitation.

We developed a screen for small molecules that protect oleate fatty acid vesicles from disruption by $Mg^{2+}$. We used two assays to monitor the leakage of either a small charged molecule (calcein) or a larger oligonucleotide, allowing us to distinguish between increased membrane permeability (faster calcein release with oligonucleotide retention) and generalized membrane disruption (rapid release of both calcein and the oligonucleotide) (figs. S2 to S4). We identified several chelators, including citrate, isocitrate, oxalate, nitrilotriacetic acid (NTA), and EDTA, that protect oleate vesicles in the presence of at least 10 mM $Mg^{2+}$ (figs. S5 and S6). In the presence of chelated $Mg^{2+}$, oleate vesicles remained intact but exhibited a modest increase in the permeability of a small polar molecule (Fig. 1 and fig. S7) and an even smaller increase in the leakage of an oligonucleotide. In terms of vesicle stabilization, citrate was one of the most effective chelators of $Mg^{2+}$.

We also examined the stability of model protocell membranes made of myristoleic acid:glycerol monomyristoleate (2:1) and from the more prebiotically reasonable decanoic acid:decanol:glycerol monodecanoate (4:1:1). Citrate-chelated $Mg^{2+}$ caused only a small amount of leakage from these vesicles, and the stabilizing effect of citrate was seen for both calcein and oligonucleotides (Fig. 1 and figs. S8 to S13).

We then asked whether these chelators were compatible with the $Mg^{2+}$ catalysis of nonenzymatic template-directed RNA primer extension. We measured the rate at which an RNA primer was elongated when annealed to an oligonucleotide with a templating region of C nucleotides, in the presence of an excess of the activated G monomer guanosine 5′-phosphor(2-methyl)imidazolide (2MeImpG) (Fig. 2). We examined citric acid, EDTA, NTA, and a weakly stabilizing chelator (isocitric acid). In the presence of 50 mM unchelated $Mg^{2+}$, the primer-extension reaction proceeded at a rate of 1.4 $hour^{-1}$, compared to 0.03 $hour^{-1}$ in the absence of $Mg^{2+}$ ions. The addition of four equivalents of EDTA or NTA resulted in complete abolition of $Mg^{2+}$ catalysis (Fig. 2 and figs. S14 and S15), indicating that the $Mg^{2+}$ in these samples is chelated in a fashion incompatible with promoting primer extension. In contrast, four equivalents of citrate only decreased the rate of primer extension to 0.67 $hour^{-1}$. For comparison, isocitric acid does not fully protect vesicles (figs. S16 and S17) but also does not affect the primer extension reaction.

To see whether citrate would allow nonenzymatic RNA copying to proceed within fatty acid vesicles, we encapsulated an RNA primer-template complex inside oleate vesicles, added $Mg^{2+}$ and citrate, and removed unencapsulated RNA by size exclusion chromatography. We then added the activated G monomer 2MeImpG, heated the sample briefly to allow for rapid monomer permeation (*7*), and then incubated it at room temperature for times up to 24 hours to allow

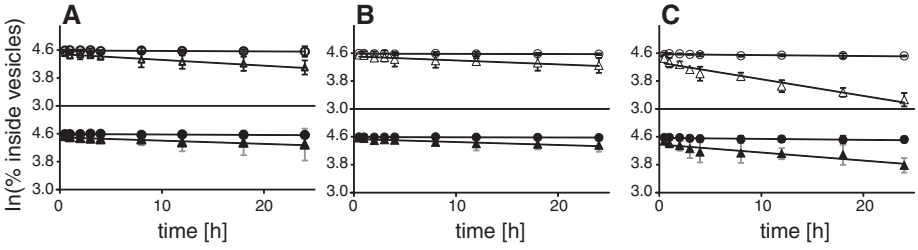


**Fig. 1. Citrate stabilizes fatty acid vesicles in the presence of $Mg^{2+}$ ions.** Leakage of a small charged molecule (calcein, open symbols) and a larger nine-oligomer oligodeoxynucleotide (solid symbols) from fatty acid vesicles is shown. (**A**) Oleate vesicles; (**B**) myristoleate:glycerol monomyristoleate 2:1 vesicles; (**C**) decanoate:decanol:glycerol monodecanoate 4:1:1 vesicles. Circles, no $MgCl_2$, no citrate; triangles, 50 mM $MgCl_2$, 200 mM $Na^+$-citrate. The assay used to obtain these data is described in fig. S3. Lines are linear fits, coefficient of determination ($R^2$) ≥ 0.97. All experiments were repeated twice; error bars are mean ±2 SE.

[1]Howard Hughes Medical Institute, Department of Molecular Biology, and Center for Computational and Integrative Biology, Massachusetts General Hospital, Boston, MA 02114, USA. [2]Dipartimento di Biologia, Università degli Studi di Roma Tre, Rome, Italy.

*Corresponding author at Howard Hughes Medical Institute, Department of Molecular Biology, and Center for Computational and Integrative Biology, 7215 Simches Research Center, Massachusetts General Hospital, 185 Cambridge Street, Boston, MA 02114, USA. E-mail: szostak@molbio.mgh.harvard.edu

the monomer to take part in template-copying chemistry inside the vesicles. Analysis of the reaction products showed that after 24 hours of incubation, most of the primer had been extended by the addition of six G residues, with a smaller fraction extended to full length by the addition of a seventh G residue (Fig. 3). In parallel experiments with vesicles composed of mixtures of shorter-chain lipids, the brief heating step was not

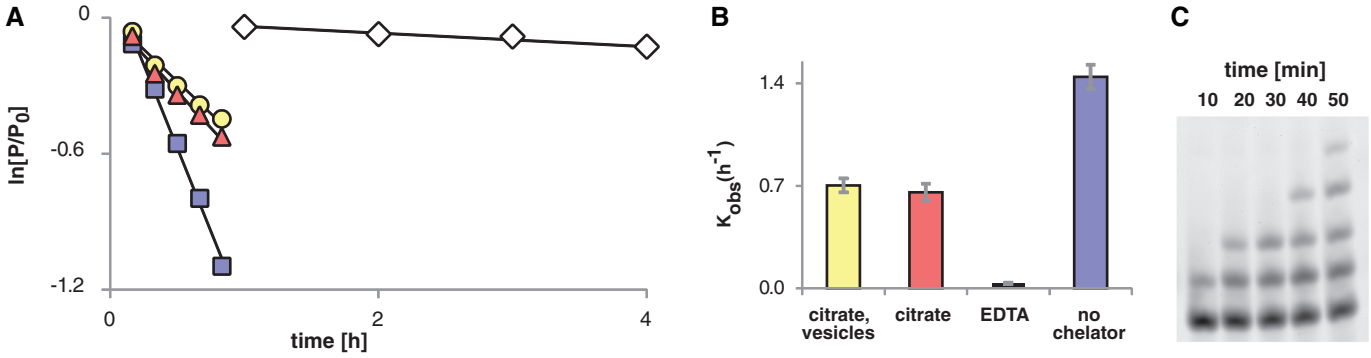


**Fig. 2. The rate of RNA template-directed primer extension in the presence or absence of $Mg^{2+}$ chelators and fatty acid vesicles.** (**A**) Time courses of primer extension on a templating region of four C residues, expressed as a fraction of unextended primer remaining versus time. Squares, no chelators; triangles, 200 mM $Na^+$-citrate; circles, 200 mM $Na^+$-citrate and 100 mM oleate vesicles; diamonds, 200 mM EDTA. Lines are linear fits, $R^2 \geq 0.97$; the slope is $k_{obs}$ ($hour^{-1}$). (**B**) Rates of primer extension under the indicated conditions; each kinetic experiment was performed in duplicate, and rates are determined as an average of the three separate runs. Error bars indicate SEM, $n = 3$ independent repetitions. (**C**) Typical polyacrylamide gel electrophoresis (PAGE) analysis of a template-directed primer extension experiment. Primer extension was carried out in the presence of 200 mM $Na^+$-citrate. For the gel analysis of the reactions used to obtain this data, see fig. S15.

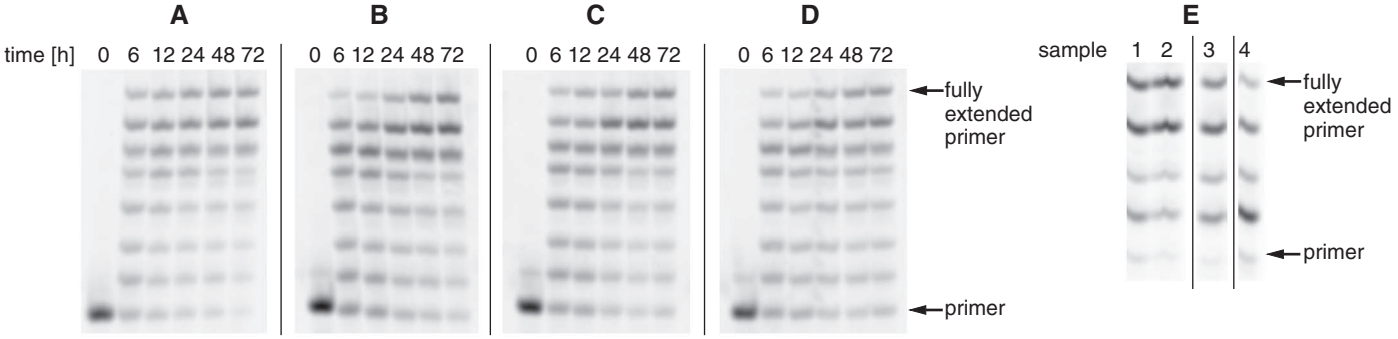


**Fig. 3. RNA template copying inside model protocell vesicles.** (**A** to **D**) Primer extension on a templating region of seven C residues. (A) Control reaction in solution; (B) inside oleate vesicles; (C) inside myristoleate:glycerol monomyristoleate 2:1 vesicles; (D) inside decanoate:decanol:glycerol monodecanoate 4:1:1 vesicles. (**E**) Extension of labeled RNA primer annealed to a mixed base template, templating region sequence GCCG. Sample 1, reaction inside myristoleate:glycerol monomyristoleate 2:1 vesicles; sample 2, reaction inside decanoate:decanol:glycerol monodecanoate 4:1:1 vesicles. Both sample 1 and 2 reactions were performed inside a liposome dialyzer (see the supplementary materials for the description of the liposome dialyzer) with a total of 13 buffer exchanges. Sample 3, control reaction in solution with daily addition of fresh portion of activated monomers, without removing the hydrolyzed monomers. Sample 4, control reaction in solution, without the addition of fresh monomer.

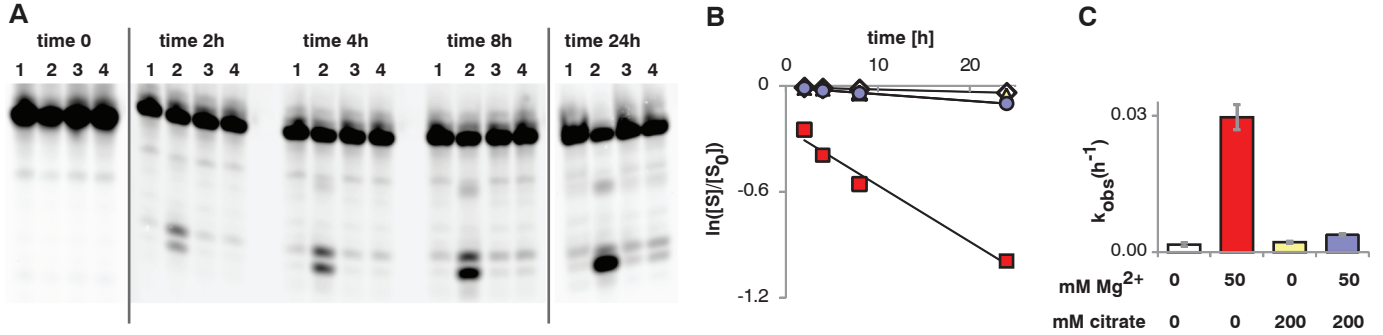


**Fig. 4. Citrate protects RNA from $Mg^{2+}$-catalyzed degradation.** (**A**) PAGE analysis of cleavage of a DNA oligonucleotide at the site of a single internal ribonucleotide, at indicated time points; lane 1, no $Mg^{2+}$, no citrate; lane 2, 50 mM $Mg^{2+}$, no citrate; lane 3, no $Mg^{2+}$, 200 mM citrate; lane 4, 50 mM $Mg^{2+}$, 200 mM citrate. (**B**) Quantitation of strand cleavage, expressed as a fraction of the intact substrate over total substrate versus time. Diamonds, no $Mg^{2+}$, no citrate; triangles, no $Mg^{2+}$, 200 mM citrate; circles, 50 mM $Mg^{2+}$, 200 mM citrate; squares, 50 mM $Mg^{2+}$, no citrate. Lines are linear fits, $R^2 \geq 0.97$. (**C**) Rates of strand cleavage at the *ribo* linkage with and without $Mg^{2+}$ and citrate. Error bars indicate SEM, $n = 3$ independent repetitions.

necessary, because of the higher permeability of such membranes to nucleotide monomers. It is noteworthy that RNA primer extension occurred efficiently inside vesicles made of decanoic acid: decanol:glycerol monodecanoate (4:1:1) (Fig. 3), because short-chain saturated amphiphilic compounds are more prebiotically plausible than longer-chain unsaturated fatty acids such as oleate or myristoleate. When we encapsulated the RNA primer-template complex inside POPC vesicles, no primer extension was observed, because of the impermeability of phospholipid vesicles to the 2MeImpG monomer (even with a heat pulse) (fig. S18).

The efficiency of nonenzymatic RNA replication can be greatly enhanced by the periodic addition of fresh portions of activated monomer to a primer-extension reaction occurring on templates immobilized by covalent linkage to beads (*8*). We sought to reproduce this effect by mimicking the flow of an external solution of fresh monomers over vesicles, by periodic dialysis of model protocells against a solution of fresh activated monomers (see the supplementary materials for a description of the liposome reactor dialyzer). The control primer-extension reaction in solution shows that the yield of full-length primer-extension product from copying a GCCG template is very low, even if fresh monomers are added to the reaction periodically (Fig. 3E). In contrast, after repeated exchanges of external solution by dialysis, the proportion of full-length product was much greater (Fig. 3E).

The high thermal stability of the RNA duplex is a major problem for prebiotic RNA replication (*5*). Because $Mg^{2+}$ greatly increases the melting temperature ($T_m$) of RNA duplexes, we asked whether the chelating properties of citrate would prevent the increase in the $T_m$ of RNA duplexes caused by the presence of free $Mg^{2+}$ ions. We observed a small but reproducible decrease in $T_m$ in the presence of citrate when compared to samples containing unchelated $Mg^{2+}$ (table S1 and figs. S19 and S20). For example, in the presence of 50 mM $Mg^{2+}$ with four equivalents of citrate, the $T_m$ of the RNA duplex was 71°C, whereas in the control sample without citrate the $T_m$ was 75°C.

Citrate also stabilizes RNA by preventing the $Mg^{2+}$ catalysis of RNA degradation. Incubating a 13-oligomer oligodeoxynucleotide with one *ribo* linkage at 75°C, with and without $Mg^{2+}$ and citrate, results in significant strand cleavage at the site of the single *ribo* linkage. Four equivalents of citrate, relative to $Mg^{2+}$, abolished the $Mg^{2+}$-catalyzed degradation (Fig. 4). The observed rate constant ($k_{obs}$) for cleavage at the *ribo* linkage, at 75°C in the presence of 50 mM $Mg^{2+}$ was 0.03 $hour^{-1}$, whereas in the presence of a fourfold excess of citrate, the rate decreased to 0.004 $hour^{-1}$.

The chelation of $Mg^{2+}$ by citrate exhibits two protective effects in the context of model protocells: Protocell membranes based on fatty acids are protected from the disruption caused by the precipitation of fatty acids as $Mg^{2+}$ salts, and single-stranded RNA oligonucleotides are protected from $Mg^{2+}$-catalyzed degradation. Based on the known affinity of citrate for $Mg^{2+}$ (*9*, *10*), it is clear that the RNA synthesis observed in the presence of $Mg^{2+}$ and citrate cannot be due to residual free $Mg^{2+}$ (less than 1 mM) and must be due to catalysis by the $Mg^{2+}$-citrate complex. The crystal structure of $Mg^{2+}$-citrate (*11*) shows that the $Mg^{2+}$ ion is coordinated by the hydroxyl and two carboxylates of citrate, so that three of the six coordination sites of octahedral $Mg^{2+}$ are occupied by citrate, while the remaining three are free to coordinate with water or other ligands. The clear implication is that coordination of $Mg^{2+}$ by at most three sites is sufficient for catalysis of template-directed RNA synthesis, but not for catalysis of RNA degradation or for the precipitation of fatty acids. In the absence of a prebiotic citrate synthesis pathway [but see (*12*) for a recent advance], it is of interest to consider prebiotically plausible alternatives to citrate that could potentially confer similar effects, such as short acidic peptides. Just such a peptide constitutes the heart of cellular RNA polymerases, where it binds and presents the catalytic $Mg^{2+}$ ion in the active site of the enzyme.

### References and Notes


1. W. Gilbert, *Nature* **319**, 618 (1986).
2. G. F. Joyce, *Nature* **338**, 217–224 (1989).
3. J. M. Gebicki, M. Hicks, *Nature* **243**, 232–234 (1973).
4. D. W. Deamer, J. P. Dworkin, *Top. Curr. Chem.* **259**, 1–27 (2005).
5. J. W. Szostak, The eightfold path to non-enzymatic RNA replication. *J. Sys. Chem.* **3:2** (2012).
6. J. C. Bowman, T. K. Lenz, N. V. Hud, L. D. Williams, *Curr. Opin. Struct. Biol.* **22**, 262–272 (2012).
7. S. S. Mansy, J. W. Szostak, *Proc. Natl. Acad. Sci. U.S.A.* **105**, 13351–13355 (2008).
8. C. Deck, M. Jauker, C. Richert, *Nat. Chem.* **3**, 603–608 (2011).
9. A. K. Covington, E. Y. Danish, *J. Solution Chem.* **38**, 1449–1462 (2009).
10. M. Walser, *J. Phys. Chem.* **65**, 159–161 (1961).
11. C. K. Johnson, *Acta Crystallogr.* **18**, 1004–1018 (1965).
12. C. Butch *et al.*, *J. Am. Chem. Soc.* **135**, 13440–13445 (2013).



**Acknowledgments:** We thank A. Engelhart, C. Hentrich, A. Larsen, N. Kamat, and A. Björkbom for discussions and help with manuscript preparation and A. Gifford for help with vesicle leakage experiments. This work was supported in part by NASA Exobiology grant NNX07AJ09G. J.W.S. is an investigator of the Howard Hughes Medical Institute. Raw data are presented in the supplementary materials. The instructions for assembling the Liposome Dialyzer are available at http://molbio.mgh.harvard.edu/szostakweb/.


### Supplementary Materials

www.sciencemag.org/content/342/6162/1098/suppl/DC1
Materials and Methods
Supplementary Text
Figs. S1 to S21
Tables S1 to S3
Liposome Dialyzer Instructions
References (*13*–*15*)


13 June 2013; accepted 25 September 2013
10.1126/science.1241888


# Primate Transcript and Protein Expression Levels Evolve Under Compensatory Selection Pressures


**Zia Khan,[1]* Michael J. Ford,[2] Darren A. Cusanovich,[1] Amy Mitrano,[1] Jonathan K. Pritchard,[1,3]*† Yoav Gilad[1]***



**Changes in gene regulation have likely played an important role in the evolution of primates. Differences in messenger RNA (mRNA) expression levels across primates have often been documented; however, it is not yet known to what extent measurements of divergence in mRNA levels reflect divergence in protein expression levels, which are probably more important in determining phenotypic differences. We used high-resolution, quantitative mass spectrometry to collect protein expression measurements from human, chimpanzee, and rhesus macaque lymphoblastoid cell lines and compared them to transcript expression data from the same samples. We found dozens of genes with significant expression differences between species at the mRNA level yet little or no difference in protein expression. Overall, our data suggest that protein expression levels evolve under stronger evolutionary constraint than mRNA levels.**


Measurements of mRNA levels have revealed substantial differences across primate transcriptomes (*1*–*3*) and have led to the identification of putatively adaptive changes in transcript expression (*4*). Traditionally, measurements of divergence in mRNA levels are assumed to be good proxies for divergence in protein levels. However, there are numerous mechanisms by which protein expression may be regulated independently of mRNA levels (*5*, *6*). If transcript and protein expression levels are often uncoupled, mRNA levels may evolve under reduced constraint as changes at the transcript level could be buffered or compensated for at the


[1]Department of Human Genetics, University of Chicago, Chicago, IL 60637, USA. [2]MS Bioworks, LLC, 3950 Varsity Drive, Ann Arbor, MI 48108, USA. [3]Howard Hughes Medical Institute, University of Chicago, Chicago, IL 60637, USA.

*Corresponding author. E-mail: zia@uchicago.edu (Z.K.); pritch@stanford.edu (J.K.P); gilad@uchicago.edu (Y.G.)
†Present address: Departments of Genetics and Biology, Stanford University, Stanford, CA 94305, USA.

protein level (*7*–*9*). To date, however, genome-wide studies of protein expression in primates have been limited (*10*, *11*).

We collected a comparative proteomic data set with SILAC [stable isotope labeling by amino acids in cell culture (*12*)]. Using high-resolution, quantitative mass spectrometry (*13*), we measured peptide expression levels in lymphoblastoid cell lines (LCLs) from five human, five chimpanzee, and five rhesus macaque individuals (fig. S1 and table S1). We analyzed the peptide expression data in the context of orthologous gene models (*14*) to obtain comparative protein expression measurements from all three species (table S2). We obtained measurements for 4157 proteins in at least three human and three chimpanzee individuals, and 3688 proteins were quantified in at least three individuals from all three species (table S2 and fig. S1). We also collected RNA-sequence (RNA-seq) data from the same samples and estimated mRNA expression levels using reads that map to orthologous exons (fig. S1 and table S3). We thus obtained both mRNA and protein expression levels for 3390 genes in at least three individuals from each of the three species (fig. S2 and table S4).

Focusing on differences between human and chimpanzee, we classified 1151 genes as differentially expressed (DE) between species at the mRNA and/or protein expression levels, independently [likelihood ratio test, false discovery rate (FDR) = 1%, table S5]. The number of interspecies DE genes at the mRNA level was higher (815) than the number of DE proteins (571; Fig. 1, A and B). By accounting for incomplete power to detect interspecies differences in gene expression (*15*), we estimated that 266 genes (33%) are DE between humans and chimpanzees at the mRNA level but not at the protein level. We observed a similar pattern for comparisons that include the rhesus macaque data (table S5).

These observations may reflect a slower rate of divergence in protein levels or higher levels of within-species variation in protein than mRNA expression levels. To distinguish between these possibilities, we compared estimates of mRNA and protein divergence (Fig. 1C). Among genes whose interspecies mRNA and protein divergence differ (FDR = 1%), interspecies variation at the mRNA level is higher than at the protein level much more often than the reverse pattern (Fig. 1D). This indicates that protein expression levels might evolve under greater evolutionary constraint than mRNA expression levels.

The accuracy of SILAC has been established by biochemical means (*16*); yet, it is difficult to exclude all possible technical explanations for our observations. We thus conducted a large number of quality-control analyses. First, we observed

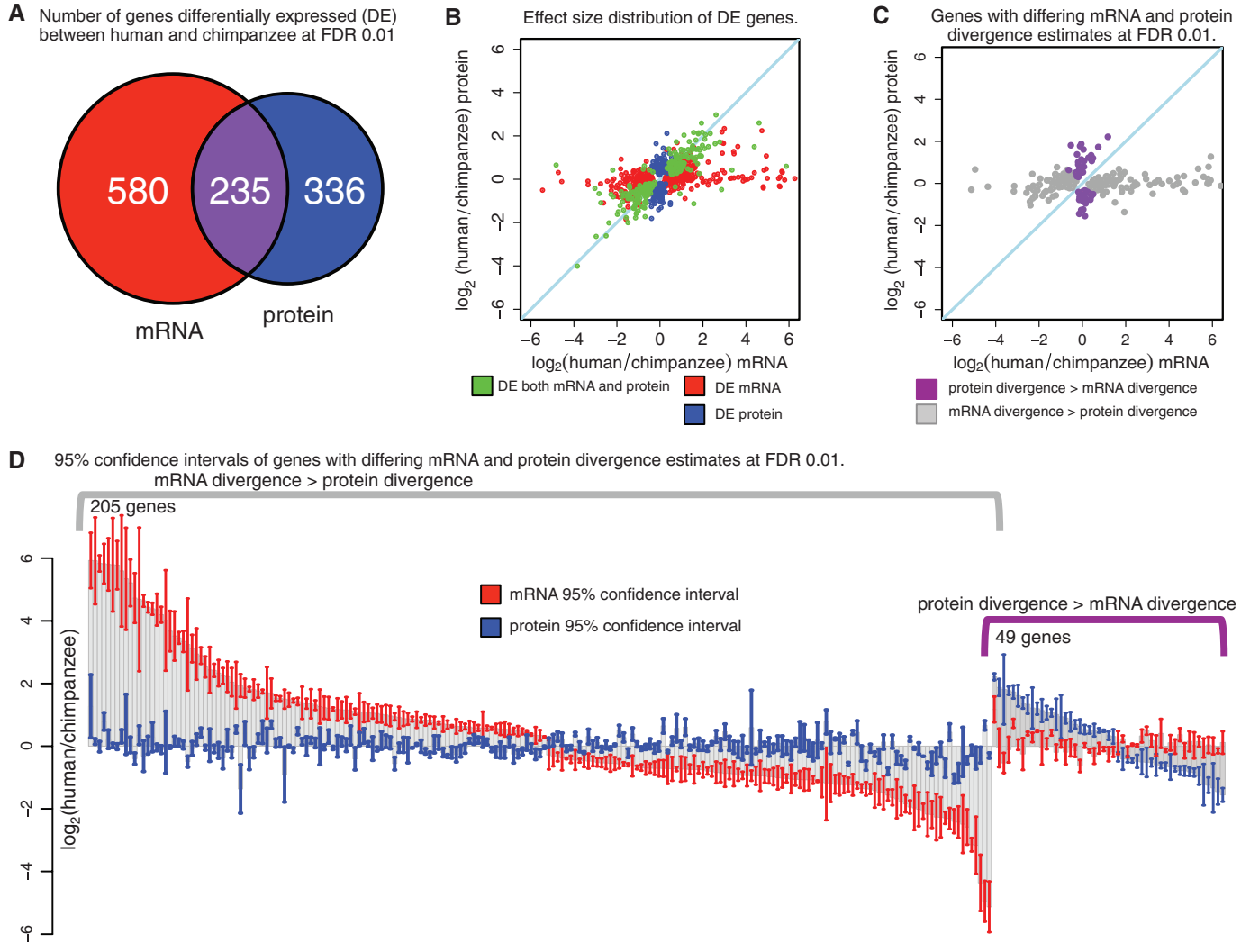


**Fig. 1. Protein expression levels evolve under greater evolutionary constraint than mRNA expression levels.** (**A**) A Venn diagram of the numbers of mRNAs (red) and proteins (blue) classified as differentially expressed (DE). (**B**) Mean effect size of the interspecies difference in expression for genes classified as DE as mRNA-only, protein-only, or both. Each point corresponds to a single DE gene. (**C**) Scatterplot of median mRNA and protein divergence of genes where estimates of mRNA and protein divergence between human and chimpanzee differed significantly (FDR = 1%). (**D**) Ninety-five percent confidence intervals around estimates of mean mRNA and protein divergence of genes in (C).

that the consistency of protein measurements is at least as good as that for mRNA (fig. S3). Additionally, biological variation associated with the mRNA and protein measurements, regardless of species, is comparable (fig. S4). We then proceeded to demonstrate that the protein measurements have a higher dynamic range than the mRNA measurements, and hence, our results are conservative with respect to this property of the data (fig. S5). We also confirmed that the observation of lower divergence of protein levels relative to mRNA levels could not be explained by insufficient quantification of protein expression (fig. S6) and is robust to differences in the approach used to summarize multiple peptide measurements into a single estimate of protein expression level (fig. S7). Finally, we established that our observations are robust by restricting our analysis only to the subset of genes with similar RNA-seq read depth across orthologous exons; only to genes with low interindividual variation both at the mRNA and protein levels; only to genes whose protein and mRNA levels were measured in all five individuals from each species; only to genes whose protein expression levels were measured by two peptides or more; by excluding the top 2% of most highly expressed genes at the transcript level; and by excluding all genes with RNA-seq reads per kilobase per million mapped reads (RPKM) of less than 1. These analyses all produced consistent results (figs. S8 to S13).

To gain further insight into the differences in evolutionary pressures acting on mRNA and protein expression in primates, we used data from all three species to identify genes whose regulation might have evolved under natural selection. We applied an empirical approach to identify expression patterns that are consistent with the action of stabilizing or directional selection on gene regulation (*2*, *17*). The rationale of our approach is similar to that used in empirical scans of selection on nucleotide sequence data (*18*). We scanned for expression patterns on the basis of our expectations given different evolutionary scenarios. For example, patterns of low variation in expression levels, both within and between species, are consistent with a scenario of stabilizing selection on gene regulation (fig. S14A). In turn, a lineage-specific shift in expression level associated with high within-species variation is consistent with relaxation of evolutionary constraint (fig. S14B). A lineage-specific shift in expression level coupled with low within-species variation is consistent with directional selection acting on gene regulation in a particular lineage (fig. S14C).

We considered the transcript and protein comparative expression data independently. Among the 300 genes with the least varied protein expression levels within and between species, consistent with the action of stabilizing selection, we found enrichment of genes involved in conserved cellular processes including translation, splicing, and transcriptional regulation (table S6). Compared to genes not in this set (Fig. 2), these 300 genes also evolve under stronger evolutionary constraint at the amino acid level (Wilcoxon rank sum, $P < 10^{-9}$), have higher expression levels ($P < 10^{-5}$), have shorter 3′ untranslated regions (3′UTRs) ($P < 10^{-5}$), have more reported protein-protein interactions ($P < 10^{-15}$), and are expressed in more tissues ($P < 10^{-8}$). We found that these properties are also associated with the 300 genes with the least varied mRNA levels: stronger evolutionary constraint on amino acid sequence ($P < 0.003$); larger number of protein-protein interactions ($P < 10^{-4}$); and higher absolute expression levels ($P < 0.02$), as has been noted (*1*, *19*). Yet, all of these associations are stronger when genes are ranked by conservation of protein expression than when ranked by conservation of mRNA expression. Our observations are robust to arbitrary choices in cutoffs (fig. S15) and suggest that these regulatory and sequence properties are more coupled to protein expression levels.

We next focused on lineage-specific differences in gene regulation. We found that a subset of genes with lineage-specific expression differences were also associated with a lineage-specific increase in within-species variation in expression levels; this pattern is consistent with lineage-specific relaxation of evolutionary constraint on gene regulation. We classified 85 genes (one-sided F-test; $P < 0.05$) with expression patterns consistent with either human- or chimpanzee-specific relaxation of constraint on transcript expression levels but only 20 genes with regulatory patterns consistent with relaxation of constraint on protein expression levels. This observation provides further evidence that protein levels might evolve under greater evolutionary constraint than mRNA levels. Lineage-specific shifts in protein expression levels might also be associated with low within-species variation, consistent with directional selection on gene regulation. We classified 196 and 161 such patterns in human or chimpanzee, respectively (table S7).

We then considered the protein and mRNA data jointly. As expected, in most cases, the patterns of mRNA and protein expression levels are consistent with the same evolutionary scenario. We found a few genes whose mRNA expression patterns are consistent with the action of stabilizing selection, whereas the patterns of their protein expression levels are consistent with lineage-specific directional selection in either human (14 genes, Fig. 3A) or chimpanzee (10 genes). These patterns can potentially be explained by lineage-specific changes that specifically affect posttranscriptional regulation. We also identified 40 and 20 genes whose mRNA expression patterns are consistent with the action of lineage-specific directional selection in human or chimpanzee, respectively, yet their protein levels are consistent with the action of stabilizing selection (Fig. 3B). These observations may indicate that protein expression levels of these genes are buffered against changes in mRNA levels (*20*) or that these genes are evolving under compensatory selection pressures. Genes whose mRNA and protein expression levels are consistent with this pattern have slightly longer 5′UTRs (one-sided Wilcoxon rank sum; $P < 0.03$), a greater number of known ubiquitination sites ($P < 0.0002$), and, among those with a human-specific decrease in mRNA levels, more phosphorylation sites ($P < 0.006$). Put together, these are all properties typically common to genes that evolve under strong evolutionary constraint.

In summary, our data suggest that protein expression levels evolve under greater evolution-

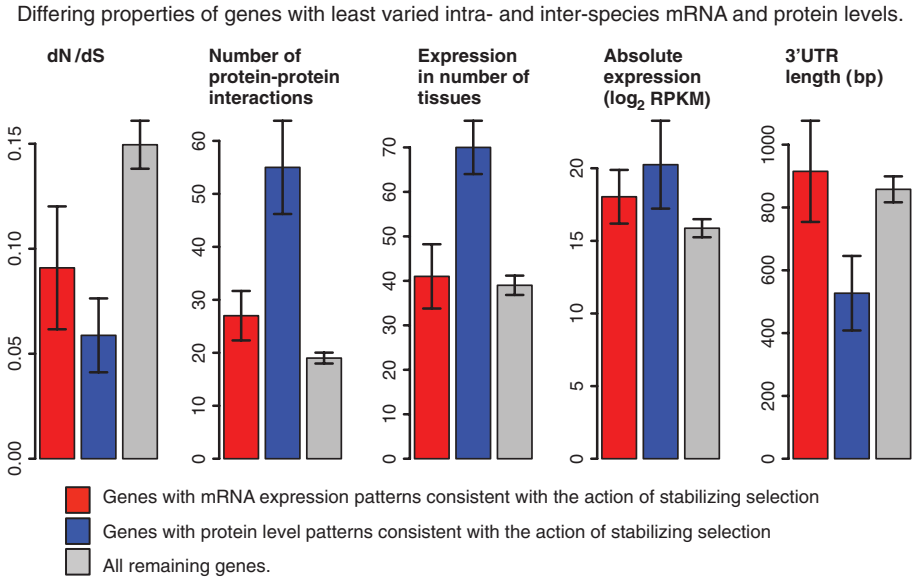


**Fig. 2. Properties of genes whose protein and mRNA expression levels are inferred to have evolved under stabilizing selection.** Error bars represent the 95% confidence intervals around the mean. Data are shown for the top 300 genes with the least varied mRNA (red) or protein (blue) expression levels between and within species. Gray bars correspond to all other genes.

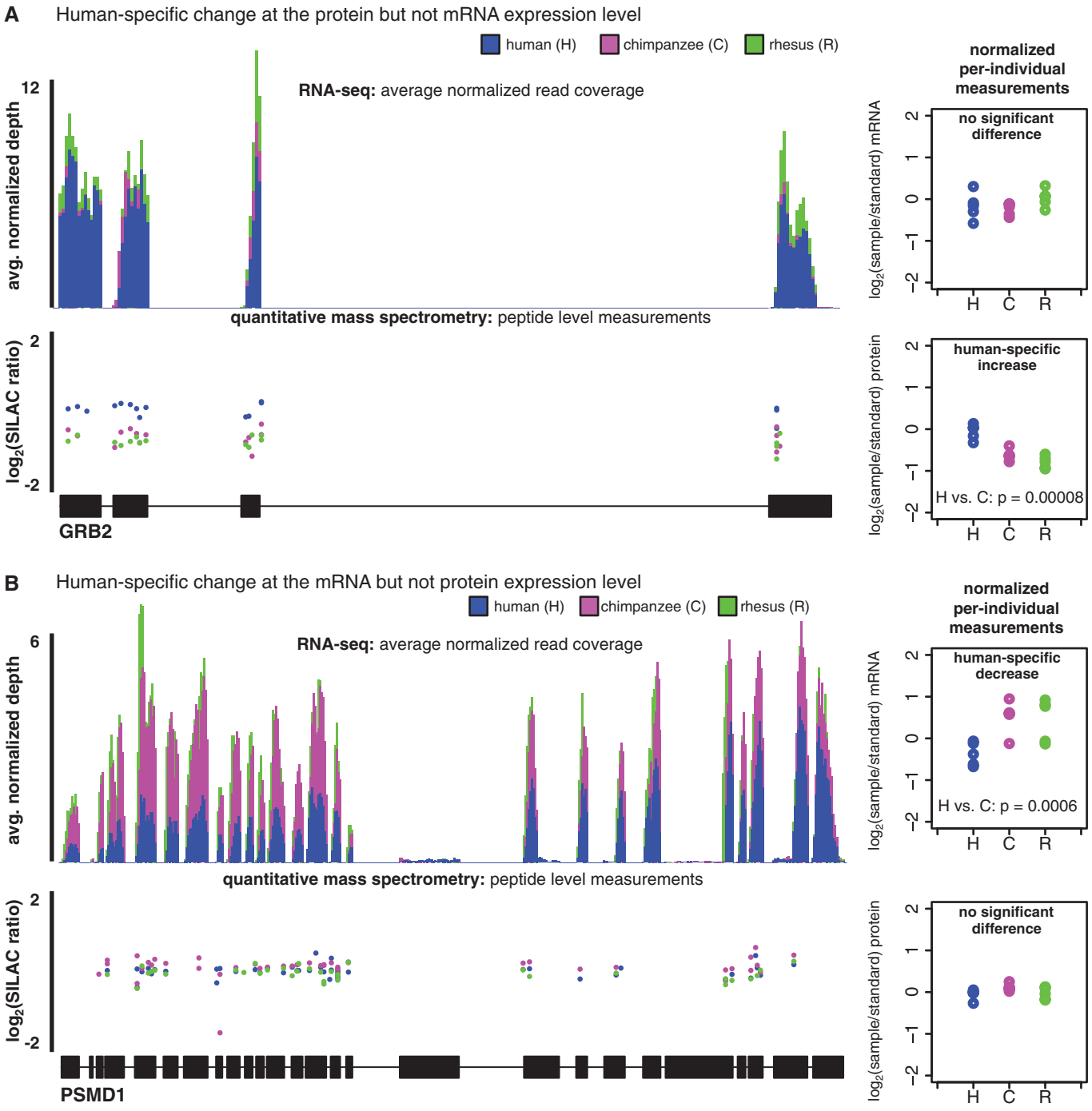


**Fig. 3. Examples of genes whose mRNA and protein expression levels are consistent with different evolutionary scenarios.** (**A**) A gene whose mRNA and protein expression levels are consistent with a lineage-specific change in posttranscriptional regulation. (**B**) A gene whose interspecies mRNA levels are consistent with buffering or compensation at the protein expression level. In both cases, RNA-seq coverage is standardized to per million mapped reads and averaged across all five individuals. Protein measurements are plotted at the starting genomic position of the peptides. The plots on the right are of mRNA and protein expression levels from all individuals, normalized relative to the internal standard cell line.

ary constraint than mRNA levels. It seems likely that for many genes, evolutionary changes in mRNA levels may be effectively neutral, if buffered or compensated for at the protein level. As protein levels are presumably more relevant to understanding how the genotype gives rise to the phenotype than mRNA levels of protein-coding genes, insight into the interplay between transcriptional and posttranscriptional regulatory differences may greatly advance our understanding of human-specific adaptations.

### References and Notes


1. P. Khaitovich *et al.*, *Science* **309**, 1850–1854 (2005).
2. Y. Gilad, A. Oshlack, G. K. Smyth, T. P. Speed, K. P. White, *Nature* **440**, 242–245 (2006).
3. D. Brawand *et al.*, *Nature* **478**, 343–348 (2011).
4. I. G. Romero, I. Ruvinsky, Y. Gilad, *Nat. Rev. Genet.* **13**, 505–516 (2012).
5. C. Vogel, E. M. Marcotte, *Nat. Rev. Genet.* **13**, 227–232 (2012).
6. B. Cox *et al.*, *Mol. Syst. Biol.* **3**, 109 (2007).
7. J. M. Laurent *et al.*, *Proteomics* **10**, 4209–4212 (2010).
8. S. P. Schrimpf *et al.*, *PLOS Biol.* **7**, e48 (2009).
9. L. Wu *et al.*, *Nature* **499**, 79–82 (2013).
10. N. Fu *et al.*, *PLOS ONE* **2**, e216 (2007).
11. W. Enard *et al.*, *Science* **296**, 340–343 (2002).

12. S.-E. Ong *et al.*, *Mol. Cell. Proteomics* **1**, 376–386 (2002).
13. M. Mann, N. L. Kelleher, *Proc. Natl. Acad. Sci. U.S.A.* **105**, 18132–18138 (2008).
14. R. Blekhman, J. C. Marioni, P. Zumbo, M. Stephens, Y. Gilad, *Genome Res.* **20**, 180–189 (2010).
15. J. D. Storey, J. E. Taylor, D. Siegmund, *J. R. Stat. Soc. Series B Stat. Methodol.* **66**, 187–205 (2004).
16. S. Hanke, H. Besir, D. Oesterhelt, M. Mann, *J. Proteome Res.* **7**, 1118–1130 (2008).
17. C. D. Meiklejohn, J. Parsch, J. M. Ranz, D. L. Hartl, *Proc. Natl. Acad. Sci. U.S.A.* **100**, 9894–9899 (2003).
18. J. M. Akey, *Genome Res.* **19**, 711–722 (2009).
19. B. Lemos, B. R. Bettencourt, C. D. Meiklejohn, D. L. Hartl, *Mol. Biol. Evol.* **22**, 1345–1354 (2005).
20. S. L. Rutherford, *Bioessays* **22**, 1095–1105 (2000).

**Acknowledgments:** We thank members of our labs for helpful discussions. Funded by NIH grant GM077959 to Y.G. and by Howard Hughes Medical Institute funds to J.K.P. Z.K. is supported by National Research Service Award F32HG006972. Z.K., J.K.P., and Y.G. conceived of the study and designed it; M.J.F. acquired the mass spectrometry data; Z.K. conducted the computational analyses with input from D.A.C., J.K.P., and Y.G. M.J.F. acknowledges assistance from colleagues at MS Bioworks LLC. A.M. cultured cells and prepared protein samples. Z.K., J.K.P., and Y.G. wrote the paper with contributions from all authors. RNA-seq data have been deposited to the Gene Expression Omnibus (GSE49682). The mass spectrometry proteomics data have been deposited to the ProteomeXchange Consortium via the PRIDE partner repository (PXD000419). J.K.P. is on the scientific advisory boards for 23andMe and DNANexus with stock options.

**Supplementary Materials**
www.sciencemag.org/content/342/6162/1100/suppl/DC1
Materials and Methods
Figs. S1 to S16
Tables S1 to S7
References (*21*–*28*)

25 June 2013; accepted 25 September 2013
Published online 17 October 2013;
10.1126/science.1242379

# Phycobilisomes Supply Excitations to Both Photosystems in a Megacomplex in Cyanobacteria

**Haijun Liu,[1,2] Hao Zhang,[2,3] Dariusz M. Niedzwiedzki,[2] Mindy Prado,[1,2] Guannan He,[2,3] Michael L. Gross,[3] Robert E. Blankenship[1,2,3]***

**In photosynthetic organisms, photons are captured by light-harvesting antenna complexes, and energy is transferred to reaction centers where photochemical reactions take place. We describe here the isolation and characterization of a fully functional megacomplex composed of a phycobilisome antenna complex and photosystems I and II from the cyanobacterium *Synechocystis* PCC 6803. A combination of in vivo protein cross-linking, mass spectrometry, and time-resolved spectroscopy indicates that the megacomplex is organized to facilitate energy transfer but not intercomplex electron transfer, which requires diffusible intermediates and the cytochrome $b_6f$ complex. The organization provides a basis for understanding how phycobilisomes transfer excitation energy to reaction centers and how the energy balance of two photosystems is achieved, allowing the organism to adapt to varying ecophysiological conditions.**

In cyanobacteria and red algae, phycobilisomes (PBSs) (*1*–*3*) absorb light and transfer its energy to chlorophylls in photosystem II (PSII) and photosystem I (PSI), where charge separation occurs. This process of light capture by the PBS greatly expands the natural solar spectrum energy use under varying and sometimes extreme light conditions (*4*). Although spatial orientations of the chromophores in the PBS and chlorophylls in the reaction centers (RCs) dictate an efficient energy transfer, the exact PBS-RCs interactions are as yet unclear.

To address how the three protein complexes structurally interact, we examined chemically cross-linked PBS, PSII, and PSI by using liquid chromatography and tandem mass spectrometry (LC-MS/MS) (*5*–*8*) and analyzed the data by using two different searching methods (*9*, *10*). Application of membrane-permeable, chemical cross-linkers to the living cells essentially captures the weak interactions between these components (*5*). This is made possible by the introduction of a polyhistidine tag on the C terminus of PSII subunit O (PsbO), in which, without cross-linking reactions, only PSII complexes are isolated (Fig. 1 and fig. S2).

Several observations are consistent with the formation of a larger, multicomponent complex. Key components from both PSII and PSI are present as per immunological analysis (fig. S4, A and B); oxygen evolution (PSII) and oxygen consumption (PSI) activities were observed (table S2); not only PBS but PSII and PSI components (table S3) are also present, as demonstrated by LC-MS/MS; additionally, multiple cross-linking occurs between PBS-PSII and PBS-PSI (see below). PSII isolation using affinity chromatography is routine and substantially reduces PSI contamination (fig. S5, A and B) (*5*). The blue-green band collected from the preparation (fig. S3A) shows characteristic fluorescence emission peaks from PBS, PSII (691 nm), and PSI (720 nm) (fig. S5). Taken together, these observations indicate that we have isolated a protein complex that contains PBS, PSII, and PSI. Considering the cumulative mass of PBS, PSII, and PSI is in the range of several megadaltons, we named this complex the PBS-PSII-PSI megacomplex (MCL).

LC-MS/MS identified all the major components from PBS, PSII, and PSI (table S3). Systematic analysis of the cross-linked MCL identified 26 protein interlinks (table S4). Notably, five interlinks were consistently found between the PSII components and ApcE (allophycocyanin E), a key component of the PBS (Fig. 2A and table S4F). [The PSII and PSI peptide sequence numbering used in this study (*Synechocystis* 6803) has its basis in the 3ARC and 1JB0 crystal structures, respectively (*11*, *12*).] In PSII, $Lys^{227}$ is in the loop D of PsbB ($^{227}$K:PsbB) and is cross-linked to $^{87}$K:ApcE (Fig. 2A and figs. S6 and S7) (*5*). ApcE, is a multidomain protein responsible for the assembly of the PBS core (*13*). The N-terminal portion of ApcE (phycobilinprotein, or PB domain) shares high similarity to ApcA (fig. S8) (*14*). The PB domain, however, is interrupted by a dispensable PB-loop insertion (*13*, *15*). We also found that $^{23}$K:PsbD (or D2) is linked to $^{317}$K:ApcE (Fig. 2A). Spatial proximity of $^{23}$K:PsbD and $^{227}$K:PsbB seems likely (10.4 Å, fig. S9), but the cross-links were not found. Furthermore, both $^{457}$K:PsbC and $^{35}$K:PsbI are cross-linked to $^{523}$K:ApcE, which is located on the Arm 2 domain of ApcE (Fig. 2A). PsbI, a binding partner for PsbA (D1), is known to play an important role in stabilizing PsbC in the PSII assembly process (*16*).

We identified cross-links between $^{11}$K:PsaA (Psa for PSI and Psb for PSII) and $^{48}$K:ApcD and between $^{49}$K:ApcD and $^{76}$K:PsaD (Fig. 2E, table S4), in line with the concept that energy absorbed by the PBS is delivered to PSI as well as to PSII (*17*, *18*). Our results locate ApcD on the edge area of PSI through a domain formed by PsaA and PsaD (Fig. 2C). Additionally, LC-MS/MS analysis showed cross-links between $^{17}$K:ApcB and $^{30}$K:PsaA and between $^{58}$K:ApcB and $^{10}$K:PsaD (Fig. 2, D and E; fig. S7; and table S4). These data support a docking model in which $^{17}$K:ApcB (β) is from one monomer (ApcDβ), and $^{58}$K:ApcB (β) is from another (αβ), instead of from one β subunit (fig. S10). These chemical cross-linking data in combination with results from protein modeling (fig. S10B) support a side-on orientation of the PBS core to PSI through a cove formed by PsaD and PsaA (Fig. 2D). Our structural model predicts a closest distance of about 22 Å from PCB (phycocyanobilin) to the cytoplasmic layer of chlorophylls in the PsaA (fig. S11). Although early studies demonstrated the involvement of ApcD in energy transfer from PBS to PSI (*19*, *20*), the route by which

[1]Department of Biology, Washington University in St. Louis, St. Louis, MO 63130, USA. [2]Photosynthetic Antenna Research Center, Washington University in St. Louis, St. Louis, MO 63130, USA. [3]Department of Chemistry, Washington University in St. Louis, St. Louis, MO 63130, USA.

*Corresponding author. E-mail: blankenship@wustl.edu

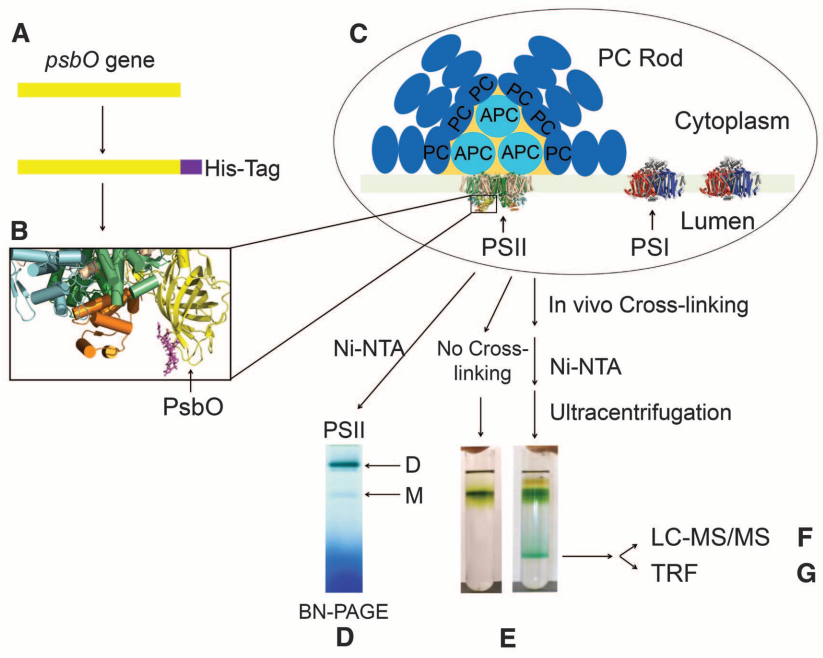


**Fig. 1. Schematic outline of the experimental workflow established for the genetic modification, isolation, and preliminary characterization of the MCL.** (**A**) Genetic modification of PsbO protein at C terminus [PsbOH strain (*5*)]. (**B**) Luminal side of the PSII monomer, indicating the solvent-accessible PsbO C terminus with $His_6$ tag (purple) introduction. PsbO is colored yellow; PsbU, orange; PsbV, light blue; and loop E of CP43, lime. (**C**) In vivo model of PBS and photosystems. NTA, nitrilotriacetic acid. (**D**) BN-PAGE (blue native polyacrylamide gel electrophoresis) analysis of isolated PSII (PsbOH), dimer (D), and monomer (M). (**E**) Ultracentrifugation isolation of MCL after affinity chromatography. (**F** and **G**) LC-MS/MS and TRF spectroscopy of the MCL.

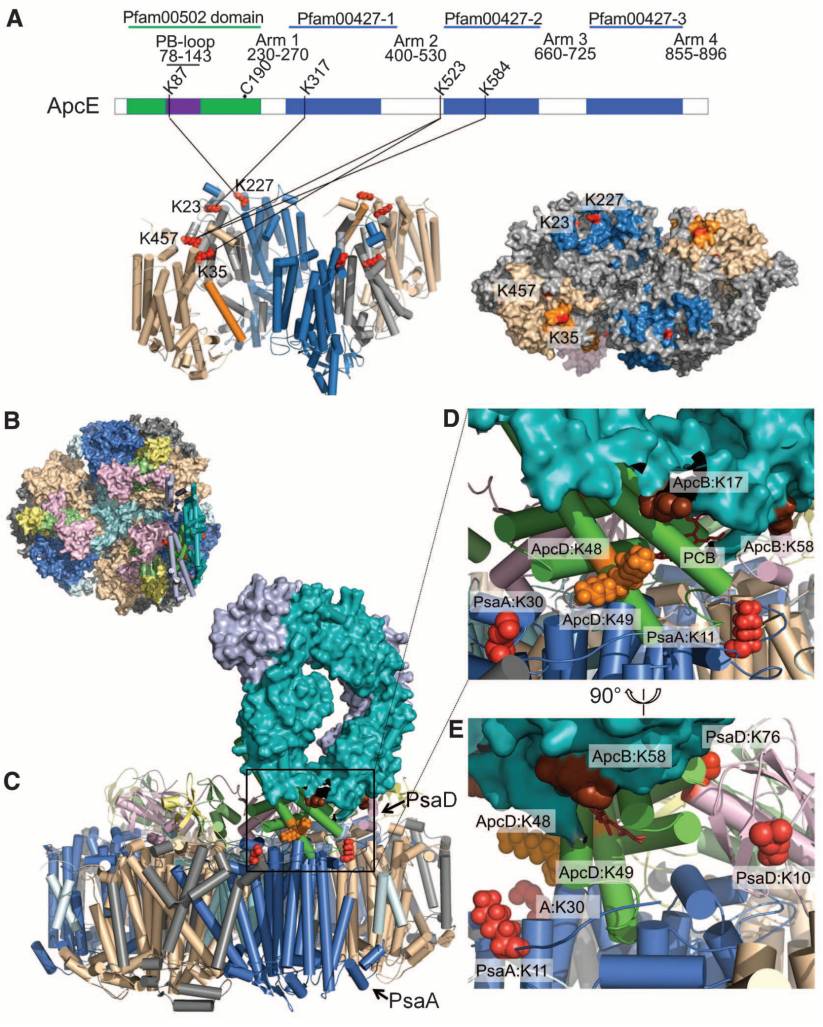


**Fig. 2. Identification of interprotein cross-links between PBS and two photosystems.** (**A**) ApcE-PSII cross-links. The N-terminal domain of ApcE is the only phycobilin-attached region in linker proteins ($Cys^{190}$). Five cross-links were found between ApcE and PSII. PsbB, sky blue; PsbC, wheat; PsbD, light gray; PsbI, orange. All lysines ($^{227}$K:PsbB, $^{457}$K:PsbC, $^{35}$K:PsbI, and $^{23}$K:PsbD) are represented as spheres. (**B**) Docking model of ApcD to PSI trimmer (cytoplasmic view) based on the identified cross-links presented in (**C**). PsaA, marine; PsaB, wheat; PsaC, lime; PsaD, light pink; PsaE, yellow; PsaF, gray; PsaL, cyan; ApcD, green; ApcA, light blue; ApcB, teal. (**D** and **E**) Close-up views of the model shown in (C) and PCB (red sticks). Cross-links were found between $^{48}$K:ApcD (orange) and $^{11}$K:PsaA, $^{17}$K:ApcB and $^{30}$K:PsaA, $^{58}$K:ApcB and $^{10}$K:PsaD, and $^{49}$K:ApcD and $^{76}$K:PsaD. Lysine residues from PSI, ApcD, and ApcB are presented as red, orange, and chocolate spheres, respectively.

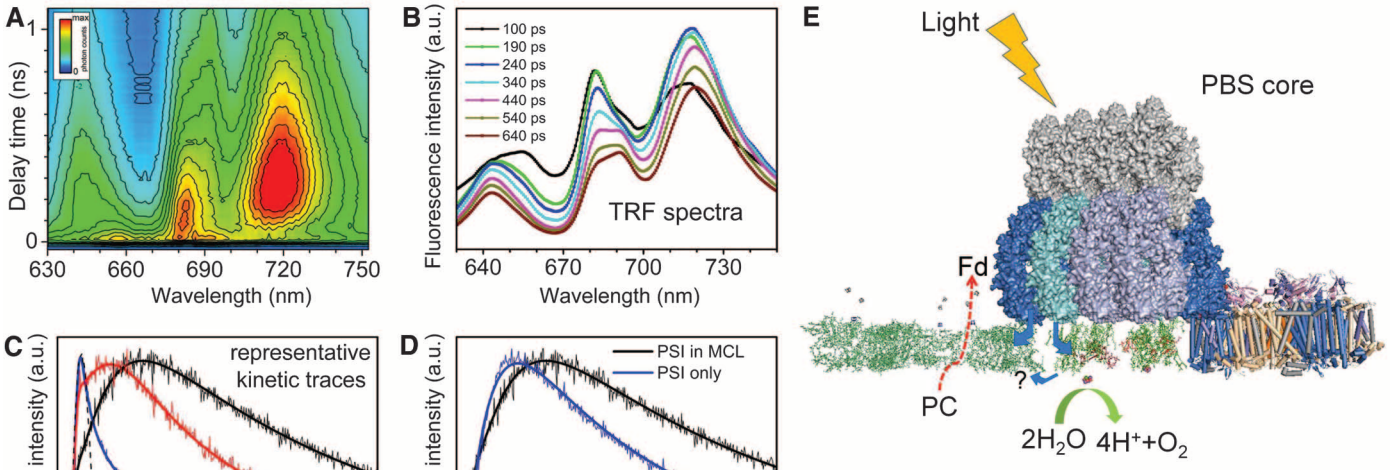


**Fig. 3. Time-resolved fluorescence of the MCL at 77 K, fluorescence decay analysis, and model of the PBS-PSII-PSI association in the MCL.** (**A**) Two-dimensional profile of TRF recorded in 1-ns time windows after excitation at 550 nm. (**B**) Representative TRF spectra taken at various delay times after excitation. a.u., arbitrary unit. (**C**) Representative fluorescence decay traces taken at three distinct bands (PC, PSII, and PSI) accompanied with fits. IRF, instrument response function. (**D**) Rise and decay of fluorescence at 720 nm (PSI) recorded for the MCL and the isolated PSI. (**E**) The MCL model of the PBS-PSII-PSI association, showing that PSII is fully covered by close association with the PBS core, whereas PSI is associated with ApcD through a side-on orientation.

the energy migrates from PBS to PSI has been elusive (*21*). Docking ApcD onto the cove formed by PsaA and PsaD causes no apparent steric clashes on ferredoxin (fig. S12) (*12*).

We then applied time-resolved fluorescence (TRF) spectroscopy at 77 K to study energy transfer between structurally coupled components of the MCL (Fig. 3). Two-dimensional TRF profiles and representative TRF spectra taken at various delay times after excitation at 550 nm (Fig. 3, A and B) show three distinct emission bands with maxima of 645, 685, and 720 nm associated with fluorescence from phycocyanin (PC), PSII, and PSI, respectively, suggesting that energy transfer from PBS to both photosystems takes place. TRF of the MCL does not show a signature of $APC_{680}$ (terminal energy emitter) fluorescence as in isolated PBS (fig. S13). This may not be surprising if the MCL is functionally intact. The absence of PBS fluorescence around this region and the almost instantaneous rise of the PSII chlorophyll a (Chl a) fluorescence (Fig. 3C) demonstrate efficient energy transfer from PBS to PSII, consistent with the PBS core sitting directly on top of the PSII dimer (Fig. 2A).

The rise of fluorescence associated with the PSI in MCL is not instantaneous (Fig. 3, C and D) but rather delayed compared with the others (figs. S14 to S20), suggesting that PBS-PSII and PBS-PSI energy transfer rates are different. Emission at ~720 nm originates from excitation traps—clusters of Chl a pigments with the strongest excitonic interactions located in the PsaA and PsaB PSI subunits (*22*). These traps effectively serve as excitation donors to the P700 dimer at physiological temperatures, demonstrating multidecay character at 77 K (*23*, *24*) (figs. S18 and S19). If energy transfer from the PBS to PSI is slow, the rise of fluorescence at 720 nm should be delayed in the MCL with respect to the isolated PSI, as is demonstrated by the data in Fig. 3D. The delayed rise of the PSI fluorescence may be associated with decreased PBS-to-PSI excitation-energy transfer owing either to side-on orientation of PBS and PSI or to a chemical cross-linking modification effect. We do not exclude the possibility of energy spillover from PSII (*25*). (Fig. 3E). However, undetectable long-lived PSI fluorescence (*26*) may indicate that the delayed rise of PSI fluorescence is associated with slow excitation-energy transfer between the PBS and PSI, as indicated by the structural interactions between PsaA and ApcD (terminal energy emitter) (Fig. 2C).

Previous studies have suggested that physical interactions between the PBS core and PSII and I are essential for efficient excitation energy migration from low-energy allophycocyanin (APC) in the PBS core to Chl a in RCs (*20*, *27*). However, the enigmatic "supercomplex" comprising PBS-RCs has never been consistently detected and isolated (*21*), owing to weak and easily disrupted interactions between these complexes. Our study demonstrates that if cells are gently cross-linked in vivo, the weak interactions can be captured and identified. The isolated complex contains PSI but not the cytochrome $b_6f$ complex, which connects PSI and PSII by mobile-electron carriers. Thus, the MCL is best considered as an energy-transfer complex that directs excitations to one or the other photosystem (Fig. 3E) and not as a complex that includes the complete electron-transport chain.

The isolation of the MCL allows us to witness the merger of three intensely studied photosynthetic events of light harvesting and two light-driven photochemistry reactions in one module. There are still many unresolved issues, including the molecular mechanism that governs the assembly of the MCL and the means by which the excitation energy is delivered to the two photosystems by the PBS. For instance, the orange carotenoid protein is directly involved in the fluorescence quenching of PBS and possibly in the regulation of energy transfer between PBS and the photosystems (*28*).

### References and Notes


1. E. Gantt, S. F. Conti, *Brookhaven Symp. Biol.* **19**, 393–405 (1966).
2. A. N. Glazer, *Annu. Rev. Biophys. Biophys. Chem.* **14**, 47–77 (1985).
3. N. T. de Marsac, G. Cohen-bazire, *Proc. Natl. Acad. Sci. U.S.A.* **74**, 1635–1639 (1977).
4. M. Chen, R. E. Blankenship, *Trends Plant Sci.* **16**, 427–431 (2011).
5. Materials and methods are available as supplementary materials on *Science* Online.
6. E. V. Petrotchenko, C. H. Borchers, *Mass Spectrom. Rev.* **29**, 862–876 (2010).
7. A. Sinz, *Mass Spectrom. Rev.* **25**, 663–682 (2006).
8. C. Zheng *et al*, *Mol. Cell. Proteomics* **10**, M110.006841 (2011).
9. H. Xu, M. A. Freitas, *Proteomics* **9**, 1548–1555 (2009).
10. T. Walzthoeni *et al*., *Nat. Methods* **9**, 901–903 (2012).
11. Y. Umena, K. Kawakami, J. R. Shen, N. Kamiya, *Nature* **473**, 55–60 (2011).
12. P. Jordan *et al*., *Nature* **411**, 909–917 (2001).
13. J. Houmard, V. Capuano, M. V. Colombano, T. Coursin, N. Tandeau de Marsac, *Proc. Natl. Acad. Sci. U.S.A.* **87**, 2152–2156 (1990).
14. V. Capuano, A. S. Braux, N. Tandeau de Marsac, J. Houmard, *J. Biol. Chem.* **266**, 7239–7247 (1991).
15. G. Ajlani, C. Vernotte, *Eur. J. Biochem.* **257**, 154–159 (1998).
16. M. Dobáková, M. Tichy, J. Komenda, *Plant Physiol.* **145**, 1681–1691 (2007).
17. D. Bruce, J. Biggins, *Biochim. Biophys. Acta* **810**, 295–301 (1985).

18. C. W. Mullineaux, *Biochim. Biophys. Acta* **1100**, 285–292 (1992).
19. J. Zhao, J. Zhou, D. A. Bryant, in *Research in Photosynthesis*, N. Murata, Ed. (Kluwer Academic Publishers, Dordrecht, Netherlands, 1992), vol. 1, pp. 25–32.
20. A. N. Glazer, D. A. Bryant, *Arch. Microbiol.* **104**, 15–22 (1975).
21. C. W. Mullineaux, *Photosynth. Res.* **95**, 175–182 (2008).
22. V. Soukoulis, S. Savikhin, W. Xu, P. R. Chitnis, W. S. Struve, *Biophys. J.* **76**, 2711–2715 (1999).
23. B. Gobets *et al*., *Biophys. J.* **81**, 407–424 (2001).
24. G. Hastings, F. A. M. Kleinherenbrink, S. Lin, R. E. Blankenship, *Biochemistry* **33**, 3185–3192 (1994).
25. J. Biggins, D. Bruce, *Photosynth. Res.* **20**, 1–34 (1989).
26. M. Yokono, A. Murakami, S. Akimoto, *Biochim. Biophys. Acta* **1807**, 847–853 (2011).
27. T. Redlinger, E. Gantt, *Plant Physiol.* **68**, 1375–1379 (1981).
28. D. Kirilovsky, C. A. Kerfeld, *Photochem. Photobiol. Sci.* **12**, 1135–1143 (2013).
29. J. A. Vizcaíno *et al*., *Nucleic Acids Res.* **41**, D1063–D1069 (2013).

**Acknowledgments:** We thank T. Bricker and H. Pakrasi for the HT3 strain, G. Ajlani and D. Kirilovsky for the ΔAB strain, all the other members of the Gross and Blankenship laboratories for collegial discussions, and H. Rohrs and M. Plasencia for help with LC-MS/MS instrumentation. The research was supported by the Photosynthetic Antenna Research Center (PARC), an Energy Frontier Research Center funded by the U.S. Department of Energy (DOE), Office of Basic Energy Science (grant no. DE-SC 0001035 to R.E.B) and National Institute of General Medical Science (grant no. 8 P41 GM103422-35 to M.L.G). H.L., D.M.N, M.P., and G.H. were funded by the DOE grant, H.Z. was funded equally by the DOE and NIH grants, and instrumentation was made available from both DOE and NIH grants. Additional data are available in the supplementary materials. The mass spectrometry proteomics data have been deposited to the ProteomeXchange Consortium (http://proteomecentral.proteomexchange.org) via the PRIDE (Proteomics Identifications Database) partner repository (*29*) with the data set identifier PXD000545.

**Supplementary Materials**

www.sciencemag.org/content/342/6162/1104/suppl/DC1
Materials and Methods
Figs. S1 to S20
Tables S1 to S5
References (*30*–*58*)

24 June 2013; accepted 16 October 2013
10.1126/science.1242321

# Long-Distance Integration of Nuclear ERK Signaling Triggered by Activation of a Few Dendritic Spines

**Shenyu Zhai,[1] Eugene D. Ark,[1] Paula Parra-Bueno,[2] Ryohei Yasuda[1,2,3]***

**The late phase of long-term potentiation (LTP) at glutamatergic synapses, which is thought to underlie long-lasting memory, requires gene transcription in the nucleus. However, the mechanism by which signaling initiated at synapses is transmitted into the nucleus to induce transcription has remained elusive. Here, we found that induction of LTP in only three to seven dendritic spines in rat CA1 pyramidal neurons was sufficient to activate extracellular signal–regulated kinase (ERK) in the nucleus and regulate downstream transcription factors. Signaling from individual spines was integrated over a wide range of time (>30 minutes) and space (>80 micrometers). Spatially dispersed inputs over multiple branches activated nuclear ERK much more efficiently than clustered inputs over one branch. Thus, biochemical signals from individual dendritic spines exert profound effects on nuclear signaling.**

Activity-dependent gene transcription is essential for the maintenance of long-term potentiation (LTP) and memory consolidation (*1*, *2*). Induction of LTP in single dendritic spines activates signaling that can either be restricted to the stimulated spine or spread into the parent dendrite over 5 to 10 μm (*3*–*5*). However, it is not known whether signaling initiated at single dendritic spines can be transmitted into the nucleus to regulate gene transcription. Extracellular signal–regulated kinase (ERK) is important, both for signaling within the stimulated spine and adjacent dendrites (*3*, *6*, *7*) and also for activating transcription factors in the nucleus during LTP (*2*, *8*–*11*). Thus, ERK signaling may play an important role in relaying signals from the stimulated spines to the nucleus.

To monitor the activity of ERK in the nucleus, we ballistically transfected cultured organotypic hippocampal slices of rats with nuclear-targeted ERK activity reporter ($EKAR_{nuc}$) (*12*) and imaged CA1 pyramidal neurons with two-photon fluorescence lifetime imaging microscopy (2pFLIM). The expression of $EKAR_{nuc}$ was highly localized to the nucleus (*12*). Using the weak EKAR expression in the cytosol, we employed fluorescence intensity measurements to monitor structural plasticity of dendritic spines on secondary and tertiary apical dendritic branches (Fig. 1).

When a single spine was stimulated with a low-frequency train (1Hz, 60 s) (Fig. 1A) of two-photon glutamate uncaging pulses in the absence of $Mg^{2+}$, the spine volume increased rapidly by 275 ± 18% in 1 to 2 min (transient phase), which decayed to a sustained level 61 ± 4% larger than the original volume that lasted more than 1 hour (sustained phase) (Fig. 1, C and E), as expected (*3*–*5*, *13*). The volume increase was similar to that induced in neurons expressing monomeric enhanced green fluorescent protein (mEGFP) (Fig. 1E). This structural LTP (sLTP) of spines is known to be associated with electrophysiological LTP (*3*–*5*, *13*). Repeating this protocol in different spines one by one (at ~60-s intervals) (Fig. 1A), we induced sLTP sequentially in seven spines on three to five different dendritic branches (Fig. 1, B and C). After the seven-spine stimulation, we observed a slow and sustained elevation of ERK activity in the nucleus, as indicated by a gradual (over ~30 min) shortening of the fluorescence lifetime of $EKAR_{nuc}$ (~−0.02 ns) that was maintained for at least the following 40 min (Fig. 1, D and F). Pharmacological inhibition of ERK with ERK inhibitor FR180204 (50 μM) completely prevented the fluorescence lifetime decrease respectively (Fig. 1, F and G). Inhibition of the classical upstream molecules Ras and mitogen-activated protein kinase kinase (MEK) (*14*) with dominant-negative Ras (dnRas) expression and MEK inhibitor U0126 prevented the fluorescence lifetime decrease, respectively (Fig. 1J and fig. S5). Thus, the change in fluorescence lifetime of $EKAR_{nuc}$ acted as a reliable reporter of ERK activation in the nucleus.

We further confirmed that our seven-spine stimulation protocol activates nuclear ERK by two methods independent of 2pFLIM imaging of $EKAR_{nuc}$. First, we performed immunostaining of phosphorylated ERK in CA1 neurons expressing mEGFP. Consistent with the $EKAR_{nuc}$ results, the level of phosphorylated ERK in the nucleus was persistently elevated after seven-spine stimulation (*15*) (Fig. 1H and fig. S1). Second, we performed live imaging of mEGFP-tagged ERK2 in organotypic slices. Under basal conditions, mEGFP-ERK2 was localized predominantly to the cytoplasm but slowly translocated into the nucleus after seven-spine stimulation (Fig. 1I and fig. S2) (*8*, *15*). Thus, nuclear ERK is activated by sequential activation of a few spines.

Next, we determined the source of intracellular $Ca^{2+}$ elevation that leads to nuclear ERK activation. Uncaging-induced $Ca^{2+}$ elevation was largely restricted to the stimulated spines, and spreading along the dendrite was limited to 2 to 3 μm (figs. S3 and S4) (*15*, *16*). This local $Ca^{2+}$ elevation was dependent mainly on *N*-methyl-D-aspartate-type glutamate receptors (NMDARs); there was negligible contribution from voltage-sensitive $Ca^{2+}$ channels (VSCCs), metabotropic glutamate receptor (mGluR)–mediated internal $Ca^{2+}$ release, or $Ca^{2+}$-permeable α-amino-3-hydroxy-5-methyl-4-isoxazolepropionic acid receptors (fig. S4F). Inhibition of NMDARs with 2-amino-5-phosphonopentanoic acid (APV) (50 μM) completely prevented nuclear ERK activation (Fig. 1J and fig. S5A), as well as sLTP (Fig. 1, K and L) (*13*). In contrast, blockade of VSCCs with $CdCl_2$ (200 μM) did not prevent nuclear ERK activation

[1]Department of Neurobiology, Duke University Medical Center, Durham, NC 27710, USA. [2]Max Planck Florida Institute for Neuroscience, Jupiter, FL 33458, USA. [3]Howard Hughes Medical Institute, Duke University Medical Center, Durham, NC 27710, USA.

*Corresponding author. E-mail: ryohei.yasuda@mpfi.org

(Fig. 1J and fig. S5A), although the sustained phase of sLTP was partially inhibited (Fig. 1, K and L). Thus, uncaging-induced nuclear ERK activation was not caused by direct membrane depolarization in close proximity to the nucleus and resultant $Ca^{2+}$ entry through VSCCs. Indeed, uncaging-evoked excitatory postsynaptic potential recordings showed only small somatic voltage changes during uncaging (1.5 to 4 mV) (fig. S3). Inhibition of mGluRs with α-methyl-4-carboxyphenylglycine (MCPG) (1 mM) or 2-quinoxaline-carboxamide-*N*-adamantan-1-yl (NPS 2390) (20 μM) attenuated the nuclear ERK activation (Fig. 1J and fig. S5, B and C). However, inhibition of mGluRs did not affect sLTP (*13*) (Fig. 1, K and L). Thus, the requirement for nuclear ERK activation is different from that for $Ca^{2+}$ elevation or sLTP. Because group I mGluR activation increases the production of diacylglycerol, which leads to activation of protein kinase C (PKC) (*17*), we further tested if PKC is required for the sustained nuclear ERK activation. Because PKC inhibitor blocks sLTP (*3*), we applied PKC inhibitor bisindolylmaleimide I (BIM) (0.2 μM) ~60 min after induction of nuclear ERK activation. Surprisingly, this delayed application of BIM caused nuclear ERK activity to gradually return to the basal level (fig. S6), suggesting that sustained PKC activity is required for maintaining nuclear ERK activation.

What is the spatial pattern of synaptic activation required for nuclear ERK activation? We first tested how many synapses are required for nuclear ERK activation. We stimulated different numbers (i.e., one, three, seven) of spines at a fixed density (i.e., one to three spines per dendritic branch, separated by more than 10 μm)

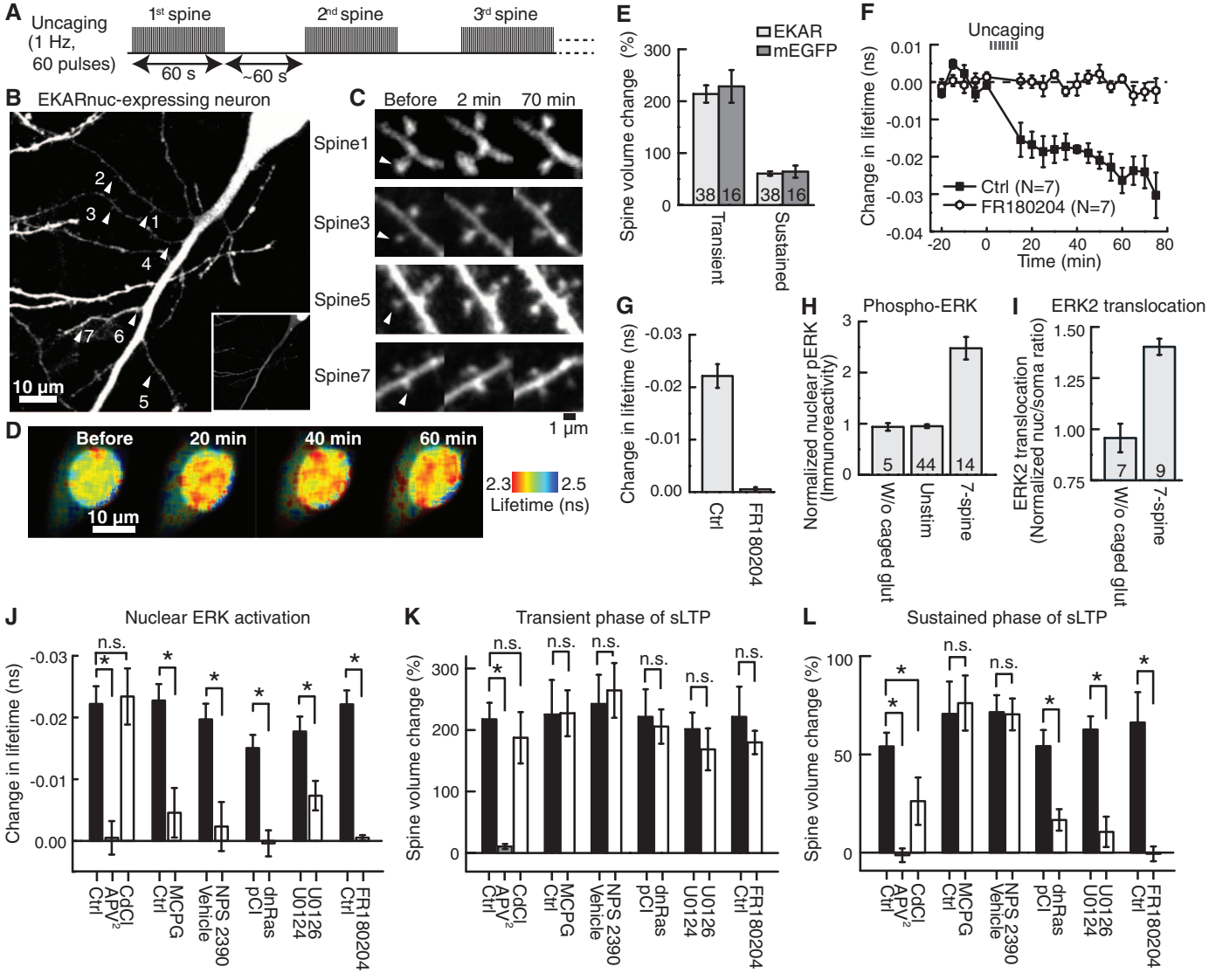


**Fig. 1. Stimulation of seven spines in a sequential fashion triggers activation of ERK in the nucleus.** (**A**) Schematic for seven-spine stimulation. (**B**) A neuron transfected with $EKAR_{nuc}$. Arrowheads indicate the locations of seven stimulated spines. (Inset) Low-brightness view of the same neuron shows nuclear localization of $EKAR_{nuc}$. (**C**) Representative images of spine sLTP induced by glutamate uncaging in the neuron shown in (B). (**D**) Fluorescence lifetime images of $EKAR_{nuc}$ before and after seven-spine stimulation in the same neuron as in (B) and (C). (**E**) Quantification of the transient (1 to 2 min) and sustained (~70 min) phases of sLTP after seven-spine stimulation in $EKAR_{nuc}$-expressing neurons and in mEGFP-expressing neurons. The number of neurons (*N*) is indicated at the bottom of each bar. (**F**) Time course of change in fluorescence lifetime of $EKAR_{nuc}$ after seven-spine stimulation in the absence (Ctrl) or presence of ERK inhibitor FR180204. (**G**) Quantification of change in fluorescence lifetime averaged over 40 to 70 min in (F). (**H** to **I**) Stimulation of seven spines leads to increased nuclear phospho-ERK level (pERK) (H) and ERK2 nuclear translocation (I). (**J** to **L**) Effects of pharmacological agents and genetic manipulation on nuclear ERK activation (J) and the transient (1 to 2 min) (K) and sustained (~70 min) (L) phases of sLTP. Fluorescence lifetime change averaged over 40 to 70 min was quantified for experiments shown in fig. S5 and (F). *$P < 0.05$; n.s., not significant. $N = 14$ for Ctrl and 7 for APV and $CdCl_2$, 6 for Ctrl and MCPG, 6 for vehicle and NPS 2390, 7 for pCl and 8 for dnRas, and 7 for U0124 and U0126. Error bars denote SEM.

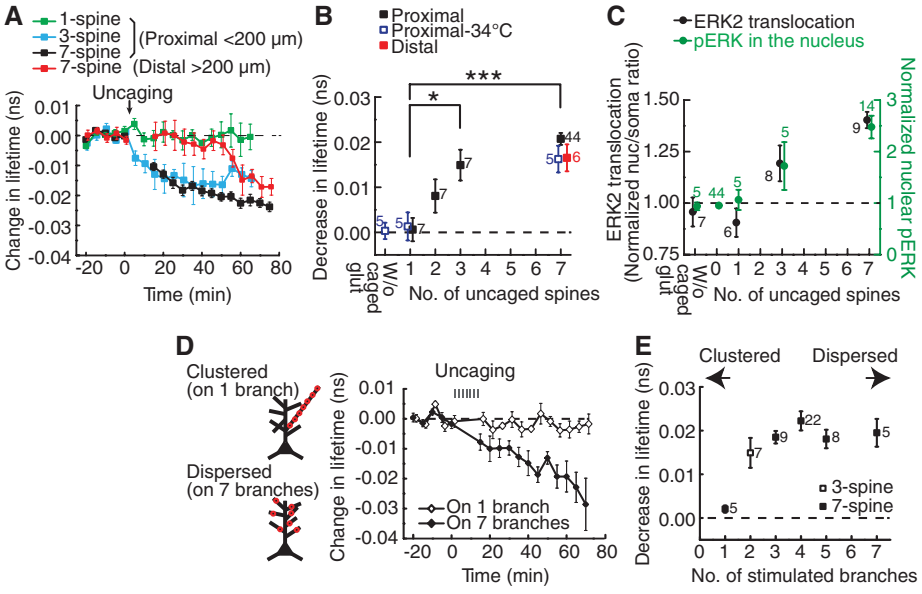


**Fig. 2. Spatial stimulation pattern required for nuclear ERK activation.** (**A**) Time course of fluorescence lifetime change of $EKAR_{nuc}$ after stimulation of varied numbers of spines under a fixed density of stimulation. Three-spine stimulation was on two separated dendritic branches. Proximal dendrites (<200 μm from the nucleus) were stimulated in most of the experiments, but distal dendrites (<200 μm) were stimulated in some experiments (red). (**B**) Quantification of the sustained fluorescence lifetime change (averaged over 40 to 70 min for proximal seven-spine stimulation, 30 to 60 min for one- and three-spine stimulations, and 65 to 75 min for distal seven-spine stimulation). As a negative control, seven-spine stimulation experiments without caged glutamate were performed (W/o caged glut). *N* for each condition is indicated next to the data points; $*P < 0.05$, $***P < 0.001$. (**C**) Dependency of the magnitudes of nuclear translocation of mEGFP-ERK2 (black) and pERK in the nucleus (green) on the number of stimulated dendritic spines. The level of pERK was measured 75 min after stimulation (see fig. S1). The nuclear/somatic ratio was averaged over 55 to 70 min for one-spine stimulation and 60 to 75 min for other groups (see fig. S2). (**D**) Time course of fluorescence lifetime change of $EKAR_{nuc}$ after stimulation of seven spines that reside on the same branch or on seven different branches. (**E**) Quantification of the sustained fluorescence lifetime change after stimulation of varied numbers of dendritic branches. Data are presented as mean ± SEM (error bars).

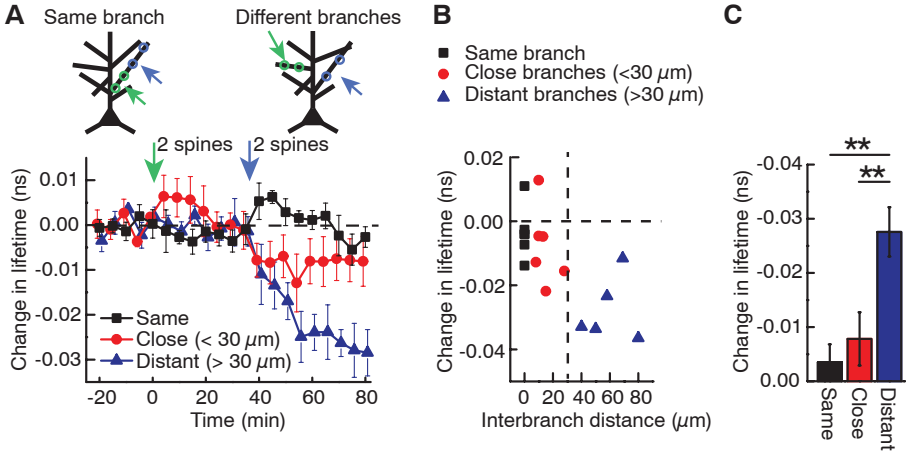


**Fig. 3. Wide-range spatiotemporal integration of ERK signaling from different branches.** (**A**) Time course of $EKAR_{nuc}$ fluorescence lifetime in response to sequential stimulation of two spines on a branch (green arrows), which does not cause any nuclear ERK activation (as predicted from Fig. 2D), followed by stimulation of two additional spines 30 min after the first stimulation (blue arrows). When the second stimulation was on the same branch or a close branch (interbranch distance <30 μm), ERK was not activated in the nucleus. However, when the second stimulation was applied to a dendritic branch well apart from the first stimulated branch (interbranch distance >30 μm), significant activation occurred. (*N* = six, six, and five neurons for same, close, and distant, respectively.) (**B**) Relation between change in fluorescence lifetime [averaged over 70 to 80 min from data shown in (A)] and interbranch distance measured along the primary dendrite. (**C**) Quantification of ERK signaling shown in (B). $**P <$ 0.01. Data are presented as mean ± SEM (error bars).

(Fig. 1, A and B). Glutamate uncaging at a single spine failed to cause any detectable signal in the nucleus, whereas glutamate uncaging at three spines led to significantly elevated nuclear ERK activity (Fig. 2, A and B). For $EKAR_{nuc}$ signal at a near-physiological temperature (34°C), we found a similar correlation with the number of stimulated spines (Fig. 2B and fig. S7), as well as for the levels of nuclear phospho-ERK and ERK2 translocation into the nucleus (Fig. 2C and figs. S1 and S2).

In most of the experiments, we stimulated proximal branches within 200 μm from the soma. However, when we stimulated distal branches at more than 200 μm away from the soma, ERK activation showed a long delay (~40 min) before it started to increase to the level similar to that caused by proximal stimulation (Fig. 2, A and B). This slow process suggests that fast biochemical processes such as $Ca^{2+}$ waves (*18*) and electrochemical signaling (*2*, *19*) are unlikely to underlie the nuclear ERK activation induced by activating a few spines.

Next, we varied the number of dendritic branches on which the stimulated spines reside to find out which input pattern—clustered or dispersed—produces nuclear ERK activation more efficiently. Clustered stimulation of all seven spines on a single branch failed to induce any nuclear ERK activity increase (Fig. 2, D and E). In contrast, stimulating three or seven spines distributed over two to seven branches resulted in marked activation of nuclear ERK (Fig. 2, D and E; all $P < 0.05$). Thus, signal integration over multiple dendritic branches is required to induce nuclear activation of ERK. We further investigated why dispersed stimulation is more efficient by imaging ERK activation at the branching point in the primary dendritic trunk after stimulating within a dendritic branch (fig. S8). ERK activity at the branching point was saturated when we stimulated two spines within a dendritic branch. Thus, additional stimulation to a branch should not cause additional ERK activation in the primary dendrite or in the nucleus.

What is the range of the spatiotemporal integration of the nuclear ERK activation? To address this question, we stimulated two spines in a dendritic branch first, waited for 30 min, and then stimulated two additional spines in the same branch or another dendritic branch 5 to 80 μm away from the first branch (Fig. 3A). As expected, the first set of stimulation did not activate nuclear ERK because both stimulated spines were on the same branch (see Fig. 2D). However, the second set of stimulation, when applied to another branch separated by more than 30 μm, significantly increased nuclear ERK activity (Fig. 3). Thus, nuclear ERK signaling can integrate synaptic stimulation over more than 30 min. When the second set of stimulation was applied to the same branch or a nearby branch (within 30 μm), we did not observe a significant increase in nuclear ERK activity (Fig. 3). Thus, nuclear ERK is activated more efficiently by a spatially distributed pattern of stimulation.

Is nuclear ERK activation induced by stimulation of a few dendritic spines sufficient to regulate gene transcription? To address this question, we used immunostaining to measure the activity of two transcription factors—cyclic adenosine monophosphate response element–binding protein (CREB) and E26-like transcription factor-1 (Elk-1) (Fig. 4)—because these molecules are known to be activated by neuronal activity via ERK activation (*14*). After glutamate uncaging at seven spines of mEGFP-expressing CA1 neurons, the slices were immunostained for CREB phosphorylated at $Ser^{133}$ (Fig. 4, A and B) or Elk-1 phosphorylated at $Ser^{383}$ (Fig. 4, D and E), the phosphorylation sites required for their transcriptional activity (*20*, *21*). The levels of phosphorylated CREB and Elk-1 were higher in uncaged neurons than in surrounding untransfected neurons at 45 and 90 min after uncaging (Fig. 4, B and E). In contrast, mEGFP-positive, unstimulated neurons in the same slices did not show any increase in phosphorylated CREB and Elk-1 (Fig. 4). Furthermore, CREB and Elk-1 phosphorylation was abolished when ERK inhibitor FR180204 was applied before stimulation (Fig. 4, C and F). Thus, stimulation of a few spines regulates activities of transcription factors CREB and Elk-1 through ERK.

Induction of structural LTP in three to seven spines led to nuclear ERK activation and subsequent regulation of downstream transcription factors CREB and Elk-1. Because each CA1 pyramidal neuron has roughly 10,000 synapses, activation of only a tiny fraction (<0.1%) of its synapses can activate nuclear signaling that regulates gene transcription. Many studies have demonstrated that somatonuclear $Ca^{2+}$ transients, caused by somatic depolarization and $Ca^{2+}$ wave propagation, play an important role in regulation of activity-dependent gene transcription [(*19*, *22*), reviewed by (*23*)]. However, under our experimental condition, this mechanism is unlikely to play a role. Our sLTP induction protocol produced $Ca^{2+}$ elevation highly restricted to the vicinity of the stimulated spines and only small somatic voltage changes. In addition, activation of VSCCs was not required for nuclear ERK activation. Moreover, the slow signal transmission strongly suggests that biochemical messengers relay information from activated synapses to the nucleus (*10*, *11*, *24*–*27*). Because Ras activity is known to spread over ~10 μm upon single-spine stimulation (*3*), downstream ERK may diffuse further and invade the nucleus as a result of multiple-spine stimulation. Consistent with this hypothesis, we observed that ERK2 translocates into the nucleus in response to stimulation of a few spines. Further, the onset of ERK activation in response to distal dendrite stimulation was consistent with the speed of ERK diffusion (*15*). Considering that the size of the nucleus is ~2000 times larger than that of an average spine (*2*) and that the phosphatase-rich cytosol needs to be traversed by phosphorylated ERK, additional mechanisms such as a PKC-ERK positive feedback loop and physical protection would be required to aid the long-distance, persistent synapse-to-nucleus ERK signaling (*27*, *28*).

The long-distance spatiotemporal integration in inducing nuclear ERK activation may have important implications for the functional organization of dendritic inputs. Many studies have shown that synaptic potentiation tends to occur in a spatially clustered fashion (*29*–*31*) due to electrical integration and biochemical cross talk within a short stretch of dendrite (*32*–*35*). However, because potentiated synapses would recruit stronger local membrane depolarization and biochemical signaling in the surrounding region in a positive-feedback manner, this mechanism potentially leads to accumulation of potentiated synapses in one dendritic branch (*36*). The nuclear signaling efficiently induced by spatially dispersed inputs may be important for counterbalancing the tendency to accumulate potentiated spines in one branch and developing balanced spatial distribution of synaptic weights.

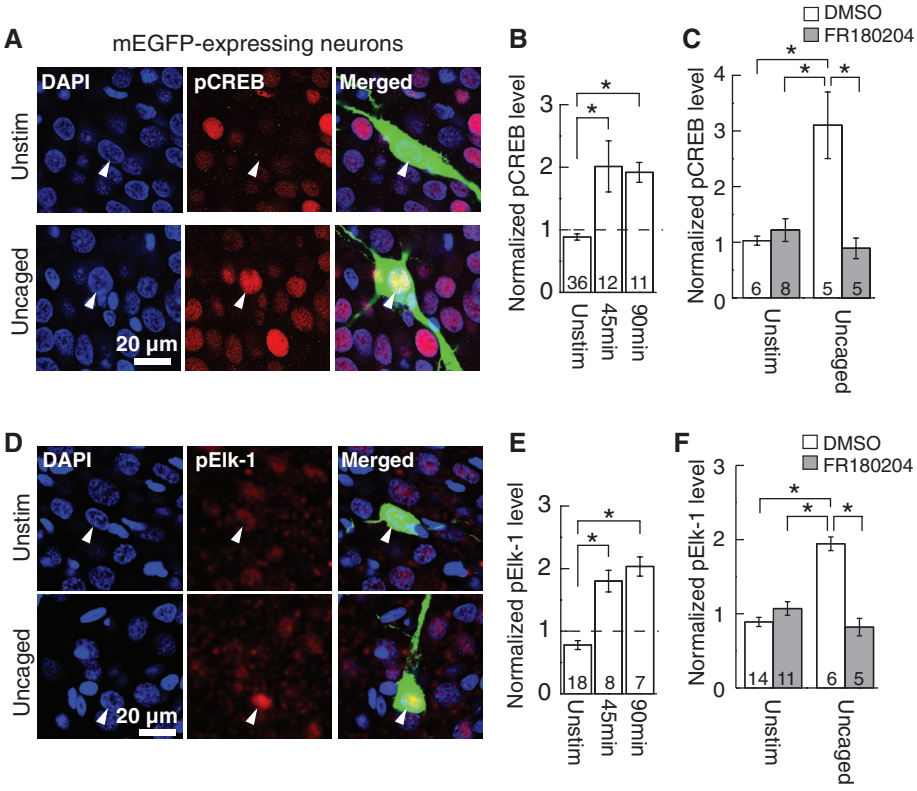


**Fig. 4. Transcription factors are phosphorylated in response to seven-spine stimulation in an ERK-dependent fashion.** (**A**) Immunofluorescent images of phosphorylated CREB (pCREB) (red). Seven spines of a neuron expressing mEGFP (green) were stimulated, and the slice was fixed 45 min after the stimulation (Uncaged). An unstimulated mEGFP neuron in the same slices is also shown as negative control (Unstim). The nuclei were stained with 4′,6-diamidino-2-phenylindole (DAPI) (blue). The relatively high basal level of pCREB in a subpopulation of neurons is probably due to spontaneous circuit activity (*7*). (**B**) Quantification of the fluorescence intensity of pCREB in the nuclei identified with DAPI. The fluorescence in the nucleus of each mEGFP-expressing neuron was normalized to the average fluorescence in the nuclei of five surrounding untransfected neurons. Uncaged neurons were always paired with unstimulated neurons in the same slices (*15*). The numbers of neurons are indicated at the bottom of the bars. $*P < 0.05$. (**C**) ERK inhibitor FR180204 blocks uncaging-induced CREB phosphorylation. Dimethyl sulfoxide (DMSO) was used as vehicle control. (**D** to **F**) Same as (A) to (C), except phosphorylated Elk-1 (pElk-1) was analyzed instead of pCREB. Arrowheads in (A) and (D) indicate unstimulated or uncaged mEGFP-expressing neurons. Data are presented as mean ± SEM (error bars).


**References and Notes**

1. P. V. Nguyen, T. Abel, E. R. Kandel, *Science* **265**, 1104–1107 (1994).
2. J. P. Adams, S. M. Dudek, *Nat. Rev. Neurosci.* **6**, 737–743 (2005).
3. C. D. Harvey, R. Yasuda, H. Zhong, K. Svoboda, *Science* **321**, 136–140 (2008).
4. S.-J. R. Lee, Y. Escobedo-Lozoya, E. M. Szatmari, R. Yasuda, *Nature* **458**, 299–304 (2009).
5. H. Murakoshi, H. Wang, R. Yasuda, *Nature* **472**, 100–104 (2011).
6. M. A. Patterson, E. M. Szatmari, R. Yasuda, *Proc. Natl. Acad. Sci. U.S.A.* **107**, 15951–15956 (2010).
7. J. J. Zhu, Y. Qin, M. Zhao, L. Van Aelst, R. Malinow, *Cell* **110**, 443–455 (2002).
8. S. Impey *et al.*, *Neuron* **21**, 869–883 (1998).
9. A. E. West, E. C. Griffith, M. E. Greenberg, *Nat. Rev. Neurosci.* **3**, 921–931 (2002).
10. K. C. Martin *et al.*, *Neuron* **18**, 899–912 (1997).

11. K. Deisseroth, P. G. Mermelstein, H. Xia, R. W. Tsien, *Curr. Opin. Neurobiol.* **13**, 354–365 (2003).
12. C. D. Harvey *et al.*, *Proc. Natl. Acad. Sci. U.S.A.* **105**, 19264–19269 (2008).
13. M. Matsuzaki, N. Honkura, G. C. R. Ellis-Davies, H. Kasai, *Nature* **429**, 761–766 (2004).
14. G. M. Thomas, R. L. Huganir, *Nat. Rev. Neurosci.* **5**, 173–183 (2004).
15. See materials and methods and other supplementary materials on *Science* Online.
16. J. Noguchi, M. Matsuzaki, G. C. Ellis-Davies, H. Kasai, *Neuron* **46**, 609–622 (2005).
17. C. M. Niswender, P. J. Conn, *Annu. Rev. Pharmacol. Toxicol.* **50**, 295–322 (2010).
18. T. Nakamura, J. G. Barbara, K. Nakamura, W. N. Ross, *Neuron* **24**, 727–737 (1999).
19. S. M. Dudek, R. D. Fields, *Proc. Natl. Acad. Sci. U.S.A.* **99**, 3962–3967 (2002).
20. B. Mayr, M. Montminy, *Nat. Rev. Mol. Cell Biol.* **2**, 599–609 (2001).
21. A. Besnard, B. Galan-Rodriguez, P. Vanhoutte, J. Caboche, *Front. Neurosci.* **5**, 35 (2011).
22. G. E. Hardingham, F. J. Arnold, H. Bading, *Nat. Neurosci.* **4**, 261–267 (2001).
23. A. M. Hagenston, H. Bading, *Cold Spring Harb. Perspect. Biol.* **3**, a004564 (2011).
24. P. F. Worley *et al.*, *J. Neurosci.* **13**, 4776–4786 (1993).
25. M. K. Meffert, J. M. Chang, B. J. Wiltgen, M. S. Fanselow, D. Baltimore, *Nat. Neurosci.* **6**, 1072–1078 (2003).
26. K. R. Thompson *et al.*, *Neuron* **44**, 997–1009 (2004).
27. A. Karpova *et al.*, *Cell* **152**, 1119–1133 (2013).
28. K. Tanaka, G. J. Augustine, *Neuron* **59**, 608–620 (2008).
29. H. Makino, R. Malinow, *Neuron* **72**, 1001–1011 (2011).
30. M. De Roo, P. Klauser, D. Muller, *PLOS Biol.* **6**, e219 (2008).
31. M. Fu, X. Yu, J. Lu, Y. Zuo, *Nature* **483**, 92–95 (2012).
32. A. Govindarajan, I. Israely, S.-Y. Huang, S. Tonegawa, *Neuron* **69**, 132–146 (2011).
33. A. Losonczy, J. K. Makara, J. C. Magee, *Nature* **452**, 436–441 (2008).
34. S. Gasparini, J. C. Magee, *J. Neurosci.* **26**, 2088–2100 (2006).
35. C. D. Harvey, K. Svoboda, *Nature* **450**, 1195–1200 (2007).
36. J. Goldberg, K. Holthoff, R. Yuste, *Trends Neurosci.* **25**, 433–435 (2002).



**Acknowledgments:** We thank A. West, S. Dudek, S. Soderling, K. Tanaka, and G. Augustine for discussion; N. Hedrick and L. Colgan for comments on the manuscript; A. Wan for preparing cultured slices; and D. Kloetzer for laboratory management. This study was funded by Howard Hughes Medical Institute, National Institute of Mental Health, and National Institute of Neurological Disorders and Stroke. The authors made the following contributions: S.Z. and R.Y. designed experiments, S.Z. collected the majority of the data, E.D.A. performed the GCaMP imaging with pharmacological inhibitors, P.P.-B. performed the patch clamp experiments, S.Z. and R.Y. analyzed the data and wrote the paper, and all authors discussed the results and commented on the manuscript.


**Supplementary Materials**

www.sciencemag.org/content/342/6162/1107/suppl/DC1
Materials and Methods
Figs. S1 to S8
References (*37*–*49*)


6 September 2013; accepted 17 October 2013
10.1126/science.1245622


# Neural Activity in Human Hippocampal Formation Reveals the Spatial Context of Retrieved Memories


**Jonathan F. Miller,[1]* Markus Neufang,[2]* Alec Solway,[3] Armin Brandt,[2] Michael Trippel,[2] Irina Mader,[2] Stefan Hefft,[2] Max Merkow,[3] Sean M. Polyn,[3] Joshua Jacobs,[1] Michael J. Kahana,[3]†‡ Andreas Schulze-Bonhage[2]†‡**



**In many species, spatial navigation is supported by a network of place cells that exhibit increased firing whenever an animal is in a certain region of an environment. Does this neural representation of location form part of the spatiotemporal context into which episodic memories are encoded? We recorded medial temporal lobe neuronal activity as epilepsy patients performed a hybrid spatial and episodic memory task. We identified place-responsive cells active during virtual navigation and then asked whether the same cells activated during the subsequent recall of navigation-related memories without actual navigation. Place-responsive cell activity was reinstated during episodic memory retrieval. Neuronal firing during the retrieval of each memory was similar to the activity that represented the locations in the environment where the memory was initially encoded.**


When one encounters an old friend and remembers the time they last met, often the place of meeting and surrounding circumstances come to mind. This is the hallmark of episodic memory: the capacity to store and later retrieve memories that are bound to a particular place and time (*1*). Theories of episodic memory posit that the brain supports this ability by continually maintaining an updated representation of the current spatiotemporal context, which is a neural representation of space, time, and other aspects of one's current cognitive milieu (*2*). When the brain forms a new episodic memory, these theories predict that the content of the experience becomes associated with the current spatial and temporal context. When the memory is retrieved, this prior context is partially reinstated, focusing one's thoughts on the time and place of the remembered episode. This reinstatement not only provides the phenomenological experience of remembering, but also helps to cue other memories experienced within the same or related contexts.

Although it is well established that the hippocampus and surrounding medial-temporal-lobe (MTL) structures play a central role in the formation and retrieval of context-mediated memories (*3*–*5*), we know far less about how these memory processes manifest in the activities of individual MTL neurons. Much of what is known about the neural coding properties of hippocampal and MTL neurons comes from studies of rodent spatial navigation, where individual neurons respond preferentially at specific locations within a given contextually defined spatial environment (*6*, *7*). Similar neuronal responses have also been identified in the human hippocampus during virtual spatial navigation (*8*, *9*). The context-dependent firing of these neurons (*10*, *11*) and their dependence on the animal's goal state or past history of experienced cues (*12*, *13*) have led some to speculate that the neural representation of space in the hippocampus is part of a broader network of neurons that encode episodic memories more generally (*14*–*17*). This hypothesis suggests that the same neural structures and computations that enable the learning of a spatial layout via place-cell activity also facilitate the encoding of episodic memories. However, according to a prominent alternative account, the spatial coding functions of the hippocampus are part of a context module that operates independently of the computations that encode the content of a memory (*18*, *19*).

We designed a virtual-reality memory game in which participants played the role of a delivery person, driving through a virtual town and delivering items to stores. Our participants were patients with drug-resistant epilepsy who were implanted with depth electrodes to localize the focus of their seizures and to map cognitive function in surrounding healthy tissue. In an initial phase of the game, participants explored the town using a computer controller to navigate from store to store as they attempted to learn the layout of the environment illustrated in Fig. 1A. After this initial familiarization phase, during which participants visited each store twice, a series of "delivery days" began. On each delivery day, participants were instructed to travel from store to store, visiting 13 randomly chosen stores (of the 16 total) in a randomly determined order. Upon their arrival at each store, participants were presented with an item [either visually for 2 s for participants one to five or aurally for participants six and seven (*20*)]. Upon arrival at the final (13th) store, no item was presented. Instead, the screen


[1]Drexel University, Philadelphia, PA 19104, USA. [2]Epilepsy Center, University Medical Center, Freiburg, Germany. [3]University of Pennsylvania, Philadelphia, PA 19104, USA.

*These authors contributed equally to this work.
†These authors contributed equally to this work.
‡Corresponding author. E-mail: andreas.schulze-bonhage@uniklinik-freiburg.de (A.S.-B.); kahana@psych.upenn.edu (M.J.K.)

went black and participants were prompted to vocally recall as many of the 12 delivered items as they could remember in any order (participants recalled 5.2 items, on average). After being given 90 s for free recall, participants could advance to a new delivery day, in which they would deliver a distinct but randomly determined set of items to a random sequence of 13 stores and then attempt to recall the new set of items. Consistent with earlier work (*21*), participants exhibited a significant ($P = 0.008$) tendency to consecutively recall items delivered to more spatially proximate locations (see supplementary text).

We first sought to identify patterns of neuronal activity that represented participants' location within the virtual town. We identified place-responsive cells as the neurons that exhibited significantly increased firing at a particular location in the virtual environment (*20*). Figure 2A depicts the activity of one example place-responsive cell, which increased its firing rate when the participant was positioned at a location on the left side of the virtual environment and facing north. The majority of the identified place-responsive cells were direction-dependent (72%) and did not exhibit significant place fields when direction of traversal was not taken into account. This is similar to earlier findings of directionally oriented place cells in environments with clearly defined routes, in contrast to open environments, where omnidirectional place cells are prevalent (*8*, *22*). These directionally oriented place cells were not generally responsive to place-invariant view information (see supplementary text). Figure 2B shows the firing rate of a place-responsive cell from the entorhinal cortex, which activated at a location in the south part of the environment during eastward movements. In total, we identified 95 place-responsive cells, making up 25.6% of all observed neurons. There were significant numbers of place-responsive cells in the hippocampus, entorhinal cortex, and amygdala and in anterior MTL regions of ambiguous localization (*20*) (binomial test with $P < 0.01$ for each region) (Fig. 2C and tables S1 and S2).

To determine whether spontaneous retrieval of items during free recall reinstated the spatial context associated with the item's encoding, we calculated the neural similarity between ensemble place-responsive cell activity during navigation and during item retrieval [see (*20*) and fig. S1 for further details]. We partitioned the environment into three regions for each recalled item: regions close to the delivery location, regions of intermediate distance, and regions that were far from the delivery location. We then asked whether the ensemble place-cell activity at the time of retrieval was more similar to navigational epochs that were closer to the delivery location. A high degree of similarity would indicate the reinstatement of the spatial context associated with the item. To protect against potential confounding between item and spatial context, we excluded navigational epochs surrounding the delivery of an item.

We found significant spatial context reinstatement surrounding the time of item vocalization (time course illustrated in Fig. 3A). The level of neural similarity between recall activity and navigation activity was ordered such that areas of the environment near an item's encoding location exhibited the highest similarity scores, intermediate spatial distances exhibited middling similarity scores, and far spatial distances exhibited the lowest similarity scores (this effect was strongest over the interval of –300 to 700 ms, illustrated

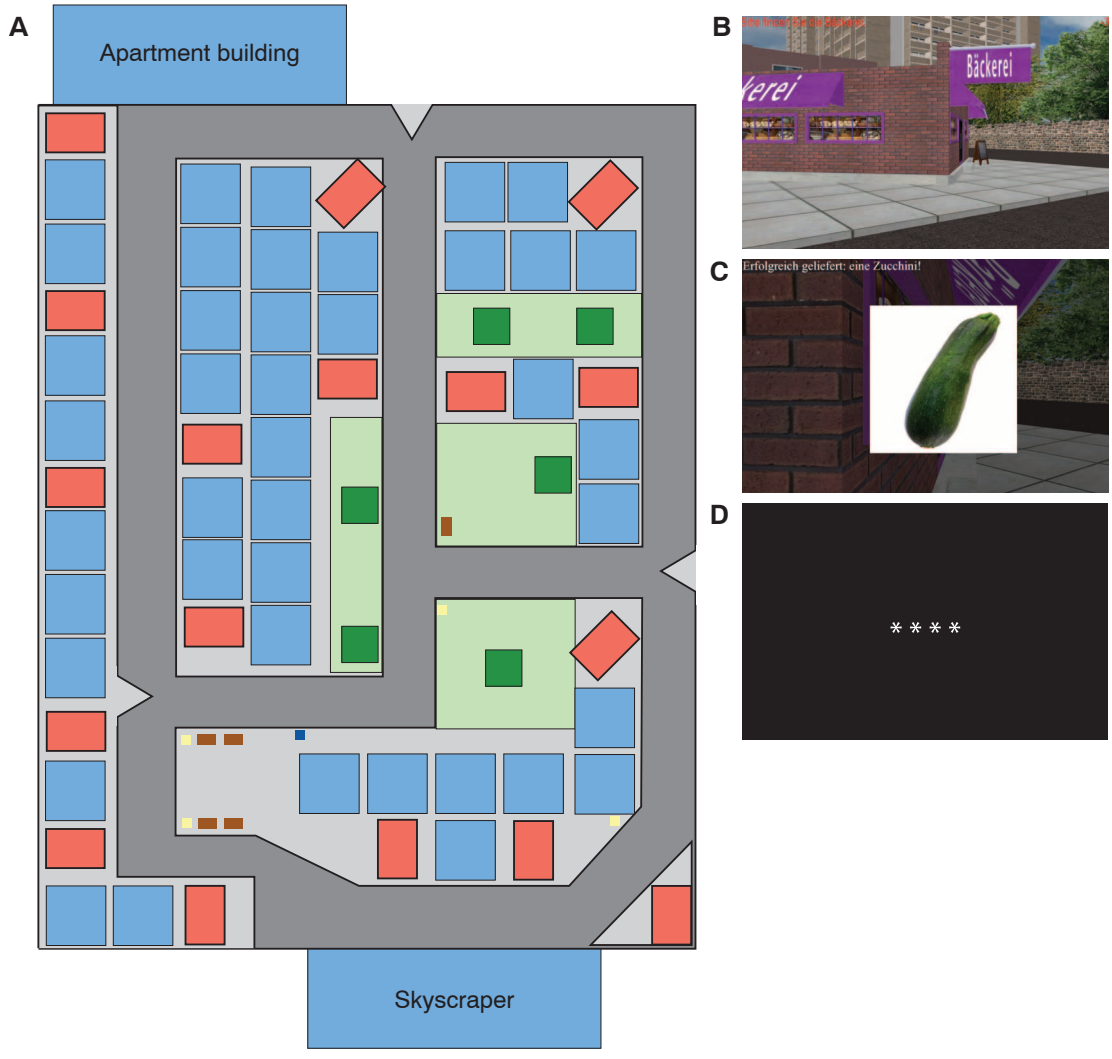


**Fig. 1. The behavioral task.** (**A**) Overhead map of the virtual environment. Red rectangles, store locations; blue squares, locations of nonstore buildings; green areas, grass and trees; small dark blue, brown, and yellow boxes; mailboxes, benches, and street lights. (**B**) An example storefront that a participant might encounter. (Translation of text at top left: "Please find the bakery.") (**C**) The presentation of an item (a zucchini) upon arrival at the target store (bakery). (Translation of text at top left: "Successfully delivered: a zucchini.") (**D**) The initiation of the recall period, as indicated by a black screen with asterisks.

in Fig. 3B). An analysis of variance (ANOVA) indicated a significant effect of distance on the level of neural similarity ($F_{2,300} = 7.6$, $P < 0.001$). Performing this latter analysis across participants rather than recall events revealed that neural similarity within the near distance bin was significantly greater than that within the far distance bin (Fig. 3C) [$t(5) = 4.0$, $P = 0.009$].

During the spontaneous recall of an item, place-responsive cells exhibited firing patterns similar to those shown during exploration of the region of the town where the item was previously delivered. Thus, recalling an episodic memory involves recovery of its spatial context, as seen in the activity of place-responsive cells in the human hippocampal formation and surrounding MTL regions. If the item delivery occurred in or near a cell's place field, characterized by a firing rate that is significantly higher than the baseline level, then recalling the item should also produce an increase in firing rate. We calculated the firing rate of place-responsive cells when participants were navigating inside and outside of each cell's place field, as well as the firing rate when participants recalled items that were presented near to or far from each cell's respective place field (Fig. 4) [see (*20*) and fig. S2 for further details]. The average in-field firing rate (3.8 Hz) was substantially higher than the out-of-field firing rate [1.9 Hz; $t(32) = 5.9$, $P < 10^{-5}$]. The average firing rate during the recall of items presented near a place field was 2.2 Hz, which was significantly higher than the 1.8-Hz firing rate during recall of items presented far from a place field [$t(32) = 2.2$, $P = 0.03$].

Unlike traditional list-recall studies of episodic memory, in which items unfold only in time, the present experiment provided a distinct spatial context for each item. This allowed us to leverage the spatial-coding properties of hippocampal neurons in the study of the neural basis of episodic recollection. Spatially sensitive neural activity in the hippocampal formation became reactivated during episodic retrieval, when no visual cues were present. At the time of recall, participants simply vocalized the names of the delivered items in the order in which they came to mind, yet the neurons responsive to spatial information reactivated during the time just before and during vocalization. This reactivation implies that each experienced item is bound to its spatial context, which in turn may be reinstated when the item comes to mind during recall.

Because human neural recordings are rarely possible, little is known about the neural substrates of spontaneous verbal recall. Nonetheless, several recent studies have established the general phenomena of content reinstatement, whereby the attributes of an item at encoding become reinstated just before recall. This has been shown for human hippocampal neurons that are selective for taxonomic categories, or possibly individual items (*23*), and also for distributed patterns

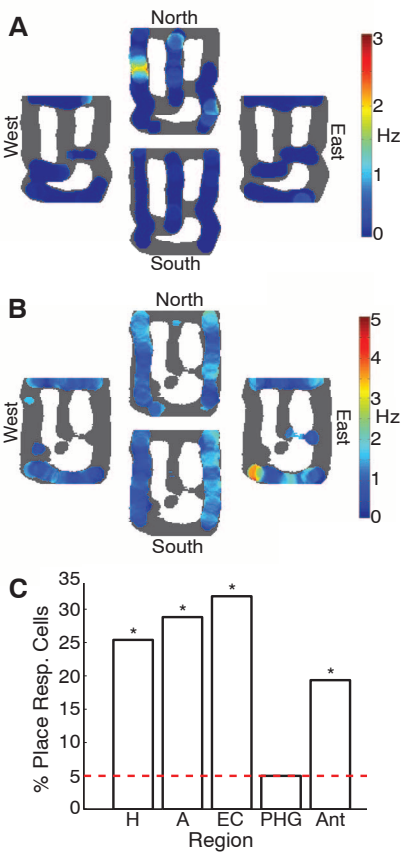


**Fig. 2. Place-responsive cells.** (**A**) Firing-rate map for a cell responsive to northward traversals located in participant six's hippocampus, shown separately for each cardinal direction. Gray represents all areas traversed by the participant, regardless of the direction of travel. (**B**) A cell responsive to eastward traversals recorded from participant one's entorhinal cortex. (**C**) Regional distribution of place-responsive cells in the entire data set of 371 single units (H, hippocampus; A, amygdala; EC, entorhinal cortex; PHG, parahippocampal gyrus; Ant, anterior medial temporal lobe). The red dashed line indicates the false-positive rate of 5%. Asterisks denote brain regions where the number of place-responsive cells significantly exceeded chance levels.

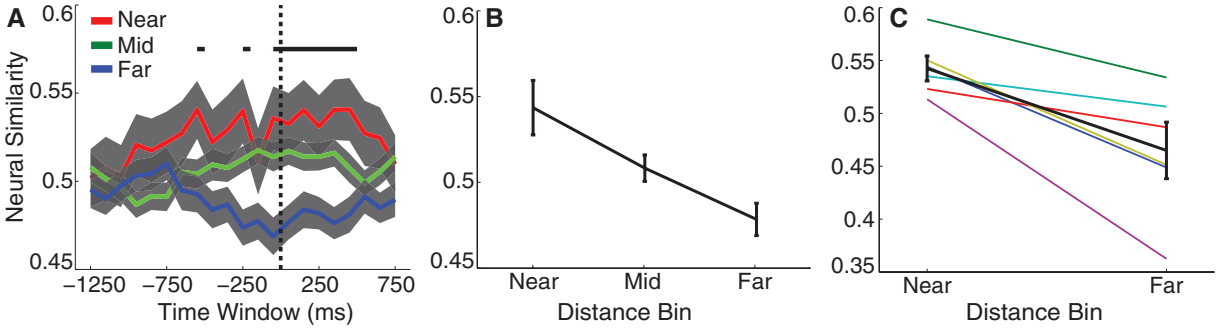


**Fig. 3. Spatial context reinstatement.** (**A**) Time courses of neural similarity between ensemble place-cell activity during navigation and during item recall are shown for near, middle, and far spatial distance bins. Time courses, shown relative to recall onset, were computed in overlapping 500-ms windows (*x* values indicate the center of the window). Similarity is defined as the cosine of the angle between ensemble activity during recall and navigation, normalized as a rank score (*20*). Shaded regions indicate SEM across recalled items. The horizontal bar indicates statistically significant time points, as determined by ANOVA with a false-discovery rate–adjusted significance threshold of 0.017. The vertical dotted line at 0 ms denotes the onset of the vocalization. (**B**) Average neural similarity for near, middle, and far spatial distance bins is shown for the time period of −300 to 700 ms relative to recall onset. Error bars indicate SEM across recalled items. (**C**) Neural similarity for near and far spatial distance bins for each of the included participants (thin colored lines) and the participant average (thick black line) is shown for the time period of −300 to 700 ms relative to recall onset. Error bars indicate SEM across participants.

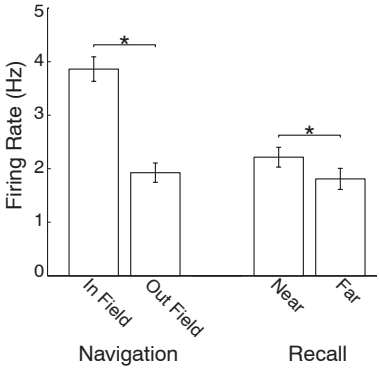


**Fig. 4. Place-responsive cell activity during navigation and recall. (Left)** Navigation. "In Field" indicates the average place-responsive cell firing rate when navigating within a cell's place field, whereas "Out Field" indicates the average place-responsive cell firing rate at locations outside of a place field ($*P < 10^{-5}$). **(Right)** Recall. "Near" indicates the average place-responsive cell firing rate in the time period from 1.5 s before to 1 s after recall onset of items that were initially presented in or close to the center of a place field. In contrast, "Far" represents the average place-responsive cell firing rate in the same time window for recall of items that were initially presented far from the center of a place field ($*P = 0.03$). Error bars indicate SEM.

of intracranial electroencephalography and hemodynamic activity (*24*, *25*). Reinstatement is not specific to an individual item but also activates neighboring items, as would be expected if those neighboring items provide an abstract temporal context for the recalled item (*26*, *27*). Such a temporal context signal may be reflected in the recent discovery of individual neurons in the rodent hippocampus that appear to encode the relative times of behaviorally important events (*28*, *29*).

Our finding that spontaneous recall of an item reactivates its spatial context provides direct neural evidence for theories of episodic memory that postulate context reinstatement as the basis for recollection (*2*, *30*). This result also implies that the spatial coding identified with the hippocampal place-cell system is part of a more general engine of episodic memory in which items become associated with their spatiotemporal contexts, and retrieval of items reinstates those contexts to help cue other context-appropriate memories.

### References and Notes


1. E. Tulving, *Elements of Episodic Memory* (Oxford Univ. Press, New York, 1983).
2. S. M. Polyn, M. J. Kahana, *Trends Cogn. Sci.* **12**, 24–30 (2008).
3. W. B. Scoville, B. Milner, *J. Neurol. Neurosurg. Psychiatry* **20**, 11–21 (1957).
4. H. Eichenbaum, *Neuron* **44**, 109–120 (2004).
5. L. Davachi, *Curr. Opin. Neurobiol.* **16**, 693–700 (2006).
6. J. O'Keefe, L. Nadel, *The Hippocampus as a Cognitive Map* (Oxford Univ. Press, New York, 1978).
7. B. L. McNaughton, F. P. Battaglia, O. Jensen, E. I. Moser, M.-B. Moser, *Nat. Rev. Neurosci.* **7**, 663–678 (2006).
8. A. D. Ekstrom *et al.*, *Nature* **425**, 184–188 (2003).
9. J. Jacobs, M. J. Kahana, A. D. Ekstrom, M. V. Mollison, I. Fried, *Proc. Natl. Acad. Sci. U.S.A.* **107**, 6487–6492 (2010).
10. R. U. Muller, J. L. Kubie, *J. Neurosci.* **7**, 1951–1968 (1987).
11. S. Leutgeb, J. K. Leutgeb, M. B. Moser, E. I. Moser, *Curr. Opin. Neurobiol.* **15**, 738–746 (2005).
12. E. R. Wood, P. A. Dudchenko, R. J. Robitsek, H. Eichenbaum, *Neuron* **27**, 623–633 (2000).
13. J. Ferbinteanu, M. L. Shapiro, *Neuron* **40**, 1227–1239 (2003).
14. H. Eichenbaum, P. Dudchenko, E. Wood, M. Shapiro, H. Tanila, *Neuron* **23**, 209–226 (1999).
15. G. Buzsáki, *Hippocampus* **15**, 827–840 (2005).
16. M. W. Howard, M. S. Fotedar, A. V. Datey, M. E. Hasselmo, *Phys. Rev.* **112**, 75–116 (2005).
17. G. Buzsáki, E. I. Moser, *Nat. Neurosci.* **16**, 130–138 (2013).
18. L. Davachi, J. P. Mitchell, A. D. Wagner, *Proc. Natl. Acad. Sci. U.S.A.* **100**, 2157–2162 (2003).
19. E. L. Hargreaves, G. Rao, I. Lee, J. J. Knierim, *Science* **308**, 1792–1794 (2005).
20. Materials and methods are available as supplementary materials on *Science* Online.
21. J. F. Miller, E. M. Lazarus, S. M. Polyn, M. J. Kahana, *J. Exp. Psychol. Learn. Mem. Cogn.* **39**, 773–781 (2013).
22. R. U. Muller, E. Bostock, J. S. Taube, J. L. Kubie, *J. Neurosci.* **14**, 7235–7251 (1994).
23. H. Gelbard-Sagiv, R. Mukamel, M. Harel, R. Malach, I. Fried, *Science* **322**, 96–101 (2008).
24. J. R. Manning, M. R. Sperling, A. Sharan, E. A. Rosenberg, M. J. Kahana, *J. Neurosci.* **32**, 8871–8878 (2012).
25. S. M. Polyn, V. S. Natu, J. D. Cohen, K. A. Norman, *Science* **310**, 1963–1966 (2005).
26. J. R. Manning, S. M. Polyn, G. H. Baltuch, B. Litt, M. J. Kahana, *Proc. Natl. Acad. Sci. U.S.A.* **108**, 12893–12897 (2011).
27. M. W. Howard, I. V. Viskontas, K. H. Shankar, I. Fried, *Hippocampus* **22**, 1833–1847 (2012).
28. E. Pastalkova, V. Itskov, A. Amarasingham, G. Buzsáki, *Science* **321**, 1322–1327 (2008).
29. C. J. MacDonald, K. Q. Lepage, U. T. Eden, H. Eichenbaum, *Neuron* **71**, 737–749 (2011).
30. S. M. Polyn, K. A. Norman, M. J. Kahana, *Psychol. Rev.* **116**, 129–156 (2009).


**Acknowledgments:** This work was sponsored by NIH grant MH-061975, the Brain and Behavior Research Foundation, German Research Foundation (Deutsche Forschungsgemeinschaft) grant SFB 780-TP3, and Federal Ministry of Education and Research (Bundesministerium für Bildung, Wissenschaft, Forschung und Technologie, Germany) grant BCNT TP B3. We are most grateful to J. Stein and H. Urbach for help with localizing electrode locations in postoperative magnetic resonance imaging. We thank the patients and their families for their participation in this research.

### Supplementary Materials

www.sciencemag.org/content/342/6162/1111/suppl/DC1
Materials and Methods
Supplementary Text
Figs. S1 to S3
Tables S1 and S2
References

31 July 2013; accepted 28 October 2013
10.1126/science.1244056

# BTBD3 Controls Dendrite Orientation Toward Active Axons in Mammalian Neocortex

**Asuka Matsui, May Tran, Aya C. Yoshida, Satomi S. Kikuchi, Mami U, Masaharu Ogawa, Tomomi Shimogori***

Experience-dependent structural changes in the developing brain are fundamental for proper neural circuit formation. Here, we show that during the development of the sensory cortex, dendritic field orientation is controlled by the BTB/POZ domain–containing 3 (BTBD3). In developing mouse somatosensory cortex, endogenous Btbd3 translocated to the cell nucleus in response to neuronal activity and oriented primary dendrites toward active axons in the barrel hollow. Btbd3 also directed dendrites toward active axon terminals when ectopically expressed in mouse visual cortex or normally expressed in ferret visual cortex. BTBD3 regulation of dendrite orientation is conserved across species and cortical areas and shows how high-acuity sensory function may be achieved by the tuning of subcellular polarity to sources of high sensory activity.

Proper neural circuit development is important for the newborn animal to receive, process, and respond to information from the external sensory environment. This process critically depends on the patterning of individual neurons to shape the postsynaptic dendritic field for assembly with presynaptic axons. Dendritic remodeling is a conserved process in which postsynaptic dendrites are pruned in response to presynaptic activity during metamorphosis in *Drosophila* (*1*) and during the development of hippocampal CA1, cerebellar Purkinje cells, and retinal ganglion cells in mouse (*2*). In the rodent primary somatosensory cortex, layer IV spiny stellate neurons are concentrated around barrel walls, forming cell-sparse barrel hollows and pyramidal neuron dense septa that delineate individual barrels. In mouse somatosensory barrel cortex, spiny stellate neurons orient their dendrites toward barrel hollows during the first postnatal week to enable efficient synapse formation with thalamocortical axons from the ventrobasal thalamic nucleus (*3*). Neuronal activity and monoamine uptake in the synaptic junction contribute to this process (*4*, *5*). We pursued the mechanism of dendrite orientation by

RIKEN Brain Science Institute, Laboratory for Molecular Mechanisms of Thalamus Development, 2-1 Hirosawa Wako, Saitama 351-0198, Japan.

*Corresponding author. E-mail: tshimogori@brain.riken.jp

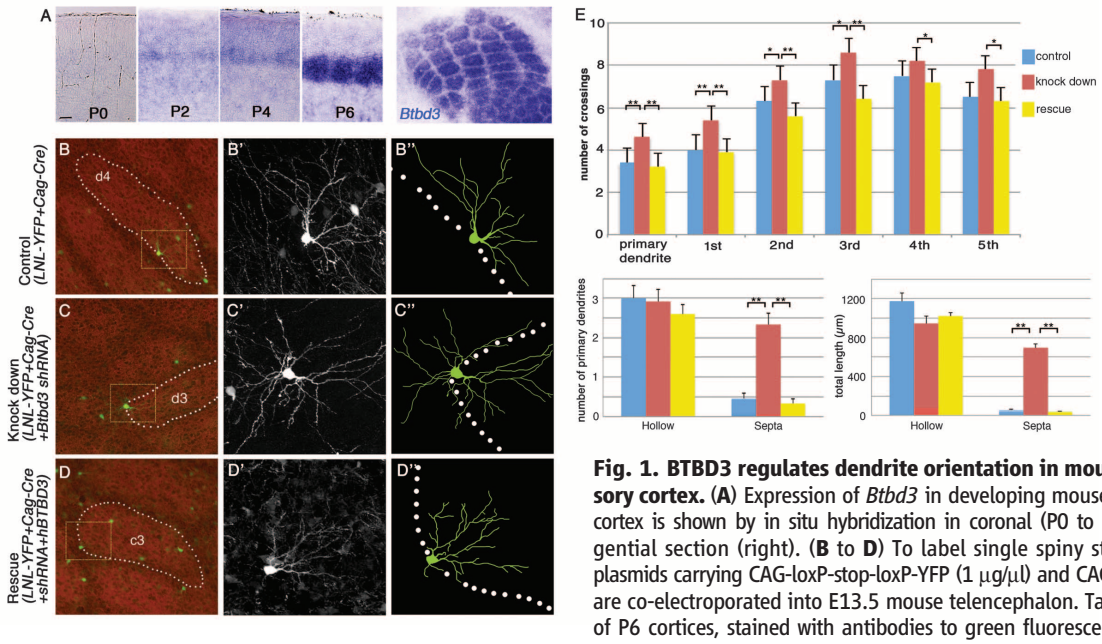


**Fig. 1. BTBD3 regulates dendrite orientation in mouse somatosensory cortex.** (**A**) Expression of *Btbd3* in developing mouse somatosensory cortex is shown by in situ hybridization in coronal (P0 to P6) and P6 tangential section (right). (**B** to **D**) To label single spiny stellate neurons, plasmids carrying CAG-loxP-stop-loxP-YFP (1 μg/μl) and CAG-Cre (0.1 ng/μl) are co-electroporated into E13.5 mouse telencephalon. Tangential section of P6 cortices, stained with antibodies to green fluorescent protein (GFP) and vGlut2 to reveal the location of barrels and sparsely labeled spiny stellate neurons. (**B′** to **D′** and **B″** to **D″**) Confocal images and corresponding schematic traces of neurons indicated by the yellow box in (B) to (D). (**E**) Quantification of dendritic parameters of spiny stellate cells. Sholl analysis: Histograms represent the mean number of dendrites crossing concentric rings drawn at 10-μm intervals from the cell soma (schema in fig. S2). Dendrite distribution is analyzed by counting primary dendrites in the barrel hollow and the barrel septa, respectively. Quantification of dendritic length is also demonstrating dendrite distribution. Analysis of variance (ANOVA) shows a significant difference in Btbd3 knock-down cells compared with control and rescue cells. **P* < 0.05, ***P* < 0.01, *t* test. Scale bars are 150 μm in (A); 50 μm in (B), (C), and (D); and 12.5 μm in (B′), (C′), and D′.

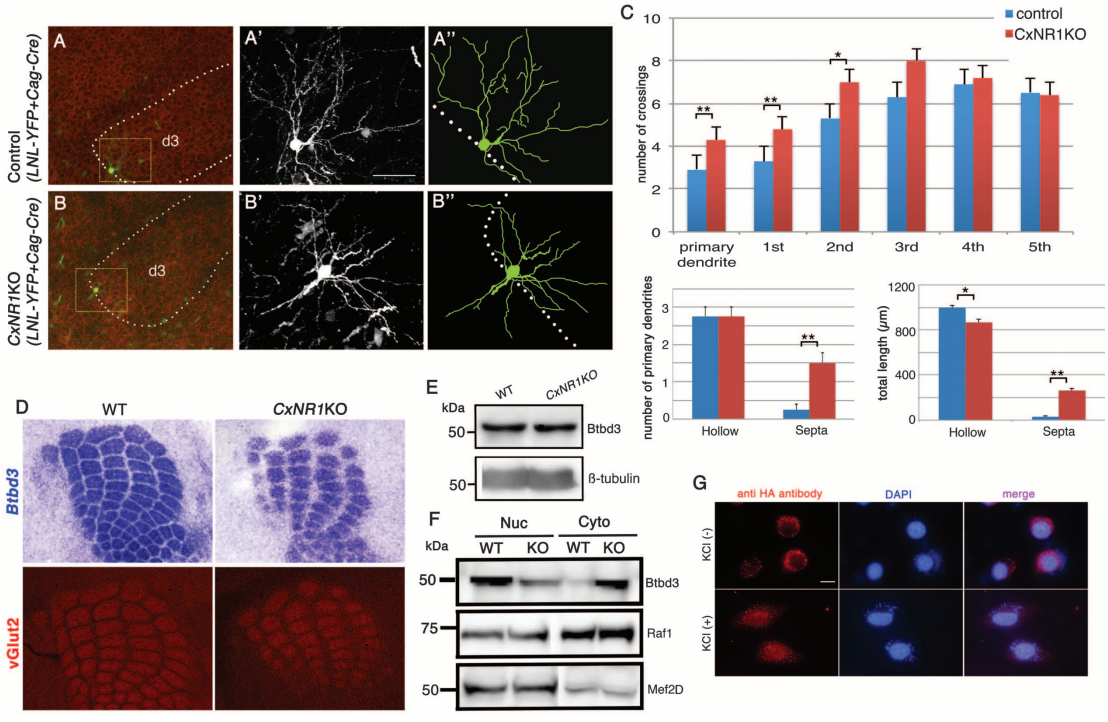


**Fig. 2. Neuronal activity–dependent nuclear translocation of BTBD3 is required for proper dendritic patterning.** (**A** and **B**) Tangential sections of P6 cortices of wild-type (WT) (A) and CxNR1KO (B), stained with antibodies to GFP and vGlut2 after sparse labeling of spiny stellate neurons by YFP electroporation at E13.5. (**A′** to **B″**) Confocal images and corresponding schematic traces of neurons. (**C**) Dendrite distribution is quantified by Sholl analysis, distribution of primary dendrites, and dendritic length. **P* < 0.05, ***P* < 0.01, *t* test. (**D**) Expression of *Btbd3* by in situ hybridization and immunostaining of antibodies to vGlut2 in tangential sections of WT and CxNR1KO cortices at P6. (**E**) Western blot analysis of BTBD3 protein from somatosensory cortex. (**F**) Western blot analysis of BTBD3 in nuclear (Nuc) and cytosolic (Cyto) cellular fractions. Markers for the cytosolic (Raf1) and nuclear fraction (Mef2D) are indicated. (**G**) Depolarization of the Neuro2A cell line promotes Btbd3-HA nuclear translocation. Scale bars are 150 μm in (A) and (B); 50 μm in (A′), (A″), (B′), and (B″); 500 μm in (D); and 10 μm in (G).

searching for molecules with selective expression in mouse somatosensory cortex and found that BTB/POZ domain–containing 3 (*Btbd3*) is localized exclusively in spiny stellate neurons during barrel formation (Fig. 1A). The BTB/POZ (Broad complex, Tramtrack, and Bric-à-brac/Poxvirus and zinc finger) proteins comprise a family of putative transcription factors with essential roles in development, differentiation, and oncogenesis (*6*). The BTB/POZ domain mediates homo- and/or heterodimerization in a transcriptional repression complex by the recruitment of co-repressors (*7*). The BTB domain is also contained within proteins such as Abrupt, which controls dendrite formation in *Drosophila* (*8*, *9*). We hypothesized that the observed *Btbd3* expression in spiny stellate neurons of the mouse somatosensory cortex could regulate the formation of dendritic field patterning.

In early postnatal somatosensory cortex, *Btbd3* mRNA is not expressed at postnatal day (P) 0 (Fig. 1A); however, weak expression is observed at P2, coincident with innervation by thalamocortical axons into layer IV cortex, followed by a barrel-like expression pattern established over the next few days (Fig. 1A and fig. S1). To test the function of BTBD3 in somatosensory neurons, we transfected a Btbd3 short hairpin–mediated RNA (shRNA) construct by in utero electroporation, resulting in ~70% reduction in gene expression compared with control brain (fig. S2). We imaged wild-type spiny stellate neurons with confocal microscopy at P6, which is electroporated with yellow fluorescent protein (YFP)–expressing plasmid at embryonic day 13.5 (E13.5), and observed on average 3 to 4 primary dendrites (Fig. 1E) with a unidirectional orientation (Fig. 1, B to B″). With Btbd3 knockdown, there was an increase in the number of primary dendrites and misoriented dendrites (Fig. 1, C to C″ and E). The altered dendritic morphology was rescued by a human BTBD3 construct, the expression of which is not suppressed by the shRNA (fig. S2), suggesting that the observed defects are due to a specific suppression of Btbd3 by the shRNA (Fig. 1, D to D″ and E). In early postnatal mouse brain development, spiny stellate neuron morphology undergoes a transient increase in the number of primary dendrites without a preferred orientation (fig. S2), and the time at which the greatest number of nonpolarized dendrites is evident (P2) correlates with the onset of *Btbd3* expression in the barrel (Fig. 1A).

Neuronal activity from thalamocortical axons is required for morphological changes in dendrites of spiny stellate cells in the somatosensory cortex (*10*–*12*). Therefore, we examined *Btbd3* expression in the NMDAR1 (N-methyl-D-aspartate receptor) cortex-specific conditional mutant mouse, where spiny stellate neurons have disoriented dendritic fields (Fig. 2, A to C) (*13*). In the somatosensory cortex of these mice at P6, although thalamocortical axons had extensive arbors compared with wild type, their terminals in cortical layer IV were arranged in normal, barrel-like clus-

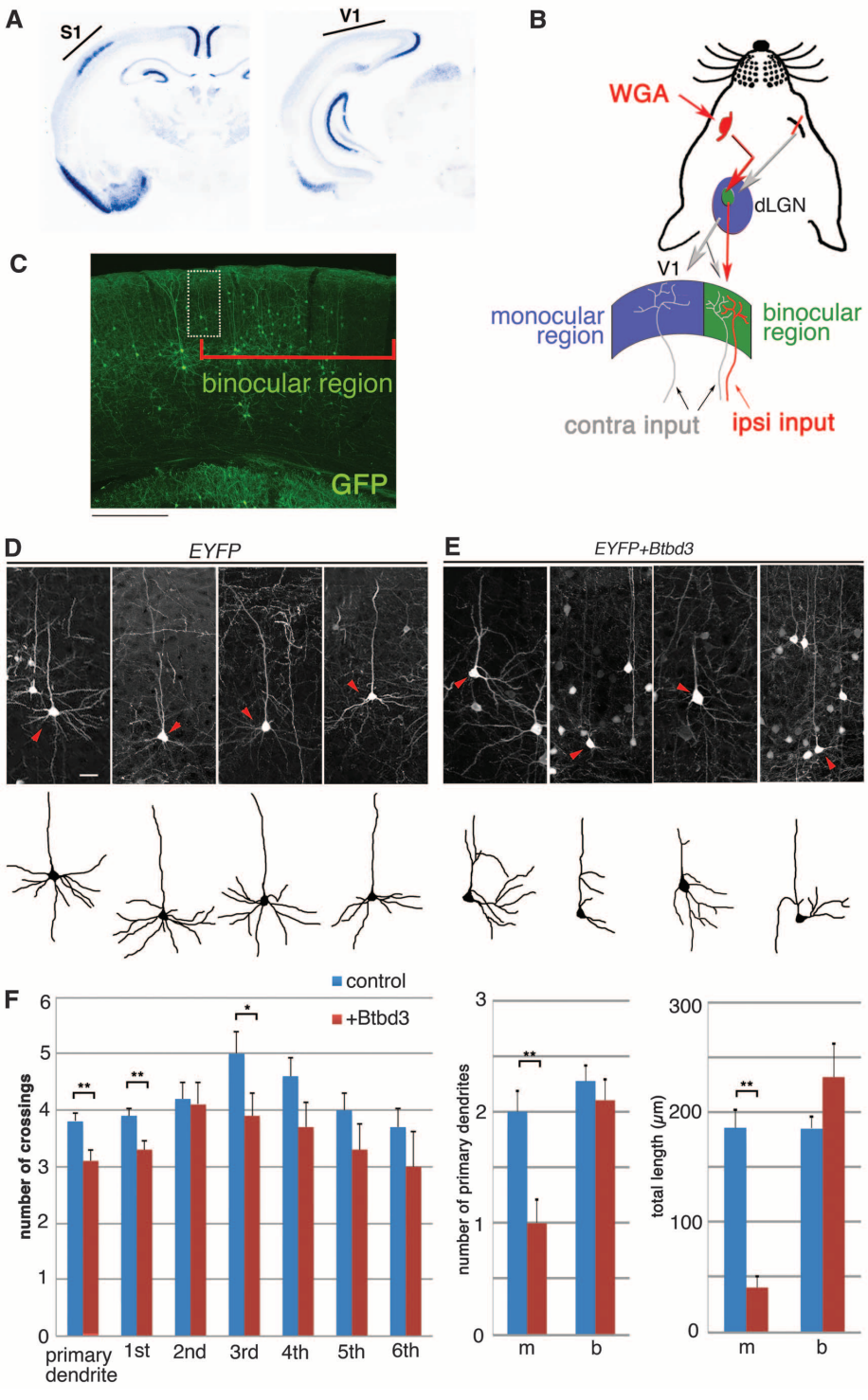


**Fig. 3. Ectopic BTBD3 orients the dendritic field in mouse visual cortex.** (**A**) In situ hybridization of *Btbd3* in the mouse somatosensory and visual cortexes at P6. (**B**) Schema of the experimental procedure. In utero electroporation was conducted at E13.5 in the occipital lobe. Pups were raised to P14, and the contralateral eye was enucleated for monocular enucleation (ME). (**C**) GFP antibody staining of the binocular region of the YFP-transfected brain. The binocular region is indicated by the red bracket, and analyzed neurons are indicated by the yellow box. (**D** and **E**) Confocal images and corresponding schematic traces of neurons (red arrowhead) in control (D) and *Btbd3*-transfected neurons (E). (**F**) Dendrite distribution was quantified by Sholl analysis, distribution of primary dendrites, and dendritic length. *$P < 0.05$, **$P < 0.01$, *t* test. m, monocular region; b, binocular region. Scale bars are 1 mm in (A), 200 μm in (C), and 20 μm in (D) and (E).

ters (*14*) containing normal *Btbd3* expression (Fig. 2D). Total BTBD3 protein levels in somatosensory cortex did not differ between control and NMDAR1 mutant mice (Fig. 2E). However, the subcellular localization of BTBD3 in wild-type brain partitioned to the nuclear fraction, whereas BTBD3 in mutant brain was found selectively in the cytosolic fraction (Fig. 2F). To study subcellular localization dynamics, we tagged Btbd3 with

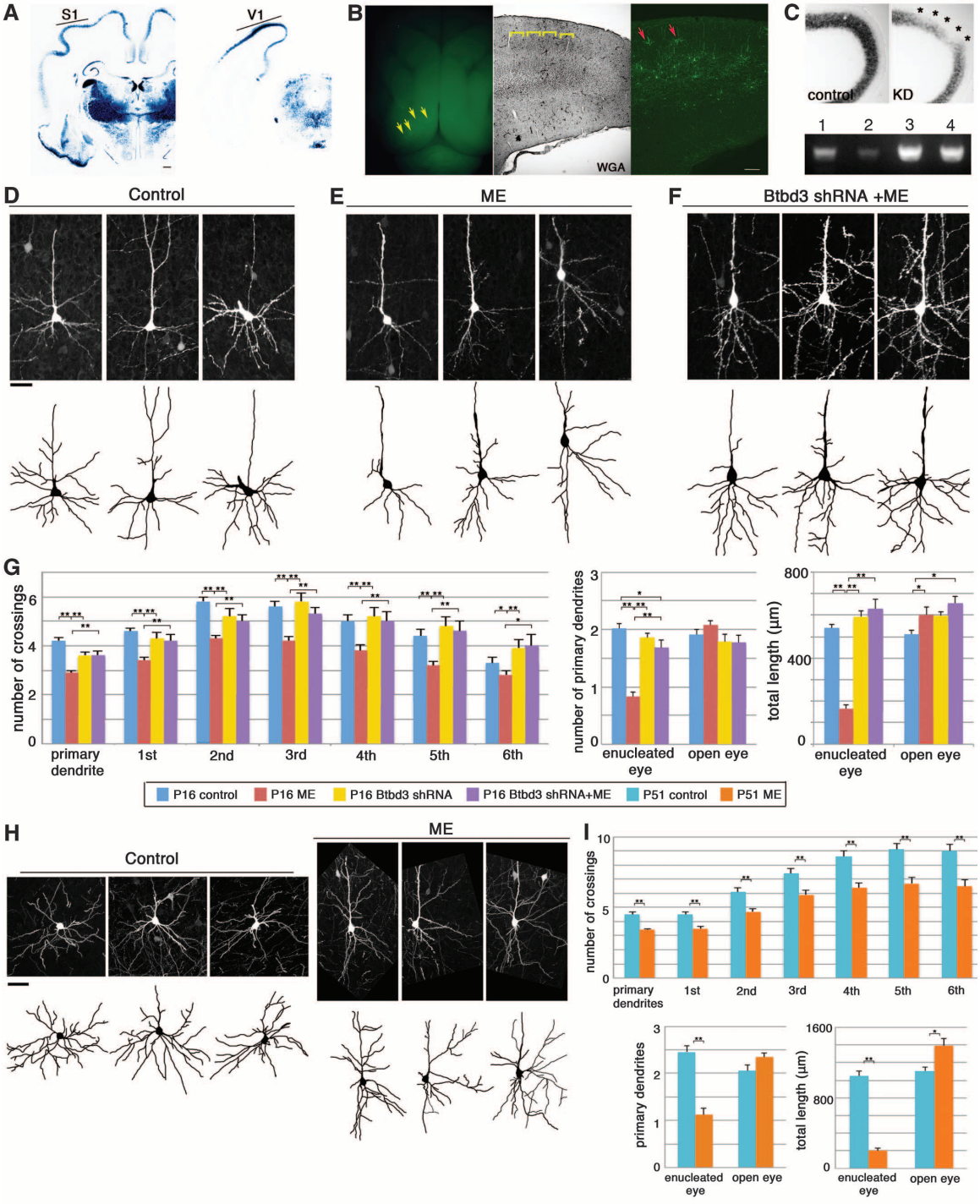


**Fig. 4. BTBD3 controls dendrite orientation in ferret visual cortex.** (**A**) In situ hybridization of *BTBD3* in the ferret brain at P16. (**B**) Dorsal view of P16 ferret brain that shows transfected neurons in the visual cortex (yellow arrows, left). The WGA-positive axon terminus is observed in the primary visual cortex (yellow bracket, middle). Positions of analyzed YFP-positive layer IV neurons are indicated by red arrows (right). (**C**) Reduction of *BTBD3* mRNA by shRNA electroporation was tested by in situ hybridization (top, asterisks), and by quantitative real-time fluorescence polymerase chain reaction, (bottom). Lane 1, *BTBD3* in control brain; lane 2, *BTBD3* in shRNA electroporated knock-down brain; lane 3, *B-ACTIN* in control brain; lane 4, *B-ACTIN* in shRNA electroporated knock-down brain. (**D** to **F**) Confocal images and schematic traces of neurons in control (D), 3 days after monocular enucleation (E) and monocular enucleation brain after *BTBD3* knock-down (F). (**G**) Dendrite distribution was quantified by Sholl analysis, distribution of primary dendrites, and dendritic length. $*P < 0.05$, $**P < 0.01$, *t* test. (**H**) Dendrite morphology in control brain and monocular enucleation brain were observed at P51. (**I**) Dendrite distribution was quantified by Sholl analysis, distribution of primary dendrites, and dendritic length. $*P < 0.05$, $**P < 0.01$, *t* test. Scale bars are 1 mm in (A), 250 μm in (B) and (C), 25 μm in (D) to (F), and 50 μm in (H).

hemagglutinin (HA) and transfected Neuro2A cells (Fig. 2G). Under control, nonstimulating conditions, Btbd3-HA was localized in the cytoplasm, but after KCl depolarization, Btbd3-HA had translocated to the nucleus (Fig. 2G). Based on these results, we conclude that neuronal activity triggers the translocation of BTBD3 from the cytosol to the nucleus, where it may control transcriptional programs to trim excess dendrites in developing mouse somatosensory cortex.

We adopted a gain-of-function approach to investigate whether BTBD3 can remodel dendrite orientation toward active axons by ectopic expression of BTBD3 in mouse primary visual cortex, which does not express BTBD3 nor mediate high-acuity vision (Fig. 3A). After electroporating *Btbd3* into primary visual cortex at E13.5, the contrast of neuronal activity was increased in the binocular region with monocular enucleation and eyelid suturing to effect visual deprivation at P14 before eye opening (Fig. 3B). After 4 days, we analyzed cortical organization by trans-synaptic wheat germ agglutinin (WGA) injected into the ipsilateral eye (Fig. 3C). To determine whether BTBD3 could reorient the dendritic field in visual cortex toward the binocular region, which contains active ipsilateral inputs, YFP-positive neurons close to the WGA-positive binocular region were observed (Fig. 3C). In control YFP-expressing neurons, basal dendrites showed a symmetrical branched pattern (Fig. 3D). In contrast, *Btbd3*-electroporated cortical neurons showed a highly polarized, unidirectional dendrite pattern directed toward the binocular region (Fig. 3E). We analyzed the number of primary dendrites and the distribution of the dendrites on the right and left side in YFP-positive neurons (Fig. 3F). In control brain (15 neurons from three animals), the average number of primary dendrites was significantly higher than in *Btbd3*-electroporated neurons (24 neurons from four animals), suggesting that dendrite removal was stimulated in these cells (Fig. 3F). To show that neurons had a unidirectional dendritic field, we quantified the number of dendrites in the monocular region (silenced area) and binocular region (active region) and showed that neurons ectopically expressing BTBD3 have fewer dendrites in the low neural activity area (Fig. 3F). These results support the conclusion that BTBD3 preferentially orients dendritic processes toward active axon terminals in vivo.

*BTBD3* is expressed strongly in the primary visual cortex of neonatal common marmoset (*Callithrix jacchus*), a brain region that mediates high-acuity vision via ocular dominance columns (*15*). This observation suggested a conserved function for BTBD3 in dendritic remodeling in the visual cortex of animals with high-resolution vision mediated by ocular dominance columns (*16*, *17*). To test this hypothesis, we analyzed *BTBD3* expression in developing ferret primary visual cortex (*18*, *19*) where Btbd3 is observed in visual cortex layer IV neurons (Fig. 4A). High-resolution dendrite morphology in the ferret visual cortex was achieved by targeted electroporation (Fig. 4B, yellow arrows). WGA was injected into the contralateral eye to label ocular dominance columns (Fig. 4B, yellow bracket) and their peripheral neurons (Fig. 4B, red arrows). Btbd3 shRNA was transfected into the ferret visual cortex to reduce endogenous *BTBD3* expression (Fig. 4C). The basal dendrites of control cortical neurons showed a symmetrical pattern, but after monocular enucleation, an asymmetric morphology was observed, with neurons observed to orient their dendrites toward the open eye column (Fig. 4, D and E). To determine whether BTBD3 regulates dendrite orientation, Btbd3 shRNA was co-electroporated with YFP into visual cortex, followed by monocular enucleation. There were no morphological differences observed, similar to the control non–monocular enucleation group, suggesting that BTBD3 is required for dendrite remodeling toward active axon terminals (Fig. 4, F and G). To address whether the changes in dendrite orientation in the early postnatal developmental critical period were transient or persistent, we assessed dendritic morphology at P51 (*20*). In control brain, apical dendrites were shorter and difficult to distinguish from basal dendrites (*21*), and the complexity of dendritic branching was increased. However, the number of primary dendrites and the unilateral morphology of the basal dendrites remained similar to those during P16 (Fig. 4, G and I). These results further support a role for BTBD3 in dendrite orientation toward afferents with high neuronal activity.

Dendritic refinement is known to operate by cytoskeletal modification and membrane-initiated activity-dependent pathways through molecules including neurexin-neuroligin, Wnt, and EphB-ephrinB (*22*–*24*). Here, we define a role for Btbd3 as a nuclear regulator of activity-dependent dendritic refinement. In mouse, *Btbd3* is also expressed in the mouse olfactory bulb, piriform cortex, and hippocampus (Fig. 3), where dendritic field formation of mitral cells, piriform pyramidal cells, and CA1 neurons are altered or delayed when presynaptic input is altered (*25*, *26*). This observation suggests that BTBD3 or a related family member may control dendrite remodeling in different areas of the brain. We propose that the acquisition of BTBD3 expression in a specific cortical area could provide the ability to streamline the flow of sensory information in neuronal circuits by remodeling dendritic fields to optimally respond to sensory activity. In consequence, high-acuity sensory function may have been enabled by the evolution of BTBD3 and related BTB/POZ family members in cortical development. This idea is supported by the selective expression of *BTBD3* in the visual and auditory cortex of the common marmoset, a species that relies heavily on high-acuity vocal and visual communication for survival (*17*), and in the mouse, where it is expressed in high-acuity tactile and olfactory areas but not in low-acuity visual cortex. Thus, BTBD3 expression and function may help to index the evolution of precise columnar organization in many cortical regions of the mammalian brain.

## References and Notes


1. Y. N. Jan, L. Y. Jan, *Nat. Rev. Neurosci.* **11**, 316–328 (2010).
2. R. O. L. Wong, A. Ghosh, *Nat. Rev. Neurosci.* **3**, 803–812 (2002).
3. T. A. Woolsey, H. Van der Loos, *Brain Res.* **17**, 205–242 (1970).
4. C. Lebrand *et al*., *J. Comp. Neurol.* **401**, 506–524 (1998).
5. T. Iwasato *et al*., *Nature* **406**, 726–731 (2000).
6. O. M. Siggs, B. Beutler, *Cell Cycle* **11**, 3358–3369 (2012).
7. S.-U. Lee, T. Maeda, *Immunol. Rev.* **247**, 107–119 (2012).
8. K. Sugimura, D. Satoh, P. Estes, S. Crews, T. Uemura, *Neuron* **43**, 809–822 (2004).
9. W. Li, F. Wang, L. Menut, F. B. Gao, *Neuron* **43**, 823–834 (2004).
10. T. Iwasato *et al*., *Neuron* **19**, 1201–1210 (1997).
11. J. S. Espinosa, D. G. Wheeler, R. W. Tsien, L. Luo, *Neuron* **62**, 205–217 (2009).
12. N. Narboux-Nême *et al*., *J. Neurosci.* **32**, 6183–6196 (2012).
13. A. Datwani, T. Iwasato, S. Itohara, R. S. Erzurumlu, *Mol. Cell. Neurosci.* **21**, 477–492 (2002).
14. L. J. Lee, T. Iwasato, S. Itohara, R. S. Erzurumlu, *J. Comp. Neurol.* **485**, 280–292 (2005).
15. H. Mashiko *et al*., *J. Neurosci.* **32**, 5039–5053 (2012).
16. A. Kossel, S. Löwel, J. Bolz, *J. Neurosci.* **15**, 3913–3926 (1995).
17. Y. Nakagami, A. Watakabe, T. Yamamori, *Front. Neural Circuits* **7**, 43 (2013).
18. H. Kawasaki, L. Iwai, K. Tanno, *Mol. Brain* **5**, 24 (2012).
19. J. C. Crowley, L. C. Katz, *Science* **290**, 1321–1324 (2000).
20. M. Sur, C. A. Leamey, *Nat. Rev. Neurosci.* **2**, 251–262 (2001).
21. E. M. Callaway, V. Borrell, *J. Neurosci.* **31**, 7456–7470 (2011).
22. M. Packard *et al*., *Cell* **111**, 319–330 (2002).
23. S. X. Chen, P. K. Tari, K. She, K. Haas, *Neuron* **67**, 967–983 (2010).
24. N.-J. Xu, S. Sun, J. R. Gibson, M. Henkemeyer, *Nat. Neurosci.* **14**, 1421–1429 (2011).
25. B. Bathellier, T. W. Margrie, M. E. Larkum, *J. Neurosci.* **29**, 12641–12652 (2009).
26. D. M. Lin *et al*., *Neuron* **26**, 69–80 (2000).



**Acknowledgments:** We thank C. Yokoyama, A. Kania, T. Young, and A. Terashima for critical reading. We also thank Y. Takahashi, S. Tonegawa, S. Blackshaw, and S. Itohara for providing plasmids and mouse line, and F. Matsuzaki, D. Konno, T. Suetsugu, H. Mashiko, and Y. Maeda for technical assistance. This work was supported by the RIKEN Brain Science Institute, MEXT Strategic Research Program for Brain Science (SRPBS), Center of Novel Science Initiative Brain Science Project, Funding Program for World-Leading Innovative R&D on Science and Technology (FIRST), and the Human Frontier Science Program (HFSP). M.T. is funded by the Japan-U.S. Educational Commission (Fulbright Japan).


## Supplementary Materials

www.sciencemag.org/content/342/6162/1114/suppl/DC1
Materials and Methods
Figs. S1 and S2
References (*27*–*30*)


9 August 2013; accepted 17 October 2013
Published online 31 October 2013;
10.1126/science.1244505

# Though They May Be Unaware, Newlyweds Implicitly Know Whether Their Marriage Will Be Satisfying

James K. McNulty,[1]* Michael A. Olson,[2] Andrea L. Meltzer,[3] Matthew J. Shaffer[2]

For decades, social psychological theories have posited that the automatic processes captured by implicit measures have implications for social outcomes. Yet few studies have demonstrated any long-term implications of automatic processes, and some scholars have begun to question the relevance and even the validity of these theories. At baseline of our longitudinal study, 135 newlywed couples (270 individuals) completed an explicit measure of their conscious attitudes toward their relationship and an implicit measure of their automatic attitudes toward their partner. They then reported their marital satisfaction every 6 months for the next 4 years. We found no correlation between spouses' automatic and conscious attitudes, which suggests that spouses were unaware of their automatic attitudes. Further, spouses' automatic attitudes, not their conscious ones, predicted changes in their marital satisfaction, such that spouses with more positive automatic attitudes were less likely to experience declines in marital satisfaction over time.

Getting married is typically associated with high levels of satisfaction and optimism regarding the future. But for many people, such positive sentiments are ultimately replaced by feelings of dissatisfaction and despair (*1*). When asked directly about their likelihood of success, however, newlyweds are unable to accurately predict whether they will remain satisfied or join the ranks of the unfulfilled (*2*). Indeed, spouses' strong motivations to perceive their relationship in a positive light can lead to biased evaluations of the relationship (*3*) that prevent them from accurately forecasting their fate.

But new spouses may know more than they are able to report. Although the motivation to see the relationship in a positive light may distort spouses' explicit, conscious evaluations of their relationship, their implicit, automatic evaluations of the relationship appear to be relatively impervious to such motivations (*4*, *5*). And dual-process models of social cognition suggest that how people approach and respond to others is guided not only by their conscious evaluations of those others, but also by these automatic evaluations (*6*). For example, the Motivation and Opportunity as Determinants (MODE) model of attitude-behavior processes (*7*) posits that automatic attitudes facilitate (i) attention to attitude-consistent features of attitude objects, (ii) attitude-consistent interpretations of attitude objects, and (iii) attitude-consistent behavior toward attitude objects. Accordingly, even though people may be unwilling or unable to recognize any deep-seated discontent they have toward their partners, that discontent may nonetheless shape their relationship outcomes.

Empirical research supports this perspective (*8*). In one particularly relevant set of studies (*9*), participants' automatic attitudes toward various faces were made more or less accessible (i.e., likely to be activated) through an attitude rehearsal manipulation. Then participants were again shown the faces, some of which had been changed by partially morphing them with other unseen faces. Participants whose automatic attitudes toward the original faces had been made more accessible were less likely to perceive that the faces had changed.

If newly married spouses' automatic attitudes have similar implications for their perceptions of their marriages, spouses with more positive automatic attitudes may be less likely to perceive undesirable changes in their relationships and thus more likely to maintain their initial levels of satisfaction over time. Although several studies have examined the implications of automatic attitudes for interpersonal outcomes over intervals of 1 year or less (*5*, *10*–*14*), no studies have examined the extent to which automatic attitudes predict the development of a marriage over an interval longer than 1 year; in fact, we are not aware of any study that has examined the extent to which any automatic attitude predicts any outcome over such an extended period.

To examine the extent to which spouses' initial automatic attitudes toward their partner predicted the trajectory of their marital satisfaction, we recruited 135 newlywed couples in eastern Tennessee as participants in a 4-year, eight-wave longitudinal study. We predicted that spouses with more positive automatic attitudes toward their partner would demonstrate less substantial declines in their marital satisfaction because, consistent with the MODE model, they would perceive fewer undesirable changes in the marriage.

At baseline (June 2006 to October 2007), and every 6 months for the next 4 years, both members of these couples reported their relationship satisfaction and the severity of their specific relationship problems. Also at baseline, spouses completed an explicit measure of their conscious attitudes toward the relationship and an implicit measure of their automatic attitudes toward their partner. The explicit measure was an oft-used semantic differential (*15*) that asked spouses to report the extent to which they would describe their marriage using 15 pairs of opposing adjectives (e.g., "good" versus "bad," "satisfied" versus "dissatisfied"). The implicit measure was a version of an associative priming task (*16*) that required spouses to indicate as quickly as possible the valence of positively and negatively valenced words after being exposed to 300-ms primes of photographs of their partner and various control individuals. An index of spouses' automatic attitudes was formed by subtracting the time it took them to indicate the valence of the positive words from the time it took them to indicate the valence of the negative words. Both attitude indexes were standardized before analyses. Higher scores on both measures indicate more positive attitudes. We also assessed several notable covariates: implicit and explicit self-esteem, neuroticism, automatic attitudes toward alternatives, barriers to leaving the marriage, partner facial and body attractiveness, and attachment insecurity (*17*).

A two-level analysis indicated that spouses' reports of their conscious attitudes were not correlated with their automatic attitudes [$r$ = 0.00, not significant (n.s.)], which suggests that spouses were unaware of their automatic attitudes. Consistent with other research on newlyweds (*1*), a

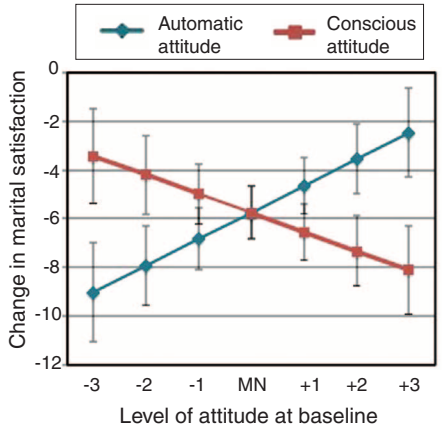


**Fig. 1. Changes in marital satisfaction as a function of automatic and conscious attitudes.** The blue line depicts the significantly positive association between automatic attitudes and changes in marital satisfaction. The red line depicts the nonsignificant association between conscious attitudes and changes in marital satisfaction. The two associations are significantly different from one another. MN, arithmetic mean.

[1]Department of Psychology, Florida State University, Tallahassee, FL 32306, USA. [2]Department of Psychology, University of Tennessee, Knoxville, TN 37996, USA. [3]Department of Psychology, Southern Methodist University, Dallas, TX 75275, USA.

*Corresponding author. E-mail: mcnulty@psy.fsu.edu

three-level growth curve analysis indicated that spouses' marital satisfaction declined significantly over the 4 years of the study [$B = -0.60$, SE = 0.11, $t(133) = -5.36$, $P < 0.001$]. The primary analysis used both indexes of attitudes to account for initial levels of and changes in marital satisfaction.

Although spouses' automatic attitudes were not significantly associated with their initial reports of marital satisfaction [$B = 0.20$, SE = 0.14, $t(250) = 1.44$, n.s.; effect size $r = 0.09$], spouses' automatic attitudes were positively associated with changes in their marital satisfaction over time [$B = 0.14$, SE = 0.07, $t(250) = 2.02$, $P = 0.044$; effect size $r = 0.13$]. The blue line in Fig. 1 depicts the significant association between automatic attitudes and changes in marital satisfaction over time. As can be seen, the more positive spouses' automatic attitudes were at baseline, the less their marital satisfaction declined over time. Notably, this effect remained significant controlling for all covariates [$B = 0.14$, SE = 0.06, $t(232) = 2.15$, $P = 0.032$; effect size $r = 0.14$].

Spouses' conscious attitudes, in contrast, were positively associated with initial levels of marital satisfaction [$B = 2.48$, SE = 0.21, $t(250) = 11.72$, $P < 0.001$; effect size $r = 0.60$] but were not significantly associated with changes in satisfaction over time [$B = -0.10$, SE = 0.06, $t(250) = -1.53$, n.s.; effect size $r = 0.10$]. For comparison purposes, the red line in Fig. 1 depicts the nonsignificant association between spouses' conscious attitudes at baseline and changes in their marital satisfaction over time. Although the association between conscious attitudes and changes in marital satisfaction was not significantly different from zero, a test that constrained that association to be equal to the positive association between automatic attitudes and changes in satisfaction indicated that the two effects were significantly different from one another [$B = 0.23$, SE = 0.08, $\chi^2(1) = 7.64$, $P < 0.01$; effect size $r = 0.17$].

We next tested whether spouses' perceptions of their marital problems mediated the effects of their automatic attitudes on changes in their marital satisfaction. This required conducting two additional analyses (*18*). In the first, we examined whether spouses' automatic attitudes predicted their perceptions of marital problems over the intervening years of the study by repeating the growth curve analysis, except this time substituting the seven reports of problem severity that preceded the predicted changes in marital satisfaction for those reports of satisfaction, and once again entering both the automatic and conscious attitude indexes to account for the level-2 intercepts and slopes. Additionally, to more rigorously demonstrate that spouses' automatic attitudes were associated with perceptions of fewer problems (rather than actually developing fewer problems), we controlled for the variance common to both partners' reports of problem severity by including spouses' partners' reports of problem severity as a time-varying covariate.

Spouses' automatic attitudes were not significantly associated with their initial perceptions of their marital problems [$B = 0.04$, SE = 0.05, $t(250) = 0.75$, n.s.; effect size $r = 0.05$]. Nonetheless, consistent with the first criterion necessary to establish mediation, spouses' automatic attitudes were negatively associated with changes in their perceptions of marital problems over time [$B = -0.04$, SE = 0.02, $t(250) = -2.44$, $P = 0.016$; effect size $r = 0.15$], indicating that spouses with more positive automatic attitudes reported perceiving fewer problems over time. Spouses' reports of their conscious attitudes were not significantly associated with changes in their perceptions of their problems [$B = 0.00$, SE = 0.02, $t(250) = 0.25$, n.s.; effect size $r = 0.02$].

In the second analysis, we examined the extent to which spouses' perceptions of their marital problems predicted changes in their marital satisfaction by entering spouses' reports of problem severity as a time-lagged level-1 predictor of satisfaction, controlling for time-lagged partner reports of problems and time-lagged reports of own satisfaction at level 1 and spouses' automatic and explicit attitudes at level 2. Consistent with the second criterion necessary to establish mediation, spouses' perceptions of their marital problems at each assessment significantly negatively predicted changes in their satisfaction from that assessment to the next [$B = -0.54$, SE = 0.15, $t(133) = -3.69$, $P < 0.001$].

Finally, we multiplied these two effects together, which yielded an indirect effect of $B = 0.02$, and estimated the 95% confidence interval (CI) for this indirect effect (0.003, 0.046), which was significant. Thus, automatic attitudes toward one's partner appear to protect marital satisfaction by desensitizing oneself to undesirable changes in the relationship.

We also estimated equivalent models testing the alternative possibility that changes in satisfaction mediated the effect of automatic attitudes on changes in perceived problems. Although automatic attitudes directly predicted changes in marital satisfaction over the first seven waves of the study [$B = 0.19$, SE = 0.08, $t(250) = 2.36$, $P = 0.019$; effect size $r = 0.15$], these reports of marital satisfaction did not predict subsequent perceptions of problems [$B = 0.01$, SE = 0.01, $t(133) = 1.41$, n.s.; effect size $r = 0.12$], and thus the indirect effect ($B = 0.002$) was not significant [95% CI, (–0.001, 0.006)].

For decades, social psychological theories have posited that the automatic processes captured by implicit measures have important implications for social outcomes (*19*). Yet few studies have demonstrated any long-term implications of automatic processes outside of the laboratory, leading some to question the relevance and even the validity of these theories (*20*–*22*). Our findings demonstrate not only the validity of automatic processes as a theoretical construct, but also their practical importance. Although spouses' explicit reports of their conscious attitudes toward their relationships at the time of marriage were unrelated to changes in their satisfaction over time, their automatic reactions to 300-ms exposures of pictures of their partner positively predicted changes in their relationship satisfaction over the course of 4 years. In sum, although they may be largely unwilling or unable to verbalize them, people's automatic evaluations of their partners predict one of the most important outcomes of their lives—the trajectory of their marital satisfaction.

### References and Notes


1. J. K. McNulty, E. M. O'Mara, B. R. Karney, *J. Pers. Soc. Psychol.* **94**, 631–646 (2008).
2. J. A. Lavner, B. R. Karney, T. N. Bradbury, *J. Fam. Psychol.* **27**, 531–540 (2013).
3. S. L. Murray *et al.*, *Psychol. Sci.* **22**, 619–626 (2011).
4. A. Dijksterhuis, L. W. Albers, K. C. Bongers, in *Attitudes: Insights from the New Implicit Measures*, R. E. Petty, R. H. Fazio, P. Briñol, Eds. (Erlbaum, Mahwah, NJ, 2009), pp. 229–250.
5. A. Scinta, S. L. Gable, *Pers. Soc. Psychol. Bull.* **33**, 1008–1022 (2007).
6. S. Chaiken, Y. Trope, Eds., *Dual-Process Theories in Social Psychology* (Guilford, New York, 1999).
7. R. H. Fazio, *Adv. Exp. Soc. Psychol.* **23**, 75–109 (1990).
8. M. A. Olson, R. H. Fazio, in *Attitudes: Insights from the New Implicit Measures*, R. E. Petty, R. H. Fazio, P. Briñol, Eds. (Erlbaum, Mahwah, NJ, 2009), pp. 19–64.
9. R. H. Fazio, J. E. Ledbetter, T. Towles-Schwen, *J. Pers. Soc. Psychol.* **78**, 197–210 (2000).
10. E. P. LeBel, L. Campbell, *J. Exp. Soc. Psychol.* **45**, 1291–1294 (2009).
11. E. P. LeBel, L. Campbell, *Soc. Psychol. Pers. Sci.* **4**, 167–174 (2013).
12. S. Lee, R. D. Rogge, H. T. Reis, *Psychol. Sci.* **21**, 857–864 (2010).
13. S. L. Murray, S. Gomillion, J. G. Holmes, B. Harris, V. Lamarche, *J. Pers. Soc. Psychol.* **104**, 305–334 (2013).
14. T. Towles-Schwen, R. H. Fazio, *J. Exp. Soc. Psychol.* **42**, 698–705 (2006).
15. C. E. Osgood, G. J. Suci, P. H. Tannenbaum, *The Measurement of Meaning* (Univ. of Illinois Press, Urbana, IL, 1957).
16. R. H. Fazio, J. R. Jackson, B. C. Dunton, C. J. Williams, *J. Pers. Soc. Psychol.* **69**, 1013–1027 (1995).
17. See supplementary materials on *Science* Online.
18. D. Tofighi, D. P. MacKinnon, *Behav. Res. Methods* **43**, 692–700 (2011).
19. R. H. Fazio, M. A. Olson, *Annu. Rev. Psychol.* **54**, 297–327 (2003).
20. H. R. Arkes, P. E. Tetlock, *Psychol. Inq.* **15**, 257–278 (2004).
21. S. Doyen, O. Klein, C. L. Pichon, A. Cleeremans, *PLOS ONE* **7**, e29081 (2012).
22. H. Pashler, N. Coburn, C. R. Harris, *PLOS ONE* **7**, e42510 (2012).


**Acknowledgments:** Supported by National Institute of Child Health and Human Development grant RHD058314A and NSF grant BCS-1251520 (J.K.M.). We thank D. Atkins, R. Baumeister, and J. Maner for their helpful comments regarding this research. Data are available from the first author upon request.

### Supplementary Materials

www.sciencemag.org/content/342/6162/1119/suppl/DC1
Materials and Methods
Tables S1 and S2
References (*23*–*28*)

12 July 2013; accepted 17 October 2013
10.1126/science.1243140

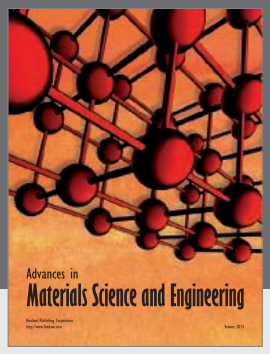


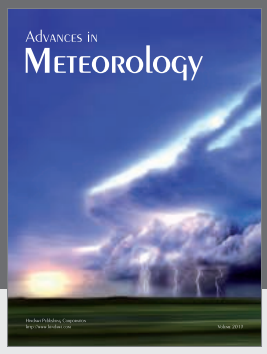


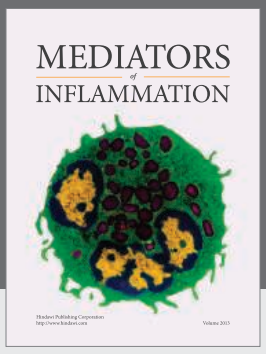


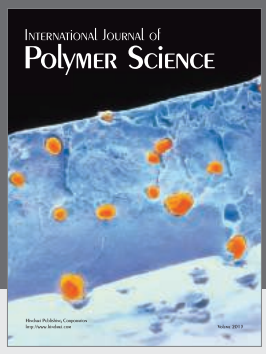


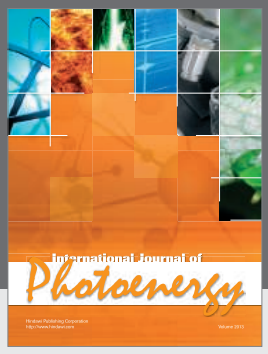


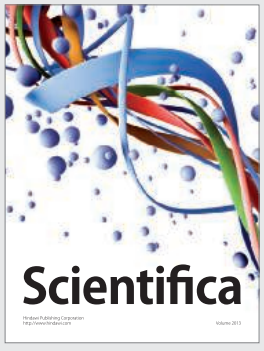



Hindawi

Submit your manuscripts at
http://www.hindawi.com


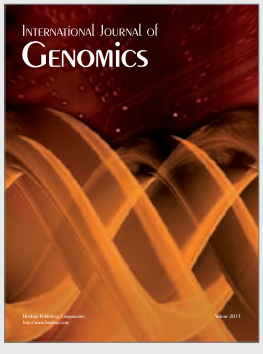




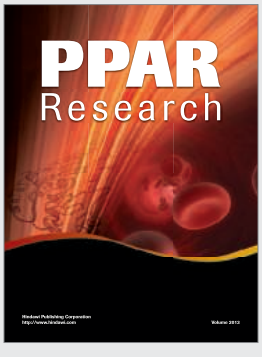


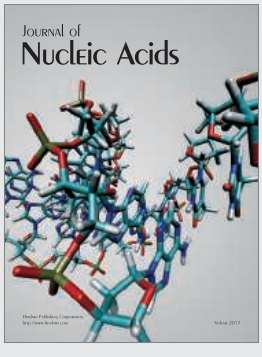


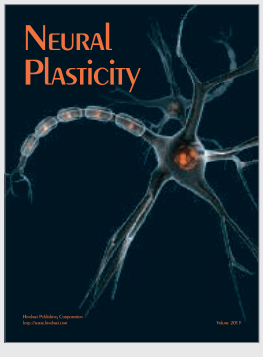


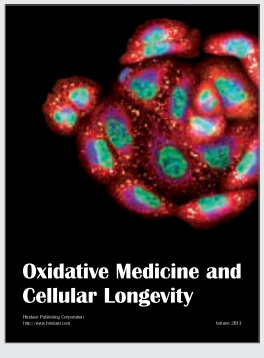


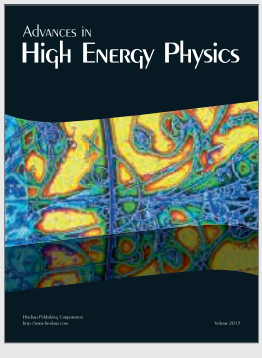


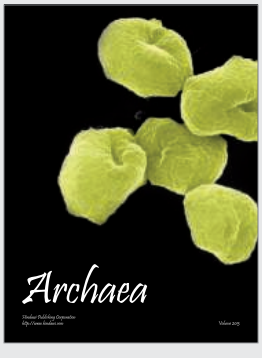



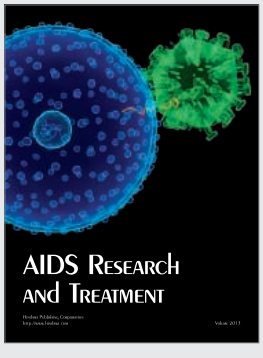

# Better results — on any sequencing platform

## Get the most from your NGS

### Discover new and innovative solutions, dedicated for use with any NGS workflow

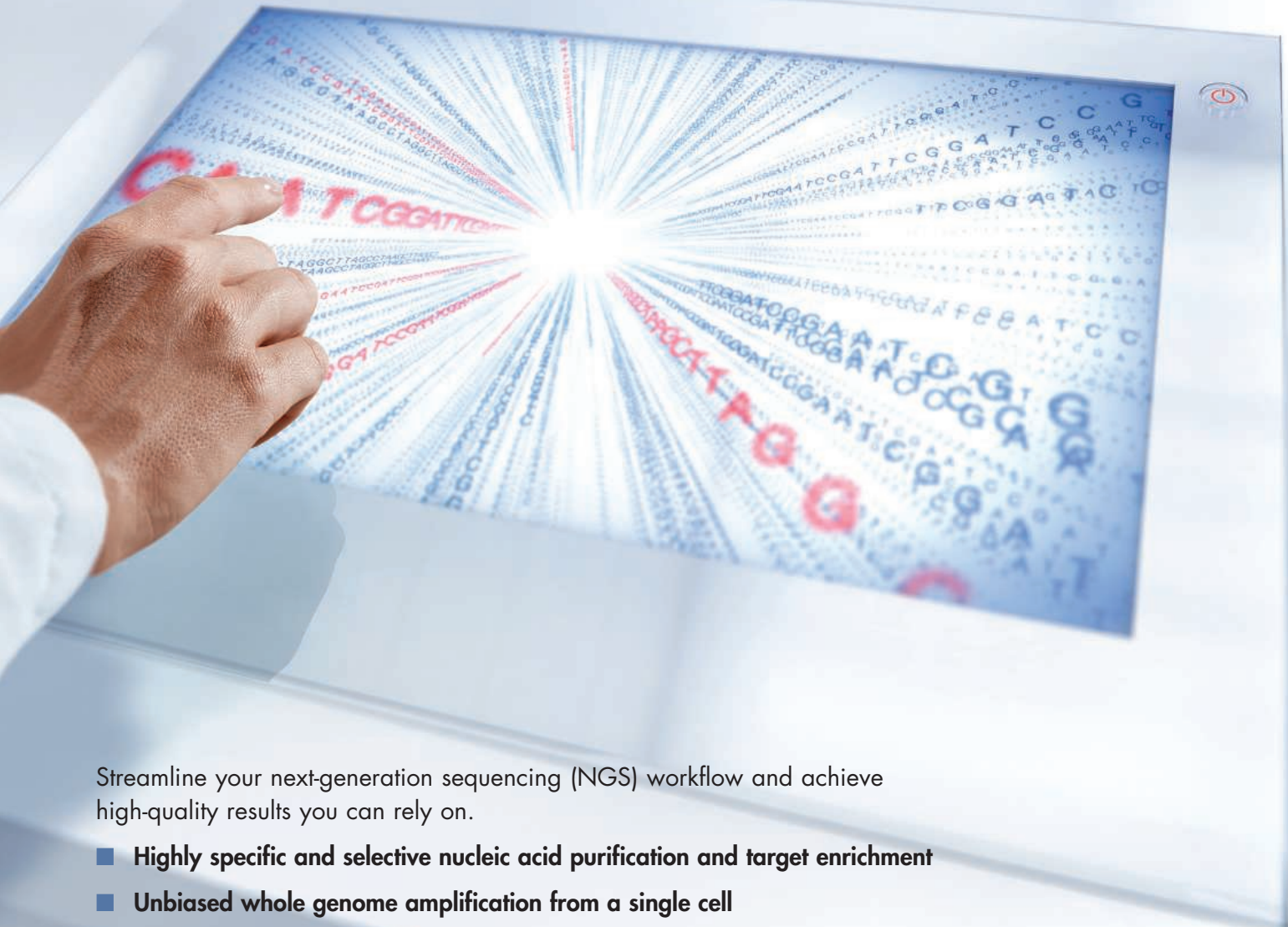

Streamline your next-generation sequencing (NGS) workflow and achieve high-quality results you can rely on.

- **Highly specific and selective nucleic acid purification and target enrichment**
- **Unbiased whole genome amplification from a single cell**
- **High DNA library yields using optimized workflows that allow ~50% time-savings**
- **Outstanding results on any sequencing platform**
- **Intuitive, knowledge-based data interpretation for deeper insight into NGS results**

Visit www.qiagen.com/goto/NGS to learn more!

QIAGEN®

Sample & Assay Technologies

NGS1113S1WW

# Science Signaling

**The Leading Journal for Cell Signaling**

Publishing key findings of broad relevance in the multidisciplinary field of cell signaling

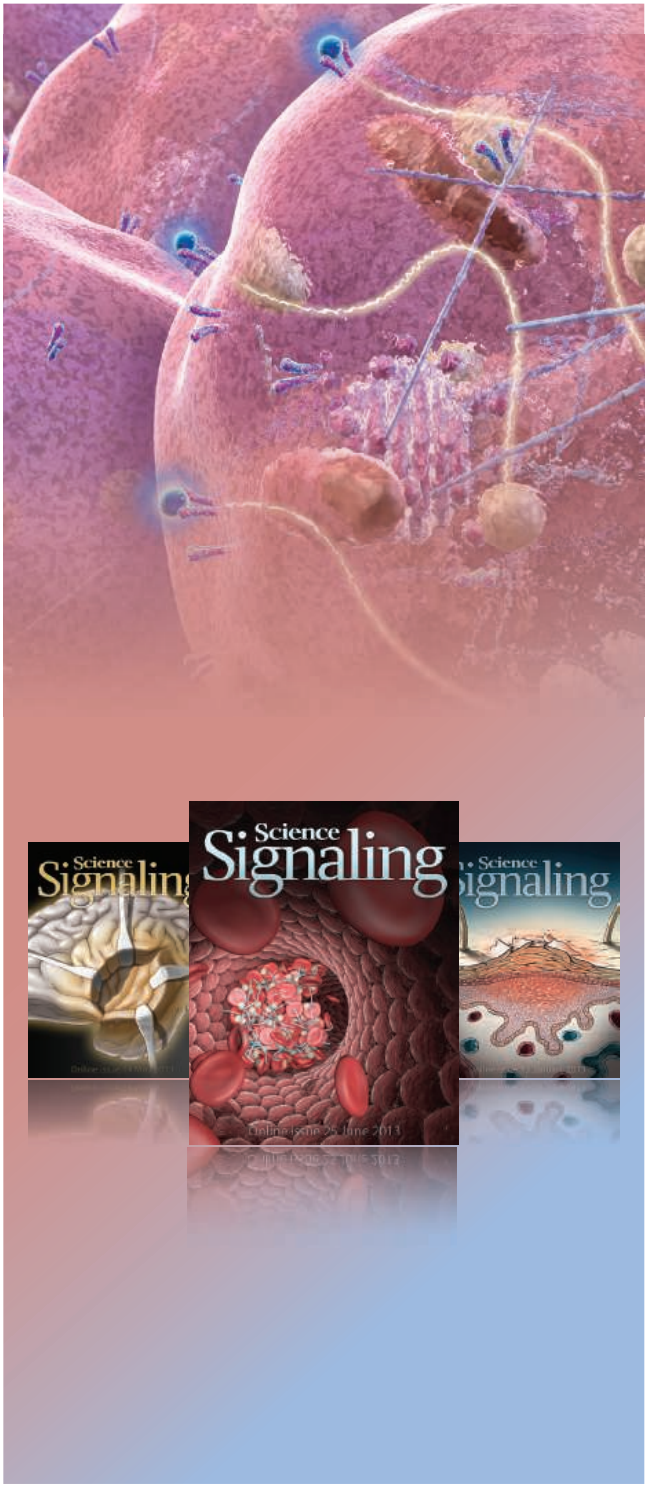


## Submit your research

ScienceSignaling.org

## Recommend to your library

ScienceOnline.org/recommend

### Join the ranks of high-profile papers published in *Science Signaling*:

**Cancer Biology**
Vemurafenib Potently Induces Endoplasmic Reticulum Stress–Mediated Apoptosis in BRAFV600E Melanoma Cells
D. Beck *et al.* (F. Meier), *Sci. Signal.* **6**, ra7 (2013)

**Neuroscience**
Requirement for Nuclear Calcium Signaling in *Drosophila* Long-Term Memory
J.-M. Weislogel *et al.* (H. Bading), *Sci. Signal.* **6**, ra33 (2013)

**Cell and Molecular Biology**
A Nontranscriptional Role for HIF-1α as a Direct Inhibitor of DNA Replication
M. E. Hubbi *et al.* (G. L. Semenza), *Sci. Signal.* **6**, ra10 (2013)

**Immunology**
Monovalent and Multivalent Ligation of the B Cell Receptor Exhibit Differential Dependence upon Syk and Src Family Kinases
S. Mukherjee *et al.* (A. Weiss), *Sci. Signal.* **6**, ra1 (2013)

**Computational and Systems Biology**
Cross-Species Protein Interactome Mapping Reveals Species-Specific Wiring of Stress Response Pathways
J. Das *et al.* (H. Yu), *Sci. Signal.* **6**, ra38 (2013)



Science Signaling
AAAS

sciencesignalingeditors@aaas.org

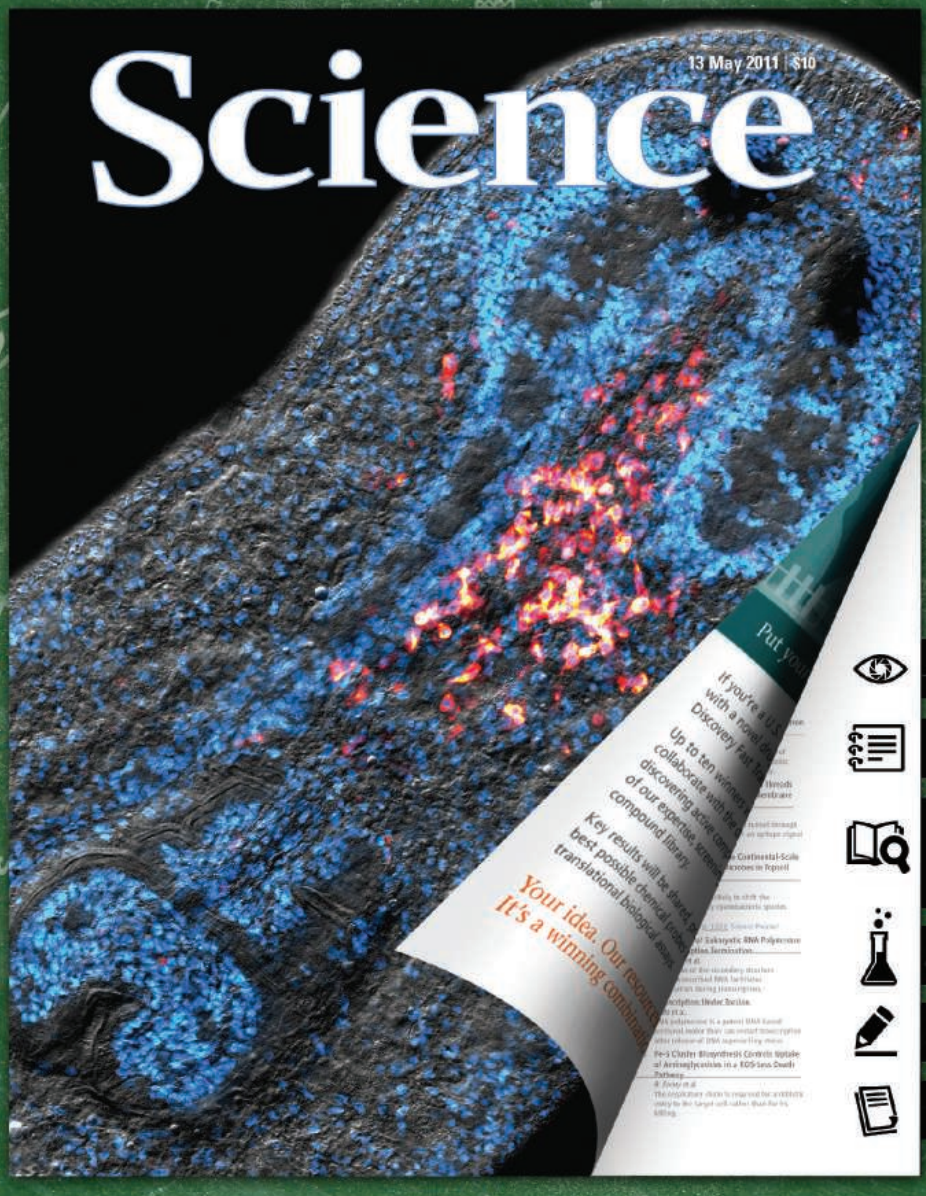


Science

Online tools to help your students analyze a professional research paper!

**Tell me and I forget. Teach me and I remember. Involve me and I learn.** -- Benjamin Franklin

Featuring over 6 research papers at any given time, *Science* in the Classroom is specifically designed to help young researchers understand the structure and workings of professional scientific research.

Learn for yourself how *Science* in the Classroom can help your students deepen their understanding of scientific research. **Visit scienceintheclassroom.org today.**

AAAS
ADVANCING SCIENCE, SERVING SOCIETY

## PERFIX REAGENT KITS


PerFix-Expose and PerFix-nc are innovative new reagent kits for intracellular staining, which minimize sample manipulation for a streamlined workflow that delivers high-quality results. Developed for use on Beckman Coulter's Gallios and Navios series flow cytometers and compatible with all Beckman Coulter Life Sciences' fluorochromes, the kits enable a clear focus on the cytoplasmic and nuclear compartments of the cell. PerFix-Expose (phospho-epitope exposure kit), which helps scientists identify and explore complex intracellular signaling pathways disrupted by cancer and other diseases, allows fluorochrome-coupled antibodies and other probes to enter into cells, their nuclei, and other cell compartments, where they bind to proteins relevant to signaling pathways that have been disrupted by disease. Cell fixation is accomplished using a cross-linking agent, while permeabilization of white blood cells and lysis of red blood cells is achieved using a detergent. A denaturing agent "unmasks" proteins bound to other proteins or DNA.

**Beckman Coulter Life Sciences**
For info: 800-742-2345 | www.beckmancoulter.com

## NOVEL GENE FUSIONS

Oncomine Next Gen Sequencing Power Tools are an analytics offering that will allow cancer researchers to explore results from in-depth analysis of next generation sequencing (NGS) data, including data from The Cancer Genome Atlas. In total, more than 4,500 paired tumor and normal samples have been analyzed to date. Oncomine NGS Power Tools constitutes a suite of software tools that enable cancer researchers to easily survey novel predicted driver mutations and gene fusions across all cancers and within two-dozen specific cancers types as well as explore simple summary analyses that integrate multiple types of gene and pathway aberrations with clinical data. In addition to basic research applications, the NGS tools also provide a foundation for specialized biomarker services to pharma and biotech customers in their efforts to evaluate NGS data for biomarker and companion diagnostic development.

**Life Technologies**
For info: 800-955-6288 | www.lifetechnologies.com

## TRANSFECTION SYSTEM

The *Trans*IT-X2 Dynamic Delivery System is an innovative polymeric system for high-efficiency nucleic acid delivery. *Trans*IT-X2 can be used for independent or simultaneous delivery of DNA and siRNA. The *Trans*IT-X2 Dynamic Delivery System offers researchers: efficiency with an exceptional broad spectrum transfection; versatility with cutting-edge delivery of plasmid DNA and/or siRNA; and technology with novel nonliposomal polymeric delivery. This system provides superior delivery of plasmid DNA and siRNA into a vast array of cell types.

**Mirus Bio**
For info: 608-229-1416 | www.thetransfectionexperts.com

## CROSSLINKERS

Ease of use and unmatched accuracy make the XL-1000 UV crosslinker ideal for many applications including: elimination of polymerase chain reaction contamination, crosslinking of DNA and RNA, nicking ethidium-bromide-stained DNA, gene mapping, RecA mutation screening and testing, ultraviolet (UV) sterilization, UV-induced polymerization, UV intensity monitoring, and many other UV-dosage applications. Researchers appreciate the XL-1000's "smart" microprocessor controller and unique, true UV-monitoring circuitry, which allows users to obtain error-free results faster, safer, and more accurately than previously possible. The Spectrolinker ensures reliable crosslinking in record time by covalently binding nucleic acids to membranes in less than 30 seconds. The UV-monitoring circuitry guarantees that the set dosage is always delivered, protecting important test results from washout damage. The Spectrolinker greatly increases the visibility of samples on autoradiograms, which results in superior analysis and extra-sharp, extremely clear, publication-quality photodocumentation. The XL-1000 has four operation modes, built-in "help" messages, and an auto-repeat function.

**Spectroline**
For info: 800-274-8888 | www.spectroline.com

## SCANNING ELECTRON MICROSCOPE

The next generation of the EVO series scanning electron microscope (SEM) is designed for material and life science applications. Customer productivity and imaging performance are dramatically increased by the SEM's workflow automation, beam deceleration technology, and class leading HD BSE detector. EVO reduces a typical workflow from over 400 steps to just 15. Workflow productivity is improved by automated image settings such as the beam alignment, magnification and focus, allowing the imaging of areas of interest in the shortest possible time. A user-friendly mid-column click-stop aperture changer is introduced for reliable and reproducible results. EVO allows imaging of exceptionally fine surface details with crisp contrast. Beam deceleration technology and a high definition BSE detector provide images rich in topographical information. The EVO series continues to offer full environmental capabilities, three chamber sizes, and class-leading X-ray geometry.

**Carl Zeiss**
For info: 800-233-2343 | www.zeiss.com

# Science Translational Medicine

**Integrating Science, Engineering, and Medicine**

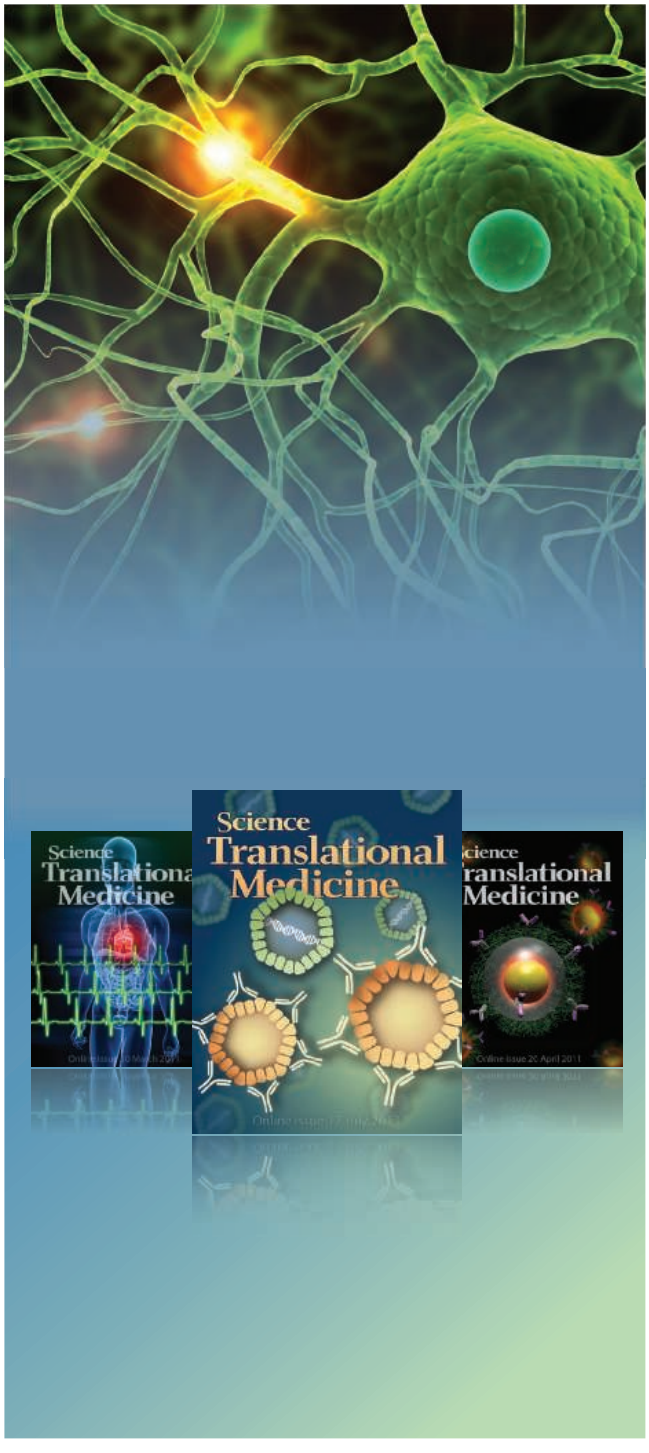


Publishing results that harness the basic sciences to advance human health in all areas of medicine

## Submit your research

ScienceTranslationalMedicine.org

## Recommend to your library

ScienceOnline.org/recommend

**Join the ranks of high-profile papers published in *Science Translational Medicine*:**

**Neurology**

A Theoretically Based Index of Consciousness Independent of Sensory Processing and Behavior

A. G. Casali *et al.* (M. Massimini), *Sci. Transl. Med.* **5** 198ra105 (2013)

**Immunology**

TGFβ Receptor Mutations Impose a Strong Predisposition for Human Allergic Disease

P.A. Frischmeyer-Guerrerio *et al.* (H. Dietz), *Sci. Transl. Med.* **5** 195ra94 (2013)

**Bioengineering**

A Human Disease Model of Drug Toxicity-Induced Pulmonary Edema in a Lung-on-a-Chip Microdevice

D. Huh *et al.* (D. Ingber), *Sci. Transl. Med.* **5** 159ra147 (2012)

**Cancer**

Genome-Wide Mutational Signatures of Aristolochic Acid and its Application as a Screening Tool

S.L. Poon *et al.* (B. T. Teh), *Sci. Transl. Med.* **5** 197ra101 (2013)

**Tissue Engineering**

Human Cartilage Repair with a Photoreactive Adhesive-Hydrogel Composite

B. Sharma *et al.* (J.J. Elisseeff), *Sci. Transl. Med.* **5** 167 ra6 (2013)



Science Translational Medicine AAAS

scitranslmededitors@aaas.org

NEW ENGLAND BioLabs® Inc.
*enabling technologies in the life sciences*

# Make ends meet.

## Gibson Assembly® Cloning Kit

New England Biolabs has revolutionized your laboratory's standard cloning methodology. The Gibson Assembly Cloning Kit combines the power of the Gibson Assembly Master Mix with NEB 5-alpha Competent *E. coli*, enabling fragment assembly and transformation in just under two hours. Save time, without sacrificing efficiency.

Making ends meet is now quicker and easier than ever before, with the Gibson Assembly Cloning Kit from NEB.

**NEBuilder™ for Gibson Assembly**

Visit **NEBGibson.com** to view the latest tutorials and to try our primer design tool.

Gibson Assembly Cloning Kit provides robust transformation efficiencies

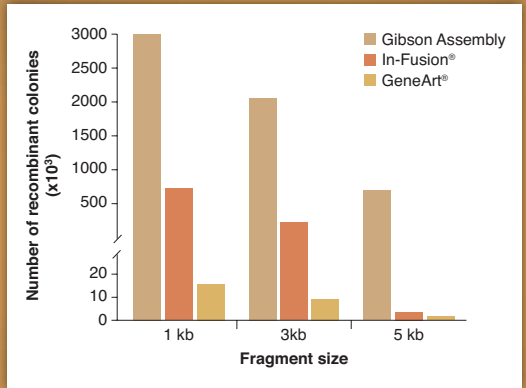


*Assembly reactions containing 25 ng of linear pUC19 vector and 0.04 pmol of each fragment were performed following individual suppliers' recommended protocols and using the competent cells provided with the kit. The total number of recombinant colonies was calculated per 25 ng of linear pUC19 vector added to the assembly reaction.*



SGI-DNA

## Meharry Medical College - Vanderbilt Ingram Cancer Center - Tennessee State University Cancer Partnership

## Senior Biostatistician

The Meharry Medical College-Vanderbilt-Ingram Cancer Center-Tennessee State University (MMC-VICC-TSU) Cancer Partnership in Nashville, TN is looking for a qualified individual for a full time faculty appointment as a Senior Biostatistician to work with cancer research investigators within the partnership institutions. This cancer partnership is in its 12th year of continuous funding by the NCI U54 grant mechanism.

**APPOINTMENT:** The successful candidate will be recruited as a tenure track/tenured faculty at Meharry Medical College at a rank that is commensurate with qualifications and experience that meet our APT guidelines. While the primary appointment at Meharry Medical College will be in the school of medicine, because this is a joint recruitment with the School of Graduate Studies and Research (SOGSR) in Meharry Medical College, the successful candidate will have a joint appointment in both schools. He/she will become a member of the Meharry Medical College-Vanderbilt-Ingram Cancer Center-Tennessee State University cancer partnership. The successful candidate will also have a either full or associate membership status at the Vanderbilt-Ingram Comprehensive Cancer Center as well as have full access to all core facilities at the cancer center. Also, the individual will have access to Bio-informatics and Biostatistics Cores in the partnership institutions.

**SPECIFIC RESPONSIBILITIES:** The Senior Biostatistician works with social science and clinical investigators on a cancer disparities research plan for the U-54 Community Outreach Program; the design and conduct of cancer disparities studies; and the evaluation, interpretation, and reporting of study results.

As part of a research team, collaborates in the preparation and review of the cancer disparities research plan. For assigned cancer disparities projects, provides statistically sound experimental design and data analysis input to meet project objectives and statistical requirements. Reviews all project protocols, authors' protocol statistical analysis sections, and generates study randomization. Reviews study methods and data collection forms to ensure protocol objectives are met and project standards are maintained. Develops study analysis plans as a team member and leads this effort for selected studies. Develops statistical programs as necessary to perform analyses and prepare data displays. Authors results sections of cancer disparities study reports. Provides support for publication of cancer disparities study results. Keeps abreast of new developments in statistics, cancer health disparities, and community engaged research through literature review, attendance at workshops and professional meetings, and consistent participation in relevant community meetings and events.

**REQUIREMENTS: Ph.D.** in Statistics/Biostatistics with at least 3-5 years of cancer disparities and/or cancer control research-related experience. Experience with statistical software packages such as SAS, SPSS and S-Plus. The individual should possess sound knowledge of theoretical and applied statistics. Possess clear understanding and commitment to community-engaged research among racially/ethnically diverse populations. Effective skills in team collaboration and communication to diverse stakeholders (academic and lay audiences) are required. Racial/ethnic minority and female candidates are encouraged to apply. Interested applicants should send full applications containing (1) current full CV, a list of references and a cover letter to: **Ms. Ketia Barnes, Senior Program Coordinator, MMC-VICC-TSU Cancer Partnership, Department of Biochemistry and Cancer Biology, Meharry Medical College, 1005 D. B. Todd Blvd, Nashville, TN 37208.** Or email application in PDF to: **kbarnes@mmc.edu**

---

## The Sarah and Daniel Hrdy Fellowship in Conservation Biology
## Department of Organismic and Evolutionary Biology
## Harvard University

***Application deadline: January 1, 2013***

The Department of Organismic and Evolutionary Biology at Harvard University invites applications or nominations for the Sarah and Daniel Hrdy Visiting Fellowship in Conservation Biology. The Hrdy Fellowship is open to faculty at any rank, and supports visits of either one or two semesters.

The Hrdy Fellowship is awarded to an individual who will engage in scientific study in the Department of Organismic and Evolutionary Biology. Recipients of this fellowship are expected to have a strong and transformative effect on the study of conservation biology at Harvard University. The research of previous Hrdy Fellows has included conservation paleobiology, marine evolution and conservation, conservation biology of amphibians and reptiles, and the impact of human activities on the environment. Information about previous fellows is available here: **http://www.oeb.harvard.edu/employment/hrdy.html**.

**Eligibility:** Applications are sought from faculty whose research focuses on contemporary issues in conservation biology. Applicants should be well positioned to conduct original, independent research and to publish their findings in peer-reviewed publications. Applicants are expected to be fluent in English and have a record of effective teaching.

**Fellowship Details:** The Hrdy Fellowship award provides a stipend of up to $80,000 per year, depending on professional status, need, and duration of the fellowship. Modest support is also available for research and travel costs. Hrdy Fellows are ordinarily employees of Harvard University during their tenure and are eligible for health insurance benefits. Fellows must be in residence for the full term of the Fellowship. Primarily, the Hrdy Fellow is expected to engage in leading-edge research, where possible in collaboration with members of the Harvard community. Additional responsibilities include a public lecture by the Fellow in any area of conservation biology. Finally, the Fellow is required to teach a one-semester, seminar-style course aimed at upper-level undergraduates (for more information on teaching, contact OEB Chair John Wakeley, at wakeley@fas.harvard.edu).

**Application Process:** Applicants should contact a faculty sponsor with whom they will collaborate, before applying. Interested individuals with general questions about the program may contact Chris Preheim, Academic Programs Coordinator, at **cpreheim@oeb.harvard.edu**.
Fellowships are awarded through a competitive review process. To be considered for a fellowship, applicants should submit a concise proposal in PDF format that includes the following:

- **Cover letter:** The cover letter should clearly state (i) the applicant's interest in the fellowship; (ii) the length of the term desired by the applicant and potential start-date; and (iii) the applicant's contact information.
- **Research Statement:** The statement should be no longer than 4 pages, single-spaced, and should clearly describe the research project. The statement should detail: (i) the nature and scope of the proposed research project, (ii) the approach and methods to be employed, (iii) how Harvard resources would be utilized, (iv) all laboratory and equipment requirements, and (v) how the project will advance knowledge about conservation biology.
- **Research Budget:** A modest level of funding is available for research and travel costs. Applicants should submit a simple, one-page budget which itemizes the research and travel costs associated with the proposed project.
- **Curriculum vitae.**
- **Three letters of recommendation:** Letters of recommendation should clearly indicate the name, title, mailing address, phone, and email address of the person providing the recommendation. Letters may be sent under separate cover, provided they meet the deadline.

All four components should be submitted to **http://academicpositions.harvard.edu/postings/5051**

*The Sarah and Daniel Hrdy Fellowship in Conservation Biology is made possible by the generosity of Sarah and Daniel Hrdy. Harvard University is an Affirmative Action/Equal Opportunity Employer and requires pre-employment reference and background screening.*

COLUMBIA | ENGINEERING
The Fu Foundation School of Engineering and Applied Science

## Faculty Positions in the Department of Chemical Engineering

Columbia Engineering's Department of Chemical Engineering at Columbia University in New York City invites applications for tenured or tenure-track faculty positions. Appointments at the assistant professor, associate professor and full professor, will be considered.

Applications are specifically sought in any area of chemical engineering research with particular emphasis on, but not limited to "big data" approaches.

Candidates must have a Ph.D. or its professional equivalent by the starting date of the appointment. Applicants for this position at the Assistant Professor and Associate Professors without tenure must have the potential to do pioneering research and to teach effectively. Applicants for this position at the tenured level (Associate or Full Professor) must have a demonstrated record of outstanding research accomplishments, excellent teaching credentials and established leadership in the field.

The successful candidate should contribute to the advancement of the department in these areas by developing an externally funded research program, contributing to the undergraduate and graduate educational mission of the Department and is expected to establish multidisciplinary research and educational collaborations with academic departments and units across Columbia University. The Department is especially interested in qualified candidates who can contribute, through their research, teaching, and/or service, to the diversity and excellence of the academic community.

For additional information and to apply, please see: http://engineering.columbia.edu/faculty-job-opportunities. Applications should be submitted electronically and include the following: curriculum-vitae including a publication list, a description of research accomplishments, a statement of research/teaching interests and plans, contact information for three people who can provide letters of recommendation, and up to three pre/reprints of scholarly work. The positions will close no sooner than November 30, 2013, and will remain open until filled.

Applicants can consult http://cheme.columbia.edu/ for more information about the department.

Columbia University is an affirmative action/equal opportunity employer.

## American Philosophical Society Postdoctoral Fellowship in Advanced Materials

Benjamin Franklin founded the American Philosophical Society (APS) in 1743 as the nation's first learned society. For many years the APS served as the nation's de facto science academy and patent office and is today the administrator of the nation's oldest scientific prize (the Magellanic Premium, first awarded in 1790).

In conjunction with its longstanding tradition of supporting the research of early career scientists and scholars in all disciplines, the APS is pleased to offer a two-year postdoctoral fellowship. Sponsored by the Ewing Marion Kauffman Foundation, the fellowship, to be awarded by a committee made up of eminent members of the American Philosophical Society, will support innovative research projects in fields that change each year. The first competition supported a project in molecular biology, biochemistry, and/or the life sciences. This year's competition will focus on the field of advanced materials.

**Eligibility:** Applicants must have received the Ph.D. from an institution in the United States. Applicants should be either entering or already affiliated with a U.S. institution at the postdoctoral level and should have received the Ph.D. after July 1, 2012. Applications will be judged on their innovative nature. Applications for academic year 2014–2015, eligible for renewal in academic year 2015–2016, will be based on existing problems in advanced materials and can include projects concentrated in such areas as meta materials, nano materials, green energy materials, biomaterials, and similar fields.

**Award:** Stipends for the fellowship are $55,000 for the first year and $60,000 for the second year upon approval of a renewal request.

**Details and Application:** Complete information on the program, the requirements, and the application materials are available at the APS website (www.amphilsoc.org/grants/advancedmaterials).

**Deadline and Notification:** The application and the letters of support must be received by February 1, 2014. The committee's decision will be communicated by June 2014.

Questions may be directed to APS Director of Grants and Fellowships **Linda Musumeci**, at **LMusumeci@amphilsoc.org** or **215-440-3429**.

MUSC
MEDICAL UNIVERSITY of SOUTH CAROLINA

## CECILIA AND VINCENT PENG ENDOWED CHAIR IN MELANOMA AND CUTANEOUS ONCOLOGY

The Hollings Cancer Center of the Medical University of South Carolina (MUSC) in Charleston, South Carolina's only NCI-designated cancer center, is actively soliciting applications for the Cecilia and Vincent Peng Endowed Chair in Melanoma and Cutaneous Oncology. In addition to the endowed chair, the successful candidate would have a dual appointment including the department representing his/her own specialty (eg. medical or surgical oncology) and the Vice Chair for Research in the Department of Dermatology and Dermatologic Surgery. The Department has a thriving cutaneous oncology franchise that would fit especially well with an individual whose major interests lie in or interface with the fields of cutaneous carcinogenesis, tumor biology, and immunotherapy, especially with regard to melanoma and nonmelanoma skin cancer. MUSC's Departments of Surgery and Immunology have a strong, well-funded research presence in these areas, as well as a cell therapy and growth facility. MUSC has made a major commitment to expand its research footprint, as evidenced by the recent opening of the Clyburn Research Center, housing 78 labs and other facilities in 211,481 square feet. For this position, we are seeking an experienced NIH/NCI-funded investigator (MD, PhD, or MD/PhD) to strengthen our basic and translational research efforts and collaborate with the many excellent scientists in other clinical and basic science departments. Applications are welcome from all disciplines interfacing with melanoma research. This position is made even more attractive by the opportunity to live in a thriving and historic coastal city where the quality of life is voted by national publications to be among the best in the country. The position posting can be found at **https://www.jobs.musc.edu/postings/22208**.

Interested candidates should send their CV and a letter of interest detailing their clinical and research experience to **Bruce H. Thiers, MD, Chair, Department of Dermatology and Dermatologic Surgery, Medical University of South Carolina, 135 Rutledge Avenue, MSC 578, Charleston, SC 29425. E-mail: thiersb@musc.edu, Website: http://clinicaldepartments.musc.edu/dermatology**.

**MUSC is an EO/AA Employer.**

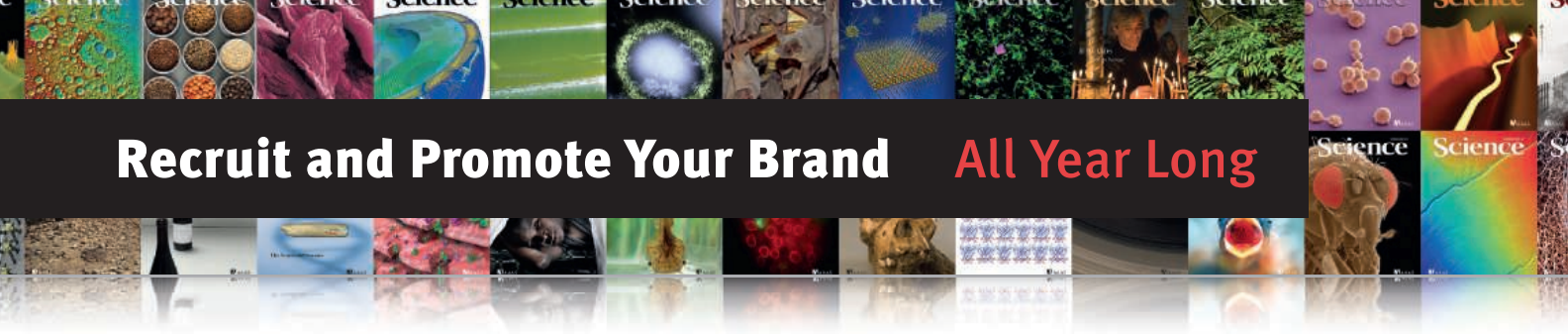

# Recruit and Promote Your Brand All Year Long

## *Science* Careers will publish a 2014 Career Directory that will be promoted and distributed all year long.

A combination of career development content alonside your branding ads makes this the pefect place to promote your organization's mission and the areas where you typically recruit. With bonus distributions to meetings and career fairs throughout the year and push marketing including banner ads and e-mail blasts to potential candidates, your company receives ongoing exposure to scientists eager to know about career opportunities.

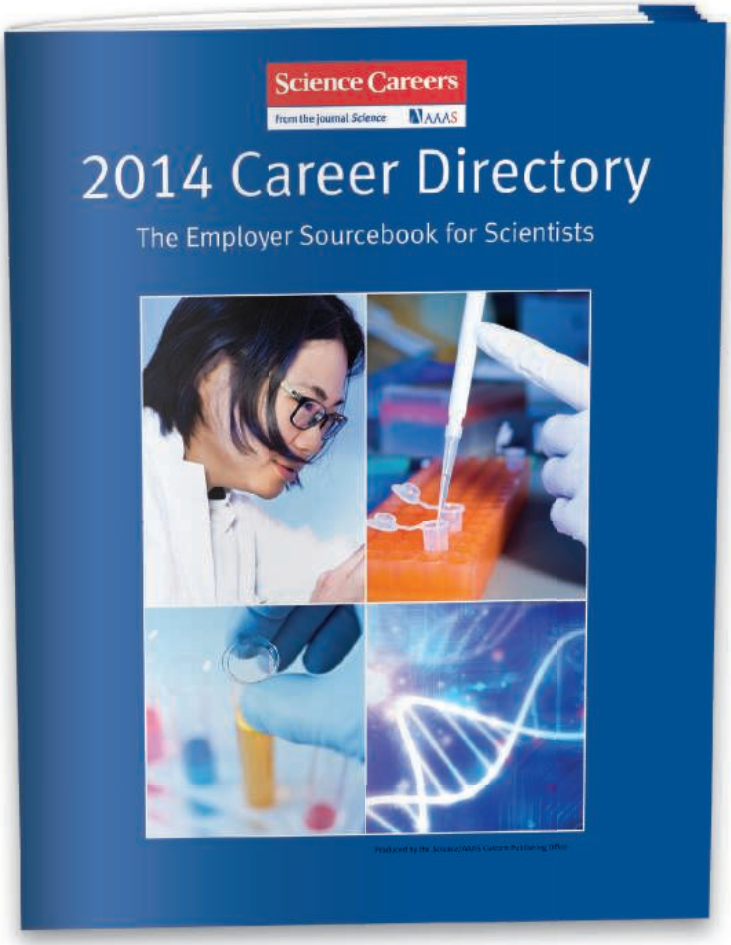


### Benefits to your company

- Opportunity to brand your organization to scientists beyond your normal reach.
- Print bonus distribution of 3,500 copies to career fairs and meetings around the globe.
- Digital copy e-mailed to 100,000 scientists including all *Science* Careers registrants.
- Your logo included in two Career Path newsletters.
- A PDF of the booklet will also be posted on *Science* Careers for one year with marketing to drive readers to the booklet. Marketing includes banners, e-mail blasts, and promotion across AAAS/*Science* newsletters.

**To book your ad or for more information:**
E-mail: advertise@sciencecareers.org

Or telephone us:
**US/Canada/South America:**
202-326-6582

**Europe/India/Australia/New Zealand/Rest of World:** +44 (0) 1223 326500

**Japan:** +81-(0)90-9110-1719

**China/Korea/Singapore/Taiwan/Thailand:** +86-1367-1015-294

**Reserve space by December 20, 2013**
**Ad materials due January 10, 2014**
**Rate: US$2,995**

For recruitment in science, there's only one Science

Produced by the *Science*/AAAS Custom Publishing Office

Science Careers
From the journal *Science* AAAS

ScienceCareers.org

NYIT
College of
Osteopathic Medicine

## FACULTY POSITION: BASIC SCIENCE MICROBIOLOGY EDUCATOR/RESEARCHER

New York Institute of Technology-College of Osteopathic Medicine (NYIT-COM), seeks an Assistant Professor for its Biomedical Sciences Department. Senior level applicants with extramural funding are also encouraged to apply. Under new leadership, the Department has established research strengths in cardiovascular diseases, neuroscience, and kidney development. The successful candidate is expected to establish a competitive research program with assigned **teaching in microbiology, immunology, or infectious disease**. The new faculty will have access to research facilities including an animal care facility (rats, mice, zebrafish), cell culture core, a microscopy core including two confocal microscopes, and a physiology core.

The successful candidate will possess a PhD, D.O., M.D., or D.V.M., and 2+ years of post-doctoral research experience. We offer research startup funds, a competitive benefits package including tuition remission, and a professional environment designed to enhance career development. To apply, please e-mail cover letter and resume to: **Dr. A. Martin Gerdes, Chair of Biomedical Sciences at agerdes@nyit.edu,** or mail to **NYIT-COM, PO Box 8000, Northern Blvd, Old Westbury, NY 11568-8000**.

*EOE M/F/D/V.*

GRU CANCER CENTER
GEORGIA REGENTS UNIVERSITY

## Group Leader in Tumor Angiogenesis

Cancer research at Georgia Regents University (GRU) is undergoing unprecedented expansion in line with the GRU Cancer Center's initiative to achieve NCI designation. Following successful completion of Phase 1 of this expansion, the GRU Cancer Center is seeking a leader in **Tumor Angiogenesis** who will pioneer a highly interactive program with the nationally recognized Vascular Biology Center within the GRU Medical College of Georgia and also develop this theme within the Cancer Center's Signaling and Angiogenesis Program. The selected candidate will work closely with clinical research oncologists to promote translational research. Applicants must have active extramural research funding (preferably from NCI) and a strong track record of independent research. The ideal candidate will have conducted research in an NCI-designated Cancer Center and is well-funded in areas of tumor angiogenesis research such as, targeted therapeutics for neovascularization, the relationship between tumor angiogenesis and inflammation, or novel approach to targeting neovascularization in tumor development. A competitive salary and start-up package are available, commensurate with experience and academic qualifications. For questions, please contact **Dr. John Cowell** (**jcowell@gru.edu**), **Dr. David Munn** (**dmunn@gru.edu**), or **Dr. Andy Mellor** (**amellor@gru.edu**). Please send a summary of research interests, curriculum vitae, and names of three references to **Dr. Rhea-Beth Markowitz** at **rbmarkowitz@gru.edu** and apply online at **www.gru.edu/facultyjobs**, referencing position number **10854**.

## Basic Cancer Research Scientists – Tumor Angiogenesis

As part of Phase 2 of its expansion of the basic sciences programs, the GRU Cancer Center invites applications for positions at **Assistant**, **Associate**, and **Full Professor** levels from interested individuals having expertise in the general area of **tumor angiogenesis**. Applicants must have active extramural research funding (preferably from NCI) and a strong track record of independent research. Ideal candidates will have conducted research in an NCI-designated Cancer Center. Successful applicants will join a collaborative Program that works closely with clinical research oncologists to promote translational research. A competitive salary and start-up package are available, commensurate with experience and academic qualifications. For questions, please contact **Dr. John Cowell** (**jcowell@gru.edu**), **Dr. David Munn** (**dmunn@gru.edu**), or **Dr. Andy Mellor** (**amellor@gru.edu**). Please send a summary of research interests, curriculum vitae, and names of three references to **Dr. Rhea-Beth Markowitz** at **rbmarkowitz@gru.edu** and apply online at **www.gru.edu/facultyjobs**, referencing position number **18051**.

*Georgia Regents University is an Equal Opportunity Affirmative Action, and Equal Access Employer. Georgia Regents University has a strong interest in promoting diversity in its faculty and women and minority candidates are encouraged to apply.*

JOHNS HOPKINS BLOOMBERG SCHOOL of PUBLIC HEALTH

## Faculty Position Biochemistry and Molecular Biology

The Department of Biochemistry and Molecular Biology at the Bloomberg School of Public Health of Johns Hopkins University invites applications for a tenure-track faculty position, preferably at the Assistant Professor level. We seek outstanding applicants with a demonstrated ability to study problems of major public health relevance at the cellular, molecular, and/or structural level. Areas of highest priority for this search include DNA repair and genome integrity. Applicants interested in stress response biology, chronic diseases and cancer biology should also apply. Successful applicants will be expected to establish an outstanding research program, be strongly committed to graduate level training and education, and contribute to the success of the department and school. Visit **http://www.jhsph.edu/departments/biochemistry-and-molecular-biology/faculty-openings/** for information about the application process and recent faculty hires. Applications will be accepted until **January 15, 2014**.

*We actively encourage applications from women and minority candidates. The Johns Hopkins University is an Equal Opportunity/Affirmative Action Employer.*

UNIVERSITY OF NEVADA •Reno

## Department of Biology Functional Genomics and Bioinformatics Faculty Positions

The Department of Biology seeks two faculty positions, one in **FUNCTIONAL GENOMICS** and one in **BIOINFORMATICS**, at the assistant professor level, tenure-track. For the functional genomic position, we are seeking candidates using functional genomic and bioinformatic approaches to investigate cellular and neural functions, but any other areas of focus will be considered. Of particular interest are candidates who integrate innovative high-throughput sequencing and bioinformatics-based experimental approaches to examine neural functions through detailed analysis of the genome and/or transcriptome. For the bioinformatics position, we are interested in candidates whose research seeks to develop and apply computational and quantitative methods to interrogate large data sets in the study of biology. Possible areas include, but are not limited to, genomic and transcriptomic data analysis, regulatory networks, biological systems, and should address fundamental questions in biology, including biomedical, evolutionary and ecological fields. The successful candidates will be expected to develop an innovative, extramurally-funded, research program, and teach at the undergraduate and graduate levels. The Department recently hired a genome biologist and is currently recruiting two Neurobiologists, who together with the new faculty hires in functional genomics and bioinformatics would generate synergistic interactions with the diverse faculty in the Biology Department including faculty supported by a Neuroscience and Cell Signaling COBRE.

The University of Nevada, Reno, offers competitive start-up support, in addition to an interactive research environment, including outstanding core facilities in proteomics, genomics, microscopy, bioinformatics and flow cytometry. The Biology Department is home to 26 faculty members that maintain nationally recognized, extramurally funded research programs, mentor 50 graduate students, and participate in undergraduate teaching. The Department has a growing neuroscience, developmental biology and evolutionary genomics research clusters, focusing on neural development, behavioral genetics, speciation and adaptation. Faculty members in the Department of Biology have close ties to the University of Nevada School of Medicine and over $60 million of NIH funds have recently been targeted for biomedical research development on campus. Reno is located in the Sierra Nevada mountains near Lake Tahoe, and was recently rated one of the best small cities in the US for outdoor recreation and overall quality of life.

Go to **http://jobs.unr.edu** to submit application materials, including an application letter, CV, research plans, teaching interests, and contact information for three references. Applications received by **January 10, 2014** will receive full consideration.

*Equal Employment Opportunity/Affirmative Action.*
*Women and underrepresented groups are encouraged to apply.*

**Nontraditional Careers:** Opportunities Away From the Bench

Webinar

Want to learn more about exciting and rewarding careers outside of academic/industrial research? View a roundtable discussion that looks at the various career options open to scientists and strategies you can use to pursue a nonresearch career.

**Now Available On Demand**
**www.sciencecareers.org/webinar**

Produced by the *Science*/AAAS Business Office.

Science Careers
From the journal *Science* AAAS

## POSITIONS OPEN

### BINGHAMTON UNIVERSITY
### State University of New York (SUNY)

Anthropology Department seeks a biological anthropologist specializing in epidemiology for a tenure-track appointment at the Assistant Professor level to begin August 2014. Applicants must have a Ph.D., demonstrated teaching experience, an active research program, and publications. The areas of expertise within epidemiology should include one or more of the following: evolutionary medicine, international health, genetic epidemiology, and/or the epidemiology of chronic and infectious diseases. The candidate is expected to develop an active research program with field-based and/or laboratory-based research, and with plans to incorporate students in her/his research. This position must support the Biomedical Anthropology M.S. Degree program by teaching core courses for the MS, as well as advising Biomedical M.S. students, and providing teaching support for pre-med students who need to meet the new competency requirements for the MCAT exams. Applicants should review the graduate and undergraduate programs and other faculty interests at **website: http://www.binghamton.edu/anthropology/.**

Formal review of applications will begin December 2, 2013 and will continue until the position is filled. Applications consisting of a cover letter addressing teaching and research interests, curriculum vitae, and contact information for three references must be sent electronically by visiting **website: http://binghamton.interviewexchange.com.** In addition, hard copies should be sent to: **Chair, Biological Anthropology Search Committee, Department of Anthropology, Binghamton University, P.O. Box 6000, Binghamton, NY 13902-6000.** Questions about the position may be directed to **e-mail: anthsrch@binghamton.edu.**

*Binghamton University is an Equal Opportunity/Affirmative Action Employer.*

---

### POSTDOCTORAL POSITION AVAILABLE
### Obesity and Type 2 Diabetes

A postdoctoral position is available at the Hallett Center for Diabetes and Endocrinology of Alpert Medical School of Brown University.

Requirement: Ph.D. degree with extensive experience in cellular and molecular biology as well as mouse physiology. Background in obesity-related research, particularly in liver and adipose tissue energy homeostasis. A strong publication record. Skills such as primary hepatocyte and adipocyte isolation as well as hyperinsulinemic-euglycemic clamp are necessary. The applicant will study the role of MAP kinase phosphatase 3 in hepatic and adipose energy homeostasis in obese state. For more information regarding our research, please visit the PI's **website: http://research.brown.edu/myresearch/Haiyan_Xu.** Successful applicant will be generously offered with NIH guideline-based salary and fringe benefits. Please send curriculum vitae and the contact information of three references to: **Haiyan Xu MD, Ph.D., Associate Professor of Medicine, Alpert Medical School of Brown University, Hallett Center for Diabetes and Endocrinology, 55 Claverick Street, Rm 318, Providence, RI 02903; telephone: 401-444-0347; fax. 401-444-3784; e-mail: haiyan_xu@brown.edu.**

---

Two **POSTDOCTORAL POSITIONS** are available. First position will investigate the Keap1/INrf2 signaling and role in cancer and metastasis. Second position will investigate the role of Nrf2 downstream NQO1 and NQO2 in control of growth/differentiation/proliferation factors in prevention of Breast Cancer Metastasis.

The positions will involve studying protein-protein interaction, protein modifications and degradation, apoptosis, cell proliferation and knockout/transgenic mice disease models. Experience in biochemical and molecular biology techniques and working with mice disease models is essential. Applicants should submit curriculum vitae, names, addresses, telephone numbers, and e-mail addresses of three references. Contact: **Anil Jaiswal, Ph.D., Professor, Department of Pharmacology, University of Maryland School of Medicine, 655 West Baltimore Street, Baltimore, MD 21201** or **e-mail: ajaiswal@som.umaryland.edu.**

## POSITIONS OPEN

### INTERDISCIPLINARY:
### Research Computational Biologist or Research Molecular Biologist or Research Geneticist (Plants)

The U.S. Department of Agriculture, Agricultural Research Service, Plant Gene Expression Center (PGEC) (**e-mail: pgec@ars.usda.gov**) in Albany, California invites applications for a Research Scientist position with expertise in plant biology and bioinformatics, GS-12/13/14. PGEC research is conducted through a close collaborative partnership with the University of California, Berkeley. The successful candidate will be responsible for developing a research program that addresses a key challenge in modern plant biology to develop and deploy new genomic and computational tools for integrating "big data" in order to accelerate rates of gain in crop performance through genomics-enhanced breeding for cereals and perennial grasses. The successful applicant will be considered for an Adjunct Faculty appointment in the Department of Plant and Microbial Biology, University of California, Berkeley. This is a permanent, full time position. U.S. Citizenship is required. The salary range is $81,460.00 to $148,806.00 per annum, which is commensurate with experience/qualifications. A comprehensive Federal benefits package is available. For application instructions, see **website: http://www.usajobs.gov. Keyword: ARS-XW14-0015.** Announcement closes January 10, 2014.

*The USDA/ARS is an Equal Opportunity Employer and Provider.*

---

### BIOLOGY

The Department of Biology at The College of Wooster invites applications for a three-year **VISITING POSITION** in Molecular Physiology to teach introductory biology and upper level courses in cellular and molecular biology. Preference will be given to candidates who can also teach Human or Plant Physiology. Will direct undergraduate research in the College's required Independent Study Program. Applicants should have a Ph.D.; postdoctoral research and/or teaching experience preferred. Send curriculum vitae, statements of research and teaching philosophy, transcripts, and three letters of recommendation to **Beth Snyder,** Administrative Coordinator (**e-mail: biology@wooster.edu**). Questions should be directed to **M. D. Loveless,** Chair of Biology, The College of Wooster, Wooster, OH (**e-mail: mloveless@wooster.edu**). Electronic applications are preferred, and should be received by January 6, 2014, for full consideration.

*Wooster seeks to ensure diversity by its policy of employing persons without regard to age, sex, color, race, creed, religion, national origin, disability, veteran status, sexual orientation, or political affiliation. The College of Wooster is an Equal Opportunity/Affirmative Action Employer.*

Help employers find you. Post your resume/cv.

Science Careers
From the journal *Science* AAAS

www.ScienceCareers.org

## MARKETPLACE